Strategies to Improve Non-Viral Gene Delivery and the Preclinical Investigation of Nanomedicines

Inauguraldissertation

zur
Erlangung der Würde eines Doktors der Philosophie
vorgelegt der
Philosophisch-Naturwissenschaftlichen Fakultät der
Universität Basel
von

Jonas Buck

2021

Genehmigt von der Philosophisch-Naturwissenschaftlichen Fakultät

Auf Antrag von

Prof. Dr. Jörg Huwyler

Prof. Dr. Alex Odermatt

Prof. Dr. Paola Luciani

Basel, 21. April 2020

Prof. Dr. Martin Spiess (Dekan)

Nothing has such power to broaden the mind as the ability to investigate systematically and truly all that comes under thy observation in life.

Marcus Aurelius

Contents

1 Zusammenfassung für Laien

Konventionelle medikamentöse Therapien basieren auf der Verabreichung therapeutischer Moleküle über verschiedene Verabreichungswege (z.B. orale, parenterale oder topische Verabreichung). Alle diese Routen haben eine Gemeinsamkeit: Durch die Verabreichung wird der ganze Organismus dem therapeutischen Molekül ausgesetzt. Dies führt dazu, dass diese Moleküle auch mit Zellen und Geweben interagieren, mit denen sie nicht interagieren sollten. Dies ist einer der Hauptgründe für beobachtete Nebenwirkungen. Um die notwendige Konzentration am Wirkort zu erreichen wird daher eine viel höhere Dosis als nötig verabreicht, da die verabreichte Dosis sich im Körper verteilt.

Eine Lösung dieses Problems besteht darin, die therapeutischen Moleküle direkt zu ihrem Wirkort zu führen. Einerseits führt dieser Ansatz - in Fachkreisen "targeted drug delivery" genannt - dazu, dass weniger Moleküle am falschen Ort landen, was Nebenwirkungen bereits reduzieren kann. Andererseits kann durch diesen Ansatz die Dosis, die verabreicht werden muss, bei gleichbleibender Wirkung drastisch reduziert werden, weil die Moleküle direkt zum Wirkort geführt und nicht auf den ganzen Körper verteilt werden. Verschiedene Strategien ermöglichen die gezielte Verabreichung von therapeutischen Molekülen, doch die am weitesten verbreitete Strategie basiert auf der Verwendung von Nanopartikeln. Aufgrund ihrer extrem kleinen Grösse ($\leq$100 nm) können diese Nanopartikel von Zellen aufgenommen werden und ermöglichen dadurch die intrazelluläre Freisetzung der therapeutischen Moleküle. Unter den verschiedenen Typen von synthetischen (nicht-viralen) Nanopartikeln sind lipidbasierte Nanopartikel die am besten charakterisierten und am weitesten verbreiteten Systeme. Nanopartikel werden in der Regel zusätzlich dekoriert mit Molekülen, die eine lange Zirkulation im Blutkreislauf ermöglichen, sowie mit sogenannten targeting Molekülen, die eine gezielte Verabreichung erst ermöglichen und die

Nanopartikel zu spezifischen Zellpopulationen führen.

Die Verkapselung innerhalb von Nanopartikeln ist besonders wichtig für therapeutische Nukleinsäuren (z.B. DNA), da nackte Nukleinsäuren in der Blutbahn umgehend von Serumnukleasen abgebaut werden. Dies kann durch Verkapselung verhindert werden. Die Verabreichung therapeutischer Geninformation (Gentherapie) zeigt dabei einige Vorteile gegenüber konventionellen medikamentösen Therapien. Viele genetische Erkrankungen manifestieren sich aufgrund eines Defekts in der genetischen Information, die als Blaupause für die Herstellung von Enzymen dient, welche wiederum für die Aufrechterhaltung der normalen Körperfunktionen verantwortlich sind. Aufgrund des Defekts in der Blaupause können die entsprechenden Enzyme nicht oder nur in einer Form mit reduzierter Enzymaktivität hergestellt werden. Wird der Zelle jedoch die korrekte Geninformation (z.B. in Form von DNA) zugeführt, können die negativen Einflüsse des defekten nativen Enzyms ausgeglichen werden. Die folgenden Vorteile treten daher besonders zutage: Erstens ist die konventionelle medikamentöse Therapie oftmals nicht in der Lage, die Ursachen der Erkrankung zu beheben, sondern behandelt nur die Symptome. Zweitens kann eine Zelle, wenn mit der korrekten Blaupause versorgt, das Enzym selber herstellen. Drittens wurde für einige genetische Erkrankungen gezeigt, dass schon Bruchteile der natürlichen Aktivität eines Enzyms ausreichen, damit betroffene Personen symptomfrei leben können. Viertens sorgt die lange Persistenz von DNA im Zellkern dazu, dass die Anzahl therapeutischer Interventionen massiv reduziert werden kann (z.B. halbjährliche Intervention gegenüber täglicher).

Trotz dieser Vorteile bleibt dieses Forschungsgebiet ein komplexes Thema und viele der zugrunde liegenden Mechanismen entziehen sich bisher unserer Kenntnis. Aus diesem Grund ist es das Ziel des ersten Teils der vorliegenden Doktorarbeit, die Effizienz einer klinisch relevanten Nanopartikelformulierung zu erhöhen und das Verständins molekularer Strukturen für eine erfolgreiche

Gentherapie zu vertiefen. Weiter zeigt die Arbeit im zweiten Teil Möglichkeiten auf, wie man die molekularen Wechselwirkungen zwischen DNA und Nanopartikeln mittels einer fluoreszenzbasierten Methode bestimmen kann. Im Dritten Teil geht die Arbeit auf die Möglichkeit ein, virale Strukturen als targeting Moleküle auszunutzen und wie eine lange Zirkulationszeit im Blutkreislauf erreicht werden kann, ohne eine Immunantwort zu provozieren.
Im letzen Teil wird ein neues Tiermodell präsentiert und diskutiert. Das Tiermodell bedient sich der Embryos des Zebrafisches, um neue antibiotische Substanzen und neue Therapieansätze zu testen. Aufgrund ihrer Transparenz können fluoreszenzbasierte Methoden verwendet werden und die hohe Reproduktionsrate ermöglicht einen hohen experimentellen Durchsatz bei der Suche nach neuen antibiotischen Substanzen.

2 Summary

Conventional drug therapy relies on the introduction of therapeutic molecules into the body through various routes of administration (*e.g.*, oral, parenteral, or topical). However, all these applications share a serious drawback: Following administration, the whole organism is exposed to the therapeutic molecule. Consequently, therapeutic molecules can interact with cells or tissues they were not intended to interact with, which is a major driver of side effects. To account for the distribution in the body, much higher doses than necessary are administered to ensure a sufficiently high concentration of the therapeutic molecule at the target site.

A solution to this problem is to direct the therapeutic molecules to the specific cells where they are needed. On the one hand, this approach, called targeted drug delivery, reduces the number of molecules that end up in the wrong place in the body, thereby reducing side effects. On the other hand, this enables a drastic reduction of the required dose while maintaining the same effect because the therapeutic molecules are directed to the site where they are required instead of being distributed all across the body. There are several strategies to achieve targeted drug delivery but the use of nanoparticles is one of the most common approaches. Due to their small size ($\leq$100 nm), nanoparticles are taken up by cells and therefore, enable the intracellular release of therapeutic molecules. Among the different types of nanoparticles of synthetic (non-viral) origin, lipid-based nanoparticles are the best characterized and most used ones. Nanoparticles are usually decorated with molecules that enable prolonged circulation in the bloodstream and with targeting molecules that direct the nanoparticle to a specific cell population.

The benefits offered by encapsulation into targeted nanoparticles are even more pronounced for nucleic acids (*e.g.*, DNA) because naked nucleic acids are rapidly degraded in the blood circulation by serum nucleases which is pre-

vented by encapsulation. Gene therapy offers a number of advantages. Many genetic diseases manifest due to defects in the genetic information that is the blueprint for enzymes responsible for maintenance of normal body functions. Due to the defect in the blueprint, the enzyme cannot be produced or its activity is reduced. The introduction of the correct genetic information (blueprint) in the form of DNA or other nucleic acids can counterbalance the negative effects of the defective native enzyme. This approach is very attractive due to several reasons: First, conventional drug therapy is usually unable to cure genetic diseases but only treats or attenuates the symptoms. Second, with the correct blueprint at hand, the cells own "enzyme factory" can produce the "cure". Third, the restoration of only a small proportion of the native activity of the enzyme is often sufficient for the patients to live without symptoms. Fourth, the long persistence of DNA molecules in the cell nucleus ensures prolonged expression of the enzyme, thereby drastically reducing the number of therapeutic interventions compared to conventional drug therapy (*e.g.*, once every six months compared to daily intake).

Despite these promises, the field of non-viral drug and gene delivery is a very complex topic and the underlying mechanisms and important factors for therapeutic success often remain elusive. Therefore, the first part of this PhD thesis aimed to improve the efficiency of a clinically relevant lipid nanoparticle formulation for gene delivery, as well as our understanding of molecular structures important for successful gene delivery (Chapter 1). Furthermore, the interactions between lipid nanoparticles and DNA molecules are investigated using a fluorescence-based method. The method provides a means to determine the number of DNA molecules per nanoparticle, a question that has only been addressed theoretically so far (Chapter 2). The proposed method enables researchers to draw more precise conclusions from their gene delivery experiments. The third part of the thesis focuses on the improvement of targeting and

blood circulation properties of lipid-based drug delivery vehicles. A novel targeting molecule derived from the hepatitis B virus enables highly efficient and selective liposome delivery to hepatocytes whereas a novel nanoparticle shielding molecule demonstrated enhanced blood circulation properties comparable to the gold standard (PEG) while avoiding immune responses associated with PEG (Chapter 3).

Finally, a transparent animal infection model (zebrafish embryo) for the investigation of novel antibiotic compounds is discussed (Chapter 4). The transparency allows the application of fluorescence-based methods to evaluate antibiotic compounds, thereby improving our understanding of antibiotic therapy according to the proverb "seeing is believing". Furthermore, the high reproduction rate and the relatively low regulatory requirements enable the screening of a large number of compounds, thereby possibly accelerating research in the field of antibacterial drug therapy.

3 Introduction

3.1 The Goals of Gene Delivery

The delivery of therapeutic nucleic acids is a promising strategy to treat or even cure inherited genetic diseases and possibly also acquired diseases. In fact, many inherited genetic diseases such as severe-combined immunodeficiency (SCID), haemophilia, Crigler-Najjar syndrome, Gilbert's syndrome, Niemann-Pick disease, or α1-antitrypsin deficiency [1–7] are associated with genetic defects leading to loss of function of proteins or very low levels of enzyme activity. Using gene therapy, several approaches can be envisioned to treat such conditions. First, small interfering RNA (siRNA) can be introduced into cells to modify or inhibit the protein expression level by means of RNA interference (RNAi). [8] As a double-stranded oligonucleotide of around 19-25 base pairs in length, siRNA binds to the RNA-induced silencing complex (RISC), allowing the cleavage of the targeted messenger RNA (mRNA) thereby inhibiting translation of the targeted mRNA into proteins. [9] Another approach is the introduction of genetic material (*e.g.*, plasmid DNA) encoding for a functional version of the protein. With the correct blueprint for the protein provided in the form of RNA or DNA, the cells' own (transcription)/translation machinery is then capable to produce the functional variant of the dysfunctional protein. In some cases (*e.g.*, cystic fibrosis) such interventions seem very promising due to the fact that only a small fraction ($\leq$10%) of the native enzyme activity needs to be restored for the affected patients to live symptom-free. [10] Moreover, the transient nature of this gene delivery approach circumvents issues associated with gene therapies relying on insertion of the delivered DNA into the host cell's genome. Generally, plasmid DNA exists as an episomal entity that is not integrated into host chromosomal DNA and replicated seperately, [11,12] although plasmid DNA can also be designed to promote chromosomal integra-

tion. [13, 14] The third possible intervention is relying on gene editing. Genetic information *e.g.*, plasmid DNA encoding for gene editing tools such as CRISPR/Cas9 can be introduced using gene delivery systems to modify the target cell's genome. Gene editing holds the promise to cure genetic diseases on a genomic level but is also associated with more severe ethical concerns compared to transient gene delivery due to the long-term implications of insertion of exogenous genetic material into the genome. [15]

3.2 Strategies to Delivery Genetic Material

Nucleic acids (such as DNA, or especially RNA) are unstable in the blood circulation when injected intravenously [16, 17] and need to be protected from noxious agents such as serum nucleases. An attractive approach to protect nucleic acids relies on encapsulation of the nucleic acids into nanocarriers that mimic viral structures. In the field of gene delivery, we can identify several nanocarrier-based delivery strategies (in contrast to physical methods such as microinjection or electroporation, which offer no protection because these are not carrier-based approaches):

As a result of millions of years of evolution, viruses represent a naturally evolved vector that is able to transfer exogenous nucleic acids (DNA, RNA) to human (or other) cells in a very efficient manner. [18] It is therefore not surprising that gene therapy was pioneered by viral carriers due to these properties since the advent of this therapeutic option. Despite their efficiency, viral vectors carry several drawbacks such as immunogenicity, high costs, oncogenicity and the risk for insertional mutagenesis, as well as the limited size of DNA that can be encapsulated by viruses. [19, 20]

As an alternative to viral vectors, synthetic non-viral nanoparticulate drug delivery systems can be used to encapsulate therapeutic agents. Non-viral

delivery vehicles can be divided into inorganic materials, polymeric materials, and lipid or lipid-like materials. While inorganic materials were the first non-viral gene delivery vehicles to be discovered, [21] they are often only suitable for *in vitro* experiments. Polymeric materials are very versatile, allow for targeting approaches and efficiently condense DNA into nanoparticles but have their drawbacks in their high batch-to-batch variability and cytotoxicity. For polymeric compounds, it is key to find the balance between efficiency and cytotoxicity. For example, it was reported that both delivery efficiency and cytotoxicity increase with polymer length. [19] Finally, lipid-based non-viral gene delivery systems are the most thoroughly investigated non-viral gene delivery systems, [22] show low immunogenicity and toxicity, [23] allow for targeting approaches, and can incorporate large nucleic acid molecules. While lipid based systems are probably the best of the "artificial" transfection systems, they also suffer from some drawbacks such as higher cytotoxicity than viral vectors, [24] a possible colloidal instability in biologically relevant media, [25–27] rapid clearance from the blood compartment due to unspecific interactions with membranes or serum proteins when unshielded, [28] and a general lack of efficiency and specificity compared to viral vectors. [29, 30] However, there are several approaches to tackle the drawbacks of lipid-based gene delivery vehicles as discussed later on. For example, surface modification of the nanoparticles with sterically hindering and hydrophilic polymeric compounds such as polyethylene glycol (PEG) increases colloidal stability and reduces clearance of lipid-based nanoparticulate gene delivery systems when they are administered intraveniously, while the use of targeting moieties increases efficiency and specificity. Due to the aforementioned advantages and the presented strategies to circumvent drawbacks of lipid-based gene delivery systems, this thesis focuses on liposomes and lipid nanoparticles. Different lipid-based non-viral gene delivery vehicles and the most important influence

factors for gene delivery are discussed in detail in **Chapter 1.1**, [31] while a straightforward one-pot synthetis to obtain aminolipids for lipid-based gene delivery is described in **Chapter 1.2**. [32] The proposed synthesis described in this thesis is in stark contrast to many other described synthesises in that it comprises a one-pot reaction as opposed to complicated multi-step reactions often seen in literature. [33, 34] Moreover, avoidance of a cationic charge can circumvent cytotoxicity issues because interactions between the cationic lipid and cellular proteins, membranes and serum proteins can account for cytotoxicity, inflammatory toxicity, reduced cellular uptake, accelerated blood clearance, or even hemolysis [24, 35]

3.3 Nucleic Acids for Gene Delivery

In addition to the composition of the nanoparticle, the type of nucleic acids used to carry the genetic information of interest can influence the interaction with the gene delivery system [36, 37] and thereby the outcome of the experiment or therapy. For example, RNA moieties do not need to be delivered to the nucleus and offer pharmacological effects without nuclear entry, which is an important hurdle in DNA delivery. Thus, it is sufficient to deliver RNA moieties to the cytosol where they can either be translated into proteins (mRNA) or inhibit or modify protein expression by a process called RNAinterference (siRNA). Plasmid DNA, however, needs to be translocated to the nucleus to be transcribed and translated into proteins. Despite the additional hurdle of having to enter the cell nucleus, plasmid DNA is able to introduce the genetic blueprint for the prolonged expression of therapeutic proteins (up to several months). In stark contrast, these effects are short-lived in the case of RNA-based strategies. [37, 38] In view of this, plasmid DNA-based strategies seem to be beneficial when the long-term expression of a protein is desired because

the number of administrations can be reduced, resulting in increased compliance. However, due to their bacterial origin, plasmids contain sequences not necessary for, or even detrimental to, successful gene delivery. In addition to the expression cassette, which contains the gene of interest (GOI) as well as an eukaryotic promoter and a polyadenylation (polyA) sequence, plasmid DNA also comprises a bacterial backbone including a bacterial origin of replication (ORI), and antibiotic resistance genes. [11, 39] This bacterial backbone can be recognized by the immune system and is subjected to epigenetic silencing, leading to a complete loss of expression of the desired protein in the long-term. [39–41] To reduce or even eliminate this time-dependent epigenetic silencing, a miniaturized plasmid moiety was proposed: minicircle DNA. Minicircle DNA is devoid of bacterial backbone sequences and is therefore both, smaller in size and less prone to epigenetic silencing. [42] This results in increased delivery efficiency and transgene expression levels, as well as in a prolonged transgene expression. For example, long-term treatment of murine phenylketonuria with minicircle DNA encoding for murine phenylalanine hydroxylase led to a normalized blood phenylalanine level and reversed hypopigmentation for more than 1 year, whereas phenylalanine clearance rapidly declined after treatment with the corresponding parental plasmid. [43] There is a consensus in the literature that minicircle DNA is superior to its corresponding larger parental plasmid DNA. However, the implications for the formation of nanoparticle/minicircle DNA complexes are still a matter of debate. To improve the understanding of the interactions between nanoparticles and different DNA molecules, a straightforward, fluorescence-based method (fluorescence cross-correlation spectroscopy, FCCS) is discussed in **Chapter 2.1**. [44] Because confocal imaging is a standard method for the assessment of gene delivery efficiency, many laboratories in principle possess the capability to perform FCCS experiments. Therefore, this method can be used to gather

additional information on the formation of nanoparticle/DNA complexes and to improve the quality of conclusions drawn from transfection experiments.

3.4 Targeting of Gene Delivery Vehicles

The delivery of therapeutic agents to specific cell populations or tissues has been the goal of targeted drug delivery approaches for a long time. [45, 46] Therapeutic agents other than nucleic acids that also profit from a targeted drug delivery approach include, but are not limited to, small molecules, [47] and large biomolecules such as enzymes. [48,49] Targeting of therapeutic agents can be achieved by several ways, for example by direct coupling of a targeting moiety to the therapeutic agent or by encapsulation of the therapeutic agent into a nanocarrier vehicle and subsequent modification of the vehicle with targeting moieties. [48] While direct coupling of targeting moieties to the therapeutic agent can be an attractive approach for large but stable biomolecules, encapsulation into nanocarriers is the preferred option for small molecules or nucleic acids. Moieties suitable for targeting include for example small molecules, [50, 51] sugars, [52, 53] peptides, [54, 55] non-immune proteins, [56–59] or antibodies or fragments thereof. [60–62] An interesting approach is to exploit naturally occuring mechanisms for selective targeting strategies such as mechanisms used by pathogens. An example of such a mechanism is provided by the hepatitis B virus (HBV). It was shown that less than 10 virus particles are sufficient to induce a pathogenic HBV infection in chimpanzees. [63] The large HBV envelope protein (HBVpreS) was shown to contain a highly specific amino acid sequence responsible for the efficient and specific targeting of hepatocytes. [64, 65] The applicability of this approach to specifically target hepatocytes using HBVpreS peptide variants as a targeting moiety is discussed in **Chapter 3.1**. [66]

3.5 Avoiding Recognition by the Immune System

For successful targeting strategies, it is important to optimize the circulation behavior of nanoparticles. Unshielded nanoparticles are prone to unspecific interactions with *e.g.*, cell membranes or serum proteins [28, 67, 68] due to charge interactions. Such interactions lead to opsonization of the nanoparticle surface and aggregation of nanoparticles due to impaired colloidal stability. Large aggregates or opsonized nanoparticles are then rapidly cleared *e.g.*, by macrophages of the mononuclear phagocytic system (MPS), also called the reticuloendothelial system (RES). [69–71] To avoid opsonization and clearance from the blood circulation, decoration of nanoparticles with PEG (*e.g.*, using 1,2-distearoyl-sn-glycero-3-phosphoethanolamine-N-[methoxy(polyethylene glycol)-2000], DSPE-mPEG2k) turned out to be the gold standard since 1990. [72–76] However, despite improved circulation properties offered by PEGylation, the emergence of Anti-PEG antibodies has raised concerns towards this strategy. It is believed that increased exposure to PEG, which is contained in many products (such as cosmetics) that are used in everyday life, is at least in part responsible for the emergence of Anti-PEG antibodies even in healthy individuals. [77] The emergence of Anti-PEG antibodies is especially detrimental to therapeutic interventions that require repeated dose administration of PEGylated moieties due to the drop in efficiency observed for the second and following interventions. [78–81] Because both, the phospholipid that anchors PEG in the nanoparticle and PEG itself are considered to cause immune reactions, [82] it is not sufficient to replace only the hydrophilic part of DSPE-mPEG2k but a replacement of the anchor is also needed. As a superior alternative to DSPE-mPEG2k, the use of bisalkyl polysarcosines (BA-pSar), where the DSPE anchor is replaced by bisalkyl chains and the mPEG2k moiety is

replaced by polysarcosines is discussed in **Chapter 3.2**. [83]

3.6 *In Vivo* Assessment of Nanoparticulate Drug Delivery Vehicles and Small Molecule Drugs

The assessment of the circulation behavior of BA-pSar-modified liposomes and of HBVpreS-modified liposomes was carried out in the zebrafish (*Danio rerio*) embryo animal model in these studies The zebrafish embryo is a fast-reproducing organism that allows for high-throughput screenings in a vertebrate animal model. Its transparency makes it especially suitable for fluorescence-based methods thereby providing qualitative data with respect to circulation behavior or macrophage clearance. There is a large variety of genetic variants of zebrafish that express different fluorescent proteins in different tissues, for example the kdrl:eGFP (fluorescent vasculature) or the mpeg:kaede (fluorescent macrophages) fish lines. Another important consideration in animal trials is the administrative effort required to rectify animal experiments. The zebrafish embryo is classified as cell culture trial up to 5 days (120 h) post-fertilization, [84] avoiding the need for approval of animal trials and thereby increasing the possible experimental throughput as well. Moreover, assessments in the zebrafish embryo model, implemented in our lab by excellent work of Dr. Sandro Sieber, were shown to be highly predictive of the situation in rodents (mice, rats). [85] Consequently, the zebrafish embryo offers the unique possibility to pre-select interesting candidates for animal trials and discard candidates with poor circulation behavior, thereby reducing the number of animals needed for animal trials. However, the zebrafish embryo can not only be used to determine the circulation behavior of nanoparticulate drug delivery systems but also to assess the efficiency of treatment of small molecule drugs. In the field of bacterial infections, emergence of antibiotic resistance

(ABR) is a serious problem. [86] Increasing spread of resistance genes renders conventional antibiotic therapies inefficient. There are several mechanisms by which pathogenic bacteria can counter or evade antibiotic treatment. The most prominent of these mechanisms is the inheritance of antibiotic resistance by either mutagenesis or lateral gene transfer between microorganisms by means of plasmid DNA. [87,88] Another mechanism involves the emergence of dormant forms of bacteria, called persister cells. These non-dividing cells are not per-se resistant to the antibiotic intervention but are almost insusceptible to such therapies due to their dormancy. [89–92] Furthermore, a number of pathogenic microorganisms including *Salmonella* species are able to survive and replicate within so-called *Salmonella* containing vacuoles (SCV) in macrophages. [93–96] The microorganisms not only evade the innate immune system by this mechanism but also antibiotic treatment, especially in the case of antibiotics that do not cross cell membranes such as tobramycin. A similar strategy is also found in *Mycobacterium* species. [97–99] Consequently, the search for novel antibiotic compounds and antibiotic adjuvants, or novel treatment approaches is a major focus of current research efforts. The applicability of the zebrafish embryo animal model to tackle these problems is discussed in **Chapter 4.1** [100]. Maximizing the effect of already marketed antibiotics using alkylresorcinols as an antibiotic adjuvant (**Chapter 4.2**), [101] and nanoparticle-based delivery of antibiotics directly to macrophages are two possible ways by which the ABR problem can be reduced. The zebrafish embryo animal model could be an interesting model organism to test the two approaches *in vivo* due to the high throughput (alkylresorcinols), and the transparency (macrophage targeting) offered by this animal model.

4 Aim of the Thesis

Lipid-based delivery systems are very promising candidates for the delivery of both, nucleic acids, and conventional small drug molecules. However, the mechanisms involved in successful delivery often remain elusive. It was therefore the aim of this PhD thesis to develop optimized gene delivery systems, to investigate mechanisms important for lipid-based drug and gene delivery, and to apply the zebrafish as a proof-of-concept animal model. The following questions were addressed:

- **Evaluation of lipid-based gene delivery vehicles**

What is the influence of the molecular structure of lipids on gene delivery?
What factors are important for successful *in vitro* and *in vivo* gene delivery?
How to simplify lipid synthesis?

- **Evaluation of lipid nanoparticle (LNP)-DNA interactions**

What is the influence of nucleic acid size on LNP-DNA interaction?
Is minicircle DNA superior to parental plasmid DNA?
Does the superiority of minicircle DNA derive from larger numbers of plasmids per nanoparticle?

- **Improvement of lipid nanoparticle-based delivery**

Are viral proteins suitable for targeting purposes?
Is there an alternative to PEG to improve circulation behavior?

- **Novel applications for the zebrafish embryo model**

Can we use the zebrafish as a predictive vertebrate model for antibiotic treatment?
Can macrophage-targeted liposomes improve antibiotic treatment?

5 Results

The present PhD thesis has led to seven publications and is separated into four major working packages (Chapter 1-4):

Chapter 1

1.1 Lipid-Based DNA Therapeutics: Hallmarks of Non-Viral Gene Delivery

1.2 Improvement of DNA Vector Delivery of DOTAP Lipoplexes by Short Chain Aminolipids

Chapter 2

2.1 Characterization and Optimization of Lipoplexes: How to standardize Assays and avoid Pitfalls

Chapter 3

3.1 Optimization-by-design of hepatotropic lipid nanoparticles targeting the sodium-taurocholate cotransporting polypeptide

3.2 Poly(Sarcosine) Surface Modification Imparts Stealth-Like Properties to Liposomes

Chapter 4

4.1 Bacteria vs. Antibiotics – Bridging Infection Modeling in Danio rerio

4.2 The Use of 4-Hexylresorcinol as Antibiotic Adjuvant

5.1 Chapter 1

5.1.1 Chapter 1.1

Lipid-Based DNA Therapeutics: Hallmarks of Non-Viral Gene Delivery

Jonas Buck, Philip Grossen, Pieter R. Cullis, Jörg Huwyler, Dominik Witzigmann

ACS Nano. 2019 Apr 23;13(4):3754–82.
doi: 10.1021/acsnano.8b07858

Highlights: Lipid-based gene delivery systems are among the most promising non-viral gene delivery systems. This review gives a thorough overview over the historic milestones in lipid-based non-viral gene delivery. We summarize factors important for nanoparticle formulation, as well as for *in vitro* and *in vivo* applications. The latest developments in the field of lipid-based gene delivery systems are discussed and an overview over clinical trials involving lipid-based gene delivery is provided.

ACS NANO
Cite This: ACS Nano 2019, 13, 3754−3782
www.acsnano.org

REVIEW

Lipid-Based DNA Therapeutics: Hallmarks of Non-Viral Gene Delivery

Jonas Buck,[†] Philip Grossen,[†] Pieter R. Cullis,[‡] Jörg Huwyler,[*,†] and Dominik Witzigmann[*,†,‡]

[†]Division of Pharmaceutical Technology, Department of Pharmaceutical Sciences, University of Basel, Klingelbergstrasse 50, 4056 Basel, Switzerland

[‡]Department of Biochemistry and Molecular Biology, University of British Columbia, 2350 Health Sciences Mall, Vancouver, British Columbia V6T 1Z3, Canada

ABSTRACT: **Gene therapy is a promising strategy for the treatment of monogenic disorders. Non-viral gene delivery systems including lipid-based DNA therapeutics offer the opportunity to deliver an encoding gene sequence specifically to the target tissue and thus enable the expression of therapeutic proteins in diseased cells. Currently, available gene delivery approaches based on DNA are inefficient and require improvements to achieve clinical utility. In this Review, we discuss state-of-the-art lipid-based DNA delivery systems that have been investigated in a preclinical setting. We emphasize factors influencing the delivery and subsequent gene expression *in vitro*, *ex vivo*, and *in vivo*. In addition, we cover aspects of nanoparticle engineering and optimization for DNA therapeutics. Finally, we highlight achievements of lipid-based DNA therapies in clinical trials.**

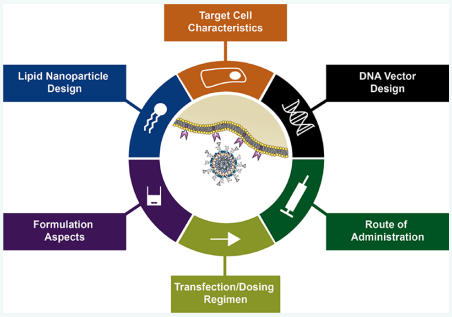

KEYWORDS: *non-viral gene delivery, lipid nanoparticles, DNA, gene therapy, nanomedicine, transfection, nucleic acid delivery, genetic disorders, clinical trials*

Inherited genetic diseases represent a considerable public health burden. Gene therapy offers great potential for the treatment of various orphan monogenic disorders.[1] However, the translation from *in vitro* to *in vivo* remains a major hurdle for most nucleic acid delivery systems due to poor *in vitro*−*in vivo* correlation and lack of both efficient and safe carrier systems.[2] So far, only 4.2% of all clinical trials involving gene therapy approaches reached a late clinical phase.[3] The majority of all initiated clinical studies use viral vectors. The low success rate was often attributed to key limitations of viral systems with respect to immunogenicity and generalized toxicity.[4] Consequently, non-viral lipid-based gene delivery systems have gained much attention due to their reduced immunogenicity, large payloads, safety, and ease of manufacturing.[5−8] They offer the possibility to transport large biomolecules including nucleic acids with reasonable specificity to diseased target cells.

The term "nucleic acids" here includes various types of nucleic acid polymers such as (but not exclusively) plasmid DNA (pDNA), messenger RNA (mRNA), small interfering RNA (siRNA), or anti-sense oligonucleotides (ASOs). During the last decades, a wide range of nanoparticulate gene delivery systems have been developed. Promising results for RNA interference (RNAi) therapeutics using lipid-based nanoparticles have been achieved and several companies have initiated clinical trials.[9−11] The first RNAi therapeutic (Onpattro, formerly known as patisiran) to receive FDA approval (August 2018) uses a lipid-based nanoparticle delivery system.[12] However, these systems do not allow the introduction and subsequent expression of therapeutic proteins. In addition, the induced pharmacological effects obtained by most of these siRNA-based strategies are short-lived, *i.e.*, in the range of days and weeks, in contrast to months, for gene delivery using a DNA expression vector.[13] Therefore, the use of DNA-based therapeutics offers a favorable option for the induction of long-term therapeutic effects without the need for insertion into the genome and accompanying off-target effects. (The term "DNA therapeutics" is solely used in this Review article as an umbrella term to describe delivery systems for DNA expression vectors. Other DNA therapeutics such as antisense oligonucleotides, aptamers, or DNAzymes are not considered.) Theoretically, nanoparticulate gene delivery systems can accommodate large DNA polynucleotides with a size of up to 52.5 kbp (see the DNA Vector Encoding Gene of Interest section). However, smaller polynucleotides are considered to be more easily encapsulated or more easily translocated to the nucleus (in the case of pDNA). It was shown that plasmids up to a size of 20 kbp can be encapsulated and delivered without hampering the transfection efficiency.[14] Using pDNA expression vectors, it is thus possible to transfer both a gene of interest ("gene delivery" including "knock-in" strategies)

Received: October 15, 2018
Accepted: March 25, 2019
Published: March 25, 2019

DOI: 10.1021/acsnano.8b07858
ACS Nano 2019, 13, 3754−3782

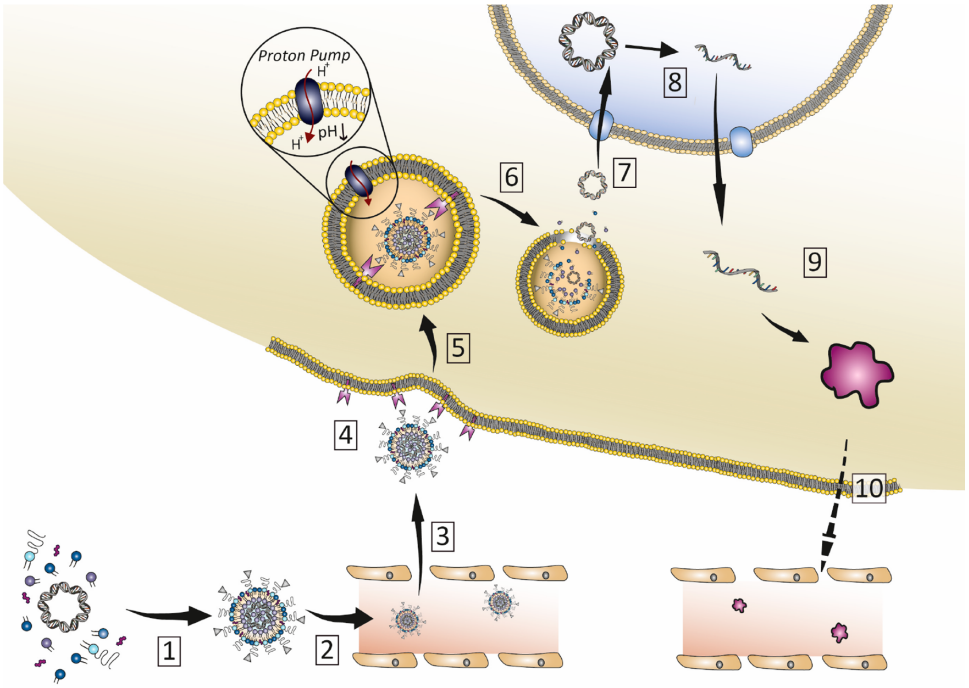

Figure 1. Schematic representation of different hurdles for systemically administered non-viral DNA therapeutics *in vivo*. (1) Production of stable DNA-loaded lipid-based nanoparticles. (2) After intravenous injection, DNA therapeutics need to circulate in the blood compartment. (3) After the passage of fenestrated blood vessels, (4) nanoparticles bind to the target cells. Cellular uptake of DNA nanoparticles is an active transport process. (5) After endosomal escape (triggered by a pH decrease within the endosome), (6) the DNA is released from the nanoparticle into the cytoplasm. (7) Nuclear trafficking results in (8) transcription of the gene. (9) Finally, the mRNA is transported into the cytoplasm, where the exogenous protein is translated. (10) Further processing results in a mature protein, which performs its function inside the host cell or after release into circulation.

Table 1. Comparison between Lipid- and Polymer-Based Gene-Delivery Systems[a]

type of delivery system	advantages	disadvantages
lipid-based	most thoroughly investigated non-viral delivery systems	toxicity of permanently charged cationic lipids
	incorporation of hydrophilic and hydrophobic substances possible	an be colloidally unstable systems resulting in low half-life stability on storage
	low toxicity	rapid sequestration by the RES unless PEG coating
	low immunogenicity	historically low transfection efficiency compared to viral vectors
	surface modification allows targeting (e.g., ligands) and extended blood circulation time (e.g., PEGylation)	
	biodegradable	
	stable incorporation of large DNA molecules	
	transfection of a wide variety of cell types	
	preparation of stimuli-responsive systems	
	lipid-based delivery systems that have already been approved by FDA and other regulatory agencies	
polymer-based	wide variety of chemically diverse structures	cytotoxicity of highly cationic polymers
	strong DNA condensation capacities	biodegradability issues for certain polymers
	targeting possible *via* site-specific attachment of ligands	immune response to polymers
	biodegradability of many polymers such as chitosan, PLGA, or PLL	significant influence of the molecular weight for certain polymers (e.g., PEI) or the generation number of *e.g.*, polyamidoamine dendrimers
	stable to aggregation under physiological conditions	no polymer-based delivery system in late clinical stages
	strong buffering capacity (e.g., PEI)	poorly defined systems of variable size and molecular weight

[a]Expert opinion summarizing the most important advantages and disadvantages of both lipid- and polymer-based gene-delivery systems.

DOI: 10.1021/acsnano.8b07858
ACS Nano 2019, 13, 3754−3782

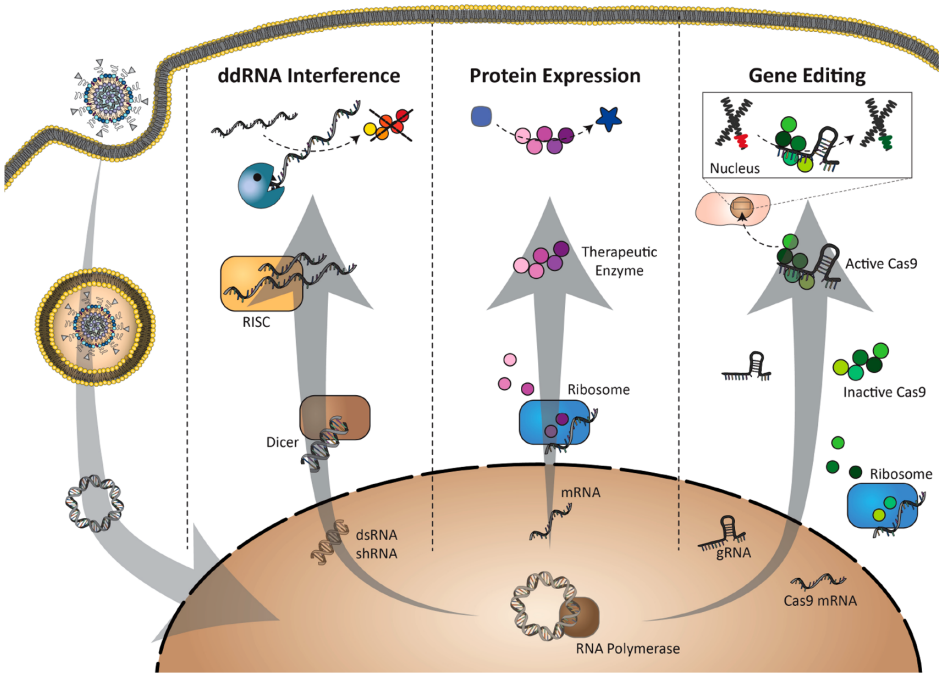

Figure 2. Therapeutic applications for lipid-based DNA therapeutics. (1) DNA-directed RNA interference (ddRNA Interference) can be used to knock down protein expression. The DNA encodes for a shRNA (short hairpin RNA) or dsRNA (double-stranded RNA), which is processed in the cytoplasm by Dicer (an endoribonuclease) to siRNA. Together with argonaute proteins, siRNAs build the RNA interference silencing complex (RISC), which cleaves mRNA of interest and thereby inhibits protein expression. (2) The DNA can also encode for a transgene, which is transcribed into mRNA and translated by ribosomes to a protein of interest such as a therapeutic enzyme. This strategy can be used for enzyme replacement therapy. (3) Gene editing using Zinc finger, TALENs, or CRISPR-Cas technology offers the possibility to genetically modify the host genome and thereby stably express or knock out a protein of interest.

leading to the expression of a functional protein or to "knock-down" target genes by gene silencing using DNA-directed RNA interference (ddRNAi).

For the successful systemic delivery of DNA and subsequent expression of the encoded exogenous protein, many hurdles have to be overcome: (I) efficient nucleic acid packaging, (II) long plasma circulation, (III) extravasation from systemic circulation, (IV) cellular internalization, (V) endosomal escape, (VI) intracellular DNA release, and (VII) nuclear entry.[15] A schematic representation of these hurdles *in vivo* is given in Figure 1.

It is important to note that non-viral gene therapeutics optimized for one type of nucleic acid, *e.g.*, siRNA or mRNA, cannot simply be translated to another type (*i.e.*, DNA vector). This can be due to differences in physical properties such as size or the need for different types of nucleic acids to be delivered to different intracellular sites of action, *i.e.*, cytosol (RNA) *versus* nucleus (DNA). Kauffman *et al.* have shown significant differences for the translation of siRNA delivery systems to mRNA therapeutics.[16] Kulkarni *et al.* observed that lipid-based formulations optimized for RNA delivery are not optimal for pDNA delivery.[17]

In this Review, we discuss recent developments in the field of lipid-based gene delivery systems with a focus on DNA therapeutics. Other therapeutic strategies such as siRNA (RNA knock-down), oligonucleotides (RNA knock-down, translation inhibition, or RNA processing such as splice switch), or mRNA (protein expression), are not covered by this Review but are summarized in several excellent reviews.[18−22] We summarize most important key factors for the design of efficient and safe DNA delivery systems. In addition, we address opportunities to develop next-generation DNA therapeutics and discuss their anticipated clinical use.

DNA DELIVERY SYSTEMS

DNA delivery systems can be divided into three different categories: (i) physical methods, (ii) viral delivery systems, and (iii) non-viral delivery systems, which are the topic of this Review. Non-viral DNA delivery systems can be subdivided into another three categories: inorganic materials such as calcium phosphate, lipid or lipid-like materials, and polymeric materials. Although the first reports on gene transfer used calcium phosphate precipitation (see the Historic Milestones towards Lipid-Based DNA Delivery section), current research in the area of gene delivery mainly focuses on lipid(-like) and polymeric compounds. Advantages and disadvantages of both lipid- and polymer-based gene delivery systems are summarized in Table 1. A detailed comparison of all gene delivery systems including viral vectors and physical methods as well as inorganic materials can be found elsewhere.[23,24]

LIPID-BASED DNA DELIVERY SYSTEMS

DNA Vectors and Their Mode of Action. The delivery of DNA vectors offers the possibility for three different therapeutic applications: (i) inhibition of protein expression by RNAi, (ii) transient protein production by expression vetors, or (iii) stable

DOI: 10.1021/acsnano.8b07858
ACS Nano 2019, 13, 3754−3782

protein expression or knockout by gene editing. These three approaches (Figure 2) can be summarized as follows: ddRNAi is a technology in which DNA vectors encode for short-hairpin RNAs (shRNA), which enable the long-term silencing of specific mRNAs and thus inhibition of protein expression. The intracellular processing in ddRNAi is similar to the endogenous microRNA (miRNA) pathway.[25] After the successful delivery of DNA, shRNA is transcribed in the nucleus, processed by the ribonuclease Drosha and exported into the cytoplasm *via* Exportin 5. In the cytoplasm, Dicer processes the shRNA to siRNA, which is subsequently loaded together with argonaute proteins into the RNA-induced silencing complex (RISC). Depending on sequence complementary, the RISC cleaves the target mRNA (in case of perfect complementary between siRNA and mRNA sequence) or represses the translation into the protein (imperfect complementary). This approach offers an advantage for various diseases because, in contrast to direct siRNA delivery, these effects are long-lasting.

The delivery of DNA vectors in enzyme-replacement or cancer therapy result in long-term transgene expression of an exogenous protein in the target cell. Transgenes encoded on the DNA vector will be transcribed to mRNA and translated into the protein of interest. This protein or enzyme can act intracellularly or extracellularly.

Gene editing or genome engineering is a technique to insert, replace, or delete specific DNA sequences in the genome of host cells. A total of four different nucleases have been used for this strategy: meganucleases, zinc finger nucleases (ZFN), transcription activator-like effector-based nucleases (TALEN), and the clustered regularly interspaced short palindromic repeats (CRISPR)-associated protein (Cas) system. In the case of CRISPR-Cas, a DNA vector can simultaneously encode for the Cas9 protein and a target-sequence specific guide RNA (gRNA). After the transcription of gRNA and translation of Cas9 mRNA, the Cas9/gRNA ribonucleoprotein (RNP) complex will create site-specific double-strand breaks in the genome and insert the transgene by homology directed repair (HDR) mechanisms. Alternatively, a gene can also be silenced or deleted by this technology following nonhomologous end joining (NHEJ).[26] Advances in CRISPR-Cas9 technology have been discussed in detail in several recent reviews.[27−29]

From Research Tool to Therapy. DNA vectors can be applied in a broad range of medical applications ranging from their use as important *in vitro* research tool to *in vivo* applications in patients.

For *in vitro* applications, identifying new drug targets and characterizing the relevance of these targets in early drug discovery are important steps toward development of medicines. In recent years, gene editing techniques such as CRISPR-Cas9 have been used as powerful tools for implementation of such screening and mechanistic studies.[30] Furthermore, CRISPR-Cas9 technology can *e.g.*, be used subsequently to generate relevant *in vitro* and *in vivo* disease models.[26] Efficient delivery to a wide range of target cells *in vitro* is, however, a prerequisite for these applications. Lipid-based DNA delivery can be a valuable alternative to viral vectors in generating these preclinical models.[30] In addition, these systems offer the possibility to co-deliver DNA, RNA (e.g., mRNA or gRNA) and/or proteins to target cells in a coordinated manner.[31]

For *ex vivo* applications, modification of patient-derived cells *ex vivo* has been explored during the recent decade. Major achievements have been made in cancer immunotherapy resulting in the approval of personalized CAR-T cell therapies. Whereas some technologies were developed to introduce macromolecules to isolated cells without the need for transfection reagents (e.g., microfluidics and electroporation), lipid-based vehicles offer the possibility to efficiently introduce target DNA sequences into patient cells in an *ex vivo* setting to express target proteins or to modify the host cell genome,[32] resulting in safe and reproducible transfection.[33−35]

For *in vivo* applications, whereas *in vitro* or *ex vivo* applications aim for high delivery efficiencies and low toxicity, *in vivo* applications additionally require favorable pharmacokinetic properties and accumulation in target tissues (see the Factors Important for in Vivo Gene Delivery section). Several candidates have reached clinical development in recent years and a summary of major achievements is provided in the DNA Therapeutics in Clinical Trials section.

Historic Milestones toward Lipid-Based DNA Delivery. The basic process of gene therapy is called transfection and describes the transfer of exogenous genetic material (e.g., DNA) into a cell to exert a therapeutic effect.[36] The first attempts toward non-viral gene delivery using chemical reagents were made by Szybalska and Szybalski in the 1960s when they observed an improved "DNA-mediated genetic transformation" in D98 cells upon the addition of spermine to the DNA prior to incubation of the cells.[37] However, chemical analysis of spermine revealed that it was contaminated with about 10% calcium. This resulted in calcium phosphate/DNA complexes, which facilitated the delivery of DNA into cells.[38] Then, 3 years later, Vaheri and Pagano demonstrated the potential of polymeric substances such as diethylaminoethyl dextran (DEAE dextran) to transfer pDNA to cells.[39] In 1973, Graham and Van Der Eb published a detailed study on the effects of calcium phosphate-mediated transfection,[40] which is generally cited to be the primary source for this transfection technique.[41] A total of 5 years later, Mukherjee *et al.* showed a successful delivery of metaphase chromosomes from hypoxanthine guanine phosphoribosyltransferase (HGPRT) positive cells to HGPRT negative cells using a mixture of unsaturated phosphatidylcholine (PC) and cholesterol 7:2 (w/w) as the transfection reagent.[42] In 1979, Fraley *et al.* demonstrated delivery of DNA to bacteria using a mixture of PC and phosphatidylglycerol (PG),[43] whereas Lurquin showed delivery of DNA to plant cells using either PC or PC/cholesterol, 7:2 (w/w) lipid-based nanoparticles.[44] A total of 1 year later, again, Fraley *et al.* reported successful delivery of pDNA to African green monkey kidney cells using PC:PG 10:1 (w/w) lipid-based nanoparticles.[45] The possibility for stable gene transfer using lipid-based nanoparticles was demonstrated by Schaefer-Ridder *et al.* in 1982.[46] In 1983, Nicolau *et al.* demonstrated successful insulin expression in the liver of rats transfected with intravenously (i.v.) injected nanoparticles consisting of a plasmid encoding for rat preproinsulin I and a mixture of PC/phosphatidylserine/cholesterol 8:2:10 (mol/mol) as transfection reagent.[47]

The term lipofection, which describes the transfection of cells using lipid-based transfection reagents, was created in 1987 by Felgner *et al.* when they demonstrated the formation of cationic lipid-based nanoparticles and their use for successful gene transfer and subsequent transgene expression in various cell lines. They synthesized the cationic lipid *N*-[1-(2,3-dioleyloxy)-propyl]-*N*,*N*,*N*-trimethylammonium chloride (DOTMA) and combined it with the helper lipid dioleoylphosphatidylethanolamine (DOPE). After complexation with DNA, they observed fusion of the lipoplexes with the cell membrane of tissue culture

DOI: 10.1021/acsnano.8b07858
ACS Nano 2019, 13, 3754−3782

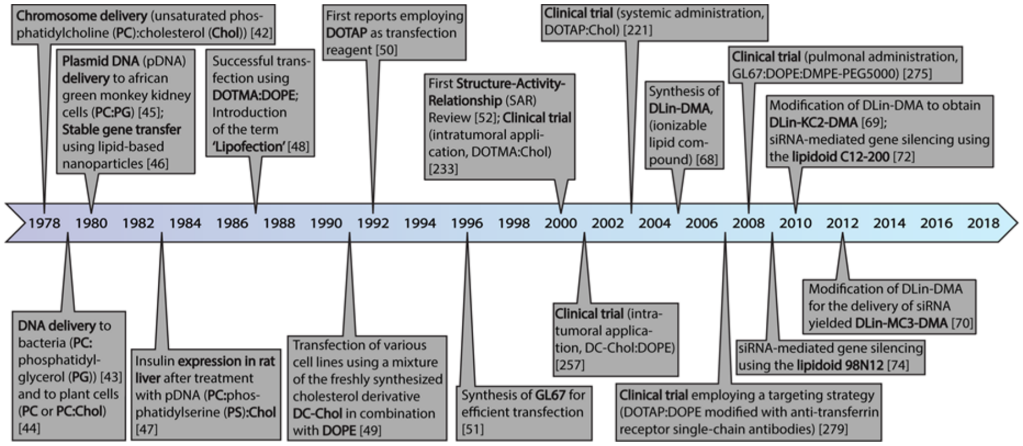

Figure 3. Historic milestones in lipid-based DNA delivery. The timeline displays the historic milestones in lipid-based DNA delivery that are summarized in this review. Each milestone is displayed together with respective references.

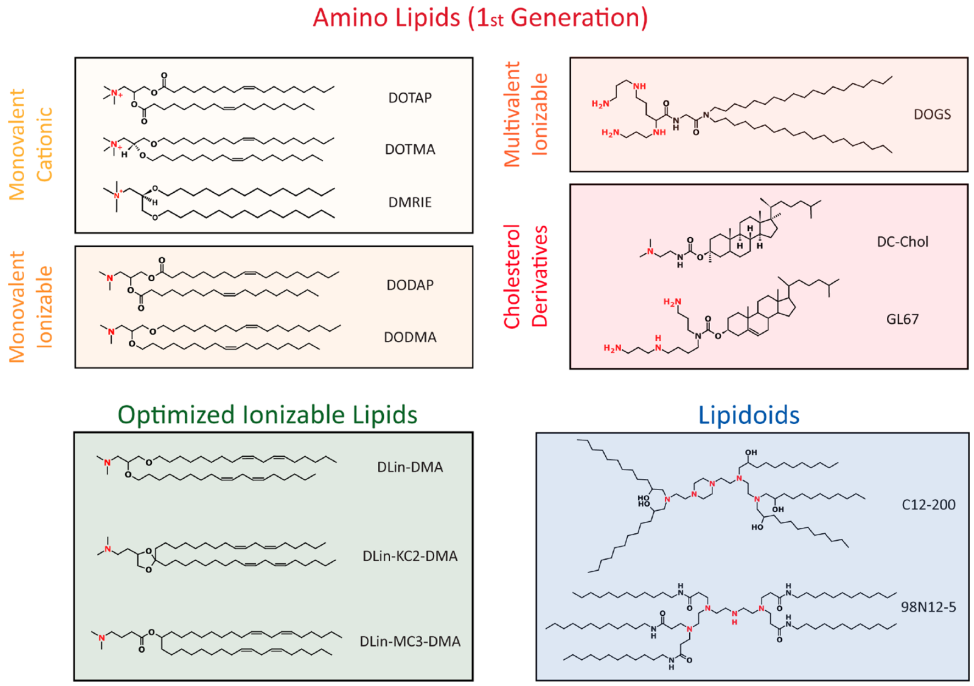

Figure 4. Chemical structures of lipids or lipid-like materials used for the delivery of nucleic acids. Various lipid-based materials have been investigated for the delivery of nucleic acids including RNA and DNA. In general, three different categories have been identified, *i.e.*, first-generation amino lipids, optimized ionizable lipids, and lipidoids. First-generation amino lipids can be grouped into monovalent or multivalent lipids and cholesterol derivatives. All amines with a permanent positive charge (*i.e.*, quaternary amines of monovalent amino lipids) or which are protonated at low pH (such as encounters in the endosomal or lysosomal compartment) are highlighted in red color. A pK_a of around 6.4 is favorable for the endosomal and lysosomal escape of nucleic acids into the cytoplasm.

cells and subsequent diffusion of fluorescent rhodamine-conjugated DOPE throughout the intracellular membranes.[48] In 1991, Gao and Huang reported successful synthesis of 3β-[*N*-(*N*′,*N*′-dimethylaminoethane) carbamoyl] cholesterol (DC-Chol) and demonstrated efficient transfection of various cell lines using this cationic cholesterol derivative.[49] A total of 1 year later, one of the first studies employing 1,2-dioleoyl-3-(trimethylammonium) propane (DOTAP) for DNA transfection was published.[50] Because this study focused on vesicular transport rather than transfection, the technique was used as a tool but was not the focus of the study. In the following decades, many modifications and combinations of these first generation transfection reagents were reported, such as GL67 in 1996,[51] but the basic processes behind gene transfer were poorly understood despite the successful modification of lipids for transfection. The

DOI: 10.1021/acsnano.8b07858
ACS Nano 2019, 13, 3754−3782

historic milestones summarized in this section are displayed in Figure 3.

It took until the next millennium until more detailed mechanistic insights were provided (see ref 52). However, the molecular mechanisms of nucleic acid delivery employing cationic lipids are still controversial. DNA often stays at the surface of cells when lipoplexes interact with the plasma membrane.[53,54] It has been suggested that fusion with the plasma membrane and nanoparticle entry into cells is mediated by the so-called "fusogenic" lipid DOPE.[55] Consequently, to promote intracellular delivery of DNA, DOPE is included in several commercially available transfection reagents such as Lipofectin (a 1:1 (w/w) mixture of DOTMA and DOPE)[56] or Lipofectamine (a 3:1 (w/w) mixture of 2,3-dioleyloxy-*N*-[2-spermine carboxamide] ethyl-*N*,*N*-dimethyl-1-propanammonium trifluoroacetate (DOSPA) and DOPE).[57,58]

Key Components of Lipid-Based Gene Delivery Systems. Lipid-based nanoparticles consist of lipids or lipid-like materials to bind DNA, helper lipids to increase transfection efficiency, and a DNA vector encoding for the gene of interest. The chemistry and function of these components are discussed in the following sections.

(Ionizable) Cationic Lipids or Lipid-Like Materials. After initial experiments using phosphatidylserine-based liposomes for DNA delivery,[45] a vast number of structurally different lipid-based materials have been developed over the last four decades to improve gene-transfer efficiency and safety of resulting lipid nanoparticles.

Three primary categories can be identified, *i.e.*, first generation permanently positively charged amino lipids, optimized ionizable lipids, and lipidoids. All of these share common structural elements such as a hydrophobic moiety that is linked to a hydrophilic headgroup containing cationic or ionizable amine moieties. Examples of the various types of lipid and lipid-like compounds used in gene therapy are discussed in the following sections (Figure 4). Lipids and lipidoids used for RNA delivery have been reviewed recently.[22,59]

Cationic and Ionizable Amino Lipids (First Generation). In 1987, Felgner and colleagues developed synthetic permanently positively charged cationic lipids for complexation and delivery of DNA.[48] Even 30 years after their discovery as gene-delivery vehicles, lipids with permanently positively charged headgroups remain the dominant lipid-based gene delivery agents for *in vitro* applications as discussed elsewhere.[60,61] The positively charged headgroup of cationic lipids can bind and condense the anionic phosphate groups of the DNA backbone *via* electrostatic interactions. The cationic surface charge of such lipoplexes mediates efficient DNA delivery and cellular internalization through interactions with the negatively charged plasma membrane of target cells. Furthermore, positive charges of the lipids in combination with negative charges of anionic lipids in the endosomal membrane promote endosomal escape and, thus, DNA release to the cytosol.[62]

A large number of cationic headgroup structures have been investigated for lipids used in gene delivery. Headgroups can be categorized in 6 classes: permanently positively charged moieties such as quaternary amines, ionizable amines, amino acids or peptides, guanidiniums, heterocyclic headgroups, and others (*i.e.*, unusual headgroups).[63] The ionizable lipids were introduced to achieve systems that exhibited little surface charge at physiological pH, which can lead to severely toxic side effects *in vivo*. Further optimization has led to identification of ionizable lipids with optimized apparent acid dissociation constant (pK_a) properties that enhance transfection potency (see the Optimized Ionizable Lipids section). The hydrophobic tail of cationic lipids for transfection is usually composed of either saturated or unsaturated alkyl chains or steroids. Unsaturated alkyl chains are beneficial with respect to transfection efficiency due to increased lipid membrane fluidity.[64,65] The first generation of cationic and ionizable lipids can be classified according to their molecular structure as follows (Figure 4):[66]

(1) monovalent aliphatic lipids characterized by a single positively charged amine moiety in their headgroup such as (a) permanently positively charged cationic lipids, *e.g.*, DOTAP, DOTMA, 1,2-dimyristyloxypropyl-3-dimethyl-hydroxy ethylammonium bromide (DMRIE) or (b) ionizable cationic lipids that only exist in a positively charged form at pH values below their pK_a, where they are protonated, *e.g.*, 1,2-dioleoyl-3-dimethylammonium propane (DODAP) and 1,2-dioleoyl-3-dimethylammonium propane (DODMA);

(2) multivalent aliphatic lipids that contain two or more amine functions in their headgroup such as dioctadecylamidoglycylspermine (DOGS); and

(3) cationic cholesterol derivatives such as DC-Chol and GL67.

Optimized Ionizable Lipids. Whereas cationic lipids can be used to achieve high transfection efficiencies *in vitro*, they are characterized by a relatively high cytotoxicity and unfavorable pharmacokinetic properties *in vivo* (*i.e.*, short half-life in blood circulation and nonspecific binding to cell surfaces). To overcome these limitations, ionizable lipids with optimized pK_a properties have been designed. Ideally, they should (i) be positively charged during lipid nanoparticle formation to allow for nucleic acid complexation, (ii) be neutral at physiological pH for systemic (*e.g.*, intravenous) administration, and (iii) become charged again when accumulating in the endosomal compartment to promote efficient endosomal escape.[61] The first demonstration that an ionizable cationic lipid could be used to encapsulate nucleic acid polymers (*i.e.*, ASO) was made by Semple *et al.*[67] using DODAP. Subsequently, Heyes *et al.*[68] developed 1,2-dilinoleyloxy-3-dimethylaminopropane (DLinDMA) and Semple *et al.*[69] used a structure−activity relationship (SAR) approach to rationally design lipids with improved gene silencing activity (*i.e.*, siRNA delivery capacity) *in vivo*. The optimized ionizable lipid DLin-KC2-DMA (Figure 4) showed promising results and exceeded the gene silencing capacity of the precursor lipid DLinDMA by a factor of 10.

Further investigations demonstrated a SAR between the pK_a of the ionizable headgroup and the gene silencing efficiency *in vivo*. The most promising compound, DLin-MC3-DMA (Figure 4) with a pK_a of 6.44 was developed[70] that is now the gold standard for siRNA delivery platforms. In contrast to siRNA, DLin-KC2-DMA-based lipid nanoparticles showed a significantly higher DNA delivery potential as compared to DLin-MC3-DMA-based lipid nanoparticles.[17] This indicates the potential of ionizable DLin-DMA-based lipids for DNA delivery; however, structure−activity relations obtained for RNA do not necessarily apply to DNA delivery.

Lipidoids. Lipid-like materials (*i.e.*, lipidoids) can be synthesized by conjugation of alkyl-acrylates or alkyl-acrylamides to primary or secondary amines.[71] This reaction works in the absence of solvents or catalysts and has, therefore, the advantage that no protection and deprotection steps are needed, which makes this one-pot synthesis straightforward. Akinc *et al.*

DOI: 10.1021/acsnano.8b07858
ACS Nano 2019, 13, 3754−3782

synthesized a lipidoid library consisting of 1200 structurally diverse lipid-like compounds.[71] Further modifications of similar lipids and expansion of lipidoid libraries led to the identification of formulations for siRNA-mediated gene silencing *in vivo*, with C12-200 and 98N12-5 as most promising compounds (Figure 4).[72−74] A structure−function relationship based on four structural and pK_a criteria was established to predict *in vivo* gene silencing efficiency.[73] Notably, lipidoids have also been used for *in vitro* pDNA delivery.[75] Some compounds exceeded the pDNA delivery efficiency of Lipofectamine 2000 by a factor of 4.[75] Again, compounds optimized for RNA delivery are not necessarily the best for DNA delivery.

Advances in the Development of Lipids for Gene Delivery. Recent advances in the field of gene therapeutics have resulted in several highly potent and biodegradable lipids optimized for mRNA delivery. Sabnis *et al.* synthesized a library of lipids with improved safety profile and enhanced endosomal escape properties.[76] In addition, several biotechnology companies have initiated screening programs combined with SAR analysis. This has resulted in lipids for mRNA delivery that are orders of magnitude more potent as compared to MC3 (*i.e.*, gold standard for siRNA delivery).[77] In the future, these advanced lipids need to be tested for DNA vectors to see whether similar benefits are possible.

Lipid Library Screens to Elucidate Structure−Activity-Relationships. Combinatorial synthesis and high-throughput screening (HTS) enable the rapid synthesis and testing of a large number (e.g., hundreds to thousands) of structurally diverse lipid or lipid-like compounds to further unravel structural parameters important for successful nucleic acid delivery. Because RNA-based strategies are currently at the forefront of nucleic acid-based therapeutics, these techniques were mainly applied to materials for RNA delivery rather than DNA. However, both types of nucleic acids share common requirements and findings for RNA can act as a starting point for optimization of DNA therapeutics. Generally, library screens focus on three functional moieties: headgroup−linker−lipid tail.[78]

Headgroup. The cationic (ionizable) headgroup not only is responsible for the interaction with the negatively charged nucleic acids (e.g., nucleic acid condensation) but also affects nanoparticle characteristics such as the surface charge. In this regard, dimethylamino-based headgroups showed superior transfection efficiencies compared to higher substituted moieties.[69,79,80] Substitution by diethylamino, piperazino, morpholino, or trimethylamino-based headgroups increases steric hindrance as well as the pK_a resulting in decreased activity.[69,80] In addition, there are reports that indicate headgroups with more than one amine group to be superior.[71] Importantly, several studies demonstrated that a pK_a between 5.5 and 6.5 (optimum of 6.44, but depending on the formulation) is associated with maximal potency *in vivo*.[33,70,73,81] This ionizable characteristic plays two important roles. First, the headgroup is relatively neutral at physiological pH thereby improving pharmacokinetics (PK) and decreasing toxic effects. Second, the headgroup must exhibit a positive charge in an acidified endosome (pH of ∼5−6) to interact with endogenous anionic lipids thereby destabilizing the endosomal membrane to deliver the nucleic acid payload.[70] Of note, the pK_a is not relevant for permanently positively charged quaternary ammonium-based headgroups.[80]

Linker. The next important functional moiety is the linker that connects the headgroup with its tail group(s). Interestingly, the linker affects not only the global pK_a of ionizable lipids but also the flexibility for charge presentation or biodegradability of the delivery system. Several groups reported that amide linkers are associated with higher transfection efficiencies *in vitro* as compared to other linkers such as ester or hydroxyl linkers.[71,75] For ionizable lipids, a gradually decreasing transfection efficiency was reported when alkoxy linkers were replaced for an ester linker. Notably, ester linkers are highly prone to hydrolysis thereby risking to lose activity of the delivery system.[75] Inclusion of carbamate and thioether linkers resulted as well in poor activity *in vivo*. Only linkers with a ketal function showed increased transfection efficiency when replacing the two alkoxy linkers.[69] Besides the functional group of the linker, also the spacing between the headgroup and the linker is crucial. A distance between the headgroup functionality and the linker functionality of two carbon atoms promotes the highest efficiency.[69,81] Further increase or decrease of carbon atoms negatively influences the activity. First, the substitution length of the linker amine can influence the pK_a of amines and thereby alter the global pK_a and subsequent efficiency.[81] Second, the distance between the linker and the headgroup affects the size of the headgroup, which can affect the formation of nonbilayer structures and subsequent destabilization of the endosomal bilayer.[69]

Lipid Tail. The third important functional moiety is the tail group, which generally possesses long hydrophobic carbon chains and is therefore responsible for the "lipid properties". Lipid tail saturation, length, substitution, and number of tail groups affect the transfection efficiency. Unsaturated tails demonstrated to improve the efficiency of gene delivery systems.[70] With respect to the tail length, no clear SAR can be summarized. Whereas a tail length in the range of 8−12 carbon atoms demonstrated highest transfection efficiencies in some studies,[71,73] another library screening showed that increasing the tail length from 14 to 18 carbon atoms increased the transfection efficiency.[79] The optimal tail length may, therefore, vary among different headgroups or linkers. Tail substitution is another crucial factor. The inclusion of one tail containing a secondary amine is critical for transfection[71] and tails with 3 or more substitution sites, tails containing tertiary and secondary amines, alcohols, branched or linear chains are still effective, while ethers and rings are ineffective.[73] Recently, a study demonstrated that branched-tails enhance the potency of lipid nanoparticles due to increased surface ionization at acidic pH (e.g., in endosomes).[82] Finally, the number of tail groups needs to be considered. Lipid-like molecules that are substituted with only one tail result in poor efficiency compared to their bi-tailed counterparts. However, a synergistic effect could be observed when mixing mono- and bi-tailed lipids at different ratios.[79,83] Monotailed lipids increase the surface charge, whereas bi-tailed lipids decrease lipid nanoparticle size and increase stability.[79] In the field of lipidoid synthesis, attachment of more than two alkyl tails is considered to be very important to promote high gene delivery efficiencies.[71,73]

Additional Lipid Components. As mentioned above, lipid nanoparticles are typically multicomponent formulations. Cationic or ionizable lipid-based materials are often combined with so-called helper lipids. The term "helper lipids" covers a range of charge neutral substances that are included in lipid nanoparticle formulations to improve the performance of the delivery system *e.g.*, by stabilizing the nanoparticle or by improvement of intracellular trafficking.[84,85] The role of helper

DOI: 10.1021/acsnano.8b07858
ACS Nano 2019, 13, 3754−3782

Table 2. Formulation Aspects Influencing Nanoparticle Properties[a]

influence factor	effect on	general influence
size of encoding DNA sequence	size of the nanoparticle	plasmid size correlated with lipoplex nanoparticle size when using the cationic lipid RPR120535
		no correlation found for Lipopolyamine/DNA nanoparticles
gene delivery system-to-DNA ratio (N/P)	DNA condensation and protection	high N/P ratios increase DNA condensation within the nanoparticle
	nanoparticle size	increasing the N/P ratio decreases nanoparticle size
		N/P ratios leading to net neutral ζ potential (±5 mV) promote rapid agglomeration
ionic strength	colloidal stability	impaired self-assembly and colloidal stability
	size	larger nanoparticle size (>150 mM NaCl)
		smaller nanoparticle size (<20 mM NaCl)
impact of proteins	colloidal stability	reduced agglomeration of nanoparticles (protein opsonization)
	nanoparticle size	reduced nanoparticle size in the presence of serum
complexation volume	transfection efficiency	volumes that are too low may hinder DNA condensation
ζ potential	colloidal stability	highly positive (>+30 mV) or negative (←30 mV) ζ potential hinders nanoparticle agglomeration and therefore improves its stability; neutral ζ potential (±5 mV) leads to agglomeration

[a]A summary of main factors influencing nanoparticle properties (e.g., size and colloidal stability) is provided. The factors are ordered in accordance to the chapters of this Review. Detailed information on the ζ potential is provided in the ζ Potential section of this Review.

lipids in lipid nanoparticles has recently been discussed in detail elsewhere.[86]

Cholesterol is a natural component of biological membranes[87] and is a major contributor to the cell membrane fluidity, leading to membrane condensation.[88] Incorporation of cholesterol into lipid-based DNA formulations has been shown to improve stability and transfection efficiency *in vitro*[89] and *in vivo*.[90,91] In contrast, replacement of cholesterol with DOPE led to rapid lipoplex dissociation upon contact with serum.[89] DOPE can induce the non-bilayer inverted hexagonal (H_{II}) lipid phase, which can result in bilayer disruption. This effect is attributed to the small polar headgroup in combination with the two unsaturated oleoyl chains leading to a cone-like shape compatible with the H_{II} phase structure.[86]

Other commonly used helper lipids include phospholipids such as 1,2-dioleyl-*sn*-glycerol-3-phosphatidylcholine (DOPC), 1,2-distearoyl-*sn*-glycero-3-phosphocholine (DSPC), or 1-stearoyl-2-oleoyl-*sn*-glycero-3-phosphocholine (SOPC). Interestingly, Kulkarni *et al.* demonstrated a dramatic increase in reporter gene expression when replacing DSPC with DOPC or SOPC, suggesting that unsaturated lipid chains such as oleoyl chains improve the transfection efficiency compared to saturated lipid chains of the same length.[17] A pair of other studies revealed improved transfection efficiencies when replacing DOPC with DOPE *in vitro*[85] and *in vivo*,[84] suggesting an enhanced intracellular trafficking for this type of lipid nanoparticles due to the fusogenic properties of DOPE.

The recognition of DNA therapeutics by immune cells and subsequent clearance from systemic circulation after intravenous administration is a major hurdle for effective therapies. Thus, many lipid-based DNA delivery systems have been modified with a hydrophilic corona to inhibit plasma protein binding and uptake by macrophages. The most common approach to enhance circulation half-life is the concept of PEGylation, *i.e.*, modification of nanoparticles with polyethylene glycol (PEG). These stealth, long-circulating, sterically stabilized systems can be created by incorporation of lipids containing a PEG modification. Notably, neutral and positively charged PEG lipids such as distearoyl-rac-glycerol-PEG (PEG-DSG), 1,2-dimyristoyl-rac-glycero-3-methoxy-PEG (PEG-DMG), and PEG-ceramide are superior to PEG lipids with a net negative charge for non-viral gene delivery systems.[92] Importantly, PEGylation can dramatically reduce transfection efficiency of lipid nanoparticles due to reduced cellular internalization. This "PEG dilemma" (*i.e.*, improved PK *versus* reduced uptake) has been shown for several nucleic acid delivery systems.[93−95]

The targeting of cell-specific membrane receptors is a promising strategy to enhance cellular uptake of DNA therapeutics. Targeting can either be achieved by endogenous ligands or synthetic exogenous ligands. For example, lipid nanoparticles containing ionizable lipids can serve as siRNA delivery systems for hepatocyte-specific targeting *via* low-density lipoprotein (LDL) or asialoglycoprotein (ASGP) receptors.[96] Endogenous mechanisms rely on binding of apolipoprotein E (ApoE) present in the blood circulation to the surface of lipid nanoparticles containing ionizable lipids. This subsequently triggers nanoparticle internalization *via* lipoprotein receptors such as the LDL receptor. Exogenous mechanisms are often based on the modification of lipid-based nanoparticles using a targeting ligand covalently attached to synthetic PEG-lipid. The most advanced strategy for hepatocyte targeting is conjugation of a trivalent *N*-acetylgalactosamine (GalNAc) moiety. This mediates specific binding to the ASGP receptor and subsequent clathrin-mediated internalization.

The concept of active targeting has also been investigated for the delivery of DNA. First clinical trials using single-chain antibody modified nanoparticles to target the transferrin receptor of tumor cells have been initiated (for details, see the Immuno-lipoplexes section). In general, many different targeting ligands based on sugars, peptides, proteins, aptamers or antibodies have been investigated, and all of these have different advantages and disadvantages. In addition, various receptors have been evaluated for cell-type specific targeting. Challenges and advances of active targeted nanoparticles have been discussed in detail in several recent reviews.[5,97]

DNA Vector Encoding Gene of Interest. The efficiency of lipid-based DNA therapeutics is highly dependent on the DNA vector design. Modifications of the DNA vector influence the physicochemical properties of resulting lipid nanoparticles and have direct impact on gene expression efficiency and persistency. As a general rule, a small DNA vector size leads to higher transfection efficiencies. For example, the transfection efficiency of lipid nanoparticles increased by a factor of 6 when the DNA size was reduced from 52 000 to 900 bp.[98] The use of so-called minicircle DNA (mcDNA), lacking the bacterial backbone (e.g., bacterial origin of replication and antibiotic resistance genes) is, therefore, a promising strategy to improve the therapeutic

DOI: 10.1021/acsnano.8b07858
ACS Nano 2019, 13, 3754−3782

Table 3. Formulation Aspects Influencing Transfection Efficiency[a]

influence factor	effect on	general influence
size of encoding DNA sequence	duration of transgene expression	prolonged transgene expression using mcDNA
	transfection efficiency	increased transfection efficiency using smaller DNA sequences or mcDNA
gene delivery system to DNA ratio (N/P)	binding to and uptake by cells	increased cell membrane binding and uptake of nanoparticles with increased N/P ratios (unspecific binding also increased)
	DNA condensation and protection	high N/P ratios protect DNA from nucleases due to condensation
		high N/P ratios might impair DNA dissociation from the nanoparticles after their internalization by cells
	endolysosomal escape	increased endolysosomal escape for higher N/P ratios
	toxicity	high N/P ratios lead to increased cytotoxicity
	transfection efficiency	increasing transfection efficiencies up to an optimized N/P ratio
complexation pH	transfection efficiency	increased transfection efficiency at lower pH (DNA condensation is improved)
ionic strength	transfection efficiency	controversial
impact of proteins and cholesterol	binding and uptake by cells	reduced binding and uptake if lipoplexes formed in the presence of serum
		accumulation in large intracellular vesicles if lipoplexes formed under serum-free conditions
		accumulation in small intracellular vesicles if lipoplexes formed in the presence of serum
		opsonization promotes macrophage uptake
	cell viability	very low or very high serum concentrations detrimental
	endolysosomal escape	endolysosomal membrane destabilization by HSA
	transfection efficiency	reduced transfection efficiency in the presence of serum
		cholesterol promotes transfection efficiency
complexation volume	transfection efficiency	increased transfection efficiency using larger volumes

[a]A summary of formulation factors influencing DNA delivery and subsequent transgene expression (*e.g.*, DNA vector design, formulation strategy) is provided. The factors are ordered in accordance to the chapters of this Review.

performance of DNA vectors.[99] Beneficial effects of mcDNA *versus* conventional pDNA on the transfection efficiency were demonstrated in several studies.[100,101] Moreover, mcDNA vectors resulted in long-term transgene expression *in vitro* and *in vivo*.[101] Importantly, these effects are not dependent on the type of transfection reagent or cell type and have been described for various targets and application routes *in vivo*.[100−102] Possible reasons for these findings are an increased diffusion coefficient and an improved nuclear internalization, a more efficient transcription of gene expression cassettes when mcDNA is used, and a higher number of plasmid copies per amount of DNA as compared to large parenteral plasmids.[100,102−105] Consequently, small DNA vectors (e.g., mcDNA) can be associated with higher transfection efficiencies *in vitro* and *in vivo*. This offers the possibility of reducing the concentration of used transfection reagents to minimize lipid-associated cytotoxicity of these substances.

KEY ASPECTS FOR LIPID-BASED NANOPARTICLE FORMULATION

Besides inherent characteristics of the DNA vector, the formulation (*i.e.*, the mixture of lipid components and DNA vector) is a key factor for efficient non-viral gene transfer. For optimal performance, formulation aspects such as lipid-to-DNA ratio, formulation buffer and production volumes need to be optimized. These factors are summarized and discussed in the following sections. Overviews of formulation aspects influencing nanoparticle properties (Table 2) and gene expression (Table 3) are provided.

Gene Delivery System-to-DNA Ratio. The system-to-DNA (N/P) ratio is defined as the ratio of nitrogen atoms of the lipid headgroup to phosphate atoms of the DNA backbone. At the time point of nanoparticle formation, most of the lipid headgroups must be positively charged to associate with nucleic acid phosphates. The N/P ratio strongly influences the physico- and electrochemical properties of resulting nanoparticles (e.g., size, ζ potential, DNA condensation), cellular internalization, endolysosomal escape, cytotoxicity, PK and biodistribution, and, finally, transfection efficiency.

After endocytosis, nanoparticles are trafficked *via* early and late endosomes to lysosomes for degradation. Endosomal membranes contain vacuolar ATPase proton pumps (V ATPases) and anionic lipids.[106] In the presence of adenosine triphosphate (ATP), V-ATPases shuttle protons and Cl^- into these subcellular compartments. Nanoparticles that contain proton-accepting functional groups (e.g., primary, secondary, or tertiary amines) can capture protons and become positively charged. Association of exogenous cationic lipids with endogenous anionic lipids results in membrane disruptive nonlamellar structures that subsequently lead to rupture of the endosomal membrane (shape hypothesis).[21,107] Thus, high N/P ratios (*i.e.*, high number of exogenous cationic lipids) can enhance this lipid interaction and increase subsequent endolysosomal escape.[69]

Chen *et al.* investigated the N/P-ratio-dependent transfection efficiency of lipid nanoparticles encapsulating siRNA. When the N/P ratio was increased from 1 to 12, the transfection efficiency also increased up to a N/P ratio of 6. Further increase of the N/P ratio yielded only a minor improvement of the transfection efficiency. The authors concluded that a minimum amount of excess cationic (ionizable) lipid is necessary to maximize endolysosomal escape.[108] Similar findings were made for pDNA delivery.[15]

In general, low N/P charge ratios lead to poor transgene expression.[109] High N/P ratios lead to increased cytotoxic effects due to noncomplexed cationic lipids that can damage cells.[110−112] Furthermore, high N/P ratios reduce circulation lifetimes and nonhepatic biodistribution of lipid nanoparticles and can result in toxicity *in vivo*. For example, binding to erythrocytes causes aggregation in lung capillaries and subsequently leads to lung embolism.[113,114] Interestingly, the N/P ratio inversely correlates with the nanoparticle size of

DOI: 10.1021/acsnano.8b07858
ACS Nano 2019, 13, 3754−3782

DOTAP/DOPE, DC-Chol/DOPE, or KC2/helper lipid containing nanoparticles.[17,115] Similar findings were made with other types of gene-delivery systems.[116,117] Moreover, a high N/P ratio increases the ζ potential[115] and by this increases the homogeneity and stability of lipid nanoparticles due to electrostatic repulsive forces that prevent aggregation.[117,118] High N/P ratios furthermore protect DNA from degradation by DNase I due to increased DNA condensation.[15,115] It was shown that fully condensed pDNA is protected against nucleases, *e.g.*, cytosolic nucleases.[119] However, very high N/P ratios can impair the dissociation of the DNA after cellular internalization, and therefore, reduce transfection efficiency.[34,120]

Taken together, these findings indicate that the N/P ratio is closely associated not only with nanoparticle size, ζ potential, and DNA condensation capability but also with toxicity. Increasing N/P charge ratios were found to correlate with decreased cell viability but also with increased transfection efficiency. In general, the transfection efficiency shows a maximum at a certain N/P ratio. There is, however, no optimal N/P ratio that can be used for all types of cationic lipids. Whereas the highest transfection efficiency for cholesterol-derived lipoplexes was found at a N/P ratio of 3:1,[34] other types of lipids required much higher N/P ratios.[48]

Formulation Buffer. *Complexation pH.* In this Review, the complexation pH is defined as the pH at which the lipids and the DNA vector are mixed. The complexation pH can affect the lipid nanoparticle formation depending on the pK_a values of the lipids used. This factor is of special importance when electrostatic interactions between lipids and DNA are the main driver for lipid nanoparticle formation.[121] In general, complexation at lower pH increases DNA binding capacity and resulting transfection efficiency.[122,123] This is due to higher protonation of the cationic lipids leading to stronger electrostatic interactions with negatively charged phosphate moieties of DNA. For example, higher N/P ratios are needed to obtain lipoplexes with high transfection efficiencies at pH 8 as compared to pH 7 when using the lipids RPR 120535 and RPR 12276.[124] In the case of optimized ionizable lipids such as KC2 or MC3, DNA is efficiently encapsulated at pH 4, where the lipid is positively charged. Subsequent dialysis of formulated lipid nanoparticles against pH 7.4 results in nanoparticles with low surface charge.

Ionic Strength. The salt concentration during mixing of lipids and DNA can influence the complex formation and the transfection efficiency. High electrolyte concentrations in the complexation medium can shield the charge of cationic lipids and DNA and thus decrease the electrostatically driven self-assembly of lipid nanoparticles.[124] In addition, the colloidal stability of the solution is reduced.

When lipid nanoparticles with the cationic lipid RPR120535 are prepared at high salt concentrations (150 mM NaCl), the resulting size is larger as compared to formulations prepared at low (20 mM NaCl) salt concentrations.[124] In general, replacement of saline by glucose in the complexation medium reduces the lipid nanoparticle size.[116,118] The effect on the resulting transfection efficiency is, however, not conclusive. Whereas for some transfection reagents, high salt concentrations (*i.e.*, up to 600 mM NaCl) increase transfection efficiency,[125] other reagents show a higher transfection efficiency when produced at low ionic strength (*i.e.*, 10 mM NaCl).[123]

Impact of Proteins and Cholesterol. Serum is a collective term for a mixture of various plasma protein components (e.g., albumin), inorganic constituents (e.g., bicarbonate), amino acids, nonprotein nitrogen components (e.g., creatine) and their low-molecular metabolites, carbohydrates, fats and their derivatives, as well as vitamins, hormones, and pigments.[126] Notably, the composition of serum varies among different species.

It is important to note that serum can strongly influence the performance of DNA delivery systems on different levels: the complex formation and the complex stability as well as the characteristics of cells during *in vitro* experiments. This factor needs to be considered because many cell lines require serum-containing medium for growth and differentiation.

When lipid nanoparticles are formed in serum-containing complexation medium, a reduced binding to plasma membranes, cellular internalization, and transfection efficiency can be observed. In addition, lipid nanoparticles formed in serum containing medium and buffer are often smaller in size.[109] When preformed lipid nanoparticles are diluted, the presence of serum can prevent lipid nanoparticle aggregation due to protein adsorption onto the nanoparticle surface.[118,127] Lipoplexes formed by cationic lipids RPR 120535 and RPR 121653, for example, show reduced agglomeration in serum-containing medium. However, presence of serum reduces their transfection efficiency *in vitro* by a factor of 100 although the intracellular pDNA concentration is only reduced 2- to 3-fold. The larger lipoplex nanoparticles obtained in serum free conditions were found in large, homogeneous intracellular vesicles, whereas the smaller lipoplex nanoparticles accumulated in small vesicles. Thus, different uptake and intracellular trafficking mechanisms seem to contribute to the difference in transfection efficiencies observed.[128] Decreased transfection efficiencies upon serum addition during formulation were reported for various lipid nanoparticles. The decrease in transfection efficiency was not significantly affected by the serum type or concentration (e.g., 10% *versus* 30% fetal bovine serum). Interestingly, complexes containing cholesterol such as DOTAP/cholesterol (DOTAP/Chol) or DOTAP/DOPE/Chol are less sensitive to serum.[120]

Although the exact mechanism is not known yet, it is tempting to speculate that neutral cholesterol reduces the overall electrostatic interactions with negatively charged serum components, thereby reducing the negative influence of serum on the lipid nanoparticle system. In addition, cholesterol increases the packing of phospholipids in lipid bilayers. Dalmen *et al.* showed that high-density lipoproteins (HDL) and LDL trigger release of liposomal drug payload. However, when cholesterol is incorporated into the liposome formulation, the transfer of phospholipids from liposomes to HDL is reduced. As a consequence, the stability of the phospholipid bilayer is increased and drug retention within the liposomes improved.[129] In addition, a decrease in ζ potential can be observed when positively charged nanoparticles are mixed with serum-containing medium.[130]

Because serum consists of a protein mixture, one needs to consider that not only the extent of protein adsorption but also the types of proteins adsorbed to the nanoparticle surface are critical parameters. *In vivo*, certain serum proteins promote recognition and uptake of nanoparticles by macrophages of the mononuclear phagocytic system (MPS), *i.e.*, opsonins, whereas others such as human serum albumin (HSA) or immunglobulin A (IgA) can prolong the blood circulation time of nanoparticles (*i.e.*, dysopsonins).[131,132] Moreover, HSA can promote membrane fusion under acidic conditions and increase endolysosomal escape by facilitating membrane destabilization.[133] By pre-incubating nanoparticles prior to incubation or injection, this effect can be exploited to improve the gene delivery efficiency.

DOI: 10.1021/acsnano.8b07858
ACS Nano 2019, 13, 3754−3782

Table 4. Factors Influencing Transfection Efficiency *in Vitro*[a]

influence factor	effect on	general influence
nanoparticle size	transfection efficiency	efficiency is increased for pDNA when size is increased
		efficiency is decreased for siRNA when size is increased
	cellular uptake	size influences the uptake pathway and speed of uptake but not the amount of internalized NPs expressed as μg NP/cell
		>1 μm: phagocytosis
		≤200 nm: clathrin or caveolae-mediated
	intracellular trafficking	≥500 nm: avoidance of lysosomes and endolysosomes
		smaller NPs are associated with more but smaller NP-containing vesicles in the cytoplasm
ζ potential	interaction with target cell membranes	positive ζ potentials are associated with stronger interactions with the negatively charged cell membrane
DNA quantity	toxicity	increased cytotoxicity at higher DNA dosage due to correlating high dose of transfection reagent required
	transfection efficiency	increased transfection efficiency for increased amounts of DNA
transfection volume and nanoparticle concentration	nutrient supply	faster nutrient depletion in low transfection volumes
	toxicity	increased cell viability in larger volumes
	transfection efficiency	increased transfection efficiency in lower transfection volumes
incubation time	colloidal stability	agglomeration of lipoplexes over time
	lipoplex internalization	amount of internalized lipoplexes decreases over time
	nutrient supply	nutrient depletion during longer incubation times
	toxicity	increased cell viability after shorter incubation times
	transfection efficiency	increased transfection efficiency for longer incubation times
cell lines	cell division rate	higher transfection efficiency in rapidly dividing cells
		rapidly dividing cells might show a faster nutrient depletion in cell culture media
		experiments can be conducted in a shorter time when using rapidly dividing cell lines
	cell surface decoration	differences in cell surface protein expression of various *e.g.*, receptors allow for targeting
	endocytic capacity	varies among different cell lines
		higher endocytic capacities associated with higher transfection efficiency
		ability for micropinocytosis associated with higher transfection efficiency
	membrane repair capacity	higher membrane repair capacity for primary cells
		lower membrane repair capacity for cancer cells and immortalized cell lines
	secretion pattern	secretion of certain molecules such as pulmonary surfactant may impair transfection efficiency of cationic lipid-based delivery systems
	transfection efficiency	primary cells harder to transfect
		immortalized cell lines easier to transfect
		differences when using different transfection reagents in different cell lines
	uptake	rate-limiting step in primary cells
		not rate-limiting step in immortalized cell lines
cell density	cell growth behavior	faster cell growth at higher densities (above 50%)
		slower cell growth at lower densities (below 30%)
		recovery of exponential growth after passaging is slower when cells grew 100% confluent prior to passaging
	toxicity	higher toxicities at lower cell densities due to higher amount of cationic lipid per cell
		lower toxicities at higher cell densities due to lower amount of cationic lipid per cell
plate coating	cell viability	increased viability for *e.g.*, hepatocytes when cultured on collagen-coated culture dishes
	transfection efficiency	increased transfection efficiency for weakly adherent cells after coating of the culture dish with cationic polymers or ECM proteins

[a]A summary of main factors (in addition to formulation aspects; Table 3) influencing the delivery of DNA and subsequent gene expression *in vitro* is provided. Influence factors are listed in accordance to chapters of this Review.

Simões *et al.* pre-incubated DOTAP/DOPE liposomes with HSA prior to complexation with DNA. HSA coating significantly improved transfection efficiency and transgene expression of lipoplexes. These results were obtained in several cell lines (HeLa, COS-7, the Hut-78 T-cell line derived H9 cell line, B-lymphocytic TF228.1.16 cells, and human peripheral blood monocyte-derived macrophages), as well as *in vivo* in mice. Moreover, HSA coating dramatically reduced the negative effects of serum-containing medium on transfection efficiency. In contrast, non-modified lipoplexes almost completely lost their transfection activity upon contact with serum. The cell viability, however, remained unaffected, suggesting that HSA coating is safe.[134] Similar studies showed beneficial effects on the toxicity profile of nanoparticles, most likely due to the shielding of the positive charge by protein adsorption.[135,136]

Complexation Volume. The complexation volume is defined as the volume in which the lipid components and the DNA are mixed to form the gene delivery system. It should not be confounded with the transfection volume *in vitro*. The complexation volume affects the formation of complexes, and although most formulations are diluted prior to application *in vitro* or *in vivo*, the complexation volume heavily influences the transfection efficiency. High concentrations of DNA, for example, might not allow for a proper condensation and lead to only partially formed nanoparticles or trigger particle aggregation.[111]

DOI: 10.1021/acsnano.8b07858
ACS Nano 2019, 13, 3754−3782

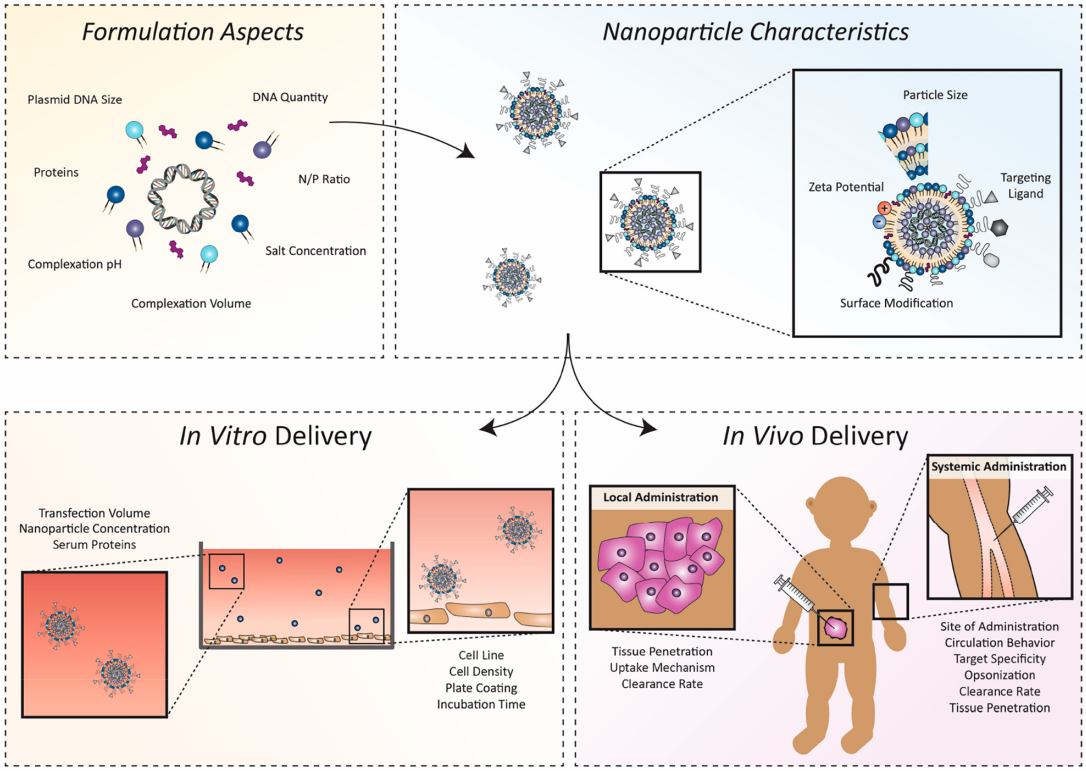

Figure 5. Schematic representation of various factors influencing the gene delivery and gene expression of lipid-based DNA therapeutics. (1) During the formulation process, several aspects have to be considered that influence nanoparticle characteristics and gene delivery efficiency. Complexation pH, volume, salts, and proteins can be influenced using an optimized formulation buffer. DNA characteristics and lipid-to-DNA ratio influence gene expression. (2) Optimized physicochemical properties of lipid-based DNA therapeutics are essential for an efficient gene delivery and need to be adjusted for a cell-type or tissue-specific gene expression. (3) *In vitro*, cell medium and cell characteristics are two important factors influencing gene delivery efficiency. Cell-dependent factors include cell type, cell density (*i.e.*, nanoparticles per cell), cell attachment, and time for nanoparticle uptake. (4) *In vivo* gene delivery is mainly influenced by the route of administration and the nanoparticle PK (*i.e.*, circulation behavior, clearance rate, tissue penetration, targeting capacity, and cellular uptake).

For example, DOTAP/Chol DNA lipoplexes were formed in complexation volumes ranging from 3.2 to 102.2 μL. Although all formulations were diluted to a final volume of 102.2 μL prior to *in vitro* transfection experiments, a significant increase in transfection efficiency was observed when DOTAP/Chol lipoplexes were formed in larger complexation volumes.[137] However, this effect is dependent on factors such as initial DNA concentration, transfection reagent, and N/P ratio.[137,138] When DOTAP/Chol lipoplexes are formed at a high N/P ratio, the effect of the complexation volume becomes negligible.[137]

Although higher complexation volumes might be advantageous for certain transfection reagents, the volume for *in vitro* (cell culture dish) and *in vivo* (injection volume) administrations is limited. Protocols such as hydrodynamic injection (8−10% of total body weight) for gene delivery to hepatocytes may be applied in rodents, its application in the clinical setting is, however, limited. The standard protocol for animal experiments involves a normodynamic i.v. injection of a total volume up 5 mL/kg (1.25% of total body weight).[139−141]

FACTORS IMPORTANT FOR *IN VITRO* AND *EX VIVO* TRANSFECTION

The efficiency of lipid-based DNA delivery and subsequent gene expression *in vitro* and *ex vivo* is dependent on various factors. In the following sections, we summarize and discuss the influence of nanoparticle design, transfection protocol, and target cell type. An overview of factors influencing the nanoparticle properties, and the transfection efficiency *in vitro* is provided in Table 4 and Figure 5.

Nanoparticle Design. The physicochemical properties (e.g., size and surface charge) of lipid-based DNA delivery systems strongly influence their transfection efficiency *in vitro*. Therefore, optimization of physicochemical characteristics is of crucial importance to enhance DNA delivery and subsequent transgene expression. In the following section, we discuss these key factors, their importance for the design of lipid-based DNA nanoparticles and their influence on gene transfer *in vitro*.

Size. The size of lipid-based DNA nanoparticles is a key characteristic that influences the transfection efficiency *in vitro*. This parameter depends on multiple factors such as the type of cationic or ionizable lipid used,[110,118,142] N/P ratio,[115,120] pH of the transfection medium,[143] preparation method,[144] time frame

DOI: 10.1021/acsnano.8b07858
ACS Nano 2019, 13, 3754−3782

for maturation after complex formation,[142] presence of serum,[109,118,120,127,128,130] or salt concentration during complex formation.[116,118,124,125] Consequently, nanoparticle size has to be monitored during particle preparation, during storage under different assay conditions, and before use. Despite such precautions, nanoparticle size may increase after addition to cell medium due to binding of plasma proteins and the formation of a biocorona.[132,145,146]

There is no consensus on whether larger or smaller lipid nanoparticles are more effective (*in vitro*). Some authors hypothesize that large particles sediment *in vitro* onto cultured cells, leading to a higher exposure.[118,120] In addition, a higher amount of DNA vectors can be incorporated within larger nanoparticles as compared to their smaller counterparts.[120] Indeed, several research groups reported a positive correlation between nanoparticle size and transfection efficiency in *in vitro* experiments.[118,120,127] In line with these reports, Almofti *et al.* found that larger lipoplexes resulted in higher transfection efficiencies *in vitro*. Furthermore, lipoplex size was the only nanoparticle characteristic that correlated with transfection efficiency.[109] However, detailed studies revealed that the amount of DNA internalized by cells is independent of nanoparticle size.[124,147] This finding suggests that not the total amount of delivered DNA is decisive but rather the intracellular processing of nanoparticles and their cargo. Indeed, large intracellular vesicles might be more prone to vesicular disruption than smaller vesicles associated with smaller nanoparticles.[109,124,128] This might favor endosomal escape and appearance of a higher number of smaller-sized nanoparticles in the cytoplasm.[148]

With respect to intracellular trafficking, nanoparticle size heavily influences cellular internalization and intracellular processing.[145] For example, microparticles larger than 1 μm are internalized by antigen presenting cells (APCs) such as macrophages and dendritic cells through phagocytosis, whereas these particles are internalized inefficiently in nonphagocytic cells.[149] Nanoparticles smaller than 200 nm were shown to be rapidly internalized by murine melanoma cells B16−F10 *via* clathrin-mediated endocytosis, whereas larger nanoparticles (*i.e.*, 500 nm) were slowly internalized *via* other pathways. Consequently, smaller nanoparticles accumulated in late endosomes and lysosomes, whereas nanoparticles with a size of 500 nm did not reach the lysosomal compartment.[150]

ζ Potential. The ζ potential of a nanoparticle is a measure of the electrokinetic potential between the surface of a tightly bound ion layer (shear plane) and the electroneutral region of the surrounding solution. The ζ potential has practical implications for the colloidal stability of systems containing dispersed particles because this potential, rather than the Nernst potential, governs the degree of repulsion between dispersed particles and the interaction with biological membranes. The ζ potential is mainly influenced by the lipid composition and the N/P ratio. In general, the ζ potential increases with increasing N/P ratio.[115,151]

On the one hand, it was shown that nanoparticles with a highly positive or negative ζ potential (±30 mV) have a high colloidal stability due to electrostatic repulsive forces that prevent aggregation.[120,151] In sharp contrast, nanoparticles with a nearly neutral (±5 mV) ζ potential rapidly agglomerate.[152] On the other hand, a high positive ζ potential can increase the adsorption of negatively charged plasma proteins to the nanoparticle surface. All of these effects influence nanoparticle size and thus transfection efficiency. Strategies for improved colloidal stability, such as surface modification with the hydrophilic polymer PEG, were already discussed in the Additional Lipid Components section of this Review.

Transfection Protocol. *DNA Quantity.* The total amount of DNA used during *in vitro* experiments markedly influences the transfection efficiency. As a general rule, higher amounts of DNA result in higher transfection efficiencies. For example, increasing the dose of pDNA per well from 0.5 to 4 μg significantly increased transfection efficiencies in various cell lines when integrin-targeted cationic lipid-based/pDNA nanoparticles were used.[102] Similar findings were made for other types of transfection reagents and cell lines.[110,153] In transfection experiments with Lipofectamine, lipofectin, cellfectin, and DMRIE-cholesterol, high *in vitro* transfection efficiencies were obtained when pDNA concentrations above 1.33 μg/mL were used. Lower pDNA concentrations resulted in dramatically decreased transfection efficiencies.[154] It should be noted, however, that very high pDNA doses may also increase cytotoxicity due to the co-administered high doses of cationic lipids. This has been demonstrated by Gao *et al.*, who reported a bell-shaped curve for transfection efficiency *versus* DNA dosage.[143]

Transfection Volume and Nanoparticle Concentration. The transfection volume is defined as the total volume in which cells are incubated with lipid-based nanoparticles for transfection. For practical reasons, the transfection volume is, in most cases, the sum of culture medium and its nutrients accessible for cultured cells during incubation and a constant amount of transfection reagent.

For many lipid-based transfection reagents, low transfection volumes are associated with an increased transfection efficiency due to a higher apparent concentration of DNA nanoparticles. However, not all transfection reagents profit from higher concentrations (*i.e.*, lower transfection volumes). The commercially available lipid-based transfection reagent Lipofectamine 2000 is hardly affected by varying transfection volumes in a certain range while maintaining the same quantity of lipid-based nanoparticles added to cells.[155]

In general, decreasing the transfection volume leads to a decreased amount of nutrients and growth factors in cell culture and higher concentrations of transfection reagents. This may result in increased cytotoxicity. Malloggi *et al.* clearly demonstrated that the cell viability increased with increased transfection volumes, irrespective of the transfection agent used.[156] High lipid nanoparticles concentrations can thus reduce transfection efficiency due to reduced cell viability and inefficient transgene expression as also shown for lipid nanoparticles consisting of optimized ionizable lipids.[17] This balance needs to be optimized for each lipid nanoparticle system and experimental setting. A common strategy to reduce toxic effects of high lipid nanoparticle concentrations is to keep the incubation times short and to exchange the cell culture medium.

Incubation Time. The incubation time of cells with lipid nanoparticles strongly influences the transfection efficiency and cytotoxicity. In this Review, the incubation time is referred to as the time frame during which the cells are in contact with the lipid-based DNA complexes (*i.e.*, until medium exchange or assay readout). As a general rule, long incubation times increase the transfection efficiency. However, they may as well lead to cytotoxicity,[110] nutrient depletion during the incubation,[154] and aggregation of lipid nanoparticles. In particular, lipoplexes suffer from a rather low colloidal stability. To minimize aggregation of

DOI: 10.1021/acsnano.8b07858
ACS Nano 2019, 13, 3754−3782

lipoplexes during transfection, an incubation time frame of 24 h is typically not exceeded.[111]

It was demonstrated that transfection efficiencies of DOTAP or DOTAP/DOPE-based systems reached a maximum after 24−48 h of incubation, whereas shorter or longer incubation times led to reduced transfection efficiencies.[102] DOTAP/pDNA lipoplexes showed a luciferase activity that was 2 orders of magnitude higher 24 h after transfection as compared to 80 h post-transfection.[102] The transfection efficiency of lipofectin/pDNA lipoplexes in MRC5E- and 293E-cells increased when the incubation time increased from 20 min to 4 h.[102] Similar findings were made for other types of transfection reagents.[156] It was demonstrated that longer incubation times are associated with higher amounts of internalized lipid nanoparticles.[157] However, short incubation times reduce the interaction between cells and the DNA/lipid complex and thereby reduce the transfection efficiency.

Target Cells. *Cell Lines.* In general, cell lines can be separated into primary cells and cultured cells. Primary cells are often more difficult to transfect and the resulting transfection efficiencies are low,[158] whereas immortalized cultured cells such as COS-7, NIH 3T3, HeLa, HEK 293, and CHO often show high transfection efficiencies.

While lipid nanoparticle uptake is rather fast in most cultured cells, membrane binding and cellular internalization seems a rate limiting factor for high transfection efficiencies in primary cells.[54] Vercauteren *et al.* showed that the slow and inefficient cellular internalization of lipoplexes in primary bovine cells (BRPE) correlated with a low transfection efficiency of these cells, whereas cultured retinal pigment epithelial cell lines (ARPE-19 cells) were efficiently transfected after a rapid lipoplex internalization. Indeed, the low metabolic activity of primary cells (leading to significantly lower cellular growth rates for primary cells as compared to cultured cell lines)[159] results in a low endocytic activity. However, not all cultured cell lines can be transfected efficiently. Differences in the expression pattern of extracellular receptors and intracellular mediators, endocytic activity, and cell division rate can influence the gene delivery efficiency to various cell types. For example, COS-7 cells expressed a luciferase reporter gene 165-fold more efficient as compared to HEK-293 cells using similar DNA delivery conditions. The authors hypothesized that COS-7 cells may have an increased nuclear translocation of inserted DNA due to a markedly increased cell division rate.[148] The synthesis and secretion pattern of various molecules is another cell-line-dependent factor. For example, A549 human lung epithelium carcinoma cells are known to be able to synthesize and secrete saturated PC, an important component of pulmonary surfactant. Secreted lipids can interfere with DNA transfection *in vitro* by disrupting lipid−DNA complexes.[151,160,161] Replacement of the culture medium prior to transfection may therefore be advisable if epithelial cells are transfected and if the lipid nanoparticles are sensitive to disruption. Similarly, the expression of collagen by cultured and isolated cells can vary between 0.001% and 50% of the total protein content among different cell lines.[162,163] In addition, differences in endocytic capacity and cell division rate may influence transfection efficiencies *in vitro*. Furthermore, cell lines that express sufficient levels of target receptors should be chosen when actively targeted DNA delivery systems are evaluated. For example, cells that express a high level of the galactose-binding ASGP receptor will show higher transfection efficiencies when nanoparticles are modified with galactose moieties.[164]

It should be noted that the extent of many of these phenomena depend on the type of delivery system used. For example, transfection efficiency in C6 rat glioma cells[127] or caprine and ovine fibroblasts[154] is higher with Lipofectine as compared to DMRIE, whereas the opposite was found in bovine fibroblasts[154] and COS cells.[165] All of these findings highlight the importance to carefully choose a suitable *in vitro* cell model for a specific question to be addressed.

Cell Density. The cell density strongly influences the transfection efficiency and lipid nanoparticle-mediated toxicity *in vitro*. A low cell number results in a high dose of nanoparticles per cell that may result in higher transfection efficiencies.[110,111] When cells with a confluence of 30%, 60%, and 90% were transfected at a constant lipid nanoparticle concentration, transfection efficiencies of 45%, 27.6%, and 6.5% were achieved.[154] In addition, cells in an exponential growth phase often show a higher protein expression as compared to confluent (resting) cells.[158] However, cytotoxicity may be dramatically increased when a (too-) low cell density is chosen for transfection experiments. This is due to reduced growth rates at low cell densities (e.g., below 50%)[111] and the increased relative dose of lipid nanoparticles per cell. Consequently, commercially available transfection reagents are often recommended in combination with cells that show a high confluence (e.g., 90−95% for Lipofectamine 2000).

Plate Coating. The type and surface coating of cell culture plates is another factor that influences transfection efficiency. The substrate on which cells are cultured has an impact on, *e.g.*, cell polarity, morphology, proliferation, differentiation, viability, and responsiveness to signaling molecules.[166] In general, cells in suspension are harder to transfect compared to adherent cells.[167] Adherent cultured cells need to attach to a substrate to survive and divide.[162,168] Whereas positively charged surfaces represents the easiest and most frequently used substrate for culturing strongly adherent cells such as fibroblasts, a pretreatment of the culture plate may be required for other cell types.[169] Typical examples of coating reagents are extracellular matrix (ECM) proteins such as collagen, fibronectin, and laminin[162,166] or cationic polymers such as poly-L-lysine (PLL), polyornithine,[170,171] or polyethylenimine (PEI).[172,173] The coating of wells with cationic polymers or ECM proteins increased the DNA delivery efficiency in weakly adherent HEK-293 and PC-12 cells up to 6-fold. However, no increase in transfection efficiency by coating was observed for strongly adherent primary fibroblasts.[169] Increase in transfection efficiency by plate coating in weakly adherent cells may be a result of decreased detachment of cells (when culture medium is aspirated) and increased cell membrane surface area.[174]

FACTORS IMPORTANT FOR *IN VIVO* GENE DELIVERY

***In Vitro* to *in Vivo* Translation.** A major bottleneck in the development of lipid-based DNA therapeutics is the weak correlation between results observed *in vitro* and the actual situation *in vivo*.[2] Cultured cells are in direct contact with lipid nanoparticles during incubation. However, *in vivo* additional factors such as PK, tissue distribution, safety and tolerability, interactions with the host immune system, and metabolic stability of injected nanoparticles have to be considered. Recently, more than 100 different cationic lipids were investigated for siRNA delivery to hepatocytes *in vitro* and *in vivo*. Surprisingly, physicochemical properties such as ζ potential and the nanoparticle size (when <300 nm) could not be used to directly correlate *in vitro*−*in vivo* transfection efficiencies.[175]

DOI: 10.1021/acsnano.8b07858
ACS Nano 2019, 13, 3754−3782

Table 5. Factors Important for *in Vivo* Gene Delivery[a]

influence factor	effect on	general influence
nanoparticle size	blood circulation time	reduced blood circulation time for smaller NPs
	tissue penetration	enhanced tissue penetration for smaller NPs
	pharmacokinetic behavior	increased NP uptake in spleen and liver for larger NPs
	opsonization	increased serum protein opsonization for smaller NPs with higher specific surface area
ζ potential	interaction with serum proteins	positive ζ potentials favor serum protein opsonization
	pharmacokinetic behavior	positive ζ potentials (>20 mV) as well as negative ζ potentials (←20 mV) may lead to off-target tissue accumulation
		cationic nanoparticles accumulate in lungs, and anionic nanoparticles are sequestered by liver endothelial cells and spleen
route of administration	pharmacokinetic behavior	accumulation at the site of injection for nanoparticles with poor diffusion capacity
	side effects/toxicity	related to tissue distribution or increased risk after local deposition of cationic lipids

[a]Summary of most important factors (in addition to formulation aspects; see Table 3) influencing the lipid-based delivery of DNA and subsequent gene expression *in vivo*. Influence factors are listed in accordance to chapters of this Review.

Classical 2D cell culture models often fail to mimic the *in vivo* situation and fail to predict nanoparticle biodistribution.[2] However, early screening of hundreds of formulation candidates in preclinical animal models is costly and time-consuming and raises ethical concerns. The limited *in vitro* to *in vivo* translation depicts a key limitation in the development of efficacious lipid-based gene delivery systems. Noteworthy, several recent developments have the potential to bridge this gap by either using non-rodent screening models or by increasing the experimental power of single *in vivo* studies. Increasing number of evidence is highlighting zebrafish (and their embryos) as a model to screen nanoparticle circulation and biodistribution,[176−179] to analyze nanoparticle toxicity[177] and to assess their therapeutic potential in various disease models.[180,181] These assays can be performed in high-throughput and the transparency of zebrafish embryos enables whole-body imaging using fluorescence-based techniques.[176] Sieber *et al.* systemically injected liposomal formulations in zebrafish embryos and analyzed the circulation behavior (*i.e.*, PK)[176] and macrophage uptake[178] to optimize lipid composition as well as type and extent of PEGylation.

Other preclinical screening strategies aim to increase the experimental throughput and were optimized for parallel formulation assessment in rodents. The so-called barcoding of nanoparticles using DNA codes allows the injection of hundreds of formulation candidates in the same animal.[2,182−184] Subsequent decoding by high-throughput techniques such as next generation sequencing (NGS) allows the tracing back of the DNA signal and sequence to a formulation composition. Furthermore, this technique has the main advantage that it can be considered label-free because the drug payload (*e.g.*, pDNA) is directly quantified. This technique allows reducing the number of animals and analytical efforts used for PK and biodistribution by orders of magnitude.

Factors Important for Lipid Nanoparticle Design. An overview of factors important for *in vivo* gene delivery is provided in Table 5 and Figure 5. Several nanoparticle-related characteristics can be optimized to obtain efficient gene delivery *in vivo*. Physicochemical properties such as size and ζ potential need to be considered early in nanoparticle design. Factors such as the route of administration, dosing scheme, or target tissue and cell type are important design restraints. In the following section, these nanoparticle- and therapy-related factors will be discussed in more detail. Because results from *in vitro* cannot be accurately translated to the *in vivo* situation, advanced preclinical screening tools are of increased interest (see the In Vitro to in Vivo Translation section).

Size. After administration into the body, lipid nanoparticles need to reach their target tissue. Major hurdles for target tissue accumulation are several tissue and cell specific hurdles, efficient internalization, and release of the nucleic acid payload.[185]

Nanoparticles with a hydrodynamic diameter below 6 nm can be excreted *via* renal filtration.[145,186] Interestingly, nanoparticles consisting of positively charged lipids were shown to be excreted *via* urine even if their size exceeds the glomerular filtration cutoff. For example, lipoplexes that self-assemble *via* electrostatic forces can be destabilized by negatively charged proteoglycans (*e.g.*, heparin sulfate) at the glomerular basement membrane in the kidneys.[187] It was shown that sterically stabilized (*i.e.*, PEGylated) lipid-based nanoparticles with a size of less than 150 nm in diameter are able to accumulate in the bone marrow of rabbits. In contrast, nanoparticles with a size of 250 nm are more efficiently sequestered by the reticuloendothelial system (RES) including spleen and liver-resident macrophages, *i.e.*, Kupffer cells, whereas only a small fraction can be found in the bone marrow.[188]

The physiological role of the spleen is the removal of aged or damaged red blood cells and other particles from the blood. Notably, the spleen is endowed with interendothelial cell slits of approximately 200−500 nm, and nanoparticles exceeding this size threshold act as splenotropic agents.[189,190] Thus, further increase in size (and positive ζ potentials) enhances nanoparticles accumulation in the spleen.[191] In addition, increased protein accumulation and opsonization results in enhanced uptake by phagocytic Kupffer cells in the liver.[132,189,192] These processes finally result in a reduced plasma half-life and decreased gene delivery efficiency to the target cell.

For tissue- or cell-type-specific targeting, nanoparticle size is a key parameter. For example, the fenestrae of human hepatic sinusoidal capillaries have an average diameter of 105 nm with a size range between 50−180 nm.[193] Notably, these fenestrae parameters might show variations due to pathological conditions.[194,195] Thus, the delivery of nucleic acids to hepatocytes is unlikely if the diameter of the nanoparticles markedly exceeds that of the fenestrae. Other targets are not (*e.g.*, central nervous system) or not efficiently accessible *via* the central blood circulation (*e.g.*, solid tumors) and require deep tissue penetration. It was shown that smaller nanoparticles and particles with a high aspect ratio exhibit enhanced tissue

DOI: 10.1021/acsnano.8b07858
ACS Nano 2019, 13, 3754−3782

Table 6. Lipid-Based DNA Therapeutics in Clinical Trials[a]

delivery system	gene	combination therapy	delivery route	indication	phase	status	ClinicalTrials identifier (first received)	ref
DOTAP	FUS1 gene		i.v.	advanced non-small-cell lung cancer (NSCLC)	I	completed	NCT00059605 (2003)	220−224
	FUS1 gene (INGN-401)	combination with erlotinib	i.v.	stage IV lung cancer (NSCLC)	I/II	recruiting	NCT01455389 (2011)	225−227
	BikDD gene (C-VISA)		i.v.	advanced pancreatic cancer	I	withdrawn	NCT00968604 (2009)	228−232
	CFTR gene		nasal application	cystic fibrosis	I	completed		267
DOTMA	interleukin-2 gene		i.t. injections	squamous cell carcinoma of the head and neck (stage III/IV)	II	completed	NCT00006033 (2004)	233−235
DMRIE	CFTR gene		nasal application	cystic fibrosis	I pilot	completed	NCT00004471 (1999)	237−240
					I	completed	NCT00004806 (2000)	
	interleukin-2 gene (Leuvectin)		i.t. injections	prostate cancer	I/II	Terminated (prostate cancer)	NCT00004050 (2003) NCT00005072 (2003)	241−245, 268
	HLA-B7 and β2-macroglobulin gene (Allovectin)		i.t. injections	metastatic melanoma	II	completed	NCT00044356 (2002)	246−252
				head and neck cancer	III	completed	NCT00050388 (2002)	
				melanoma	II	completed	NCT00003646 (2004)	
					III	completed	NCT00003647 (2004)	
					pivotal III	completed	NCT00395070 (2006)	
EDMPC	CFTR gene		nasal application	cystic fibrosis				253−255
DC-Chol	EGFR Antisense DNA		i.t. weekly for 4 weeks	advanced oral squamous cell carcinoma (head and neck cancer)	I	completed	NCT00009841 (2001)	256−260
	CFTR gene		nasal application	cystic fibrosis	I	completed		269−272
	HLA-A2 gene		injection into nodules	cervical and ovarian carcinoma	I	completed		261, 262
GL67	CFTR gene		administered to the nose and lungs	cystic fibrosis	I/II	completed	NCT00789867 (2008)	273−275
	CFTR gene		nasal application	cystic fibrosis	IIb	completed	NCT01621867 (2012)	263−266
transferrin-receptor-targeted lipoplexes	P53 (SGT-53, scFv transferrin receptor antibody)	docetaxel	systemic i.v. administration	advanced solid tumors	I	completed	NCT00470613 (2007)	276−280
		temozolomide		recurrent glioblastoma	II	recruiting	NCT02340156 (2014)	281
		topotecan and cyclophosphamide		recurrent or refractory solid tumors	I	recruiting	NCT02354547 (2014)	282
		gemcitabine/nab-paclitaxel		metastatic pancreatic cancer	II	recruiting	NCT02340117 (2014)	283
	RB94 (SGT-94, scFv transferrin receptor antibody)		systemic i.v. administration	solid tumors	I	completed	NCT01517464 (2012)	284−286

[a]Lipid-based nanoparticles for the expression of therapeutic genes are used in several clinical trials. Most approaches are based on passive targeted systems. Recently, transferrin-receptor-targeted lipid-based nanoparticles were evaluated. Different routes of administration were investigated, *i.e.*, intravenous (i.v.), intratumoral (i.t.), and pulmonary or nasal application. Clinical trials are grouped by delivery system and listed chronologically.

3769
DOI: 10.1021/acsnano.8b07858
ACS Nano 2019, 13, 3754−3782

penetration.[108,186,196,197] Nanoparticle size is therefore a critical design parameter to achieve efficient gene delivery *in vivo*.

ζ Potential. The ζ potential can influence to which extent nanoparticles interact with serum proteins. As a consequence of opsonization, nanoparticles are removed from the bloodstream by phagocytotic cells.[198] For example, Xiao *et al.* demonstrated that micellar nanoparticles with either highly positive or highly negative surface charge are cleared by macrophages following opsonization.[199] Besides influence on macrophage clearance, the ζ potential was also shown to influence the biodistribution of nanoparticles. Cationic nanoparticles interact with negatively charged biological membranes, leading to adsorptive mediated endocytosis and a high systemic plasma clearance *in vivo*. Anionic nanoparticles, however, are at risk to be cleared *via* Stab-2-dependent stabilin scavenger receptors of mammalian liver sinusoidal endothelial cells.[179] Kranz *et al.* demonstrated that a highly positive ζ potential (>20 mV) is associated with predominant nanoparticle accumulation in the lungs, whereas negative ζ potentials (←20 mV) led to almost-exclusive nanoparticle accumulation in the spleen.[200] Similarly, Levchenko *et al.* demonstrated an increased liver accumulation of negatively charged lipid-based nanoparticles.[201] A possibility to overcome difficulties associated with high surface charges is decoration of the nanoparticle surface with PEG.[202] However, several issues are associated with PEGylation of DNA therapeutics. First, the use of more than 8 mol % DSPE-PEG2000 for the preparation of PEGylated lipid nanoparticles is associated with an increased risk for liposome destabilization.[203] Second, the PEGylation of nanoparticles may lead to immune responses against PEG, especially in the case of multiple dosing.[204] Finally, excessive PEGylation might result in decreased therapeutic efficacy (PEG-dilemma).[93−95]

Route of Administration. *Systemic Administration.* Several nanoparticle-related characteristics can result in rapid clearance of nanoparticles from the bloodstream. The lung is the first organ encountered by intravenously injected nanoparticles. Consequently, the i.v. injection of (large) cationic nanoparticles or particle agglomerates leads to first-pass filtration in the lung and is likely to provoke severe side effects such as embolism. At later time points, a substantial fraction of cationic nanoparticles can be found in liver or spleen. Cellular uptake is preferentially mediated by endothelial cells (lung) or Kupffer cells (liver).[205−207] Thus, besides the spatial distribution, a temporal distribution takes place after i.v. administration.[205,208] Several strategies were introduced to overcome these limitations.[191]

Local Administration. Besides chemical modification of lipids and synthesis of new lipid (-like) materials, local administration is another promising approach to avoid issues related to systemic administration. Lipid-based nanoparticles are invasively deposited within diseased organs or tissues to achieve a (local) therapeutic effect. Due to the focused delivery, the administered dose of the lipid-based DNA therapeutics can be reduced. This strategy is especially favorable for nanoparticles with poor pharmacokinetic properties because the nanoparticles remain at the site of administration.[205] Examples of successful local administration of lipid nanoparticles are provided in the following section.

Many solid tumors are characterized by a high interstitial fluid pressure and therefore, systemically administered nanoparticles show a reduced accumulation due to a pressure gradient that limits diffusion.[209,210] When positively charged GL67/DOPE/1,2-dimyristoyl-sn-glycero-3-posphoethanolamine conjugated PEG (DMPE-PEG) liposomes were injected intratumorally, a 2000-fold increased expression of a chloramphenicol acetyltransferase (CAT) reporter gene was achieved as compared to systemic administration.[211] In this respect, lipid-to-DNA ratio and total DNA amount are the major influence factors on transgene expression levels, followed by the injection volume and the injection technique.[212] However, the therapeutic success after intratumoral injection can vary significantly among different tumor models. The optimization of treatment procedures and schemes should thus be performed for every tumor model treated.[205] The choice of an adequate preclinical disease (*i.e.*, tumor) model is considered as critical step in the translation of preclinical data to the patient situation.[185] Similar to the intratumoral injection, lipid-based nanoparticles can be administered locally to other tissues such as muscle (intramuscular) and skin (intradermal) *via* local injection or to the gastrointestinal tract *via* the oral route.[213,214] For example, intramuscular injection of lipid nanoparticles coding for viral antigens was able to stimulate a humoral and cellular antiviral immune response (*i.e.*, genetic vaccination).[215,216] Other strategies aim to locally administer lipid-based nanoparticles to lung or nasal mucosa and local application of lipid nanoparticles was able to improve mucosal immunity.[205,217] However, the colloidal stability and thus gene delivery efficiency of lipid nanoparticles on epithelial barriers may be impaired due to protective layers of mucus or surfactants.[205] Many transfection reagents show a dose-dependent cytotoxicity. Therefore, local side effects may be observed upon local administration. For example, the production of reactive oxygen species was reported upon local lung delivery.[218]

DNA THERAPEUTICS IN CLINICAL TRIALS

In recent years, several lipid-based DNA delivery systems, administered *via* various administration routes, have been investigated in clinical trials mainly focusing on the expression of therapeutic proteins for cancer therapy or treatment of cystic fibrosis (summarized in Table 6). Notably, none of these DNA therapeutics have advanced to a late clinical phase. In the following sections lipid-based DNA therapeutics in clinical trials (registered with ClinicalTrials.gov) are described in detail. Formulation aspects, compositions, and important nanoparticle characteristics are provided.

DOTAP. The first application of DOTAP-based lipoplexes for systemic DNA delivery and subsequent gene expression was published in 1997.[219] Since then, many preclinical and several clinical tests were performed. In the following section, two DOTAP/Chol-based gene delivery approaches for cancer therapy are described in detail.

FUS1 Gene. TUSC2/FUS1 is a tumor suppressor gene that mediates apoptosis in cancer cells. However, in many lung cancer patients, FUS1 protein is reduced or lost.[220] The first clinical trial on *FUS1* gene delivery using DOTAP/Chol lipoplexes (DC-FUS1) in patients with lung cancer was published in 2012.[221,222] DC-FUS1 was prepared in two steps, resulting in lipoplexes with a mean particle size around 300 nm.[223,224] First, cationic liposomes consisting of DOTAP/Chol (20 mM: 18 mM) were formulated using a combination of film rehydration (sterile 5% dextrose), sonication, and sequential extrusion. Second, DOTAP/Chol liposomes were mixed with FUS1 pDNA in equal volumes to a final concentration of 4 mM DOTAP and 0.5 mg/mL pDNA. DC-FUS1 were administered *via i.v.* infusion every 3 weeks at 0.01−0.09 mg/kg (dose escalation). Patients received dexamethasone and diphenhydramine prior to injection to suppress inflammatory responses.[223]

DOI: 10.1021/acsnano.8b07858
ACS Nano 2019, 13, 3754−3782

Most common toxicities were hypophosphatemia and fever. Five patients of this platinum-pretreated study cohort achieved a stable disease. Interestingly, transcribed FUS1 mRNA and translated protein were detected in tumor specimen and several genes in the intrinsic pro-apoptosis pathway were changed. In 2011, a phase I/II trial was initiated to investigate the combination of DC-FUS1 nanoparticles with the epidermal growth factor receptor (EGFR) inhibitor Erlotinib.[225−227]

BikDD Gene. *BikDD* is a potent pro-apoptotic gene with antitumor effect. Xie *et al.* investigated this approach for the treatment of pancreatic cancer.[228] In preclinical animal models, *i.e.*, xenograft and syngeneic orthotopic mouse model, *BikDD* gene delivery using DOTAP:Chol lipoplexes resulted in significant antitumor effects. Gene expression was controlled by the pancreatic-cancer-specific promotor VISA. DOTAP:Chol lipoplexes were produced according to Templeton *et al.* (procedure as described above for DC-FUS1),[219] *i.e.*, extruded DOTAP/Chol liposomes were mixed with pDNA resulting in complexes between 200 to 450 nm in size. Notably, *BikDD*-based gene therapies showed promising preclinical results in the treatment of various other cancers such as hepatocellular carcinoma, lung cancer, breast cancer, or prostate cancer.[229−232] However, an initiated phase I clinical trial has been withdrawn prior to enrollment (last updated in May 2015).

DOTMA. DOTMA is the first cationic lipid that resulted in efficient transfection *in vitro*. Consequently, the first clinical trials for the delivery of DNA were based on liposomes consisting of DOTMA combined with cholesterol (equimolar ratio).

Interleukin-2 (IL-2). Interleukin-2 is a potent activator of immune responses. To maximize antitumor response in cancer treatment, the immune-stimulatory effects of IL-2 were investigated.[233] Cationic DOTMA/Chol liposomes (prepared by microfluidization) were complexed with pDNA encoding for IL-2 at a DNA-to-lipid weight ratio of 1:1 in a solution containing 10% lactose. Resulting lipoplexes were characterized by a mean particle below 200 nm.[136,234] Patients with squamous cell carcinoma of the head and neck received multiple intratumoral injections.[235] Interestingly, the exogenous pDNA nonspecifically induced interferon (IFN)-γ and IL-12 cytokines. A synergistic effect of IL-2, IFN- γ, and IL-12 within the tumor environment was observed.[233] Because one patient demonstrated a tumor reduction, phase II clinical studies were initiated. The most-common adverse events were fever and nausea.

DMRIE. In 1993, the potential use of DMRIE for gene therapy applications was demonstrated in combination with DOPE (1:1 molar ratio).[236]

CFTR. Because DMRIE/DOPE-DNA lipoplexes resulted in effective transgene expression with minor toxicity in several preclinical studies, the efficacy and safety of lipid-mediated transfer of the cystic fibrosis transmembrane conductance regulator (CFTR) gene by intranasal instillation in patients with cystic fibrosis was evaluated.[237−240] However, information on physicochemical characteristics of tested lipoplexes and clinical results is scarce. Of note, others reported that DMRIE/DOPE-DNA lipoplexes were characterized by a heterogeneous size distribution with dimensions of at least 100 nm or larger.[239]

Interleukin-2. In several preclinical studies, pDNA encoding IL-2 complexed with cationic DMRIE/DOPE-based liposomes (product name: Leuvectin/VCL-1102) showed significant reduction in tumor growth.[207,241,242] Therefore, this cancer immunotherapy was investigated in several phase I/II studies in patients with metastatic melanoma, renal cell carcinoma (RCC), and sarcoma. Lipoplexes were prepared immediately prior to injection by vortexing of pDNA with liposomes at a DNA:lipid mass ratio of 5:1 resulting in mean diameters of 200−500 nm.[243] Leuvectin was injected with escalating doses ranging from 0.75 to 4 mg into multiple sites throughout the tumor.[244,245] In around 75% of all tumors, IL-2 pDNA, IL-2 protein, and infiltrating CD81 were detected. No grade 4 toxicities and only one grade 3 toxicity were observed. Interestingly, two patients with RCC and one with melanoma have achieved partial responses, and around 25% of patients had a stable disease.

Major Histocompatibility Complex (MHC). The delivery of pDNA encoding MHC molecules enables the stimulation of antitumor immune responses. This approach was investigated in patients with metastatic melanoma or hepatic metastasis using DNA encoding HLA-B7 and β2-macroglobulin complexed with cationic DMRIE/DOPE liposomes (Allovectin-7/VCL-1005).[246−248] Multilamellar liposomes were prepared by lipid film rehydration using lactated Ringer's solution followed by vortexing. Prior to injection, cationic DMRIE/DOPE liposomes were mixed with pDNA by repeated inversion. Patients received direct injections into tumor lesions with escalating doses up to 250 μg. In a phase I immunotherapy study of patients with hepatic metastases of colorectal carcinoma, the pDNA (93%), mRNA (33%), and protein (63%) were detected.[247] No serious toxicity was observed. In a phase II study of direct intralesional gene transfer in patients with metastatic melanoma, patients received up to 10 μg of Allovectin-7.[248] Only mild to moderate adverse events were observed, and 18% of patients achieved a regression. Several other clinical trials were initiated including a phase III trial with 390 melanoma patients.[249,250] Unfortunately, the rate of responses was unexpectedly low, and the drug was discontinued.[251,252]

EDMPC. The first study demonstrating the potential of the cationic lipid EDMPC to deliver DNA to pulmonary cells was published in 1997.[253]

CFTR. Due to promising preclinical results, a first-in-human trials in patients with cystic fibrosis was initiated.[254,255] Liposomes consisting of EDMPC and cholesterol (1:1 molar ratio) were prepared by sonication in 5% dextrose and subsequently mixed with CFTR DNA resulting in lipoplexes above 200 nm. A total of 11 patients received up to 4 mg of DNA using a nasal spray. No adverse events were observed. However, lipoplexes did also not show any activity. No vector-specific mRNA was detected, most probably due to the low efficiency of these lipoplexes in the nasal epithelium.

DC-Chol. The cationic derivative of cholesterol, DC-Chol, was published in 1991 by Xiang Gao and Leaf Huang.[49] Since then, DC-Chol/DOPE-containing liposomes were investigated for several DNA delivery approaches.

EGFR Inhibition. In squamous cell carcinoma the EGFR is often up-regulated. Therefore, the potential of an EGFR antisense gene therapy was investigated to directly block the production of EGFR in contrast to common inhibitory approaches using monoclonal antibodies. To complex the EGFR antisense DNA, cationic liposomes consisting of DC-Chol and DOPE (produced by microfluidization at a 3:2 molar ratio)[256] were mixed with DNA using 1 nmol of liposomes per μg of DNA.[257] Similar studies revealed that final complexes had a relatively large size above 200 nm.[258,259] In 2009, the results of the first human application were published.[260] DC-Chol-based nanoparticles were injected intratumorally at 60 to 1920 μg of DNA per injection (dose escalation). One-third of the patients

DOI: 10.1021/acsnano.8b07858
ACS Nano 2019, 13, 3754−3782

achieved a clinical response, and importantly, no severe toxicities (grades 3 and 4) were observed.

HLA-A2 Gene. The activation of tumor-specific immunity is a promising strategy in the management of various malignant disorders. Therefore, DC-Chol/DOPE lipoplexes containing DNA encoding nonsyngeneic MHC antigens, *i.e.*, the HLA-A2 gene, were investigated in a pair of phase I/II trials.[261,262] Lipoplexes were prepared by simple mixing of DC-Chol/DOPE cationic liposomes (150−200 nm) and DNA in lactated Ringer's solution. Late-stage cancer patients received four weekly injections into cutaneous nodules with up to 80 μg of DNA. The majority of patients with metastatic cervical or ovarian carcinoma had subsequent local immune responses. However, all patients had progressive malignancies.

GL67. GL-67 is a multivalent cholesterol derivative that was developed for the delivery of pDNA to the lung. Stabilized lipoplexes consisting of GL67, DOPE, DMPE-PEG5000 (1:2:0.05 molar ratio), and pDNA were successfully delivered *via* aerosolization.[263]

CFTR. Delivery of DNA encoding the CFTR is a promising strategy for the treatment of cystic fibrosis. Several clinical trials have been initiated investigating different lipid-based delivery systems as discussed elsewhere in great detail.[264] Lee *et al.* performed a detailed screening of cationic lipids for efficient gene transfer to airway epithelia.[51] The most-effective lipid was GL67, *i.e.*, 100-fold more active than DC-Chol. After intensive optimization of the formulation, a phase I clinical trial was initiated in 2008 followed by phase II clinical trials by the UK cystic fibrosis consortium (www.cfgenetherapy.org.uk).[263−266] The incorporation of small amounts of DMPE-PEG5000 enabled the preparation of concentrated lipoplexes with an optimal cationic lipid:pDNA ratio of 0.75:1 for aerosolization. Patients (n = 78) received the nebulized lipoplex once per month for 1 year. Lung function was modestly stabilized in some individuals, and no significant adverse effects were observed.[266]

Immuno-lipoplexes. In recent years, several active targeted gene therapeutics have been developed for the treatment of cancer. To increase specificity and transfection efficiency, active targeting of immunocomplexes to the transferrin receptor is one strategy.[276] This strategy was used in clinical trials for the delivery of pDNA encoding for p53 and RB94 *via i.v.* infusion. To deliver the pDNA, cationic immuno-lipoplexes consisting of DOTAP and DOPE were modified with antitransferrin receptor single-chain antibodies (TfRscFv) to target tumor cells more efficiently and trigger internalization. Immuno-lipoplexes were prepared in a three-step procedure.[277,278] First, liposomes composed of a 1:1 molar ratio of DOTAP and DOPE (including 5 mol % MPB-DOPE for TfRscFv conjugation) were prepared using ethanol injection method. Second, the reduced TfRscFv was conjugated to the cationic liposomes *via* maleimide chemistry. Third, cationic immunoliposomes were mixed with pDNA. The final complexes had a size of around 100 nm in diameter.[276]

p53. The tumor protein p53 is one of the most important tumor suppressors and is frequently mutated in human cancers. Thus, expression of p53 is an interesting approach to prevent cancer formation and progression. In 2007, the first human clinical trial using liposomal nanoparticles targeted by a single-chain antibody fragment to the transferrin receptor (SGT-53) were used to restore the normal human p53 gene.[279] In general, only minimal side effects were observed. Fever and hypotension were the most common low-grade toxicities. A prophylactic regimen including histamine blockade was used. Patients with different types of cancer were included, and the majority demonstrated a stable disease. Exogenous p53 expression in tumor samples was detected by polymerase chain reaction (PCR) and Western blot analysis. In recent years, several clinical trials have been initiated to combine SGT-53 with standard chemotherapy (*e.g.*, temozolomide, gemcitabine, docetaxel, and topotecan) to achieve tumor regression.[280,281,283]

RB94. RB94 is a truncated version of the retinoblastoma protein RB110 and functions as a potent tumor suppressor.[284] Because human bladder cancers show a high transferrin receptor expression, systemically administered targeted nanoparticles (SGT-94) encapsulating a plasmid encoding RB94 were investigated in preclinical studies.[285] The first human clinical trial in patients with genitourinary cancers showed evidence of clinical activity.[286] Only minimal side effects were observed. Selective expression of RB94 in metastases was demonstrated by PCR and Western blot analysis.

Lessons Learned from Clinical Trials: Successes, Challenges, and Current Limitations. The aim of all nucleic acid−based non-viral systems is to lead to a clinically useful therapeutic. This has now been demonstrated for a lipid nanoparticle formulation encapsulating siRNA. The approval of Onpattro by the U.S. Food and Drug Administration is a watershed event for non-viral gene therapy approaches. Not only did the drug inhibit further progression of a deadly disease that usually leads to death within 5 years of diagnosis, but also, significant improvements were observed.[287] This drug, which contains the optimized ionizable cationic lipid DLin-MC3-DMA and an siRNA to silence a gene called transthyretin (TTR), inhibits the production of TTR in the liver following i.v. administration. Mutations in TTR can lead to formation of fibrils that deposit in amyloid plaques in nerve and cardiac tissue, causing progressive neurotoxicity and cardiotoxicity. Onpattro now provides an essentially curative therapy for this monogenic disease. Further, the safety profile of Onpattro is encouraging, with readily managed edema and occasional immunogenic responses on injection that can be managed by slowing injection rates and co-administration of immunosuppressants.[288]

Onpattro provides validation that clinically effective non-viral nucleic acid therapeutics can be developed. Recent work extending these findings to mRNA for vaccine and gene editing applications suggests this promise extends to most, if not all forms of gene therapy.[289−291] However, there remain significant challenges. First, the only tissue that is available intravenously is the liver. Lipid-based nanoparticle systems that can deliver nucleic acid therapeutics to immune cells, endothelial cell, tumors, and bone marrow are not yet developed. Second, the differing requirements for small (siRNA) and large (mRNA and pDNA) non-viral formulations are not yet understood, and the molecular mechanisms whereby these systems induce transfection remain obscure. Third, the applicability of these non-viral systems to other tissues available by direct injection have not been characterized. This includes brain, ocular, subcutaneous, and other tissues. Finally, these systems are not yet specific enough. Systems developed for nonhepatic tissues are likely to also be able to transfect hepatocytes, leading to off-target effects, for example.

These issues aside the future is bright for non-viral gene therapies including lipid-based DNA therapeutics. They offer promising approaches to treat most diseases as well as straightforward manufacturing, stability, and other requirements necessary for developing a drug.

DOI: 10.1021/acsnano.8b07858
ACS Nano 2019, 13, 3754−3782

Safety Concerns and Adverse Events in Gene Therapy Clinical Trials. Although several clinical studies reported low toxicity after administration of lipid-based DNA therapeutics to humans, substantial clinical adverse responses have been observed.[292] Systemic administration of lipid-based DNA therapeutics induced inflammation, hematologic, and serologic changes in a dose-dependent fashion.[273,293] Therefore, strategies to suppress inflammation and expand the therapeutic window are crucial.[223] Systemic administration of small molecule inhibitors to suppress nanoparticle-mediated inflammation such as naproxen or dexamethasone have shown clinical significance. To circumvent the co-administration of potent immunosuppressive agents, successful incorporation of hydrophobic dexamethasone prodrugs into lipid-based nanoparticles containing nucleic acids has recently been demonstrated, thereby providing effective immunosuppression.[294] Further development will allow the incorporation of such strategies into future clinical trials. In addition, optimization of DNA vectors to reduce inflammatory responses, *e.g.,* by CpG reduction, are necessary.[295] This will ultimately also increase the magnitude and duration of transgene expression.

Pharmacokinetic Properties and Physiological Barriers. An important limitation for most lipid-based DNA therapeutics tested in clinical trials are their unfavorable physicochemical nanoparticle properties including high surface charge and large size. After systemic delivery, most cationic complexes predominantly accumulate in the lungs, and large nanoparticles get sequestered by the RES.[200,219] Taking into consideration that these characteristics impact blood circulation lifetimes, cellular binding, and internalization pathways, future studies need to focus on optimized nanoparticles for delivery to particular tissues. Physiological barriers represent another rate limiting factor for lipid-based DNA therapeutics. For example, in cystic fibrosis patients, DNA therapeutics need to be highly efficient at penetrating the viscoelastic and adhesive mucus layer in the lungs.[296,297]

Intracellular Barriers. In addition to pharmacokinetic properties, intracellular barriers represent a major hurdle for lipid-based DNA therapeutics impeding their clinical performance. Once internalized into target cells and released into cytoplasm, nuclear trafficking of DNA vectors is fundamental. In contrast to RNA therapeutics, this step represents a potentially rate-limiting barrier for lipid-based DNA therapeutics. The nuclear envelope completely seals the nucleus from the cytoplasm, while the nuclear pore complexes (NPCs) enable the import and export of molecules. Molecules smaller than 50 kDa can freely cross the NPC by passive diffusion, while macromolecules that exceed 50 kDa need to be transported actively across the NPC. Because a double-stranded 20 bp oligomer is reported to have an approximately equivalent size to a 13 kDa polypeptide, pDNA generally exceeds the size limit for passive diffusion into the nucleus and therefore requires active transport mechanisms.[298] To increase the likelihood of DNA therapeutics to overcome nuclear barriers, a wide variety of substances including nuclear localization sequences (NLS) were investigated as reviewed elsewhere.[299,300] In the future, it will be crucial to develop a better understanding of the intracellular trafficking and to design strategies overcoming this bottleneck.

Controlled and Scalable Manufacturing. Manufacturing of lipid-based DNA therapeutics is technically challenging and represents a major challenge for a clinical translation and ultimately commercialization. Cationic complexes tested in clinical trials have mostly been prepared by simple mixing of cationic liposomes with DNA, which does not guarantee process control and results in batch-to-batch variations. Identification of a robust and scalable manufacturing process to produce monodispersed and size-specific nanoparticles in a reproducible and rapid manner is essential. Microfluidic mixing techniques might represent a controllable process resulting in high entrapment efficiencies and narrow size distributions as shown for siRNA.[301]

CONCLUDING REMARKS

In recent decades, tremendous efforts have been made for the development of non-viral gene therapies. Several lipid-based DNA delivery systems have been developed and excellent results have been achieved in clinical trials for siRNA systems leading to the first approved RNAi therapeutic. Nevertheless, the widespread use of DNA vectors in clinical care is still hampered by low transfection efficiency for certain tissues, imprecise targeting, and unwanted activation of the immune system. Thus, continued research on potent and biocompatible nanomaterials for specific delivery of DNA to target cells and efficient transgene expression is required. The continuous and successful development of next-generation lipids made in the field of RNA therapeutics is an excellent example for the optimization of DNA therapeutics.[302] Non-viral gene therapy represents one of the most promising options for the treatment of cancer or monogenic disorders. In the future, this technology can potentially be used for several clinical applications. Examples in the fight against cancer might include ddRNAi and the expression of pro-apoptotic and oncotoxic proteins or tumor suppressors. Patients with orphan monogenic disorders (*i.e.,* rare diseases) would highly benefit from disease-modifying therapeutic options, which replace the mutated enzyme by delivery of their encoding DNA sequences. Finally, the delivery of large nucleic acids can enable the implementation of promising gene editing approaches such as the CRISPR/Cas9 or zinc-finger technology for *in vivo* applications.

AUTHOR INFORMATION

Corresponding Authors

*E-mail: joerg.huwyler@unibas.ch.
*E-mail: dominik.witzigmann@unibas.ch.

ORCID

Pieter R. Cullis: 0000-0001-9586-2508
Dominik Witzigmann: 0000-0002-8197-8558

Notes

The authors declare the following competing financial interest(s): P.R.C. has financial interests in Acuitas Therapeutics and Precision NanoSystems. The remaining authors declare no conflict of interest.

ACKNOWLEDGMENTS

We thank all collaborators for helpful discussions and apologize to all scientists whose work was not cited in this Review due to space constraints. In addition, we acknowledge the financial support of the "Novartis University Basel Excellence Fellowship for Life Sciences", "FAG Basel", and the "Swiss National Science Foundation" (SNF grants No. 174975 and No. 173057). DW and JH have equally contributed as senior scientists to the present work.

DOI: 10.1021/acsnano.8b07858
ACS Nano 2019, 13, 3754−3782

GLOSSARY

transfection, introduction of genetic material of foreign origin into cells using biological, chemical, or physical methods to obtain genetically modified (*i.e.*, transgenic) cells; **gene therapy**, treatment of various disorders based on the delivery of nucleic acids to modulate gene expression at DNA or RNA level; **gene silencing**, inhibition of endogenous protein expression based on the delivery of nucleic acid drugs modulating the degradation of mRNA or alternative splicing of pre-mRNA; **gene expression**, expression of therapeutic proteins based on the delivery of nucleic acid drugs encoding the gene of interest; **gene editing**, altering gene expression based on the delivery of nucleic acid drugs encoding nucleases to mediate insertion, deletion, modification, or replacement of DNA sequences in the genome; **ionizable cationic lipids**, lipids containing amine moieties with optimized acid dissociation constant resulting in a net-positive charge at acidic pH (e.g., during formulation or intracellularly) but net-neutral charge at physiological pH (*e.g.*, in circulation)

REFERENCES

(1) Mulligan, R. C. The Basic Science of Gene Therapy. *Science* **1993**, *260*, 926−932.

(2) Paunovska, K.; Sago, C. D.; Monaco, C. M.; Hudson, W. H.; Castro, M. G.; Rudoltz, T. G.; Kalathoor, S.; Vanover, D. A.; Santangelo, P. J.; Ahmed, R.; Bryksin, A. V.; Dahlman, J. E. A Direct Comparison of *in Vitro* and *in Vivo* Nucleic Acid Delivery Mediated by Hundreds of Nanoparticles Reveals a Weak Correlation. *Nano Lett.* **2018**, *18*, 2148−2157.

(3) Gene Therapy Clinical Trials Worldwide Home Page. http://www.abedia.com/wiley/phases.php (accessed February 5, 2019).

(4) Niidome, T.; Huang, L. Gene Therapy Progress and Prospects: Nonviral Vectors. *Gene Ther.* **2002**, *9*, 1647−1652.

(5) Wicki, A.; Witzigmann, D.; Balasubramanian, V.; Huwyler, J. Nanomedicine in Cancer Therapy: Challenges, Opportunities, and Clinical Applications. *J. Controlled Release* **2015**, *200*, 138−157.

(6) Pack, D. W.; Hoffman, A. S.; Pun, S.; Stayton, P. S. Design and Development of Polymers for Gene Delivery. *Nat. Rev. Drug Discovery* **2005**, *4*, 581−593.

(7) Palivan, C. G.; Fischer-Onaca, O.; Delcea, M.; Itel, F.; Meier, W. Protein-Polymer Nanoreactors for Medical Applications. *Chem. Soc. Rev.* **2012**, *41*, 2800−2823.

(8) Kataoka, K.; Harada, A.; Nagasaki, Y. Block Copolymer Micelles for Drug Delivery: Design, Characterization and Biological Significance. *Adv. Drug Delivery Rev.* **2001**, *47*, 113−131.

(9) Kanasty, R.; Dorkin, J. R.; Vegas, A.; Anderson, D. Delivery Materials for siRNA Therapeutics. *Nat. Mater.* **2013**, *12*, 967−977.

(10) Lorenzer, C.; Dirin, M.; Winkler, A.-M.; Baumann, V.; Winkler, J. Going Beyond the Liver: Progress and Challenges of Targeted Delivery of siRNA Therapeutics. *J. Controlled Release* **2015**, *203*, 1−15.

(11) Sehgal, A.; Vaishnaw, A.; Fitzgerald, K. Liver as a Target for Oligonucleotide Therapeutics. *J. Hepatol.* **2013**, *59*, 1354−1359.

(12) FDA News Release. FDA approves first-of-its kind targeted RNA-based therapy to treat a rare disease. https://www.fda.gov/NewsEvents/Newsroom/PressAnnouncements/ucm616518.htm (accessed February 5, 2019).

(13) Scholz, C.; Wagner, E. Therapeutic Plasmid DNA *versus* siRNA Delivery: Common and Different Tasks for Synthetic Carriers. *J. Controlled Release* **2012**, *161*, 554−565.

(14) Fink, T. L.; Klepcyk, P. J.; Oette, S. M.; Gedeon, C. R.; Hyatt, S. L.; Kowalczyk, T. H.; Moen, R. C.; Cooper, M. J. Plasmid Size up to 20 Kbp Does Not Limit Effective *in Vivo* Lung Gene Transfer Using Compacted DNA Nanoparticles. *Gene Ther.* **2006**, *13*, 1048−1051.

(15) Witzigmann, D.; Wu, D.; Schenk, S. H.; Balasubramanian, V.; Meier, W.; Huwyler, J. Biocompatible Polymer−Peptide Hybrid-Based DNA Nanoparticles for Gene Delivery. *ACS Appl. Mater. Interfaces* **2015**, *7*, 10446−10456.

(16) Kauffman, K. J.; Dorkin, J. R.; Yang, J. H.; Heartlein, M. W.; DeRosa, F.; Mir, F. F.; Fenton, O. S.; Anderson, D. G. Optimization of Lipid Nanoparticle Formulations for mRNA Delivery *in Vivo* with Fractional Factorial and Definitive Screening Designs. *Nano Lett.* **2015**, *15*, 7300−7306.

(17) Kulkarni, J. A.; Myhre, J. L.; Chen, S.; Tam, Y. Y. C.; Danescu, A.; Richman, J. M.; Cullis, P. R. Design of Lipid Nanoparticles for *in Vitro* and *in Vivo* Delivery of Plasmid DNA. *Nanomedicine* **2017**, *13*, 1377−1387.

(18) Aagaard, L.; Rossi, J. J. RNAi Therapeutics: Principles, Prospects and Challenges. *Adv. Drug Delivery Rev.* **2007**, *59*, 75−86.

(19) Whitehead, K. A.; Langer, R.; Anderson, D. G. Knocking Down Barriers: Advances in siRNA Delivery. *Nat. Rev. Drug Discovery* **2009**, *8*, 129−138.

(20) Yin, H.; Kanasty, R. L.; Eltoukhy, A. A.; Vegas, A. J.; Dorkin, J. R.; Anderson, D. G. Non-Viral Vectors for Gene-Based Therapy. *Nat. Rev. Genet.* **2014**, *15*, 541−555.

(21) Cullis, P. R.; Hope, M. J. Lipid Nanoparticle Systems for Enabling Gene Therapies. *Mol. Ther.* **2017**, *25*, 1467−1475.

(22) Hajj, K. A.; Whitehead, K. A. Tools for Translation: Non-Viral Materials for Therapeutic mRNA Delivery. *Nat. Rev. Mater.* **2017**, *2*, 17056.

(23) Nayerossadat, N.; Maedeh, T.; Ali, P. A. Viral and Nonviral Delivery Systems for Gene Delivery. *Adv. Biomed. Res.* **2012**, *1*, 27.

(24) Jin, L.; Zeng, X.; Liu, M.; Deng, Y.; He, N. Current Progress in Gene Delivery Technology Based on Chemical Methods and Nano-Carriers. *Theranostics* **2014**, *4*, 240−255.

(25) Winter, J.; Jung, S.; Keller, S.; Gregory, R. I.; Diederichs, S. Many Roads to Maturity: MicroRNA Biogenesis Pathways and Their Regulation. *Nat. Cell Biol.* **2009**, *11*, 228−234.

(26) Fellmann, C.; Gowen, B. G.; Lin, P.-C.; Doudna, J. A.; Corn, J. E. Cornerstones of CRISPR−Cas in Drug Discovery and Therapy. *Nat. Rev. Drug Discovery* **2017**, *16*, 89−100.

(27) Hsu, P. D.; Lander, E. S.; Zhang, F. Development and Applications of CRISPR-Cas9 for Genome Engineering. *Cell* **2014**, *157*, 1262−1278.

(28) Doudna, J. A.; Charpentier, E. Genome Editing. The New Frontier of Genome Engineering with CRISPR-Cas9. *Science* **2014**, *346*, 1258096.

(29) Liu, C.; Zhang, L.; Liu, H.; Cheng, K. Delivery Strategies of the CRISPR-Cas9 Gene-Editing System for Therapeutic Applications. *J. Controlled Release* **2017**, *266*, 17−26.

(30) Ahmad, G.; Amiji, M. Use of CRISPR/Cas9 Gene-Editing Tools for Developing Models in Drug Discovery. *Drug Discovery Today* **2018**, *23*, 519−533.

(31) Wang, M.; Zuris, J. A.; Meng, F.; Rees, H.; Sun, S.; Deng, P.; Han, Y.; Gao, X.; Pouli, D.; Wu, Q.; Georgakoudi, I.; Liu, D. R.; Xu, Q. Efficient Delivery of Genome-Editing Proteins Using Bioreducible Lipid Nanoparticles. *Proc. Natl. Acad. Sci. U. S. A.* **2016**, *113*, 2868−2873.

(32) Zhu, X.; Cai, H.; Zhao, L.; Ning, L.; Lang, J. CAR-T Cell Therapy in Ovarian Cancer: From the Bench to the Bedside. *Oncotarget* **2017**, *8*, 64607−64621.

(33) Maier, M. A.; Jayaraman, M.; Matsuda, S.; Liu, J.; Barros, S.; Querbes, W.; Tam, Y. K.; Ansell, S. M.; Kumar, V.; Qin, J.; et al. Biodegradable Lipids Enabling Rapidly Eliminated Lipid Nanoparticles for Systemic Delivery of RNAi Therapeutics. *Mol. Ther.* **2013**, *21*, 1570−1578.

(34) Ju, J.; Huan, M.-L.; Wan, N.; Hou, Y.-L.; Ma, X.-X.; Jia, Y.-Y.; Li, C.; Zhou, S.-Y.; Zhang, B.-L. Cholesterol Derived Cationic Lipids as Potential Non-Viral Gene Delivery Vectors and Their Serum Compatibility. *Bioorg. Med. Chem. Lett.* **2016**, *26*, 2401−2407.

(35) Rak, M.; Ochalek, A.; Bielecka, E.; Latasiewicz, J.; Gawarecka, K.; Sroka, J.; Czyz, J.; Piwowarczyk, K.; Masnyk, M.; Chmielewski, M.; Chojnacki, T.; Swiezewska, E.; Madeja, Z. Efficient and Non-Toxic Gene Delivery by Anionic Lipoplexes Based on Polyprenyl Ammonium Salts and Their Effects on Cell Physiology. *J. Gene Med.* **2016**, *18*, 331−342.

DOI: 10.1021/acsnano.8b07858
ACS Nano 2019, 13, 3754−3782

(36) Zhao, Q.-Q.; Chen, J.-L.; Lv, T.-F.; He, C.-X.; Tang, G.-P.; Liang, W.-Q.; Tabata, Y.; Gao, J.-Q. N/P Ratio Significantly Influences the Transfection Efficiency and Cytotoxicity of a Polyethylenimine/Chitosan/DNA Complex. *Biol. Pharm. Bull.* **2009**, *32*, 706−710.
(37) Szybalska, E. H.; Szybalski, W. Genetics of Human Cell Lines, IV. DNA-Mediated Heritable Transformation of a Biochemical Trait. *Proc. Natl. Acad. Sci. U. S. A.* **1962**, *48*, 2026−2034.
(38) Szybalska, E. H.; Szybalski, W. A Forerunner of Monoclonal-Antibodies and Human Gene-Therapy - A Citation-Classic Commentary on Genetics of Human Cell-Lines 0.4. DNA-Mediated Heritable Transformation of a Biochemical Trait. *CC/LIFE SCI.* **1991**, No. 46, 11. Szybalska, E. H.; Szybalski, W. Genetics of human cell lines.IV. DNA-mediated heritable transformation of a biochemical train. *Proc. Natl. Acad. Sci. U.S.A.* **1962**, *48*, 2026−34.
(39) Vaheri, A.; Pagano, J. S. Infectious Poliovirus RNA: A Sensitive Method of Assay. *Virology* **1965**, *27*, 434−436.
(40) Graham, F. L.; van der Eb, A. J. A New Technique for the Assay of Infectivity of Human Adenovirus 5 DNA. *Virology* **1973**, *52*, 456−467.
(41) Wolff, J. A.; Lederberg, J. An Early History of Gene Transfer and Therapy. *Hum. Gene Ther.* **1994**, *5*, 469−480.
(42) Mukherjee, A. B.; Orloff, S.; Butler, J. D.; Triche, T.; Lalley, P.; Schulman, J. D. Entrapment of Metaphase Chromosomes into Phospholipid Vesicles (Lipochromosomes): Carrier Potential in Gene Transfer. *Proc. Natl. Acad. Sci. U. S. A.* **1978**, *75*, 1361−1365.
(43) Fraley, R. T.; Fornari, C. S.; Kaplan, S. Entrapment of a Bacterial Plasmid in Phospholipid Vesicles: Potential for Gene Transfer. *Proc. Natl. Acad. Sci. U. S. A.* **1979**, *76*, 3348−3352.
(44) Lurquin, P. F. Entrapment of Plasmid DNA by Liposomes and Their Interactions with Plant Protoplasts. *Nucleic Acids Res.* **1979**, *6*, 3773−3784.
(45) Fraley, R.; Subramani, S.; Berg, P.; Papahadjopoulos, D. Introduction of Liposome-Encapsulated SV40 DNA into Cells. *J. Biol. Chem.* **1980**, *255*, 10431−10435.
(46) Schaefer-Ridder, M.; Wang, Y.; Hofschneider, P. H. Liposomes as Gene Carriers: Efficient Transformation of Mouse L Cells by Thymidine Kinase Gene. *Science* **1982**, *215*, 166−168.
(47) Nicolau, C.; Le Pape, A.; Soriano, P.; Fargette, F.; Juhel, M. F. *In Vivo* Expression of Rat Insulin after Intravenous Administration of the Liposome-Entrapped Gene for Rat Insulin I. *Proc. Natl. Acad. Sci. U. S. A.* **1983**, *80*, 1068−1072.
(48) Felgner, P. L.; Gadek, T. R.; Holm, M.; Roman, R.; Chan, H. W.; Wenz, M.; Northrop, J. P.; Ringold, G. M.; Danielsen, M. Lipofection: A Highly Efficient, Lipid-Mediated DNA-Transfection Procedure. *Proc. Natl. Acad. Sci. U. S. A.* **1987**, *84*, 7413−7417.
(49) Gao, X.; Huang, L. A Novel Cationic Liposome Reagent for Efficient Transfection of Mammalian Cells. *Biochem. Biophys. Res. Commun.* **1991**, *179*, 280−285.
(50) Kurzchalia, T. V.; Dupree, P.; Parton, R. G.; Kellner, R.; Virta, H.; Lehnert, M.; Simons, K. VIP21, a 21-KD Membrane Protein Is an Integral Component of Trans-Golgi-Network-Derived Transport Vesicles. *J. Cell Biol.* **1992**, *118*, 1003−1014.
(51) Lee, E. R.; Marshall, J.; Siegel, C. S.; Jiang, C.; Yew, N. S.; Nichols, M. R.; Nietupski, J. B.; Ziegler, R. J.; Lane, M. B.; Wang, K. X.; Wan, N. C.; Scheule, R. K.; Harris, D. J.; Smith, A. E.; Cheng, S. H. Detailed Analysis of Structures and Formulations of Cationic Lipids for Efficient Gene Transfer to the Lung. *Hum. Gene Ther.* **1996**, *7*, 1701−1717.
(52) Chesnoy, S.; Huang, L. Structure and Function of Lipid-DNA Complexes for Gene Delivery. *Annu. Rev. Biophys. Biomol. Struct.* **2000**, *29*, 27−47.
(53) Elouahabi, A.; Thiry, M.; Pector, V.; Ruysschaert, J.-M.; Vandenbranden, M. *Calorimetry of Cationic Liposome−DNA Complex and Intracellular Visualization of the Complexes*; Enzymology, B.-M. in, Ed.; Liposomes, Part C; Academic Press: Boca Raton, FL, 2003; Vol. 373, pp 312−332.
(54) Elouahabi, A.; Ruysschaert, J.-M. Formation and Intracellular Trafficking of Lipoplexes and Polyplexes. *Mol. Ther.* **2005**, *11*, 336−347.
(55) Lv, H.; Zhang, S.; Wang, B.; Cui, S.; Yan, J. Toxicity of Cationic Lipids and Cationic Polymers in Gene Delivery. *J. Controlled Release* **2006**, *114*, 100−109.
(56) Zhu, L.; Lu, Y.; Miller, D. D.; Mahato, R. I. Structural and Formulation Factors Influencing Pyridinium Lipid-Based Gene Transfer. *Bioconjugate Chem.* **2008**, *19*, 2499−2512.
(57) Zugates, G. T. Synthesis and Chemical Modification of Degradable Polymers to Enhance Gene Delivery. Thesis, Massachusetts Institute of Technology, 2006. http://hdl.handle.net/1721.1/38970 (accessed February 5, 2019).
(58) Swaney, W. P.; Sorgi, F. L.; Bahnson, A. B.; Barranger, J. A. The Effect of Cationic Liposome Pretreatment and Centrifugation on Retrovirus-Mediated Gene Transfer. *Gene Ther.* **1997**, *4*, 1379−1386.
(59) Kulkarni, J. A.; Cullis, P. R.; van der Meel, R. Lipid Nanoparticles Enabling Gene Therapies: From Concepts to Clinical Utility. *Nucleic Acid Ther.* **2018**, *28*, 146.
(60) Zhao, Y.; Huang, L. Lipid Nanoparticles for Gene Delivery. *Adv. Genet.* **2014**, *88*, 13−36.
(61) Wang, Y.; Miao, L.; Satterlee, A.; Huang, L. Delivery of Oligonucleotides with Lipid Nanoparticles. *Adv. Drug Delivery Rev.* **2015**, *87*, 68−80.
(62) Xu, Y.; Szoka, F. C. Mechanism of DNA Release from Cationic Liposome/DNA Complexes Used in Cell Transfection. *Biochemistry* **1996**, *35*, 5616−5623.
(63) Zhi, D.; Zhang, S.; Cui, S.; Zhao, Y.; Wang, Y.; Zhao, D. The Headgroup Evolution of Cationic Lipids for Gene Delivery. *Bioconjugate Chem.* **2013**, *24*, 487−519.
(64) Felgner, J. H.; Kumar, R.; Sridhar, C. N.; Wheeler, C. J.; Tsai, Y. J.; Border, R. Enhanced Gene Delivery and Mechanism Studies with a Novel Series of Cationic Lipid Formulations. *J. Biol. Chem.* **1994**, *28*, 2550−2561.
(65) Yuba, E.; Nakajima, Y.; Tsukamoto, K.; Iwashita, S.; Kojima, C.; Harada, A.; Kono, K. Effect of Unsaturated Alkyl Chains on Transfection Activity of Poly(Amidoamine) Dendron-Bearing Lipids. *J. Controlled Release* **2012**, *160*, 552−560.
(66) Morille, M.; Passirani, C.; Vonarbourg, A.; Clavreul, A.; Benoit, J.-P. Progress in Developing Cationic Vectors for Non-Viral Systemic Gene Therapy against Cancer. *Biomaterials* **2008**, *29*, 3477−3496.
(67) Semple, S. C.; Klimuk, S. K.; Harasym, T. O.; Hope, M. J. Lipid-Based Formulations of Antisense Oligonucleotides for Systemic Delivery Applications. *Methods in Enzymology; Antisense Technology Part A: General Methods, Methods of Delivery, and RNA Studies*; Academic Press: Boca Raton, FL, 2000, *313*, 322−341.
(68) Heyes, J.; Palmer, L.; Bremner, K.; MacLachlan, I. Cationic Lipid Saturation Influences Intracellular Delivery of Encapsulated Nucleic Acids. *J. Controlled Release* **2005**, *107*, 276−287.
(69) Semple, S. C.; Akinc, A.; Chen, J.; Sandhu, A. P.; Mui, B. L.; Cho, C. K.; Sah, D. W. Y.; Stebbing, D.; Crosley, E. J.; Yaworski, E.; et al. Rational Design of Cationic Lipids for siRNA Delivery. *Nat. Biotechnol.* **2010**, *28*, 172−176.
(70) Jayaraman, M.; Ansell, S. M.; Mui, B. L.; Tam, Y. K.; Chen, J.; Du, X.; Butler, D.; Eltepu, L.; Matsuda, S.; Narayanannair, J. K.; Rajeev, K. G.; Hafez, I. M.; Akinc, A.; Maier, M. A.; Tracy, M. A.; Cullis, P. R.; Madden, T. D.; Manoharan, M.; Hope, M. J. Maximizing the Potency of siRNA Lipid Nanoparticles for Hepatic Gene Silencing *In Vivo*. *Angew. Chem., Int. Ed.* **2012**, *51*, 8529−8533.
(71) Akinc, A.; Zumbuehl, A.; Goldberg, M.; Leshchiner, E. S.; Busini, V.; Hossain, N.; Bacallado, S. A.; Nguyen, D. N.; Fuller, J.; Alvarez, R.; et al. A Combinatorial Library of Lipid-like Materials for Delivery of RNAi Therapeutics. *Nat. Biotechnol.* **2008**, *26*, 561−569.
(72) Love, K. T.; Mahon, K. P.; Levins, C. G.; Whitehead, K. A.; Querbes, W.; Dorkin, J. R.; Qin, J.; Cantley, W.; Qin, L. L.; Racie, T.; Frank-Kamenetsky, M.; Yip, K. N.; Alvarez, R.; Sah, D. W. Y.; de Fougerolles, A.; Fitzgerald, K.; Koteliansky, V.; Akinc, A.; Langer, R.; Anderson, D. G. Lipid-like Materials for Low-Dose, *in Vivo* Gene Silencing. *Proc. Natl. Acad. Sci. U. S. A.* **2010**, *107*, 1864−1869.
(73) Whitehead, K. A.; Dorkin, J. R.; Vegas, A. J.; Chang, P. H.; Veiseh, O.; Matthews, J.; Fenton, O. S.; Zhang, Y.; Olejnik, K. T.; Yesilyurt, V.

DOI: 10.1021/acsnano.8b07858
ACS Nano 2019, 13, 3754−3782

Degradable Lipid Nanoparticles with Predictable *in Vivo* siRNA Delivery Activity. *Nat. Commun.* **2014**, *5*, 1.
(74) Nguyen, D. N.; Chen, S. C.-Y.; Lu, J.; Goldberg, M.; Kim, P.; Sprague, A.; Novobrantseva, T.; Sherman, J.; Shulga-Morskaya, S.; de Fougerolles, A.; Chen, J.; Langer, R.; Anderson, D. G. Drug Delivery–Mediated Control of RNA Immunostimulation. *Mol. Ther.* **2009**, *17*, 1555–1562.
(75) Sun, S.; Wang, M.; Knupp, S. A.; Soto-Feliciano, Y.; Hu, X.; Kaplan, D. L.; Langer, R.; Anderson, D. G.; Xu, Q. Combinatorial Library of Lipidoids for *In Vitro* DNA Delivery. *Bioconjugate Chem.* **2012**, *23*, 135–140.
(76) Sabnis, S.; Kumarasinghe, E. S.; Salerno, T.; Mihai, C.; Ketova, T.; Senn, J. J.; Lynn, A.; Bulychev, A.; McFadyen, I.; Chan, J.et al. A Novel Amino Lipid Series for mRNA Delivery: Improved Endosomal Escape and Sustained Pharmacology and Safety in Non-Human Primates. *Mol. Ther.* **2018**.261509
(77) *Acuitas Non-Confidential Presentation*. https://acuitastx.com/wp-content/uploads/2018/09/Acuitas-non-confidential-presentation-2017.pdf (accessed February 5, 2019).
(78) Molla, M. R.; Levkin, P. A. Combinatorial Approach to Nanoarchitectonics for Nonviral Delivery of Nucleic Acids. *Adv. Mater.* **2016**, *28*, 1159–1175.
(79) Li, L.; Wang, F.; Wu, Y.; Davidson, G.; Levkin, P. A. Combinatorial Synthesis and High-Throughput Screening of Alkyl Amines for Nonviral Gene Delivery. *Bioconjugate Chem.* **2013**, *24*, 1543–1551.
(80) Miller, J. B.; Kos, P.; Tieu, V.; Zhou, K.; Siegwart, D. J. Development of Cationic Quaternary Ammonium Sulfonamide Amino Lipids for Nucleic Acid Delivery. *ACS Appl. Mater. Interfaces* **2018**, *10*, 2302–2311.
(81) Hao, J.; Kos, P.; Zhou, K.; Miller, J. B.; Xue, L.; Yan, Y.; Xiong, H.; Elkassih, S.; Siegwart, D. J. Rapid Synthesis of a Lipocationic Polyester Library *via* Ring-Opening Polymerization of Functional Valerolactones for Efficacious siRNA Delivery. *J. Am. Chem. Soc.* **2015**, *137*, 9206–9209.
(82) Hajj, K. A.; Ball, R. L.; Deluty, S. B.; Singh, S. R.; Strelkova, D.; Knapp, C. M.; Whitehead, K. A. Branched-Tail Lipid Nanoparticles Potently Deliver mRNA *In Vivo* Due to Enhanced Ionization at Endosomal pH. *Small* **2019**, *15*, 1805097.
(83) Wu, Y.; Li, L.; Chen, Q.; Su, Y.; Levkin, P. A.; Davidson, G. Single-Tailed Lipidoids Enhance the Transfection Activity of Their Double-Tailed Counterparts. *ACS Comb. Sci.* **2016**, *18*, 43–50.
(84) Hattori, Y.; Suzuki, S.; Kawakami, S.; Yamashita, F.; Hashida, M. The Role of Dioleoylphosphatidylethanolamine (DOPE) in Targeted Gene Delivery with Mannosylated Cationic Liposomes *via* Intravenous Route. *J. Controlled Release* **2005**, *108*, 484–495.
(85) Farhood, H.; Serbina, N.; Huang, L. The Role of Dioleoyl Phosphatidylethanolamine in Cationic Liposome Mediated Gene Transfer. *Biochim. Biophys. Acta, Biomembr.* **1995**, *1235*, 289–295.
(86) Cheng, X.; Lee, R. J. The Role of Helper Lipids in Lipid Nanoparticles (LNPs) Designed for Oligonucleotide Delivery. *Adv. Drug Delivery Rev.* **2016**, *99*, 129–137.
(87) Tenchov, B. G.; MacDonald, R. C.; Siegel, D. P. Cubic Phases in Phosphatidylcholine-Cholesterol Mixtures: Cholesterol as Membrane "Fusogen. *Biophys. J.* **2006**, *91*, 2508–2516.
(88) de Meyer, F.; Smit, B. Effect of Cholesterol on the Structure of a Phospholipid Bilayer. *Proc. Natl. Acad. Sci. U. S. A.* **2009**, *106*, 3654–3658.
(89) Zhang, Y.; Anchordoquy, T. J. The Role of Lipid Charge Density in the Serum Stability of Cationic Lipid/DNA Complexes. *Biochim. Biophys. Acta, Biomembr.* **2004**, *1663*, 143–157.
(90) Hong, K.; Zheng, W.; Baker, A.; Papahadjopoulos, D. Stabilization of Cationic Liposome-Plasmid DNA Complexes by Polyamines and Poly(Ethylene Glycol)-Phospholipid Conjugates for Efficient *in Vivo* Gene Delivery. *FEBS Lett.* **1997**, *400*, 233–237.
(91) Li, S.; Rizzo, M. A.; Bhattacharya, S.; Huang, L. Characterization of Cationic Lipid-Protamine-DNA (LPD) Complexes for Intravenous Gene Delivery. *Gene Ther.* **1998**, *5*, 930–937.
(92) Akinc, A.; Goldberg, M.; Qin, J.; Dorkin, J. R.; Gamba-Vitalo, C.; Maier, M.; Jayaprakash, K. N.; Jayaraman, M.; Rajeev, K. G.; Manoharan, M.; Koteliansky, V.; Röhl, I.; Leshchiner, E. S.; Langer, R.; Anderson, D. G. Development of Lipidoid-siRNA Formulations for Systemic Delivery to the Liver. *Mol. Ther.* **2009**, *17*, 872–879.
(93) Xia, Y.; Tian, J.; Chen, X. Effect of Surface Properties on Liposomal siRNA Delivery. *Biomaterials* **2016**, *79*, 56–68.
(94) Harvie, P.; Wong, F. M.; Bally, M. B. Use of Poly(Ethylene Glycol)-Lipid Conjugates to Regulate the Surface Attributes and Transfection Activity of Lipid-DNA Particles. *J. Pharm. Sci.* **2000**, *89*, 652–663.
(95) Song, L. Y.; Ahkong, Q. F.; Rong, Q.; Wang, Z.; Ansell, S.; Hope, M. J.; Mui, B. Characterization of the Inhibitory Effect of PEG-Lipid Conjugates on the Intracellular Delivery of Plasmid and Antisense DNA Mediated by Cationic Lipid Liposomes. *Biochim. Biophys. Acta, Biomembr.* **2002**, *1558*, 1–13.
(96) Akinc, A.; Querbes, W.; De, S.; Qin, J.; Frank-Kamenetsky, M.; Jayaprakash, K. N.; Jayaraman, M.; Rajeev, K. G.; Cantley, W. L.; Dorkin, J. R.; Butler, J. S.; Qin, L.; Racie, T.; Sprague, A.; Fava, E.; Zeigerer, A.; Hope, M. J.; Zerial, M.; Sah, D. W.; Fitzgerald, K.; et al. Targeted Delivery of RNAi Therapeutics with Endogenous and Exogenous Ligand-Based Mechanisms. *Mol. Ther.* **2010**, *18*, 1357–1364.
(97) van der Meel, R.; Vehmeijer, L. J. C.; Kok, R. J.; Storm, G.; van Gaal, E. V. B. Ligand-Targeted Particulate Nanomedicines Undergoing Clinical Evaluation: Current Status. *Adv. Drug Delivery Rev.* **2013**, *65*, 1284–1298.
(98) Kreiss, P.; Mailhe, P.; Scherman, D.; Pitard, B.; Cameron, B.; Rangara, R.; Aguerre-Charriol, O.; Airiau, M.; Crouzet, J. Plasmid DNA Size Does Not Affect the Physicochemical Properties of Lipoplexes but Modulates Gene Transfer Efficiency. *Nucleic Acids Res.* **1999**, *27*, 3792–3798.
(99) Gaspar, V.; Melo-Diogo, D. de; Costa, E.; Moreira, A.; Queiroz, J.; Pichon, C.; Correia, I.; Sousa, F. Minicircle DNA Vectors for Gene Therapy: Advances and Applications. *Expert Opin. Biol. Ther.* **2015**, *15*, 353–379.
(100) Darquet, A. M.; Cameron, B.; Wils, P.; Scherman, D.; Crouzet, J. A New DNA Vehicle for Nonviral Gene Delivery: Supercoiled Minicircle. *Gene Ther.* **1997**, *4*, 1341–1349.
(101) Munye, M. M.; Tagalakis, A. D.; Barnes, J. L.; Brown, R. E.; McAnulty, R. J.; Howe, S. J.; Hart, S. L. Minicircle DNA Provides Enhanced and Prolonged Transgene Expression Following Airway Gene Transfer. *Sci. Rep.* **2016**, *6*, 23125.
(102) White, R. E.; Wade-Martins, R.; Hart, S. L.; Frampton, J.; Huey, B.; Desai-Mehta, A.; Cerosaletti, K. M.; Concannon, P.; James, M. R. Functional Delivery of Large Genomic DNA to Human Cells with a Peptide-Lipid Vector. *J. Gene Med.* **2003**, *5*, 883–892.
(103) Zhou, R.; Geiger, R. C.; Dean, D. A. Intracellular Trafficking of Nucleic Acids. *Expert Opin. Drug Delivery* **2004**, *1*, 127–140.
(104) Lukacs, G. L.; Haggie, P.; Seksek, O.; Lechardeur, D.; Freedman, N.; Verkman, A. S. Size-Dependent DNA Mobility in Cytoplasm and Nucleus. *J. Biol. Chem.* **2000**, *275*, 1625–1629.
(105) Mieruszynski, S.; Digman, M. A.; Gratton, E.; Jones, M. R. Characterization of Exogenous DNA Mobility in Live Cells through Fluctuation Correlation Spectroscopy. *Sci. Rep.* **2015**, *5*, 13848.
(106) Nelson, N. Structure, Function, and Evolution of Proton-ATPases. *Plant Physiol.* **1988**, *86*, 1–3.
(107) Tam, Y. K.; Madden, T. D.; Hope, M. J. Pieter Cullis' Quest for a Lipid-Based, Fusogenic Delivery System for Nucleic Acid Therapeutics: Success with siRNA so What about mRNA? *J. Drug Target.* **2016**, *24*, 774–779.
(108) Chen, S.; Tam, Y. Y. C.; Lin, P. J. C.; Sung, M. M. H.; Tam, Y. K.; Cullis, P. R. Influence of Particle Size on the *in Vivo* Potency of Lipid Nanoparticle Formulations of siRNA. *J. Controlled Release* **2016**, *235*, 236–244.
(109) Almofti, M. R.; Harashima, H.; Shinohara, Y.; Almofti, A.; Li, W.; Kiwada, H. Lipoplex Size Determines Lipofection Efficiency with or without Serum. *Mol. Membr. Biol.* **2003**, *20*, 35–43.

DOI: 10.1021/acsnano.8b07858
ACS Nano 2019, 13, 3754–3782

(110) Kunath, K.; von Harpe, A.; Fischer, D.; Petersen, H.; Bickel, U.; Voigt, K.; Kissel, T. Low-Molecular-Weight Polyethylenimine as a Non-Viral Vector for DNA Delivery: Comparison of Physicochemical Properties, Transfection Efficiency and *in Vivo* Distribution with High-Molecular-Weight Polyethylenimine. *J. Controlled Release* **2003**, *89*, 113−125.
(111) Hsu, C. Y. M.; Uludağ, H. A Simple and Rapid Nonviral Approach to Efficiently Transfect Primary Tissue-Derived Cells Using Polyethylenimine. *Nat. Protoc.* **2012**, *7*, 935−945.
(112) Godbey, W. T.; Wu, K. K.; Hirasaki, G. J.; Mikos, A. G. Improved Packing of Poly(Ethylenimine)/DNA Complexes Increases Transfection Efficiency. *Gene Ther.* **1999**, *6*, 1380−1388.
(113) Mansour, H. M.; Rhee, Y.-S.; Wu, X. Nanomedicine in Pulmonary Delivery. *Int. J. Nanomed.* **2009**, *4*, 299−319.
(114) Sakurai, F.; Nishioka, T.; Yamashita, F.; Takakura, Y.; Hashida, M. Effects of Erythrocytes and Serum Proteins on Lung Accumulation of Lipoplexes Containing Cholesterol or DOPE as a Helper Lipid in the Single-Pass Rat Lung Perfusion System. *Eur. J. Pharm. Biopharm.* **2001**, *52*, 165−172.
(115) Chen, Y.; Sun, J.; Lu, Y.; Tao, C.; Huang, J.; Zhang, H.; Yu, Y.; Zou, H.; Gao, J.; Zhong, Y. Complexes Containing Cationic and Anionic pH-Sensitive Liposomes: Comparative Study of Factors Influencing Plasmid DNA Gene Delivery to Tumors. *Int. J. Nanomed.* **2013**, *8*, 1573−1593.
(116) Mao, S.; Neu, M.; Germershaus, O.; Merkel, O.; Sitterberg, J.; Bakowsky, U.; Kissel, T. Influence of Polyethylene Glycol Chain Length on the Physicochemical and Biological Properties of Poly(Ethylene Imine)-Graft-Poly(Ethylene Glycol) Block Copolymer/siRNA Polyplexes. *Bioconjugate Chem.* **2006**, *17*, 1209−1218.
(117) Jiang, H.-L.; Kim, Y.-K.; Arote, R.; Nah, J.-W.; Cho, M.-H.; Choi, Y.-J.; Akaike, T.; Cho, C.-S. Chitosan-Graft-Polyethylenimine as a Gene Carrier. *J. Controlled Release* **2007**, *117*, 273−280.
(118) Ogris, M.; Steinlein, P.; Kursa, M.; Mechtler, K.; Kircheis, R.; Wagner, E. The Size of DNA/Transferrin-PEI Complexes Is an Important Factor for Gene Expression in Cultured Cells. *Gene Ther.* **1998**, *5*, 1425.
(119) Lechardeur, D.; Sohn, K. J.; Haardt, M.; Joshi, P. B.; Monck, M.; Graham, R. W.; Beatty, B.; Squire, J.; O'Brodovich, H.; Lukacs, G. L. Metabolic Instability of Plasmid DNA in the Cytosol: A Potential Barrier to Gene Transfer. *Gene Ther.* **1999**, *6*, 482−497.
(120) Faneca, H.; Simões, S.; Pedroso de Lima, M. C. Evaluation of Lipid-Based Reagents to Mediate Intracellular Gene Delivery. *Biochim. Biophys. Acta, Biomembr.* **2002**, *1567*, 23−33.
(121) Guo, C.; Gemeinhart, R. A. Assessment of a Modular Transfection System Based upon Cellular Localization of DNA. *Mol. Pharmaceutics* **2004**, *1*, 309−316.
(122) Agirre, M.; Zarate, J.; Puras, G.; Ojeda, E.; Pedraz, J. L. Improving Transfection Efficiency of Ultrapure Oligochitosan/DNA Polyplexes by Medium Acidification. *Drug Delivery* **2015**, *22*, 100−110.
(123) Pavan, G. M.; Monteagudo, S.; Guerra, J.; Carrión, B.; Ocaña, V.; Rodríguez-Lopez, J.; Danani, A.; Pérez-Martínez, F. C.; Ceña, V. Role of Generation, Architecture, pH and Ionic Strength on Successful siRNA Delivery and Transfection by Hybrid PPV-PAMAM Dendrimers. *Curr. Med. Chem.* **2012**, *19*, 4929−4941.
(124) Turek, J.; Dubertret, C.; Jaslin, G.; Antonakis, K.; Scherman, D.; Pitard, B. Formulations Which Increase the Size of Lipoplexes Prevent Serum-Associated Inhibition of Transfection. *J. Gene Med.* **2000**, *2*, 32−40.
(125) Sang, Y.; Xie, K.; Mu, Y.; Lei, Y.; Zhang, B.; Xiong, S.; Chen, Y.; Qi, N. Salt Ions and Related Parameters Affect PEI−DNA Particle Size and Transfection Efficiency in Chinese Hamster Ovary Cells. *Cytotechnology* **2015**, *67*, 67−74.
(126) Krebs, H. A. Chemical Composition of Blood Plasma and Serum. *Annu. Rev. Biochem.* **1950**, *19*, 409−430.
(127) Masotti, A.; Mossa, G.; Cametti, C.; Ortaggi, G.; Bianco, A.; Grosso, N. D.; Malizia, D.; Esposito, C. Comparison of Different Commercially Available Cationic Liposome−DNA Lipoplexes: Parameters Influencing Toxicity and Transfection Efficiency. *Colloids Surf., B* **2009**, *68*, 136−144.
(128) Escriou, V.; Ciolina, C.; Lacroix, F.; Byk, G.; Scherman, D.; Wils, P. Cationic Lipid-Mediated Gene Transfer: Effect of Serum on Cellular Uptake and Intracellular Fate of Lipopolyamine/DNA Complexes. *Biochim. Biophys. Acta, Biomembr.* **1998**, *1368*, 276−288.
(129) Damen, J.; Regts, J.; Scherphof, G. Transfer and Exchange of Phospholipid between Small Unilamellar Liposomes and Rat Plasma High Density Lipoproteins Dependence on Cholesterol Content and Phospholipid Composition. *Biochim. Biophys. Acta, Lipids Lipid Metab.* **1981**, *665*, 538−545.
(130) Arukuusk, P.; Pärnaste, L.; Margus, H.; Eriksson, N. K. J.; Vasconcelos, L.; Padari, K.; Pooga, M.; Langel, Ü. Differential Endosomal Pathways for Radically Modified Peptide Vectors. *Bioconjugate Chem.* **2013**, *24*, 1721−1732.
(131) Liu, F.; Frick, A.; Yuan, X.; Huang, L. Dysopsonin Activity of Serum DNA-Binding Proteins Favorable for Gene Delivery. *J. Pharmacol. Exp. Ther.* **2010**, *332*, 500−504.
(132) Immordino, M. L.; Dosio, F.; Cattel, L. Stealth Liposomes: Review of the Basic Science, Rationale, and Clinical Applications, Existing and Potential. *Int. J. Nanomedicine* **2006**, *1*, 297−315.
(133) Schenkman, S.; Araujo, P. S.; Dukman, R.; Quina, F. H.; Chaimovich, H. Effects of Temperature and Lipid Composition on the Serum Albumin-Induced Aggregation and Fusion of Small Unilamellar Vesicles. *Biochim. Biophys. Acta, Biomembr.* **1981**, *649*, 633−641.
(134) Simões, S.; Slepushkin, V.; Pires, P.; Gaspar, R.; Pedroso de Lima, M. C.; Düzgüneş, N. Human Serum Albumin Enhances DNA Transfection by Lipoplexes and Confers Resistance to Inhibition by Serum. *Biochim. Biophys. Acta, Biomembr.* **2000**, *1463*, 459−469.
(135) Fumoto, S.; Kawakami, S.; Shigeta, K.; Higuchi, Y.; Yamashita, F.; Hashida, M. Interaction with Blood Components Plays a Crucial Role in Asialoglycoprotein Receptor-Mediated *in Vivo* Gene Transfer by Galactosylated Lipoplex. *J. Pharmacol. Exp. Ther.* **2005**, *315*, 484−493.
(136) Sakurai, F.; Nishioka, T.; Saito, H.; Baba, T.; Okuda, A.; Matsumoto, O.; Taga, T.; Yamashita, F.; Takakura, Y.; Hashida, M. Interaction between DNA-Cationic Liposome Complexes and Erythrocytes Is an Important Factor in Systemic Gene Transfer *via* the Intravenous Route in Mice: The Role of the Neutral Helper Lipid. *Gene Ther.* **2001**, *8*, 677−686.
(137) Nchinda, G.; Zschörnig, O.; Überla, K. Increased Non-Viral Gene Transfer Levels in Mice by Concentration of Cationic Lipid DNA Complexes Formed under Optimized Conditions. *J. Gene Med.* **2003**, *5*, 712−722.
(138) Hellgren, I.; Gorman, J.; Sylvén, C. Factors Controlling the Efficiency of Tat-Mediated Plasmid DNA Transfer. *J. Drug Target.* **2004**, *12*, 39−47.
(139) Suda, T.; Liu, D. Hydrodynamic Gene Delivery: Its Principles and Applications. *Mol. Ther.* **2007**, *15*, 2063−2069.
(140) Liu, F.; Song, Y.; Liu, D. Hydrodynamics-Based Transfection in Animals by Systemic Administration of Plasmid DNA. *Gene Ther.* **1999**, *6*, 1258−1266.
(141) Diehl, K. H.; Hull, R.; Morton, D.; Pfister, R.; Rabemampianina, Y.; Smith, D.; Vidal, J. M.; van de Vorstenbosch, C. European Federation of Pharmaceutical Industries Association and European Centre for the Validation of Alternative Methods. A Good Practice Guide to the Administration of Substances and Removal of Blood, Including Routes and Volumes. *J. Appl. Toxicol.* **2001**, *21*, 15−23.
(142) Wightman, L.; Kircheis, R.; Rössler, V.; Carotta, S.; Ruzicka, R.; Kursa, M.; Wagner, E. Different Behavior of Branched and Linear Polyethylenimine for Gene Delivery *in Vitro* and *in Vivo*. *J. Gene Med.* **2001**, *3*, 362−372.
(143) Gao, Y.; Xu, Z.; Chen, S.; Gu, W.; Chen, L.; Li, Y. Arginine-Chitosan/DNA Self-Assemble Nanoparticles for Gene Delivery: *In Vitro* Characteristics and Transfection Efficiency. *Int. J. Pharm.* **2008**, *359*, 241−246.
(144) Meisel, J. W.; Gokel, G. W. A Simplified Direct Lipid Mixing Lipoplex Preparation: Comparison of Liposomal-, Dimethylsulfoxide-, and Ethanol-Based Methods. *Sci. Rep.* **2016**, *6*, 27662.

DOI: 10.1021/acsnano.8b07858
ACS Nano 2019, 13, 3754−3782

(145) Huwyler, J.; Kettiger, H.; Schipanski, A.; Wick, P. Engineered Nanomaterial Uptake and Tissue Distribution: From Cell to Organism. *Int. J. Nanomed.* **2013**, *8*, 3255−69.
(146) Ishida, T.; Harashima, H.; Kiwada, H. Liposome Clearance. *Biosci. Rep.* **2002**, *22*, 197−224.
(147) Densmore, C. L.; Giddings, T. H.; Waldrep, J. C.; Kinsey, B. M.; Knight, V. Gene Transfer by Guanidinium-Cholesterol: Dioleoylphosphatidyl-Ethanolamine Liposome-DNA Complexes in Aerosol. *J. Gene Med.* **1999**, *1*, 251−264.
(148) Prabha, S.; Zhou, W.-Z.; Panyam, J.; Labhasetwar, V. Size-Dependency of Nanoparticle-Mediated Gene Transfection: Studies with Fractionated Nanoparticles. *Int. J. Pharm.* **2002**, *244*, 105−115.
(149) Luten, J.; van Nostrum, C. F.; De Smedt, S. C.; Hennink, W. E. Biodegradable Polymers as Non-Viral Carriers for Plasmid DNA Delivery. *J. Controlled Release* **2008**, *126*, 97−110.
(150) Rejman, J.; Oberle, V.; Zuhorn, I. S.; Hoekstra, D. Size-Dependent Internalization of Particles *via* the Pathways of Clathrin- and Caveolae-Mediated Endocytosis. *Biochem. J.* **2004**, *377*, 159−169.
(151) Birchall, J. C.; Kellaway, I. W.; Mills, S. N. Physico-Chemical Characterisation and Transfection Efficiency of Lipid-Based Gene Delivery Complexes. *Int. J. Pharm.* **1999**, *183*, 195−207.
(152) Honary, S.; Zahir, F. Effect of Zeta Potential on the Properties of Nano-Drug Delivery Systems - A Review (Part 1). *Trop. J. Pharm. Res.* **2013**, *12*, 255−264.
(153) Mao, H.-Q.; Roy, K.; Troung-Le, V. L.; Janes, K. A.; Lin, K. Y.; Wang, Y.; August, J. T.; Leong, K. W. Chitosan-DNA Nanoparticles as Gene Carriers: Synthesis, Characterization and Transfection Efficiency. *J. Controlled Release* **2001**, *70*, 399−421.
(154) Oliveira, R. R.; Carvalho, D. M. de; Lisauskas, S.; Mello, E.; Vianna, G. R.; Dode, M. A. N.; Rumpf, R.; Aragão, F. J. L.; Rech, E. L. Effectiveness of Liposomes to Transfect Livestock Fibroblasts. *Genet. Mol. Res. GMR* **2005**, *4*, 185−196.
(155) Hashemi, A.; Roohvand, F.; Ghahremani, M. H.; Aghasadeghi, M. R.; Vahabpour, R.; Motevali, F.; Memarnejadian, A. Optimization of Transfection Methods for Huh-7 and Vero Cells: Comparative Study. *Cytol. Genet.* **2012**, *46*, 347−353.
(156) Malloggi, C.; Pezzoli, D.; Magagnin, L.; De Nardo, L.; Mantovani, D.; Tallarita, E.; Candiani, G. Comparative Evaluation and Optimization of Off-the-Shelf Cationic Polymers for Gene Delivery Purposes. *Polym. Chem.* **2015**, *6*, 6325−6339.
(157) Zuhorn, I. S.; Kalicharan, R.; Hoekstra, D. Lipoplex-Mediated Transfection of Mammalian Cells Occurs through the Cholesterol-Dependent Clathrin-Mediated Pathway of Endocytosis. *J. Biol. Chem.* **2002**, *277*, 18021−18028.
(158) Dalby, B.; Cates, S.; Harris, A.; Ohki, E. C.; Tilkins, M. L.; Price, P. J.; Ciccarone, V. C. Advanced Transfection with Lipofectamine 2000 Reagent: Primary Neurons, siRNA, and High-Throughput Applications. *Methods* **2004**, *33*, 95−103.
(159) Vercauteren, D.; Piest, M.; van der Aa, L. J.; Al Soraj, M.; Jones, A. T.; Engbersen, J. F. J.; De Smedt, S. C.; Braeckmans, K. Flotillin-Dependent Endocytosis and a Phagocytosis-like Mechanism for Cellular Internalization of Disulfide-Based Poly(Amido Amine)/DNA Polyplexes. *Biomaterials* **2011**, *32*, 3072−3084.
(160) Duncan, J. E.; Whitsett, J. A.; Horowitz, A. D. Pulmonary Surfactant Inhibits Cationic Liposome-Mediated Gene Delivery to Respiratory Epithelial Cells *in Vitro*. *Hum. Gene Ther.* **1997**, *8*, 431−438.
(161) Tsan, M. F.; Tsan, G. L.; White, J. E. Surfactant Inhibits Cationic Liposome-Mediated Gene Transfer. *Hum. Gene Ther.* **1997**, *8*, 817−825.
(162) Kleinman, H. K.; Klebe, R. J.; Martin, G. R. Role of Collagenous Matrices in the Adhesion and Growth of Cells. *J. Cell Biol.* **1981**, *88*, 473−485.
(163) Dehm, P.; Prockop, D. J. Synthesis and Extrusion of Collagen by Freshly Isolated Cells from Chick Embryo Tendon. *Biochim. Biophys. Acta, Nucleic Acids Protein Synth.* **1971**, *240*, 358−369.
(164) Morimoto, K.; Nishikawa, M.; Kawakami, S.; Nakano, T.; Hattori, Y.; Fumoto, S.; Yamashita, F.; Hashida, M. Molecular Weight-Dependent Gene Transfection Activity of Unmodified and Galactosylated Polyethyleneimine on Hepatoma Cells and Mouse Liver. *Mol. Ther.* **2003**, *7*, 254−261.
(165) El Ouahabi, A.; Thiry, M.; Pector, V.; Fuks, R.; Ruysschaert, J. M.; Vandenbranden, M. The Role of Endosome Destabilizing Activity in the Gene Transfer Process Mediated by Cationic Lipids. *FEBS Lett.* **1997**, *414*, 187−192.
(166) Kleinman, H. K.; Luckenbill-Edds, L.; Cannon, F. W.; Sephel, G. C. Use of Extracellular Matrix Components for Cell Culture. *Anal. Biochem.* **1987**, *166*, 1−13.
(167) Guerra-Crespo, M.; Charli, J.-L.; Rosales-Garcia, V. H.; Pedraza-Alva, G.; Pérez-Martinez, L. Polyethylenimine Improves the Transfection Efficiency of Primary Cultures of Post-Mitotic Rat Fetal Hypothalamic Neurons. *J. Neurosci. Methods* **2003**, *127*, 179−192.
(168) Shin, S. I.; Freedman, V. H.; Risser, R.; Pollack, R. Tumorigenicity of Virus-Transformed Cells in Nude Mice Is Correlated Specifically with Anchorage Independent Growth *in Vitro*. *Proc. Natl. Acad. Sci. U. S. A.* **1975**, *72*, 4435−4439.
(169) Vancha, A. R.; Govindaraju, S.; Parsa, K. V.; Jasti, M.; González-García, M.; Ballestero, R. P. Use of Polyethyleneimine Polymer in Cell Culture as Attachment Factor and Lipofection Enhancer. *BMC Biotechnol.* **2004**, *4*, 23.
(170) Yavin, E.; Yavin, Z. Attachment and Culture of Dissociated Cells from Rat Embryo Cerebral Hemispheres on Polylysine-Coated Surface. *J. Cell Biol.* **1974**, *62*, 540−546.
(171) Letourneau, P. C. Possible Roles for Cell-to-Substratum Adhesion in Neuronal Morphogenesis. *Dev. Biol.* **1975**, *44*, 77−91.
(172) Rüegg, U. T.; Hefti, F. Growth of Dissociated Neurons in Culture Dishes Coated with Synthetic Polymeric Amines. *Neurosci. Lett.* **1984**, *49*, 319−324.
(173) Lelong, I. H.; Petegnief, V.; Rebel, G. J. Neuronal Cells Mature Faster on Polyethyleneimine Coated Plates than on Polylysine Coated Plates. *J. Neurosci. Res.* **1992**, *32*, 562−568.
(174) Walum, E.; Peterson, A. Acute Toxicity Testing in Cultures of Mouse Neuroblastoma Cells. *Acta Pharmacol. Toxicol.* **1983**, *52* (2), 100−114.
(175) Whitehead, K. A.; Matthews, J.; Chang, P. H.; Niroui, F.; Dorkin, J. R.; Severgnini, M.; Anderson, D. G. The *in Vitro* − *in Vivo* Translation of Lipid Nanoparticles for Hepatocellular siRNA Delivery. *ACS Nano* **2012**, *6*, 6922−6929.
(176) Sieber, S.; Grossen, P.; Detampel, P.; Siegfried, S.; Witzigmann, D.; Huwyler, J. Zebrafish as an Early Stage Screening Tool to Study the Systemic Circulation of Nanoparticulate Drug Delivery Systems *in Vivo*. *J. Controlled Release* **2017**, *264*, 180−191.
(177) Sieber, S.; Grossen, P.; Bussmann, J.; Campbell, F.; Kros, A.; Witzigmann, D.; Huwyler, J. Zebrafish as a Preclinical *in Vivo* Screening Model for Nanomedicines. *Adv. Drug Delivery Rev.* **2019**, 1 DOI: 10.1016/j.addr.2019.01.001.
(178) Sieber, S.; Grossen, P.; Uhl, P.; Detampel, P.; Mier, W.; Witzigmann, D.; Huwyler, J. Zebrafish as a Predictive Screening Model to Assess Macrophage Clearance of Liposomes *in Vivo*. *Nanomedicine* **2019**, *17*, 82.
(179) Campbell, F.; Bos, F. L.; Sieber, S.; Arias-Alpizar, G.; Koch, B. E.; Huwyler, J.; Kros, A.; Bussmann, J. Directing Nanoparticle Biodistribution through Evasion and Exploitation of Stab2-Dependent Nanoparticle Uptake. *ACS Nano* **2018**, *12*, 2138−2150.
(180) Chakraborty, C.; Sharma, A. R.; Sharma, G.; Lee, S.-S. Zebrafish: A Complete Animal Model to Enumerate the Nanoparticle Toxicity. *J. Nanobiotechnol.* **2016**, *14*, 65.
(181) Haque, E.; Ward, A. C. Zebrafish as a Model to Evaluate Nanoparticle Toxicity. *Nanomaterials* **2018**, *8*, 561.
(182) Sago, C. D.; Lokugamage, M. P.; Islam, F. Z.; Krupczak, B. R.; Sato, M.; Dahlman, J. E. Nanoparticles That Deliver RNA to Bone Marrow Identified by *in Vivo* Directed Evolution. *J. Am. Chem. Soc.* **2018**, *140*, 17095−17105.
(183) Sago, C. D.; Lokugamage, M. P.; Paunovska, K.; Vanover, D. A.; Monaco, C. M.; Shah, N. N.; Gamboa Castro, M.; Anderson, S. E.; Rudoltz, T. G.; Lando, G. N.; Munnilal Tiwari, P.; Kirschman, J. L.; Willett, N.; Jang, Y. C.; Santangelo, P. J.; Bryksin, A. V.; Dahlman, J. E. High-Throughput *in Vivo* Screen of Functional mRNA Delivery

DOI: 10.1021/acsnano.8b07858
ACS Nano 2019, 13, 3754−3782

Identifies Nanoparticles for Endothelial Cell Gene Editing. *Proc. Natl. Acad. Sci. U. S. A.* **2018**, *115*, E9944−E9952.
(184) Paunovska, K.; Gil, C. J.; Lokugamage, M. P.; Sago, C. D.; Sato, M.; Lando, G. N.; Gamboa Castro, M.; Bryksin, A. V.; Dahlman, J. E. Analyzing 2000 *in Vivo* Drug Delivery Data Points Reveals Cholesterol Structure Impacts Nanoparticle Delivery. *ACS Nano* **2018**, *12*, 8341−8349.
(185) Bertrand, N.; Wu, J.; Xu, X.; Kamaly, N.; Farokhzad, O. C. Cancer Nanotechnology: The Impact of Passive and Active Targeting in the Era of Modern Cancer Biology. *Adv. Drug Delivery Rev.* **2014**, *66*, 2−25.
(186) Jain, R. K.; Stylianopoulos, T. Delivering Nanomedicine to Solid Tumors. *Nat. Rev. Clin. Oncol.* **2010**, *7*, 653−664.
(187) Zuckerman, J. E.; Choi, C. H. J.; Han, H.; Davis, M. E. Polycation-siRNA Nanoparticles Can Disassemble at the Kidney Glomerular Basement Membrane. *Proc. Natl. Acad. Sci. U. S. A.* **2012**, *109*, 3137−3142.
(188) Porter, C. J. H.; Moghimi, S. M.; Illum, L.; Davis, S. S. The Polyoxyethylene/Polyoxypropylene Block Co-Polymer Poloxamer-407 Selectively Redirects Intravenously Injected Microspheres to Sinusoidal Endothelial Cells of Rabbit Bone Marrow. *FEBS Lett.* **1992**, *305*, 62−66.
(189) Almeida, J. P. M.; Chen, A. L.; Foster, A.; Drezek, R. *In Vivo* Biodistribution of Nanoparticles. *Nanomedicine* **2011**, *6*, 815−835.
(190) Moghimi, S. M.; Hunter, A. C.; Murray, J. C. Long-Circulating and Target-Specific Nanoparticles: Theory to Practice. *Pharmacol. Rev.* **2001**, *53*, 283−318.
(191) Blanco, E.; Shen, H.; Ferrari, M. Principles of Nanoparticle Design for Overcoming Biological Barriers to Drug Delivery. *Nat. Biotechnol.* **2015**, *33*, 941−951.
(192) Longmire, M.; Choyke, P. L.; Kobayashi, H. Clearance Properties of Nano-Sized Particles and Molecules as Imaging Agents: Considerations and Caveats. *Nanomedicine* **2008**, *3*, 703−717.
(193) Sarin, H. Physiologic Upper Limits of Pore Size of Different Blood Capillary Types and Another Perspective on the Dual Pore Theory of Microvascular Permeability. *J. Angiog. Res.* **2010**, *2*, 14.
(194) Mori, T.; Okanoue, T.; Sawa, Y.; Hori, N.; Ohta, M.; Kagawa, K. Defenestration of the Sinusoidal Endothelial Cell in a Rat Model of Cirrhosis. *Hepatology* **1993**, *17*, 891−897.
(195) Wisse, E.; De Zanger, R. B.; Charels, K.; Van Der Smissen, P.; McCuskey, R. S. The Liver Sieve: Considerations Concerning the Structure and Function of Endothelial Fenestrae, the Sinusoidal Wall and the Space of Disse. *Hepatology* **1985**, *5*, 683−692.
(196) Cabral, H.; Matsumoto, Y.; Mizuno, K.; Chen, Q.; Murakami, M.; Kimura, M.; Terada, Y.; Kano, M. R.; Miyazono, K.; Uesaka, M.; Nishiyama, N.; Kataoka, K. Accumulation of Sub-100 nm Polymeric Micelles in Poorly Permeable Tumours Depends on Size. *Nat. Nanotechnol.* **2011**, *6*, 815−823.
(197) Huo, S.; Ma, H.; Huang, K.; Liu, J.; Wei, T.; Jin, S.; Zhang, J.; He, S.; Liang, X.-J. Superior Penetration and Retention Behavior of 50 nm Gold Nanoparticles in Tumors. *Cancer Res.* **2013**, *73*, 319−330.
(198) Owens, D. E., III; Peppas, N. A. Opsonization, Biodistribution, and Pharmacokinetics of Polymeric Nanoparticles. *Int. J. Pharm.* **2006**, *307*, 93−102.
(199) Xiao, K.; Li, Y.; Luo, J.; Lee, J. S.; Xiao, W.; Gonik, A. M.; Agarwal, R. G.; Lam, K. S. The Effect of Surface Charge on *in Vivo* Biodistribution of PEG-Oligocholic Acid Based Micellar Nanoparticles. *Biomaterials* **2011**, *32*, 3435−3446.
(200) Kranz, L. M.; Diken, M.; Haas, H.; Kreiter, S.; Loquai, C.; Reuter, K. C.; Meng, M.; Fritz, D.; Vascotto, F.; Hefesha, H.; Grunwitz, C.; Vormehr, M.; Hüsemann, Y.; Selmi, A.; Kuhn, A. N.; Buck, J.; Derhovanessian, E.; Rae, R.; Attig, S.; Diekmann, J.; et al. Systemic RNA Delivery to Dendritic Cells Exploits Antiviral Defence for Cancer Immunotherapy. *Nature* **2016**, *534*, 396−401.
(201) Levchenko, T. S.; Rammohan, R.; Lukyanov, A. N.; Whiteman, K. R.; Torchilin, V. P. Liposome Clearance in Mice: The Effect of a Separate and Combined Presence of Surface Charge and Polymer Coating. *Int. J. Pharm.* **2002**, *240*, 95−102.
(202) Sadzuka, Y.; Hirotsu, S.; Hirota, S. Effect of Liposomalization on the Antitumor Activity, Side-Effects and Tissue Distribution of CPT-11. *Cancer Lett.* **1998**, *127*, 99−106.
(203) Ernsting, M. J.; Murakami, M.; Roy, A.; Li, S.-D. Factors Controlling the Pharmacokinetics, Biodistribution and Intratumoral Penetration of Nanoparticles. *J. Controlled Release* **2013**, *172*, 782−794.
(204) Judge, A.; McClintock, K.; Phelps, J. R.; Maclachlan, I. Hypersensitivity and Loss of Disease Site Targeting Caused by Antibody Responses to PEGylated Liposomes. *Mol. Ther.* **2006**, *13*, 328−337.
(205) Audouy, S. A. L.; de Leij, L. F. M. H.; Hoekstra, D.; Molema, G. *In Vivo* Characteristics of Cationic Liposomes as Delivery Vectors for Gene Therapy. *Pharm. Res.* **2002**, *19*, 1599−1605.
(206) McLean, J. W.; Fox, E. A.; Baluk, P.; Bolton, P. B.; Haskell, A.; Pearlman, R.; Thurston, G.; Umemoto, E. Y.; McDonald, D. M. Organ-Specific Endothelial Cell Uptake of Cationic Liposome-DNA Complexes in Mice. *Am. J. Physiol. - Heart Circ. Physiol.* **1997**, *273*, H387−H404.
(207) Parker, S. E.; Ducharme, S.; Norman, J.; Wheeler, C. J. Tissue Distribution of the Cytofectin Component of a Plasmid−DNA/Cationic Lipid Complex Following Intravenous Administration in Mice. *Hum. Gene Ther.* **1997**, *8*, 393−401.
(208) Niven, R.; Pearlman, R.; Wedeking, T.; Mackeigan, J.; Noker, P.; Simpson-Herren, L.; Smith, J. G. Biodistribution of Radiolabeled Lipid−DNA Complexes and DNA in Mice. *J. Pharm. Sci.* **1998**, *87*, 1292−1299.
(209) Navalitloha, Y.; Schwartz, E. S.; Groothuis, E. N.; Allen, C. V.; Levy, R. M.; Groothuis, D. R. Therapeutic Implications of Tumor Interstitial Fluid Pressure in Subcutaneous RG-2 Tumors. *Neuro-Oncol.* **2006**, *8*, 227−233.
(210) Wu, M.; Frieboes, H. B.; McDougall, S. R.; Chaplain, M. A. J.; Cristini, V.; Lowengrub, J. The Effect of Interstitial Pressure on Tumor Growth: Coupling with the Blood and Lymphatic Vascular Systems. *J. Theor. Biol.* **2013**, *320*, 131−151.
(211) Mohr, L.; Yoon, S.-K.; Eastman, S. J.; Chu, Q.; Scheule, R. K.; Scaglioni, P. P.; Geissler, M.; Heintges, T.; Blum, H. E.; Wands, J. R. Cationic Liposome-Mediated Gene Delivery to the Liver and to Hepatocellular Carcinomas in Mice. *Hum. Gene Ther.* **2001**, *12*, 799−809.
(212) Clark, P. R.; Stopeck, A. T.; Ferrari, M.; Parker, S. E.; Hersh, E. M. Studies of Direct Intratumoral Gene Transfer Using Cationic Lipid-Complexed Plasmid DNA. *Cancer Gene Ther.* **2000**, *7*, 853−860.
(213) Ball, R. L.; Bajaj, P.; Whitehead, K. A. Oral Delivery of siRNA Lipid Nanoparticles: Fate in the GI Tract. *Sci. Rep.* **2018**, *8*, 2178.
(214) Ball, R. L.; Knapp, C. M.; Whitehead, K. A. Lipidoid Nanoparticles for siRNA Delivery to the Intestinal Epithelium: *In Vitro* Investigations in a Caco-2 Model. *PLoS One* **2015**, *10*, e0133154.
(215) Hartikka, J.; Bozoukova, V.; Ferrari, M.; Sukhu, L.; Enas, J.; Sawdey, M.; Wloch, M. K.; Tonsky, K.; Norman, J.; Manthorpe, M.; Wheeler, C. J. Vaxfectin Enhances the Humoral Immune Response to Plasmid DNA-Encoded Antigens. *Vaccine* **2001**, *19*, 1911−1923.
(216) Perrie, Y.; Frederik, P. M.; Gregoriadis, G. Liposome-Mediated DNA Vaccination: The Effect of Vesicle Composition. *Vaccine* **2001**, *19*, 3301−3310.
(217) Klavinskis, L. S.; Barnfield, C.; Gao, L.; Parker, S. Intranasal Immunization with Plasmid DNA-Lipid Complexes Elicits Mucosal Immunity in the Female Genital and Rectal Tracts. *J. Immunol. Baltim. Md 1950* **1999**, *162*, 254−262.
(218) Dokka, S.; Toledo, D.; Shi, X.; Castranova, V.; Rojanasakul, Y. Oxygen Radical-Mediated Pulmonary Toxicity Induced by Some Cationic Liposomes. *Pharm. Res.* **2000**, *17*, 521−525.
(219) Templeton, N. S.; Lasic, D. D.; Frederik, P. M.; Strey, H. H.; Roberts, D. D.; Pavlakis, G. N. Improved DNA: Liposome Complexes for Increased Systemic Delivery and Gene Expression. *Nat. Biotechnol.* **1997**, *15*, 647−652.
(220) Prudkin, L.; Behrens, C.; Liu, D. D.; Zhou, X.; Ozburn, N. C.; Bekele, B. N.; Minna, J. D.; Moran, C.; Roth, J. A.; Ji, L.; Wistuba, I. I. Loss and Reduction of FUS1 Protein Expression Is a Frequent

DOI: 10.1021/acsnano.8b07858
ACS Nano 2019, 13, 3754−3782

Phenomenon in the Pathogenesis of Lung Cancer. *Clin. Cancer Res.* **2008**, *14*, 41−47.
(221) Lu, C.; Stewart, D. J.; Lee, J. J.; Ji, L.; Ramesh, R.; Jayachandran, G.; Nunez, M. I.; Wistuba, I. I.; Erasmus, J. J.; Hicks, M. E.; Grimm, E. A.; Reuben, J. M.; Baladandayuthapani, V.; Templeton, N. S.; McMannis, J. D.; Roth, J. A. Phase I Clinical Trial of Systemically Administered TUSC2(FUS1)-Nanoparticles Mediating Functional Gene Transfer in Humans. *PLoS One* **2012**, *7*, e34833.
(222) Roth, J.; Stewart, D.; Lu, C.; Wistuba, I.; Yan, S.; Nunez, M. I. Fus1/Tusc2 Therapies. WO2012119095A1, September 7, 2012.
(223) Gopalan, B.; Ito, I.; Branch, C. D.; Stephens, C.; Roth, J. A.; Ramesh, R. Nanoparticle Based Systemic Gene Therapy for Lung Cancer: Molecular Mechanisms and Strategies to Suppress Nanoparticle-Mediated Inflammatory Response. *Technol. Cancer Res. Treat.* **2004**, *3*, 647−657.
(224) Ramesh, R.; Saeki, T.; Smyth Templeton, N.; Ji, L.; Stephens, L. C.; Ito, I.; Wilson, D. R.; Wu, Z.; Branch, C. D.; Minna, J. D.; Roth, J. A. Successful Treatment of Primary and Disseminated Human Lung Cancers by Systemic Delivery of Tumor Suppressor Genes Using an Improved Liposome Vector. *Mol. Ther.* **2001**, *3*, 337−350.
(225) Dai, B.; Yan, S.; Lara-Guerra, H.; Kawashima, H.; Sakai, R.; Jayachandran, G.; Majidi, M.; Mehran, R.; Wang, J.; Bekele, B. N.; Baladandayuthapani, V.; Yoo, S. Y.; Wang, Y.; Ying, J.; Meng, F.; Ji, L.; Roth, J. A. Exogenous Restoration of TUSC2 Expression Induces Responsiveness to Erlotinib in Wildtype Epidermal Growth Factor Receptor (EGFR) Lung Cancer Cells through Context Specific Pathways Resulting in Enhanced Therapeutic Efficacy. *PLoS One* **2015**, *10*, e0123967.
(226) Xiaobo, C.; Majidi, M.; Feng, M.; Shao, R.; Wang, J.; Zhao, Y.; Baladandayuthapani, V.; Song, J.; Fang, B.; Ji, L.; Mehran, R.; Roth, J. A. TUSC2(FUS1)-Erlotinib Induced Vulnerabilities in Epidermal Growth Factor Receptor(EGFR) Wildtype Non-Small Cell Lung Cancer(NSCLC) Targeted by the Repurposed Drug Auranofin. *Sci. Rep.* **2016**, *6*, 35741.
(227) Rimkus, T.; Sirkisoon, S.; Harrison, A.; Lo, H.-W. Tumor Suppressor Candidate 2 (TUSC2, FUS-1) and Human Cancers. *Discovery Med.* **2017**, *23*, 325−330.
(228) Xie, X.; Xia, W.; Li, Z.; Kuo, H.-P.; Liu, Y.; Li, Z.; Ding, Q.; Zhang, S.; Spohn, B.; Yang, Y.; Wei, Y.; Lang, J.-Y.; Evans, D. B.; Chiao, P. J.; Abbruzzese, J. L.; Hung, M.-C. Targeted Expression of BikDD Eradicates Pancreatic Tumors in Noninvasive Imaging Models. *Cancer Cell* **2007**, *12*, 52−65.
(229) Li, L.-Y.; Dai, H.-Y.; Yeh, F.-L.; Kan, S.-F.; Lang, J.; Hsu, J. L.; Jeng, L.-B.; Chen, Y.-H.; Sher, Y.-P.; Lin, W.-C.; Hung, M.-C. Targeted Hepatocellular Carcinoma Proapoptotic BikDD Gene Therapy. *Oncogene* **2011**, *30*, 1773−1783.
(230) Sher, Y.-P.; Tzeng, T.-F.; Kan, S.-F.; Hsu, J.; Xie, X.; Han, Z.; Lin, W.-C.; Li, L.-Y.; Hung, M.-C. Cancer Targeted Gene Therapy of BikDD Inhibits Orthotopic Lung Cancer Growth and Improves Long-Term Survival. *Oncogene* **2009**, *28*, 3286−3295.
(231) Xie, X.; Li, L.; Xiao, X.; Guo, J.; Kong, Y.; Wu, M.; Liu, W.; Gao, G.; Hsu, J. L.; Wei, W.; Hung, M.-C.; Xie, X. Targeted Expression of BikDD Eliminates Breast Cancer with Virtually No Toxicity in Noninvasive Imaging Models. *Mol. Cancer Ther.* **2012**, *11*, 1915−1924.
(232) Xie, X.; Kong, Y.; Tang, H.; Yang, L.; Hsu, J. L.; Hung, M.-C. Targeted BikDD Expression Kills Androgen-Dependent and Castration-Resistant Prostate Cancer Cells. *Mol. Cancer Ther.* **2014**, *13*, 1813−1825.
(233) O'Malley, B. W.; Li, D.; McQuone, S. J.; Ralston, R. Combination Nonviral Interleukin-2 Gene Immunotherapy For Head and Neck Cancer: From Bench Top to Bedside. *Laryngoscope* **2005**, *115*, 391−404.
(234) Anwer, K.; Kao, G.; Proctor, B.; Rolland, A.; Sullivan, S. Optimization of Cationic Lipid/DNA Complexes for Systemic Gene Transfer to Tumor Lesions. *J. Drug Target.* **2000**, *8*, 125−135.
(235) Morse, M. A. Technology Evaluation: Gene Therapy (IL-2), Valentis Inc. *Curr. Opin. Mol. Ther.* **2000**, *2*, 448−452.
(236) San, H.; Yang, Z.-Y.; Pompili, V. J.; Jaffe, M. L.; Plautz, G. E.; Xu, L.; Felgner, J. H.; Wheeler, C. J.; Felgner, P. L.; Gao, X.; Huang, L.; Gordon, D.; Nabel, G. J.; Nabel, E. G. Safety and Short-Term Toxicity of a Novel Cationic Lipid Formulation for Human Gene Therapy. *Hum. Gene Ther.* **1993**, *4*, 781−788.
(237) Logan, J. J.; Bebok, Z.; Walker, L. C.; Peng, S.; Felgner, P. L.; Siegal, G. P.; Frizzell, R. A.; Dong, J.; Howard, M.; Matalon. Cationic Lipids for Reporter Gene and CFTR Transfer to Rat Pulmonary Epithelium. *Gene Ther.* **1995**, *2*, 38−49.
(238) Schreier, H.; Sawyer, S. M. Liposomal DNA Vectors for Cystic Fibrosis Gene Therapy. Current Applications, Limitations, and Future Directions. *Adv. Drug Delivery Rev.* **1996**, *19*, 73−87.
(239) Zabner, J.; Fasbender, A. J.; Moninger, T.; Poellinger, K. A.; Welsh, M. J. Cellular and Molecular Barriers to Gene Transfer by a Cationic Lipid. *J. Biol. Chem.* **1995**, *270*, 18997−19007.
(240) Sorscher, E. *Cationic Lipids for CFTR Gene Therapy*. http://grantome.com/grant/NIH/R01-DK049057-02 (accessed February 5, 2019).
(241) Stopeck, A. T.; Hersh, E. M.; Brailey, J. L.; Clark, P. R.; Norman, J.; Parker, S. E. Transfection of Primary Tumor Cells and Tumor Cell Lines with Plasmid DNA/Lipid Complexes. *Cancer Gene Ther.* **1998**, *5*, 119−126.
(242) Hoffman, D. M.; Figlin, R. A. Intratumoral Interleukin 2 for Renal-Cell Carcinoma by Direct Gene Transfer of a Plasmid DNA/DMRIE/DOPE Lipid Complex. *World J. Urol.* **2000**, *18*, 152−156.
(243) Zelphati, O.; Nguyen, C.; Ferrari, M.; Felgner, J.; Tsai, Y.; Felgner, P. L. Stable and Monodisperse Lipoplex Formulations for Gene Delivery. *Gene Ther.* **1998**, *5*, 1272−1282.
(244) Galanis, E.; Hersh, E. M.; Stopeck, A. T.; Gonzalez, R.; Burch, P.; Spier, C.; Akporiaye, E. T.; Rinehart, J. J.; Edmonson, J.; Sobol, R. E.; Forscher, C.; Sondak, V. K.; Lewis, B. D.; Unger, E. C.; O'Driscoll, M.; Selk, L.; Rubin, J. Immunotherapy of Advanced Malignancy by Direct Gene Transfer of an Interleukin-2 DNA/DMRIE/DOPE Lipid Complex: Phase I/II Experience. *J. Clin. Oncol.* **1999**, *17*, 3313−3323.
(245) Galanis, E.; Burch, P. A.; Richardson, R. L.; Lewis, B.; Pitot, H. C.; Frytak, S.; Spier, C.; Akporiaye, E. T.; Peethambaram, P. P.; Kaur, J. S.; Okuno, S. H.; Unni, K. K.; Rubin, J. Intratumoral Administration of a 1,2-Dimyristyloxypropyl-3- Dimethylhydroxyethyl Ammonium Bromide/Dioleoylphosphatidylethanolamine Formulation of the Human Interleukin-2 Gene in the Treatment of Metastatic Renal Cell Carcinoma. *Cancer* **2004**, *101*, 2557−2566.
(246) Hersh, E. M.; Stopeck, A. T. Advances in the Biological Therapy and Gene Therapy of Malignant Disease. *Clin. Cancer Res.* **1997**, *3*, 2623−2629.
(247) Rubin, J.; Galanis, E.; Pitot, H. C.; Richardson, R. L.; Burch, P. A.; Charboneau, J. W.; Reading, C. C.; Lewis, B. D.; Stahl, S.; Akporiaye, E. T.; Harris, D. T. Phase I Study of Immunotherapy of Hepatic Metastases of Colorectal Carcinoma by Direct Gene Transfer of an Allogeneic Histocompatibility Antigen, HLA-B7. *Gene Ther.* **1997**, *4*, 419−425.
(248) Stopeck, A. T.; Jones, A.; Hersh, E. M.; Thompson, J. A.; Finucane, D. M.; Gutheil, J. C.; Gonzalez, R. Phase II Study of Direct Intralesional Gene Transfer of Allovectin-7, an HLA-B7/Beta2-Microglobulin DNA-Liposome Complex, in Patients with Metastatic Melanoma. *Clin. Cancer Res.* **2001**, *7*, 2285−2291.
(249) Gonzalez, R.; Hutchins, L.; Nemunaitis, J.; Atkins, M.; Schwarzenberger, P. O. Phase 2 Trial of Allovectin-7 in Advanced Metastatic Melanoma. *Melanoma Res.* **2006**, *16*, 521−526.
(250) Bedikian, A. Y.; Richards, J.; Kharkevitch, D.; Atkins, M. B.; Whitman, E.; Gonzalez, R. A Phase 2 Study of High-Dose Allovectin-7 in Patients with Advanced Metastatic Melanoma. *Melanoma Res.* **2010**, *20*, 218−226.
(251) Williams, R. Discontinued in 2013: Oncology Drugs. *Expert Opin. Invest. Drugs* **2015**, *24*, 95−110.
(252) Nouri, N.; Garbe, C. Intralesional Immunotherapy as a Strategy to Treat Melanoma. *Expert Opin. Biol. Ther.* **2016**, *16*, 619−626.
(253) Gorman, C. M.; Aikawa, M.; Fox, B.; Fox, E.; Lapuz, C.; Michaud, B.; Nguyen, H.; Roche, E.; Sawa, T.; Wiener-Kronish, J. P. Efficient *in Vivo* Delivery of DNA to Pulmonary Cells Using the Novel Lipid EDMPC. *Gene Ther.* **1997**, *4*, 983−992.

DOI: 10.1021/acsnano.8b07858
ACS Nano 2019, 13, 3754−3782

(254) Noone, P. G.; Hohneker, K. W.; Zhou, Z.; Johnson, L. G.; Foy, C.; Gipson, C.; Jones, K.; Noah, T. L.; Leigh, M. W.; Schwartzbach, C.; Efthimiou, J.; Pearlman, R.; Boucher, R. C.; Knowles, M. R. Safety and Biological Efficacy of a Lipid−CFTR Complex for Gene Transfer in the Nasal Epithelium of Adult Patients with Cystic Fibrosis. *Mol. Ther.* **2000**, *1*, 105−114.
(255) McDonald, R. J.; Liggitt, H. D.; Roche, L.; Nguyen, H. T.; Pearlman, R.; Raabe, O. G.; Bussey, L. B.; Gorman, C. M. Aerosol Delivery of Lipid:DNA Complexes to Lungs of Rhesus Monkeys. *Pharm. Res.* **1998**, *15*, 671−679.
(256) Sorgi, F. L.; Huang, L. Large Scale Production of DC-Chol Cationic Liposomes by Microfluidization. *Int. J. Pharm.* **1996**, *144*, 131−139.
(257) Thomas, S. M.; Zeng, Q.; Dyer, K. F.; Suscovich, T. J.; Kanter, P. M.; Whalen, J. D.; Watkins, S. F.; Grandis, J. R. Tissue Distribution of Liposome-Mediated Epidermal Growth Factor Receptor Antisense Gene Therapy. *Cancer Gene Ther.* **2003**, *10*, 518−528.
(258) Ciani, L.; Ristori, S.; Salvati, A.; Calamai, L.; Martini, G. DOTAP/DOPE and DC-Chol/DOPE Lipoplexes for Gene Delivery: Zeta Potential Measurements and Electron Spin Resonance Spectra. *Biochim. Biophys. Acta, Biomembr.* **2004**, *1664*, 70−79.
(259) Zhang, Y.; Li, H.; Sun, J.; Gao, J.; Liu, W.; Li, B.; Guo, Y.; Chen, J. DC-Chol/DOPE Cationic Liposomes: A Comparative Study of the Influence Factors on Plasmid pDNA and siRNA Gene Delivery. *Int. J. Pharm.* **2010**, *390*, 198−207.
(260) Lai, S. Y.; Koppikar, P.; Thomas, S. M.; Childs, E. E.; Egloff, A. M.; Seethala, R. R.; Branstetter, B. F.; Gooding, W. E.; Muthukrishnan, A.; Mountz, J. M.; Lui, V. W.; Shin, D. M.; Agarwala, S. S.; Johnson, R.; Couture, L. A.; Myers, E. N.; Johnson, J. T.; Mills, G.; Argiris, A.; Grandis, J. R. Intratumoral Epidermal Growth Factor Receptor Antisense DNA Therapy in Head and Neck Cancer: First Human Application and Potential Antitumor Mechanisms. *J. Clin. Oncol.* **2009**, *27*, 1235−1242.
(261) Nabel, G. J.; Nabel, E. G.; Yang, Z. Y.; Fox, B. A.; Plautz, G. E.; Gao, X.; Huang, L.; Shu, S.; Gordon, D.; Chang, A. E. Direct Gene Transfer with DNA-Liposome Complexes in Melanoma: Expression, Biologic Activity, and Lack of Toxicity in Humans. *Proc. Natl. Acad. Sci. U. S. A.* **1993**, *90*, 11307−11311.
(262) Hui, K. M.; Ang, P. T.; Huang, L.; Tay, S. K. Phase I Study of Immunotherapy of Cutaneous Metastases of Human Carcinoma Using Allogeneic and Xenogeneic MHC DNA−Liposome Complexes. *Gene Ther.* **1997**, *4*, 783−790.
(263) Eastman, S. J.; Lukason, M. J.; Tousignant, J. D.; Murray, H.; Lane, M. D.; St George, J. A.; Akita, G. Y.; Cherry, M.; Cheng, S. H.; Scheule, R. K. A Concentrated and Stable Aerosol Formulation of Cationic Lipid:DNA Complexes Giving High-Level Gene Expression in Mouse Lung. *Hum. Gene Ther.* **1997**, *8*, 765−773.
(264) Alton, E. W.; Armstrong, D. K.; Ashby, D.; Bayfield, K. J.; Bilton, D.; Bloomfield, E. V.; Boyd, A. C.; Brand, J.; Buchan, R.; Calcedo, R.; Carvelli, P.; Chan, M.; Cheng, S. H.; Collie, D. S.; Cunningham, S.; Davidson, H. E.; Davies, G.; Davies, J. C.; Davies, L. A.; Dewar, M. H. et al. A Randomised, Double-Blind, Placebo-Controlled Trial of Repeated Nebulisation of Non-Viral Cystic Fibrosis Transmembrane Conductance Regulator (CFTR) Gene Therapy in Patients with Cystic Fibrosis; *Efficacy and Mechanism Evaluation*; NIHR Journals Library: Southampton, UK, 2016; DOI: 10.3310/eme03050.
(265) Eastman, S. J.; Tousignant, J. D.; Lukason, M. J.; Murray, H.; Siegel, C. S.; Constantino, P.; Harris, D. J.; Cheng, S. H.; Scheule, R. K. Optimization of Formulations and Conditions for the Aerosol Delivery of Functional Cationic Lipid:DNA Complexes. *Hum. Gene Ther.* **1997**, *8*, 313−322.
(266) Alton, E. W. F. W.; Armstrong, D. K.; Ashby, D.; Bayfield, K. J.; Bilton, D.; Bloomfield, E. V.; Boyd, A. C.; Brand, J.; Buchan, R.; Calcedo, R.; Carvelli, P.; Chan, M.; Cheng, S. H.; Collie, D. S.; Cunningham, S.; Davidson, H. E.; Davies, G.; Davies, J. C.; Davies, L. A.; Dewar, M. H.; et al. Repeated Nebulisation of Non-Viral CFTR Gene Therapy in Patients with Cystic Fibrosis: A Randomised, Double-Blind, Placebo-Controlled, Phase 2b Trial. *Lancet Respir. Med.* **2015**, *3*, 684−691.
(267) Porteous, D. J.; Dorin, J. R.; McLachlan, G.; Davidson-Smith, H.; Davidson, H.; Stevenson, B. J.; Carothers, A. D.; Wallace, W. a. H.; Moralee, S.; Hoenes, C.; Kallmeyer, G.; Michaelis, U.; Naujoks, K.; Ho, L. P.; Samways, J. M.; Imrie, M.; Greening, A. P.; Innes, J. A. Evidence for Safety and Efficacy of DOTAP Cationic Liposome Mediated CFTR Gene Transfer to the Nasal Epithelium of Patients with Cystic Fibrosis. *Gene Ther.* **1997**, *4*, 210−218.
(268) Kaushik, A. Leuvectin Vical Inc. *Curr. Opin. Investig. Drugs London Engl. 2000* **2001**, *2*, 976−981.
(269) Middleton, P. G.; Caplen, N. J.; Gao, X.; Huang, L.; Gaya, H.; Geddes, D. M.; Alton, E. W. Nasal Application of the Cationic Liposome DC-Chol:DOPE Does Not Alter Ion Transport, Lung Function or Bacterial Growth. *Eur. Respir. J.* **1994**, *7*, 442−445.
(270) Caplen, N. J.; Alton, E. W. F. W.; Mddleton, P. G.; Dorin, J. R.; Stevenson, B. J.; Gao, X.; Durham, S. R.; Jeffery, P. K.; Hodson, M. E.; Coutelle, C.; Huang, L.; Porteous, D. J.; Williamson, R.; Geddes, D. M. Liposome-Mediated CFTR Gene Transfer to the Nasal Epithelium of Patients with Cystic Fibrosis. *Nat. Med.* **1995**, *1*, 39−46.
(271) Gill, D. R.; Southern, K. W.; Mofford, K. A.; Seddon, T.; Huang, L.; Sorgi, F.; Thomson, A.; MacVinish, L. J.; Ratcliff, R.; Bilton, D.; Lane, D. J.; Littlewood, J. M.; Webb, A. K.; Middleton, P. G.; Colledge, W. H.; Cuthbert, A. W.; Evans, M. J.; Higgins, C. F.; Hyde, S. C. A Placebo-Controlled Study of Liposome-Mediated Gene Transfer to the Nasal Epithelium of Patients with Cystic Fibrosis. *Gene Ther.* **1997**, *4*, 199−209.
(272) Hyde, S. C.; Southern, K. W.; Gileadi, U.; Fitzjohn, E. M.; Mofford, K. A.; Waddell, B. E.; Gooi, H. C.; Goddard, C. A.; Hannavy, K.; Smyth, S. E.; Egan, J. J.; Sorgi, F. L.; Huang, L.; Cuthbert, A. W.; Evans, M. J.; Colledge, W. H.; Higgins, C. F.; Webb, A. K.; Gill, D. R. Repeat Administration of DNA/Liposomes to the Nasal Epithelium of Patients with Cystic Fibrosis. *Gene Ther.* **2000**, *7*, 1156−1165.
(273) Ruiz, F. E.; Clancy, J. P.; Perricone, M. A.; Bebok, Z.; Hong, J. S.; Cheng, S. H.; Meeker, D. P.; Young, K. R.; Schoumacher, R. A.; Weatherly, M. R.; Wing, L.; Morris, J. E.; Sindel, L.; Rosenberg, M.; van Ginkel, F. W.; McGhee, J. R.; Kelly, D.; Lyrene, R. K.; Sorscher, E. J. A Clinical Inflammatory Syndrome Attributable to Aerosolized Lipid−DNA Administration in Cystic Fibrosis. *Hum. Gene Ther.* **2001**, *12*, 751−761.
(274) Zabner, J.; Cheng, S. H.; Meeker, D.; Launspach, J.; Balfour, R.; Perricone, M. A.; Morris, J. E.; Marshall, J.; Fasbender, A.; Smith, A. E.; Welsh, M. J. Comparison of DNA-Lipid Complexes and DNA Alone for Gene Transfer to Cystic Fibrosis Airway Epithelia *in Vivo*. *J. Clin. Invest.* **1997**, *100*, 1529−1537.
(275) Alton, E.; Stern, M.; Farley, R.; Jaffe, A.; Chadwick, S.; Phillips, J.; Davies, J.; Smith, S.; Browning, J.; Davies, M.; Hodson, M. E.; Durham, S. R.; Li, D.; Jeffery, P. K.; Scallan, M.; Balfour, R.; Eastman, S. J.; Cheng, S. H.; Smith, A. E.; Meeker, D.; et al. Cationic Lipid-Mediated CFTR Gene Transfer to the Lungs and Nose of Patients with Cystic Fibrosis: A Double-Blind Placebo-Controlled Trial. *Lancet* **1999**, *353*, 947−954.
(276) Xu, L.; Tang, W. H.; Huang, C. C.; Alexander, W.; Xiang, L. M.; Pirollo, K. F.; Rait, A.; Chang, E. H. Systemic P53 Gene Therapy of Cancer with Immunolipoplexes Targeted by Anti-Transferrin Receptor ScFv. *Mol. Med.* **2001**, *7*, 723−734.
(277) Xu, L.; Huang, C.-C.; Huang, W.; Tang, W.-H.; Rait, A.; Yin, Y. Z.; Cruz, I.; Xiang, L.-M.; Pirollo, K. F.; Chang, E. H. Systemic Tumor-Targeted Gene Delivery by Anti-Transferrin Receptor ScFv-Immunoliposomes. *Mol. Cancer Ther.* **2002**, *1*, 337−346.
(278) Kim, S.-S.; Rait, A.; Kim, E.; Pirollo, K. F.; Nishida, M.; Farkas, N.; Dagata, J. A.; Chang, E. H. A Nanoparticle Carrying the P53 Gene Targets Tumors Including Cancer Stem Cells, Sensitizes Glioblastoma to Chemotherapy and Improves Survival. *ACS Nano* **2014**, *8*, 5494−5514.
(279) Senzer, N.; Nemunaitis, J.; Nemunaitis, D.; Bedell, C.; Edelman, G.; Barve, M.; Nunan, R.; Pirollo, K. F.; Rait, A.; Chang, E. H. Phase I Study of a Systemically Delivered P53 Nanoparticle in Advanced Solid Tumors. *Mol. Ther.* **2013**, *21*, 1096−1103.
(280) Pirollo, K. F.; Nemunaitis, J.; Leung, P. K.; Nunan, R.; Adams, J.; Chang, E. H. Safety and Efficacy in Advanced Solid Tumors of a

Targeted Nanocomplex Carrying the P53 Gene Used in Combination with Docetaxel: A Phase 1b Study. *Mol. Ther.* **2016**, *24*, 1697−1706.
(281) Kim, S.-S.; Rait, A.; Kim, E.; Pirollo, K. F.; Chang, E. H. A Tumor-Targeting P53 Nanodelivery System Limits Chemoresistance to Temozolomide Prolonging Survival in a Mouse Model of Glioblastoma Multiforme. *Nanomedicine* **2015**, *11*, 301−311.
(282) A Study of SGT-53 in Children With Refractory or Recurrent Solid Tumors. https://clinicaltrials.gov/ct2/show/NCT02354547 (accessed February 5, 2019).
(283) Camp, E. R.; Wang, C.; Little, E. C.; Watson, P. M.; Pirollo, K. F.; Rait, A.; Cole, D. J.; Chang, E. H.; Watson, D. K. Transferrin Receptor Targeting Nanomedicine Delivering Wild-Type P53 Gene Sensitizes Pancreatic Cancer to Gemcitabine Therapy. *Cancer Gene Ther.* **2013**, *20*, 222−228.
(284) Zhou, J.; Zhang, X.-Q.; Ashoori, F.; McConkey, D. J.; Knowles, M. A.; Dong, L.; Benedict, W. F. Early RB94-Produced Cytotoxicity in Cancer Cells Is Independent of Caspase Activation or 50 Kb DNA Fragmentation. *Cancer Gene Ther.* **2009**, *16*, 13−19.
(285) Pirollo, K. F.; Rait, A.; Zhou, Q.; Zhang, X.; Zhou, J.; Kim, C.-S.; Benedict, W. F.; Chang, E. H. Tumor-Targeting Nanocomplex Delivery of Novel Tumor Suppressor RB94 Chemosensitizes Bladder Carcinoma Cells *In Vitro* and *In Vivo*. *Clin. Cancer Res.* **2008**, *14*, 2190−2198.
(286) Siefker-Radtke, A.; Zhang, X.; Guo, C. C.; Shen, Y.; Pirollo, K. F.; Sabir, S.; Leung, C.; Leong-Wu, C.; Ling, C.-M.; Chang, E. H.; Millikan, R. E.; Benedict, W. F. A Phase l Study of a Tumor-Targeted Systemic Nanodelivery System, SGT-94, in Genitourinary Cancers. *Mol. Ther.* **2016**, *24*, 1484−1491.
(287) Adams, D.; Gonzalez-Duarte, A.; O'Riordan, W. D.; Yang, C.-C.; Ueda, M.; Kristen, A. V.; Tournev, I.; Schmidt, H. H.; Coelho, T.; Berk, J. L.; Lin, K.-P.; Vita, G.; Attarian, S.; Planté-Bordeneuve, V.; Mezei, M. M.; Campistol, J. M.; Buades, J.; Brannagan, T. H.; Kim, B. J.; Oh, J.; et al. Patisiran, an RNAi Therapeutic, for Hereditary Transthyretin Amyloidosis. *N. Engl. J. Med.* **2018**, *379*, 11−21.
(288) Szebeni, J. Complement Activation-Related Pseudoallergy: A Stress Reaction in Blood Triggered by Nanomedicines and Biologicals. *Mol. Immunol.* **2014**, *61*, 163−173.
(289) Pardi, N.; Secreto, A. J.; Shan, X.; Debonera, F.; Glover, J.; Yi, Y.; Muramatsu, H.; Ni, H.; Mui, B. L.; Tam, Y. K.; Shaheen, F.; Collman, R. G.; Karikó, K.; Danet-Desnoyers, G. A.; Madden, T. D.; Hope, M. J.; Weissman, D. Administration of Nucleoside-Modified mRNA Encoding Broadly Neutralizing Antibody Protects Humanized Mice from HIV-1 Challenge. *Nat. Commun.* **2017**, *8*, 14630.
(290) Pardi, N.; Hogan, M. J.; Pelc, R. S.; Muramatsu, H.; Andersen, H.; DeMaso, C. R.; Dowd, K. A.; Sutherland, L. L.; Scearce, R. M.; Parks, R.; Wagner, W.; Granados, A.; Greenhouse, J.; Walker, M.; Willis, E.; Yu, J. S.; McGee, C. E.; Sempowski, G. D.; Mui, B. L.; Tam, Y. K.; et al. Zika Virus Protection by a Single Low-Dose Nucleoside-Modified mRNA Vaccination. *Nature* **2017**, *543*, 248−251.
(291) Finn, J. D.; Smith, A. R.; Patel, M. C.; Shaw, L.; Youniss, M. R.; van Heteren, J.; Dirstine, T.; Ciullo, C.; Lescarbeau, R.; Seitzer, J.; Shah, R. R.; Shah, A.; Ling, D.; Growe, J.; Pink, M.; Rohde, E.; Wood, K. M.; Salomon, W. E.; Harrington, W. F.; Dombrowski, C.; et al. A Single Administration of CRISPR/Cas9 Lipid Nanoparticles Achieves Robust and Persistent *In Vivo* Genome Editing. *Cell Rep.* **2018**, *22*, 2227−2235.
(292) Oliveira, C.; Ribeiro, A. J.; Veiga, F.; Silveira, I. Recent Advances in Nucleic Acid-Based Delivery: From Bench to Clinical Trials in Genetic Diseases. *J. Biomed. Nanotechnol.* **2016**, *12*, 841−862.
(293) Tousignant, J. D.; Gates, A. L.; Ingram, L. A.; Johnson, C. L.; Nietupski, J. B.; Cheng, S. H.; Eastman, S. J.; Scheule, R. K. Comprehensive Analysis of the Acute Toxicities Induced by Systemic Administration of Cationic Lipid:Plasmid DNA Complexes in Mice. *Hum. Gene Ther.* **2000**, *11*, 2493−2513.
(294) Chen, S.; Zaifman, J.; Kulkarni, J. A.; Zhigaltsev, I. V.; Tam, Y. K.; Ciufolini, M. A.; Tam, Y. Y. C.; Cullis, P. R. Dexamethasone Prodrugs as Potent Suppressors of the Immunostimulatory Effects of Lipid Nanoparticle Formulations of Nucleic Acids. *J. Controlled Release* **2018**, *286*, 46−54.
(295) Hyde, S. C.; Pringle, I. A.; Abdullah, S.; Lawton, A. E.; Davies, L. A.; Varathalingam, A.; Nunez-Alonso, G.; Green, A.-M.; Bazzani, R. P.; Sumner-Jones, S. G.; et al. CpG-Free Plasmids Confer Reduced Inflammation and Sustained Pulmonary Gene Expression. *Nat. Biotechnol.* **2008**, *26*, 549−551.
(296) Suk, J. S.; Kim, A. J.; Trehan, K.; Schneider, C. S.; Cebotaru, L.; Woodward, O. M.; Boylan, N. J.; Boyle, M. P.; Lai, S. K.; Guggino, W. B.; Hanes, J. Lung Gene Therapy with Highly Compacted DNA Nanoparticles That Overcome the Mucus Barrier. *J. Controlled Release* **2014**, *178*, 8−17.
(297) Duncan, G. A.; Jung, J.; Hanes, J.; Suk, J. S. The Mucus Barrier to Inhaled Gene Therapy. *Mol. Ther.* **2016**, *24*, 2043−2053.
(298) Talcott, B.; Moore, M. S. Getting across the Nuclear Pore Complex. *Trends Cell Biol.* **1999**, *9*, 312−318.
(299) Joris, F.; De Smedt, S. C.; Raemdonck, K. Small Molecules Convey Big Messages: Boosting Non-Viral Nucleic Acid Delivery with Low Molecular Weight Drugs. *Nano Today* **2017**, *16*, 14−29.
(300) Dean, D. A. Import of Plasmid DNA into the Nucleus Is Sequence Specific. *Exp. Cell Res.* **1997**, *230*, 293−302.
(301) Belliveau, N. M.; Huft, J.; Lin, P. J.; Chen, S.; Leung, A. K.; Leaver, T. J.; Wild, A. W.; Lee, J. B.; Taylor, R. J.; Tam, Y. K.; Hansen, C. L.; Cullis, P. R. Microfluidic Synthesis of Highly Potent Limit-Size Lipid Nanoparticles for *In Vivo* Delivery of siRNA. *Mol. Ther.–Nucleic Acids* **2012**, *1*, e37.
(302) Rietwyk, S.; Peer, D. Next-Generation Lipids in RNA Interference Therapeutics. *ACS Nano* **2017**, *11*, 7572−7586.

DOI: 10.1021/acsnano.8b07858
ACS Nano 2019, 13, 3754−3782

5.1.2 Chapter 1.2

Improvement of DNA Vector Delivery of DOTAP Lipoplexes by Short Chain Aminolipids

Jonas Buck, Dennis Mueller, Ute Mettal, Miriam Ackermann, Hiu-Man Grisch-Chan, Beat Thöny, Andreas Zumbuehl, Jörg Huwyler, Dominik Witzigmann

Revised manuscript under review (ACS Omega).

Highlights: Lipid-based gene delivery systems often require sophisticated lipid synthesises including multi-step reactions with low yield. This study shows that short chain aminolipids can be synthesized in a straigthforward one-pot approach. The synthesized aminolipids successfully improved DNA vector delivery and cytotoxicity of DOTAP-based lipoplexes. Structure-Activity-Relation demonstrated the superiority of C_{12} lipid tails and methoxy headgroups over C_{10} lipid tails and hydroxy headgroups. The pharmacokinetic behavior of DOTAP-based lipoplexes was not altered *in vivo* in the zebrafish embryo animal model after incorporation of aminolipids.

ACS OMEGA

http://pubs.acs.org/journal/acsodf

Article

Improvement of DNA Vector Delivery of DOTAP Lipoplexes by Short-Chain Aminolipids

Jonas Buck, Dennis Mueller, Ute Mettal, Miriam Ackermann, Hiu Man Grisch-Chan, Beat Thöny, Andreas Zumbuehl, Jörg Huwyler,* and Dominik Witzigmann

Cite This: *ACS Omega* 2020, 5, 24724−24732

Read Online

ACCESS | Metrics & More | Article Recommendations | Supporting Information

ABSTRACT: Cellular delivery of DNA vectors for the expression of therapeutic proteins is a promising approach to treat monogenic disorders or cancer. Significant efforts in a preclinical and clinical setting have been made to develop potent nonviral gene delivery systems based on lipoplexes composed of permanently cationic lipids. However, transfection efficiency and tolerability of such systems are in most cases not satisfactory. Here, we present a one-pot combinatorial method based on double-reductive amination for the synthesis of short-chain aminolipids. These lipids can be used to maximize the DNA vector delivery when combined with the cationic lipid 1,2-dioleoyl-3-trimethylammonium propane (DOTAP). We incorporated various aminolipids into such lipoplexes to complex minicircle DNA and screened these systems in a human liver-derived cell line (HuH7) for gene expression and cytotoxicity. The lead aminolipid AL-A12 showed twofold enhanced gene delivery and reduced toxicity compared to the native DOTAP:cholesterol lipoplexes. Moreover, AL-A12-containing lipoplexes enabled enhanced transgene expression *in vivo* in the zebrafish embryo model.

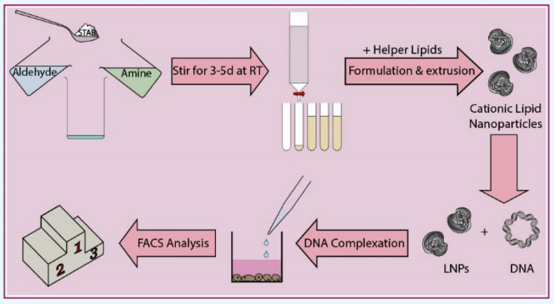

INTRODUCTION

Delivery of genetic material to diseased cells is of growing clinical interest. Many inherited liver diseases including Crigler−Najjar syndrome or Gilbert's syndrome are associated with genetic defects leading to loss of function of proteins or low levels of enzymatic activity.[1−8] Gene therapy enables the introduction of genetic material (*e.g.*, DNA vectors) encoding for a therapeutic protein, thereby restoring physiological functions. Alternatively, the expression of tumor suppressors, proapoptotic or oncotoxic proteins, offers an interesting option for the treatment of malignant disorders.[9−16]

In recent years, various nonviral delivery systems have been investigated in preclinical and clinical settings for the delivery of recombinant DNA.[17] Electrostatic interaction of cationic lipids and negatively charged DNA vectors of virtually any size induces condensation. The resulting lipoplexes are formed spontaneously. Their preparation and handling are simple and cost-effective. Moreover, lipoplexes allow for a straightforward transfer "from bench to large-scale production" compared to viral vectors[18] without the risk for insertion of genetic material into the host's genome as shown for adeno-associated virus vectors.[19−21] Although cationic lipids overcome some of the limitations described for viral vectors, they encompass some disadvantages: The permanent positive charge of cationic lipids is associated with cytotoxicity,[22] and lipoplex systems generally lack efficiency compared to viral vectors.[23,24] As a result, only a few types of cationic lipids have entered clinical trials. In 2017, lipofection (*i.e.*, the introduction of exogenous genetic material by means of lipid-based transfection reagents) accounted for only 4.5% of all clinical trials involving gene therapy.[25] As one of the exceptions, 1,2-dioleoyl-3-trimethylammonium propane and cholesterol (DOTAP:chol)-based lipoplexes have been clinically investigated for the treatment of various diseases including lung cancer, breast cancer, prostate cancer, or hepatocellular carcinoma.[9,13,15,16,26,27] The cationic charge of DOTAP:chol lipoplexes enables facilitated cellular interactions and also accounts for decreased cell viability.[24,28] Therefore, as observed for many lipoplexes, the use of DOTAP:chol systems is limited by poor transfection efficiency and cytotoxic effects.[29−32]

The aim of the present study was to maximize the potency of clinically tested DOTAP:chol lipoplexes while reducing toxicity. Based on our finding that short-chain (C_8−C_{12}) amide lipidoids are potential carriers for siRNA,[33] a combination of short-chain aminolipids and DOTAP:chol-

Received: July 10, 2020
Accepted: August 21, 2020
Published: September 15, 2020

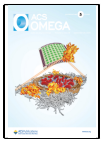

based lipoplexes was explored to enhance DNA vector delivery. It is noteworthy that enhanced gene silencing and reduced cytotoxic potential were demonstrated for polymeric nanoparticles after combination with natural polyphenols and polyphenol inspired polycatechols.[34,35] In view of these results, a combinatorial library of different types of aminolipids with chain lengths of C_{10} or C_{12} and various headgroups, including aliphatic and heterocyclic functional groups, was synthesized by double-reductive amination. The designed aminolipids were incorporated into DOTAP:chol lipoplexes and screened *in vitro* for transfection efficiency and cellular toxicity. The most promising aminolipid-containing system was then compared to DOTAP:chol lipoplexes for *in vivo* transfection efficiency in the zebrafish embryo model.

MATERIALS AND METHODS

Materials. Text adopted from Neuhaus et al.[36] The starting compounds and solvents were purchased from Sigma-Aldrich (St. Louis, MO), Honeywell Fluka (Fisher Scientific AG, Reinach, Switzerland), ABCR (Zug, Switzerland), TCI Deutschland GmbH (Eschborn, Germany), or Acros Organics (Thermo Fisher Scientific, Geel, Belgium) and were used without further purification. For reactions under inert gas conditions, the solvent dichloromethane (DCM) was dried over molecular sieves 4 Å and degassed afterward. Column chromatography was carried out using 230−400 mesh, 60 Å silica gel (Chemie Brunschwig AG, Basel, Switzerland). TLC plates (Merck, Darmstadt, Germany, Silica gel 60 F254) were developed with KMnO4 solution. ^{1}H and ^{13}C NMR spectra were recorded (as indicated) on Bruker 300, 400, or 600 MHz spectrometer (Bruker, Billerica, MA) and are reported as chemical shifts in ppm relative to TMS, calibrated to the signal of the deuterated NMR solvent (300 and 400 MHz). Spin multiplicities are reported as singlet (s), doublet (d), triplet (t), quintet (qui), with coupling constants (J) given in hertz, or multiplet (m). Broad peaks are marked as br. NMR experiments (600 MHz) were performed on a Bruker Avance III NMR spectrometer operating at 600.13 MHz proton frequency. The instrument was equipped with a direct observe 5 mm BBFO smart probe. The experiments were performed at 298 K, and the temperature was calibrated using a methanol standard showing accuracy within ±0.2 K. HRESI-MS was performed on a QSTAR Pulsar (AB Sciex Switzerland GmbH, Baden, Switzerland) spectrometer and are reported as mass-per-charge ratio m/z. IR spectra were recorded on a PerkinElmer Spectrum One Fourier transform infrared (FT-IR) spectrometer (ATR, Golden Gate, PerkinElmer, Basel, Switzerland). 1,2-Dioleoyl-3-trimethylammonium-propane (DOTAP) was obtained from Corden Pharma Switzerland LLC (Liestal, Switzerland). Glucose was purchased from Roth AG, Switzerland. Dulbecco's modified Eagle's medium (DMEM) high glucose was obtained from Sigma-Aldrich Co. (St. Louis, MO) and supplemented with 10% FCS (BioConcept, Allschwil, Switzerland) and penicillin (100 units/mL)−streptomycin (100 μg/mL) (Sigma-Aldrich Co., St. Louis, MO). Trypsin/EDTA (0.25%) was purchased from Invitrogen, Life Technologies (Zug, Switzerland). FACS buffer, composed of D-PBS (Sigma-Aldrich Co, St. Louis, MO), was supplemented with 2% FCS and 0.1% NaN_3 (Sigma-Aldrich Co., St. Louis, MO). The MTT reagent comprised a 1:10 dilution (v/v) of a 5 mg/mL 3-(4,5-dimethylthiazol-2-yl)-2,5-diphenyl tetrazolium bromide stock solution in DMEM. 3-(4,5-Dimethylthiazol-2-yl)-2,5-diphenyl tetrazolium bromide was purchased from Carl Roth (Karlsruhe, Germany). SDS was purchased from Bio-Rad Laboratories, Cressier, Switzerland. HCl and isopropanol were obtained from Merck KGaA (Darmstadt, Germany).

The extrusion equipment consisted of 100 nm polycarbonate membranes (Whatman Nuclepore Track-Etched Membranes, GE Healthcare Life Sciences, Buckinghamshire, U.K.), filter supports (Whatman Drain Disc 10 mm PE, GE Healthcare Life Sciences, Buckinghamshire, U.K.), and a hand extruder (Avanti Mini Extruder, Avanti Polar Lipids, Inc., AL). Particle size and ζ-potential measurements were performed using a Delsa Nano C Particle Analyzer (Beckman Coulter, Inc., Indianapolis, IN). Transmission electron microscopy (TEM) was conducted using a CM-100 electron microscope (Philips, Eindhoven, the Netherlands). Transfection experiments and cytotoxicity experiments were conducted in 24-well plates (TPP Tissue Culture Testplate 24, TPP Techno Plastic Products AG, Trasadingen, Switzerland) and in 96-well plates (TPP Tissue Culture Testplate 96F, TPP Techno Plastic Products AG, Trasadingen, Switzerland), respectively. The minicircle DNA was kindly provided by the University Children's Hospital Zürich, Switzerland. Statistical evaluation was carried out using OriginPro 2018 (64-bit) SR1 b9.5.1.195 (Academic) (OriginLab Corporation, Northampton, MA).

Synthesis of Aminolipids. A small library of 12 multitailed aminolipids was obtained *via* reductive amination of decanal or dodecanal with different amines, as depicted in Figure 1. Briefly, the various amines representing the headgroups of the respective aminolipids were mixed with excess aldehyde (representing the tails) in dichloromethane (DCM). The mixture was stirred for 3 h at RT, followed by the addition of sodium triacetoxyborohydride (STAB) and further stirred for 2−5 days at RT. Afterward, the solvent was evaporated under reduced pressure. The obtained aminolipids were then redissolved in 30 mL of DCM. Brine (30 mL) was added, and the aminolipids were extracted three times with DCM. The crude product was then purified using column chromatography (silica) and a gradient of an appropriate solvent system, *e.g.*, DCM/MeOH or EtOAc/MeOH (*e.g.*, 98:2

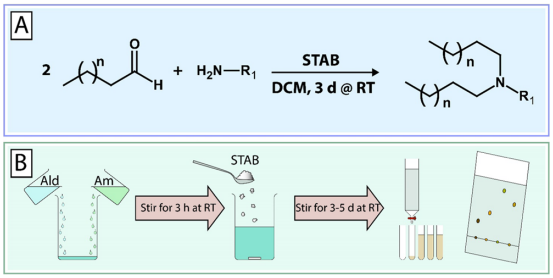

Figure 1. One-pot combinatorial synthesis of short-chain aminolipids *via* double-reductive amination. (A) Double-reductive amination of aldehydes with amines in dichloromethane (DCM) in the presence of sodium triacetoxyborohydride (STAB) as a reducing agent. (B) Briefly, amines (Am) are mixed with excess aldehyde (Ald) and stirred at RT for 3 h followed by the addition of STAB. The reaction continues under stirring at RT for 3−5 days. The obtained aminolipids are then extracted using DCM/brine and then purified by column chromatography (silica, DCM/MeOH 98:2 → 90:10). A detailed description of the chemical synthesis and experimental procedures is provided in the Supporting Information.

https://dx.doi.org/10.1021/acsomega.0c03303
ACS Omega 2020, 5, 24724−24732

to 90:10 (v/v)). The obtained aminolipid fractions were checked for the presence of aminolipid using thin-layer chromatography (TLC). Clean fractions containing the aminolipid (according to TLC) with the correct mass (determined by MS) were combined, and the solvent was evaporated under reduced pressure. For the final drying step, aminolipid samples were exposed to vacuum using an HV pump for at least 2 days. Detailed descriptions and NMR plots for each aminolipid can be found in the Supporting Information.

Preparation of Aminolipid-Based Systems. *DNA Vector Delivery.* Aminolipids in chloroform were combined with chloroform stock solutions of cholesterol, DOPE, or DOTAP (1:1 mol/mol) or a combination of either cholesterol and DOTAP, or DOPE and DOTAP (aminolipid:helper:DOTAP = 5:4:1 (mol/mol)) in a glass vial. The (amino-)lipid mixture in chloroform was subsequently dried under nitrogen flow overnight. On the next day, the components were rehydrated using 5% D(+)-glucose solution in Milli-Q ddH_2O to obtain a final DOTAP (or aminolipid-) concentration of 8 mM. Afterward, the mixtures were stirred and vortexed to ensure complete rehydration of the (amino-)lipid components. Following this step, the rehydrated mixtures were subjected to five freeze−thaw cycles (*i.e.*, frozen for 5 min using dry ice followed by thawing for 5 min in a water bath at 62 °C). After freeze−thawing, the (amino-)lipid mixtures were left at room temperature (RT) for 3 h. Subsequently, the mixtures were extruded 15 times through a Whatman Nuclepore Track-Etched Membrane with a pore size of 0.1 μm using an Avanti Mini Extruder.

Physicochemical Characterization of Aminolipid-Based Systems. Directly after extrusion, the size, polydispersity index (PDI), and ζ-potential of the aminolipid nanoparticles were measured using a Delsa Nano C Particle Analyzer at RT, as described previously.[37,38] Particle size and PDI were determined using CONTIN data conversion after measurement of the extruded nanoparticle preparation (cDOTAP = 8 mM) using a 658 nm laser. Scattered light was detected at an angle of 165°. ζ-Potential data were converted using the Smoluchowski equation after measurement of nanoparticles diluted 1:50 (v/v) in 5% glucose solution at an angle of 15°. Transmission electron microscopy (TEM) images of both pure lipid nanoparticles (LNPs) and LNPs complexed with DNA were acquired on a CM-100 electron microscope (Philips, Eindhoven, the Netherlands). Thus, samples were loaded on a carbon-coated copper grid and counterstained using 2% uranylacetate solution. Excess uranylacetate was removed and the grids were dried at RT overnight prior to TEM imaging.

Cell Culture. HuH7 cells were cultured in high-glucose DMEM, supplemented with 10% fetal calf-serum (FCS), penicillin (100 units/mL), and streptomycin (100 μg/mL) at 37 °C and 5% CO_2. For transfection experiments, the cells were detached at 80−90% confluency using 0.25% trypsin/EDTA (Invitrogen, Life Technologies, Zug, Switzerland) and seeded in 24-well plates (TPP Tissue Culture Testplate 24, TPP Techno Plastic Products AG, Trasadingen, Switzerland) at a seeding density of 5×10^4 cells per well. For cytotoxicity experiments, the cells were detached as for transfection experiments and seeded in 96-well plates (TPP Tissue Culture Testplate 96F, TPP Techno Plastic Products AG, Trasadingen, Switzerland) at a seeding density of 10^4 cells per well.

Transfection Experiments. *DNA Vector Delivery.* Twenty-four hours after seeding, the cells were transfected with minicircle DNA (mcDNA) encoding for enhanced green fluorescent protein (eGFP 1) under the control of a liver-specific p3 promoter. Aminolipid−LNPs were combined with DNA at the indicated ratios and amounts of DNA. Briefly, aminolipid−LNPs and DNA were diluted in separate 1.5 mL Eppendorf tubes in 5% glucose solution. After gentle mixing, the contents of the tubes were combined, and the mixture was left for 30 min on the bench to allow for formation of complexes between aminolipid−LNPs and DNA. After incubation of the DNA with the LNPs, 50 μL of LNP/DNA nanoparticles was added to the cell culture medium (final volume: 1 mL). The ratios of the combination of DNA with LNPs are depicted as the amount of DNA in micrograms and the final concentration of LNPs (μM) in cell culture medium during transfection experiments. The reason for this depiction is that Lipofectamine 3000, whose composition is unknown, was included in the experiment according to the manufacturer's protocol. The amount of Lipofectamine 3000 for transfection experiments was calculated based on an approach relying on the volume of Lipofectamine 3000 in microliters per weight of DNA in micrograms (v/w). This volume per weight approach was maintained throughout the whole study, resulting in a uniform depiction of all samples. Even though no concentration data is available for Lipofectamine 3000, and therefore, it is technically not correct to provide any concentrations for Lipofectamine 3000, we employed an arbitrary concentration for Lipofectamine 3000 assuming that 1 μL of Lipofectamine 3000—as used according to the manufacturer's instructions—is equivalent to 1 μL of DOTAP:chol LNPs. N/P ratios are indicated where applicable.

Transgene Expression Analysis. *Confocal Laser Scanning Microscopy.* Live-cell images were acquired on an Olympus FV-1000 inverted confocal fluorescence microscope (Olympus Ltd., Tokyo, Japan) 24 and 48 h after transfection to qualitatively assess the transfection efficiency. GFP was excited at 488 nm, and emission was recorded at 516 nm using a UPlanSApo 10× objective (numerical aperture, 0.40).

Flow Cytometry. Transfection efficiency and transgene expression were both measured using an FACS Canto II flow cytometer (Becton Dickinson, San Jose, CA) 48 h after transfection. Briefly, the cells were detached using 0.25% trypsin/EDTA (m/V) for 7 min. Subsequently, trypsin digestion was stopped by the addition of DMEM cell culture medium and the cell suspension was transferred to a 1.5 mL Eppendorf tube. The cell suspension was centrifuged (Eppendorf 5424 R Centrifuge, Eppendorf AG, Hamburg, Germany) at 200*g* for 5 min at RT. The supernatant was aspirated, the cells were suspended in FACS buffer (D-PBS, 2% FCS, 0.1% NaN_3), and %GFP-positive cells and mean fluorescence intensity (MFI) were measured after excitation at 488 nm. The fluorescence signal of cells expressing GFP was detected in fluorescence channel FL1 (505LP—530/30). Statistical evaluation of the obtained flow cytometry data was done using FlowJo Vx software (TreeStar, Ashland, OR). MFI values were calculated from GFP-positive cells.

Cytotoxicity Experiments. The HuH7 cells were treated with aminolipid−LNPs at various concentrations 24 h after seeding. Four hours after treatment, the medium containing LNPs was aspirated and replaced by a fresh medium. Twenty-four hours after treatment, the medium was aspirated and replaced by a medium containing 0.5 mg/mL 3-(4,5-

https://dx.doi.org/10.1021/acsomega.0c03303
ACS Omega 2020, 5, 24724−24732

dimethylthiazol-2-yl)-2,5-diphenyl tetrazolium bromide (MTT). The 96-well plates were then incubated (37 °C, 5% CO_2) for 2 h to allow formation of formazan crystals. Afterward, the medium was aspirated and the insoluble formazan crystals were solubilized using a mixture of 3% SDS in H_2O and 40 mM HCl in isopropanol (1:6, v/v). The plates were then shaken for 2 h, followed by absorption measurement using a 96-well plate reader (SpectraMax M2e Microplate Reader, Molecular Devices LLC, San Jose, CA) at 570 (formazan signal) and 670 nm (background).

Statistical Evaluation. Statistical evaluation was done using OriginPro 2018 (64-bit) SR1 b9.5.1.195 (Academic) Software (OriginLab Corporation, Northampton, MA). A minimum of three independent measurements were used for statistical evaluation.

Zebrafish Embryo *In Vivo* Trials. Zebrafish culture and injection were carried out as described previously.[39] Briefly, zebrafish embryos of the Tg(kdrl:EGFP)[40] line were raised under standard conditions in accordance with Swiss animal welfare regulations. Fish were maintained at 28 °C in zebrafish culture media supplemented with 1-phenyl-2-thiourea (PTU). Calibrated volumes of 1 nL sample were injected into the Duct of Cuvier (80 pg DNA, 0.64 pmol DOTAP) using a micromanipulator (Wagner Instrumentenbau KG, Schöffengrund, Germany), a pneumatic PicoPump PV830 (WPI, Sarasota, Florida), and a Leica S8APO microscope (Leica, Wetzlar, Germany). Imaging was carried out 4 and 24 h post-injection using a LEICA POINT SCANNING CONFOCAL "SP5-II-MATRIX" (Leica, Wetzlar, Germany) equipped with a 25× HCX IRAPO L (NA 0.95) objective. Image analysis was carried out using Fiji ImageJ v. 1.52n.

RESULTS AND DISCUSSION

Combinatorial Synthesis of Aminolipids. The aim of this study was the design, synthesis, and screening of novel types of short-chain aminolipids to maximize the DNA vector delivery of DOTAP:chol lipoplexes. To create a small lipid library for this proof-of-concept study, we developed a straightforward one-pot combinatorial synthesis based on a double-reductive amination strategy (Figure 1). A combination of various amines and aldehydes in the presence of the reducing agent sodium triacetoxyborohydride (STAB) resulted in the respective short-chain aminolipids with different headgroups and lipid tails.

An overview of selected building blocks as starting materials (*i.e.*, amines and aldehydes) is given in Figure 2A–C. Based on previous findings by our group that short-chain (C_8–C_{12}) lipid-like materials result in improved nucleic acid delivery, decanal (C_{10}) and dodecanal (C_{12}) were selected as building blocks for lipid tails. In addition to aliphatic amines, heterocyclic amines were selected as headgroups based on previous reports that inclusion of aromatic or heterocyclic rings into transfection reagents can increase the transfection efficiency.[41−45] To test whether these principles also apply to DNA vector delivery based on DOTAP:chol lipoplexes, different building blocks were selected and combined to afford the corresponding aminolipids (see the Supporting Information for synthesis details and aminolipid characterization). For example, aminolipid AL-A10 was synthesized using 3-methoxypropylamine (A) and decanal (C_{10}).

In summary, 12 different short-chain aminolipids were successfully synthesized in high yield using a versatile two-step one-pot procedure. This combinatorial synthesis is easy to perform and fully scalable.

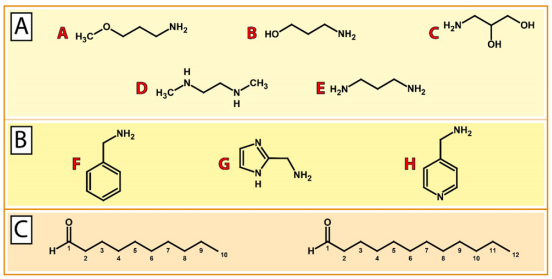

Figure 2. Building blocks for the combinatorial synthesis of aminolipids. (A) Aliphatic amine compounds including (A) 3-methoxypropylamine, (B) 3-aminopropan-1-ol, (C) 3-aminopropane-1,2-diol, (D) *N*,*N*′-dimethylethylenediamine, and (E) 1,3-diaminopropane. (B) Aromatic and heteroaromatic amine compounds including (F) benzylamine, (G) 1*H*-imidazol-2-ylmethanamine, and (H) 4-(aminomethyl)pyridine. (C) Aldehydes decanal (C_{10}) and dodecanal (C_{12}) as building blocks for lipid tails.

Physicochemical Characterization of Aminolipid-Containing Systems. The obtained aminolipids were incorporated into DOTAP-based systems in a 1:1 ratio (mol/mol) using a lipid-film rehydration and extrusion method, as described in the Supporting Information. The results of the physicochemical characterization of aminolipid:DOTAP systems are shown in Figure 3. Most aminolipid:DOTAP systems showed hydrodynamic diameters in the range of 54−79 nm along with a monodisperse size distribution, as indicated by a polydispersity index (PDI) below 0.2 (Figure 3A,B). The largest diameter was measured for the conventional formulation based on DOTAP:chol (108.2 ± 0.6 nm) followed by the AL-H10-containing system (102.0 ± 5.9 nm). The smallest diameter was measured for the AL-C10 system (53.5 ± 2.5 nm) followed by the AL-B10 system (53.8 ± 2.0 nm). Both AL-A10 and AL-A12 systems showed hydrodynamic diameters of 61.5 ± 1.0 and 63.6 ± 0.8 nm and PDI values of 0.185 and 0.181, respectively. Interestingly, incorporation of C_{10}-based aminolipids always resulted in smaller systems compared to their C_{12} counterparts. All measurements were carried out in triplicate.

The ζ-potential measurements for the obtained DOTAP-based systems revealed a positive surface charge in the range of 18−53 mV (Figure 3C). The highest ζ-potential was found for the formulation including AL-B10 with a highly positive value of 52.27 ± 2.80 mV followed by the AL-A12 system (43.66 ± 1.19 mV). The AL-B12 system showed the lowest ζ-potential with a value of 17.97 ± 4.28 mV followed by the AL-D10 system (21.29 ± 3.48 mV). The AL-A10 system showed a similar ζ-potential to DOTAP:chol (24.86 ± 3.26 *vs* 28.21 ± 4.31 mV). A highly positive ζ-potential (>30 mV) is indicative of a high colloidal stability resulting from electrostatic repulsive forces that prevent aggregation of particles.[46,47] Good colloidal stability can still be assumed for systems with ζ-potentials in the range of ±30 mV. This in contrast to a range from 0 to ±5 mV, which is indicative of particle agglomeration and instability.[48] In fact, during the time course of this study, no precipitation was observed for any formulation. All measurements were carried out in triplicate.

Representative TEM images of DOTAP:chol and the AL-A12-containing system are displayed in Figure 3D,E. Both

https://dx.doi.org/10.1021/acsomega.0c03303
ACS Omega 2020, 5, 24724−24732

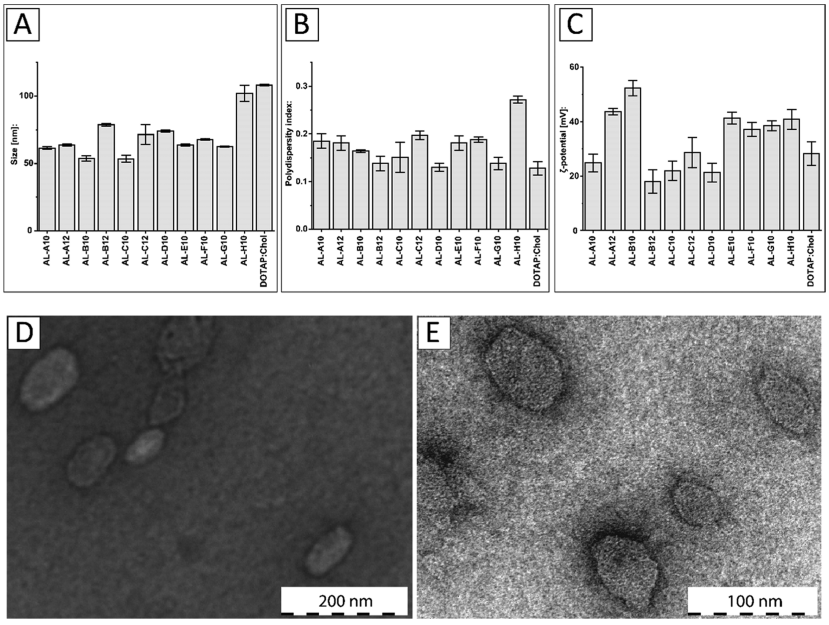

Figure 3. Physicochemical characterization of DOTAP systems combined with short-chain aminolipids. (A) Hydrodynamic diameter (nm), (B) polydispersity index (PDI), and (C) ζ-potential (mV) for aminolipid-containing DOTAP systems compared to the conventional DOTAP:cholesterol (chol) system at a 1:1 ratio (mol/mol). (D) Transmission electron microscopy (TEM) of DOTAP:chol and (E) AL-A12-containing systems.

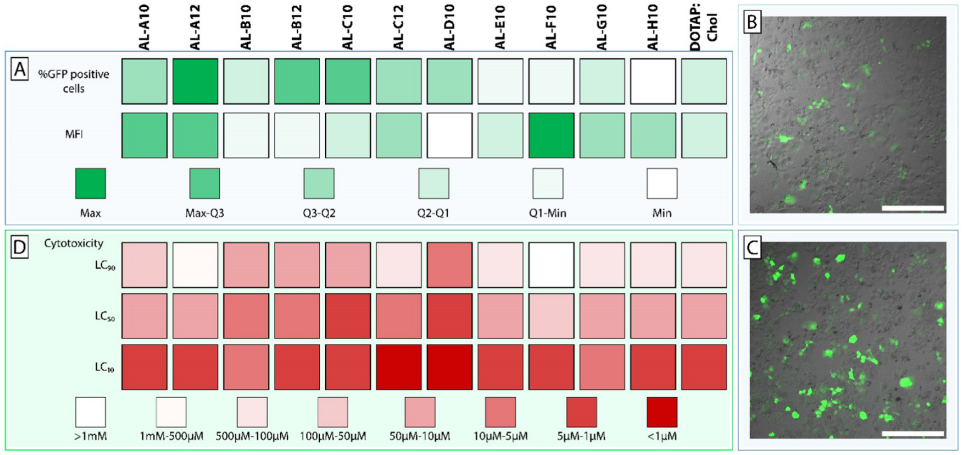

Figure 4. *In vitro* assessment of transfection efficiency and cytotoxicity of lipoplex systems. (A) Heat map representing the transfection efficiency of aminolipid-containing DOTAP lipoplexes compared to conventional DOTAP:cholesterol (chol) composed lipoplexes. Transfection efficiency was assessed by means of percentage of GFP-positive cells and mean fluorescence intensity (MFI) of GFP expression using flow cytometry. The obtained results were allocated to different groups (color code) based on the quartiles of %GFP-positive cells and MFI. Representative confocal images of HuH7 cells transfected with (B) DOTAP:chol or (C) AL-A12-containing lipoplexes entrapping minicircle DNA coding for GFP (scale bar = 400 μm). (D) Cytotoxicity of aminolipid-containing DOTAP lipoplexes compared to conventional DOTAP:chol lipoplexes by means of lethal concentrations (LC 10/50/90) resulting in 90/50/10% cell viability, respectively.

systems resulted in spherical assemblies with diameters of 82.81 ± 24.64 nm (DOTAP:chol) and 46.13 ± 8.85 nm (AL-A12 containing system), which is slightly smaller than the diameters based on dynamic light scattering (DLS). In conclusion, short-chain aminolipids can be successfully incorporated into DOTAP-based systems, thereby influencing the size and charge of the resulting particles.

Assessment of DNA Vector Delivery *In Vitro*. To assess the efficiency of DNA delivery, we selected an advanced DNA vector type, *i.e.*, minicircle DNA, which has clear advantages over plasmid DNA. Several research groups have demonstrated that the use of minicircle DNA results in high transfection efficiencies and long-lasting transgene expression.[49−51] Therefore, a minicircle DNA encoding the reporter gene for green

https://dx.doi.org/10.1021/acsomega.0c03303
ACS Omega 2020, 5, 24724−24732

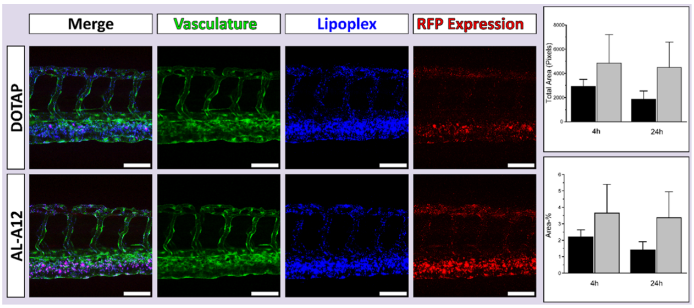

Figure 5. Assessment of *in vivo* transfection efficiency of the lead lipoplex system containing aminolipid AL-A12. Evaluation of lipoplex biodistribution and transfection efficiency *in vivo* in the zebrafish model. Confocal imaging (maximum intensity projections) of transgenic zebrafish embryos with GFP expressing vasculature endothelial cells was performed 4 and 24 h post-injection with fluorescent DOTAP:chol or AL-A12-based lipoplexes entrapping plasmid DNA encoding for RFP. Representative maximum intensity projections of a series of three images are shown (4 h post-injection). Displayed are the merged images, the vasculature expressing GFP (green), the DiD-labeled lipoplexes (blue), and the reporter gene expression (RFP, red). AL-A12 promoted a qualitatively higher gene expression than DOTAP:chol-based lipoplexes h. Scale bars = 80 μm. The right graphs show the quantitative image analysis using Fiji ImageJ of the total area in pixels (top) and the percentage of the area (bottom) of the RFP expression determined 4 and 24 h post-injection of DOTAP:chol (black) and AL-A12-based lipoplexes (gray). The results were not statistically significant at $p < 0.05$.

fluorescent protein (GFP) was complexed using DOTAP:chol and aminolipid-containing systems. The lipoplexes were not PEGylated to reduce complexity, thereby allowing us to attribute observed effects directly to the formulation components. Resulting lipoplexes were used for transfection of human liver-derived HuH7 cells *in vitro* (Table S1). A color-coded summary of the transfection screening is shown in Figure 4A. DOTAP:chol lipoplexes (at 1 μg DNA and 8 μM lipid concentration) resulted in 5.7% GFP-positive cells. Compared to the conventional DOTAP:chol system, incorporation of various aminolipids based on aliphatic amines resulted in improved transfection efficiencies (*i.e.*, AL-A to AL-D). For example, AL-B12 and AL-C12 systems resulted in 8.6 and 6.0% GFP-positive cells, respectively. The lipoplexes containing AL-A10 (7.7%) and AL-A12 (10.3%) showed a significantly increased transfection efficiency compared to DOTAP:chol ($p < 0.001$), which was even more distinct at 2 μg DNA and 16 μM lipid concentration with 28.7% (AL-A10) and 31.5% (AL-A12) compared to 13.2% (DOTAP:chol). Moreover, AL-A12 showed 72% of the transfection efficiency of Lipofectamine 3000 (47.5% GFP-positive cells). In contrast, DOTAP:chol was only 30% as efficient as Lipofectamine 3000. A statistically significant ($p < 0.001$) increase in transgene expression (*i.e.*, assessed based on mean fluorescence intensity (MFI)) compared to DOTAP:chol was only observed for AL-A12. While DOTAP:chol only resulted in 10% of the gene expression achieved with Lipofectamine 3000, AL-A12-based lipoplexes exhibited 20% of the transgene expression of Lipofectamine 3000. The replacement of aliphatic amine headgroups with heterocyclic groups (*i.e.*, AL-F10, AL-G10, and AL-H10) to improve the fusogenic properties (as previously described[52]) did not maximize the efficacy (*i.e.*, % GFP-positive cells) of DOTAP-based lipoplexes (Figure 4A). However, AL-F10 (at 1 μg DNA and 8 μM lipid concentration) resulted in the highest transgene expression among all aminolipids of the combinatorial library. It is tempting to speculate that AL-F10 enhanced the endosomal escape in transfected cells, resulting in increased GFP expression. Due to the small number of investigated heterocyclic headgroups, further studies are warranted to clarify if such a strategy is applicable for DOTAP-based lipoplexes.

To further improve the understanding of how the aminolipids' structural parameters influence the transfection efficiency, specific compounds were selected for a structure–activity relationship (SAR) study (Figure S37). Aminolipids consisting of a bifunctional methoxy headgroup (AL-A10, AL-A12) showed significantly ($p < 0.001$) higher transfection efficiencies and transgene expression levels compared to aminolipids with a bifunctional hydroxy headgroup (AL-B10, AL-B12). SAR analysis of tail groups revealed significantly higher transfection efficiencies ($p < 0.1$) and transgene expression levels ($p < 0.001$) for aminolipids consisting of C_{12} tails compared to aminolipids consisting of C_{10} tails, as demonstrated by the superiority of AL-A12 over AL-A10. Due to the poor transfection efficiency of many of the tested aminolipids, an in-depth SAR analysis focusing on headgroups could not be performed. Further experiments with an expanded range of aminolipid tail lengths and alternative headgroups are needed to improve our understanding on how small changes in lipid tail length influence the delivery of DNA vectors.

In conclusion, the highest transfection efficiency was achieved using AL-A12 lipoplexes with a 2-fold increased number of GFP-positive cells as well as significantly higher transgene expression compared to DOTAP:chol lipoplexes. Representative confocal laser scanning microscopy images of HuH7 cells transfected with DOTAP:chol lipoplexes and AL-A12-containing lipoplexes are shown in Figure 4B,C, respectively. An increased efficiency results in a lower dose of the potentially cytotoxic transfection reagent that needs to be administered while maintaining the same effect and is consequently mitigating side effects of the gene therapy. Moreover, the known composition of these lipoplexes allows for surface modification (*e.g.*, PEGylation), which is difficult to achieve for the proprietary formulation Lipofectamine 3000.

Cytotoxicity of Lipoplex Systems. Figure 4D displays the results of the cell viability assessment. Several aminolipids with aliphatic headgroups and improved transfection efficacy also resulted in enhanced cytotoxic effects (*i.e.*, AL-B to AL-D). Generally, it was observed that aminolipids derived from C_{12}

https://dx.doi.org/10.1021/acsomega.0c03303
ACS Omega 2020, 5, 24724−24732

aldehydes are less toxic than aminolipids derived from C_{10} aldehydes (Tables S2 and S3). For example, AL-A10 systems showed a toxicity comparable to DOTAP:chol while at the same time having increased DNA delivery efficacy. Interestingly, the lead aminolipid AL-A12 demonstrated lower toxicity across the entire dose range than DOTAP:chol. Up to a concentration of 16 μM total lipid, AL-A12 systems resulted in cell viabilities of approximately 80%. At 64 μM total lipid, AL-A12 still resulted in cell viabilities of up to 50%. These results clearly indicate a lower cytotoxic potential for AL-A12-containing lipoplexes than for DOTAP:chol. Lipoplex systems composed of aminolipids with heterocyclic headgroups caused similar or reduced toxicity. The lowest cytotoxic effects were observed using AL-F10-based lipoplexes, thereby confirming that inclusion of aromatic or heterocyclic rings into a transfection reagent can mitigate cytotoxic effects.[42−45]

Conclusively, the lead structures from our transfection screening AL-A12 and AL-F10 (most GFP-positive cells and highest MFI) also outperformed the other aminolipids in the cytotoxicity screening assay. This confirms the generally accepted dogma that low cytotoxic side effects are a prerequisite to achieve high transfection rates.[53]

Assessment of DNA Vector Delivery *In Vivo*. Due to its high transfection efficiency (% transfected cells) and low toxicity *in vitro*, AL-A12 was selected as lead aminolipid for the *in vivo* evaluation in the zebrafish embryo model, a validated *in vivo* tool to assess lipid-based delivery systems.[39,54−56] To assess the systemic circulation of AL-A12 and DOTAP:chol lipoplexes, the fluorescent lipid 1,1′dioctadecyl-3,3,3′,3′-tetramethylindodicarbocyanine (DiD) was incorporated as a tracer. To evaluate the utility of developed lipoplexes for *in vivo* gene delivery, lipoplexes entrapped DNA encoding for RFP. Both lipoplex systems were injected intravenously into transgenic zebrafish embryos expressing GFP in their vasculature. Biodistribution and reporter gene expression were analyzed 4 and 24 h post-injection using confocal microscopy (Figure 5).

As expected for cationic systems, both lipoplexes associated with endothelial cells with preference for venous vasculature.[57] The evaluation of reporter gene expression confirmed the fluorescence distribution patterns. AL-A12-based lipoplexes as well as DOTAP:chol resulted in RFP expression in endothelial cells 4 h post-injection with stronger expression in venous vasculature. Both qualitative confocal imaging and the image analysis confirmed a higher gene expression *in vivo* for AL-A12 compared to DOTAP-based lipoplexes. Further *in vivo* studies are needed to assess the potential to target actively growing tumor blood vessels as shown for other positively charged lipid systems.[58]

CONCLUSIONS

In recent decades, DOTAP:chol lipoplexes have been investigated in several clinical trials for the delivery of DNA vectors. However, none of these studies has advanced to a late clinical stage due to poor outcomes with respect to efficacy. The present study describes the design and one-pot synthesis of short-chain aminolipids enabling incorporation into DOTAP-based lipoplexes to maximize DNA vector delivery. The structure−activity relationship analysis revealed methoxy headgroups to be superior to hydroxy headgroups. Furthermore, C_{12} lipid tails promote higher transfection efficiencies than C_{10} tails. The DNA vector transfection ability in HuH7 cells *in vitro* was significantly increased using various aminolipids (*e.g.*, AL-A12). In addition, incorporation of selected aminolipids clearly mitigated the cytotoxicity. *In vivo* studies in zebrafish embryos showed higher gene expression using the lead lipoplex system based on AL-A12 compared to conventional DOTAP:chol lipoplexes.

In conclusion, our presented one-pot combinatorial synthesis is a versatile approach to create lipid libraries for the development of DNA delivery systems. The combination of DOTAP with short-chain aminolipids promotes efficient DNA vector delivery *in vitro* and *in vivo* as well as reduced cellular toxicity.

ASSOCIATED CONTENT

Supporting Information

The Supporting Information is available free of charge at https://pubs.acs.org/doi/10.1021/acsomega.0c03303.

Details on materials and methods; results of the synthesis, transfection, and cytotoxicity of aminolipids; and statistical data (PDF)

AUTHOR INFORMATION

Corresponding Author

Jörg Huwyler − *Division of Pharmaceutical Technology, Department of Pharmaceutical Sciences, University of Basel, 4056 Basel, Switzerland*; orcid.org/0000-0003-1748-5676; Phone: +41 61 207 15 13; Email: joerg.huwyler@unibas.ch

Authors

Jonas Buck − *Division of Pharmaceutical Technology, Department of Pharmaceutical Sciences, University of Basel, 4056 Basel, Switzerland*

Dennis Mueller − *Department of Chemistry, University of Fribourg, 1700 Fribourg, Switzerland*

Ute Mettal − *Department of Chemistry, University of Fribourg, 1700 Fribourg, Switzerland; Department of Bioresources of the Fraunhofer Institute for Molecular Biology and Applied Ecology, Institute for Insect Biotechnology, Justus-Liebig-University Giessen, 35392 Giessen, Germany*

Miriam Ackermann − *Department of Chemistry, University of Fribourg, 1700 Fribourg, Switzerland*

Hiu Man Grisch-Chan − *Division of Metabolism and Children's Research Center, University Children's Hospital Zurich, 8032 Zürich, Switzerland*

Beat Thöny − *Division of Metabolism and Children's Research Center, University Children's Hospital Zurich, 8032 Zürich, Switzerland*

Andreas Zumbuehl − *Department of Chemistry, University of Fribourg, 1700 Fribourg, Switzerland; Acthera Therapeutics Ltd., 4052 Basel, Switzerland*

Dominik Witzigmann − *Division of Pharmaceutical Technology, Department of Pharmaceutical Sciences, University of Basel, 4056 Basel, Switzerland; Department of Biochemistry and Molecular Biology, University of British Columbia, Vancouver, British Columbia V6T 1Z3, Canada*; orcid.org/0000-0002-8197-8558

Complete contact information is available at: https://pubs.acs.org/10.1021/acsomega.0c03303

Author Contributions

The manuscript was written through contributions of all authors. All authors have given approval to the final version of the manuscript. All authors contributed equally.

https://dx.doi.org/10.1021/acsomega.0c03303
ACS Omega 2020, 5, 24724−24732

Funding
Swiss National Science Foundation (SNF grant no. 173057, Sinergia grant no. CRSII5_180257). Novartis Foundation for Medical-Biological Research (#19A004).

Notes
The authors declare no competing financial interest.

■ ACKNOWLEDGMENTS

D.M. and U.M. were supported by the Swiss National Science Foundation through a stipend professorship to A.Z. In addition, we thank Daniel Häussinger (Department of Chemistry, University of Basel) for NMR and MS analyses and Nicole Rimann (University Children's Hospital Zurich) for supply with minicircle DNA. H.M.G.-C. acknowledges the support from Heidi Ras-Grant. Finally, the authors thank the Imaging Core facility (IMCF, University of Basel) and, in particular, Alexia Ferrand for the technical assistance provided on the confocal microscope for *in vivo* imaging.

■ ABBREVIATIONS

DCM:dichloromethane; DLS:dynamic light scattering; DOTAP:chol:DOTAP:cholesterol; GFP:green fluorescent protein; LC:lethal concentration; MFI:mean fluorescence intensity; PDI:polydispersity index; SAR:structure−activity relationship; STAB:sodium triacetoxyborohydride

■ REFERENCES

(1) Clayton, P. T. Inborn Errors Presenting with Liver Dysfunction. *Semin. Neonatol.* **2002**, *7*, 49−63.
(2) Jansen, P. L. M. Diagnosis and Management of Crigler-Najjar Syndrome. *Eur. J. Pediatr.* **1999**, *158*, S089−S094.
(3) Marcuello, E.; Altés, A.; Menoyo, A.; Rio, E. del.; Gómez-Pardo, M.; Baiget, M. UGT1A1gene variations and irinotecan treatment in patients with metastatic colorectalcancer. *Br. J. Cancer* **2004**, *91*, 678−682.
(4) Kadakol, A.; Ghosh, S. S.; Sappal, B. S.; Sharma, G.; Chowdhury, J. R.; Chowdhury, N. R. Genetic Lesions of Bilirubin Uridine-Diphosphoglucuronate Glucuronosyltransferase (UGT1A1) Causing Crigler-Najjar and Gilbert Syndromes: Correlation of Genotype to Phenotype. *Hum. Mutat.* **2000**, *16*, 297−306.
(5) Schuchman, E. H.; Wasserstein, M. P. Types A and B Niemann-Pick Disease. *Best Pract. Res., Clin. Endocrinol. Metab.* **2015**, *29*, 237−247.
(6) Marciniuk, D. D.; Hernandez, P.; Balter, M.; Bourbeau, J.; Chapman, K. R.; Ford, G. T.; Lauzon, J. L.; Maltais, F.; O'Donnell, D. E.; Goodridge, D.; Strange, C.; Cave, A. J.; Curren, K.; Muthuri, S. Canadian Thoracic Society COPD Clinical Assembly Alpha-1 Antitrypsin Deficiency Expert Working Group. Alpha-1 antitrypsin deficiency targeted testing and augmentation therapy: a Canadian Thoracic Society clinical practice guideline. *Can. Respir. J.* **2012**, *19* (2), 272 Erratum in: *Can Respir J.* 2012 Jul-Aug; *19* (*4*) p 272.
(7) Baruteau, J.; Waddington, S. N.; Alexander, I. E.; Gissen, P. Gene Therapy for Monogenic Liver Diseases: Clinical Successes, Current Challenges and Future Prospects. *J. Inherited Metab. Dis.* **2017**, *40*, 497−517.
(8) Boudes, P. F. Gene Therapy as a New Treatment Option for Inherited Monogenic Diseases. *Eur. J. Intern. Med.* **2014**, *25*, 31−36.
(9) Lu, C.; Stewart, D. J.; Lee, J. J.; Ji, L.; Ramesh, R.; Jayachandran, G.; Nunez, M. I.; Wistuba, I. I.; Erasmus, J. J.; Hicks, M. E.; Grimm, E. A.; Reuben, J. M.; Baladandayuthapani, V.; Templeton, N. S.; McMannis, J. D.; Roth, J. A. Phase I Clinical Trial of Systemically Administered TUSC2(FUS1)-Nanoparticles Mediating Functional Gene Transfer in Humans. *PLoS One* **2012**, *7*, No. e34833.
(10) Ramesh, R.; Saeki, T.; Smyth Templeton, N.; Ji, L.; Stephens, L. C.; Ito, I.; Wilson, D. R.; Wu, Z.; Branch, C. D.; Minna, J. D.; Roth, J. A. Successful Treatment of Primary and Disseminated Human Lung Cancers by Systemic Delivery of Tumor Suppressor Genes Using an Improved Liposome Vector. *Mol. Ther.* **2001**, *3*, 337−350.
(11) Dai, B.; Yan, S.; Lara-Guerra, H.; Kawashima, H.; Sakai, R.; Jayachandran, G.; Majidi, M.; Mehran, R.; Wang, J.; Bekele, B. N.; Baladandayuthapani, V.; Yoo, S.-Y.; Wang, Y.; Ying, J.; Meng, F.; Ji, L.; Roth, J. A. Exogenous Restoration of TUSC2 Expression Induces Responsiveness to Erlotinib in Wildtype Epidermal Growth Factor Receptor (EGFR) Lung Cancer Cells through Context Specific Pathways Resulting in Enhanced Therapeutic Efficacy. *PLoS One* **2015**, *10*, No. e0123967.
(12) Xiaobo, C.; Majidi, M.; Feng, M.; Shao, R.; Wang, J.; Zhao, Y.; Baladandayuthapani, V.; Song, J.; Fang, B.; Ji, L.; Mehran, R.; Roth, J. A. TUSC2(FUS1)-Erlotinib Induced Vulnerabilities in Epidermal Growth Factor Receptor(EGFR) Wildtype Non-Small Cell Lung Cancer(NSCLC) Targeted by the Repurposed Drug Auranofin. *Sci. Rep.* **2016**, *6*, No. 35741.
(13) Rimkus, T.; Sirkisoon, S.; Harrison, A.; Lo, H.-W. Tumor Suppressor Candidate 2 (TUSC2, FUS-1) and Human Cancers. *Discovery Med.* **2017**, *23*, 325−330.
(14) Xie, X.; Xia, W.; Li, Z.; Kuo, H.-P.; Liu, Y.; Li, Z.; Ding, Q.; Zhang, S.; Spohn, B.; Yang, Y.; Wei, Y.; Lang, J.-Y.; Evans, D. B.; Chiao, P. J.; Abbruzzese, J. L.; Hung, M.-C. Targeted Expression of BikDD Eradicates Pancreatic Tumors in Noninvasive Imaging Models. *Cancer Cell* **2007**, *12*, 52−65.
(15) Li, L.-Y.; Dai, H.-Y.; Yeh, F.-L.; Kan, S.-F.; Lang, J.; Hsu, J. L.; Jeng, L.-B.; Chen, Y.-H.; Sher, Y.-P.; Lin, W.-C.; Hung, M.-C. Targeted Hepatocellular Carcinoma Proapoptotic BikDD Gene Therapy. *Oncogene* **2011**, *30*, 1773−1783.
(16) Xie, X.; Li, L.; Xiao, X.; Guo, J.; Kong, Y.; Wu, M.; Liu, W.; Gao, G.; Hsu, J. L.; Wei, W.; Hung, M.-C.; Xie, X. Targeted Expression of BikDD Eliminates Breast Cancer with Virtually No Toxicity in Noninvasive Imaging Models. *Mol. Cancer Ther.* **2012**, *11*, 1915−1924.
(17) Buck, J.; Grossen, P.; Cullis, P. R.; Huwyler, J.; Witzigmann, D. Lipid-Based DNA Therapeutics: Hallmarks of Non-Viral Gene Delivery. *ACS Nano* **2019**, *13*, 3754−3782.
(18) Tokunaga, M.; Hazemoto, N.; Yotsuyanagi, T. Effect of Oligopeptides on Gene Expression: Comparison of DNA/Peptide and DNA/Peptide/Liposome Complexes. *Int. J. Pharm.* **2004**, *269*, 71−80.
(19) Kaiser, J. How Safe Is a Popular Gene Therapy Vector? *Science* **2020**, *367*, 131.
(20) Nault, J.-C.; Datta, S.; Imbeaud, S.; Franconi, A.; Mallet, M.; Couchy, G.; Letouzé, E.; Pilati, C.; Verret, B.; Blanc, J.-F.; Balabaud, C.; Calderaro, J.; Laurent, A.; Letexier, M.; Bioulac-Sage, P.; Calvo, F.; Zucman-Rossi, J. Recurrent AAV2-Related Insertional Mutagenesis in Human Hepatocellular Carcinomas. *Nat. Genet.* **2015**, *47*, 1187−1193.
(21) Russell, D. W.; Grompe, M. Adeno-Associated Virus Finds Its Disease. *Nat. Genet.* **2015**, *47*, 1104−1105.
(22) Cui, S.; Wang, Y.; Gong, Y.; Lin, X.; Zhao, Y.; Zhi, D.; Zhou, Q.; Zhang, S. Correlation of the Cytotoxic Effects of Cationic Lipids with Their Headgroups. *Toxicol. Res.* **2018**, *7*, 473−479.
(23) Glover, D. J.; Lipps, H. J.; Jans, D. A. Towards Safe, Non-Viral Therapeutic Gene Expression in Humans. *Nat. Rev. Genet.* **2005**, *6*, 299−310.
(24) Ramamoorth, M.; Narvekar, A. Non Viral Vectors in Gene Therapy- An Overview. *J. Clin. Diagn. Res.* **2015**, *9*, GE01−GE06.
(25) Ginn, S. L.; Amaya, A. K.; Alexander, I. E.; Edelstein, M.; Abedi, M. R. Gene Therapy Clinical Trials Worldwide to 2017: An Update. *J. Gene Med.* **2018**, *20*, No. e3015.
(26) Sher, Y.-P.; Tzeng, T.-F.; Kan, S.-F.; Hsu, J.; Xie, X.; Han, Z.; Lin, W.-C.; Li, L.-Y.; Hung, M.-C. Cancer Targeted Gene Therapy of BikDD Inhibits Orthotopic Lung Cancer Growth and Improves Long-Term Survival. *Oncogene* **2009**, *28*, 3286−3295.
(27) Xie, X.; Kong, Y.; Tang, H.; Yang, L.; Hsu, J. L.; Hung, M.-C. Targeted BikDD Expression Kills Androgen-Dependent and Castration-Resistant Prostate Cancer Cells. *Mol. Cancer Ther.* **2014**, *13*, 1813−1825.

(28) Zhang, J.-S.; Liu, F.; Huang, L. Implications of Pharmacokinetic Behavior of Lipoplex for Its Inflammatory Toxicity. *Adv. Drug Delivery Rev.* **2005**, *57*, 689−698.
(29) Lee, C.-H.; Ni, Y.-H.; Chen, C.-C.; Chou, C.-K.; Chang, F.-H. Synergistic Effect of Polyethylenimine and Cationic Liposomes in Nucleic Acid Delivery to Human Cancer Cells. *Biochim. Biophys. Acta, Biomembr.* **2003**, *1611*, 55−62.
(30) Li, W.; Szoka, F. C. Lipid-Based Nanoparticles for Nucleic Acid Delivery. *Pharm. Res.* **2007**, *24*, 438−449.
(31) Yin, H.; Kanasty, R. L.; Eltoukhy, A. A.; Vegas, A. J.; Dorkin, J. R.; Anderson, D. G. Non-Viral Vectors for Gene-Based Therapy. *Nat. Rev. Genet.* **2014**, *15*, 541−555.
(32) Zhang, Y.; Anchordoquy, T. J. The Role of Lipid Charge Density in the Serum Stability of Cationic Lipid/DNA Complexes. *Biochim. Biophys. Acta, Biomembr.* **2004**, *1663*, 143−157.
(33) Akinc, A.; Zumbuehl, A.; Goldberg, M.; Leshchiner, E. S.; Busini, V.; Hossain, N.; Bacallado, S. A.; Nguyen, D. N.; Fuller, J.; Alvarez, R.; Borodovsky, A.; Borland, T.; Constien, R.; de Fougerolles, A.; Dorkin, J. R.; Jayaprakash, K. N.; Jayaraman, M.; John, M.; Koteliansky, V.; Manoharan, M.; Nechev, L.; Qin, J.; Racie, T.; Raitcheva, D.; Rajeev, K. G.; Sah, D. W. Y.; Soutschek, J.; Toudjarska, I.; Vornlocher, H.-P.; Zimmermann, T. S.; Langer, R.; Anderson, D. G. A Combinatorial Library of Lipid-like Materials for Delivery of RNAi Therapeutics. *Nat. Biotechnol.* **2008**, *26*, 561−569.
(34) Shen, W.; Wang, Q.; Shen, Y.; Gao, X.; Li, L.; Yan, Y.; Wang, H.; Cheng, Y. Green Tea Catechin Dramatically Promotes RNAi Mediated by Low-Molecular-Weight Polymers. *ACS Cent. Sci.* **2018**, *4*, 1326−1333.
(35) Shen, W.; Wang, R.; Fan, Q.; Gao, X.; Wang, H.; Shen, Y.; Li, Y.; Cheng, Y. Natural Polyphenol Inspired Polycatechols for Efficient SiRNA Delivery. *CCS Chem.* **2020**, *2*, 146−157.
(36) Neuhaus, F.; Mueller, D.; Tanasescu, R.; Balog, S.; Ishikawa, T.; Brezesinski, G.; Zumbuehl, A. Vesicle Origami: Cuboid Phospholipid Vesicles Formed by Template-Free Self-Assembly. *Angew. Chem., Int. Ed.* **2017**, *56*, 6515−6518.
(37) Witzigmann, D.; Wu, D.; Schenk, S. H.; Balasubramanian, V.; Meier, W.; Huwyler, J. Biocompatible Polymer−Peptide Hybrid-Based DNA Nanoparticles for Gene Delivery. *ACS Appl. Mater. Interfaces* **2015**, *7*, 10446−10456.
(38) Witzigmann, D.; Sieber, S.; Porta, F.; Grossen, P.; Bieri, A.; Strelnikova, N.; Pfohl, T.; Prescianotto-Baschong, C.; Huwyler, J. Formation of Lipid and Polymer Based Gold Nanohybrids Using a Nanoreactor Approach. *RSC Adv.* **2015**, *5*, 74320−74328.
(39) Sieber, S.; Grossen, P.; Uhl, P.; Detampel, P.; Mier, W.; Witzigmann, D.; Huwyler, J. Zebrafish as a Predictive Screening Model to Assess Macrophage Clearance of Liposomes in Vivo. *Nanomedicine* **2019**, *17*, 82−93.
(40) Jin, S.-W.; Beis, D.; Mitchell, T.; Chen, J.-N.; Stainier, D. Y. R. Cellular and Molecular Analyses of Vascular Tube and Lumen Formation in Zebrafish. *Development* **2005**, *132*, 5199−5209.
(41) Liu, H.; Chang, H.; Lv, J.; Jiang, C.; Li, Z.; Wang, F.; Wang, H.; Wang, M.; Liu, C.; Wang, X.; Shao, N.; He, B.; Shen, W.; Zhang, Q.; Cheng, Y. Screening of Efficient SiRNA Carriers in a Library of Surface-Engineered Dendrimers. *Sci. Rep.* **2016**, *6*, No. 25069.
(42) Jones, C. H.; Chen, C.-K.; Ravikrishnan, A.; Rane, S.; Pfeifer, B. A. Overcoming Nonviral Gene Delivery Barriers: Perspective and Future. *Mol. Pharm.* **2013**, *10*, 4082−4098.
(43) Ilies, M. A.; Johnson, B. H.; Makori, F.; Miller, A.; Seitz, W. A.; Thompson, E. B.; Balaban, A. T. Pyridinium Cationic Lipids in Gene Delivery: An in Vitro and in Vivo Comparison of Transfection Efficiency versus a Tetraalkylammonium Congener. *Arch. Biochem. Biophys.* **2005**, *435*, 217−226.
(44) van der Woude, I.; Wagenaar, A.; Meekel, A. A.; ter Beest, M. B.; Ruiters, M. H.; Engberts, J. B.; Hoekstra, D. Novel Pyridinium Surfactants for Efficient, Nontoxic in Vitro Gene Delivery. *Proc. Natl. Acad. Sci. U.S.A.* **1997**, *94*, 1160−1165.
(45) Roosjen, A.; Šmisterová, J.; Driessen, C.; Anders, J. T.; Wagenaar, A.; Hoekstra, D.; Hulst, R.; Engberts, J. B. F. N. Synthesis and Characteristics of Biodegradable Pyridinium Amphiphiles Used for in Vitro DNA Delivery. *Eur. J. Org. Chem.* **2002**, *2002*, 1271−1277.
(46) Faneca, H.; Simões, S.; Pedroso de Lima, M. C. Evaluation of Lipid-Based Reagents to Mediate Intracellular Gene Delivery. *Biochim. Biophys. Acta, Biomembr.* **2002**, *1567*, 23−33.
(47) Birchall, J. C.; Kellaway, I. W.; Mills, S. N. Physico-Chemical Characterisation and Transfection Efficiency of Lipid-Based Gene Delivery Complexes. *Int. J. Pharm.* **1999**, *183*, 195−207.
(48) Honary, S.; Zahir, F. Effect of Zeta Potential on the Properties of Nano-Drug Delivery Systems A Review (Part 2). *Trop. J. Pharm. Res.* **2013**, *12*, 265−273.
(49) Chen, Z.-Y.; Riu, E.; He, C.-Y.; Xu, H.; Kay, M. A. Silencing of Episomal Transgene Expression in Liver by Plasmid Bacterial Backbone DNA Is Independent of CpG Methylation. *Mol. Ther.* **2008**, *16*, 548−556.
(50) Viecelli, H. M.; Harbottle, R. P.; Wong, S. P.; Schlegel, A.; Chuah, M. K.; VandenDriessche, T.; Harding, C. O.; Thöny, B. Treatment of Phenylketonuria Using Minicircle-Based Naked-DNA Gene Transfer to Murine Liver. *Hepatology* **2014**, *60*, 1035−1043.
(51) Kay, M. A. State-of-the-Art Gene-Based Therapies: The Road Ahead. *Nat. Rev. Genet.* **2011**, *12*, 316−328.
(52) Csiszár, A.; Hersch, N.; Dieluweit, S.; Biehl, R.; Merkel, R.; Hoffmann, B. NovelFusogenic Liposomes for Fluorescent Cell Labeling and Membrane Modification. *Bioconjugate Chem.* **2010**, *21*, 537−543.
(53) Durán, M. C.; Willenbrock, S.; Barchanski, A.; Müller, J.-M. V.; Maiolini, A.; Soller, J. T.; Barcikowski, S.; Nolte, I.; Feige, K.; Murua Escobar, H. Comparison of Nanoparticle-Mediated Transfection Methods for DNA Expression Plasmids: Efficiency and Cytotoxicity. *J. Nanobiotechnol.* **2011**, *9*, No. 47.
(54) Sieber, S.; Grossen, P.; Bussmann, J.; Campbell, F.; Kros, A.; Witzigmann, D.; Huwyler, J. Zebrafish as a Preclinical in Vivo Screening Model for Nanomedicines. *Adv. Drug Delivery Rev.* **2019**, *151−152*, 152−168.
(55) Sieber, S.; Grossen, P.; Detampel, P.; Siegfried, S.; Witzigmann, D.; Huwyler, J. Zebrafish as an Early Stage Screening Tool to Study the Systemic Circulation of Nanoparticulate Drug Delivery Systems in Vivo. *J. Controlled Release* **2017**, *264*, 180−191.
(56) Witzigmann, D.; Uhl, P.; Sieber, S.; Kaufman, C.; Einfalt, T.; Schöneweis, K.; Grossen, P.; Buck, J.; Ni, Y.; Schenk, S. H.; Hussner, J.; Meyer zu Schwabedissen, H. E.; Québatte, G.; Mier, W.; Urban, S.; Huwyler, J. Optimization-by-Design of Hepatotropic Lipid Nanoparticles Targeting the Sodium-Taurocholate Cotransporting Polypeptide. *eLife* **2019**, *8*, No. e42276.
(57) Campbell, F.; Bos, F. L.; Sieber, S.; Arias-Alpizar, G.; Koch, B. E.; Huwyler, J.; Kros, A.; Bussmann, J. Directing Nanoparticle Biodistribution through Evasion and Exploitation of Stab2-Dependent Nanoparticle Uptake. *ACS Nano* **2018**, *12*, 2138−2150.
(58) Schmitt-Sody, M.; Strieth, S.; Krasnici, S.; Sauer, B.; Schulze, B.; Teifel, M.; Michaelis, U.; Naujoks, K.; Dellian, M. Neovascular Targeting Therapy: Paclitaxel Encapsulated in Cationic Liposomes Improves Antitumoral Efficacy. *Clin. Cancer Res.* **2003**, *9*, 2335−2341.

https://dx.doi.org/10.1021/acsomega.0c03303
ACS Omega 2020, 5, 24724−24732

Supporting Information

Improvement of DNA Vector Delivery of DOTAP Lipoplexes by Short Chain Aminolipids

Jonas Buck[1], Dennis Mueller[2], Ute Mettal[2,3], Miriam Ackermann[2], Hiu Man Grisch-Chan[4], Beat Thöny[4], Andreas Zumbuehl[2,5], Jörg Huwyler[1]*, Dominik Witzigmann[1,6]

1 Division of Pharmaceutical Technology, Department of Pharmaceutical Sciences, University of Basel, Switzerland

2 Department of Chemistry, University of Fribourg, Switzerland

3 Institute for Insect Biotechnology, Justus-Liebig-University Giessen, Germany and Department of Bioresources of the Fraunhofer Institute for Molecular Biology and Applied Ecology, Giessen, Germany

4 Division of Metabolism and Children's Research Center, University Children's Hospital Zurich, Switzerland

5 Acthera Therapeutics Ltd., Peter Merian-Strasse 45, 4052 Basel, Switzerland

6 Department of Biochemistry and Molecular Biology, University of British Columbia, Vancouver, British Columbia, Canada.

* Corresponding author

Supporting Results

1. Synthesis of Amino Lipids

1.1 Synthesis of *N*-decyl-*N*-(3-methyoxypropyl)decan-1-amine (AL-A10)

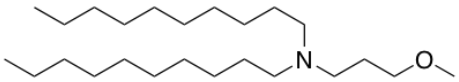

Figure S1: Chemical structure of *N*-decyl-*N*-(3-methyoxypropyl)decan-1-amine (**AL-A10**).

3-Methoxypropylamine (1.00 eq., 5.00 mmol, 0.51 mL), and decanal (2.20 eq., 11.00 mmol, 2.07 mL) were dissolved in DCM (25 mL) and stirred for 3 h. Sodium triacetoxyborohydride (2.20 eq., 11.00 mmol, 2.33 g) was added and the mixture was stirred for 2 days. The product was purified by column chromatography (Silica; EtOAc/MeOH (98:2 V/V) → EtOAc/MeOH (90:10 V/V)) to yield a yellow liquid (702 mg, 1.90 mmol, 38.0 %).

^{1}H NMR (400 MHz, $CDCl_3$) δ = 3.47 (t, *J* = 5.5 Hz, 2H), 3.33 (s, 3H), 3.14-3.08 (m, 2H), 3.00-2.95 (m, 4H), 2.16-2.09 (m, 2H), 1.82-1.78 (m, 4H,), 1.35-1.27 (m, 28H), 0.89 (t, *J* =7.0 Hz, 6H) ppm.

^{13}C NMR (100 MHz, $CDCl_3$) δ = 69.3, 58.8, 52.4, 50.5, 31.8, 29.2, 29.0, 26.8, 24.1, 23.0, 22.6, 14.1 ppm.

IR $\tilde{\nu}$ = 2924, 2853, 1718, 1579, 1466, 1379, 1256, 1119 cm^{-1}.

HRMS (ESI$^+$): m/z [M+H]$^+$: calculated for $[C_{24}H_{51}NO+H]^+$: 370.4048; found: 370.4037.

R_f (EtOAc / MeOH (9:1 V/V)) = 0.34.

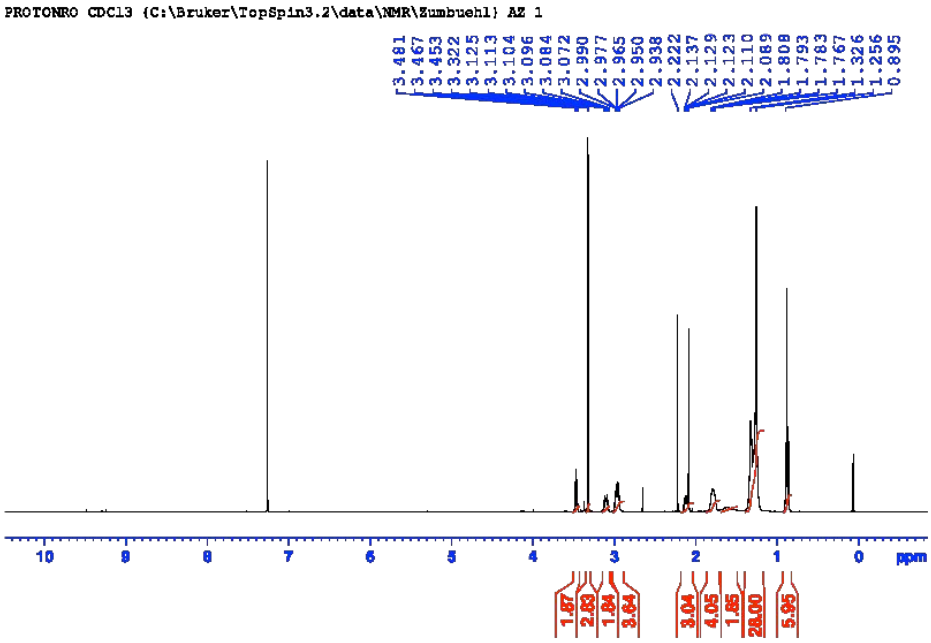

Figure S2: ^{1}H-NMR of *N*-decyl-*N*-(3-methyoxypropyl)decan-1-amine (**AL-A10**).

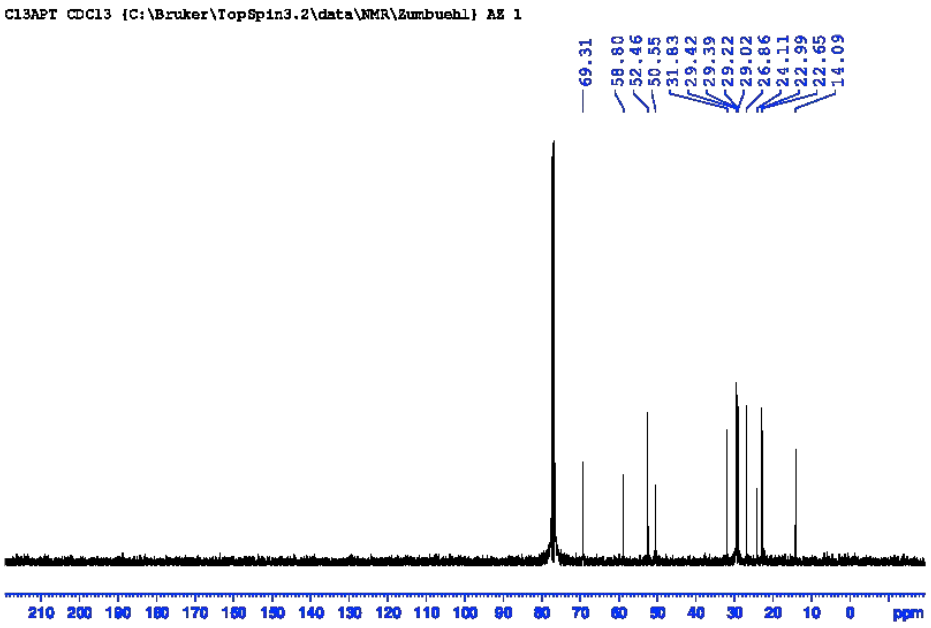

Figure S3: ^{13}C-NMR of *N*-decyl-*N*-(3-methyoxypropyl)decan-1-amine (**AL-A10**).

1.2 Synthesis of *N*-dodecyl-*N*-(3-methoxypropyl)dodecan-1-amine (AL-A12)

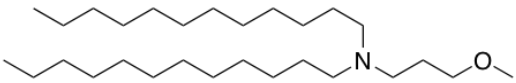

Figure S4: Chemical structure of *N*-dodecyl-*N*-(3-methoxypropyl)dodecan-1-amine (**AL-A12**).

3-Methoxypropylamine (1.00 eq., 5.00 mmol, 0.51 mL), and lauraldehyde (2.20 eq., 11.00 mmol, 2.44 mL) were dissolved in DCM (25 mL) and stirred for 3 h. Sodium triacetoxyborohydride (2.20 eq., 11.00 mmol, 2.33 g) was added and the mixture was stirred for 5 days. The product was purified by column chromatography (silica; DCM/MeOH (98:2 V/V) $\rightarrow$ DCM/MeOH 90:10 V/V)) to yield a yellow, viscous liquid (588 mg, 1.38 mmol, 28 %).

^{1}H NMR (400 MHz, $CDCl_3$) δ = 3.49-3.39 (m, 2H), 3.31 (s, 3H), 3.10-3.06 (m, 2H), 2.97-2.93 (m, 3H), 2.05-1.98 (m, 4H), 1.74-1.62 (m, 3H), 1.31-1.25 (m, 36H), 0.87 (t, *J* = 6.9 Hz, 6H) ppm.

^{13}C NMR (100 MHz, $CDCl_3$) δ = 69.5, 58.7, 52.0, 50.1, 31.9, 29.6, 29.6, 29.5, 29.3, 29.1, 26.8, 24.1, 23.0, 22.6, 14.1 ppm.

IR $\tilde{\nu}$ = 2923, 2823, 1717, 1567, 1466, 1379, 1251, 1118 cm^{-1}.

HRMS (ESI^{+}) : m/z [M+H]$^{+}$: calculated for $[C_{28}H_{59}NO+H]^{+}$: 426.4674; found: 426.4661.

R_f (DCM / MeOH (9:1 V/V)) = 0.61.

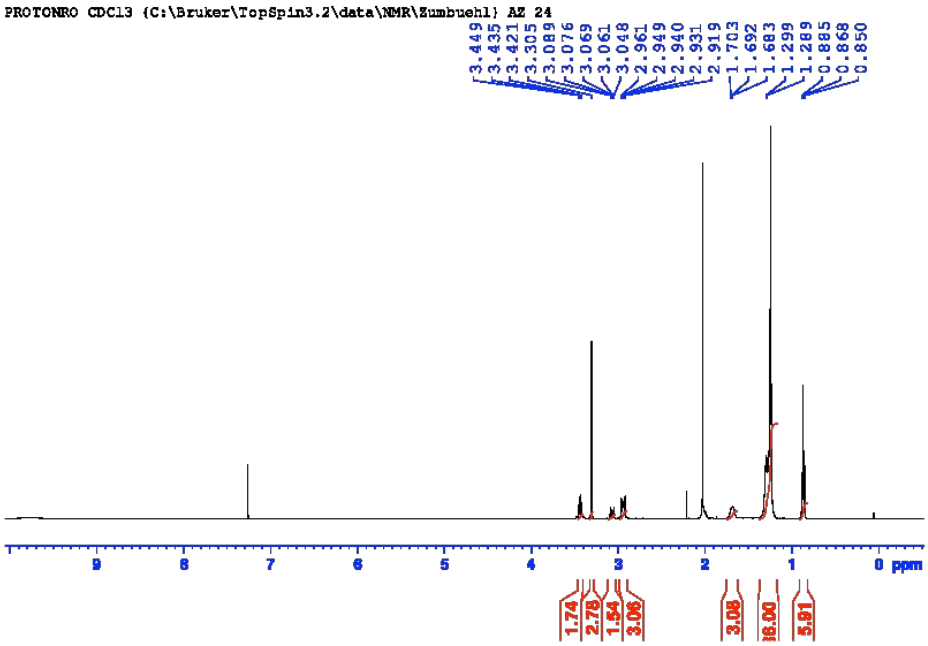

Figure S5: ^{1}H-NMR of *N*-dodecyl-*N*-(3-methoxypropyl)dodecan-1-amine (**AL-A12**).

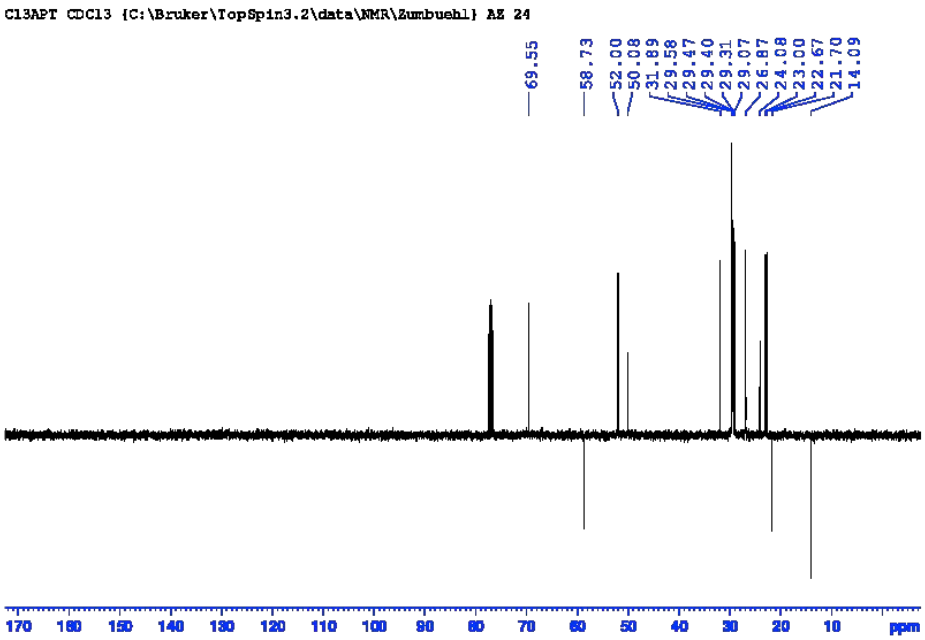

Figure S6: ^{13}C-NMR of *N*-dodecyl-*N*-(3-methoxypropyl)dodecan-1-amine (**AL-A12**).

1.3 Synthesis of 3-(didecylamino)propan-1-ol (**AL-B10**)

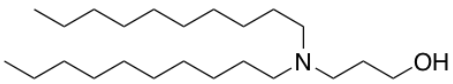

Figure S7: Chemical structure of 3-(didecylamino)propan-1-ol (**AL-B10**).

3-Amino-1-propanol (1.00 eq., 5.00 mmol, 0.38 mL) and decanal (2.20 eq., 11.00 mmol, 2.07 mL) were dissolved in DCM (25 mL) and stirred for 3 h. Sodium triacetoxyborohydride (2.20 eq., 11.00 mmol, 2.33 g) was added and the mixture was stirred for 5 days. The product was purified by column chromatography (silica; DCM/MeOH/H_2O (89:10:1 V/V/V)) to yield a slightly yellow, viscous liquid (1.380 g, 3.88 mmol, 78 %). Aldehyde is not fully reacted off.

^{1}H NMR (400 MHz, $CDCl_3$) δ = 3.75-3.72 (m, 2H), 3.14 (t, *J* =7.2 Hz, 2H), 2.97-2.93 (m, 4H), 1.92 (qui, *J* = 6.2 Hz, 2H), 1.65 (m, 4H), 1.30-1.25 (m, 28H), 0.87 (t, *J* = 6.8 Hz, 6H) ppm.

^{13}C NMR (100 MHz, $CDCl_3$) δ = 59.0, 51.9, 50.2, 31.8, 29.4, 29.4, 29.2, 29.1, 26.8, 22.9, 22.6, 22.0, 14.0 ppm.

IR $\tilde{\nu}$ = 2924, 2855, 1715, 1567, 1467, 1377, 1250, 1062, 1008 cm^{-1}.

HRMS (ESI$^+$) : m/z [M+H]$^+$: calculated for $[C_{23}H_{49}NO+H]^+$: 356.3892; found: 356.3880.

R_f (DCM / MeOH / H_2O, (89:10:1 V/V/V)) = 0.40.

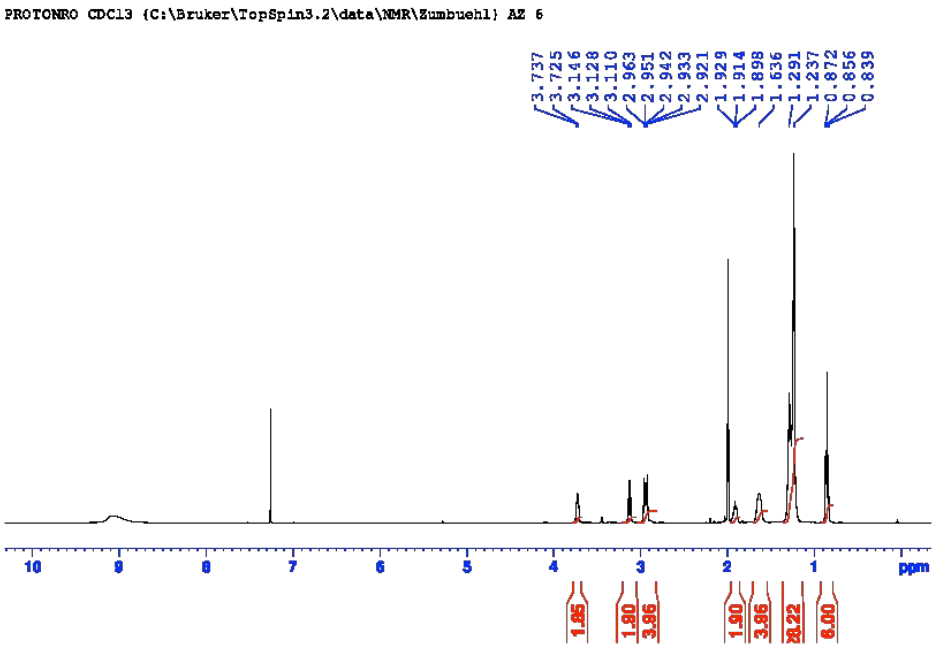

Figure S8: ^{1}H-NMR of 3-(didecylamino)propan-1-ol (**AL-B10**).

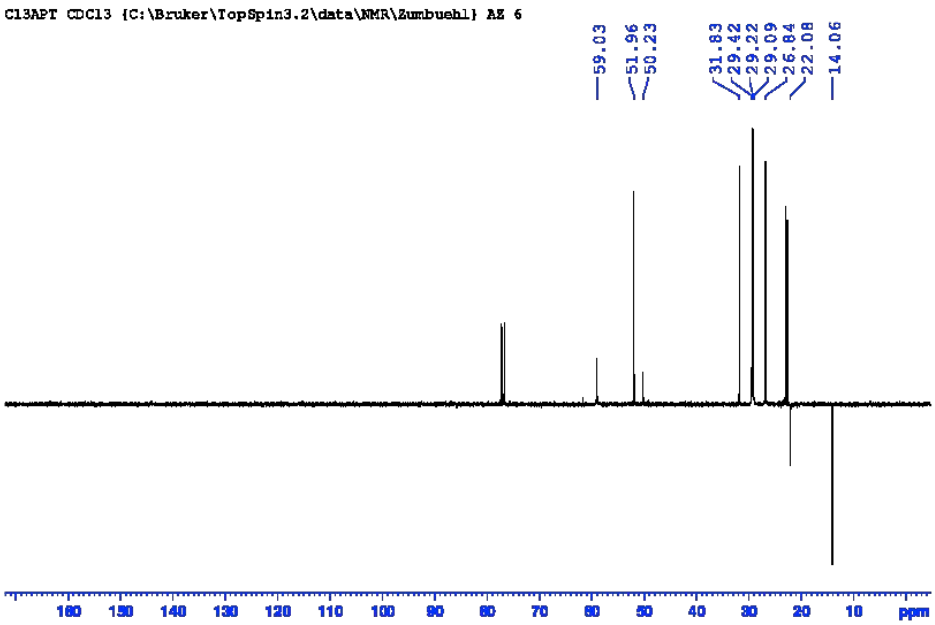

Figure S9: ^{13}C-NMR of 3-(didecylamino)propan-1-ol (**AL-B10**).

1.4 Synthesis of 3-(didodecylamino)propan-1-ol (AL-B12)

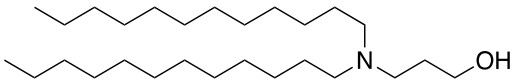

Figure S10: Chemical structure of 3-(didodecylamino)propan-1-ol (**AL-B12**).

3-Amino-1-propanol (1.00 eq., 5.00 mmol, 0.38 mL), lauraldehyde (2.20 eq, 11.00 mmol, 2.44 mL) and sodium triacetoxyborohydride (2.20 eq., 22.00 mmol, 2.33 g) were mixed in DCM and stirred for 2 days. The product was purified by column chromatography (silica, DCM/MeOH (95:5 V/V)) to yield a yellow liquid (428 mg, 1.04 mmol, 21 %). Aldehyde not fully reacted off.

^{1}H NMR (400 MHz, $CDCl_3$) δ = 3.76 (m, 2H), 3.47 (m, 1H), 3.21-3.17 (t, *J* = 7.2 Hz, 2H), 3.04-3.00 (m, 4H), 1.99-1.93 (q, *J* = 6.2 Hz, 2H), 1.68 (m, 4H), 1.30-1.24 (m, 36H), 0.88-0.85 (t, *J* = 6.7 Hz, 6H) ppm.

^{13}C NMR (100MHz, $CDCl_3$) δ = 61.4, 59.0, 52.0, 51.9, 31.8, 29.5, 29.3, 29.3, 29.0, 26.7, 26.3, 22.8, 22.6, 21.1, 14.0 ppm.

IR ν = 2924, 2855, 1713, 1379, 1237, 1008 cm^{-1}.

HRMS (ESI$^+$) : m/z [M+H]$^+$: calculated for $[C_{27}H_{57}NO + H]^+$: 412.4513; found : 412.4512

R_f (DCM/MeOH (95:5 V/V)): 0.67.

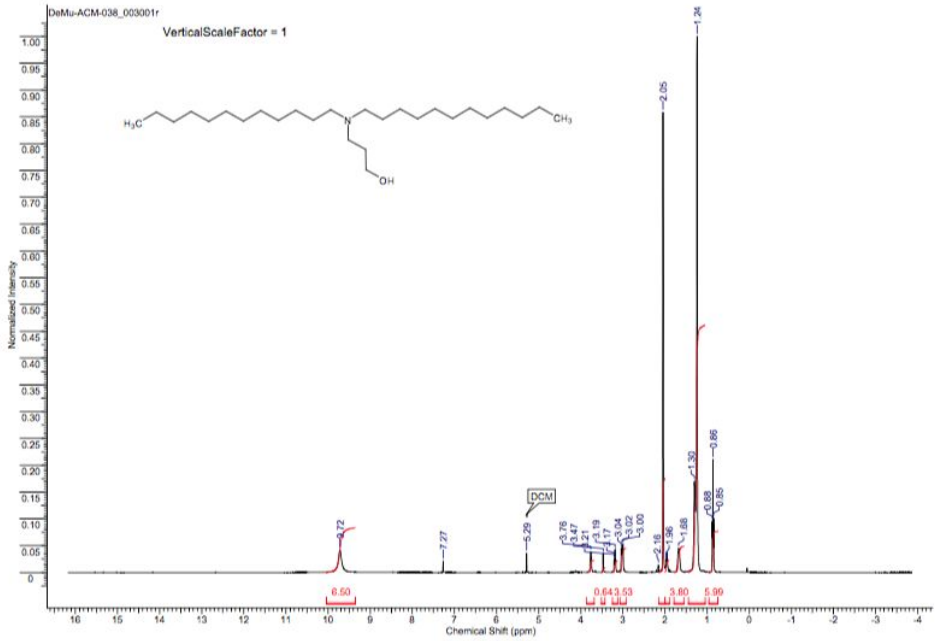

Figure S11: ^{1}H-NMR of 3-(didodecylamino)propan-1-ol (**AL-B12**).

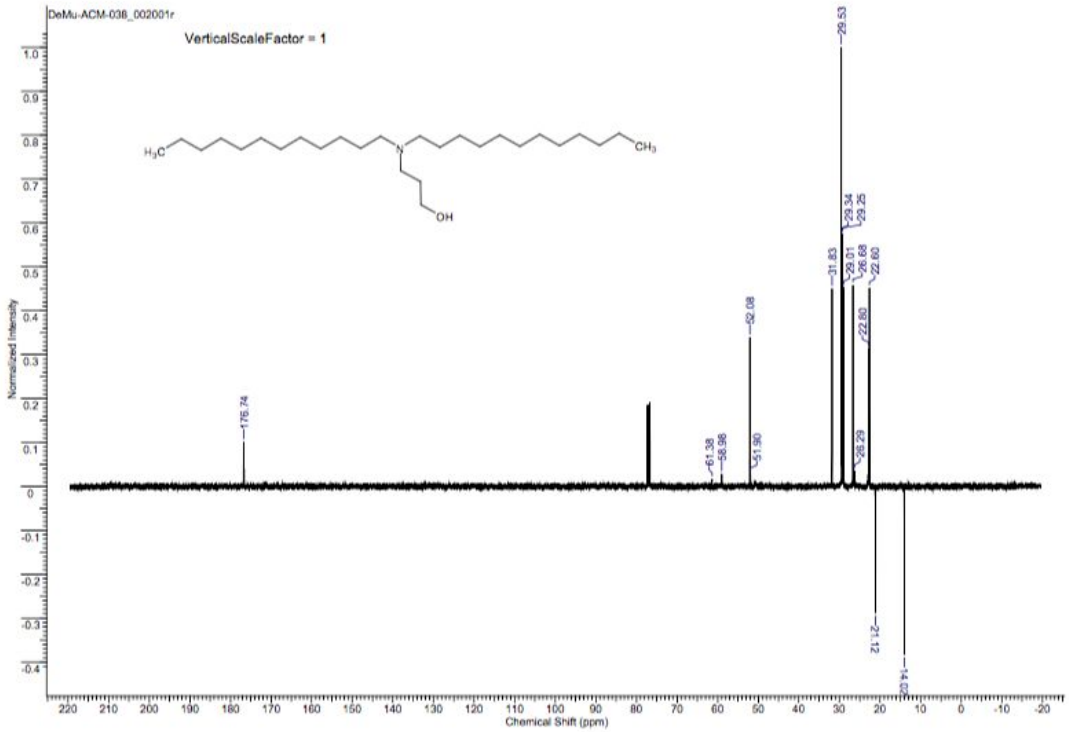

Figure S12: ^{13}C-NMR of 3-(didodecylamino)propan-1-ol (**AL-B12**).

1.5 Synthesis of 3-(didecylamino)propane-1,2-diol (**AL-C10**)

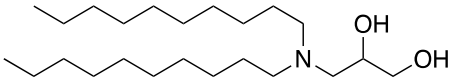

Figure S13: Chemical structure of 3-(didecylamino)propane-1,2-diol (**AL-C10**).

(±)-3-Amino-1,2-propanediol (1.00 eq., 5.00 mmol, 0.51 mL), decanal (2.20 eq, 11.00 mmol, 2.07 mL) and sodium triacetoxyborohydride (2.20 eq., 11.00 mmol, 2.33 g) were mixed in DCM and stirred for 2 days. The product was purified by column chromatography (silica; EtOAc/MeOH (98:2 V/V) → EtOAc/MeOH (90:10 V/V)) to yield a yellow liquid (773 mg, 2.081 mmol, 42 %).

NMR data still showed impurities after several purification steps.

HRMS (ESI$^+$) : m/z [M+H]$^+$: calculated for $[C_{23}H_{49}NO_2 + H]^+$: 372.3836; found : 372.3831

R_f (EtOAc/MeOH (90:10 V/V)): 0.25.

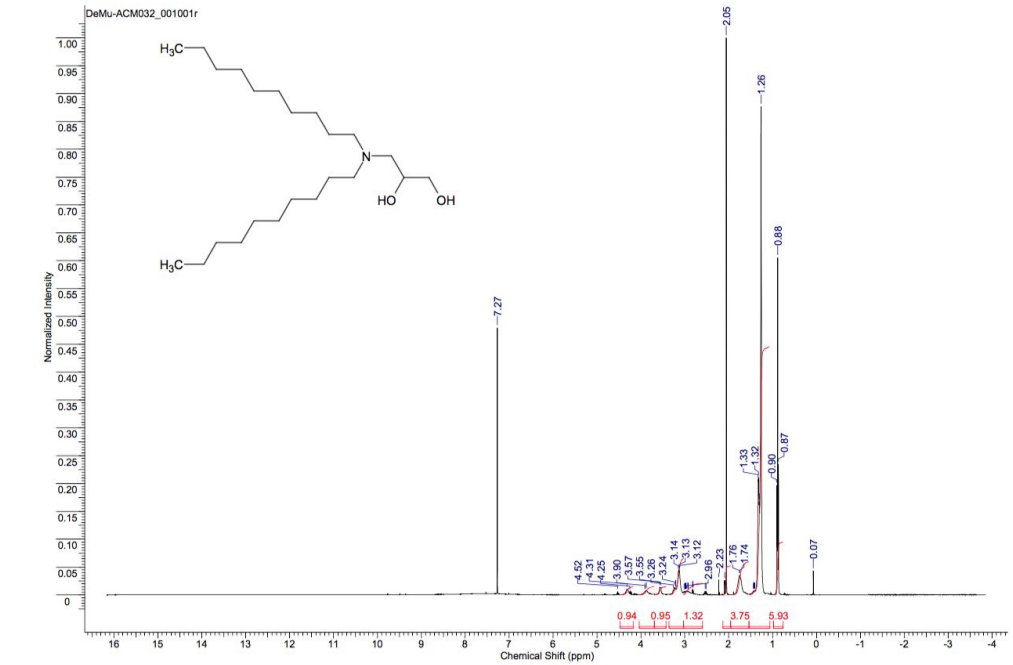

Figure S14: ^{1}H-NMR of 3-(didecylamino)propane-1,2-diol (**AL-C10**).

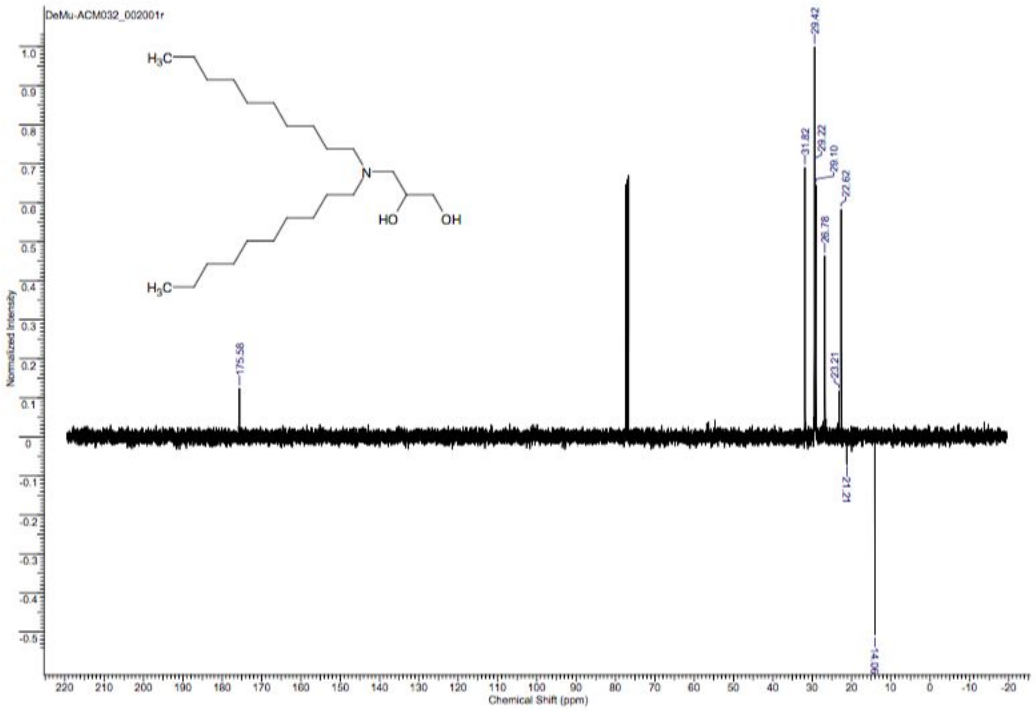

Figure S15: ^{13}C-NMR of 3-(didecylamino)propane-1,2-diol (**AL-C10**).

1.6 Synthesis 3-(didodecylamino)-1,2-propanediol (**AL-C12**)

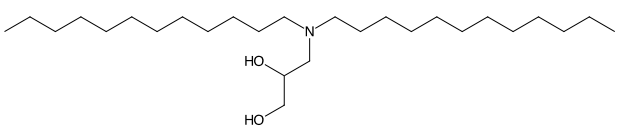

Figure S16: Chemical structure of 3-(didodecylamino)-1,2-propanediol (**AL-C12**).

(±)-3-Amino-1,2-propanediol (1.00 eq., 5.00 mmol, 0.51 mL), lauraldehyde (2.20 eq, 11.00 mmol, 2.44 mL) and sodium triacetoxyborohydride (2.20 eq., 11.00 mmol, 2.33 g) were mixed in DCM and stirred for 2 days. The product was purified by column chromatography (silica; DCM/MeOH (98:2 V/V)). The yield was too low to be determined, but still sufficient for characterization by NMR and HRMS.

^{1}H NMR (600 MHz, $CDCl_3$) δ = 4.17-4.11 (m, 1H), 3.73-3.67 (m, 1H), 3.62-3.56 (m, 1H), 3.18-2.93 (m, 5H), 1.75-1.57 (m, 2H),1.36-1.20 (m, 38H), 0.91-0.85 (m, 6H) ppm.

^{13}C NMR (150 MHz, CDCl3) δ = 66.8, 64.7, 57.3, 54.2, 32.1, 29.8, 29.8, 29.7, 29.6, 29.5, 29.4, 27.1, 23.8, 22.9, 14.3 ppm.

HRMS (ESI$^+$): m/z [M+H]$^+$: calculated for $[C_{27}H_{57}NO_2 + H]^+$: 428.4462; found: 428.4462.

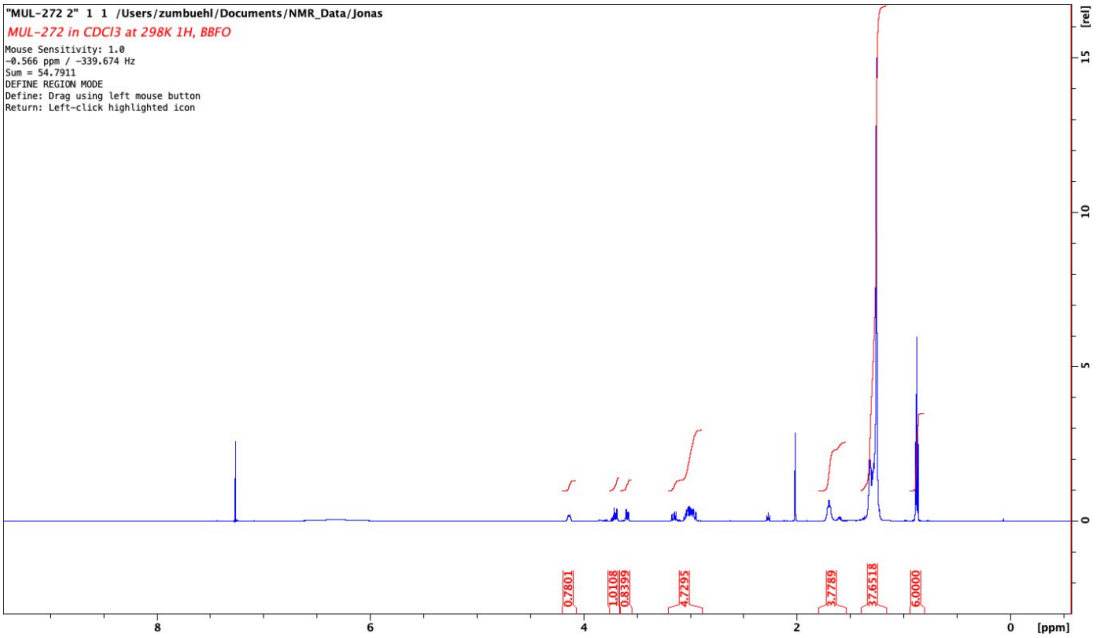

Figure S17: ^{1}H-NMR of 3-(Didodecylamino)-1,2-propanediol (**AL-C12**).

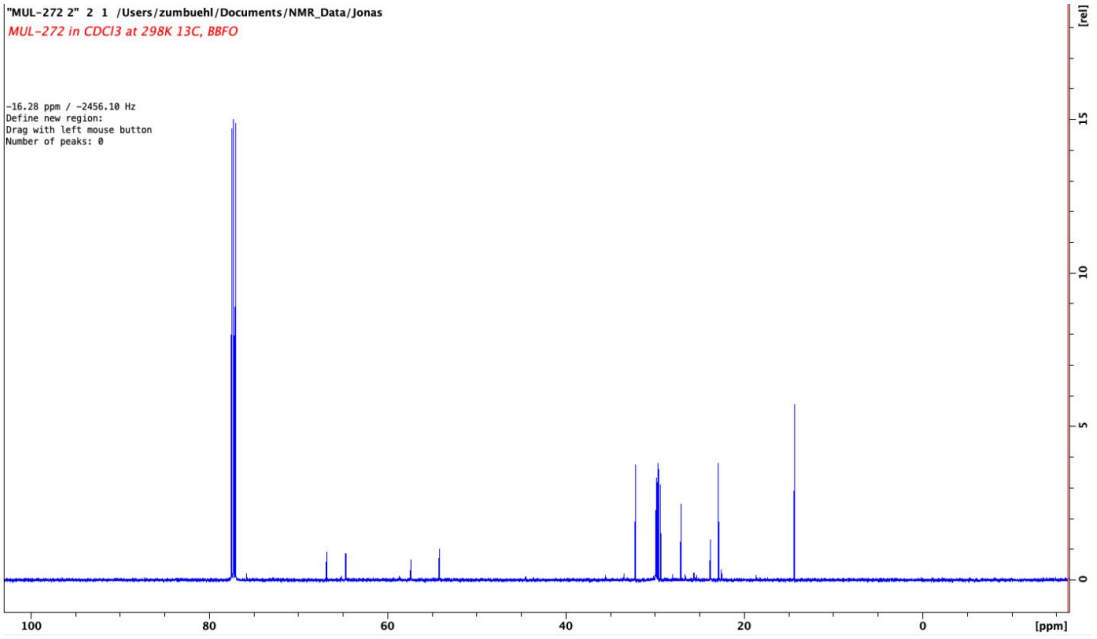

Figure S18: ^{13}C-NMR of 3-(Didodecylamino)-1,2-propanediol (**AL-C12**).

1.7 Synthesis of *N*,*N*-didecyl-*N*,*N*-dimethylethane-1,2-diamine (**AL-D10**)

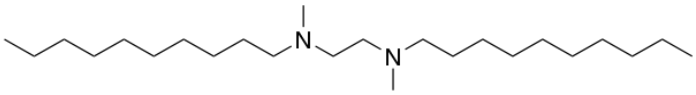

Figure S19: Chemical structure of *N*,*N*'-didecyl-*N*,*N*'-dimethylethane-1,2-diamine (**AL-D10**).

N,*N*''-Dimethylethylenediamine (1.00 eq., 5.00 mmol, 0.54 mL), and decanal (2.20 eq., 11.00 mmol, 2.07 mL) were dissolved in DCM (25 mL) and stirred for 3 h. Sodium triacetoxyborohydride (2.20 eq., 11.00 mmol, 2.33 g) was added and the reaction was stirred for 2 days. The product was purified by column chromatography (silica; DCM/MeOH/H_2O (89:10:1 V/V/V)) to yield a slightly yellow, cloudy and viscous liquid (1.924 g, 5.21 mmol). Aldehyde not fully reacted off.

^{1}H NMR (400 MHz, $CDCl_3$) δ = 3.04 (s, 4H), 2.75-2.71 (m, 4H), 2.53 (s, 6H), 1.61-1.57 (m, 4H), 1.28-1.25 (m, 28H), 0.87 (t, *J* = 6.9 Hz, 12 H) ppm.

^{13}C NMR (100 MHz, $CDCl_3$) δ = 56.8, 51.6, 40.6, 31.8, 29.4, 29.2, 27.0, 24.8, 22.6, 21.8, 14.0 ppm.

IR ν = 2924, 2854, 1713, 1568, 1466, 1406, 1377, 1257 cm^{-1}.

HRMS (ESI$^+$) : m/z [M+H]$^+$: calculated for $[C_{24}H_{52}N_2+H]^+$: 369.4209; found: 369.4209.

R_f (DCM / MeOH / H_2O, (89:10:1 V/V/V)) = 0.39.

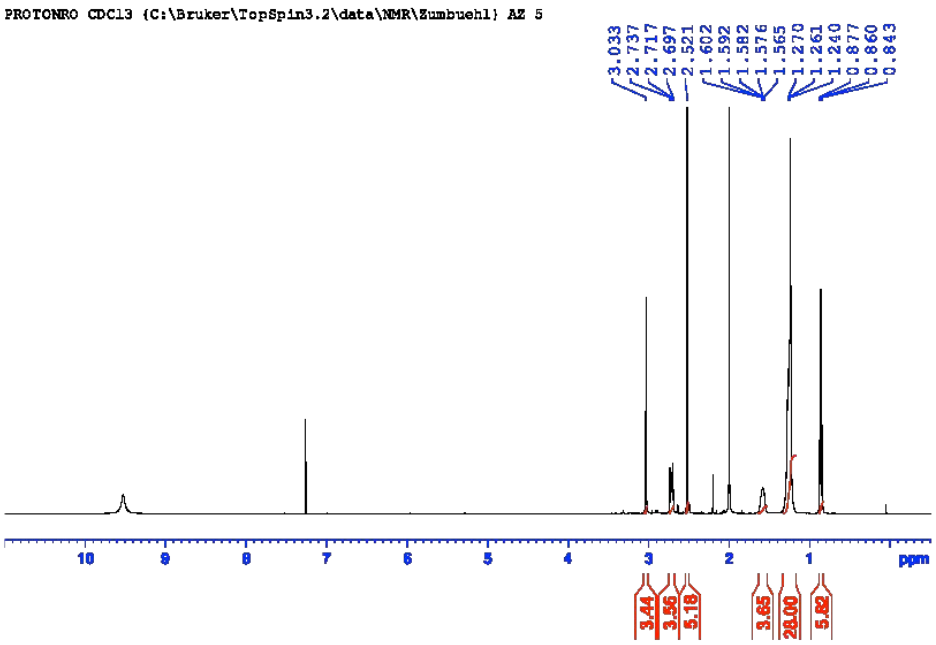

Figure S20: ^{1}H-NMR of *N,N'*-didecyl-*N,N'*-dimethylethane-1,2-diamine (**AL-D10**).

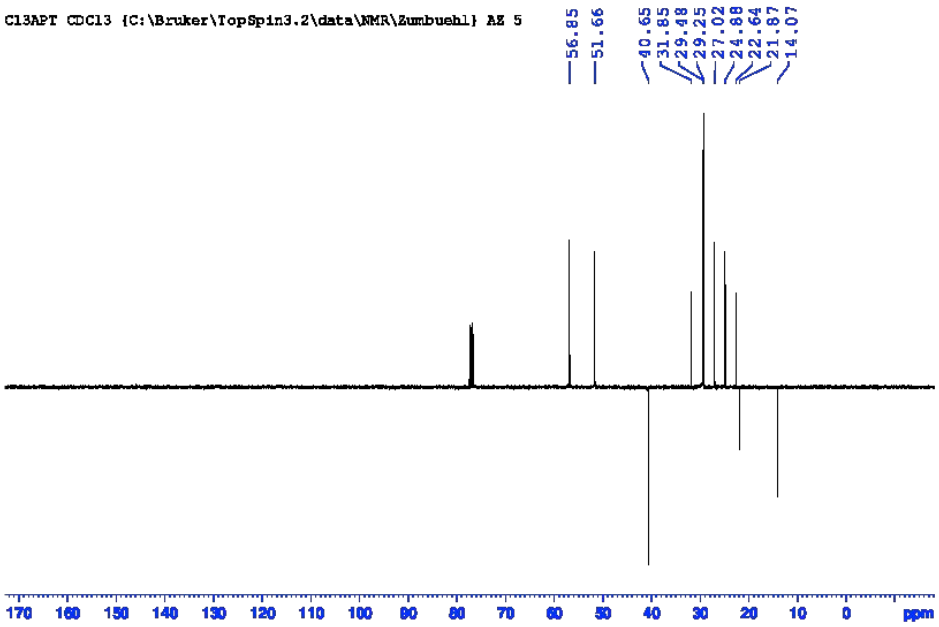

Figure S21: ^{13}C-NMR of *N,N'*-didecyl-*N,N'*-dimethylethane-1,2-diamine (**AL-D10**).

1.8 Synthesis of *N,N,N',N'*-Tetrakis(decyl)propane-1,3-diamine (**AL-E10**)

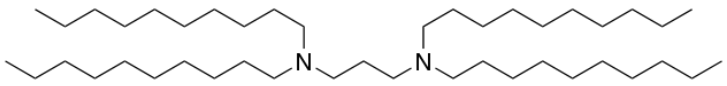

Figure S22: Chemical structure of *N,N,N',N'*-Tetrakis(decyl)propane-1,3-diamine (**AL-E10**).

1,3-Diaminopropane (1.00 eq., 5.00 mmol, 0.42 mL), and decanal (4.40 eq., 22.00 mmol, 4.14 mL) were dissolved in DCM (25 mL) and stirred for 3 h. Sodium triacetoxyborohydride (4.40 eq., 22.00 mmol, 4.66 g) was added and the reaction was stirred for 2 days. The product was purified by column chromatography (silica; EtOAc/MeOH (98:2) → EtOAc/MeOH (90:10)) to yield a slightly yellow liquid (855 mg, 1.36 mmol, 27 %).

^{1}H NMR (400 MHz, $CDCl_3$) δ = 3.10 (m, 4H), 2.95-2.91 (m, 8H), 2.43-2.39 (m, 2H), 1.77-1.66 (m, 8H), 1.33-1.27 (m, 56H), 0.89 (t *J* = 7.0 Hz, 12H) ppm.

^{13}C NMR (100 MHz, $CDCl_3$) δ = 52.5, 51.0, 31.8, 29.4, 29.4, 29.2, 29.1, 26.9, 23.4, 22.6, 14.1 ppm.

IR $\tilde{\nu}$ = 2922, 2853, 1715, 1571, 1466, 1377, 1259 cm^{-1}.

HRMS (ESI$^+$): m/z [M+H]$^+$: calculated for $[C_{43}H_{90}N_2+H]^+$: 635.7182; found: 635.7178.

R_f (EtOAc / MeOH (9:1 V/V)) = 0.54.

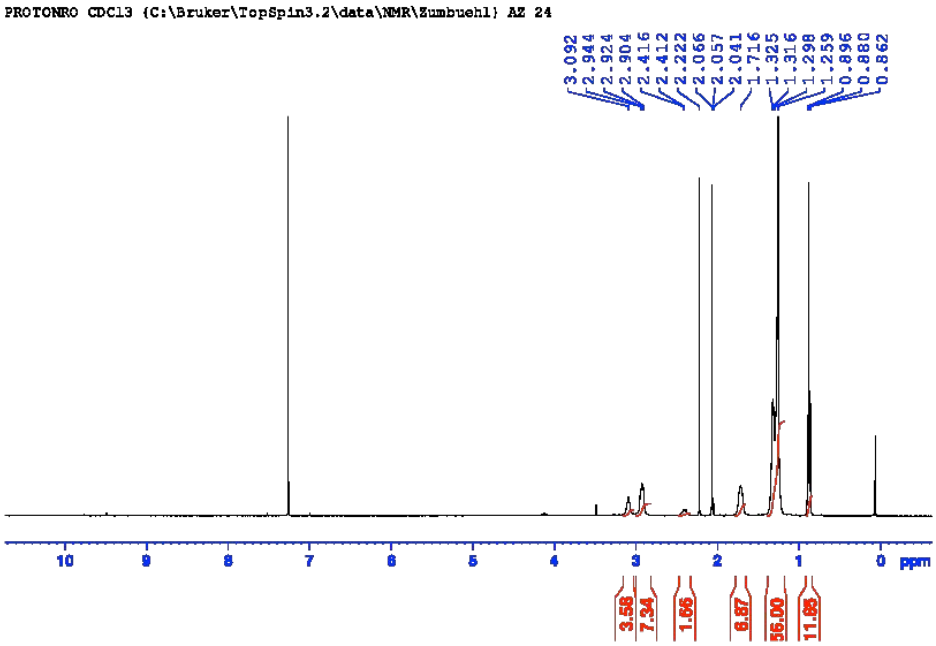

Figure S23: [1]H-NMR of *N,N,N',N'*-Tetrakis(decyl)propane-1,3-diamine (**AL-E10**).

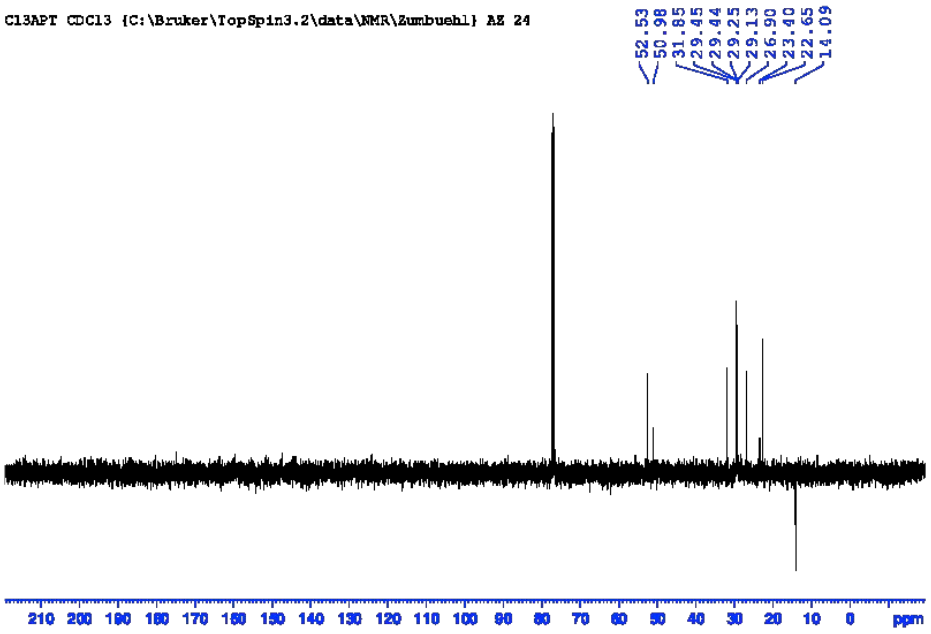

Figure S24: [13]C-NMR of *N,N,N',N'*-Tetrakis(decyl)propane-1,3-diamine (**AL-E10**).

1.9 Synthesis of *N,N,N',N'*-tetradodecylpropane-1,3-diamine (**AL-E12**)

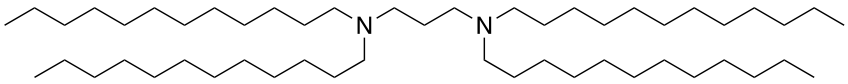

Figure S25: Chemical structure of *N,N,N',N'*-tetradodecylpropane-1,3-diamine (**AL-E12**).

1,3-Diaminopropane (1.00 eq., 5.00 mmol, 0.42 mL), lauraldehyde (4.40 eq, 22.00 mmol, 4.88 mL) and sodium triacetoxyborohydride (4.40 eq., 22.00 mmol, 4.66 g) were mixed in DCM and stirred for 5 days. The product was purified by column chromatography (silica; DCM/MeOH (98:2 V/V)) to yield a yellow liquid (26 mg, 0.04 mmol, <1 %). Aldehyde not fully reacted off.

^{1}H NMR (400 MHz, $CDCl_3$) δ = 3.10-3.06 (t, *J* = 7.8 Hz 4H), 2.96-2.92 (q, *J* = 4.2 Hz, 8H), 2.24-2.08 (m, 2H), 1.61 (m, 8H), 1.29-1.25 (m, 72H), 0.89-0.85 (t, *J* = 6.9 Hz, 12H) ppm.

^{13}C NMR (100 MHz, CDCl3) δ = 51.8, 51.6, 49.8, 31.9, 29.6, 29.3, 29.1, 26.8, 22.9, 20.0, 22.6, 21.7, 14.0 ppm.

IR ν̃ = 2923, 2854, 1714, 1565, 1467, 1361, 1252, 1008 cm^{-1}.

HRMS (ESI$^+$): m/z [M+H]$^+$: calculated for $[C_{51}H_{106}N_2 + H]^+$: 747.8429; found : 747.8426

R_f (DCM/MeOH (98:2 V/V)): 0.16.

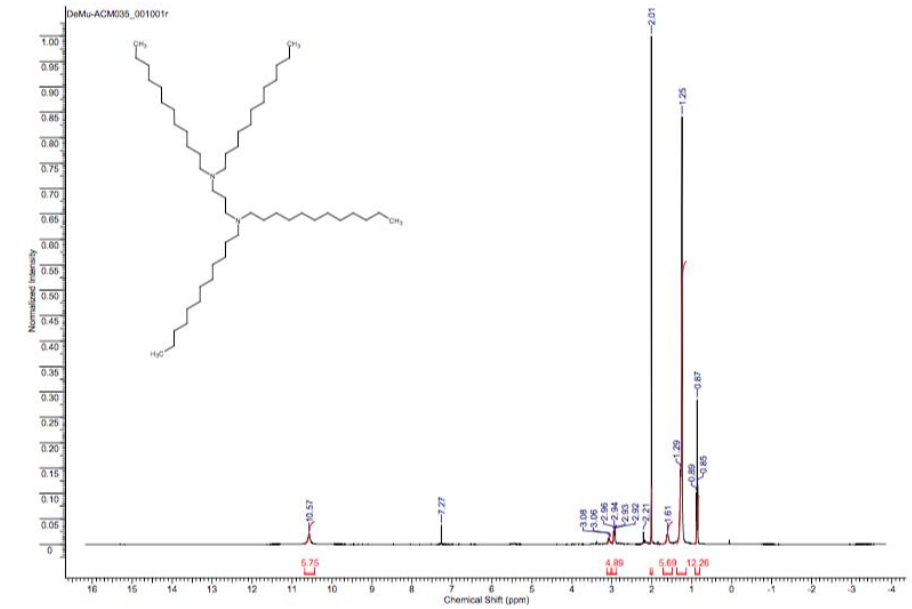

Figure S26: ^{1}H-NMR of *N,N,N'*,*N'*-tetradodecylpropane-1,3-diamine (**AL-E12**).

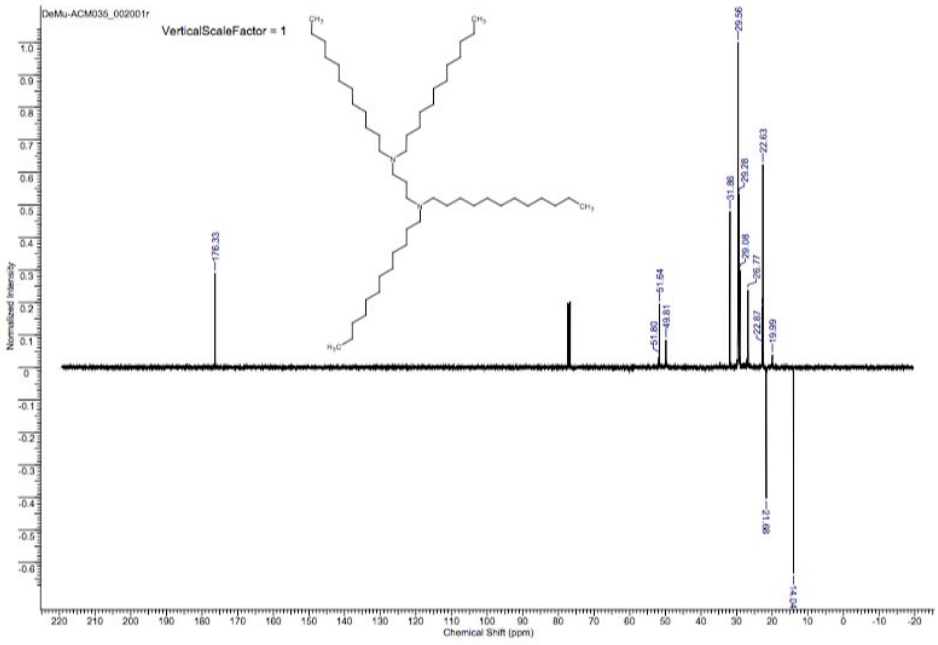

Figure S27: ^{13}C-NMR of *N,N,N'*,*N'*-tetradodecylpropane-1,3-diamine (**AL-E12**).

1.10 Synthesis of (Benzyl)didecylamine (**AL-F10**)

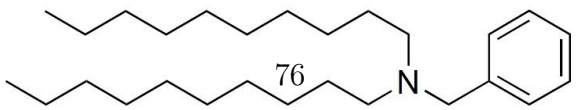

Figure S28: Chemical structure of (Benzyl)didecylamine (**AL-F10**).

Benzylamine (1.00 eq., 5.00 mmol, 0.55 mL), and decanal (2.20 eq., 11.00 mmol, 2.07 mL) were dissolved in DCM (25 mL) and stirred for 3 h. Sodium triacetoxyborohydride (2.20 eq., 11.00 mmol, 2.33 g) was added and the mixture was stirred for 2 days. The product was purified by column chromatography (Silica; EtOAc/MeOH (98:2 V/V) → EtOAc/MeOH (90:10 V/V)) to yield a dark yellow liquid (666 mg, 1.72 mmol, 34.4 %).

^{1}H-NMR (400 MHz, $CDCl_3$): δ = 7.27 – 7.10 (m, 5H), 3.46 (s, 2H), 2.36 – 2.26 (m, 4H), 1.45 – 1.31 (m, 4H), 1.17 (s, 28H), 0.81 (t, *J* = 6.8 Hz, 6H) ppm.

^{13}C-NMR (100 MHz, $CDCl_3$): δ = 140.5, 129.0, 128.2, 126.7, 58.8, 54.0, 32.1, 29.83, 29.77, 29.75, 29.5, 27.5, 27.2, 22.8, 14.3 ppm.

HRMS (ESI$^+$): m/z [M+H]$^+$: calculated for $[C_{27}H_{49}N + H]^+$: 388.3938; found : 388.3933.

R_f(DCM:MeOH (92:8 V/V)): 0.94.

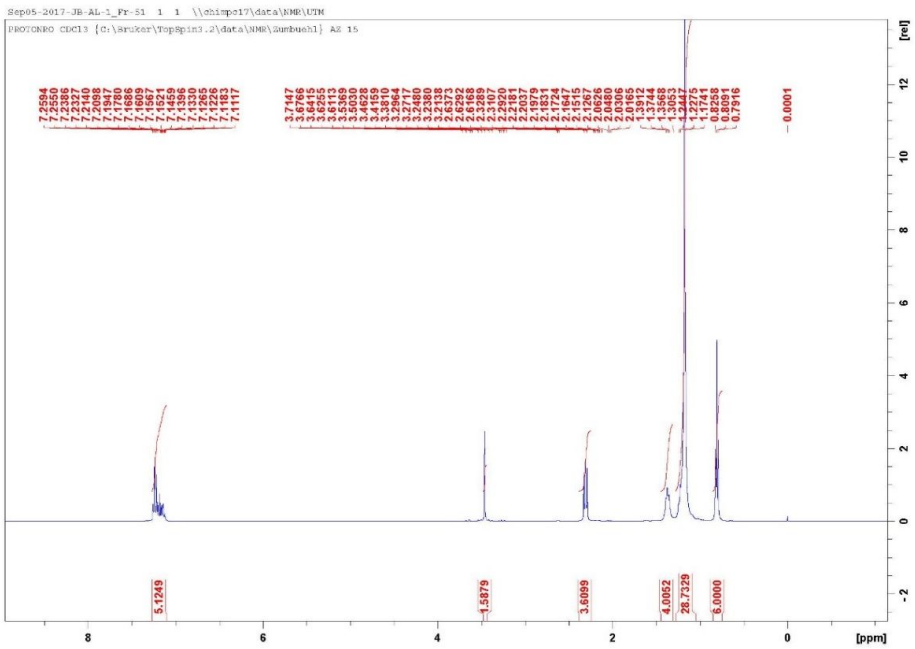

Figure S29: ^{1}H-NMR of (Benzyl)didecylamine (**AL-F10**).

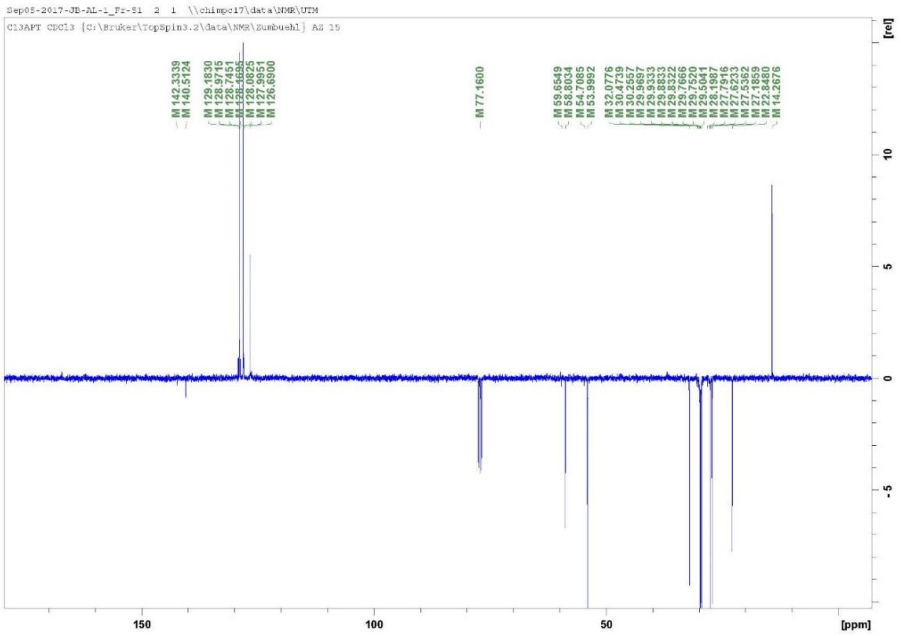

Figure S30: ^{13}C-NMR of (Benzyl)didecylamine (**AL-F10**).

1.11 Synthesis of [(1*H*-Imidazol-2-yl)methyl]didecylamine (AL-G10)

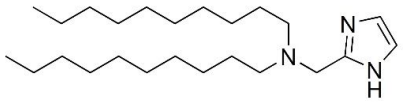

Figure S31: Chemical structure of [(1*H*-Imidazol-2-yl)methyl]didecylamine (**AL-G10**).

2-(Aminomethyl)imidazole dihydrochloride (1.00 eq., 5.00 mmol, 0.85 g), and decanal (2.20 eq., 11.00 mmol, 2.07 mL) were dissolved in DCM (25 mL) and stirred for 3 h. Sodium triacetoxyborohydride (2.20 eq., 11.00 mmol, 2.33 g) was added and the mixture was stirred for 2 days. The product was purified by column chromatography (Silica; EtOAc/MeOH (98:2 V/V) → EtOAc/MeOH (90:10 V/V)) to yield a yellow liquid (1.36 g, 3.59 mmol, 71.9 %).

^{1}H-NMR (400 MHz, $CDCl_3$): δ = 11.23 (br s, 2H), 7.01 – 6.93 (m, 2H), 5.22 (s, 1H), 4.39 (s, 1H), 3.58 – 3.55 (m, 1 H), 2.86 – 2.81 (m, 2H), 1.98 (br s, 4H), 1.58 – 1.46 (m, 3H), 1.18 (br s, 28H), 0.83 – 0.79 (m, 6H) ppm.

The integrals are not fitting well due to impurities which could not be removed by chromatography. Residual solvent peaks were found for DCM (5.33 ppm) and EtOAc 1.26 (s), 2.05 (t), 4.12 (q)

^{13}C-NMR (100 MHz, $CDCl_3$): δ = 138.1, 122.9, 63.1, 52.9, 49.5, 37.7, 34.6, 32.9, 32.0, 32.0, 29.7, 29.7, 29.6, 29.6, 29.6, 29.5, 29.4, 29.3, 29.2, 29.0, 27.3, 27.3, 26.9, 25.9, 23.4, 22.8, 22.2, 14.2 ppm.

HRMS (ESI$^+$): m/z [M+H]$^+$: calculated for $[C_{24}H_{47}N_3 + H]^+$: 378.3843; found : 378.3843.

R_f(DCM:MeOH (92:8 V/V)): 0.64.

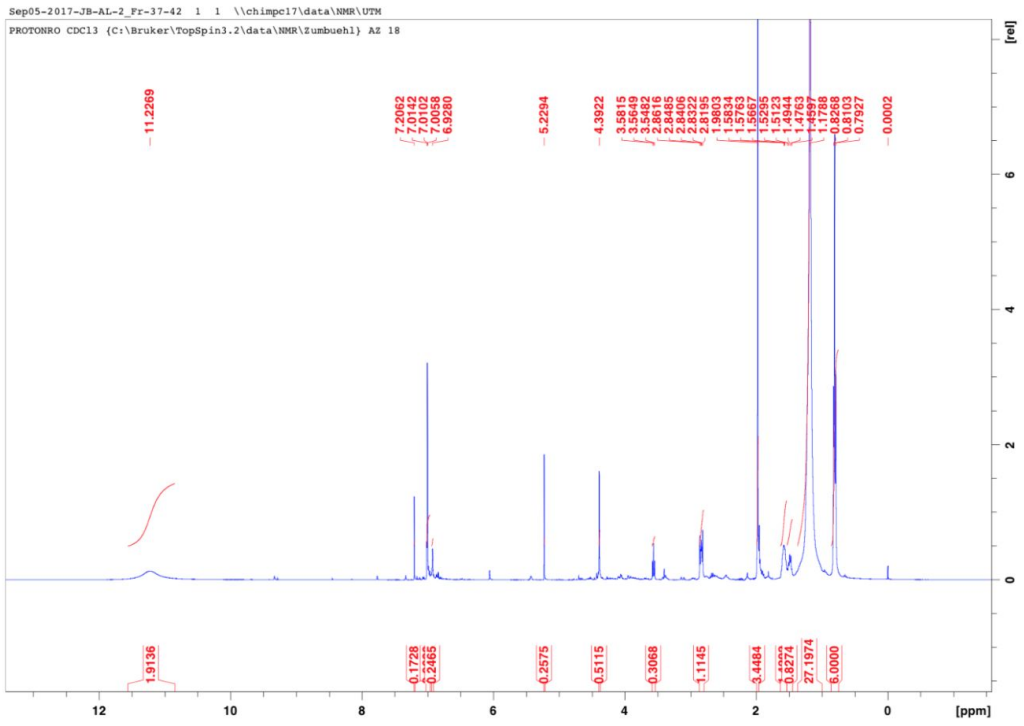

Figure S32: ^{1}H-NMR of [(1*H*-Imidazol-2-yl)methyl]didecylamine (**AL-G10**).

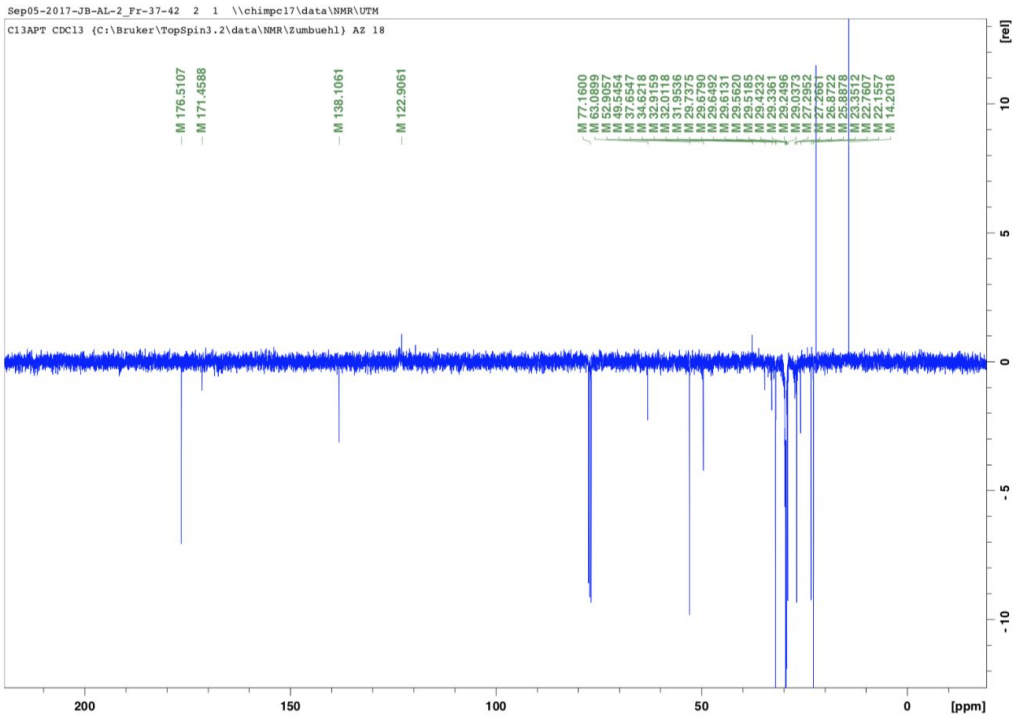

Figure S33: ^{13}C-NMR of [(1*H*-Imidazol-2-yl)methyl]didecylamine (**AL-G10**).

1.12 Synthesis [(4-Pyridyl)methyl]didecylamine (AL-H10)

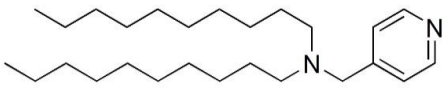

Figure S34: Chemical structure of [(4-Pyridyl)methyl]didecylamine (**AL-H10**).

4-(Aminomethyl)pyridine (1.00 eq., 5.00 mmol, 0.51 mL), and decanal (2.20 eq., 11.00 mmol, 2.07 mL) were dissolved in DCM (25 mL) and stirred for 3 h. Sodium triacetoxyborohydride (2.20 eq., 11.00 mmol, 2.33 g) was added and the mixture was stirred for 2 days. The product was purified by column chromatography (Silica; EtOAc/MeOH (98:2 V/V) → EtOAc/MeOH (90:10 V/V)) to yield a brown liquid (1.75 g, 4.51 mmol, 90.1 %). The spectrum still shows small acetic acid contaminations at approx. 2.1 ppm (^{1}H-NMR), 175 ppm, and 21 ppm (both ^{13}C-NMR) that could not be removed with column chromatography.

^{1}H-NMR (400 MHz, $CDCl_3$): δ = 8.54 – 8.49 (m, 2H), 7.32 – 7.29 (m, 2H), 3.56 (s, 2H), 2.44 – 2.36 (m, 4H), 1.49 – 1.39 (m, 4H), 1.24 (s, 28H), 0.87 (t, *J* = 6.8 Hz, 6H) ppm.

^{13}C-NMR (100 MHz, $CDCl_3$): δ = 150.3, 149.1, 124.0, 57.8, 54.2, 32.0, 29.8, 29.71, 29.66, 29.5, 27.5, 27.0, 22.8, 14.2 ppm.

HRMS (ESI^+): m/z [M+H]$^+$: calculated for $[C_{26}H_{48}N_2 + H]^+$: 389.3890; found : 389.3890.

R_f(DCM:MeOH (92:8 V/V)): 0.78.

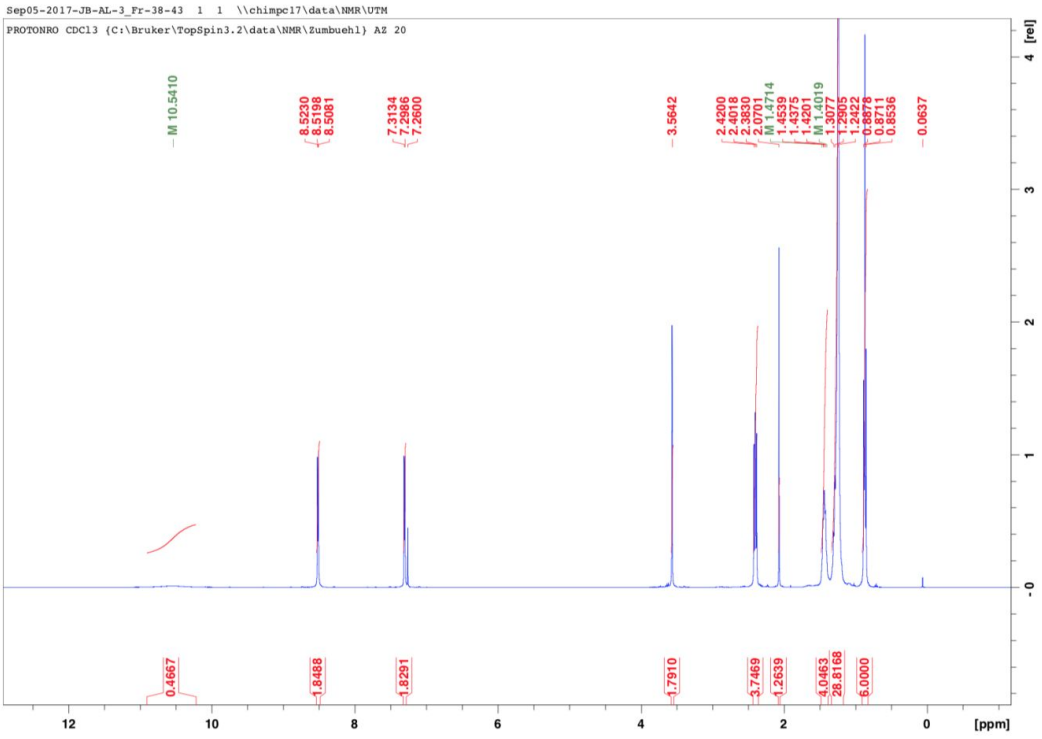

Figure S35: ^{1}H-NMR of [(4-Pyridyl)methyl]didecylamine (**AL-H10**).

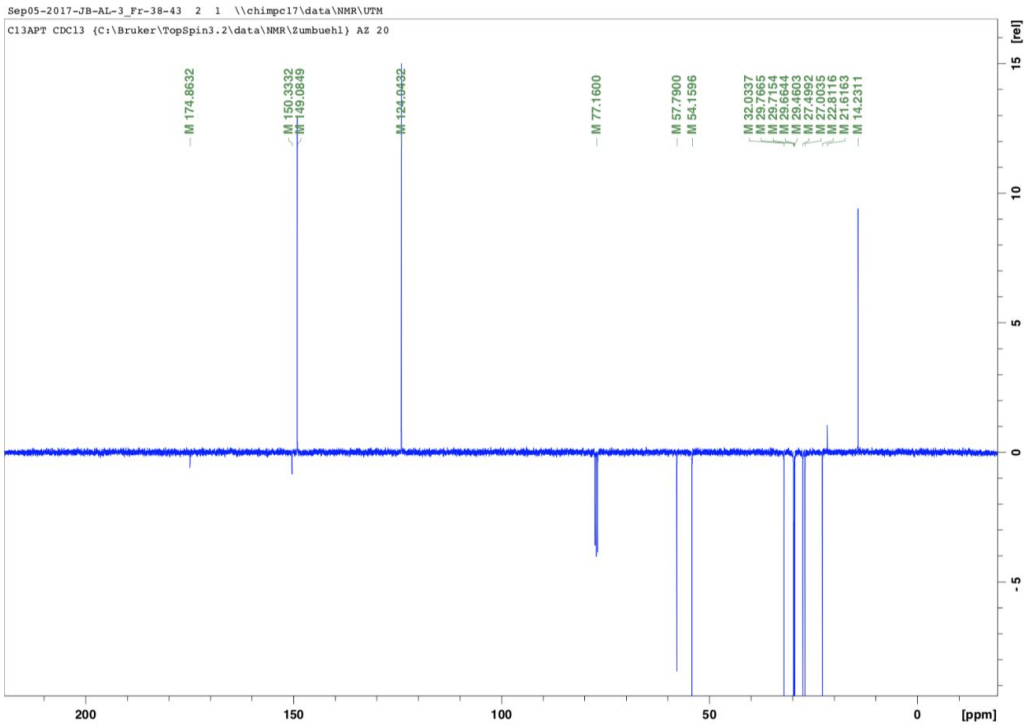

Figure S36: ^{13}C-NMR of [(4-Pyridyl)methyl]didecylamine (**AL-H10**).

2. *In vitro* experiments

2.1 Transfection experiments

Table S1: Results of transfection experiments for aminolipid- and DOTAP:chol-based lipoplexes.

Substance	Setting	GFP positive cells [%]	MFI [RFU]
AL-A10	1 µg DNA, 1:1 ratio	7.7	801
	2 µg DNA, 1:1 ratio	28.7	1033
AL-A12	1 µg DNA, 1:1 ratio	10.3	785
	2 µg DNA, 1:1 ratio	31.5	1606
AL-B10	1 µg DNA, 1:1 ratio	5.0	384
	2 µg DNA, 1:1 ratio	11.5	928
AL-B12	1 µg DNA, 1:1 ratio	8.6	469
	2 µg DNA, 1:1 ratio	8.3	358
AL-C10	1 µg DNA, 1:1 ratio	8.3	487
	2 µg DNA, 1:1 ratio	9.5	215
AL-C12	1 µg DNA, 1:1 ratio	6.0	658
	2 µg DNA, 1:1 ratio	4.2	451
AL-D10	1 µg DNA, 1:1 ratio	7.9	354
	2 µg DNA, 1:1 ratio	11.6	224
AL-E10	1 µg DNA, 1:1 ratio	4.7	577
	2 µg DNA, 1:1 ratio	11.5	928

AL-F10	1 µg DNA, 1:1 ratio	4.5	906
AL-G10	1 µg DNA, 1:1 ratio	4.7	714
AL-H10	1 µg DNA, 1:1 ratio	2.7	764
DOTAP:chol	1 µg DNA, 1:1 ratio	5.7	507
	2 µg DNA, 1:1 ratio	13.2	756
Lipofectamine 3000	1 µg DNA, 1:1 ratio	47.5	7632

2.2 Cytotoxicity experiments

Table S2: LC10, LC50, and LC90 values corresponding to 90%, 50%, and 10% cell viability for aminolipid- and DOTAP:chol-based systems. The values were calculated from MTT-assay data using the non-linear dose-response function in Origin 2018.

Substance	LC10 (90% viability) [µM]	LC50 (50% viability) [µM]	LC90 (10% viability) [µM]
AL-A10	3.7	16.8	76.5
AL-A12	4.2	43.9	456.9
AL-B10	5.4	9.3	15.9
AL-B12	4.1	9.3	21.1
AL-C10	2.2	4.8	10.4
AL-C12	0.8	9.7	120.3
AL-D10	0.9	3.0	9.5
AL-E10	1.7	20.6	251.9
AL-F10	2.2	75.3	2548.8
AL-G10	9.7	42.2	182.7
AL-H10	2.0	20.6	213.7
DOTAP:chol	2.4	24.4	254.6

Table S3: Average cell viability results of three MTT assays.

Substance	% Survival (4 µM)	% Survival (16 µM)	% Survival (25 µM)	% Survival (64 µM)	% Survival (128 µM)
AL-A10	77.5 ± 0.7	72.9 ± 1.0	65.3 ± 0.4	7.2 ± 0.3	2.5 ± 0.4
AL-A12	96.3 ± 0.7	88.9 ± 1.9	78.2 ± 2.8	48.2 ± 0.6	33.6 ± 0.5
AL-B10	79.2 ± 0.9	69.2 ± 0.6	3.4 ± 0.0	1.7 ± 0.2	1.7 ± 0.2
AL-B12	80.2 ± 1.8	67.4 ± 0.7	13.4 ± 0.2	2.0 ± 0.2	3.1 ± 1.9
AL-C10	62.8 ± 1.1	2.9 ± 0.1	1.4 ± 0.0	2.0 ± 0.6	2.2 ± 0.7
AL-C12	58.3 ± 0.2	53.6 ± 0.6	34.7 ± 0.3	3.6 ± 1.8	3.6 ± 0.1
AL-D10	36.5 ± 1.1	2.4 ± 0.1	3.3 ± 0.4	3.4 ± 0.1	3.5 ± 0.2
AL-E10	71.8 ± 1.5	62.2 ± 0.9	50.7 ± 0.9	22.5 ± 1.6	12.3 ± 1.2
AL-F10	84.7 ± 4.5	68.8 ± 2.0	69.4 ± 1.0	54.1 ± 1.6	39.1 ± 1.8
AL-G10	74.4 ± 7.9	73.4 ± 0.2	68.2 ± 0.1	29.7 ± 4.6	12.0 ± 2.4
AL-H10	80.1 ± 2.0	57.1 ± 2.5	50.5 ± 0.7	26.7 ± 0.9	11.4 ± 0.1
DOTAP:chol	78.4 ± 1.5	73.1 ± 1.1	65.3 ± 0.1	22.0 ± 0.2	17.4 ± 1.1

2.3 Structure-Activity-Relationship

The SAR was done for aminolipids AL-A10, AL-A12, AL-B10, AL-B12, and DOTAP:chol. A total of three independent measurements with three replicates each was done to obtain the data necessary for statistical evaluation. Statistical evaluation was carried out using Origin 2018 Pro (see Materials and Methods).

2.3.1 Results of the Structure-Activity-Relationship experiments

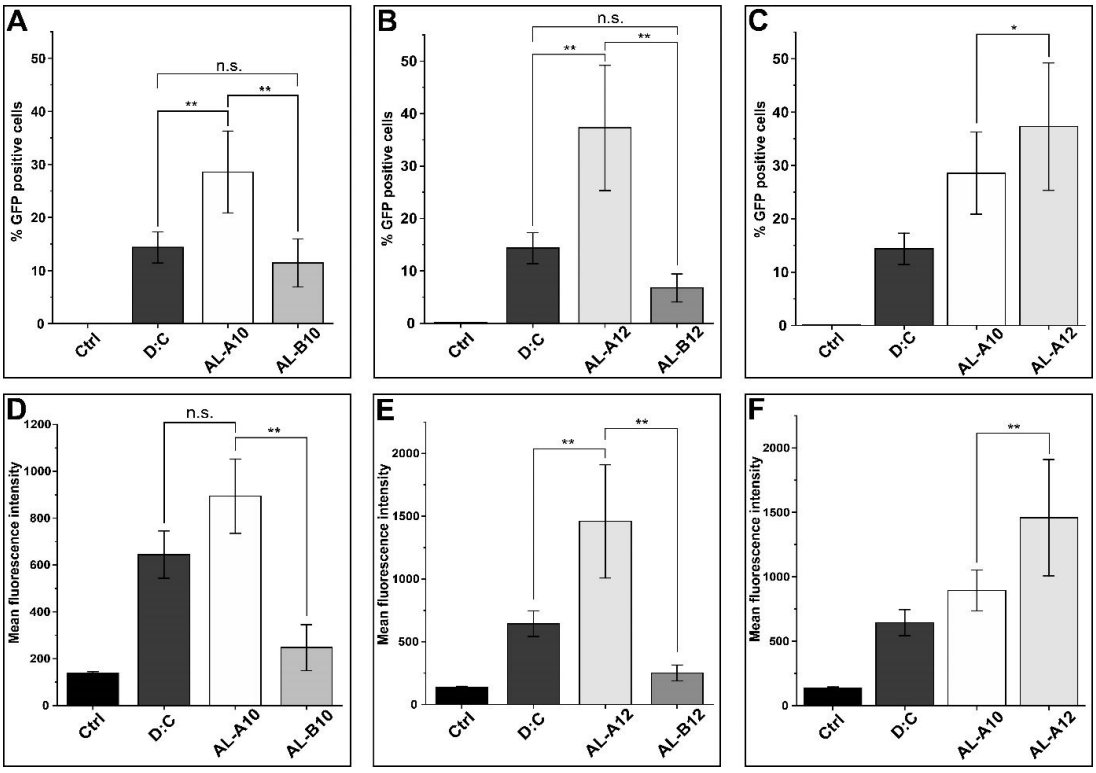

Figure S37: Structure-Activity-Relationship for the most promising aminolipids AL-A10, AL-A12, AL-B10, AL-B12, as well as DOTAP:chol. The graph shows the influence of the headgroup on transfection efficiency (A, B) and transgene expression (D, E) when the tail length stays constant and the influence of the tail length on transfection efficiency (C) and transgene expression (F) when the headgroup stays constant. Methoxy headgroups are superior to hydroxy headgroups ($p < 0.001$) and C_{12} tails are superior to C_{10} tails in both, transfection efficiency ($p < 0.1$) and transgene expression ($p < 0.001$). The data were obtained from three independent measurements with three replicates each. * $p < 0.1$, ** $p < 0.001$.

2.3.2 ANOVA Tables for GFP ($p < 0.1$)

Table S4: Descriptive statistics for the one way ANOVA for GFP ($p < 0.1$). AL 1 corresponds to AL-A10, AL 2 corresponds to AL-A12, AL 3 corresponds to AL-B10, and AL 4 corresponds to AL-B12.

	N Analysis	N Missing	Mean	Standard Deviation	SE of Mean
DOTAP/Chol 1 ug	8	1	6.0	0.7	0.3
AL 1 1 ug	9	0	7.9	1.9	0.6
AL 2 1 ug	9	0	11.2	4.2	1.4
AL 3 1 ug	9	0	4.7	2.0	0.7
AL 4 1 ug	9	0	7.6	3.1	1.0
DOTAP/Chol 2 ug	9	0	14.3	3.1	1.0
AL 1 2 ug	9	0	28.6	8.2	2.7
AL 2 2 ug	9	0	37.3	12.7	4.2
AL 3 2 ug	9	0	11.5	4.8	1.6
AL 4 2 ug	9	0	6.8	2.8	0.9

Table S5: Overall ANOVA table for the one way ANOVA for GFP ($p < 0.1$). Null Hypothesis: The means of all levels are equal. Alternative Hypothesis: The means of one or more levels are different. At the 0.1 level, the population means are significantly different.

	DF	Sum of Squares	Mean Square	F Value	Prob>F
Model	9	9374.4	1041.6	33.9	0
Error	79	2428.6	30.7		
Total	88	11803.0			

Table S6: Fit statistics for the one way ANOVA for GFP ($p < 0.1$).

	R-Square	Coeff Var	Root MSE	Data Mean
	0.794	0.406	5.545	13.661

Table S7: Means comparison Bonferroni test for one way ANOVA for GFP ($p < 0.1$). Sig equals 1 indicates that the difference of the means is significant at the 0.1 level. Sig equals 0 indicates that the difference of the means is not significant at the 0.1 level. AL 1 corresponds to AL-A10, AL 2 corresponds to AL-A12, AL 3 corresponds to AL-B10, and AL 4 corresponds to AL-B12.

	MeanDiff	SEM	t Value	Prob	Alpha	Sig	LCL	UCL
AL 1 1 ug DOTAP/Chol 1 ug	1.9	2.7	0.7	1	0.1	0	-6.6	10.4
AL 2 1 ug DOTAP/Chol 1 ug	5.2	2.7	1.9	1	0.1	0	-3.4	13.7
AL 2 1 ug AL 1 1 ug	3.2	2.6	1.2	1	0.1	0	-5.0	11.5
AL 3 1 ug DOTAP/Chol 1 ug	-1.3	2.7	-0.5	1	0.1	0	-9.8	7.2
AL 3 1 ug AL 1 1 ug	-3.2	2.6	-1.2	1	0.1	0	-11.5	5.0
AL 3 1 ug AL 2 1 ug	-6.5	2.6	-2.5	0.7	0.1	0	-14.7	1.8
AL 4 1 ug DOTAP/Chol 1 ug	1.6	2.7	0.6	1	0.1	0	-6.9	10.1
AL 4 1 ug AL 1 1 ug	-0.3	2.6	-0.1	1	0.1	0	-8.6	7.9
AL 4 1 ug AL 2 1 ug	-3.6	2.6	-1.4	1	0.1	0	-11.8	4.7
AL 4 1 ug AL 3 1 ug	2.9	2.6	1.1	1	0.1	0	-5.4	11.2
DOTAP/Chol 2 ug DOTAP/Chol 1ug	8.3	2.7	3.1	0.1	0.1	0	-0.2	16.9
DOTAP/Chol 2 ug AL 1 1 ug	6.4	2.6	2.5	0.7	0.1	0	-1.8	14.7
DOTAP/Chol 2 ug AL 2 1 ug	3.2	2.6	1.2	1	0.1	0	-5.1	11.5
DOTAP/Chol 2 ug AL 3 1 ug	9.7	2.6	3.7	0.0	0.1	1	1.4	17.9
DOTAP/Chol 2 ug AL 4 1 ug	6.8	2.6	2.6	0.5	0.1	0	-1.5	15.0
AL 1 2 ug DOTAP/Chol 1 ug	22.6	2.7	8.4	7.4E-11	0.1	1	14.0	31.1
AL 1 2 ug AL 1 1 ug	20.6	2.6	7.9	6.2E-10	0.1	1	12.4	28.9
AL 1 2 ug AL 2 1 ug	17.4	2.6	6.7	1.5E-7	0.1	1	9.1	25.7

AL 1 2 ug AL 3 1 ug	23.9	2.6	9.1	2.4E-12	0.1	1	15.6	32.2
AL 1 2 ug AL 4 1 ug	21.0	2.6	8.0	3.5E-10	0.1	1	12.7	29.2
AL 1 2 ug DOTAP/Chol 2 ug	14.2	2.6	5.4	2.6E-5	0.1	1	6.0	22.5
AL 2 2 ug DOTAP/Chol 1 ug	31.3	2.7	11.6	4.3E-17	0.1	1	22.8	39.8
AL 2 2 ug AL 1 1 ug	29.4	2.6	11.2	2.2-16	0.1	1	21.1	37.6
AL 2 2 ug AL 2 1 ug	26.1	2.6	10.0	5.1E-14	0.1	1	17.9	34.4
AL 2 2 ug AL 3 1 ug	32.6	2.6	12.5	1.1E-18	0.1	1	24.3	40.9
AL 2 2 ug AL 4 1 ug	29.7	2.6	11.4	1.3E-16	0.1	1	21.4	38.0
AL 2 2 ug DOTAP/Chol 2 ug	22.9	2.6	8.8	1.2E-11	0.1	1	14.7	31.2
AL 2 2 ug AL 1 2 ug	8.7	2.6	3.3	0.1	0.1	1	0.5	17.0
AL 3 2 ug DOTAP/Chol 1 ug	5.4	2.7	2.0	1	0.1	0	-3.1	14.0
AL 3 2 ug AL 1 1 ug	3.5	2.6	1.4	1	0.1	0	-4.7	11.8
AL 3 2 ug AL 2 1 ug	0.3	2.6	0.1	1	0.1	0	-8.0	8.6
AL 3 2 ug AL 3 1 ug	6.8	2.6	2.6	0.5	0.1	0	-1.5	15.0
AL 3 2 ug AL 4 1 ug	3.9	2.6	1.5	1	0.1	0	-4.4	12.1
AL 3 2 ug DOTAP/Chol 2 ug	-2.9	2.6	-1.1	1	0.1	0	-11.2	5.4
AL 3 2 ug AL 1 2 ug	-17.1	2.6	-6.6	2.4E-7	0.1	1	-25.4	-8.9
AL 3 2 ug AL 2 2 ug	-25.8	2.6	-9.9	8.4E-14	0.1	1	-34.1	-17.6
AL 4 2 ug DOTAP/Chol 1 ug	0.8	2.7	0.3	1	0.1	0	-7.8	9.3
AL 4 2 ug AL 1 1 ug	-1.2	2.6	-0.5	1	0.1	0	-9.4	7.1
AL 4 2 ug AL 2 1 ug	-4.4	2.6	-1.7	1	0.1	0	-12.7	3.9
AL 4 2 ug AL 3 1 ug	2.1	2.6	0.8	1	0.1	0	-6.2	10.3
AL 4 2 ug AL 4 1 ug	-0.8	2.6	-0.3	1	0.1	0	-9.1	7.4
AL 4 2 ug DOTAP/Chol 2 ug	-7.6	2.6	-2.9	0.2	0.1	0	-15.9	0.7
AL 4 2 ug AL 1 2 ug	-21.8	2.6	-8.3	8.4E-11	0.1	1	-30.1	-13.6
AL 4 2 ug AL 2 2 ug	-30.5	2.6	-11.7	3.1E-17	0.1	1	-38.8	-22.3
AL 4 2 ug AL 3 2 ug	-4.7	2.6	-1.8	1	0.1	0	-13.0	3.6

2.3.3 ANOVA Table for GFP (p < 0.001)

Table S8: Descriptive statistics for the one way ANOVA for GFP (p < 0.001). AL 1 corresponds to AL-A10, AL 2 corresponds to AL-A12, AL 3 corresponds to AL-B10, and AL 4 corresponds to AL-B12.

	N Analysis	N Missing	Mean	Standard Deviation	SE of Mean
DOTAP/Chol 1 ug	8	1	6.0	0.7	0.3
AL 1 1 ug	9	0	7.9	1.9	0.6
AL 2 1 ug	9	0	11.2	4.2	1.4
AL 3 1 ug	9	0	4.7	2.0	0.7
AL 4 1 ug	9	0	7.6	3.1	1.0
DOTAP/Chol 2 ug	9	0	14.3	3.1	1.0
AL 1 2 ug	9	0	28.6	8.2	2.7
AL 2 2 ug	9	0	37.3	12.7	4.2
AL 3 2 ug	9	0	11.5	4.8	1.6
AL 4 2 ug	9	0	6.8	2.8	1.0

Table S9: Overall ANOVA table for the one way ANOVA for GFP (p < 0.001). Null Hypothesis: The means of all levels are equal. Alternative Hypothesis: The means of one or more levels are different. At the 0.001 level, the population means are significantly different.

	DF	Sum of Squares	Mean Square	F Value	Prob>F
Model	9	9374.4	1041.6	33.9	0
Error	79	2428.6	30.7		
Total	88	11803.0			

Table S10: Fit statistics for the one way ANOVA for GFP (p < 0.001).

	R-Square	Coeff Var	Root MSE	Data Mean

	0.794	0.406	5.545	13.661

Table S11: Means comparison Bonferroni test for one way ANOVA for GFP (p < 0.001). Sig equals 1 indicates that the difference of the means is significant at the 0.001 level. Sig equals 0 indicates that the difference of the means is not significant at the 0.001 level. AL 1 corresponds to AL-A10, AL 2 corresponds to AL-A12, AL 3 corresponds to AL-B10, and AL 4 corresponds to AL-B12.

	MeanDiff	SEM	t Value	Prob	Alpha	Sig	LCL	UCL
AL 1 1 ug DOTAP/Chol 1 ug	1.9	2.7	0.7	1	0.001	0	-10.2	14.1
AL 2 1 ug DOTAP/Chol 1 ug	5.2	2.7	1.9	1	0.001	0	-7.0	17.3
AL 2 1 ug AL 1 1 ug	3.2	2.6	1.2	1	0.001	0	-8.6	15.0
AL 3 1 ug DOTAP/Chol 1 ug	-1.3	2.7	-0.5	1	0.001	0	-13.5	10.8
AL 3 1 ug AL 1 1 ug	-3.2	2.6	-1.2	1	0.001	0	-15.0	8.6
AL 3 1 ug AL 2 1 ug	-6.5	2.6	-2.5	0.7	0.001	0	-18.3	5.3
AL 4 1 ug DOTAP/Chol 1 ug	1.6	2.7	0.6	1	0.001	0	-10.6	13.7
AL 4 1 ug AL 1 1 ug	-0.3	2.6	-0.1	1	0.001	0	-12.1	11.5
AL 4 1 ug AL 2 1 ug	-3.6	2.6	-1.4	1	0.001	0	-15.4	8.2
AL 4 1 ug AL 3 1 ug	2.9	2.6	1.1	1	0.001	0	-8.9	14.7
DOTAP/Chol 2 ug DOTAP/Chol 1ug	8.3	2.7	3.1	0.1	0.001	0	-3.8	20.5
DOTAP/Chol 2 ug AL 1 1 ug	6.4	2.6	2.5	0.7	0.001	0	-5.4	18.2
DOTAP/Chol 2 ug AL 2 1 ug	3.2	2.6	1.2	1	0.001	0	-8.6	15.0
DOTAP/Chol 2 ug AL 3 1 ug	9.7	2.6	3.7	0.0	0.001	0	-2.1	21.5
DOTAP/Chol 2 ug AL 4 1 ug	6.8	2.6	2.6	0.5	0.001	0	-5.0	18.5
AL 1 2 ug DOTAP/Chol 1 ug	22.6	2.7	8.4	7.4E-11	0.001	1	10.4	34.7
AL 1 2 ug AL 1 1 ug	20.6	2.6	7.9	6.2E-10	0.001	1	8.9	32.4
AL 1 2 ug AL 2 1 ug	17.4	2.6	6.7	1.5E-7	0.001	1	5.6	29.2
AL 1 2 ug AL 3 1 ug	23.9	2.6	9.1	2.4E-12	0.001	1	12.1	35.7
AL 1 2 ug AL 4 1 ug	21.0	2.6	8.0	3.5E-10	0.001	1	9.2	32.8
AL 1 2 ug DOTAP/Chol 2 ug	14.2	2.6	5.4	2.6E-5	0.001	1	2.4	26.0
AL 2 2 ug DOTAP/Chol 1 ug	31.3	2.7	11.6	4.3E-17	0.001	1	19.1	43.4
AL 2 2 ug AL 1 1 ug	29.4	2.6	11.2	2.2E-16	0.001	1	17.6	41.1
AL 2 2 ug AL 2 1 ug	26.1	2.6	10.0	5.1E-14	0.001	1	14.3	37.9
AL 2 2 ug AL 3 1 ug	32.6	2.6	12.5	1.1E-18	0.001	1	20.8	44.4
AL 2 2 ug AL 4 1 ug	29.7	2.6	11.4	1.3E-16	0.001	1	17.9	41.5
AL 2 2 ug DOTAP/Chol 2 ug	22.9	2.6	8.8	1.2E-11	0.001	1	11.2	34.7
AL 2 2 ug AL 1 2 ug	8.7	2.6	3.3	0.1	0.001	0	-3.1	20.5
AL 3 2 ug DOTAP/Chol 1 ug	5.4	2.7	2.0	1	0.001	0	-6.7	17.6
AL 3 2 ug AL 1 1 ug	3.5	2.6	1.4	1	0.001	0	-8.3	15.3
AL 3 2 ug AL 2 1 ug	0.3	2.6	0.1	1	0.001	0	-11.5	12.1
AL 3 2 ug AL 3 1 ug	6.8	2.6	2.6	0.5	0.001	0	-5.0	18.6
AL 3 2 ug AL 4 1 ug	3.9	2.6	1.5	1	0.001	0	-7.9	15.7
AL 3 2 ug DOTAP/Chol 2 ug	-2.9	2.6	-1.1	1	0.001	0	-14.7	8.9
AL 3 2 ug AL 1 2 ug	-17.1	2.6	-6.6	2.4E-7	0.001	1	-28.9	-5.3
AL 3 2 ug AL 2 2 ug	-25.8	2.6	-9.9	8.4E-14	0.001	1	-37.6	-14.0
AL 4 2 ug DOTAP/Chol 1 ug	0.8	2.7	0.28	1	0.001	0	-11.4	12.9
AL 4 2 ug AL 1 1 ug	-1.2	2.6	-0.5	1	0.001	0	-13.0	10.6
AL 4 2 ug AL 2 1 ug	-4.4	2.6	-1.7	1	0.001	0	-16.2	7.4
AL 4 2 ug AL 3 1 ug	2.1	2.6	0.8	1	0.001	0	-9.7	13.9
AL 4 2 ug AL 4 1 ug	-0.8	2.6	-0.3	1	0.001	0	-12.6	11.0
AL 4 2 ug DOTAP/Chol 2 ug	-7.6	2.6	-2.9	0.2	0.001	0	-19.4	4.2
AL 4 2 ug AL 1 2 ug	-21.8	2.6	-8.4	8.3E-11	0.001	1	-33.6	-10.0
AL 4 2 ug AL 2 2 ug	-30.5	2.6	-11.7	3.1E-17	0.001	1	-42.3	-18.7
AL 4 2 ug AL 3 2 ug	-4.7	2.6	-1.8	1	0.001	0	-16.5	7.1

2.3.4 ANOVA Table for MFI (p < 0.1)

Table S12: Descriptive statistics for the one way ANOVA for MFI (p < 0.1). AL 1 corresponds to AL-A10, AL 2 corresponds to AL-A12, AL 3 corresponds to AL-B10, and AL 4 corresponds to AL-B12.

	N Analysis	N Missing	Mean	Standard Deviation	SE of Mean
DOTAP/Chol 1 ug	8	1	417.5	21.4	7.6
AL 1 1 ug	9	0	409.4	40.0	13.3
AL 2 1 ug	9	0	623.7	152.2	50.5
AL 3 1 ug	8	1	333.3	23.6	8.4
AL 4 1 ug	9	0	320.8	78.8	26.3
DOTAP/Chol 2 ug	9	0	644.4	107.2	35.7
AL 1 2 ug	9	0	893.9	167.7	55.9
AL 2 2 ug	9	0	1459.3	478.0	159.3
AL 3 2 ug	9	0	247.3	103.9	34.6
AL 4 2 ug	9	0	250.8	67.1	22.4

Table S13: Overall ANOVA table for the one way ANOVA for MFI (p < 0.1). Null Hypothesis: The means of all levels are equal. Alternative Hypothesis: The means of one or more levels are different. At the 0.1 level, the population means are significantly different.

	DF	Sum of Squares	Mean Square	F Value	Prob>F
Model	9	1.1E7	1.3E6	39.2	0
Error	78	2.5E6	32335.8		
Total	87	1.4E7			

Table S14: Fit statistics for the one way ANOVA for MFI (p < 0.1).

	R-Square	Coeff Var	Root MSE	Data Mean
	0.819	0.319	179.822	564.239

Table S15: Means comparison Bonferroni test for one way ANOVA for MFI (p < 0.1). Sig equals 1 indicates that the difference of the means is significant at the 0.1 level. Sig equals 0 indicates that the difference of the means is not significant at the 0.1 level. AL 1 corresponds to AL-A10, AL 2 corresponds to AL-A12, AL 3 corresponds to AL-B10, and AL 4 corresponds to AL-B12.

	MeanDiff	SEM	t Value	Prob	Alpha	Sig	LCL	UCL
AL 1 1 ug DOTAP/Chol 1 ug	-8.1	87.4	-0.1	1	0.1	0	-284.5	268.4
AL 2 1 ug DOTAP/Chol 1 ug	206.2	87.4	2.4	0.9	0.1	0	-70.3	482.6
AL 2 1 ug AL 1 1 ug	214.2	84.8	2.5	0.6	0.1	0	-53.9	482.4
AL 3 1 ug DOTAP/Chol 1 ug	-84.3	89.9	-0.9	1	0.1	0	-368.7	200.2
AL 3 1 ug AL 1 1 ug	-76.2	87.4	-0.9	1	0.1	0	-352.6	200.2
AL 3 1 ug AL 2 1 ug	-290.4	87.4	-3.3	0.1	0.1	1	-566.8	-14.0
AL 4 1 ug DOTAP/Chol 1 ug	-96.7	87.4	-1.1	1	0.1	0	-373.1	179.7
AL 4 1 ug AL 1 1 ug	-88.7	84.8	-1.0	1	0.1	0	-356.8	179.5
AL 4 1 ug AL 2 1 ug	-302.9	84.8	-3.6	0.0	0.1	1	-571.1	-34.7
AL 4 1 ug AL 3 1 ug	-12.5	87.4	-0.1	1	0.1	0	-288.9	263.9
DOTAP/Chol 2 ug DOTAP/Chol 1 ug	226.9	87.4	2.6	0.5	0.1	0	-49.5	503.4
DOTAP/Chol 2 ug AL 1 1 ug	235.0	84.8	2.8	0.3	0.1	0	-33.2	503.2
DOTAP/Chol 2 ug AL 2 1 ug	20.8	84.8	0.2	1	0.1	0	-247.4	288.9
DOTAP/Chol 2 ug AL 3 1 ug	311.2	87.4	3.6	0.0	0.1	1	34.8	587.6
DOTAP/Chol 2 ug AL 4 1 ug	323.7	84.8	3.8	0.0	0.1	1	55.5	591.8
AL 1 2 ug DOTAP/Chol 1 ug	476.4	87.4	5.5	2.5E-5	0.1	1	200.0	752.8
AL 1 2 ug AL 1 1 ug	484.4	84.8	5.7	8.6E-6	0.1	1	216.3	752.6

AL 1 2 ug AL 2 1 ug	270.2	84.8	3.2	0.1	0.1	1	2.1	538.4
AL 1 2 ug AL 3 1 ug	560.6	87.4	6.4	4.5E-7	0.1	1	284.2	837.1
AL 1 2 ug AL 4 1 ug	573.1	84.8	6.8	1.0E-7	0.1	1	304.9	841.3
AL 1 2 ug DOTAP/Chol 2 ug	249.4	84.8	2.9	0.2	0.1	0	-18.7	517.6
AL 2 2 ug DOTAP/Chol 1 ug	1041.8	87.4	11.9	1.3E-17	0.1	1	765.4	1318.3
AL 2 2 ug AL 1 1 ug	1049.9	84.8	12.4	1.9E-18	0.1	1	781.7	1318.1
AL 2 2 ug AL 2 1 ug	835.7	84.8	9.9	1.1E-13	0.1	1	567.5	1103.8
AL 2 2 ug AL 3 1 ug	1126.1	87.4	12.9	2.3E-19	0.1	1	849.7	1402.5
AL 2 2 ug AL 4 1 ug	1138.6	84.8	13.4	2.5E-20	0.1	1	870.4	1406.7
AL 2 2 ug DOTAP/Chol 2 ug	814.9	84.8	9.6	3.2E-13	0.1	1	546.7	1083.1
AL 2 2 ug AL 1 2 ug	565.4	84.8	6.7	1.5E-7	0.1	1	297.3	833.6
AL 3 2 ug DOTAP/Chol 1 ug	-170.2	87.4	-1.9	1	0.1	0	-446.6	106.3
AL 3 2 ug AL 1 1 ug	-162.1	84.8	-1.9	1	0.1	0	-430.3	106.1
AL 3 2 ug AL 2 1 ug	-376.3	84.8	-4.4	0.0	0.1	1	-644.5	-108.2
AL 3 2 ug AL 3 1 ug	-85.9	87.4	-1.0	1	0.1	0	-362.3	190.5
AL 3 2 ug AL 4 1 ug	-73.4	84.8	-0.9	1	0.1	0	-341.6	194.7
AL 3 2 ug DOTAP/Chol 2 ug	-397.1	84.8	-4.7	5.3E-4	0.1	1	-665.3	-128.9
AL 3 2 ug AL 1 2 ug	-646.6	84.8	-7.6	2.2E-9	0.1	1	-914.7	-378.4
AL 3 2 ug AL 2 2 ug	-1212.0	84.8	-14.3	7.6E-22	0.1	1	-1480.2	-943.8
AL 4 2 ug DOTAP/Chol 1 ug	-166.7	87.4	-1.9	1	0.1	0	-443.1	109.7
AL 4 2 ug AL 1 1 ug	-158.7	84.8	-1.9	1	0.1	0	-426.8	109.5
AL 4 2 ug AL 2 1 ug	-372.9	84.8	-4.4	0.0	0.1	1	-641.1	-104.7
AL 4 2 ug AL 3 1 ug	-82.5	87.4	-0.9	1	0.1	0	-358.9	193.9
AL 4 2 ug AL 4 1 ug	-70.0	84.8	-0.8	1	0.1	0	-338.2	198.2
AL 4 2 ug DOTAP/Chol 2 ug	-393.7	84.8	-4.6	6.1E-4	0.1	1	-661.8	-125.5
AL 4 2 ug AL 1 2 ug	-643.1	84.8	-7.6	2.7E-9	0.1	1	-911.3	-374.9
AL 4 2 ug AL 2 2 ug	-1208.6	84.8	-14.3	9.0E-22	0.1	1	-1476.7	-940.4
AL 4 2 ug AL 3 2 ug	3.4	84.8	0.0	1	0.1	0	-264.7	271.6

2.3.5 ANOVA Table for MFI (p < 0.001)

Table S16: Descriptive statistics for the one way ANOVA for MFI (p < 0.001). AL 1 corresponds to AL-A10, AL 2 corresponds to AL-A12, AL 3 corresponds to AL-B10, and AL 4 corresponds to AL-B12.

	N Analysis	N Missing	Mean	Standard Deviation	SE of Mean
DOTAP/Chol 1 ug	8	1	417.5	21.4	7.6
AL 1 1 ug	9	0	409.4	40.0	13.3
AL 2 1 ug	9	0	623.6	152.2	50.7
AL 3 1 ug	8	1	333.3	23.6	8.3
AL 4 1 ug	9	0	320.8	78.8	26.3
DOTAP/Chol 2 ug	9	0	644.4	107.2	35.7
AL 1 2 ug	9	0	893.9	167.7	55.9
AL 2 2 ug	9	0	1459.3	478.0	159.3
AL 3 2 ug	9	0	247.3	103.9	34.6
AL 4 2 ug	9	0	250.8	67.1	22.4

Table S17: Overall ANOVA table for the one way ANOVA for MFI (p < 0.001). Null Hypothesis: The means of all levels are equal. Alternative Hypothesis: The means of one or more levels are different. At the 0.001 level, the population means are significantly different.

	DF	Sum of Squares	Mean Square	F Value	Prob>F
Model	9	1.1E7	1.3E6	39.2	0
Error	78	2.5E6	32335.8		
Total	87	1.4E7			

Table S18: Fit statistics for the one way ANOVA for MFI (p < 0.001).

	R-Square	Coeff Var	Root MSE	Data Mean
	0.819	0.319	179.822	564.239

Table S19: Means comparison Bonferroni test for one way ANOVA for MFI (p < 0.001). Sig equals 1 indicates that the difference of the means is significant at the 0.001 level. Sig equals 0 indicates that the difference of the means is not significant at the 0.001 level. AL 1 corresponds to AL-A10, AL 2 corresponds to AL-A12, AL 3 corresponds to AL-B10, and AL 4 corresponds to AL-B12.

	MeanDiff	SEM	t Value	Prob	Alpha	Sig	LCL	UCL
AL 1 1 ug DOTAP/Chol 1 ug	-8.1	87.4	-0.1	1	0.001	0	-402.5	386.4
AL 2 1 ug DOTAP/Chol 1 ug	206.2	87.4	2.4	0.9	0.001	0	-188.2	600.6
AL 2 1 ug AL 1 1 ug	214.2	84.8	2.5	0.6	0.001	0	-168.4	596.9
AL 3 1 ug DOTAP/Chol 1 ug	-84.3	89.9	-0.9	1	0.001	0	-490.1	321.6
AL 3 1 ug AL 1 1 ug	-76.2	87.4	-0.9	1	0.001	0	-470.6	318.2
AL 3 1 ug AL 2 1 ug	-290.4	87.4	-3.3	0.1	0.001	0	-684.8	104.0
AL 4 1 ug DOTAP/Chol 1 ug	-96.7	87.4	-1.1	1	0.001	0	-491.1	297.7
AL 4 1 ug AL 1 1 ug	-88.7	84.8	-1.0	1	0.001	0	-471.3	294.0
AL 4 1 ug AL 2 1 ug	-302.9	84.8	-3.6	0.0	0.001	0	-685.5	79.7
AL 4 1 ug AL 3 1 ug	-12.5	87.4	-0.1	1	0.001	0	-406.9	381.9
DOTAP/Chol 2 ug DOTAP/Chol 1 ug	226.9	87.4	2.6	0.5	0.001	0	-167.5	621.4
DOTAP/Chol 2 ug AL 1 1 ug	235.0	84.8	2.8	0.3	0.001	0	-147.6	617.6
DOTAP/Chol 2 ug AL 2 1 ug	20.8	84.8	0.2	1	0.001	0	-361.9	403.4
DOTAP/Chol 2 ug AL 3 1 ug	311.2	87.4	3.6	0.0	0.001	0	-83.2	705.6
DOTAP/Chol 2 ug AL 4 1 ug	323.7	84.8	3.8	0.0	0.001	0	-59.0	706.3
AL 1 2 ug DOTAP/Chol 1 ug	476.4	87.4	5.5	2.5E-5	0.001	1	82.0	870.8
AL 1 2 ug AL 1 1 ug	484.4	84.8	5.7	8.6E-6	0.001	1	101.8	867.1
AL 1 2 ug AL 2 1 ug	270.2	84.8	3.2	0.1	0.001	0	-112.4	652.9
AL 1 2 ug AL 3 1 ug	560.6	87.4	6.4	4.5E-7	0.001	1	166.2	955.1
AL 1 2 ug AL 4 1 ug	573.1	84.8	6.8	1.0E-7	0.001	1	190.5	955.7
AL 1 2 ug DOTAP/Chol 2 ug	249.4	84.8	2.9	0.2	0.001	0	-133.2	632.1
AL 2 2 ug DOTAP/Chol 1 ug	1041.8	87.4	11.9	1.3E-17	0.001	1	647.4	1436.2
AL 2 2 ug AL 1 1 ug	1049.9	84.8	12.4	1.9E-18	0.001	1	667.3	1432.5
AL 2 2 ug AL 2 1 ug	835.7	84.8	9.9	1.1E-13	0.001	1	453.0	1218.3
AL 2 2 ug AL 3 1 ug	1126.1	87.4	12.9	2.3E-19	0.001	1	731.7	1520.5
AL 2 2 ug AL 4 1 ug	1138.6	84.8	13.4	2.5E-20	0.001	1	755.9	1521.2
AL 2 2 ug DOTAP/Chol 2 ug	814.9	84.8	9.6	3.2E-13	0.001	1	432.3	1197.5
AL 2 2 ug AL 1 2 ug	565.4	84.8	6.7	1.5E-7	0.001	1	182.8	948.1
AL 3 2 ug DOTAP/Chol 1 ug	-170.2	87.4	-1.9	1	0.001	0	-564.6	224.2
AL 3 2 ug AL 1 1 ug	-162.1	84.8	-1.9	1	0.001	0	-544.7	220.5
AL 3 2 ug AL 2 1 ug	-376.3	84.8	-4.4	0.0	0.001	0	-759.0	6.3
AL 3 2 ug AL 3 1 ug	-85.9	87.4	-1.0	1	0.001	0	-480.3	308.5
AL 3 2 ug AL 4 1 ug	-73.4	84.8	-0.9	1	0.001	0	-456.1	309.2
AL 3 2 ug DOTAP/Chol 2 ug	-397.1	84.8	-4.7	5.3E-4	0.001	1	-779.7	-14.5
AL 3 2 ug AL 1 2 ug	-646.6	84.8	-7.6	2.2E-9	0.001	1	-1029.2	-263.9
AL 3 2 ug AL 2 2 ug	-1212.0	84.8	-14.3	7.6E-22	0.001	1	-1594.6	-829.4
AL 4 2 ug DOTAP/Chol 1 ug	-166.7	87.4	-1.9	1	0.001	0	-561.1	227.7
AL 4 2 ug AL 1 1 ug	-158.7	84.8	-1.9	1	0.001	0	-541.3	224.0
AL 4 2 ug AL 2 1 ug	-372.9	84.8	-4.4	0.0	0.001	0	-755.5	9.7
AL 4 2 ug AL 3 1 ug	-82.5	87.4	-0.9	1	0.001	0	-476.9	311.9
AL 4 2 ug AL 4 1 ug	-70.0	84.8	-0.8	1	0.001	0	-452.6	312.6
AL 4 2 ug DOTAP/Chol 2 ug	-393.7	84.8	-4.6	6.1E-4	0.001	1	-776.3	-11.0
AL 4 2 ug AL 1 2 ug	-643.1	84.8	-7.6	2.7E-9	0.001	1	-1025.7	-260.5
AL 4 2 ug AL 2 2 ug	-1208.6	84.8	-14.3	9.0E-22	0.001	1	-1591.2	-825.9
AL 4 2 ug AL 3 2 ug	3.4	84.8	0.0	1	0.001	0	-379.2	386.1

2.3.6 Outlier Detection

Table S 20: Outlier detection for GFP at 1µg/mL DNA and a lipid-to-DNA ratio of 1. Outliers (red) were defined as values larger than the upper fence or lower than the lower fence and were excluded from analysis.Upper fence is defined by Q3 + 1.5x interquartile range (IQR) and lower fence is defined by Q1 – 1.5x IQR. Only one oulier could be identified.

Control		DOTAP:chol		AL-A10		AL-B10		AL-A12		AL-B12	
0.12	0.12	6.52	6.52	8.28	8.28	4.90	4.90	5.25	5.25	4.05	4.05
0.06	0.06	4.74	4.74	6.14	6.14	4.05	4.05	7.18	7.18	8.42	8.42
0.12	0.12	6.75	6.75	8.17	8.17	9.01	9.01	15.20	15.20	9.65	9.65
		5.98	5.98	11.50	11.50	4.28	4.28	6.34	6.34	6.34	6.34
		5.26	5.26	6.72	6.72	2.27	2.27	12.50	12.50	4.83	4.83
		6.52	6.52	7.95	7.95	5.76	5.76	15.60	15.60	9.67	9.67
		10.5		8.32	8.32	3.07	3.07	9.67	9.67	4.88	4.88
		5.78	5.78	5.00	5.00	3.16	3.16	12.60	12.60	6.66	6.66
		6.54	6.54	9.23	9.23	5.66	5.66	16.10	16.10	13.8	13.8
Q1	0.06	**Q1**	5.52	**Q1**	6.43	**Q1**	3.12	**Q1**	6.76	**Q1**	4.86
Q3	0.12	**Q3**	6.65	**Q3**	8.78	**Q3**	5.71	**Q3**	15.4	**Q3**	9.66
IQR	0.06	**IQR**	1.13	**IQR**	2.35	**IQR**	2.60	**IQR**	8.64	**IQR**	4.81
Upper Fence	0.21	**Upper Fence**	8.33	**Upper Fence**	12.29	**Upper Fence**	9.60	**Upper Fence**	28.36	**Upper Fence**	16.87
Lower Fence	-0.03	**Lower Fence**	3.83	**Lower Fence**	2.91	**Lower Fence**	-0.78	**Lower Fence**	-6.20	**Lower Fence**	-2.35
Median	0.12	**Median**	6.25	**Median**	8.17	**Median**	4.28	**Median**	12.5	**Median**	6.66
Average	0.10	**Average**	6.01	**Average**	7.92	**Average**	4.68	**Average**	11.16	**Average**	7.59
S.D.	0.03	**S.D.**	0.67	**S.D.**	1.76	**S.D.**	1.89	**S.D.**	3.95	**S.D.**	2.94
RSD	28.85	**RSD**	11.13	**RSD**	22.27	**RSD**	40.37	**RSD**	35.41	**RSD**	38.73

Table S21: Outlier detection for GFP at 2µg/mL DNA and a lipid-to-DNA ratio of 1. Outliers (red) were defined as values larger than the upper fence or lower than the lower fence and were excluded from analysis.Upper fence is defined by Q3 + 1.5x interquartile range (IQR) and lower fence is defined by Q1 – 1.5x IQR. No outlier could be identified.

Control		DOTAP:chol		AL-A10		AL-B10		AL-A12		AL-B12	
0.10	0.10	10.60	10.60	19.50	19.50	11.20	11.20	17.30	17.30	9.78	9.78
0.11	0.11	16.20	16.20	33.50	33.50	7.91	7.91	45.20	45.20	7.43	7.43
0.09	0.09	12.60	12.60	33.40	33.40	8.00	8.00	44.50	44.50	12.70	12.70
		10.60	10.60	16.70	16.70	7.92	7.92	22.00	22.00	3.99	3.99
		17.00	17.00	32.70	32.70	9.37	9.37	43.00	43.00	6.41	6.41
		16.30	16.30	37.10	37.10	8.74	8.74	53.00	53.00	4.93	4.93
		11.30	11.30	17.40	17.40	11.70	11.70	23.80	23.80	5.23	5.23
		19.10	19.10	32.80	32.80	22.20	22.20	44.60	44.60	5.91	5.91
		15.40	15.40	34.00	34.00	16.00	16.00	42.10	42.10	4.43	4.43
Q1	0.09	**Q1**	10.95	**Q1**	18.45	**Q1**	7.96	**Q1**	22.90	**Q1**	4.68
Q3	0.11	**Q3**	16.65	**Q3**	33.75	**Q3**	13.85	**Q3**	44.90	**Q3**	8.61
IQR	0.02	**IQR**	5.70	**IQR**	15.30	**IQR**	5.89	**IQR**	22.00	**IQR**	3.93
Upper Fence	0.14	**Upper Fence**	25.20	**Upper Fence**	56.70	**Upper Fence**	22.69	**Upper Fence**	77.90	**Upper Fence**	14.49
Lower Fence	0.06	**Lower Fence**	2.40	**Lower Fence**	-4.50	**Lower Fence**	-0.87	**Lower Fence**	-10.10	**Lower Fence**	-1.21
Median	0.10	**Median**	15.40	**Median**	32.80	**Median**	9.37	**Median**	43.00	**Median**	5.91
Average	0.10	**Average**	14.34	**Average**	28.57	**Average**	11.45	**Average**	37.28	**Average**	6.76
S.D.	0.01	**S.D.**	2.95	**S.D.**	7.69	**S.D.**	4.53	**S.D.**	11.95	**S.D.**	2.68
RSD	9.12	**RSD**	20.58	**RSD**	26.93	**RSD**	39.60	**RSD**	32.07	**RSD**	39.62

Table S22: Outlier detection for MFI at 1µg/mL DNA and a lipid-to-DNA ratio of 1. Outliers (red) were defined as values larger than the upper fence or lower than the lower fence and were excluded from analysis.Upper fence is defined by Q3 + 1.5x interquartile range (IQR) and lower fence is defined by Q1 – 1.5x IQR. Only two ouliers could be identified.

Control		DOTAP:chol		AL-A10		AL-B10		AL-A12		AL-B12	
182	182	409	409	379	379	333	333	424	424	294	294
127	127	398	398	395	395	354	354	451	451	290	290
147	147	461	461	426	426	420		819	819	328	328
		425	425	430	430	344	344	451	451	277	277
		401	401	477	477	313	313	582	582	291	291
		407	407	402	402	329	329	752	752	438	438
		596		392	392	291	291	714	714	224	224
		405	405	340	340	335	335	653	653	281	281
		434	434	444	444	367	367	767	767	464	464
Q1	127	**Q1**	403	**Q1**	385.5	**Q1**	321	**Q1**	451	**Q1**	279
Q3	182	**Q3**	447.5	**Q3**	437	**Q3**	360.5	**Q3**	759.5	**Q3**	383
IQR	55	**IQR**	44.5	**IQR**	51.5	**IQR**	39.5	**IQR**	308.5	**IQR**	104
Upper Fence	264.50	**Upper Fence**	514.25	**Upper Fence**	514.25	**Upper Fence**	419.75	**Upper Fence**	1222.25	**Upper Fence**	539.00
Lower Fence	44.50	**Lower Fence**	336.25	**Lower Fence**	308.25	**Lower Fence**	261.75	**Lower Fence**	-11.75	**Lower Fence**	123.00
Median	147	**Median**	408	**Median**	402	**Median**	334	**Median**	653	**Median**	291
Average	152.00	**Average**	417.50	**Average**	409.44	**Average**	333.25	**Average**	623.67	**Average**	320.78
S.D.	22.73	**S.D.**	20.04	**S.D.**	37.67	**S.D.**	22.08	**S.D.**	143.53	**S.D.**	74.33
RSD	14.95	**RSD**	4.80	**RSD**	9.20	**RSD**	6.63	**RSD**	23.01	**RSD**	23.17

Table S 23: Outlier detection for MFI at 2µg/mL DNA and a lipid-to-DNA ratio of 1. Outliers (red) were defined as values larger than the upper fence or lower than the lower fence and were excluded from analysis.Upper fence is defined by Q3 + 1.5x interquartile range (IQR) and lower fence is defined by Q1 – 1.5x IQR. No outlier could be identified.

Control		DOTAP:chol		AL-A10		AL-B10		AL-A12		AL-B12	
132	132	489	489	816	816	212	212	745	745	303	303
133	133	663	663	966	966	151	151	1972	1972	153	153
148	148	570	570	937	937	151	151	1658	1658	164	164
		531	531	694	694	308	308	968	968	238	238
		733	733	1063	1063	151	151	1492	1492	209	209
		753	753	956	956	164	164	2283	2283	253	253
		564	564	577	577	317	317	1155	1155	304	304
		774	774	1082	1082	427	427	1437	1437	354	354
		723	723	954	954	345	345	1424	1424	279	279
Q1	132	**Q1**	547.5	**Q1**	755	**Q1**	151	**Q1**	1061.5	**Q1**	186.5
Q3	148	**Q3**	743	**Q3**	1014.5	**Q3**	331	**Q3**	1815	**Q3**	303.5
IQR	16	**IQR**	195.5	**IQR**	259.5	**IQR**	180	**IQR**	753.5	**IQR**	117
Upper Fence	172.00	**Upper Fence**	1036.25	**Upper Fence**	1403.75	**Upper Fence**	601.00	**Upper Fence**	2945.25	**Upper Fence**	479.00
Lower Fence	108.00	**Lower Fence**	254.25	**Lower Fence**	365.75	**Lower Fence**	-119.00	**Lower Fence**	-68.75	**Lower Fence**	11.00
Median	133	**Median**	663	**Median**	954	**Median**	212	**Median**	1437	**Median**	253
Average	137.67	**Average**	644.44	**Average**	893.89	**Average**	247.33	**Average**	1459.33	**Average**	250.78
S.D.	7.32	**S.D.**	101.09	**S.D.**	158.10	**S.D.**	97.97	**S.D.**	450.66	**S.D.**	63.26
RSD	5.32	**RSD**	15.69	**RSD**	17.69	**RSD**	39.61	**RSD**	30.88	**RSD**	25.23

5.2 Chapter 2

5.2.1 Chapter 2.1

Characterization and Optimization of Lipoplexes: How to standardize Assays and avoid Pitfalls

Jonas Buck, Dominik Witzigmann, Susanne H. Schenk, Tomaz Einfalt, Ludovit Zweifel, Hiu-Man Grisch-Chan, Beat Thöny, Jörg Huwyler

Manuscript ready for submission.

Highlights: Interactions between DNA and nanoparticles are still poorly understood to this day. Usually, DNA and lipid-based nanoparticles are combined based on calculations and applied to cultured cells or animal models assuming that the calculations reflect the actual conditions. In our opinion, this approach is flawed because losses during preparation cannot be accounted for. In this publication, we propose the application of fluorescence cross-correlation spectroscopy (FCCS) to determine the interactions between DNA and nanoparticles. The results showed that the interactions are qualitatively and quantitatively different among the three used transfection reagents. We therefore recommend that interactions between DNA and nanoparticles should be determined for each individual formulation to reduce artifacts and to draw conclusions based on actual data rather than calculations.

Characterization and Optimization of Lipoplexes: How to standardize Assays and avoid Pitfalls

Jonas Buck[1], Dominik Witzigmann[1,2], Susanne Schenk[1], Tomaz Einfalt[1], Ludovit Zweifel[3], Hiu-Man Grisch-Chan[4], Beat Thöny[4], Jörg Huwyler[1]

1 Division of Pharmaceutical Technology, Department of Pharmaceutical Sciences, University of Basel, Basel, Switzerland

2 Department of Biochemsitry & Molecular Biology, Life Science Institute, University of British Columbia, Vancouver, Canada

3 Biozentrum, University of Basel, Basel, Switzerland

4 Division of Metabolism and Children's Research Centre, University Children's Hospital Zurich, Zurich, Switzerland

Abstract

Gene therapy aims to introduce nucleic acids into cells. Besides viral delivery, one of the most common approaches to achieve this is the use of lipid-based nanoparticles. Nucleic acids and nanoparticles are combined based on defined mixing ratios and it is generally assumed that the calculated concentrations are identical to the actual concentrations in the preparation prior to application. Herein, we apply fluorescence cross-correlation spectroscopy (FCCS) to quantify nucleic acid and nanoparticle interactions. Using FCCS, we could show that calculated concentrations do not necessarily reflect actual concentrations. The disparity was higher for a commercial formulation with unknown composition compared to self-prepared formulations. We conclude that comparisons between formulations may be misleading if they are solely based on theoretical assumptions and not on experimental data. We therefore recommend investigating interactions between nanoparticles and nucleic acids for each formulation individually to avoid this common pitfall in non-viral gene delivery.

Introduction

Gene therapy represents an attractive therapeutic option to treat various diseases. However, many aspects of molecular mechanisms involved in successful transfection of target tissues are still poorly understood.[1,2] In the field of lipid-based non-viral gene delivery, efforts are ongoing to identify lipid or lipid-like molecules, which can be used to promote successful transfer of nucleic acids into cells. Despite some setbacks, many formulations that promote high gene delivery efficiencies both *in vitro* and *in vivo* were developed in the recent years.[3–7] In many instances, researchers did thereby use an empiric approach to optimize lipid based formulations. In addition to formulations developed in the academic environment several private companies entered the marked with ready-to-use formulations (such as formulations of the Lipofectamine family) that can act as a reference system to compare different formulations with each other.[1,8,9] These commercial transfection reagents have been used by thousands of researchers so far and still see widespread application as standard

formulations for *in vitro* trials despite the fact that their precise composition is not disclosed.[10–13] Therefore, as a pragmatic approach, nucleic acids and transfection reagent are diluted separately in an appropriate buffer, combined, incubated to allow for spontaneous complexation, and finally added to target cells. It is generally assumed, that the formed lipoplexes (complexes of lipid-based transfection reagent and nucleic acid) contain the calculated amount of added ingredients. Furthermore, mixing ratios between different components of the system are believed to be precisely defined and key to a further optimization of the experimental system.[14,15] In our opinion, this procedure leads to artefacts because the formation of lipoplexes can be influenced by many factors such as the type of nucleic acid,[16] the type of lipid based constituents and the used amounts of lipoplexes.[17–19] There are some publications in which the amount of delivered nucleic acid per cell is quantified via PCR.[20–24] However, in most cases researchers just assume that the calculated amount of nucleic acids or lipoplexes used corresponds to actual quantities delivered to the target cells. We believe that the outlined approach is flawed. Transfection efficiency is not solely a function of the amount of DNA added. Furthermore, mixing ratios of all components of the used systems should be experimentally confirmed since we cannot exclude unspecific binding of lipids or lipoplexes to surfaces.

It was therefore the aim of the present project to develop a fluorescence-based method that would allow us to investigate DNA – nanoparticle interactions. Fluorescence cross-correlation spectroscopy (FCCS) was thereby identified as a promising approach to study nucleic acid-nanoparticle interactions and lipoplex formation.[25] In contrast to quantitative PCR methods, flow cytometry, or confocal microscopy, a quantitative assessment of DNA and particle interactions is possible by this method. Using FCCS, the diffusion dynamics of labeled particles within a confined confocal volume can be monitored. Based on diffusion times and signal amplitudes, the size and concentration of particles can be determined [ref]. Moreover, FCCS experiments can provide valuable insights into DNA binding patterns and amounts of labeled reagents. As a model system, small minicircle DNA (1.4 kb) and conventional parental plasmid DNA (5.4 kb) was used. Both DNA moieties were complexed with a cationic lipid (1,2-dioleoyl-3-trimethylammonium-propane, DOTAP) formulation, an ionizable lipid dilinoleylmethyl-4-dimethylaminobutyrate (DLin-MC3-DMA) formulation, as well as with a commercially available transfection reagent (Lipofectamine 3000). A design of experiment (DoE) approach was chosen to obtain data about gene delivery efficiency and transgene expression levels. The results of the FCCS measurements provided new insights in the mechanisms of interaction between DNA and lipid nanoparticles and allowed us to identify potential sources of artefacts.

Materials and Methods

Nanoparticle preparation

Lipofectamine 3000 (Invitrogen, Life Technologies, Zug, Switzerland) was used as provided by the manufacturer. DOTAP:cholesterol nanoparticles were both, extruded and prepared using microfluidics, whereas DLin-MC3-DMA nanoparticles were prepared employing a microfluidics approach only (NanoAssemblr, Precision Nanosystems, Vancouver, Canada) because extrusion was not possible with the used settings.

Extrusion

DOTAP (Corden Pharma Switzerland LLC, Liestal, Switzerland) and cholesterol (Sigma-Aldrich Co, St. Louis, MO, USA) were combined at a 1:1 ratio (mol%) using the respective ethanolic stock solutions.

The lipid film was then dried using nitrogen. Afterwards, the dried lipid film was subjected to vacuum for at least 48 h. At the day of extrusion, the dried lipid film was rehydrated with 5% glucose (Roth AG, Switzerland) solution at constant stirring and heating to 60 °C for 10 min. The rehydrated lipid film was then vortexed for 30 s and subjected to 5 freeze-thaw cycles (5 min each) using dry ice and a water bath (60 °C). After freeze-thaw, the lipid film was left for 3 h and was subsequently extruded 15 times through a 100 nm polycarbonate membrane (Whatman Nuclepore Track-Etched Membranes, GE Healthcare Life Sciences, Buckinghamshire, UK) using a hand extruder (Avanti Mini Extruder, Avanti Polar Lipids Inc, AL, USA). The size and the PDI of the resulting nanoparticles were determined using a DLS (Delsa Nano C Particle Analyzer, Beckman Coulter, Inc, Indianapolis, IN, USA)and extrusion was repeated if necessary to obtain nanoparticles with a size range of 90 – 110 nm and a PDI > 0.2.

Microfluidics

DOTAP and cholesterol (1:1), or DLin-MC3-DMA, cholesterol, and DOPC were combined at a ratio of 5:4:1 (mol%) from their ethanolic stock solutions. The lipid film was again dried using nitrogen and vacuum as described for DOTAP/cholesterol nanopartiles. At the day of nanoparticle preparation, the lipid components were redissolved in a given volume of ethanol and loaded into a syringe. Using the NanoAssemblr, the lipid fraction was combined with 5% glucose solution (DOTAP:chol) or 20 mM acetate buffer pH 4.0 (DLin-MC3-DMA) at a 1:3 ratio in a microfluidic cartridge. The resulting nanoparticles' size and PDI was determined using a DLS and the nanoparticles were subjected to dialysis overnight against 20 mM acetate buffer pH 4.0 (5% glucose in the case of DOTAP:chol) to remove the remaining ethanol. The resulting nanoparticles were used for transfection experiments. A pH below 4.0 was mandatory because DLin-MC3-DMA-based nanoparticles aggregated and precipitated in higher pH media due to the lacking stabilizing effect of PEG.[26]

Nanoparticle/DNA complex preparation

Nanoparticle/DNA complexes were prepared in 5% glucose solution. Lipofectamine 3000 was combined with DNA at indicated ratios according to the manufacturer's protocol. DOTAP:cholesterol and DLin-MC3-DMA nanoparticles were diluted in separate tubes as was DNA. The diluted samples were vortexed and spinned down for a short time frame and the content of the tube containing the diluted DNA was added to the tube containing the diluted nanoparticles. The resulting nanoparticle/DNA formulations were again vortexed and spinned down quickly and left for 30 min for complex maturation. After complex maturation, the samples were added to the cells.

Transfection

All cell lines were seeded in poly-D-lysine-coated 24-well plates (TPP Tissue Culture Testplate 24, TPP Techno Plastic Products AG, Trasadingen, Switzerland) at a seeding density of 5 x 10^4 cells per well. Cells were maintained in Dulbecco's modified Eagle's medium (DMEM, Sigma-Aldrich Co, St. Louis, MO, USA), supplemented with 10% fetal calf serum (FCS, BioConcept, Allschwil, Switzerland), as well as penicillin (100 units/mL), and streptomycin (100 µg/mL) (both from Sigma-Aldrich Co, St. Louis, MO, USA). The total volume of medium was 1 mL. Cells were then left to attach and grow for 24 h in humidified 5% CO_2 at 37 °C. The prepared nanoparticle/DNA formulations (total volume of 50 µL) were then added to the cells. The cells were incubated with the nanoparticle/DNA formulations for indicated time frames without changing the medium.

Flow cytometry

The cells were washed with 1 mL D-PBS (Sigma-Aldrich Co, St. Louis, MO, USA) and detached at indicated timepoints using 200 µL 0.25% Trypsin/EDTA (Invitrogen, Life Technologies, Zug,

Switzerland). The cells were collected and centrifuged for 5min at 200 x g. Excess medium was removed by aspiration and the cell pellet was resuspended in FACS buffer (D-PBS supplemented with 1% FCS, 0.5% EDTA, and 0.5% sodium azide, Sigma-Aldrich Co, St. Louis, MO, USA), transferred to FACS tubes and stored on ice. Flow cytometry was done using a FACS Canto II flow cytometer (Becton Dickinson, San Jose, CA) and the stopping gate was 10.000 cells. The cells were gated to obtain singlets and the percentage of GFP-positive cells (transfection efficiency) and the median fluorescence intensity (transgene expression, MFI) were recorded after excitation at 488 nm. The fluorescence signal of cells expressing GFP was detected in fluorescence channel FL1 (505LP – 530/30).. Further analysis of the obtained data was done using FlowJo Vx software (TreeStar, Ashland, OR, USA).

Design of experiment (DoE)

To screen minicircle DNA and parental plasmid DNA for transfection efficiency and transgene expression, a design of experiment (DoE) approach was applied. A full factorial (2 level) interaction model design was set up using the software MODDE v. 9.0.0.0. The design consisted of the three factors DNA concentration, lipid-to-DNA ratio, and the type of DNA molecule (minicircle DNA vs. parental plasmid DNA) and the two responses transfection efficiency (%GFP positive cells) and transgene expression (MFI). A total of 30 experimental runs per model was carried out to collect the data necessary to generate the model. Models were generated for each cell line and transfection reagent. The resulting data was log transformed where necessary (see supporting information Table S1) and data points with deviations ≥±3 SD in the normal probability plot of the Y-residuals were excluded (see supporting information Table S1). Interaction terms were kept to a minimum and were sequentially excluded to increase the model fit and predictability.

Cytotoxicity

Cytotoxicity of lipid nanoparticles alone and lipid nanoparticles combined with DNA was determined by means of MTT assay. Briefly, 50000 cells per mL were seeded in a 96-well plate (TPP Tissue Culture Testplate 96F, TPP Techno Plastic Products AG, Trasadingen, Switzerland) which was previously treated with poly-D-lysine. The final volume of the medium containing the cells was 200 µL per well resulting in 10000 cells seeded per well. After 24 hours, cells were treated with either nanoparticles alone or nanocomplexes comprising of LNPs and DNA at indicated concentrations. 24 hours later, the medium was aspirated and replaced by medium containing 0.5 mg/mL 3-(4,5-dimethylthiazol-2-yl)-2,5-diphenyl tetrazolium bromide (MTT, Carl Roth, Karlsruhe, Germany). After an incubation period of 2 hours (37°C, 5% CO_2), the medium containing the MTT reagent was aspirated. The insoluble formazan crystals formed within the cells were solubilized using a mixture of 3% SDS in H_2O and 40 mM HCl in isopropanol (1:6, V/V). The plate was then placed on a shaker for 2 hours to completely dissolve the formazan crystals. Following solubilization, absorption was measured using a 96-well plate reader (SpectraMax M2e Microplate Reader, Molecular Devices LLC, San Jose, CA, USA) at 570 nm (formazan signal) and 670 nm (background).

Transmission electron microscopy (TEM)

To acquire TEM images of the nanocomplexes, samples were prepared on copper grids. Briefly, the sample was put on the grip for 1 min and stained twice with 2% uranylacetate solution. Afterwards, the grid was washed twice with ddH_2O and left at RT for 24 hours until completely dried. TEM images were then acquired on a CM-100 electron microscope (Philips, Eindhoven, Netherlands).

Fluorescence cross-correlation spectroscopy (FCCS)

Labeling of LNPs was done by inclusion of 0.1 mol-% of 1,1'-dioctadecyl-3,3,3',3'-tetramethylindocarbocyanine perchlorate (DiI) in the formulation prior to extrusion. For Lipofectamine 3000, DiI was added in the same amount to the ready-to-use formulation. No purification step was taken because first, the DiI dye is highly fluorescent in lipophilic environments whereas it shows only weak fluorescence in hydrophilic environments[27], and second, free dye can be easily distinguished from dye bound to nanoparticles in FCCS measurements. DNA was labeled using the Cy5 Label IT® kit according to the manufacturer's protocol. The labeled DNA sample was subsequently purified using the purification columns provided with the kit. FCCS measurements were carried out according to the procedurde described by Zelmer et al. on an Olympus IX73 inverted microscope equipped with a 1.2 N.A. water-immersion 60× superapochromat objective (UplanSApo; Olympus).[28] Statistical evaluation of FCCS results was carried out using OriginPro 2018 (64-bit) SR1 b9.5.1.195 (Academic) (OriginLab Corporation, Northampton, MA, USA).

Results and Discussion

Design of experiment (DoE) and Cytotoxicity

To get a basic understanding of gene delivery efficiencies for different formulations, we employed a design of experiment (DoE) approach to determine the transfection efficiency and the amount of expressed transgene. The DNA concentration, the lipid-to-DNA ratio, and the type of plasmid (minicircle DNA vs. parental plasmid DNA) were set as the factors. The influence of those factors on the two responses transfection efficiency (%GFP positive cells) and transgene expression (MFI) was investigated using the software MODDE. As transfection reagents, we used a formulation containing a cationic lipid (DOTAP), one formulation containing an ionizable lipid (DLin-MC3-DMA), and a commercial transfection reagent (Lipofectamine 3000). The results for DOTAP:chol showed that extruded DOTAP:chol nanoparticles were associated with higher transfection efficiencies and transgene expression levels than DOTAP:chol nanoparticles manufactured by microfluidics. Therefore, the extruded nanoparticles were used for the generation of DoE data. For DLin-MC3-DMA however, extrusion was not possible due to precipitation of the lipid nanoparticles during the extrusion process. This observation can be a consequence of the negative surface charge of polycarbonate membranes at pH 4 that leads to absorption of positively charged DLin-MC3-DMA to the membrane surface.[29] Therefore, for DLin-MC3-DMA the microfluidics approach was used to prepare the nanoparticles. The obtained data allowed for generation of a DoE model using the software MODDE v.9.0. The resulting models showed high R^2 and Q^2 values (see Table 1), which were higher than expected for transfection experiments. Values above 0.5 for both parameters are acceptable and indicative of high predictability. With two exceptions (the MFI model for Lipofectamine 3000 in Hep3B cells and the GFP model for Lipofectamine 3000 in HuH7 cells), all R^2 values were above 0.65 and all Q^2 values were above 0.5. This indicates that the models reflect the actual data well and that they possess a good prediction precision. The low model validity observed for DOTAP and DLin-MC3-DMA and the response median fluorescence intensity in HuH7 cells (Figure S5, FigureS11) can be explained by the high reproducibility, leading to the validity term turning to negative values.[30] The models for Lipofectamine 3000 were characterized by a generally lower R^2 and Q^2 values compared to the other transfection reagents.

Table 1: Multiple correlation coefficients (R^2) and cross-validated R^2 (Q^2) of the generated models. The table depicts the R^2 values («goodness of fit») and the Q^2 values («predictive ability of the model») for the models generated for each cell line and transfection reagent. All results for the different cell lines and transfection reagents were fitted using partial least squares projection (PLS). Generally, a Q^2 value close to the R^2 value is indicative of a good model. R^2 and Q^2 values should be >0.5 for a good model. All models were generated from n=3 independent experiments.

Response:	Reagent:	Cell line:	Fitting method:	R^2:	Q^2:
%GFP positive cells	DOTAP	Hep3B	PLS	0.869652	0.772024
		HepG2	PLS	0.913302	0.871974
		HuH7	PLS	0.99553	0.958856
	DLin-MC3-DNA	Hep3B	PLS	0.980955	0.962263
		HepG2	PLS	0.963826	0.923392
		HuH7	PLS	0.991396	0.947793
	Lipofetamine 3000	Hep3B	PLS	0.655348	0.503689
		HepG2	PLS	0.776626	0.69747
		HuH7	PLS	0.628769	0.466982
Median fluorescence intensity	DOTAP	Hep3B	PLS	0.827971	0.754755
		HepG2	PLS	0.824154	0.749751
		HuH7	PLS	0.963571	0.946782
	DLin-MC3-DNA	Hep3B	PLS	0.750443	0.649015
		HepG2	PLS	0.830935	0.74788
		HuH7	PLS	0.974343	0.930003
	Lipofetamine 3000	Hep3B	PLS	0.294765	0.0180769
		HepG2	PLS	0.785215	0.712894
		HuH7	PLS	0.948028	0.858936

A representation of the resulting contour plots (in HuH7 cells) is shown in Figure 1. Using minicircle DNA, the highest transfection efficiencies were observed using DLin-MC3-DMA, followed by Lipofectamine 3000. This observation was consistent across all investigated cell lines (see Supporting Information Fig. S2 - Fig. S18). Nanoparticles based on DLin-MC3-DMA exhibited a remarkable efficiency in transfecting all investigated cell lines using minicircle DNA with almost 100% of the cells expressing GFP (at 2 µg/mL DNA concentration). High efficiencies using this compound were already shown previously for siRNA and in a clinical setting.[31–34] In addition to that, our results demonstrate the usefulness of DLin-MC3-DMA-based nanoparticles for the delivery of small DNA moieties. However, despite the very high transfection efficiencies, the subsequent transgene expression was lower compared to Lipofectamine 3000 which showed the highest transgene expression levels (up to 22000 RFU) across all cell lines. Still, except for Hep3B cells, DLin-MC3-DMA showed higher transgene expression levels (up to 3000 RFU) than DOTAP:chol. Therefore, DLin-MC3-DMA can be regarded as efficient transfection reagent for small DNA molecules. When using the parental plasmid DNA, however, both the transfection efficiency and the transgene expression following DLin-MC3-DMA-mediated gene delivery dropped drastically. The larger parental plasmid DNA was not delivered successfully (up to 1.25% GFP positive cells) and did not elicit a marked gene expression (<300 RFU).

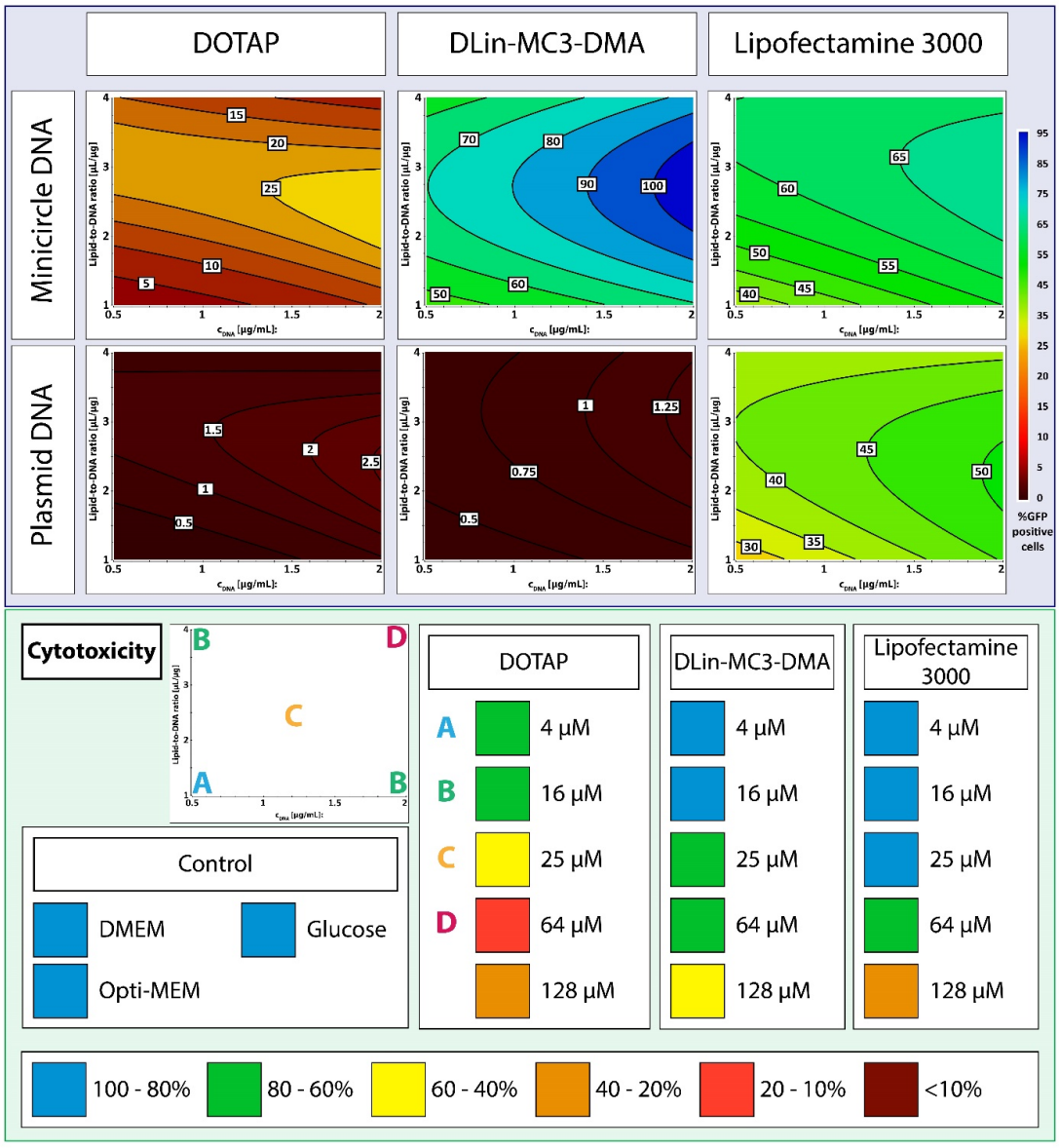

Figure 1: Comparison of the transfection efficiency of the employed nucleic acids and cytotoxicity of the applied transfection reagents in HuH7 cells. The figure displays the transfection efficiency of minicircle DNA (top row) and parental plasmid DNA (bottom row) as 2D contour plots generated by MODDE using the data of a design of experiment (DoE) in the blue box. With all employed transfection reagents, minicircle DNA is associated with markedly increased efficiency compared to parental plasmid DNA. The green box displays the cytotoxicity of the employed compounds. A concentration of 4 µM corresponds to the setting of 0.5 µg/mL DNA and a lipid-to-DNA ratio of 1µL/µg while the highest amount of lipid applied at 2 µg/mL DNA and a lipid-to-DNA ratio of 4µL/µg resulted in a final concentration of 64 µM. The highest level (128 µM) was not included in DoE runs but in cytotoxicity determination to better assess the cytotoxic potential of the used transfection reagents. The formulation containing DLin-MC3-DMA improved most following replacement of parental plasmid DNA. Lipofectamine was the least affected transfection reagent. Moreover, the DLin-MC3-DMA formulation showed the lowest cytotoxic potential of all employed transfection reagents. Data represented in the transfection box (blue box) is based on a model generated by MODDE using the data obtained during the DoE experiments (n = 3). The data in the cytotoxicity box (green box) is based on the average of six parallel measurements conducted in three independent experiments.

Consequently, DLin-MC3-DMA is highly sensitive to plasmid size. A possible explanation for this observation is the fact that DLin-MC3-DMA was optimized for delivery of siRNA leading to suboptimal interactions with large nucleic acids. A less distinct drop in efficiency was also observed for

DOTAP:Chol but not for Lipofectamine 3000. It is noteworthy that the transgene expression levels of Lipofectamine 3000 were far higher than those of DOTAP:cholesterol and DLin-MC3-DMA. Lipofectamine 3000 (except for in HepG2 cells) and DLin-MC3-DMA showed a marked influence of the dose of DNA with higher doses leading to higher percent transfected cells and transgene expression. The lipid-to-DNA ratio showed a less pronounced influence on the responses. In contrast to this, for DOTAP, a high lipid-to-DNA ratio is important for a high percentage of transfected cells, whereas a high dose of DNA is important for high transgene expression levels.

Besides transfection efficiency and transgene expression capabilities, nanoparticulate gene delivery systems also need to be well tolerated by cells and therefore, show a low cytotoxicity. A comparison between the cytotoxicity (determined by MTT assay) of nanoparticles and of nanoparticles complexed with DNA did not show significant differences. This suggests that the cytotoxicity depends on lipid moieties and cannot be attenuated by complexed DNA molecules. The cytotoxic potential of all three transfection reagents is shown in Figure 1. Both, DLin-MC3-DMA and Lipofectamine 3000 were well-tolerated up to lipid nanoparticle concentrations of 64 µM. It is noteworthy that this concentration was not exceeded in any experiment and the 128 µM data point was only included to extend the tested dose-range beyond the experimental range of the DoE. DOTAP:cholesterol nanoparticles were also well-tolerated up to a concentration of 16 µM but showed a distinct cytotoxic potential at higher concentrations. Especially in the setting employing a high dose of DNA in combination with a high lipid-to-DNA ratio, DOTAP:cholesterol shows a lower cellular survival than DLin-MC3-DMA, and Lipofectamine 3000.

DNA in lipid nanoparticles quantification

A possible explanation for the improved performance of minicircle DNA might be the number of plasmids delivered to cells. A rough calculation based on number of base pairs implies that 1 µg of minicircle DNA contains approximately 3.8 times more individual DNA molecules compared to parental plasmid DNA. If we perform experiments based on a µg/mL DNA amount and add a fixed amount of lipid nanoparticles to our DNA sample, it would be tempting to assume that minicircle DNA-based lipoplexes led to higher transfection efficiencies simply due to the fact that there are more DNA molecules present compared to parental plasmid DNA-based lipoplexes.

To improve our understanding of the properties of nanoparticles derived from either minicircle DNA or parental plasmid DNA, fluorescence cross-correlation spectroscopy (FCCS) was applied. FCCS experiments were conducted on Cy5-labeled plasmid samples, DiI-labeled nanoparticle samples, and the lipoplexes obtained after combination of plasmids and nanoparticles. Each fluorescence correlation curve is the average of three measurements and curves are lifetime corrected. The resulting molecular brightness (count per molecule) levels were used to normalize the number of DNA molecules per nanoparticle. The results of the fluorescence lifetime measurements are shown in Table 1 and the autocorrelation curves (ACFs) of DNA molecules alone and nanoparticles alone are shown in Figure S19 and Figure S20. First, FCCS data suggests that the DNA samples are clean, *i.e.*, there is no extra phase from the free dye, which was true for parental plasmid DNA as well as minicircle DNA. According to calculations, pure minicircle DNA samples (1.4 kb) should have almost four-fold higher molarity than parental plasmid DNA (5.4 kb). However, our measurements revealed 1.9 nM and 0.9 nM concentrations for both plasmids, respectively. This discrepancy can be explained by two experimental shortcomings. First, recovery of DNA was incomplete after fluorescence labeling (155 µg/ml and 393 µg/ml recovered concentrations for minicircle DNA and plasmid DNA, respectively). Second, losses of DNA during complex formation leading to an additional loss of plasmid DNA but not minicircle DNA. Thus, final concentrations of DNA in the experiment were much

smaller than expected. This emphasizes the need to carefully monitor DNA concentrations at all stages of the experiment. It is tempting to speculate that DNA losses are caused by unspecific adsorption of DNA-containing lipoplexes to surfaces. Interestingly, both effects seem to depend on plasmid size and cannot readily be explained.

Due to the differences between calculated and experimental DNA concentrations in our experiments, we had to question our initial assumption of a uniform mode of interaction between DNA molecules of different size and lipoplexes. Indeed, Cy5 lifetime measurements revealed that lipoplexes using DOTAP and DLin-MC3-DMA show a prolongation of Cy5 τ_1 lifetimes. On the other hand, τ_2 is reduced, pointing to a larger exposure or to the sensing of the different chemical environments of DOTAP and DLin-MC3-DMA. The τ_1 and τ_2 shifts for Lipofectamine 3000 interactions are qualitatively and quantitatively different, with both values shifting to shorter lifetimes. This is indicative for a different mode of interaction with DNA.

Table 2: Results of the fluorescence lifetime measurement obtained by fluorescence correlation spectroscopy (FCS).

Sample:	Fluorophore:	τ_1 fluorescence lifetime [ns]:	τ_2 fluorescence lifetime [ns]:
Minicircle DNA	Cy5	0.842 ± 0.006	1.994 ± 0.006
Minicircle DNA/DOTAP	Cy5	0.922 ± 0.009	1.803 ± 0.007
Minicircle DNA/DLin-MC3-DMA	Cy5	0.931 ± 0.006	1.746 ± 0.004
Minicircle DNA/Lipofectamine 3000	Cy5	0.577 ± 0.008	1.510 ± 0.012
Parental plasmid	Cy5	0.835 ± 0.005	1.950 ± 0.011
Parental plasmid/DOTAP	Cy5	0.919 ± 0.009	1.752 ± 0.006
Parental plasmid/DLin-MC3-DMA	Cy5	0.850 ± 0.010	1.707 ± 0.004
Parental plasmid/Lipofectamine 3000	Cy5	0.574 ± 0.005	1.404 ± 0.007
DOTAP	DiI	0.921 ± 0.011	1.650 ± 0.029
DOTAP/minicircle DNA	DiI	0.785 ± 0.009	1.416 ± 0.016
DOTAP/parental plasmid	DiI	0.780 ± 0.004	1.480 ± 0.011
DLin-MC3-DMA	DiI	0.856 ± 0.005	1.680 ± 0.013
DLin-MC3-DMA/minicircle DNA	DiI	0.792 ± 0.007	1.760 ± 0.013
DLin-MC3-DMA/parental plasmid	DiI	0.793 ± 0.005	1.806 ± 0.009
Lipofectamine 3000	DiI	0.705 ± 0.011	1.540 ± 0.043
Lipofectamine 3000/minicircle DNA	DiI	0.454 ± 0.008	1.410 ± 0.049
Lipofectamine 3000/parental plasmid	DiI	0.461 ± 0.007	1.390 ± 0.035

Lifetime measurements for DiI vary as well among the different formulations. The interaction of nanoparticles with DNA led to shifts in both measured lifetimes of DiI and are probably influenced by the change in the chemical potential in the surrounding of the nanoparticle and/or the rearrangements of molecules within the nanoparticle. In particular, shifts in τ_1 lifetimes towards shorter lifetimes suggests displacement of DiI by DNA. Shifts in the τ_2 lifetime are related to changes in chemical compositions and membrane rearrangement.

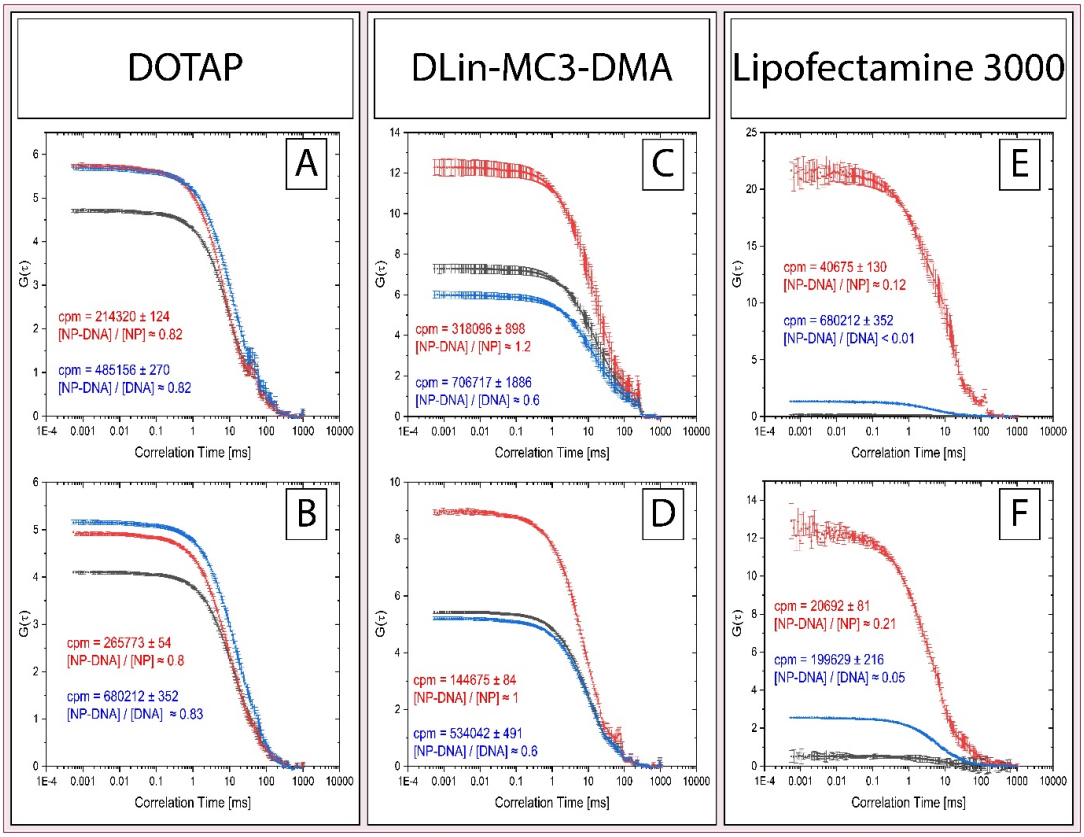

Figure 2: Autocorrelation functions (ACFs) for labeled DNA and nanoparticle samples following fluorescence cross-correlation spectroscopy (FCCS) measurements. The picture depicts the ACFs of DiI-labeled nanoparticles (red) and either Cy5-labeled mcDNA or Cy5-labeled ppDNA (blue) and the associated cross-correlation functions (black) obtained after FCCS measurements. The plots depict the results for the combination of DOTAP with either mcDNA (A) or ppDNA (B), DLin-MC3-DMA with either mcDNA (C) or ppDNA (D), and Lipofectamine 3000 with either mcDNA (E) or ppDNA (F). FCCS measurements for DOTAP indicate that at the given concentration, most (approx. 80%) of the nanoparticles are involved in interactions with DNA. DOTAP/DNA nanoparticles appear to be the most stable sample and the binding stoichiometry is approximately 2:1 (DNA:DOTAP) for both plasmid types. For DLin-MC3-DMA, basically all nanoparticles interact with DNA irrespective of the type of DNA and for both plasmid types, single DNA molecules interact with multiple nanoparticles. In contrast to this, DNA and Lipofectamine 3000 are mainly unbound, again irrespective of the type of DNA. The results indicate again for both types of plasmids that several DNA molecules interact with one nanoparticle. (n=3)

The results of the FCCS measurements are displayed in Figure 3 and allow us to calculate not only the fractions of bound and unbound particles (both nanoparticles and DNA molecules) but also the binding stoichiometry of the involved molecules. To our knowledge, these results are unique in that binding stoichiometries of nanoparticles for gene delivery were only calculated but not measured so far. The most stable nanoparticle/DNA interaction was found with DOTAP nanoparticles. The concentration ratio between bound partners and free species (*i.e.*, [NP-DNA]/[NP], and [NP-DNA]/[DNA]) can be determined in a first approximation by $G_{Complex}(0)/G_{DNA}(0)$ and $G_{Complex}(0)/G_{NP}(0)$, respectively. We conclude that at the given concentration, approximately 80% of the DNA is involved in interactions with DOTAP nanoparticles. This observation in combination with the brightness levels indicate a binding stoichiometry of approximately 2:1 (DNA:DOTAP) for both plasmids. FCCS measurements for DLin-MC3-DMA revealed that basically all of MC3 is involved in the interaction with DNA. Similar amounts of minicircle DNA or parental plasmid interact with individual DLin-MC3-DMA nanoparticles. This together with the brightness levels suggests that a single DNA molecule interacts with multiple DLin-MC3-DMA nanoparticles with a stoichiometry of approximately 0.2:1 (DNA:DLin-MC3-DMA). However, the FCCS measurements also showed that large aggregates were

formed during the measurement of DLin-MC3-DMA-based nanoparticles. Surprisingly, FCCS measurements showed that DNA is not bound to Lipofectamine 3000. There is only a small difference in binding preference with respect to DNA size. This together with the brightness levels suggests that a single Lipofectamine 3000 nanoparticle interacts (albeit weakly) with multiple DNA molecules, irrespective of the type of DNA molecule. The binding stoichiometry for Lipofectamine 3000 was calculated to be around 6:1 (DNA:Lipofectamine 3000). We conclude that neither the binding stoichiometries, nor the extent of DNA binding correlate with transfection efficiency. These findings confirm microscopic observation (i.e. formation of large agglomerates), that Lipofectamine 3000 co-precipiates with DNA triggering unspecific uptake into target cells.

To determine the number of DNA molecules per nanoparticle, the brightness of individual samples (*i.e.*,DNA molecules, nanoparticles) was normalized and compared to the brightness values of the mixtures (*i.e.*, DNA/nanoparticle complexes). The results of these calculations are shown in Figure 3. First, the average number of plasmids in the confocal volume was determined for each combination of DNA and LNP (Number of Plasmids). For DOTAP and DLin-MC3-DMA, the number of minicircle DNA in the confocal volume was slightly higher compared to the number of parental plasmid DNA. This finding was expected, although to a larger extent, because the minicircle DNA preparation should contain more DNA molecules than its parental plasmid counterpart. Moreover, the average number of DNA molecules in the confocal volume was comparable for both preparations. However, we did not see a 4-fold difference in the number of DNA molecules in the confocal volume, which is in contrast to what calculations might suggest. For Lipofectamine 3000, the number of minicircle DNA was lower compared to the number of parental plasmid DNA (Figure 3). This finding is counterintuitive. There is a possibility that DNA/LF3000 complexes interact with or attach to surfaces, therefore being depleted during FCCS measurements. An indication for this hypothesis could be the lower number of nanoparticles in the confocal volume observed for Lipofectamine 3000 nanoparticles alone. In fact, Lipofectamine 3000-based nanoparticles often formed aggregates (see above). These aggregates will sediment faster than smaller nanoparticles and might therefore lead to sample depletion during the measurement. A similar pattern was observed for the average number of nanoparticles in the confocal volume (Number of Nanoparticles). The number of nanoparticles in the confocal volume was again higher for nanoparticles containing minicircle DNA than for nanoparticles containing parental plasmid DNA in DOTAP and DLin-MC3-DMA (Figure 4). However, the number of lipid nanoparticles in the confocal volume was approximately 10 times higher for DLin-MC3-DMA than for DOTAP, explaining the approximately tenfold difference in binding stoichiometries observed in FCS measurements. Here again, Lipofectamine 3000-based nanoparticles were associated with smaller numbers of nanoparticles when complexed with minicircle DNA as compared to parental plasmid DNA. These results confirm the initial approximations with respect to the binding stoichiometry.

We conclude from these experiments (Figure 4) that the number of plasmids per nanoparticle varies considerably between formulations: the number of plasmids per nanoparticle was approximately 2.7 for DOTAP, 0.19 for DLin-MC3-DMA, and 5.8 for Lipofectamine 3000. However, irrespective of DNA size, the same number of DNA molecules is bound to nanoparticles. Consequently, the higher efficiency of minicircle DNA cannot be attributed to a higher number of DNA molecules delivered to the cells but must be influenced by more favorable properties of minicircle DNA when it comes to transfection efficiency (e.g. cytoplasmic mobility,[35–37] reduced epigenetic silencing due to a lack of bacterial backbone structures,[38–40] or enhanced nuclear translocation[41,42]). Indeed, Cy5-labeled minicircle DNA and Cy5-labeled parental plasmid DNA have different calculated hydrodynamic radii of approximately 55 nm and 100 nm, respectively (Supporting Information Figure S19). In line with this observation, Lukacs et al. showed that diffusion through the cytoplasm is highly restricted for larger DNA molecules compared with smaller ones.[37]

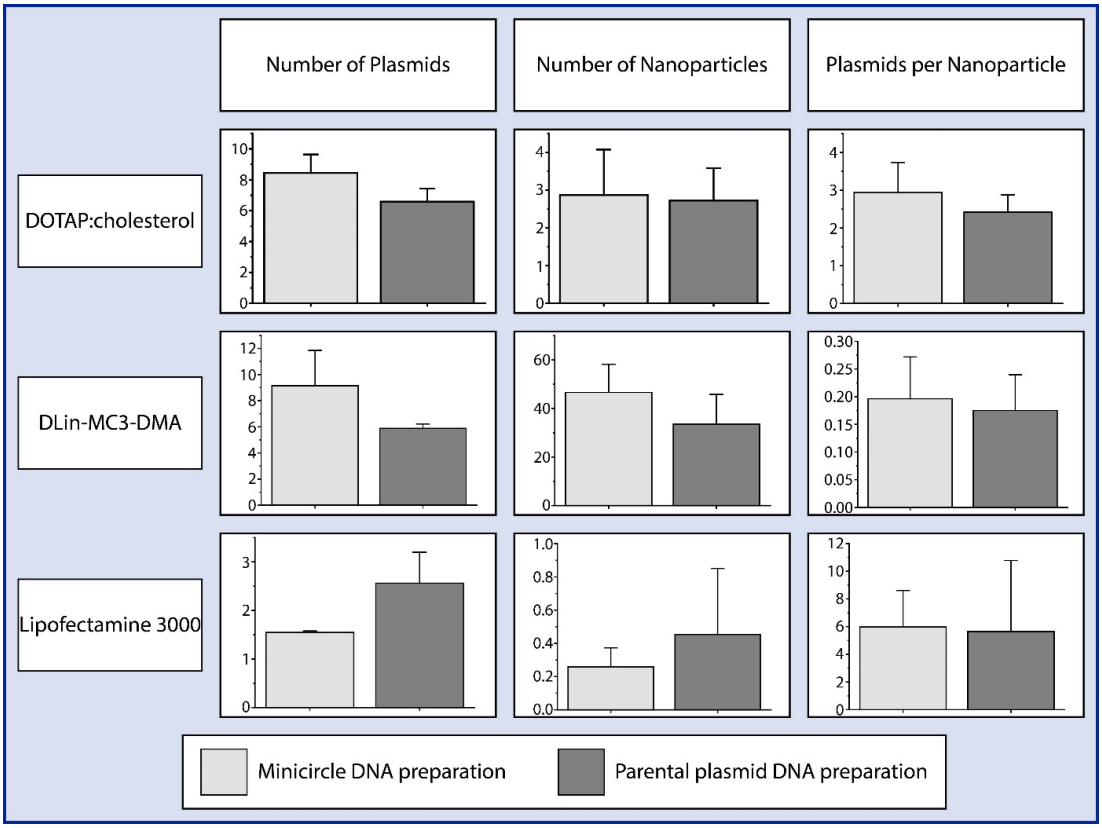

Figure 3: Quantification of plasmid molecules and nanoparticles in the confocal volume. The figure shows the number of plasmids and the number of nanoparticles in the confocal volume as well as the number of DNA molecules per nanoparticle. The panel on the left shows that the number of plasmids in the confocal volume is comparable following application of either minicircle DNA or parental plasmid DNA for DOTAP-based lipoplexes. Here are slightly more minicircle DNA molecules than parental plasmid DNA molecules in the confocal volume for DLin-MC3-DMA, while the opposite was observed for Lipofectamine 3000. The same observations as for DNA were also made for the number of nanoparticles in the confocal volume (middle panel). Therefore, the number of plasmids per nanoparticle is equal for preparations using minicircle DNA or parental plasmid DNA (right panel). Generally, the quantities were similar for the same formulation complexed with the two plasmids but differed largely between the three transfection reagents.

Results of the FCCS measurements allowed us to normalize the transfection efficiency and the transgene expression to the determined number of DNA molecules per volume unit (Figure 4). It is evident that normalization of experimental data is mandatory. This should be done using experimental data and not just calculated correction factors. Normalization based on calculated values is highly biased and would inevitably lead to misinterpretation of data. In particular, the superiority of minicircle DNA in combination with any transfection reagent could only be demonstrated using appropriate normalization procedures as recommended by this work.

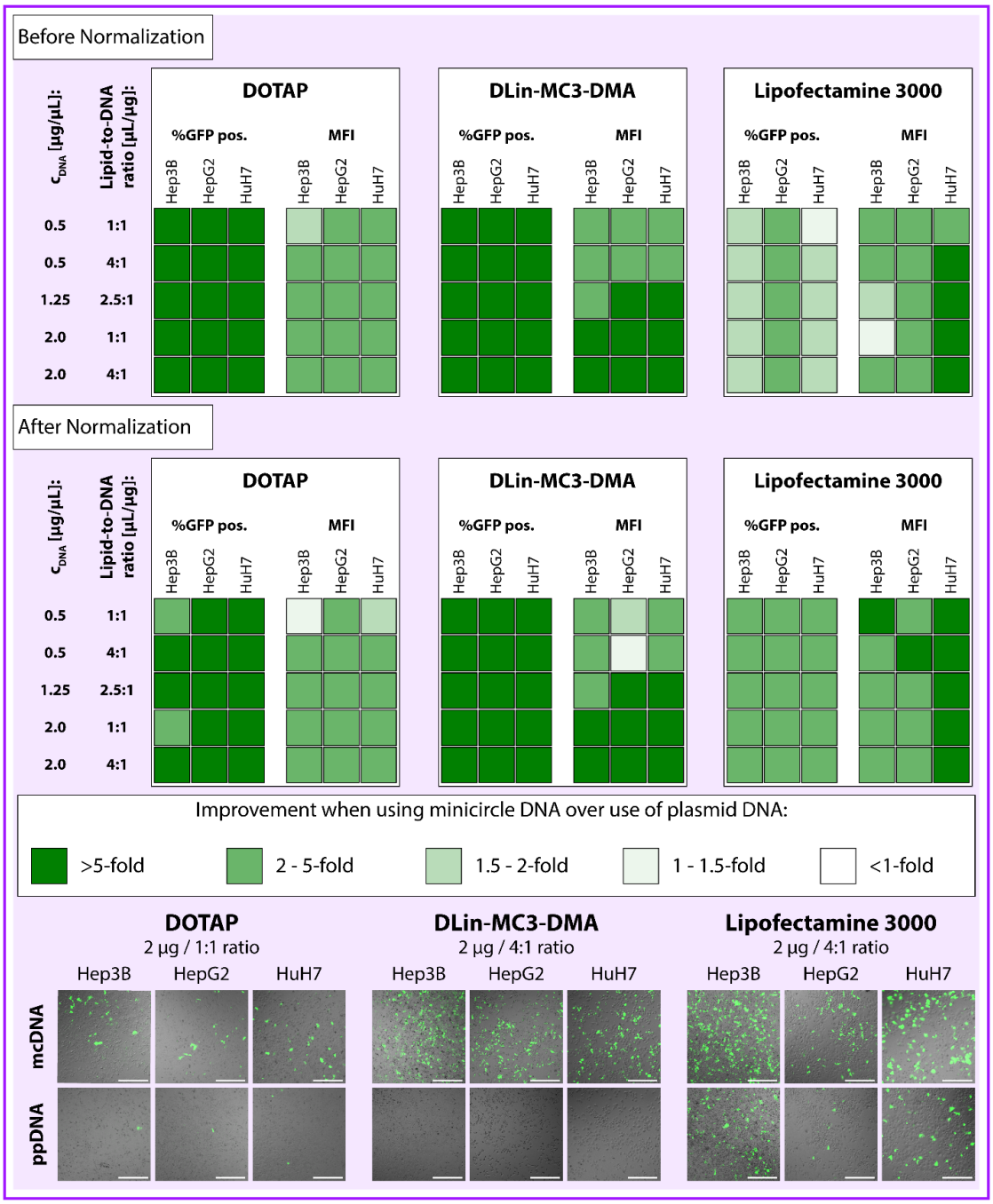

Figure 4: Improvement of transfection efficiency when using minicircle DNA instead of parental plasmid DNA before and after normalization to DNA concentration determined by FCCS. The figure shows the enhanced transfection efficiency following application of minicircle DNA compared to parental plasmid DNA for the three employed transfection reagents. The upper panel shows the improvement based on the results of the DoE, whereas the middle panel shows the improvement after normalization to the number of plasmids in the confocal volume determined by FCCS. Additionally, confocal images acquired at the settings of highest efficiency as determined by DoE are displayed for all three transfection reagents and both plasmids. Generally, the application of minicircle DNA improves transfection efficiency (%GFP positive cells) and transgene expression (mean fluorescence intensity, MFI) in all settings and with all transfection reagents by at least 1.4-fold. Both, DOTAP, and DLin-MC3-DMA profit most from the use of minicircle DNA with respect to transfection efficiency, and, in the case of DLin-MC3-DMA, also transgene expression.

Conclusion

Interactions between DNA molecules and nanoparticles seem to be more complex than anticipated. By applying FCCS we successfully implemented a fluorescence-based method to investigate such interactions. The results showed that assumptions based on calculations do not necessarily reflect the actual conditions. Furthermore, DNA/nanoparticle interactions are strongly dependent on the nanoparticle formulation whereas the size of the DNA molecule has only a minor influence. Consequently, comparisons between DNA molecules of different size, and especially between different formulations are not meaningful if these interactions are not determined for the applied formulations. Ideally such interactions are determined for each individual formulation because we could not identify a general trend that is true for all three formulations. Finally, in a comparison accounting for these observations, minicircle DNA in combination with different transfection reagents promotes higher transfection efficiencies and transgene expression levels compared to parental plasmid DNA when the number of delivered plasmids, and therefore also the number of delivered expression cassettes, is equal.

Acknowledgements

We thank Nicole Rimann of the University Children's Hospital Zurich for supply with minicircle DNA and corresponding parental plasmid DNA.

References

(1) Wu, P.; Chen, H.; Jin, R.; Weng, T.; Ho, J. K.; You, C.; Zhang, L.; Wang, X.; Han, C. Non-Viral Gene Delivery Systems for Tissue Repair and Regeneration. *J. Transl. Med.* **2018**, *16* (1), 29. https://doi.org/10.1186/s12967-018-1402-1.

(2) Buck, J.; Grossen, P.; Cullis, P. R.; Huwyler, J.; Witzigmann, D. Lipid-Based DNA Therapeutics: Hallmarks of Non-Viral Gene Delivery. *ACS Nano* **2019**, *13* (4), 3754–3782. https://doi.org/10.1021/acsnano.8b07858.

(3) Whitehead, K. A.; Dorkin, J. R.; Vegas, A. J.; Chang, P. H.; Veiseh, O.; Matthews, J.; Fenton, O. S.; Zhang, Y.; Olejnik, K. T.; Yesilyurt, V.; et al. Degradable Lipid Nanoparticles with Predictable In Vivo SiRNA Delivery Activity. *Nat. Commun.* **2014**, *5*, 4277. https://doi.org/10.1038/ncomms5277.

(4) Love, K. T.; Mahon, K. P.; Levins, C. G.; Whitehead, K. A.; Querbes, W.; Dorkin, J. R.; Qin, J.; Cantley, W.; Qin, L. L.; Racie, T.; et al. Lipid-like Materials for Low-Dose, in Vivo Gene Silencing. *Proc. Natl. Acad. Sci.* **2010**, *107* (5), 1864–1869. https://doi.org/10.1073/pnas.0910603106.

(5) Cullis, P. R.; Hope, M. J. Lipid Nanoparticle Systems for Enabling Gene Therapies. *Mol. Ther. J. Am. Soc. Gene Ther.* **2017**, *25* (7), 1467–1475. https://doi.org/10.1016/j.ymthe.2017.03.013.

(6) Kulkarni, J. A.; Myhre, J. L.; Chen, S.; Tam, Y. Y. C.; Danescu, A.; Richman, J. M.; Cullis, P. R. Design of Lipid Nanoparticles for in Vitro and in Vivo Delivery of Plasmid DNA. *Nanomedicine Nanotechnol. Biol. Med.* **2017**, *13* (4), 1377–1387. https://doi.org/10.1016/j.nano.2016.12.014.

(7) Jayaraman, M.; Ansell, S. M.; Mui, B. L.; Tam, Y. K.; Chen, J.; Du, X.; Butler, D.; Eltepu, L.; Matsuda, S.; Narayanannair, J. K.; et al. Maximizing the Potency of SiRNA Lipid Nanoparticles for Hepatic Gene Silencing In Vivo. *Angew. Chem. Int. Ed Engl.* **2012**, *51* (34), 8529–8533. https://doi.org/10.1002/anie.201203263.

(8) Jung, M.-R.; Shim, I.-K.; Kim, E.-S.; Park, Y.-J.; Yang, Y.-I.; Lee, S.-K.; Lee, S.-J. Controlled Release of Cell-Permeable Gene Complex from Poly(L-Lactide) Scaffold for Enhanced Stem Cell Tissue

Engineering. *J. Controlled Release* **2011**, *152* (2), 294–302. https://doi.org/10.1016/j.jconrel.2011.03.002.
(9) Villate-Beitia, I.; Puras, G.; Zarate, J.; Agirre, M.; Ojeda, E.; Pedraz, J. L. First Insights into Non-Invasive Administration Routes for Non-Viral Gene Therapy. *Gene Ther. - Princ. Chall.* **2015**. https://doi.org/10.5772/61060.
(10) Majidi, A.; Nikkhah, M.; Sadeghian, F.; Hosseinkhani, S. Development of Novel Recombinant Biomimetic Chimeric MPG-Based Peptide as Nanocarriers for Gene Delivery: Imitation of a Real Cargo. *Eur. J. Pharm. Biopharm.* **2016**, *107*, 191–204. https://doi.org/10.1016/j.ejpb.2016.06.017.
(11) Whittlesey, K. J.; Shea, L. D. Nerve Growth Factor Expression by PLG-Mediated Lipofection. *Biomaterials* **2006**, *27* (11), 2477–2486. https://doi.org/10.1016/j.biomaterials.2005.11.016.
(12) Rea, J. C.; Gibly, R. F.; Barron, A. E.; Shea, L. D. Self-Assembling Peptide–Lipoplexes for Substrate-Mediated Gene Delivery. *Acta Biomater.* **2009**, *5* (3), 903–912. https://doi.org/10.1016/j.actbio.2008.10.003.
(13) Kulkarni, M.; Greiser, U.; O'Brien, T.; Pandit, A. Liposomal Gene Delivery Mediated by Tissue-Engineered Scaffolds. *Trends Biotechnol.* **2010**, *28* (1), 28–36. https://doi.org/10.1016/j.tibtech.2009.10.003.
(14) Lipofectamine 3000 Reagent - CH https://www.thermofisher.com/uk/en/home/brands/product-brand/lipofectamine/lipofectamine-3000.html (accessed Feb 11, 2020).
(15) Felgner, P. L.; Gadek, T. R.; Holm, M.; Roman, R.; Chan, H. W.; Wenz, M.; Northrop, J. P.; Ringold, G. M.; Danielsen, M. Lipofection: A Highly Efficient, Lipid-Mediated DNA-Transfection Procedure. *Proc. Natl. Acad. Sci. U. S. A.* **1987**, *84* (21), 7413–7417.
(16) Darquet, A. M.; Cameron, B.; Wils, P.; Scherman, D.; Crouzet, J. A New DNA Vehicle for Nonviral Gene Delivery: Supercoiled Minicircle. *Publ. Online 04 Dec. 1997 Doi101038sjgt3300540* **1997**, *4* (12). https://doi.org/10.1038/sj.gt.3300540.
(17) Wightman, L.; Kircheis, R.; Rössler, V.; Carotta, S.; Ruzicka, R.; Kursa, M.; Wagner, E. Different Behavior of Branched and Linear Polyethylenimine for Gene Delivery in Vitro and in Vivo. *J. Gene Med.* **2001**, *3* (4), 362–372. https://doi.org/10.1002/jgm.187.
(18) Ogris, M.; Steinlein, P.; Kursa, M.; Mechtler, K.; Kircheis, R.; Wagner, E. The Size of DNA/Transferrin-PEI Complexes Is an Important Factor for Gene Expression in Cultured Cells. *Publ. Online 06 Oct. 1998 Doi101038sjgt3300745* **1998**, *5* (10). https://doi.org/10.1038/sj.gt.3300745.
(19) Kunath, K.; von Harpe, A.; Fischer, D.; Petersen, H.; Bickel, U.; Voigt, K.; Kissel, T. Low-Molecular-Weight Polyethylenimine as a Non-Viral Vector for DNA Delivery: Comparison of Physicochemical Properties, Transfection Efficiency and in Vivo Distribution with High-Molecular-Weight Polyethylenimine. *J. Controlled Release* **2003**, *89* (1), 113–125. https://doi.org/10.1016/S0168-3659(03)00076-2.
(20) Kim, E.-Y.; Schulz, R.; Swantek, P.; Kunstman, K.; Malim, M. H.; Wolinsky, S. M. Gold Nanoparticle-Mediated Gene Delivery Induces Widespread Changes in the Expression of Innate Immunity Genes. *Gene Ther.* **2012**, *19* (3), 347–353. https://doi.org/10.1038/gt.2011.95.
(21) Rahim, A. A.; Wong, A. M. S.; Howe, S. J.; Buckley, S. M. K.; Acosta-Saltos, A. D.; Elston, K. E.; Ward, N. J.; Philpott, N. J.; Cooper, J. D.; Anderson, P. N.; et al. Efficient Gene Delivery to the Adult and Fetal CNS Using Pseudotyped Non-Integrating Lentiviral Vectors. *Gene Ther.* **2009**, *16* (4), 509–520. https://doi.org/10.1038/gt.2008.186.
(22) Park, S.; Na, K. The Transfection Efficiency of Photosensitizer-Induced Gene Delivery to Human MSCs and Internalization Rates of EGFP and Runx2 Genes. *Biomaterials* **2012**, *33* (27), 6485–6494. https://doi.org/10.1016/j.biomaterials.2012.05.040.
(23) Mason, M. R.; Ehlert, E. M.; Eggers, R.; Pool, C. W.; Hermening, S.; Huseinovic, A.; Timmermans, E.; Blits, B.; Verhaagen, J. Comparison of AAV Serotypes for Gene Delivery to Dorsal Root Ganglion Neurons. *Mol. Ther.* **2010**, *18* (4), 715–724. https://doi.org/10.1038/mt.2010.19.

(24) Kim, J.-H.; Park, J. S.; Yang, H. N.; Woo, D. G.; Jeon, S. Y.; Do, H.-J.; Lim, H.-Y.; Kim, J. M.; Park, K.-H. The Use of Biodegradable PLGA Nanoparticles to Mediate SOX9 Gene Delivery in Human Mesenchymal Stem Cells (HMSCs) and Induce Chondrogenesis. *Biomaterials* **2011**, *32* (1), 268–278. https://doi.org/10.1016/j.biomaterials.2010.08.086.

(25) Braeckmans, K.; Buyens, K.; Naeye, B.; Vercauteren, D.; Deschout, H.; Raemdonck, K.; Remaut, K.; Sanders, N. N.; Demeester, J.; De Smedt, S. C. Advanced Fluorescence Microscopy Methods Illuminate the Transfection Pathway of Nucleic Acid Nanoparticles. *J. Controlled Release* **2010**, *148* (1), 69–74. https://doi.org/10.1016/j.jconrel.2010.08.029.

(26) Kulkarni, J. A.; Darjuan, M. M.; Mercer, J. E.; Chen, S.; van der Meel, R.; Thewalt, J. L.; Tam, Y. Y. C.; Cullis, P. R. On the Formation and Morphology of Lipid Nanoparticles Containing Ionizable Cationic Lipids and SiRNA. *ACS Nano* **2018**, *12* (5), 4787–4795. https://doi.org/10.1021/acsnano.8b01516.

(27) Tracers for Membrane Labeling—Section 14.4 - CH https://www.thermofisher.com/uk/en/home/references/molecular-probes-the-handbook/fluorescent-tracers-of-cell-morphology-and-fluid-flow/tracers-for-membrane-labeling.html (accessed Feb 11, 2020).

(28) Zelmer, C.; Zweifel, L. P.; Kapinos, L. E.; Craciun, I.; Güven, Z. P.; Palivan, C. G.; Lim, R. Y. H. Organelle-Specific Targeting of Polymersomes into the Cell Nucleus. *Proc. Natl. Acad. Sci.* **2020**. https://doi.org/10.1073/pnas.1916395117.

(29) Keesom, W. H.; Zelenka, R. L.; Radke, C. J. A Zeta-Potential Model for Ionic Surfactant Adsorption on an Ionogenic Hydrophobic Surface. *J. Colloid Interface Sci.* **1988**, *125* (2), 575–585. https://doi.org/10.1016/0021-9797(88)90024-0.

(30) Buck, J.; Huwyler, J.; Kühl, P.; Dischinger, A. Pediatric Dispersible Tablets: A Modular Approach for Rapid Prototyping. *Pharm. Res.* **2016**, *33* (8), 2043–2055. https://doi.org/10.1007/s11095-016-1946-9.

(31) Jayaraman, M.; Ansell, S. M.; Mui, B. L.; Tam, Y. K.; Chen, J.; Du, X.; Butler, D.; Eltepu, L.; Matsuda, S.; Narayanannair, J. K.; et al. Maximizing the Potency of SiRNA Lipid Nanoparticles for Hepatic Gene Silencing In Vivo. *Angew. Chem. Int. Ed.* **2012**, *51* (34), 8529–8533. https://doi.org/10.1002/anie.201203263.

(32) Semple, S. C.; Akinc, A.; Chen, J.; Sandhu, A. P.; Mui, B. L.; Cho, C. K.; Sah, D. W. Y.; Stebbing, D.; Crosley, E. J.; Yaworski, E.; et al. Rational Design of Cationic Lipids for SiRNA Delivery. *Nat. Biotechnol.* **2010**, *28* (2), 172–176. https://doi.org/10.1038/nbt.1602.

(33) Tam, Y. Y. C.; Chen, S.; Cullis, P. R. Advances in Lipid Nanoparticles for SiRNA Delivery. *Pharmaceutics* **2013**, *5* (3), 498–507. https://doi.org/10.3390/pharmaceutics5030498.

(34) U.S. Food and Drug Administration (FDA) Grants Alnylam Breakthrough Therapy Designation (BTD) for Patisiran for the Treatment of Hereditary ATTR (hATTR) Amyloidosis with Polyneuropathy http://investors.alnylam.com/news-releases/news-release-details/us-food-and-drug-administration-fda-grants-alnylam-breakthrough (accessed May 7, 2018).

(35) Vaughan, E. E.; DeGiulio, J. V.; Dean, D. A. Intracellular Trafficking of Plasmids for Gene Therapy: Mechanisms of Cytoplasmic Movement and Nuclear Import. *Curr. Gene Ther.* **2006**, *6* (6), 671–681.

(36) Nafissi, N.; Alqawlaq, S.; Lee, E. A.; Foldvari, M.; Spagnuolo, P. A.; Slavcev, R. A. DNA Ministrings: Highly Safe and Effective Gene Delivery Vectors. *Mol. Ther. - Nucleic Acids* **2014**, *3*. https://doi.org/10.1038/mtna.2014.16.

(37) Lukacs, G. L.; Haggie, P.; Seksek, O.; Lechardeur, D.; Freedman, N.; Verkman, A. S. Size-Dependent DNA Mobility in Cytoplasm and Nucleus. *J. Biol. Chem.* **2000**, *275* (3), 1625–1629. https://doi.org/10.1074/jbc.275.3.1625.

(38) Chen, Z.-Y.; He, C.-Y.; Ehrhardt, A.; Kay, M. A. Minicircle DNA Vectors Devoid of Bacterial DNA Result in Persistent and High-Level Transgene Expression in Vivo. *Mol. Ther.* **2003**, *8* (3), 495–500. https://doi.org/10.1016/S1525-0016(03)00168-0.

(39) Chen, Z.-Y.; Riu, E.; He, C.-Y.; Xu, H.; Kay, M. A. Silencing of Episomal Transgene Expression in Liver by Plasmid Bacterial Backbone DNA Is Independent of CpG Methylation. *Mol. Ther.* **2008**, *16* (3), 548–556. https://doi.org/10.1038/sj.mt.6300399.

(40) Gracey Maniar, L. E.; Maniar, J. M.; Chen, Z.-Y.; Lu, J.; Fire, A. Z.; Kay, M. A. Minicircle DNA Vectors Achieve Sustained Expression Reflected by Active Chromatin and Transcriptional Level. *Mol. Ther.* **2013**, *21* (1), 131–138. https://doi.org/10.1038/mt.2012.244.
(41) Akita, H.; Kurihara, D.; Schmeer, M.; Schleef, M.; Harashima, H. Effect of the Compaction and the Size of DNA on the Nuclear Transfer Efficiency after Microinjection in Synchronized Cells. *Pharmaceutics* **2015**, *7* (2), 64–73. https://doi.org/10.3390/pharmaceutics7020064.
(42) Vacik, J.; Dean, B. S.; Zimmer, W. E.; Dean, D. A. Cell-Specific Nuclear Import of Plasmid DNA. *Gene Ther.* **1999**, *6* (6), 1006–1014. https://doi.org/10.1038/sj.gt.3300924.

Supporting Information

Characterization and Optimization of Lipoplexes: How to standardize Assays and avoid Pitfalls

Jonas Buck[1], Dominik Witzigmann[1,2], Susanne Schenk[1], Tomaz Einfalt[1], Ludovit Zweifel[3], Hiu-Man Grisch-Chan[4], Beat Thöny[4], Jörg Huwyler[1]

1 Division of Pharmaceutical Technology, Department of Pharmaceutical Sciences, University of Basel, Basel, Switzerland

2 Department of Biochemsitry & Molecular Biology, Life Science Institute, University of British Columbia, Vancouver, Canada

3 Biozentrum, University of Basel, Basel, Switzerland

4 Division of Metabolism and Children's Research Centre, University Children's Hospital Zurich, Zurich, Switzerland

Table S1: Transformations and exclusions of the DoE models.

Reagent:	Cell line:	Response:	Transformation:	Exclusions (±SD):
DOTAP	Hep3B	%GFP	log	none
		MFI	log	none
	HepG2	%GFP	log	none
		MFI	none	none
	HuH7	%GFP	log	Exp. 27 (-3.0 SD)
		MFI	log	none
DLin-MC3-DMA	Hep3B	%GFP	log	none
		MFI	log	none
	HepG2	%GFP	log	Exp. 28 (-3.5 SD)
		MFI	log	Exp. 28 (-4.0 SD)
	HuH7	%GFP	log	none
		MFI	log	none
Lipofectamine 3000	Hep3B	%GFP	none	none
		MFI	none	none
	HepG2	%GFP	none	none
		MFI	none	none
	HuH7	%GFP	none	none
		MFI	log	Exp. 2 & 6 (+3.0 SD)

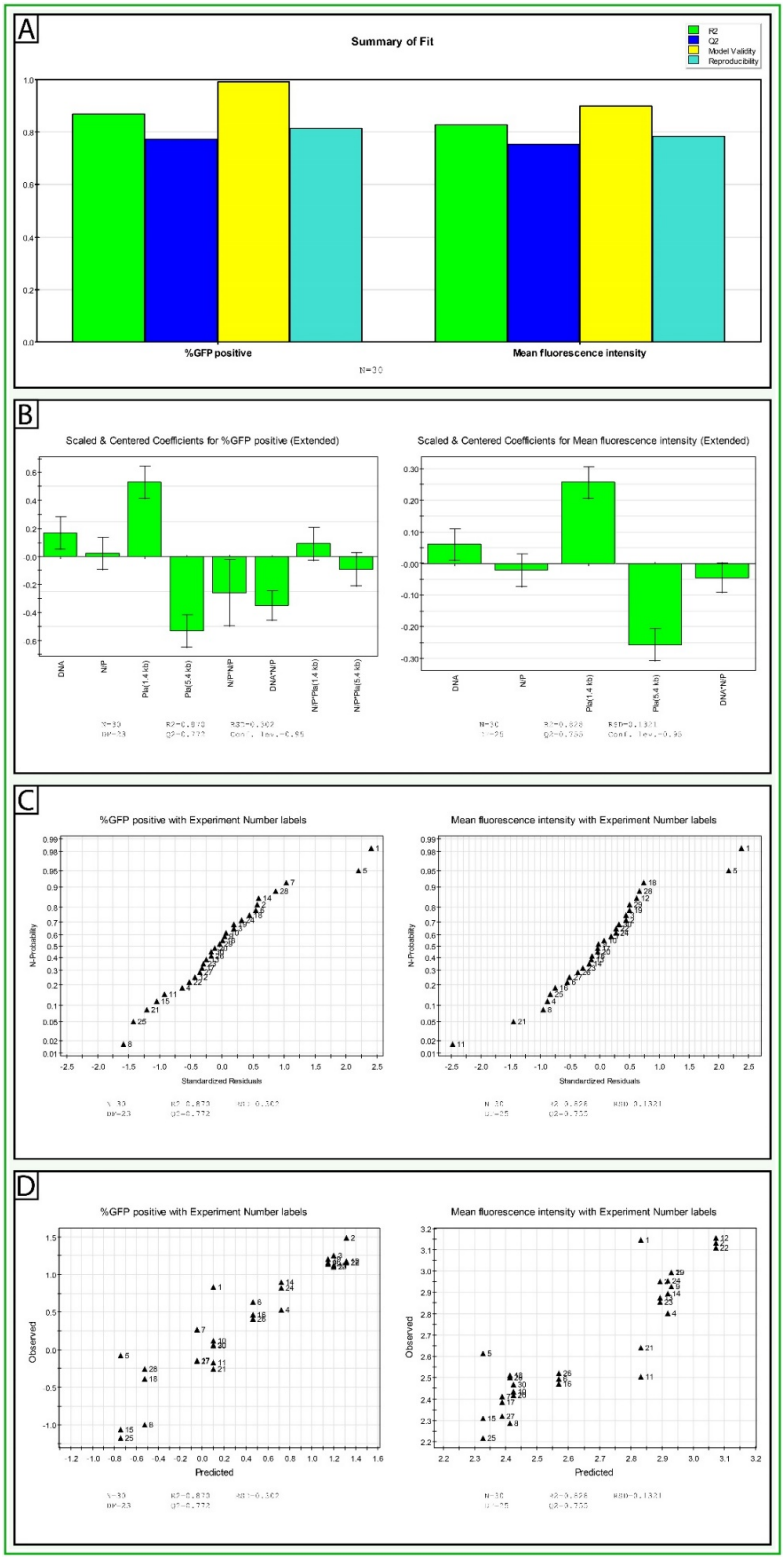

Figure S1: Model-related plots for DOTAP:cholesterol in Hep3B cells. The figure shows the summary of the generated model (A), the scaled and centered coefficents plot (B), the residuals N-plot (C), and the observed vs. predicted plot for the generated model. (A, %GFP positive cells): R^2 = 0.869652, Q^2 = 0.772024, Model validity = 0.99072, Reproducibility = 0.813567. (A, median fluorescence intensity): R^2 = 0.827971, Q^2 = 0.754755, Model validity = 0.898522, Reproducibility = 0.7853.

Table S2: Anova table for transfection efficiency (%GFP positive cells) using DOTAP:cholesterol in Hep3B cells.

%GFP positive	DF	SS	MS (variance)	F	p	SD
Total	30	20.2797	0.675991			
Constant	1	4.18185	4.18185			
Total Corrected	29	16.0979	0.555099			0.74505
Regression	6	13.9995	2.33326	25.5751	0	1.5275
Residual	23	2.09833	0.0912318			0.302046
Lack of Fit	3	0.0285525	0.00951751	0.0919665	0.964	0.0975577
(Model Error)						
Pure Error	20	2.06978	0.103489			0.321697
(Replicate Error)						
	N = 30	Q2 =	0.772	Cond. no. =	4.25	
	DF = 23	R2 =	0.87	RSD =	0.302	
	Comp. = 1	R2 Adj. =	0.836			

Table S3: Anova table for transgene expression (median fluorescence intensity) using DOTAP:cholesterol in Hep3B cells.

Mean fluorescence intensity	DF	SS	MS (variance)	F	p	SD
Total	30	217.482	7.24941			
Constant	1	214.947	214.947			
Total Corrected	29	2.53539	0.0874271			0.295681
Regression	4	2.09922	0.524806	30.081	0	0.724435
Residual	25	0.43616	0.0174464			0.132085
Lack of Fit	5	0.0607486	0.0121497	0.647274	0.667	0.110226
(Model Error)						
Pure Error	20	0.375412	0.0187706			0.137006
(Replicate Error)						
	N = 30	Q2 =	0.755	Cond. no. =	1.099	
	DF = 25	R2 =	0.828	RSD =	0.1321	
	Comp. = 1	R2 Adj. =	0.8			

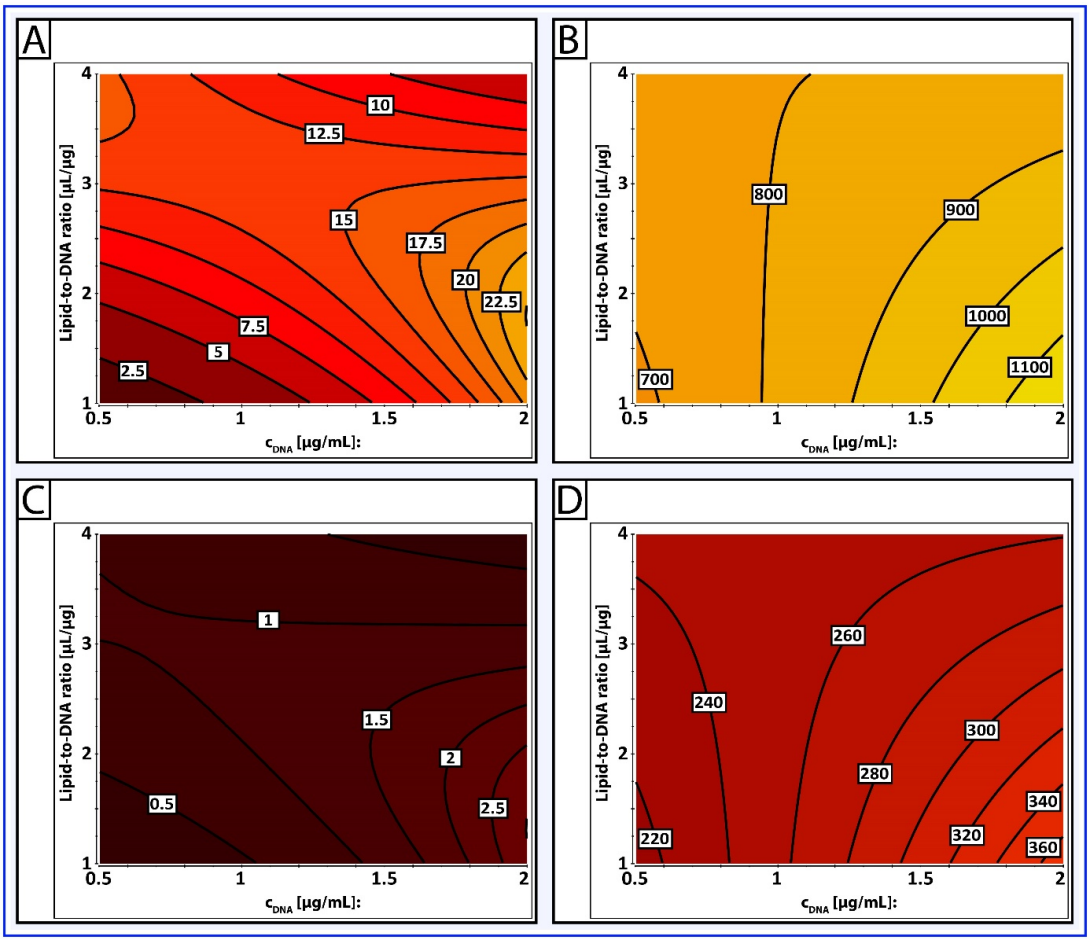

Figure S2: Predictive contour plots for DOTAP:cholesterol in Hep3B cells. The graphic shows the predictive contour plots for minicircle DNA (A, B) and parental plasmid DNA (C, D) in Hep3B cells using DOTAP:cholesterol. For both types of DNA, the transfection efficiency (A, C) by means of %GFP positive cells and the transgene expression (B, D) by means of median fluorescence intensity are provided.

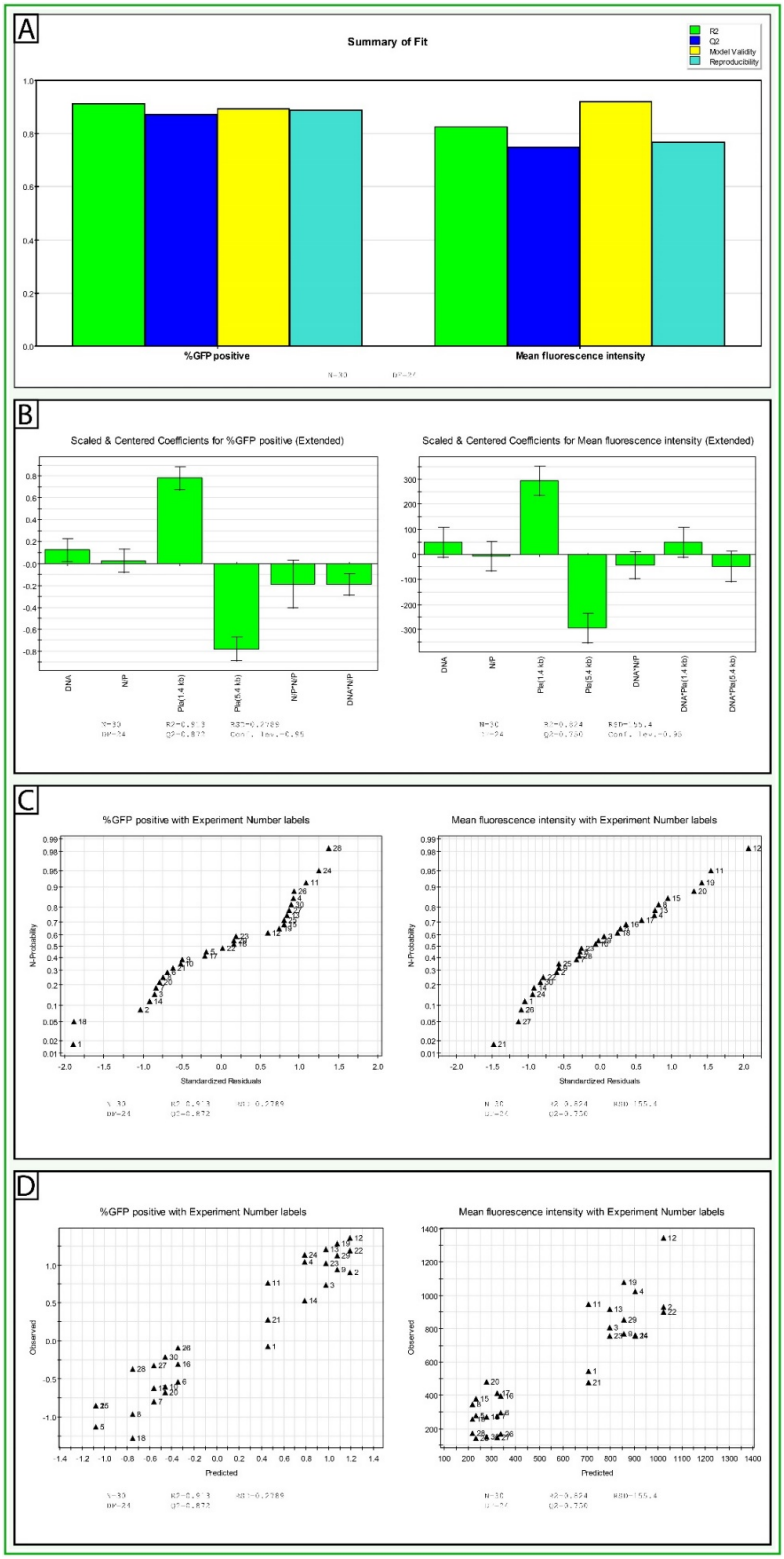

Figure S3: Model-related plots for DOTAP:cholesterol in HepG2 cells. The figure shows the summary of the generated model (A), the scaled and centered coefficents plot (B), the residuals N-plot (C), and the observed vs. predicted plot for the generated model. (A, %GFP positive cells): R^2 = 0.913302, Q^2 = 0.871974, Model validity = 0.893959, Reproducibility = 0.88812. (A, median fluorescence intensity): R^2 = 0.824154, Q^2 = 0.749751, Model validity = 0.92165, Reproducibility = 0.768489.

Table S4: Anova table for transfection efficiency (%GFP positive cells) using DOTAP:cholesterol in HepG2 cells.

%GFP positive	DF	SS	MS (variance)	F	p	SD
Total	30	22.0245	0.734149			
Constant	1	0.496636	0.496636			
Total Corrected	29	21.5278	0.742339			0.861591
Regression	5	19.6614	3.93228	50.5647	0	1.983
Residual	24	1.86641	0.0777673			0.278868
Lack of Fit	4	0.205351	0.0513378	0.618132	0.655	0.226579
(Model Error)						
Pure Error	20	1.66106	0.0830532			0.288189
(Replicate Error)						
	N = 30	Q2 =	0.872	Cond. no. =	4.25	
	DF = 24	R2 =	0.913	RSD =	0.2789	
	Comp. = 1	R2 Adj. =	0.895			

Table S5: Anova table for transgene expression (median fluorescence intensity) using DOTAP:cholesterol in HepG2 cells.

Mean fluorescence intensity	DF	SS	MS (variance)	F	p	SD
Total	30	1.30E+07	432406			
Constant	1	9.68E+06	9.68E+06			
Total Corrected	29	3.29E+06	113607			337.056
Regression	5	2.72E+06	543051	22.4966	0	736.92
Residual	24	579341	24139.2			155.368
Lack of Fit	4	53316.3	13329.1	0.506785	0.731	115.452
(Model Error)						
Pure Error	20	526025	26301.2			162.177
(Replicate Error)						
	N = 30	Q2 =	0.75	Cond. no. =	1.118	
	DF = 24	R2 =	0.824	RSD =	155.4	
	Comp. = 1	R2 Adj. =	0.788			

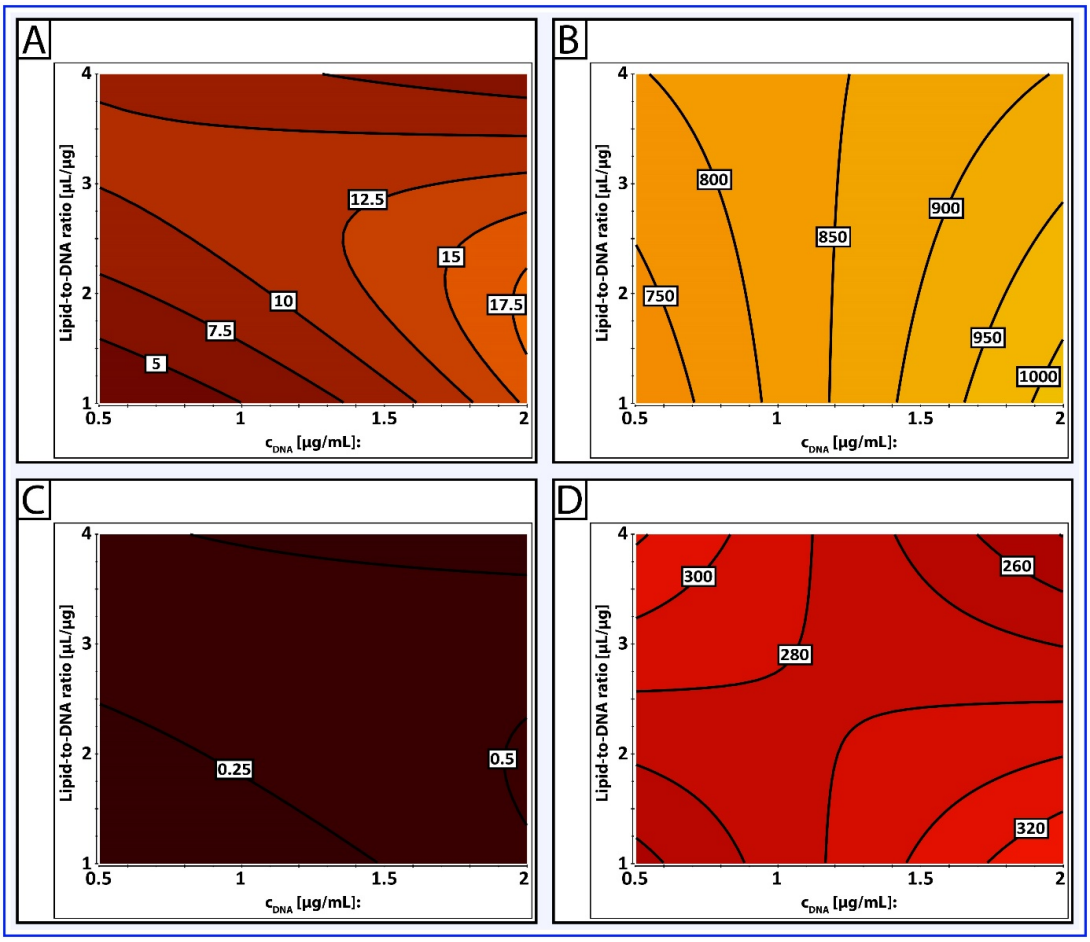

Figure S4: Predictive contour plots for DOTAP:cholesterol in HepG2 cells. The graphic shows the predictive contour plots for minicircle DNA (A, B) and parental plasmid DNA (C, D) in HepG2 cells using DOTAP:cholesterol. For both types of DNA, the transfection efficiency (A, C) by means of %GFP positive cells and the transgene expression (B, D) by means of median fluorescence intensity are provided.

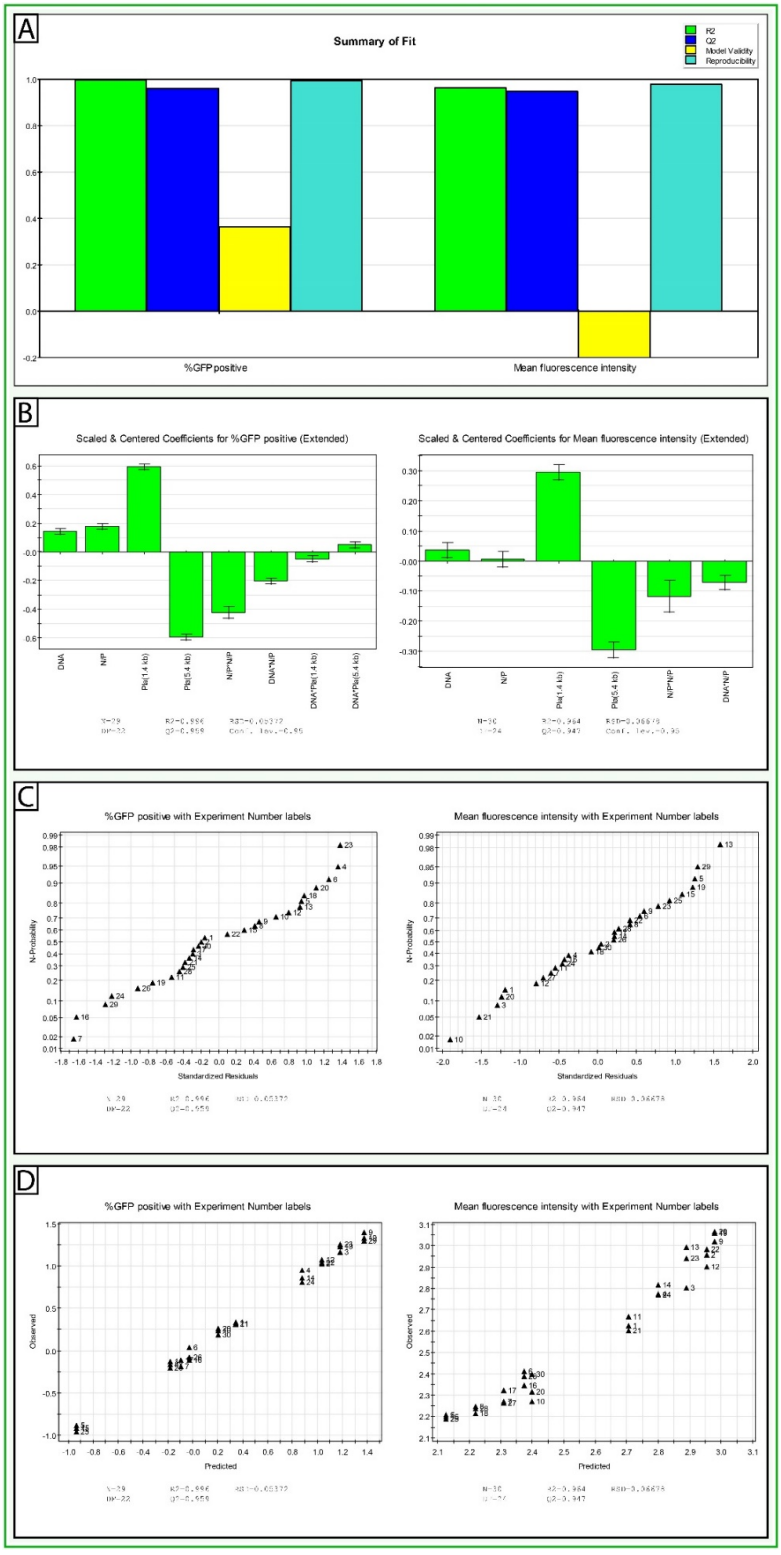

Figure S5: Model-related plots for DOTAP:cholesterol in HuH7 cells. The figure shows the summary of the generated model (A), the scaled and centered coefficents plot (B), the residuals N-plot (C), and the observed vs. predicted plot for the generated model. (A, %GFP positive cells): R^2 = 0.99553, Q^2 = 0.958856, Model validity = 0.363658, Reproducibility = 0.995353. (A, median fluorescence intensity): R^2 = 0.963571, Q^2 = 0.946782, Model validity = -0.2, Reproducibility = 0.97954.

Table S6: Anova table for transfection efficiency (%GFP positive cells) using DOTAP:cholesterol in HuH7 cells.

%GFP positive	DF	SS	MS (variance)	F	p	SD
Total	29	18.7052	0.645005			
Constant	1	4.50048	4.50048			
Total Corrected	28	14.2047	0.50731			0.712257
Regression	6	14.1412	2.35686	816.694	0	1.53521
Residual	22	0.0634889	0.00288586			0.0537202
Lack of Fit	3	0.0187001	0.00623337	2.64428	0.079	0.0789517
(Model Error)						
Pure Error	19	0.0447887	0.0023573			0.0485521
(Replicate Error)						
	N = 29	Q2 =	0.959	Cond. no. =	4.187	
	DF = 22	R2 =	0.996	RSD =	0.05372	
	Comp. = 2	R2 Adj. =	0.994			

Table S7: Anova table for transgene expression (median fluorescence intensity) using DOTAP:cholesterol in HuH7 cells.

Mean fluorescence intensity	DF	SS	MS (variance)	F	p	SD
Total	30	201.996	6.73321			
Constant	1	199.058	199.058			
Total Corrected	29	2.93829	0.10132			0.318309
Regression	5	2.83126	0.566251	126.965	0	0.752497
Residual	24	0.107038	0.00445991			0.0667825
Lack of Fit	4	0.0655766	0.0163942	7.9082	0.001	0.12804
(Model Error)						
Pure Error	20	0.0414612	0.00207306			0.0455308
(Replicate Error)						
	N = 30	Q2 =	0.947	Cond. no. =	4.25	
	DF = 24	R2 =	0.964	RSD =	0.06678	
	Comp. = 1	R2 Adj. =	0.956			

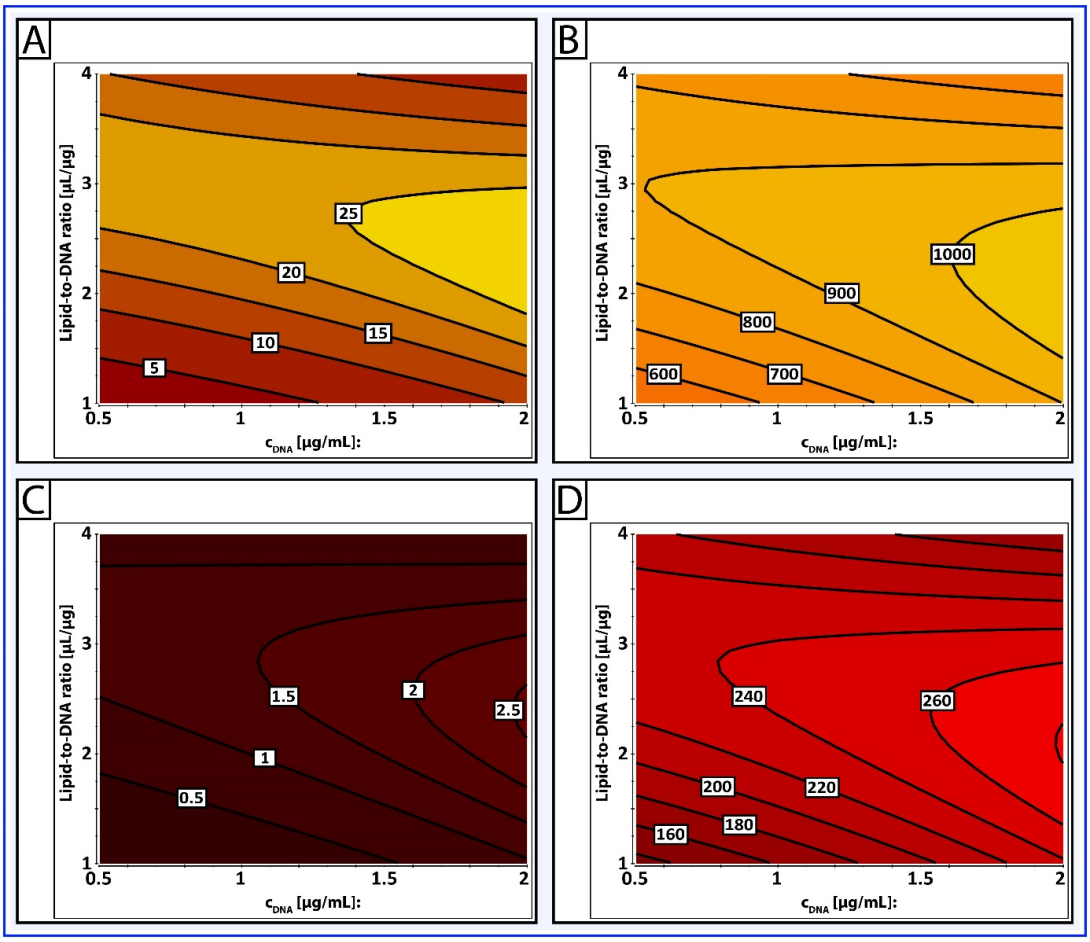

Figure S6: Predictive contour plots for DOTAP:cholesterol in HuH7 cells. The graphic shows the predictive contour plots for minicircle DNA (A, B) and parental plasmid DNA (C, D) in HuH7 cells using DOTAP:cholesterol. For both types of DNA, the transfection efficiency (A, C) by means of %GFP positive cells and the transgene expression (B, D) by means of median fluorescence intensity are provided.

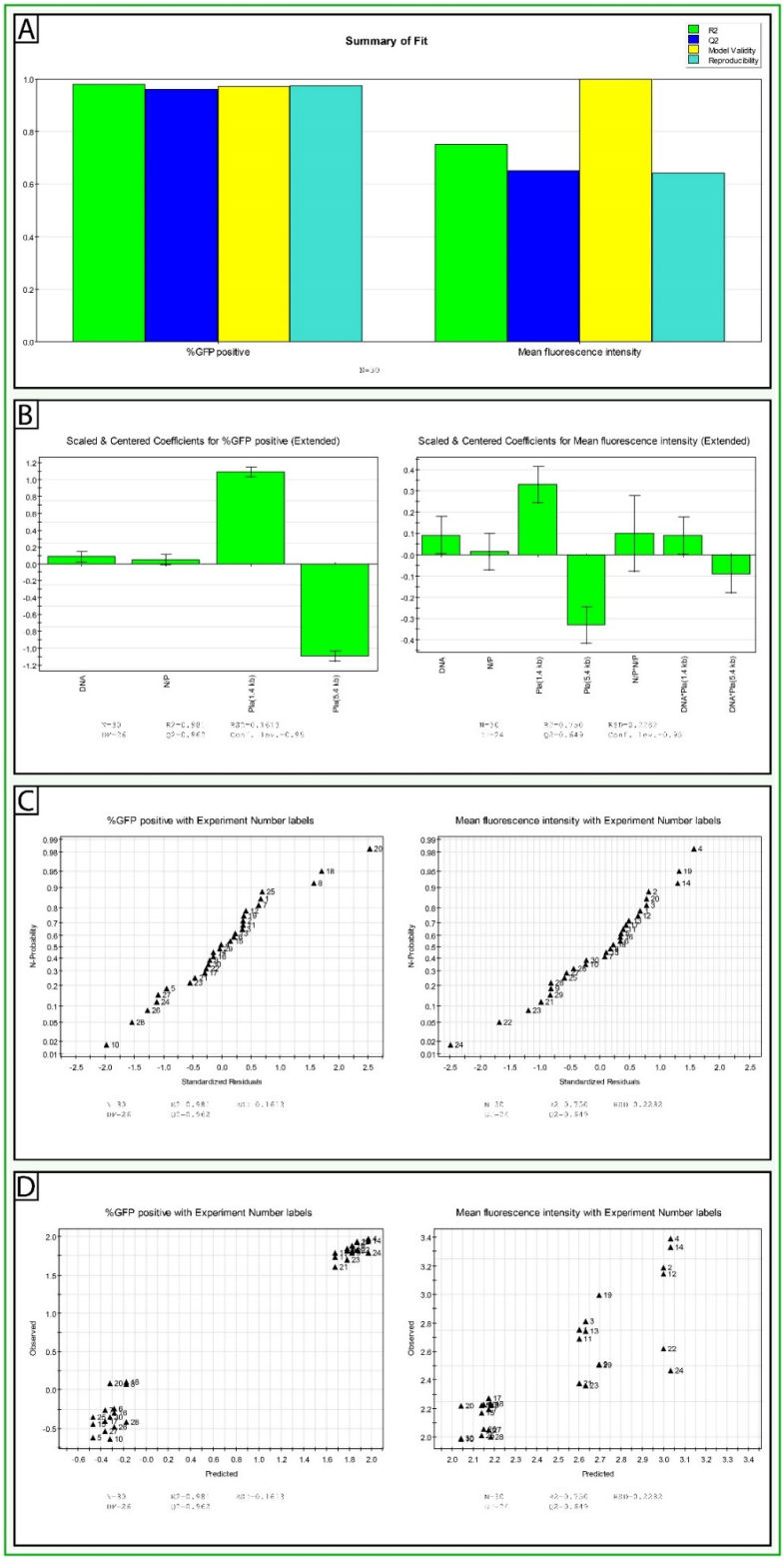

Figure S7: Model-related plots for DLin-MC3-DMA in Hep3B cells. The figure shows the summary of the generated model (A), the scaled and centered coefficents plot (B), the residuals N-plot (C), and the observed vs. predicted plot for the generated model. (A, %GFP positive cells): R^2 = 0.980955, Q^2 = 0.962263, Model validity = 0.974032, Reproducibility = 0.975009. (A, median fluorescence intensity): R^2 = 0.750443, Q^2 = 0.649015, Model validity = 0.998922, Reproducibility = 0.641428.

Table S8: Anova table for transfection efficiency (%GFP positive cells) using DLin-MC3-DMA in Hep3B cells.

%GFP positive	DF	SS	MS (variance)	F	p	SD
Total	30	52.5419	1.75139			
Constant	1	17.0383	17.0383			
Total Corrected	29	35.5036	1.22426			1.10646
Regression	3	34.8274	11.6091	446.39	0	3.40722
Residual	26	0.676174	0.0260067			0.161266
Lack of Fit	6	0.0642684	0.0107114	0.350099	0.901	0.103496
(Model Error)						
Pure Error	20	0.611906	0.0305953			0.174915
(Replicate Error)						
	N = 30	Q2 =	0.962	Cond. no. =	1.017	
	DF = 26	R2 =	0.981	RSD =	0.1613	
	Comp. = 1	R2 Adj. =	0.979			

Table S9: Anova table for transgene expression (median fluorescence intensity) using DLin-MC3-DMA in Hep3B cells.

Mean fluorescence intensity	DF	SS	MS (variance)	F	p	SD
Total	30	187.408	6.24692			
Constant	1	182.401	182.401			
Total Corrected	29	5.00687	0.172651			0.415512
Regression	5	3.75737	0.751474	14.4341	0	0.866876
Residual	24	1.2495	0.0520624			0.228172
Lack of Fit	4	0.0113467	0.00283667	0.0458211	0.996	0.0532604
(Model Error)						
Pure Error	20	1.23815	0.0619076			0.248812
(Replicate Error)						
	N = 30	Q2 =	0.649	Cond. no. =	4.25	
	DF = 24	R2 =	0.75	RSD =	0.2282	
	Comp. = 1	R2 Adj. =	0.698			

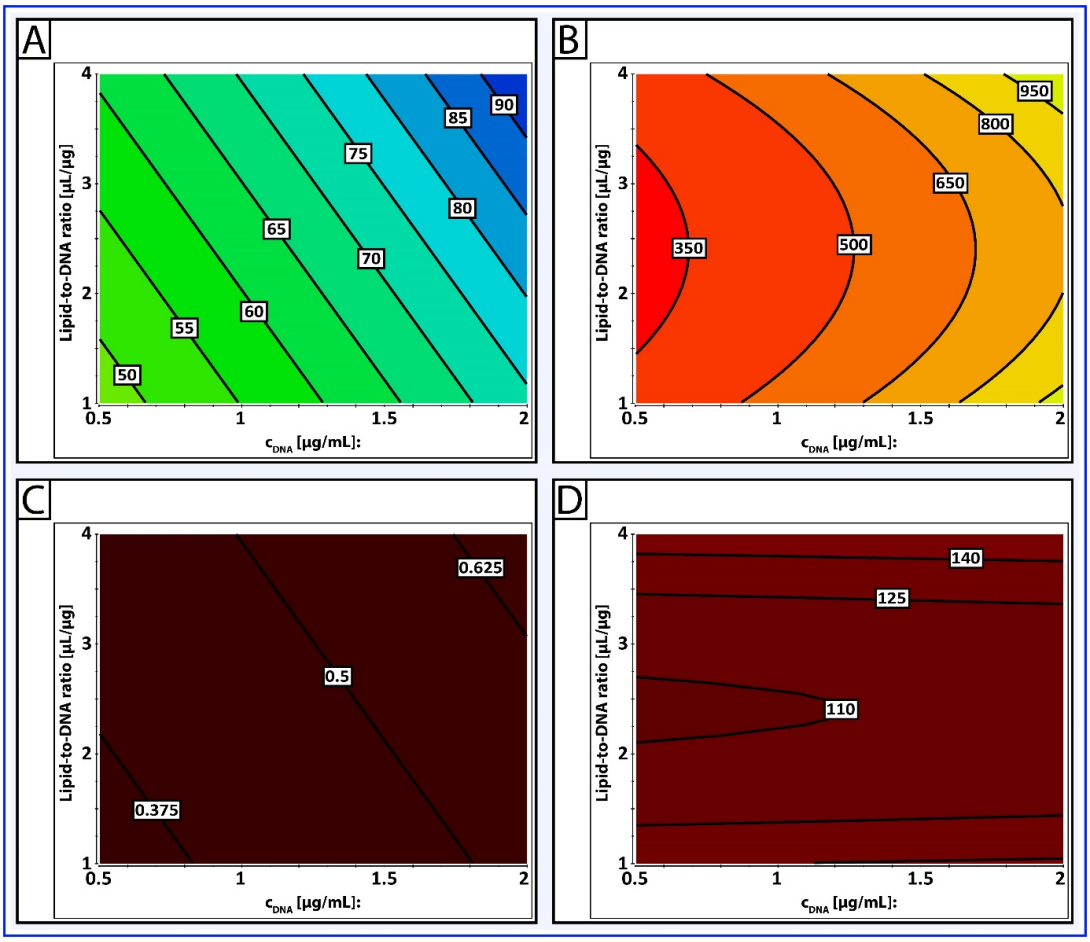

Figure S8: Predictive contour plots for DLin-MC3-DMA in Hep3B cells. The graphic shows the predictive contour plots for minicircle DNA (A, B) and parental plasmid DNA (C, D) in Hep3B cells using DLin-MC3-DMA. For both types of DNA, the transfection efficiency (A, C) by means of %GFP positive cells and the transgene expression (B, D) by means of median fluorescence intensity are provided.

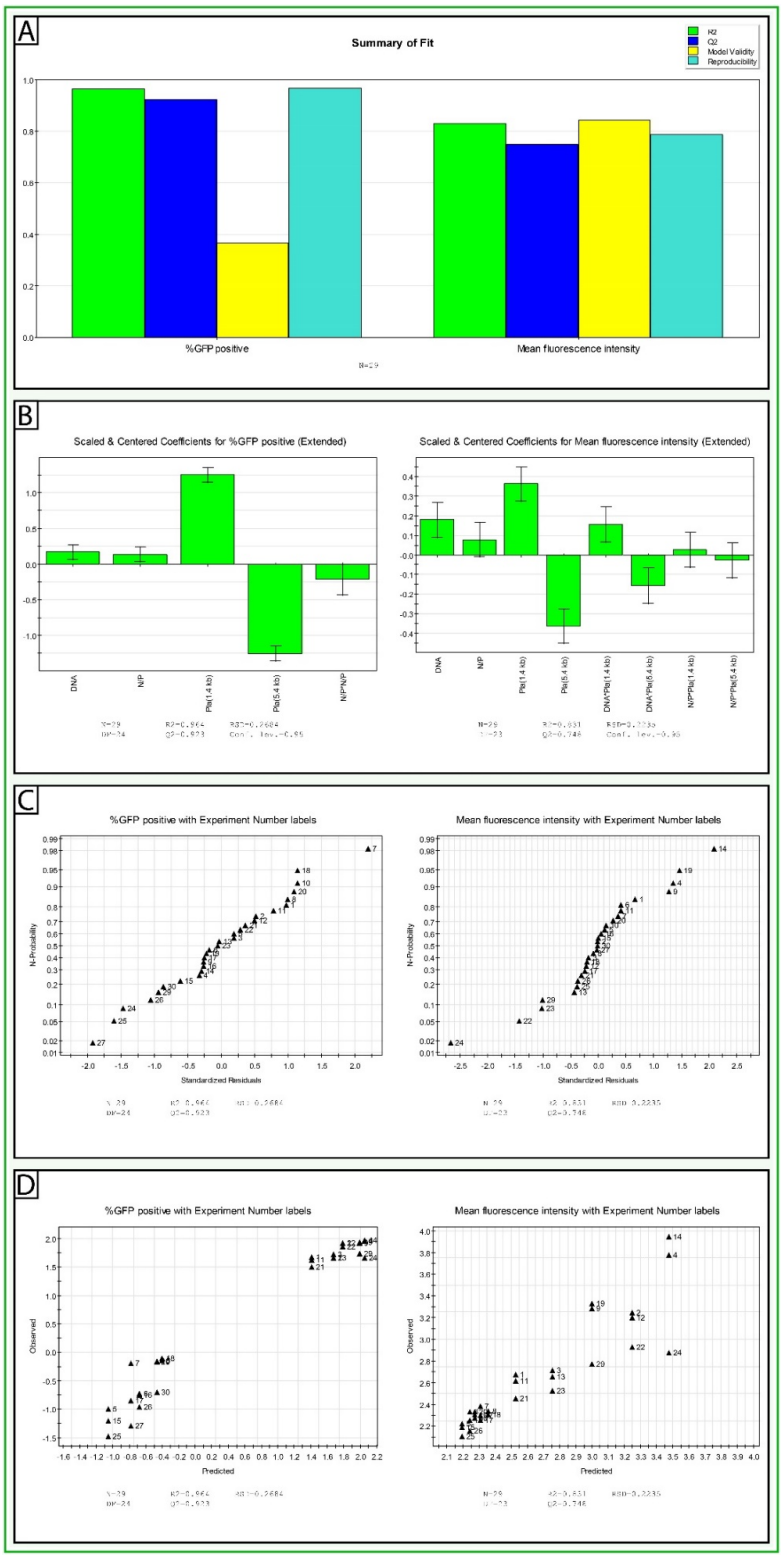

Figure S9: Model-related plots for DLin-MC3-DMA in HepG2 cells. The figure shows the summary of the generated model (A), the scaled and centered coefficents plot (B), the residuals N-plot (C), and the observed vs. predicted plot for the generated model. (A, %GFP positive cells): R^2 = 0.963826, Q^2 = 0.923392, Model validity = 0.365639, Reproducibility = 0.967122. (A, median fluorescence intensity): R^2 = 0.830935, Q^2 = 0.74788, Model validity = 0.845028, Reproducibility = 0.786867.

Table S10: Anova table for transfection efficiency (%GFP positive cells) using DLin-MC3-DMA in HepG2 cells.

%GFP positive	DF	SS	MS (variance)	F	p	SD
Total	29	57.8048	1.99327			
Constant	1	9.99406	9.99406			
Total Corrected	28	47.8108	1.70753			1.30672
Regression	4	46.0813	11.5203	159.866	0	3.39416
Residual	24	1.7295	0.0720626			0.268445
Lack of Fit	5	0.662853	0.132571	2.36146	0.079	0.364103
(Model Error)						
Pure Error	19	1.06665	0.0561394			0.236938
(Replicate Error)						
	N = 29	Q2 =	0.923	Cond. no. =	4.178	
	DF = 24	R2 =	0.964	RSD =	0.2684	
	Comp. = 2	R2 Adj. =	0.958			

Table S11: Anova table for transgene expression (median fluorescence intensity) using DLin-MC3-DMA in HepG2 cells.

Mean fluorescence intensity	DF	SS	MS (variance)	F	p	SD
Total	29	210.127	7.24575			
Constant	1	203.329	203.329			
Total Corrected	28	6.79755	0.24277			0.492716
Regression	5	5.64832	1.12966	22.6084	0	1.06286
Residual	23	1.14923	0.0499665			0.223532
Lack of Fit	4	0.166128	0.0415319	0.80267	0.538	0.203794
(Model Error)						
Pure Error	19	0.983101	0.0517422			0.227469
(Replicate Error)						
	N = 29	Q2 =	0.748	Cond. no. =	1.118	
	DF = 23	R2 =	0.831	RSD =	0.2235	
	Comp. = 2	R2 Adj. =	0.794			

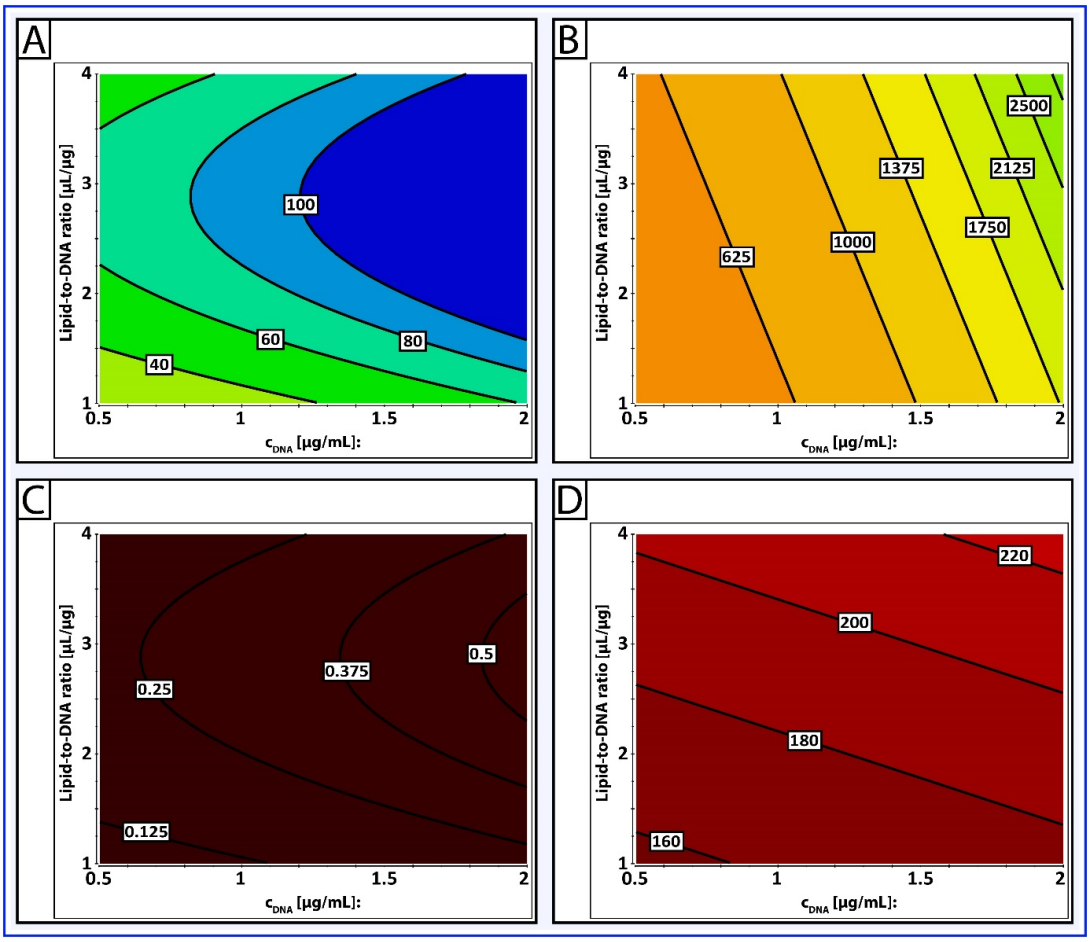

Figure S10: Predictive contour plots for DLin-MC3-DMA in HepG2 cells. The graphic shows the predictive contour plots for minicircle DNA (A, B) and parental plasmid DNA (C, D) in HepG2 cells using DLin-MC3-DMA. For both types of DNA, the transfection efficiency (A, C) by means of %GFP positive cells and the transgene expression (B, D) by means of median fluorescence intensity are provided.

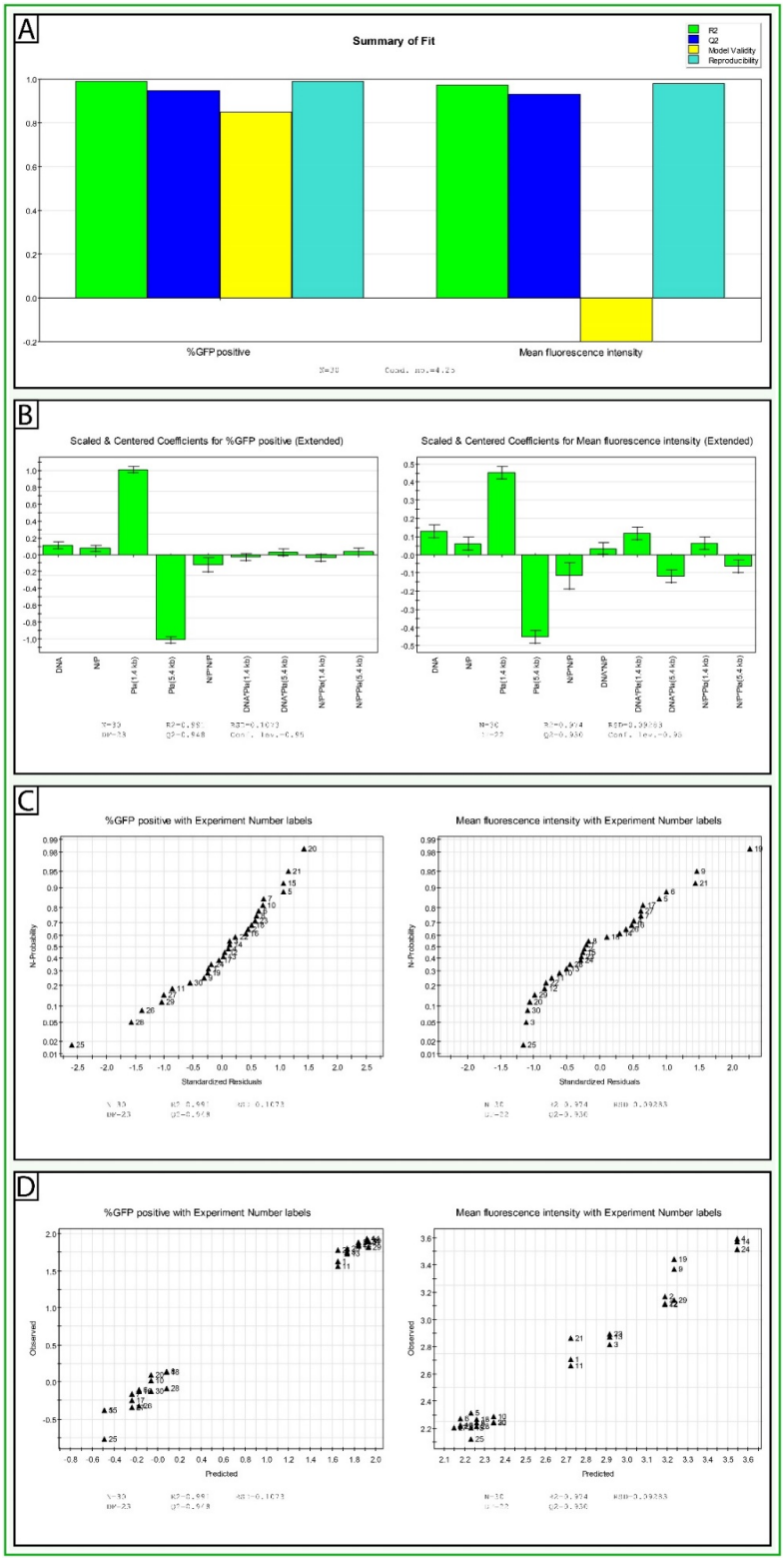

Figure S11: Model-related plots for DLin-MC3-DMA in HuH7 cells. The figure shows the summary of the generated model (A), the scaled and centered coefficents plot (B), the residuals N-plot (C), and the observed vs. predicted plot for the generated model. (A, %GFP positive cells): R^2 = 0.991396, Q^2 = 0.947793, Model validity = 0.8502, Reproducibility = 0.988746. (A, median fluorescence intensity): R^2 = 0.974343, Q^2 = 0.930003, Model validity = -0.2, Reproducibility = 0.979949.

Table S12: Anova table for transfection efficiency (%GFP positive cells) using DLin-MC3-DMA in HuH7 cells.

%GFP positive	DF	SS	MS (variance)	F	p	SD
Total	30	50.9587	1.69862			
Constant	1	20.2024	20.2024			
Total Corrected	29	30.7563	1.06056			1.02984
Regression	6	30.4917	5.08195	441.698	0	2.25432
Residual	23	0.264626	0.0115055			0.107264
Lack of Fit	3	0.0259094	0.00863648	0.723577	0.55	0.0929327
(Model Error)						
Pure Error	20	0.238716	0.0119358			0.109251
(Replicate Error)						
	N = 30	Q2 =	0.948	Cond. no. =	4.25	
	DF = 23	R2 =	0.991	RSD =	0.1073	
	Comp. = 1	R2 Adj. =	0.989			

Table S13: Anova table for transgene expression (median fluorescence intensity) using DLin-MC3-DMA in HuH7 cells.

Mean fluorescence intensity	DF	SS	MS (variance)	F	p	SD
Total	30	222.46	7.41532			
Constant	1	215.07	215.07			
Total Corrected	29	7.38931	0.254804			0.504781
Regression	7	7.19972	1.02853	119.35	0	1.01417
Residual	22	0.18959	0.00861774			0.0928318
Lack of Fit	2	0.0874066	0.0437033	8.55386	0.002	0.209053
(Model Error)						
Pure Error	20	0.102184	0.00510919			0.0714786
(Replicate Error)						
	N = 30	Q2 =	0.93	Cond. no. =	4.25	
	DF = 22	R2 =	0.974	RSD =	0.09283	
	Comp. = 1	R2 Adj. =	0.966			

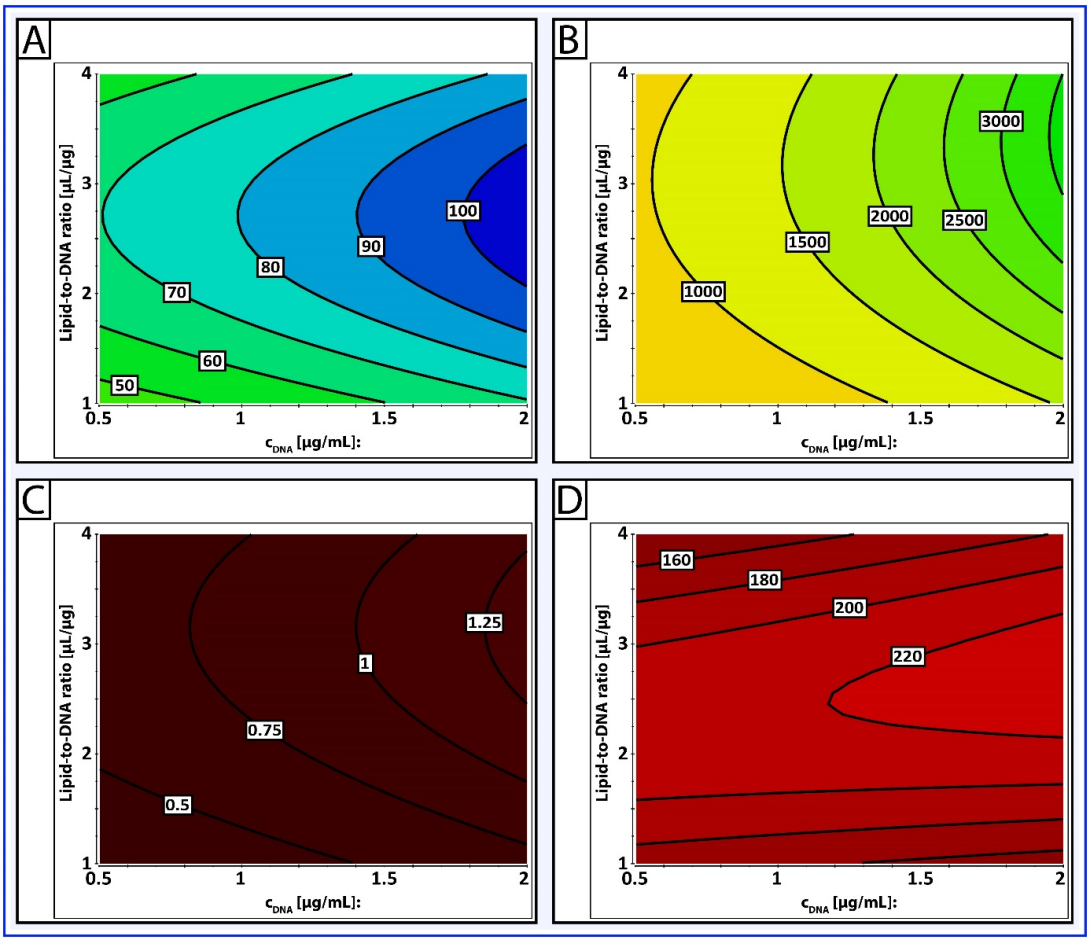

Figure S12: Predictive contour plots for DLin-MC3-DMA in HuH7 cells. The graphic shows the predictive contour plots for minicircle DNA (A, B) and parental plasmid DNA (C, D) in HuH7 cells using DLin-MC3-DMA. For both types of DNA, the transfection efficiency (A, C) by means of %GFP positive cells and the transgene expression (B, D) by means of median fluorescence intensity are provided.

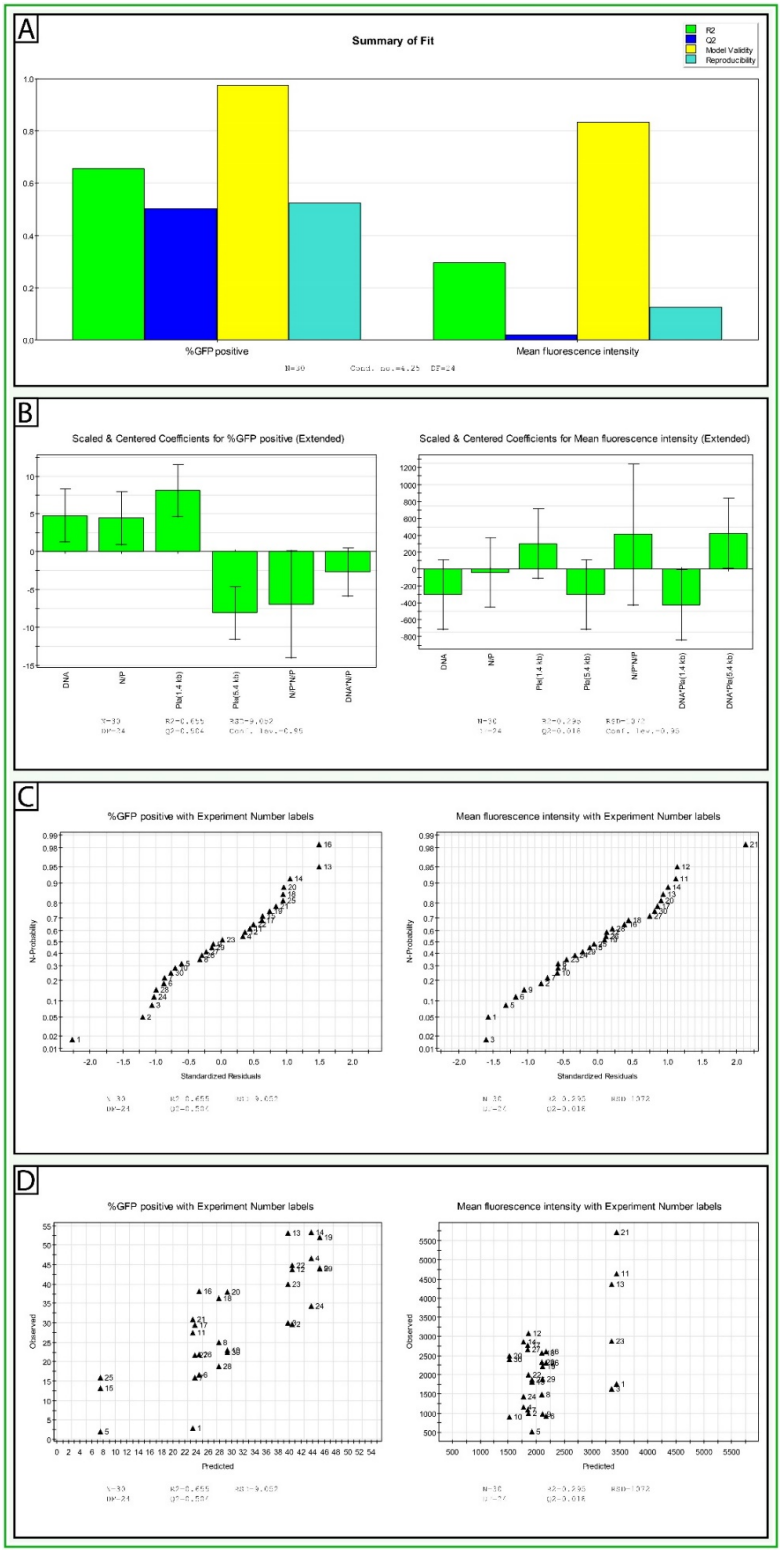

Figure S13: Model-related plots for Lipofectamine 3000 in Hep3B cells. The figure shows the summary of the generated model (A), the scaled and centered coefficents plot (B), the residuals N-plot (C), and the observed vs. predicted plot for the generated model. (A, %GFP positive cells): R^2 = 0.655348, Q^2 = 0.503689, Model validity = 0.976539, Reproducibility = 0.532411. (A, median fluorescence intensity): R^2 = 0.294765, Q^2 = 0.0180769, Model validity = 0.832221, Reproducibility = 0.125645.

Table S14: Anova table for transfection efficiency (%GFP positive cells) using Lipofectamine 3000 in Hep3B cells.

%GFP positive	DF	SS	MS (variance)	F	p	SD
Total	30	33654.3	1121.81			
Constant	1	27949	27949			
Total Corrected	29	5705.35	196.736			14.0263
Regression	5	3738.99	747.797	9.12708	0	27.3459
Residual	24	1966.36	81.9317			9.05162
Lack of Fit	4	91.1168	22.7792	0.242946	0.911	4.77276
(Model Error)						
Pure Error	20	1875.24	93.7623			9.68309
(Replicate Error)						
	N = 30	Q2 =	0.504	Cond. no. =	4.25	
	DF = 24	R2 =	0.655	RSD =	9.052	
	Comp. = 1	R2 Adj. =	0.584			

Table S15: Anova table for transgene expression (median fluorescence intensity) using Lipofectamine 3000 in Hep3B cells.

Mean fluorescence intensity	DF	SS	MS (variance)	F	p	SD
Total	30	1.86E+08	6.20E+06			
Constant	1	1.47E+08	1.47E+08			
Total Corrected	29	3.91E+07	1.35E+06			1161.79
Regression	5	1.15E+07	2.31E+06	2.00624	0.114	1519.07
Residual	24	2.76E+07	1.15E+06			1072.48
Lack of Fit	4	4.00E+06	1.00E+06	0.847689	0.512	1000.21
(Model Error)						
Pure Error	20	2.36E+07	1.18E+06			1086.35
(Replicate Error)						
	N = 30	Q2 =	0.018	Cond. no. =	4.25	
	DF = 24	R2 =	0.295	RSD =	1072	
	Comp. = 1	R2 Adj. =	0.148			

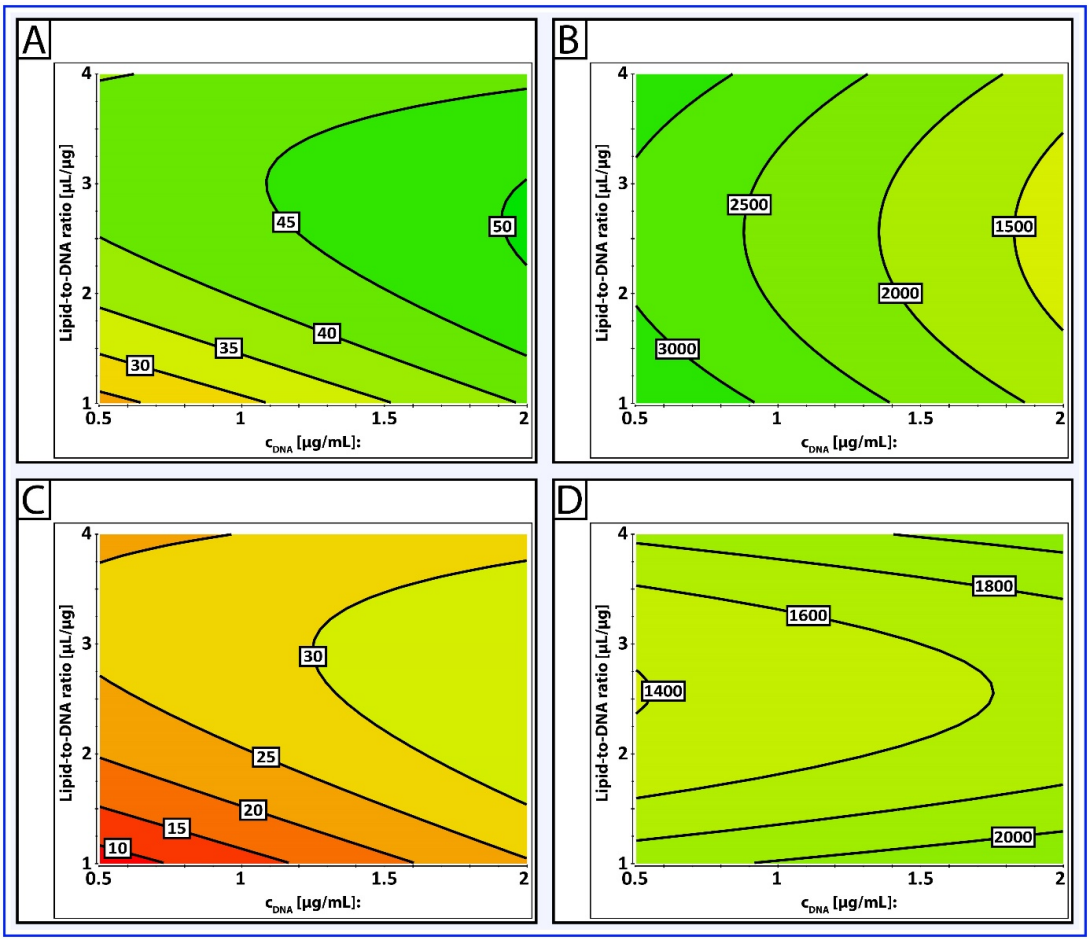

Figure S14: Predictive contour plots for Lipofectamine 3000 in Hep3B cells. The graphic shows the predictive contour plots for minicircle DNA (A, B) and parental plasmid DNA (C, D) in Hep3B cells using Lipofectamine 3000. For both types of DNA, the transfection efficiency (A, C) by means of %GFP positive cells and the transgene expression (B, D) by means of median fluorescence intensity are provided.

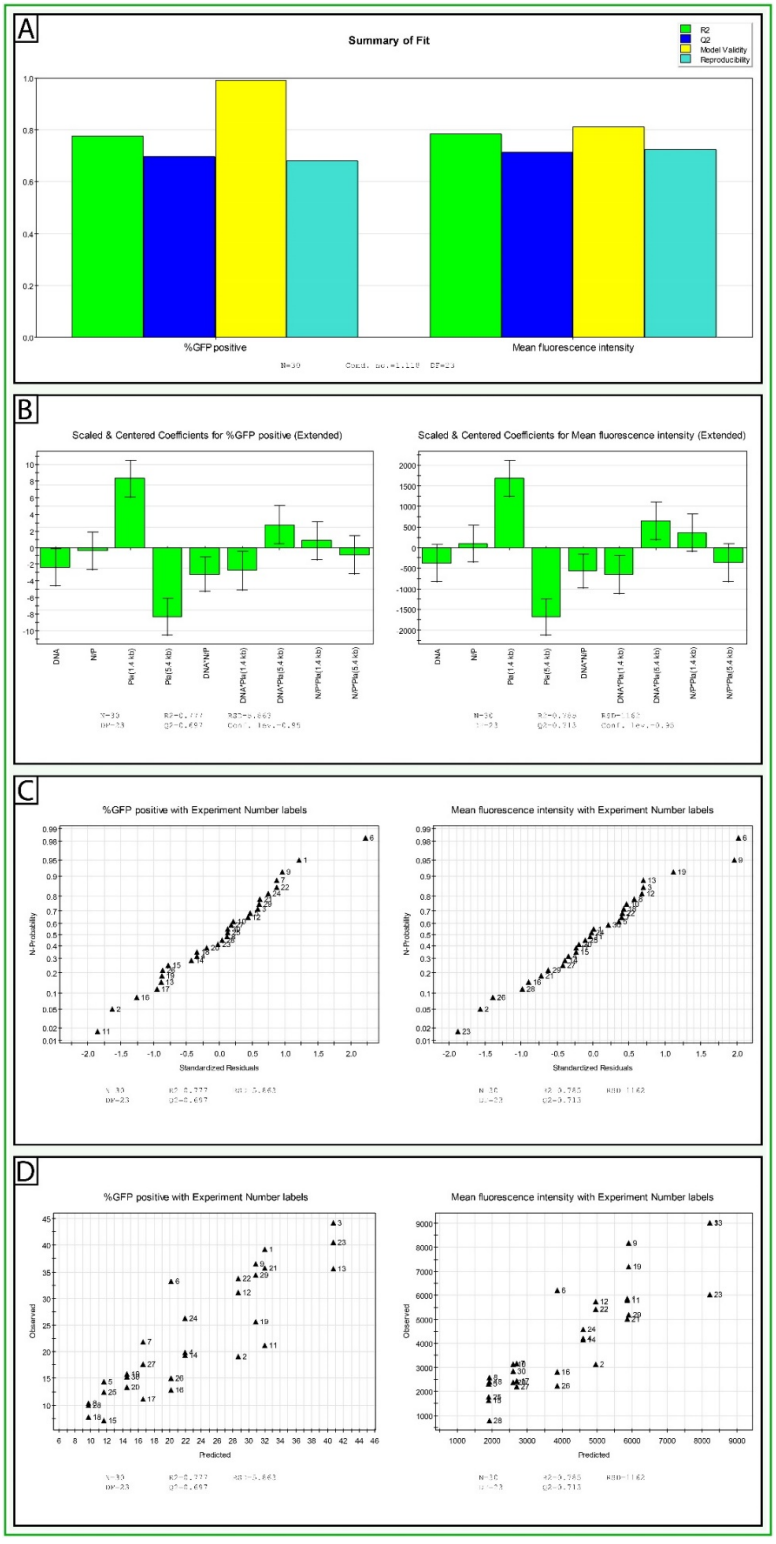

Figure S15: Model-related plots for Lipofectamine 3000 in HepG2 cells. The figure shows the summary of the generated model (A), the scaled and centered coefficents plot (B), the residuals N-plot (C), and the observed vs. predicted plot for the generated model. (A, %GFP positive cells): R^2 = 0.963826, Q^2 = 0.923392, Model validity = 0.365639, Reproducibility = 0.967122. (A, median fluorescence intensity): R^2 = 0.785215, Q^2 = 0.712894, Model validity = 0.811978, Reproducibility = 0.724596.

Table S16: Anova table for transfection efficiency (%GFP positive cells) using Lipofectamine 3000 in HepG2 cells.

%GFP positive	DF	SS	MS (variance)	F	p	SD
Total	30	18999.5	633.316			
Constant	1	15460.5	15460.5			
Total Corrected	29	3538.97	122.033			11.0469
Regression	6	2748.45	458.076	13.3277	0	21.4027
Residual	23	790.514	34.3702			5.86261
Lack of Fit	3	9.06396	3.02132	0.077326	0.972	1.73819
(Model Error)						
Pure Error	20	781.45	39.0725			6.2508
(Replicate Error)						
	N = 30	Q2 =	0.697	Cond. no. =	1.118	
	DF = 23	R2 =	0.777	RSD =	5.863	
	Comp. = 2	R2 Adj. =	0.718			

Table S17: Anova table for transgene expression (median fluorescence intensity) using Lipofectamine 3000 in HepG2 cells.

Mean fluorescence intensity	DF	SS	MS (variance)	F	p	SD
Total	30	6.87E+08	2.29E+07			
Constant	1	5.42E+08	5.42E+08			
Total Corrected	29	1.44E+08	4.98E+06			2232.21
Regression	6	1.13E+08	1.89E+07	14.014	0	4348.62
Residual	23	3.10E+07	1.35E+06			1161.64
Lack of Fit	3	3.59E+06	1.20E+06	0.872292	0.472	1094.08
(Model Error)						
Pure Error	20	2.74E+07	1.37E+06			1171.44
(Replicate Error)						
	N = 30	Q2 =	0.713	Cond. no. =	1.118	
	DF = 23	R2 =	0.785	RSD =	1162	
	Comp. = 2	R2 Adj. =	0.729			

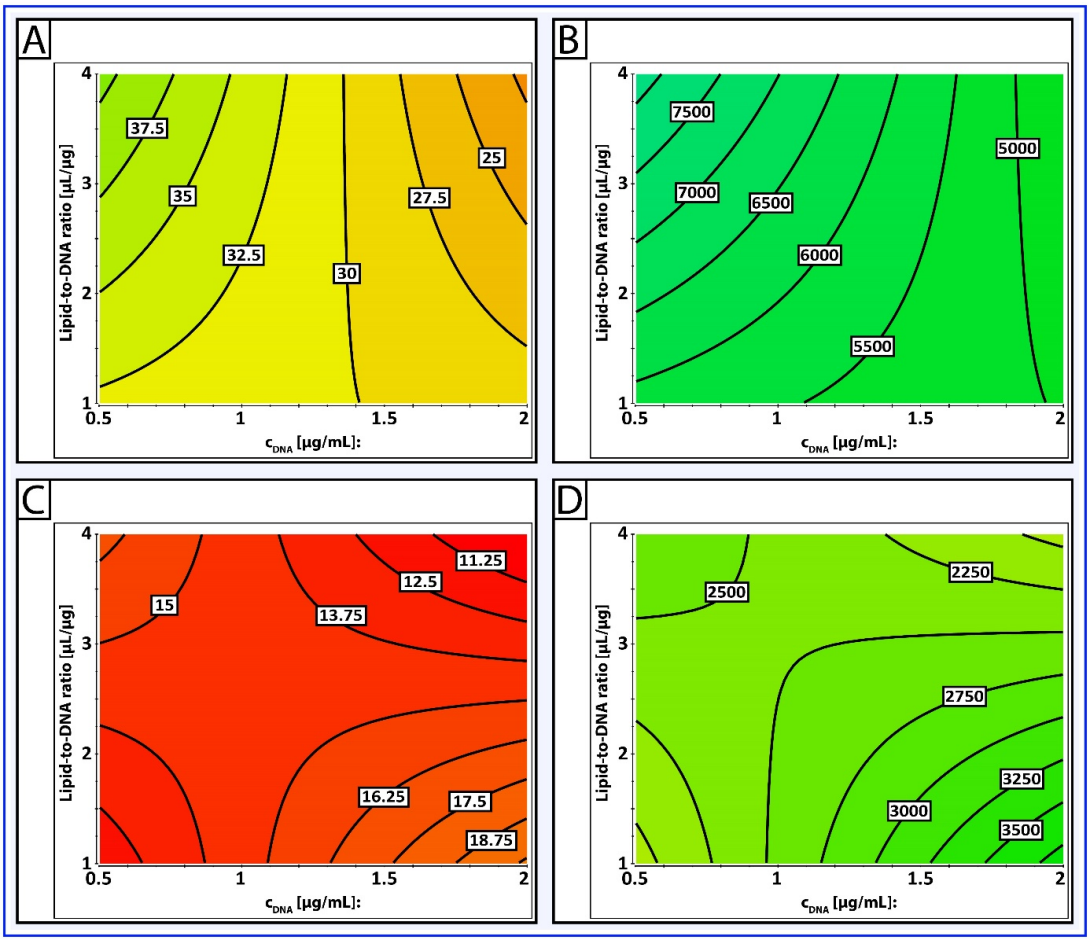

Figure S16: Predictive contour plots for Lipofectamine 3000 in HepG2 cells. The graphic shows the predictive contour plots for minicircle DNA (A, B) and parental plasmid DNA (C, D) in HepG2 cells using Lipofectamine 3000. For both types of DNA, the transfection efficiency (A, C) by means of %GFP positive cells and the transgene expression (B, D) by means of median fluorescence intensity are provided.

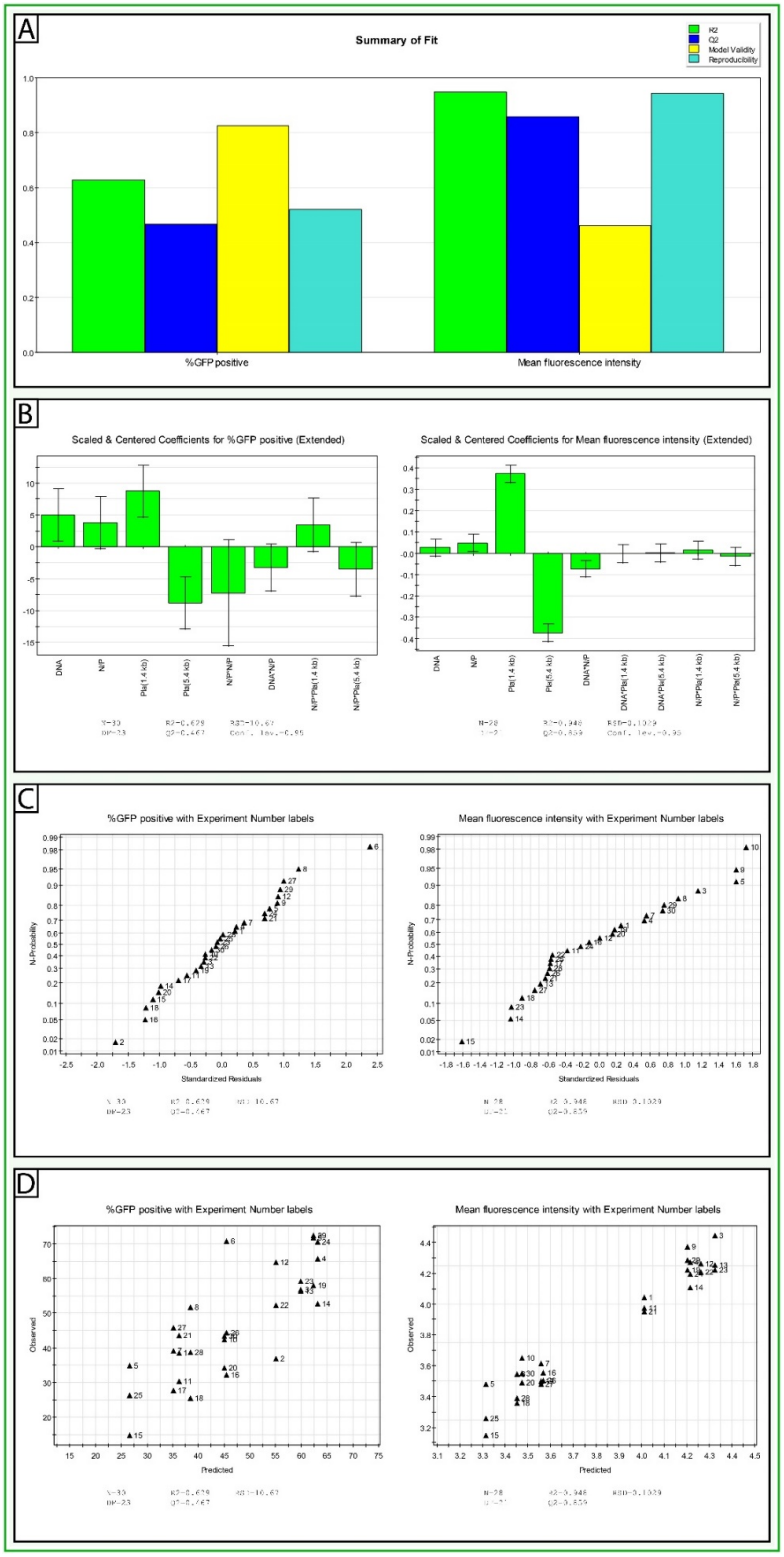

Figure S17: Model-related plots for Lipofectamine 3000 in HuH7 cells. The figure shows the summary of the generated model (A), the scaled and centered coefficents plot (B), the residuals N-plot (C), and the observed vs. predicted plot for the generated model. (A, %GFP positive cells): R^2 = 0.628769, Q^2 = 0.466982, Model validity = 0.824377, Reproducibility = 0.520949. (A, median fluorescence intensity): R^2 = 0.948028, Q^2 = 0.858936, Model validity = 0.461581, Reproducibility = 0.943364.

Table S18: Anova table for transfection efficiency (%GFP positive cells) using Lipofectamine 3000 in HuH7 cells.

%GFP positive	DF	SS	MS (variance)	F	p	SD
Total	30	72664.7	2422.16			
Constant	1	65613.6	65613.6			
Total Corrected	29	7051.11	243.142			15.593
Regression	6	4433.52	738.92	6.49268	0	27.1831
Residual	23	2617.59	113.808			10.6681
Lack of Fit	3	288.042	96.014	0.824315	0.496	9.79867
(Model Error)						
Pure Error	20	2329.55	116.477			10.7925
(Replicate Error)						
	N = 30	Q2 =	0.467	Cond. no. =	4.25	
	DF = 23	R2 =	0.629	RSD =	10.67	
	Comp. = 1	R2 Adj. =	0.532			

Table S19: Anova table for transgene expression (median fluorescence intensity) using Lipofectamine 3000 in HuH7 cells.

Mean fluorescence intensity	DF	SS	MS (variance)	F	p	SD
Total	28	415.716	14.847			
Constant	1	411.436	411.436			
Total Corrected	27	4.27994	0.158516			0.398141
Regression	6	4.0575	0.67625	63.8442	0	0.822344
Residual	21	0.222436	0.0105922			0.102918
Lack of Fit	3	0.0608363	0.0202788	2.25878	0.116	0.142404
(Model Error)						
Pure Error	18	0.1616	0.00897776			0.094751
(Replicate Error)						
	N = 28	Q2 =	0.859	Cond. no. =	1.208	
	DF = 21	R2 =	0.948	RSD =	0.1029	
	Comp. = 2	R2 Adj. =	0.933			

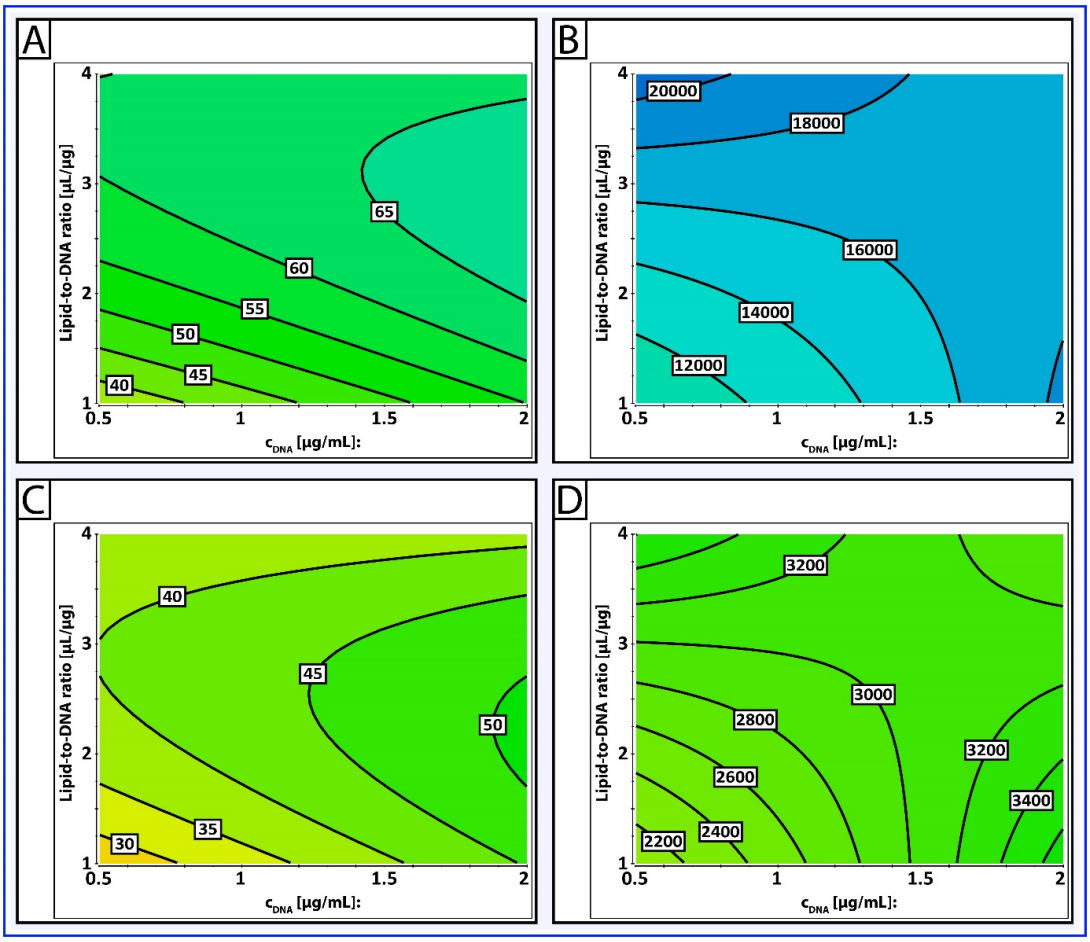

Figure S18: Predictive contour plots for Lipofectamine 3000 in HuH7 cells. The graphic shows the predictive contour plots for minicircle DNA (A, B) and parental plasmid DNA (C, D) in HuH7 cells using Lipofectamine 3000. For both types of DNA, the transfection efficiency (A, C) by means of %GFP positive cells and the transgene expression (B, D) by means of median fluorescence intensity are provided.

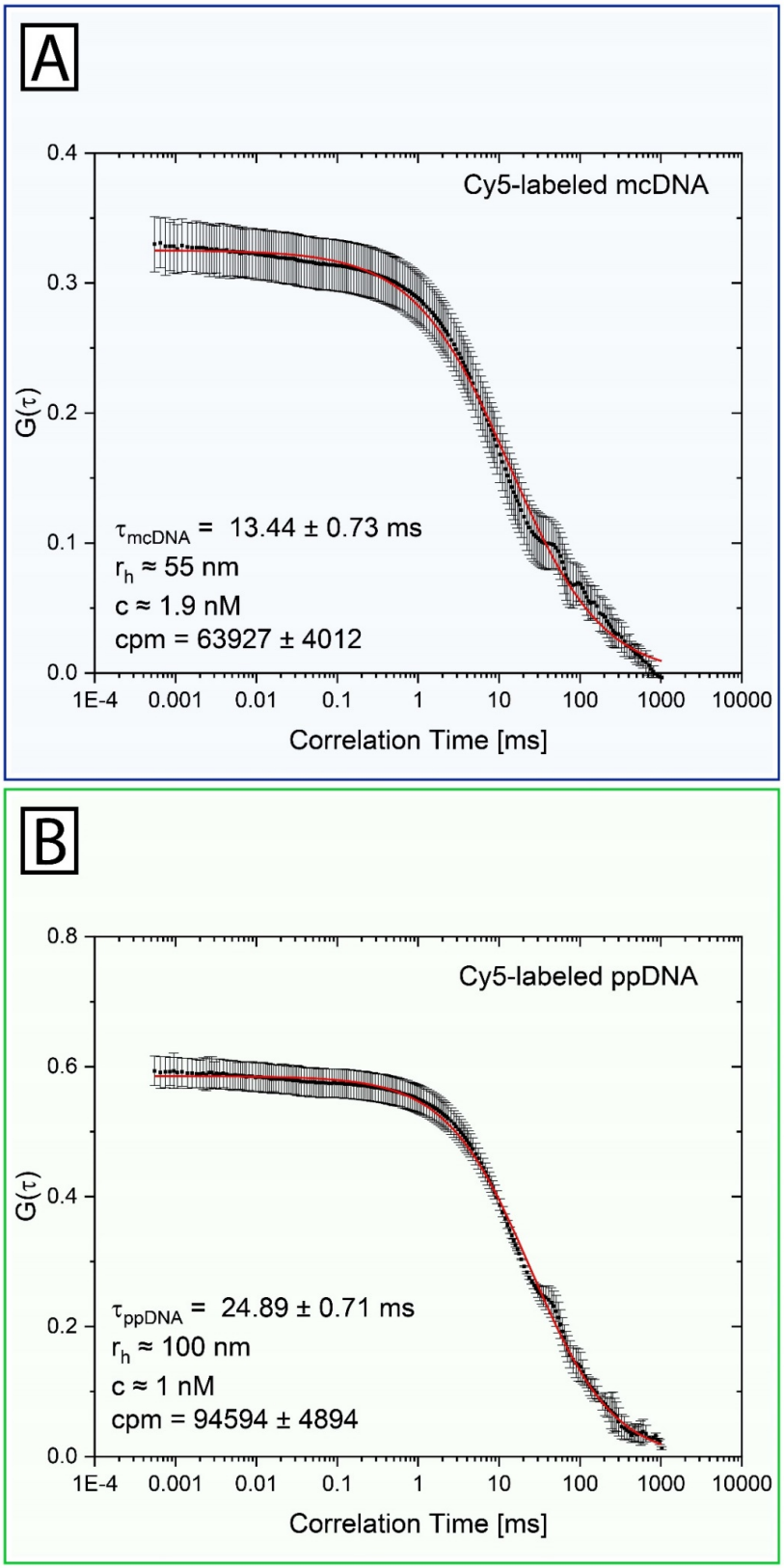

Figure S19: Autocorrelation functions (ACFs) for minicircle DNA (A) and parental plasmid DNA (B).

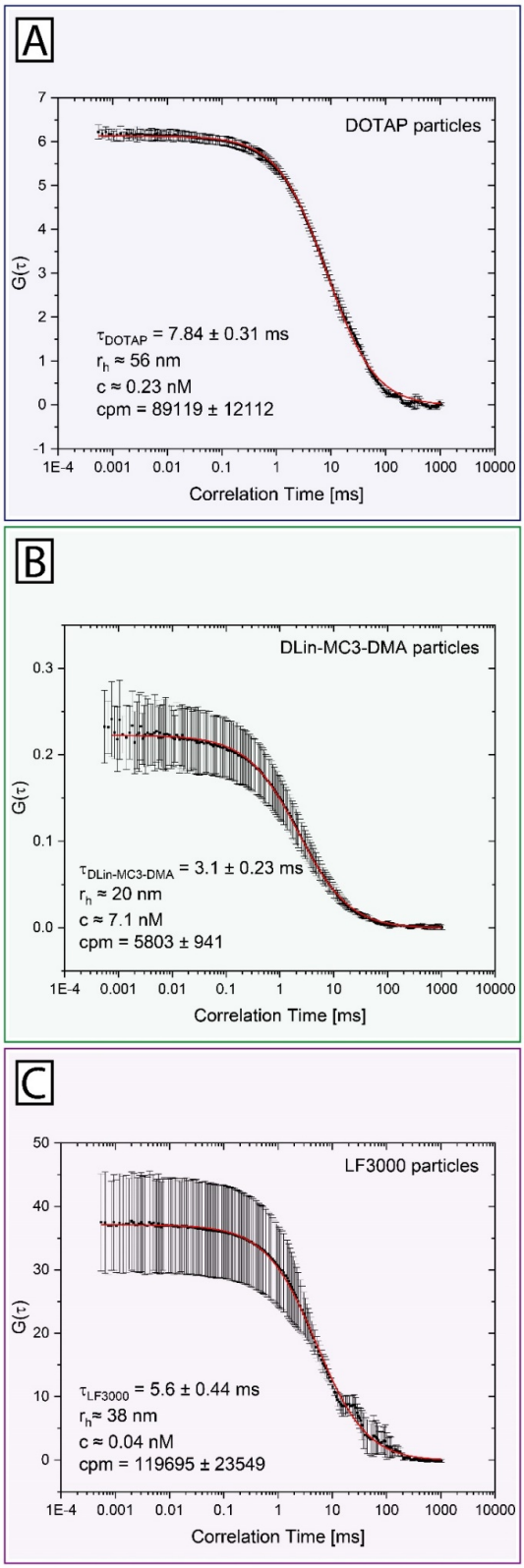

Figure S20: Autocorrelation functions (ACFs) for DOTAP (A), DLin-MC3-DMA (B), and Lipofectamine 3000 (C) lipid nanoparticles.

5.3 Chapter 3

5.3.1 Chapter 3.1

Optimization-by-design of hepatotropic lipid nanoparticles targeting the sodium-taurocholate cotransporting polypeptide

Dominik Witzigmann, Pilipp Uhl, Sandro Sieber, Christina Kaufman, Tomaz Einfalt, Katrin Schöneweis, Philip Grossen, **Jonas Buck**, Yi Ni, Susanne H. Schenk, Janine Hussner, Henriette E. Meyer zu Schwabedissen, Gabriela Québatte, Walter Mier, Stephan Urban, Jörg Huwyler

eLife. 2019 Jul 23;8:e42276.
doi: 10.7554/eLife.42276.

Highlights: Nanoparticles with prolonged blood circulation time often do not accumulate in the target tissue to a sufficient amount. To increase accumulation in specific tissues or uptake into specific cell populations, a targeting strategy is needed. In this study, we demonstrate that modification of lipid-based nanoparticles with a targeting peptide derived from the hepatitis B virus large envelope protein (HBVpreS) enables specific uptake into hepatocytes *via* the sodium-taurocholate cotransporting polypeptide (NTCP). Selection of formulations with favorable pharmacokinetics and high targeting capacity was done using the zebrafish embryo animal model. Optimized formulations showed active NTCP-mediated targeting and cellular uptake into hepatocytes of mice confirming the hepatotropic nature of these targeted nanoparticles.

eLIFE elifesciences.org

RESEARCH ARTICLE

Optimization-by-design of hepatotropic lipid nanoparticles targeting the sodium-taurocholate cotransporting polypeptide

Dominik Witzigmann[1,2]*, Philipp Uhl[3], Sandro Sieber[1], Christina Kaufman[3,4], Tomaz Einfalt[1], Katrin Schöneweis[4], Philip Grossen[1], Jonas Buck[1], Yi Ni[4], Susanne H Schenk[1], Janine Hussner[5], Henriette E Meyer zu Schwabedissen[5], Gabriela Québatte[1], Walter Mier[3], Stephan Urban[4], Jörg Huwyler[1]*

[1]Division of Pharmaceutical Technology, Department of Pharmaceutical Sciences, University of Basel, Basel, Switzerland; [2]Department of Biochemistry and Molecular Biology, University of British Columbia, Vancouver, Canada; [3]Department of Nuclear Medicine, University Hospital Heidelberg, Heidelberg, Germany; [4]Department of Infectious Diseases, Molecular Virology, University Hospital Heidelberg, INF, Heidelberg, Germany; [5]Division of Biopharmacy, Department of Pharmaceutical Sciences, University of Basel, Basel, Switzerland

Abstract Active targeting and specific drug delivery to parenchymal liver cells is a promising strategy to treat various liver disorders. Here, we modified synthetic lipid-based nanoparticles with targeting peptides derived from the hepatitis B virus large envelope protein (HBVpreS) to specifically target the sodium-taurocholate cotransporting polypeptide (NTCP; *SLC10A1*) on the sinusoidal membrane of hepatocytes. Physicochemical properties of targeted nanoparticles were optimized and NTCP-specific, ligand-dependent binding and internalization was confirmed in vitro. The pharmacokinetics and targeting capacity of selected lead formulations was investigated in vivo using the emerging zebrafish screening model. Liposomal nanoparticles modified with 0.25 mol% of a short myristoylated HBV derived peptide, that is Myr-HBVpreS2-31, showed an optimal balance between systemic circulation, avoidance of blood clearance, and targeting capacity. Pronounced liver enrichment, active NTCP-mediated targeting of hepatocytes and efficient cellular internalization were confirmed in mice by ^{111}In gamma scintigraphy and fluorescence microscopy demonstrating the potential use of our hepatotropic, ligand-modified nanoparticles.
DOI: https://doi.org/10.7554/eLife.42276.001

***For correspondence:** dominik.witzigmann@unibas.ch (DW); joerg.huwyler@unibas.ch (JöH)

Competing interests: The authors declare that no competing interests exist.

Funding: See page 23

Received: 24 September 2018
Accepted: 17 July 2019
Published: 23 July 2019

Reviewing editor: Bavesh D Kana, University of the Witwatersrand, South Africa

Introduction

The design of hepatotropic drug carriers is of great interest for the treatment of various liver disorders (***Williams et al., 2014***; ***Poelstra et al., 2012***; ***Reddy and Couvreur, 2011***). In particular if cell-type specific delivery of macromolecular therapeutic agents, selective targeting of parenchymal liver cells and internalization is needed. Previously, hepatocyte targeted nanoparticles have been developed exploiting endogenous and exogenous targeting ligand-based mechanisms using glycan, protein or antibody modifications of the nanoparticle surface (***Akinc et al., 2010***; ***Akinc et al., 2009***; ***Barrett et al., 2014***; ***Detampel et al., 2014***; ***Witzigmann et al., 2016a***). Most established systems for liver-specific drug delivery rely on targeting the hepatic asialoglycoprotein (ASGPR) or low density lipoprotein (LDLR) receptors. However, studies investigating alternative targeting strategies based on other hepatocyte-specific receptors are limited. In this respect, a promising alternative might be offered by the hepatitis B virus (HBV), which shows a pronounced efficacy to infect the human liver due to its strong affinity to hepatocytes. Less than 10 virus particles have been shown to

be sufficient to efficiently target hepatocytes of chimpanzees resulting in a pathogenic HBV infection (**Asabe et al., 2009**). The reason for its extraordinary liver tropism is a highly specific amino acid sequence in the large HBV envelope protein (*i.e.* HBVpreS1 domain), which is essential for target receptor recognition (**Meier et al., 2013**; **Schieck et al., 2013**). For decades, the specific target of HBV on the sinusoidal membrane of hepatocytes was unknown until in 2012 the interaction with the human sodium-taurocholate cotransporting polypeptide (NTCP/SLC10A1) was identified (**Yan et al., 2012**). Subsequently, Urban and colleagues performed a fine mapping of the HBVpreS sequence to identify the amino acids responsible for efficient binding (**Schulze et al., 2010**; **Ni et al., 2014**; **Schieck et al., 2013**). As a result, the first HBV/HDV entry inhibitor, a myristoylated peptide named Myrcludex B, was developed and successfully introduced in clinics (currently phase II clinical trials) (**Blank et al., 2016**; **Urban et al., 2014**). Myrcludex B binds with high affinity and specificity to human NTCP on the sinusoidal membrane of hepatocytes thereby blocking binding of virus particles to their target cells.

Based on these findings, the question arises whether Myrcludex B might serve as a targeting ligand to design a hepatotropic, NTCP-specific nanoparticle. In recent years, several groups have therefore attempted to develop targeting strategies based on HBV envelope proteins, for example recombinant HBV envelope protein particles (bio-nanocapsules) or HBV preS1-derived functionalized liposomes (**Liu et al., 2016**; **Somiya et al., 2016**; **Somiya et al., 2015**; **Zhang et al., 2015**; **Zhang et al., 2014**). However, the nanoparticulate drug delivery systems developed had physicochemical properties (e.g. size, colloidal stability, and immunogenic potential), which were sub-optimal for efficient in vivo targeting of hepatocytes. Especially the size of the nano-formulations presented a limitation. Most developed formulations had sizes above the average diameter of hepatic fenestrations in healthy humans (i.e. 100 nm) (**Wisse et al., 2008**) thereby limiting the passage through liver fenestrations and consequently the access to the space of Disse and the sinusoidal membrane of hepatocytes. Notably, the liver fenestrae diameter of rodents show high species and strain differences ranging from around 100 nm to 160 nm, possibly explaining positive liver targeting of published formulations (**Braet and Wisse, 2002**; **Steffan et al., 1987**; **Wisse et al., 2008**). In addition, a nanoparticle size above 100 nm triggers phagocytosis by cells of the reticuloendothelial system (*i.e.* hepatic Kupffer cells and spleen macrophages) resulting in rapid blood clearance (**Kettiger et al., 2013**). Both factors significantly decrease the likelihood of reaching the parenchymal liver tissue and increase the risk for potential off-target effects in untargeted tissues.

Surface properties are another important characteristic of nanoparticles. The surface charge (i.e. ζ potential) should be slightly negative (**Xiao et al., 2011**) to prevent sequestration of particles in the lung (*i.e.* due to a positive charge) (**Ishiwata et al., 2000**) or rapid clearance by cells expressing scavenger receptors (*i.e.* due to an excessive negative charge) (**Rothkopf et al., 2005**). According to the classical Derjaguin-Landau-Verwey-Overbeek (DLVO) theory of colloids, a neutral charge has to be avoided to prevent particle agglomeration. In addition to surface charge, steric stabilization by PEGylation mediates long circulating properties and prevents opsonization (**Karmali and Simberg, 2011**; **Milla et al., 2012**).

It was the aim of the present study to design and optimize a nanoparticle based on liposomes combined with derivatives of Myrcludex B to efficiently target hepatocytes while minimizing interactions with off-target cell types. Optimization of physicochemical properties of the nanoparticles included size and charge optimization and steric shielding by PEGylation. Derivatives of Myrcludex B were selected based on target binding, cellular uptake and their impact on the colloidal stability of nanoparticles. For the lipid membrane composition, we used a FDA and EMA approved multi-component lipid formulation based on Doxil (*i.e.* liposomal formulation of doxorubicin) (**Barenholz, 2012**). To design an optimal targeted system, several Myrcludex B derivatives with variations in the peptide sequence or fatty acid modification were covalently linked to the distal end of PEG-lipids. NTCP-specific and ligand-dependent uptake was confirmed in vitro using human liver-derived cell lines. Recently, Shan et al. reported huge discrepancies between in vitro systems and rodent experiments during the development of targeted nanomedicines (**Shan et al., 2015**). Therefore, we used the zebrafish as a complementary in vivo screening model based on our previous work (**Sieber et al., 2019b**; **Campbell et al., 2018**; **Einfalt et al., 2018**; **Sieber et al., 2017**). We assessed the effect of nanoparticles' ligand type and ligand density on their pharmacokinetics. To this end, human-derived cell lines lacking or expressing the human NTCP (hNTCP, *SLC10A1*) were xenotransplanted into zebrafish embryos prior to systemic administration of

nanoparticles. Finally, tissue distribution of dual-labeled nanoparticles was qualitatively (fluorescence-based) and quantitatively (radionuclide-based) investigated in vivo in mice to demonstrate the targeting potential of our hepatotropic nanoparticle platform in higher vertebrates.

Results and discussion

Design and characterization of a hepatotropic nanoparticle for NTCP-specific targeting

The aim of our study was the design of a hepatotropic, targeting ligand-modified nanoparticle. To this end, the surface of liposomal nanoparticles was modified using targeting peptides or lipopeptides derived from the preS1 domain of the HBV large envelope protein (***Figure 1A***). Based on a previous screening of 26 HBVpreS peptide variants, we selected Myrcludex B, the first HBV entry inhibitor (***Blank et al., 2016***; ***Bogomolov et al., 2016***), and five additional Myrcludex B-derived peptides to evaluate the influence of amino acid sequence variations or acyl chain modifications on targeting efficiency and thereby optimize our hepatotropic nanoparticle. All Myrcludex B derived (lipo) peptides were synthesized in high yields and purity by standard solid phase peptide synthesis using Fmoc-chemistry (***Schieck et al., 2013***; ***Schieck et al., 2010***; ***Müller et al., 2013***). Lipopeptides were N-terminally modified with the fatty acids myristic acid (saturated C14) or capric acid (saturated C10), since our previous studies have shown that fatty acid modification is key for mediating interactions with target cells. C-termini of synthesized targeting (lipo)peptides were modified with cysteine residues to allow conjugation to the distal end of PEGylated phospholipids (DSPE-PEG2000-Maleimide) integrated into sterically stabilized liposomes. Coupling was achieved by a chemically reactive maleimide, giving rise to a metabolically stable thioether bond suitable for applications in living organisms (***Figure 1A***). Successful conjugation of Myrcludex B to lipid-based nanoparticles was demonstrated by fluorescence correlation spectroscopy using Myrcludex B-Atto488. The autocorrelation curve of nanoparticle conjugated peptides showed a significant shift to longer diffusion times as compared to the free peptide, with average diffusion times of τ_d = 1639 µs and τ_d = 192 µs, respectively (***Figure 1—figure supplement 1***).

Liposome membrane partition coefficients of mono fatty acid modifications are orders of magnitudes lower as compared to di-lipid anchors. (***Sauer et al., 2006***) Therefore, the distearoyl anchor of DSPE results in a stable incorporation of the PEGylated phospholipid-targeting ligand conjugate in the lipid bilayer of liposomes (membrane partition coefficient $>10^3$ mM^{-1}), whereas the PEG linker offers a flexibility to the distally tethered lipopeptides to extend away from the liposome surface. In addition, a thermodynamically favorable backward bending insertion of the acyl chain into the liposomal membrane is possible. A slight change in transition temperature evaluated by pressure perturbation calorimetry and differential scanning calorimetry confirmed this hypothesis (data not shown). The formulation yield of modified nanoparticles after purification was dependent on the conjugated Myrcludex B derived (lipo)peptide with preS2−48 > Myr-preS2−31 > Myr-preS2-48A ≥ Myr-preS2−48 > Cap-preS2-48.

Light scattering and electron microscopy verified that all nanoparticles, that Myrcludex B-derived peptide conjugated liposomes (modified without or with C14 acyl moiety) had a spherical morphology with a small size around 90 nm, narrow size distribution (*that is* PDI <0.2), and a slightly negative zeta potential (***Figure 1B***, ***Table 1***). Only a small increase in the hydrodynamic size of about 2 nm was observed after conjugation of Myrcludex B-derived peptides (***Table 1***). The zeta potential of nanoparticles remained negative due to a negative net charge of Myrcludex B-derived lipopeptides at physiological pH. Thus, the physicochemical properties of nanoparticles were not significantly influenced by the surface modification with HBVpreS derived lipopeptides containing C14 acyl chains. Exceptions were nanoparticles modified with Cap-preS2-48, which had an average diameter of 134.28 nm and a PDI of 0.24 (***Figure 1B***, ***Table 1***).

It is tempting to speculate, that the C10 acyl chain of Cap-preS2-48 interfered with liposome membrane stability. As compared to longer acyl chains the backward bending insertion of C10 acyl chains into intra-liposomal membranes is less stable, thus promoting faster dissociation and possible interactions with neighboring liposomes due to re-association with inter-liposomal membranes. This was also indicated by formation of aggregates resulting in shorter storage stability (data not shown). Previously published studies reporting a rapid partitioning of shorter lipid anchors from liposomal

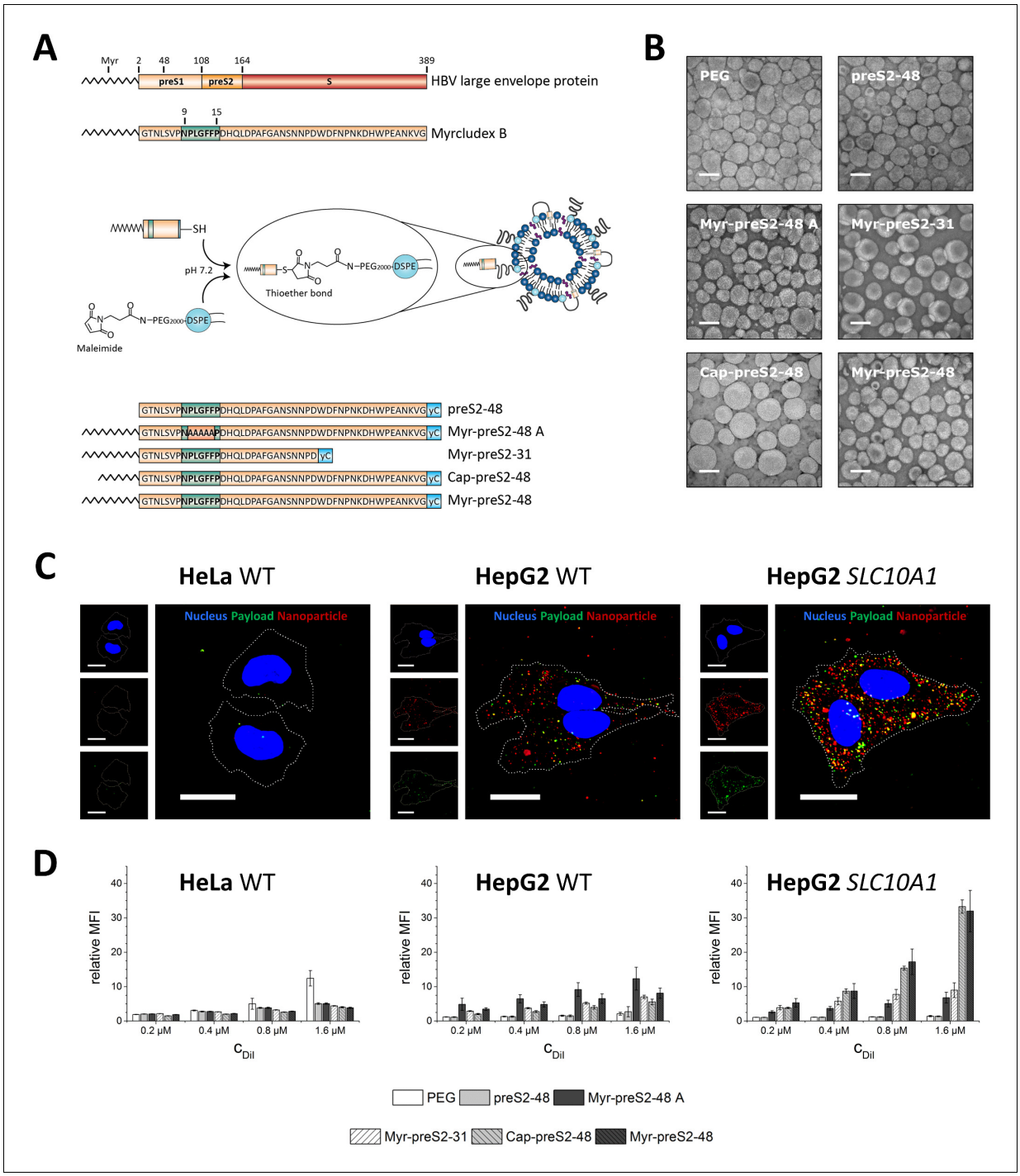

Figure 1. Hepatotropic nanoparticles based on liposomes modified with Myrcludex B-derived peptides for NTCP-specific targeting. (**A**) Schematic representation of peptides derived from Hepatitis B virus (HBV) large envelope protein including the first entry inhibitor, Myrcludex B. Different peptides were conjugated via thiol function to the distal end of PEG chains integrated in the nanoparticle structure using maleimide chemistry. The most important amino acid sequence (9-15) for NTCP-specific binding is highlighted in green color in each lipopeptide. (**B**) Representative transmission

Figure 1 continued on next page

Figure 1 continued

electron microscopy images of different Myrcludex B-derived lipopeptide conjugated nanoparticles. Scale bar = 100 nm. (**C**) Uptake of Myrcludex B-modified nanoparticles into human cells with variable NTCP expression levels. Nanoparticles have a dual fluorescent label, that is lipophilic membrane label (DiI, red) and hydrophilic payload incorporation (carboxyfluorescein, green). Representative confocal laser scanning microscopy maximum intensity projections for Myr-preS2-48 modified nanoparticles after 30 min are shown. Dotted lines indicate cell membranes. Blue signal: Hoechst stain of cell nuclei. Scale bar = 10 µm. (**D**) Flow cytometry analysis of uptake rate into non-hepatic HeLa cells, liver derived HepG2 cells and *SLC10A1* overexpressing HepG2 cells. Increasing concentrations of nanoparticles (C_{DiI}) modified with different Myrcludex B-derived peptides were evaluated. Relative mean fluorescence intensities (MFI) of DiI signals normalized to untreated cells are given. All values are shown as mean ± SD of biological replicates (n ≥ 3 independent experiments). Numerical data for all graphs are shown in ***Figure 1—source data 1***.

DOI: https://doi.org/10.7554/eLife.42276.002

The following source data and figure supplements are available for figure 1:

Source data 1. Characterization of hepatotropic nanoparticles.

DOI: https://doi.org/10.7554/eLife.42276.012

Figure supplement 1. Characterization of hepatotropic nanoparticles based on liposomes modified with Myrcludex B (Myr-preS2-48) using fluorescence correlation spectroscopy.

DOI: https://doi.org/10.7554/eLife.42276.003

Figure supplement 2. Assessment of cytocompatibility of nanoparticles modified with different Myrcludex B derived peptides using non-hepatic HeLa cells (HeLa WT), liver-derived wildtype HepG2 cells (HepG2 WT) and HepG2 cells overexpressing the human NTCP (HepG2 *SLC10A1*) by MTT assay.

DOI: https://doi.org/10.7554/eLife.42276.004

Figure supplement 3. Concentration dependent fluorescence self-quenching of 5 (6)-carboxyfluorescein.

DOI: https://doi.org/10.7554/eLife.42276.005

Figure supplement 4. Flow cytometry analysis of nanoparticle uptake rate into non-hepatic HeLa cells, liver-derived HepG2 cells and *SLC10A1* overexpressing HepG2 cells.

DOI: https://doi.org/10.7554/eLife.42276.006

Figure supplement 5. Uptake of Myrcludex B-modified nanoparticles into HuH7 liver-derived cells deficient (HuH7 WT) or overexpressing *SLC10A1* (HuH7 *SLC10A1*).

DOI: https://doi.org/10.7554/eLife.42276.007

Figure supplement 6. Time-dependent internalization of Myr-preS2-31 modified nanoparticles into *SLC10A1* overexpressing HepG2 cells.

DOI: https://doi.org/10.7554/eLife.42276.008

Figure supplement 7. Time-dependent internalization and toxicity of propidium iodide loaded nanoparticles into *SLC10A1* overexpressing HepG2 cells.

DOI: https://doi.org/10.7554/eLife.42276.009

Figure supplement 8. Time-dependent internalization and toxicity of doxorubicin loaded nanoparticles into *SLC10A1* overexpressing HepG2 cells.

DOI: https://doi.org/10.7554/eLife.42276.010

Figure supplement 9. Activity of DNA loaded lipid nanoparticles (LNP).

DOI: https://doi.org/10.7554/eLife.42276.011

Table 1. Physicochemical characteristics of nanoparticles with different surface modifications.
Hydrodynamic size [nm], polydispersity index (PDI), and zeta potential [mV] were analyzed using dynamic and electrophoretic light scattering. All values are shown as mean ± SD of n ≥ 3 independent experiments. Numerical data for all nanoparticles are shown in ***Table 1—source data 1.***.

Surface modification	Size [nm] ± SD	PDI ± SD	Zeta potential [mV] ± SD
PEG	88.53 ± 5.89	0.05 ± 0.01	−5.93 ± 0.63
preS2-48	90.74 ± 5.83	0.06 ± 0.02	−3.34 ± 1.38
Myr-preS2-48 A	90.77 ± 4.98	0.06 ± 0.04	−13.35 ± 3.08
Myr-preS2-31	89.10 ± 4.38	0.10 ± 0.02	−9.82 ± 0.87
Cap-preS2-48	134.28 ± 36.23	0.24 ± 0.04	−8.39 ± 1.13
Myr-preS2-48	92.21 ± 6.78	0.12 ± 0.08	−10.70 ± 4.25

DOI: https://doi.org/10.7554/eLife.42276.013

The following source data is available for Table 1:

Source data 1. Physicochemical characterization of nanoparticles.

DOI: https://doi.org/10.7554/eLife.42276.014

vesicles support our observation of unfavorable liposome interactions for Cap-preS2-48 (**Sauer et al., 2006**; **Webb et al., 1998**).

Cellular uptake and viability

Next, we investigated the biocompatibility and targeting capacity of our ligand-modified nanoparticles in a panel of three different cell lines in vitro, that is non-hepatic HeLa cells devoid of *SLC10A1* (negative control), liver-derived wild type HepG2 cells (HepG2 WT, hepatocyte control cell line with no detectable *SLC10A1* expression based on PCR) and HepG2 cells overexpressing the human NTCP (HepG2 *SLC10A1*). We used lentiviral transduced cells overexpressing *SLC10A1* as a positive control to confirm the specificity of our system since human liver derived cell lines such as HepG2 and HuH7 down-regulated NTCP during oncogenic transformation (i.e. NTCP expression levels are significantly decreased in hepatocellular carcinoma) (**Lempp et al., 2016**). In all cell lines, nanoparticles showed a high cytocompatibility up to the highest tested lipid concentration of 8 mM, which is far beyond liposome blood concentrations achievable in a clinical setting (**Figure 1—figure supplement 2** demonstrating no decrease of cell viability using the MTT assay) (**Barpe et al., 2010**).

In vitro uptake studies revealed that Myrcludex B-modified nanoparticles were rapidly internalized within 30 min into liver-derived HepG2 cell lines whereas no binding or cellular uptake was observed in non-hepatic HeLa cells (**Figure 1C**, representative confocal laser scanning microscopy images for Myr-preS2-48 modified nanoparticles). Both the liposomal nanoparticle (DiI signal) and the encapsulated payload (carboxyfluorescein (CF) signal), were detected intracellularly. Notably, CF was encapsulated into our nanoparticles at a fluorescence self-quenching concentration (i.e. 60 mM, **Figure 1—figure supplement 3**). Thus, CF fluorescence increases significantly after overcoming the Förster critical transfer distances, that is release of CF from nanoparticles into surrounding environment (**Chen and Knutson, 1988**). Specific uptake of nanoparticles with NTCP-binding component preS-peptide was enhanced with increasing *SLC10A1* expression levels (**Figure 1C,D** and **Figure 1—figure supplement 4**) demonstrating a high target specificity (*i.e.* HeLa WT <HepG2 *SLC10A1*). Surprisingly, the highest DiI signal (and not CF signal) in HeLa cells was observed with PEGylated nanoparticles. It is tempting to speculate that nanoparticle modification with Myrcludex B-derived lipopeptides decreases the interaction with negatively charged cell membranes of *SLC10A1*-deficient cells (*e.g.* HeLa) due to a negative net charge of lipopeptides at physiological pH and thus increased electrostatic repulsion. Uptake studies with a different liver-derived cell line (HuH7) comparing wild type and *SLC10A1* overexpressing cells confirmed the *SLC10A1* specific interaction. Overexpression of *SLC10A1* again resulted in a strong enrichment of cellular uptake ruling out an involvement of cell-line specific artifacts (**Figure 1—figure supplement 5**).

In order to demonstrate the potential application of Myr-preS2-31 modified nanoparticles as drug delivery system, we successfully incorporated small molecular payloads as well as larger compounds into nanoparticles payloads (i.e. propidium iodide, doxorubicin, FITC-labeled peptide, DNA vector) to enhance their internalization into *NTCP* expressing cells (**Figure 1—figure supplements 6**, **7**, **8** and **9**). Indeed, time-dependent uptake studies confirmed the rapid binding and internalization process of Myr-preS2-31 modified nanoparticles (**Figure 1—figure supplements 6**, **7** and **8**). Of note, propidium iodide is a cell membrane impermeable drug. Thus, NTCP-targeted nanoparticles enabled internalization into cells and successful release into cytosol indicated by nuclear counterstain (**Figure 1—figure supplement 7**). To investigate the potential application of *NTCP*-targeted lipid nanoparticles as gene delivery systems, we encapsulated a DNA vector coding for GFP into lipid nanoparticles based on a clinically approved lipid composition and modified with Myr-preS2-31. High content screening analysis demonstrated that modification of nanoparticles with Myr-preS2-31 significantly increases the transfection of *NTCP* expressing cells (**Figure 1—figure supplement 9**). These experiments highlight future applications of the developed carriers and serve as a starting point for future extended in vivo studies in different species and disease models.

Competition of NTCP-specific cellular binding and uptake of targeting ligand-modified nanoparticles

To confirm specificity of NTCP interactions with Myrcludex B derived ligands, we used pre-incubations with free Myrcludex B-Atto565 to competitively inhibit nanoparticle binding and cellular uptake (**Figure 2A**). Fluorescently labeled Myrcludex B can be considered to be a suitable blocking agent

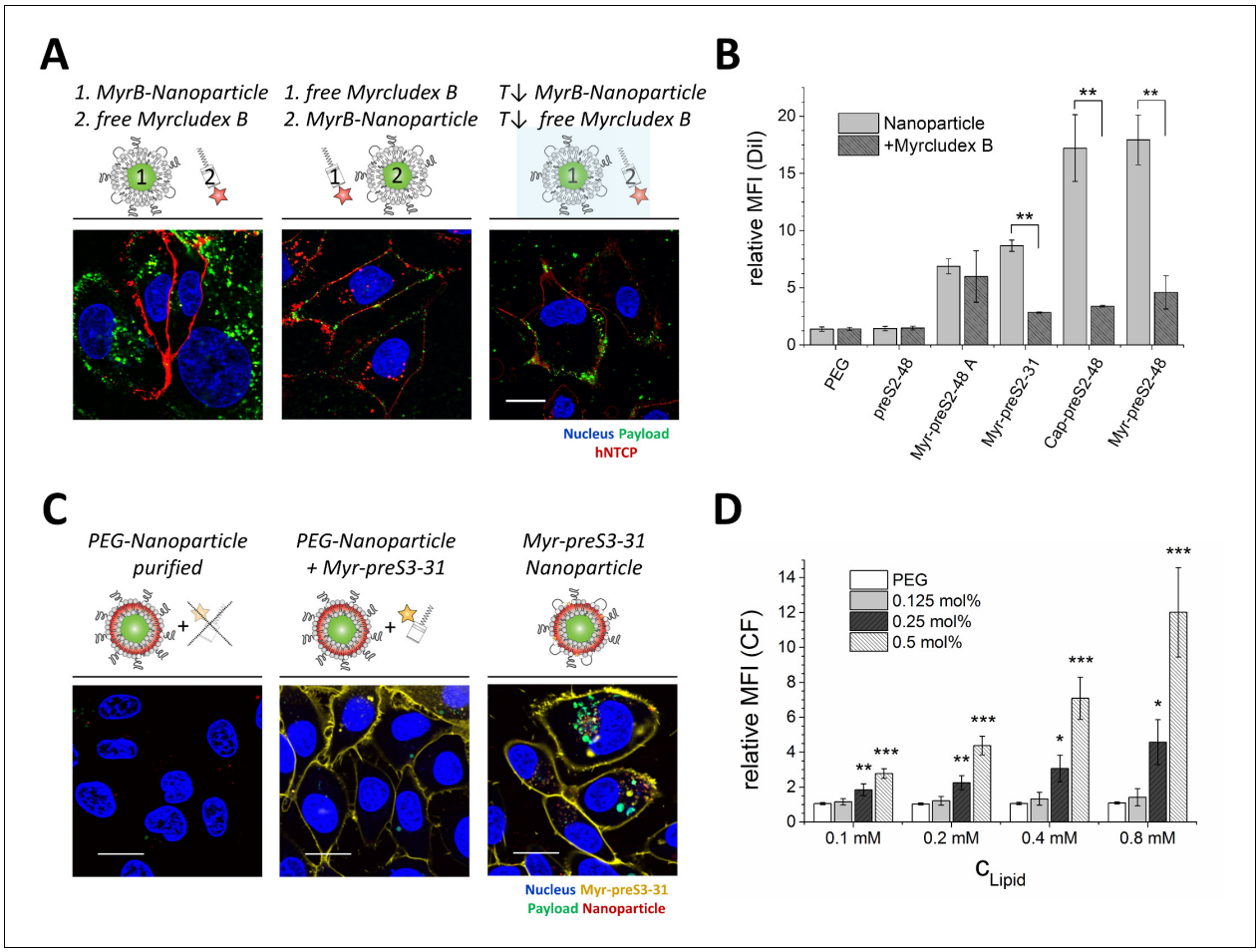

Figure 2. NTCP-specific and ligand-dependent uptake of Myrcludex B-derived lipopeptide conjugated nanoparticles into liver-derived cells in vitro. (**A**) Competitive inhibition study of Myrcludex B (MyrB)-conjugated nanoparticle uptake (carboxyfluorescein payload, green signal) into HepG2 *SLC10A1* already after 30 min. Free Atto-565 labeled Myrcludex B (red signal) was added after (left panel) or before (middle panel) nanoparticle. Uptake studies at lower temperature (T↓, 4˚C, right panel) were performed to demonstrate energy-dependent process of nanoparticle internalization. Representative confocal laser scanning microscopy images are shown. Blue signal: Hoechst stain of cell nuclei. Scale bar = 10 µm. (**B**) Quantification of nanoparticle uptake in absence or presence of free Myrcludex B dependent on different Myrcludex B derived peptide modification. All values are shown as mean ± SD of biological replicates (n = 3 independent experiments). **p<0.01. (**C**) Uptake study of nanoparticles (membrane dye, DiI, red signal) loaded with carboxyfluorescein (green signal) into HepG2 *SLC10A1* without, mixed or covalently modified with Atto-633 conjugated Myr-preS2-31 (yellow signal). Myr-preS2-31-K-Atto633 is covalently linked to surface via stable thioether bond (right panel). Representative confocal laser scanning microscopy images are shown. Blue signal: Hoechst stain of cell nuclei. Scale bar = 10 µm. (**D**) Concentration (C_{Lipid}) dependent uptake of nanoparticles modified with different amounts of Myr-preS2-31 analyzed by flow cytometry and based on CF signal. All values are shown as mean ± SD of biological replicates (n = 4 independent experiments). *p<0.05, **p<0.01, ***p<0.001. Numerical data for all graphs are shown in ***Figure 2—source data 1***.

DOI: https://doi.org/10.7554/eLife.42276.015

The following source data and figure supplements are available for figure 2:

Source data 1. Influence of ligand on cellular interactions.

DOI: https://doi.org/10.7554/eLife.42276.021

Figure supplement 1. NTCP-dependent uptake mechanism of nanoparticles.

DOI: https://doi.org/10.7554/eLife.42276.016

Figure supplement 2. Uptake of Myrcludex B-modified nanoparticles into HeLa cells transfected with empty vector (pEF6 Ctrl), *Slc10a1* or *SLC10A1*.

DOI: https://doi.org/10.7554/eLife.42276.017

Figure supplement 3. Influence of glycosaminoglycans (GAGs) on Myrcludex B binding.

Figure 2 continued on next page

Figure 2 continued

DOI: https://doi.org/10.7554/eLife.42276.018

Figure supplement 4. Uptake of nanoparticles into HepG2 WT cells in absence or presence of heparan sulfate.

DOI: https://doi.org/10.7554/eLife.42276.019

Figure supplement 5. Ligand density dependent uptake of Myrcludex B-modified nanoparticles loaded with carboxyfluorescein (payload, green).

DOI: https://doi.org/10.7554/eLife.42276.020

since its binding to NTCP expressing HepG2 *SLC10A1* cells results in a significant shift in fluorescence signal as compared to control cells (data not shown). Uptake inhibition of nanoparticles modified with Myr-preS2-31, Cap-preS2-48, and Myr-preS2-48 by free Myrcludex B-fluorescein was confirmed by flow cytometry (***Figure 2B***). In contrast, the uptake of Myr-preS2-48A modified nanoparticles was not significantly inhibited by free Myrcludex B, due to the non-specific amino acid sequence (see difference in essential amino acid sequence highlighted in ***Figure 1A***). By incubation of cells in presence of NaN_3 or at low temperature (i.e. 4˚C), we confirmed that the uptake of NTCP targeted nanoparticles is an energy-dependent process (***Figure 2A***). These results demonstrate that hepatotropism of nanoparticles is mediated by NTCP and that the cellular uptake of the carrier is an active and energy-dependent process.

Selection of the optimal hepatotropic Myrcludex B-derived lipopeptide

After evaluating the formulation yield, physicochemical characteristics (i.e. storage/colloidal stability, hydrodynamic diameter, size distribution, zeta potential) and the targeting capacity of our NTCP-specific nanoparticles in vitro, we identified Myr-preS2-48 and Myr-preS2-31 as lead structures and used these for further investigations. This choice was based on the following observations:

First, only nanoparticles modified with lipopeptides but not peptides without conjugated fatty acid (e.g. preS2-48) can bind to NTCP. This set of experiments confirmed that the acyl modification of peptides on nanoparticles' surface is a crucial prerequisite for hepatocyte binding as reported recently for free peptides (***Meier et al., 2013***; ***Schieck et al., 2013***). Only acyl modified peptides increased nanoparticle binding and internalization. Second, liposomes decorated with peptides conjugated to capric acid had a reduced colloidal stability. Their storage stability was limited due to particle aggregation. Furthermore, their size of around 134 nm exceeds the diameter of liver sinusoid fenestrations presumably limiting their access to the space of Disse. Third, Myr-preS2-48A modified nanoparticles were excluded due to poor NTCP specificity as demonstrated by the lack of binding competition by free Myrcludex B. In addition, the uptake of these nanoparticles was independent of NTCP expression levels and even higher in HepG2 wild type cells (***Figure 1D***).

Mechanistic studies on NTCP mediated cellular binding and internalization

In order to demonstrate the importance of covalent peptide attachment, we used a triple fluorescence labeling strategy (***Figure 2C***). The targeting ligand Myrcludex B was labeled with Atto633, the liposomal phospholipid bilayer was labeled with DiI, and the aqueous cargo payload of nanoparticles consisted of CF. Myr-preS2-31-K-Atto633 was labeled at an additionally introduced lysine at position 2, in order to still allow conjugation to the nanoparticle surface by the terminal cysteine. Recently, we have shown that additional N-terminal amino acids do not interfere with specific liver enrichment (for comparison Myr-preS−11-48) (***Schieck et al., 2013***).

First, CF-loaded, DiI-labeled nanoparticles were incubated with Myr-preS2-31-K-Atto633 and purified using size exclusion chromatography to remove free targeting ligand. Cell experiments confirmed successful removal of free Myr-preS2-31-K-Atto633 (no signal on cell membrane) and as expected no uptake of PEGylated nanoparticles. As a control, we added a mixture of free Myr-preS2-31-K-Atto633 and PEGylated nanoparticles to HepG2 *SLC10A1* cells without prior purification. Notably, a strong fluorescence signal on the cell membrane was observed due to specific binding of free Myr-preS2-31-K-Atto633 to *SLC10A1* indicating specific targeting despite an additional N-terminal amino acid. Free Myr-preS2-31-K-Atto633 did not interact with PEGylated nanoparticles

and thus did not trigger nanoparticle entry into HepG2 *SLC10A1* cells. Finally, we covalently linked the Myr-preS2-31-K-Atto633 to the nanoparticle surface by Michael addition of the distal cysteine residue to maleimide-functionalized PEGylated phospholipids integrated in the nanoparticle structure. A strong cellular binding and uptake of Myr-preS2-31-K-Atto633 modified nanoparticles was observed already within 1 h.

Interestingly, nanoparticles including their payload entered the target cell whereas the targeting ligand remained on the cell surface. Since Myrcludex B has a remarkably high affinity to the NTCP (K_D of 67 nM) (***Meier et al., 2013***), it is tempting to speculate that the targeting ligand is retained by NTCP on the cell surface while the dissociated liposome payload is internalized and further processed by a yet unknown mechanism. Of note, intracellular CF signals were considerably higher when compared to DiI signals. This might also indicate liposome dissociation and perhaps loss of DiI during the internalization process. Uptake experiments using pharmacological pathway inhibitors suggested a partially clathrin-dependent and caveolin-independent mechanism, which differs from the process of phagocytosis and micropinocytosis (***Figure 2—figure supplement 1***). Intriguingly, additional factors besides NTCP binding seem to contribute to this process. Non-hepatic HeLa cells transduced with mouse NTCP (mNtcp; *Slc10a1*) or *SLC10A1* can bind Myrcludex B-modified nanoparticles. However, binding is reduced as compared to binding in hepatic cell lines and no uptake is observed (***Figure 2—figure supplement 2***). Thus, additional hepatic cell dependent factors seem to play a role for efficient binding and internalization. Indeed, Verrier et al. reported recently that glypican five expression is an important co-factor for HBV entry (***Verrier et al., 2016***). Notably, uptake experiments using psgA745 cells (CHO xylosyltransferase mutants) overexpressing NTCP showed that binding of Myrcludex B alone is not influenced by glycosaminoglycans (***Figure 2—figure supplement 3***). In sharp contrast, binding of nanoparticles could be partially inhibited in HepG2 WT cells using heparan sulfate suggesting an involvement of glycosaminoglycans in the binding and subsequent internalization process of nanoparticles for hepatic cells (***Figure 2—figure supplement 4***). Therefore, it will be an important step for the design of next-generation carrier systems to elucidate such co-factors in detail and adapt the nano-sized delivery system accordingly.

To demonstrate concentration-dependent nanoparticle uptake of Myr-preS2-31 and investigate the effect of ligand density, qualitative and quantitative fluorescence techniques were used (***Figure 2D***). Therefore, we performed in vitro experiments using nanoparticles with variable amounts of coupled Myr-preS2-31 (0 mol% - 0.5 mol% initial maleimide functionalities on nanoparticle surface). With increasing targeting ligand concentration, a significant increase in cellular uptake was observed (***Figure 2D***, ***Figure 2—figure supplement 5***). Notably, we identified a threshold value of at least 0.25 mol% for efficient cell binding by qualitative confocal imaging as well as quantitative flow cytometry experiments (***Figure 2D***, ***Figure 2—figure supplement 5***). Below this value, no uptake was observed, whereas above 0.25 mol% cellular binding was improved. Stoichiometric estimations assuming a bilayer thickness of 5 nm, a phosphatidylcholine headgroup area of 0.71 nm^2 and an equal distribution of DSPE-PEG in the outer and inner nanoparticle membrane result in 157 ± 16, 79 ± 8, or 39 ± 4 maleimide moieties per liposome capable for lipopeptide conjugation corresponding to 0.5 mol%, 0.25 mol%, or 0.125 mol%, respectively (***Maurer et al., 2001***). Thus, a minimum of 80 functional maleimide moieties per nanoparticle is necessary for efficient cellular targeting after Myr-preS2-31 conjugation.

In vivo systemic circulation in the zebrafish vertebrate model

Since in vitro experimental models are not able to mimic the physiological complexity of nano-bio interactions at an organ level, we screened in the next step the effect of ligand density on pharmacokinetics of nanoparticles in vivo for Myr-preS2-48 and Myr-preS2-31 (***Figure 3***). Recently, we have reported that the zebrafish is a valuable pre-clinical tool to assess the systemic circulation and blood clearance of nanoparticulate drug delivery systems in vivo (***Sieber et al., 2017***; ***Campbell et al., 2018***; ***Sieber et al., 2019b***; ***Park, 2017***; ***Yin et al., 2018***; ***Sieber et al., 2019a***).

Thus, we injected DiI labeled nanoparticles modified with different amounts of targeting ligand (0.125 mol% - 1.0 mol%) into the duct of Cuvier of transgenic kdrl:EGFPs843 zebrafish embryos which express GFP in the vasculature endothelial cells. Already 1 h post injection, a clear qualitative difference in circulation characteristics of tested nanoparticles was detected. With increasing ligand density on the nanoparticle surface, the systemic circulation of nanoparticles decreased for both peptides (***Figure 3***) indicating that ligand modification of nanoparticles interferes with the shielding

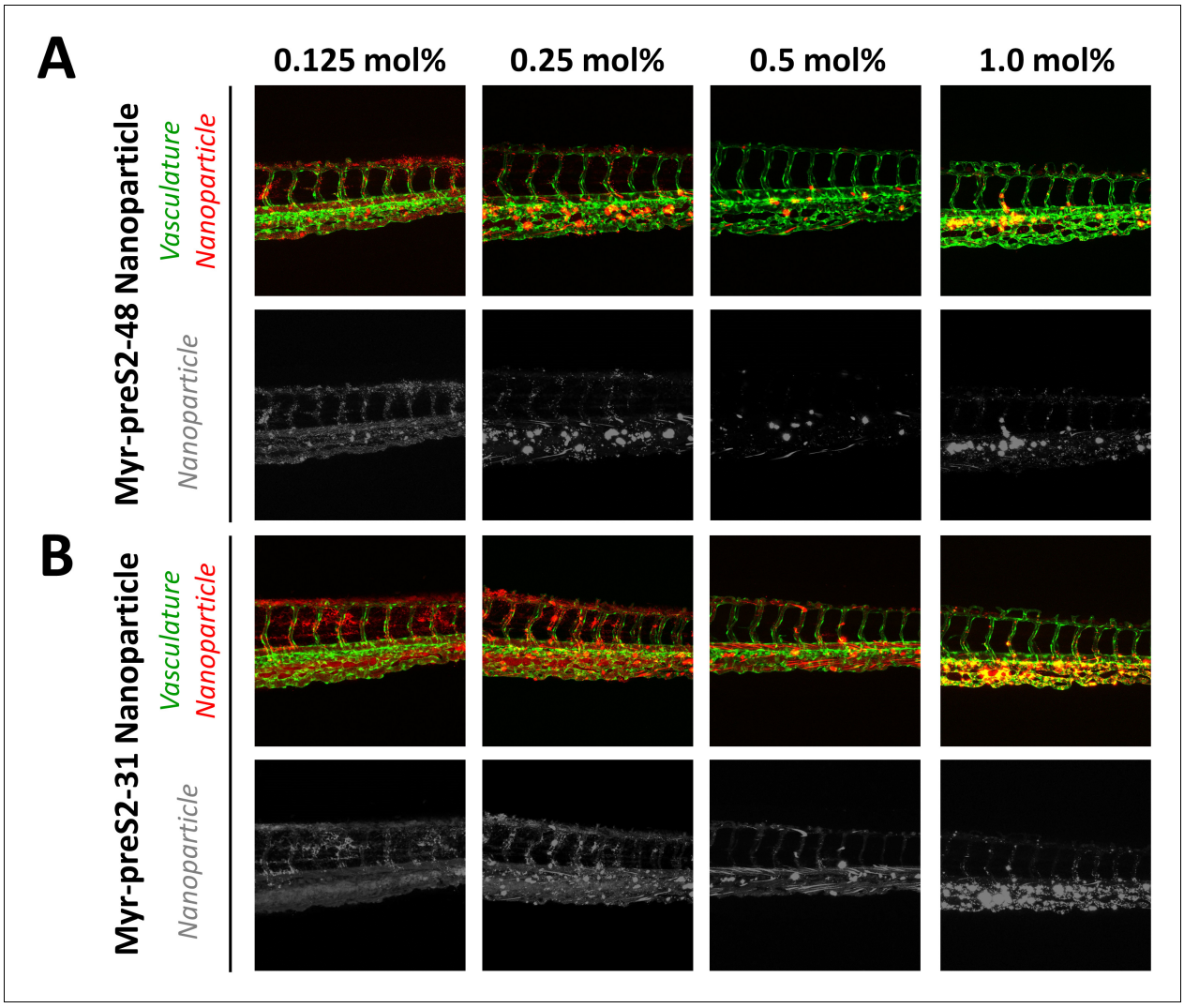

Figure 3. Systemic circulation of Myrcludex B-derived lipopeptide conjugated nanoparticles in vivo in the zebrafish model. Nanoparticles were modified with different amounts of (**A**) Myr-preS2-48 or (**B**) short Myr-preS2-31 and injected into transgenic zebrafish embryos expressing green fluorescent protein in their vasculature endothelial cells (green signal). Membrane of nanoparticles was fluorescently labeled using DiI (red signal). Representative confocal laser scanning microscopy images of tail region 1 hpost injection.

DOI: https://doi.org/10.7554/eLife.42276.022

properties of PEG. Increased blood clearance was thereby paralleled by accumulation in the posterior caudal vein region. The observed binding pattern did not match a *stabilin-2* scavenger receptor dependent nanoparticle clearance, which would be indicative for interactions with mammalian liver sinusoidal endothelial cells (LSECs) (***Campbell et al., 2018***). More likely a sequestration by macrophages is responsible for this clearance mechanism corresponding to an accumulation in the spleen of rodents (***Sieber et al., 2019b***).

Interestingly, nanoparticles modified with the shorter targeting peptide, that is Myr-preS2-31, showed increased systemic circulation (***Figure 3B***) as compared to Myr-preS2-48 modified nanoparticles (***Figure 3A***) at similar ligand densities. Thus, Myr-preS2-31 modified nanoparticles were selected for further investigations. However, nanoparticles modified with more than 0.5 mol% Myr-preS2-31 were as well excluded from further evaluation due to their poor systemic circulation and high clearance rate.

In vivo targeting ability in the zebrafish vertebrate model

In a next step, we investigated the targeting capacity of Myr-preS2-31 modified nanoparticles to human cells in vivo in the zebrafish model (***Figure 4***). In recent years, several groups have used xenografted zebrafish for various investigations including the assessment of nanoparticles (***Sieber et al.,***

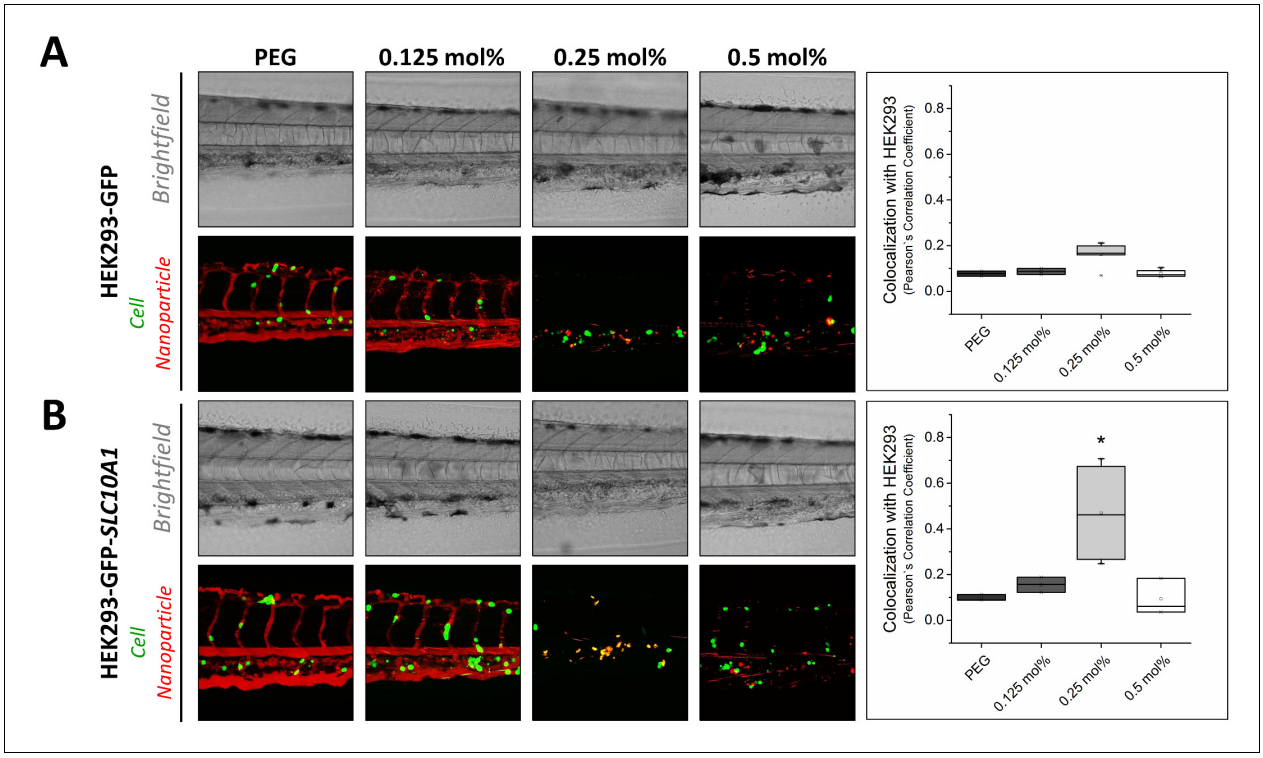

Figure 4. Targeting ability of Myr-preS2-31 conjugated nanoparticles in vivo in xenotransplanted zebrafish embryos. Nanoparticles were modified with different amounts of Myr-preS2-31 and injected into wild type zebrafish embryos xenotransplanted with human, GFP expressing HEK293 cells (green signal), (A) deficient or (B) expressing *SLC10A1*. Membrane of nanoparticles was fluorescently labeled using DiI (red signal). Yellow signals demonstrate colocalization (*i.e.* binding and internalization) of nanoparticles with HEK293-GFP cells. Representative brightfield and fluorescence images of tail region 1 h post injection are shown. Quantitative analysis of nanoparticle binding to HEK293-GFP cells is represented by Pearson´s Correlation Coefficient (PCC). All values are shown as box plots of biological replicates (n $\geq$ 2 independent experiments). *p<0.05. Numerical data for all graphs are shown in ***Figure 4—source data 1***.

DOI: https://doi.org/10.7554/eLife.42276.023

The following source data and figure supplement are available for figure 4:

Source data 1. Targeting xenotransplanted cells in the zebrafish model.

DOI: https://doi.org/10.7554/eLife.42276.025

Figure supplement 1. Targeting ability of free Myrcludex B in vivo in xenotransplanted zebrafish embryos.

DOI: https://doi.org/10.7554/eLife.42276.024

2019a; *Evensen et al., 2016*; *Wertman et al., 2016*; *Brown et al., 2017*; *He et al., 2012*; *Lin et al., 2017*; *Veinotte et al., 2014*; *Wagner et al., 2010*). Despite anatomical differences with mammals, zebrafish xenotransplantation models are an emerging preclinical tool offering several practical advantages as compared to mouse xenografting models including prolific reproduction, facilitated xenotransplantation (no immune rejection due to limited adaptive immune response), and optical transparency enabling high throughput screening. For our study, we used HEK293 cells stably expressing GFP for further genetic modification and establishment of xenotransplants (*Witzigmann et al., 2015b*). HEK293-GFP cells were transiently transfected with *SLC10A1* to express the targeting factor for our hepatotropic nanoparticles. Wild type HEK293-GFP without *SLC10A1* served as control. Both cell lines were injected into ABC/TU wild type zebrafish embryos to create human xenotranplants. The different nanoparticles were injected as soon as transgenic human cells stopped circulating and remained in the caudal vasculature tail region (*i.e.* after approximately 1 h). Interestingly, a clear difference in targeting capacity dependent on *SLC10A1* expression and ligand density was revealed. Whereas there was no significant difference in targeting capacity at different ligand densities for *SLC10A1*-deficient HEK293-GFP cells (*Figure 4A*), a significant increase in binding to HEK293-GFP cells was observed if *SLC10A1* was overexpressed as the nanoparticles could bind specifically and be readily internalized (*Figure 4B*). Most importantly, this was only valid for nanoparticles modified with 0.25 mol% Myr-preS2-31 (*Figure 4*, quantitative analysis). This illustrates that ligand density highly influences the balance between systemic circulation, systemic clearance rate and targeting efficiency of our liposome-based nanoparticles.

Nanoparticles modified with ligand densities below 0.25 mol% show a favorable systemic circulation but have an insufficient targeting ability. This also confirms our observations in vitro, where nanoparticles with a ligand density below 0.25 mol% did not significantly bind to HepG2 *SLC10A1* cells. In sharp contrast, nanoparticles modified with higher Myr-preS2-31 targeting ligand densities (*i.e.* 0.5 mol%) have increased targeting ability in vitro. However, decreased systemic circulation and a high clearance rate under in vivo conditions counteract the advantage of higher ligand densities. Nanoparticles modified with 0.25 mol% Myr-preS2-31 have the highest targeting efficiency due to an ideal balance between target affinity and long circulation time in vivo. It should be noted that nanoparticles are internalized by target cells (*Figure 4B*) whereas free Myrcludex B apparently binds with high affinity to target cells but is not internalized (*Figure 4—figure supplement 1*). This phenomenon was recently observed by our team in rodents (data not shown) and was also reported from clinical trials in humans.

In vivo liver targeting of Myr-preS2-31 conjugated nanoparticles in mice

To elucidate the influence of ligand density on hepatotropism of our nanoparticles in vivo in mammals, we evaluated the pharmacokinetic properties of Myr-preS2-31 conjugated nanoparticles in mice. For this set of experiments, we used a dual labeling approach. The radioactive nuclide indium-111 (^{111}In) was used for whole-body imaging and biodistribution studies whereas fluorescence labeling with DiI was used to evaluate intra-organ nanoparticle distribution. Importantly, we incorporated DTPA-conjugated DSPE into the lipid bilayer to chelate ^{111}In on the surface of nanoparticles. This radiolabeling strategy has distinct advantages as compared to other labeling techniques or loading of ^{111}In-oxine into nanoparticles (*van der Geest et al., 2015*). First, this radiolabeling method is robust, fast (within 45 min) and efficient with labeling efficiencies above 90%. Notably, free ^{111}In was easily removed from nanoparticle formulations prior to injection using size exclusion chromatography (NAP-5 columns). Second, DTPA-DSPE enables retention of ^{111}In in serum for at least 48 h at 37˚ C (>98% label retention) demonstrating the high stability necessary for in vivo studies of nanoparticulate drug delivery systems (*van der Geest et al., 2015*). Third, free ^{111}In is rapidly eliminated via kidneys and excreted in the urine as shown previously (*Harrington et al., 2000*; *Shih et al., 2017*). This offers an easy assessment to differentiate between non-bound and nanoparticle bound ^{111}In.

Four different lipid-based nanoparticles were prepared and injected intravenously into the tail vein of mice, that is PEGylated liposomes (negative control) and nanoparticles modified with 0.125 mol%, 0.25 mol% and 0.5 mol% Myr-preS2-31. Plasma and organs were harvested to perform a quantitative biodistribution analysis ex vivo 1 h post injection (*Figure 5A*). PEGylated nanoparticles showed the typical biodistribution of sterically stabilized nanoparticles with a strong signal in the blood (*Figure 5A*). Myr-preS2-31 conjugated liposomes demonstrated different biodistribution patterns depending on ligand density (*Figure 5A*). Modification of nanoparticles with 0.125 mol% Myr-

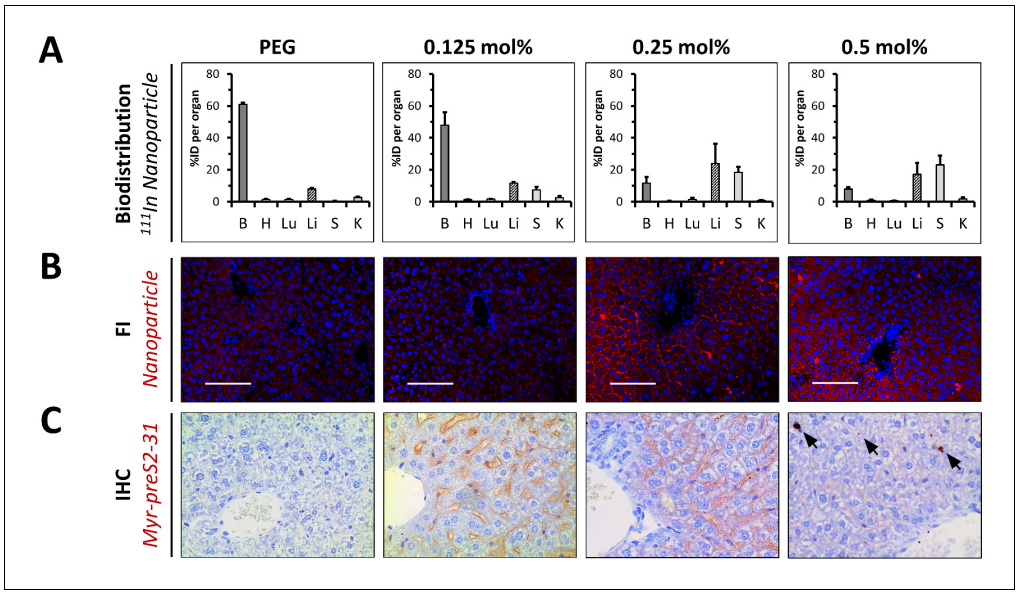

Figure 5. In vivo biodistribution and liver targeting of Myr-preS2-31 conjugated nanoparticles in mice. Nanoparticles were modified with different amounts of Myr-preS2-31 and labeled with radioactive ^{111}In and fluorescent membrane dye (DiI, red signal). (**A**) Quantitative biodistribution studies were performed 1 h post injection. Radioactivity of each organ was determined with a γ-counter and the percentage of injected dose (%ID) per organ was calculated. B = blood, H = heart, Lu = lung, Li = liver, S = spleen, K = kidney. All values are shown as mean ± SD of biological replicates (n = 4 independent experiments). Numerical data for all graphs are shown in ***Figure 5—source data 1***. (**B**) Fluorescence imaging (FI) of nanoparticles (DiI, red signal) in liver cryo-sections. Blue signal: Hoechst stain of cell nuclei. Scale bar = 100 µm. (**C**) Immunohistochemistry (IHC) of Myr-preS2-31 (red signal) in the liver sections 1 h after intravenous injection. Mice liver sections were stained with anti-Myr-preS2-31 antibody (MA18/7). Blue signals represent cell nuclei. Arrows indicate distinct localized accumulations.

DOI: https://doi.org/10.7554/eLife.42276.026

The following source data and figure supplements are available for figure 5:

Source data 1. Biodistribution in mice.

DOI: https://doi.org/10.7554/eLife.42276.036

Figure supplement 1. In vivo biodistribution and liver targeting of Myr-preS2-31 conjugated nanoparticles in mice.

DOI: https://doi.org/10.7554/eLife.42276.027

Figure supplement 2. In vivo biodistribution and ex vivo organ distribution of PEGylated nanoparticles in mice.

DOI: https://doi.org/10.7554/eLife.42276.028

Figure supplement 3. In vivo biodistribution and ex vivo organ distribution of nanoparticles with elevated Myr-preS2-31 modification.

DOI: https://doi.org/10.7554/eLife.42276.029

Figure supplement 4. Organ biodistribution of different nanoparticles in rats.

DOI: https://doi.org/10.7554/eLife.42276.030

Figure supplement 5. Organ ratios of ex vivo biodistribution analysis in mice.

DOI: https://doi.org/10.7554/eLife.42276.031

Figure supplement 6. Intra-organ distribution of Myr-preS2-31-modified nanoparticles in spleen and kidney in vivo in mice dependent on ligand density.

DOI: https://doi.org/10.7554/eLife.42276.032

Figure supplement 7. Liver targeting of Myr-preS2-31 conjugated nanoparticles in mice.

DOI: https://doi.org/10.7554/eLife.42276.033

Figure supplement 8. Specific binding of Myr-preS2-31 conjugated nanoparticles to sinusoidal membrane of hepatocytes.

DOI: https://doi.org/10.7554/eLife.42276.034

Figure supplement 9. Biodistribution of nanoparticles modified with 0.5 mol% Myr-preS2-31 in mice.

DOI: https://doi.org/10.7554/eLife.42276.035

preS2-31 did not alter the systemic circulation significantly (*i.e.* high blood pool signal). Only a minor increase in liver accumulation was observed as compared to ligand-lacking PEGylated nanoparticles (***Figure 5A***).

Interestingly, nanoparticles modified with 0.25 mol% Myr-preS2-31 significantly enriched binding to the liver (***Figure 5A***). Further increase in ligand density (0.5 mol%) resulted in an increase in spleen accumulation, that is enhanced clearance by cells of the reticuloendothelial system (***Figure 5A***). Of note, none of the nanoparticle formulation resulted in an elimination via kidneys demonstrating the high stability and retention of the DTPA-DSPE chelated ^{111}In.

Planar gamma scintigraphy imaging of injected mice and harvested organs at various time points (15 min and 60 min) confirmed these observations (***Figure 5—figure supplements 1***, ***2*** and ***3***). PEGylated nanoparticles demonstrated the typical systemic circulation with a strong signal in highly perfused organs, for example heart (***Figure 5—figure supplements 1*** and ***2***). Modification of nanoparticles with 0.25 mol% Myr-preS2-31 significantly increased the liver accumulation. Interestingly, further increase in Myr-preS2-31 modification ($\geq$0.25 mol%) resulted in dominant location of radioactivity in an elongated structure in the far-left part of the abdomen under the liver, which was identified as the spleen (***Figure 5—figure supplement 1***). In order to confirm this observation, we injected mice with excessive Myr-preS2-31 modified nanoparticles (>0.5 mol%) and performed a planar imaging (***Figure 5—figure supplement 3***). Indeed, elevated Myr-preS2-31 modification resulted in an exclusive spleen accumulation, that is enhanced clearance by cells of the reticuloendothelial system. In order to exclude species specific effects, we also performed a planar gamma scintigraphy imaging of harvested organs from injected rats (***Figure 5—figure supplement 4***). Again, elevated Myr-preS2-31 modification has negative impacts on liver accumulation.

In order to highlight the ligand-density dependent hepatotropism, we calculated ratios between the blood pool and important organs, that is liver (*i.e.* target organ), spleen (*i.e.* clearance organ), and kidney (*i.e.* control organ since nanoparticle bound ^{111}In should not show renal excretion) (***Figure 5—figure supplement 5***). Indeed, Myr-preS2-31 modification $\geq$0.25 mol% resulted in increased liver/spleen-to-blood ratios. Strikingly, nanoparticles modified with 0.25 mol% Myr-preS2-31 demonstrated a significant increase in the liver-to-kidney ratio confirming our conclusions from the zebrafish model, that 0.25 mol% Myr-preS2-31 is the optimal ligand density (***Figure 4B***).

The biodistribution studies were combined with fluorescence imaging of nanoparticle distribution (***Figure 5B***, ***Figure 5—figure supplement 6***) and immunohistochemistry of Myr-preS2-31 distribution (***Figure 5C***, ***Figure 5—figure supplements 6–9***) in liver, spleen, and kidney (*i.e.* nanoparticles and Myr-preS2-31 should not show renal excretion). PEGylated nanoparticles showed a weak fluorescent signal in the liver (***Figure 5B***). Importantly, these signals were not associated with the sinusoidal membrane of hepatocytes but arose from the high hepatic blood supply (***Figure 5—figure supplement 8***). No signals were observed in spleen and kidney (***Figure 5—figure supplement 6***). Modification of nanoparticles with 0.125 mol% Myr-preS2-31 did not result in significantly increased liver levels. A marginal binding of nanoparticles to hepatocyte membrane was visually observed (***Figure 5B,C***). This supports our hypothesis that a threshold level of targeting ligand density present on the nanoparticle surface is necessary for successful targeting. Importantly, strong signals for nanoparticles modified with 0.25 mol% Myr-preS2-31 were observed on the basolateral membrane of parenchymal liver cells (***Figure 5B,C***) demonstrating the strong hepatotropism of our nanoparticles. Further increasing the ligand density (*i.e.* 0.5 mol%) was detrimental and resulted in a diffuse hepatic staining pattern. Nanoparticles and their payload were detected as punctuated signals in the whole liver and did not show a specific membrane staining (***Figure 5B***, ***Figure 5—figure supplement 9***). Myr-preS2-31 was detected in distinct localized areas only (***Figure 5C***). We conclude that nanoparticles modified with excessive Myr-preS2-31 densities (0.5 mol%) are rapidly cleared by liver resident macrophages, *i.e.* Kupffer cells. Subsequent re-distribution phenomena result in an unspecific nanoparticle signal in the whole liver.

Competition of NTCP-specific uptake into mouse hepatocytes in vivo

Since nanoparticles modified with 0.25 mol% Myr-preS2-31 allowed highly efficient liver targeting, we next investigated the NTCP specificity and the internalization process (***Figure 6A***). Therefore, we injected either labeled nanoparticles alone or together with free unlabeled Myrcludex B into mice (***Figure 6B***). Co-injection of Myrcludex B resulted in a clear decrease in liver enrichment by competitive inhibition of NTCP-binding as demonstrated by a change of signal.

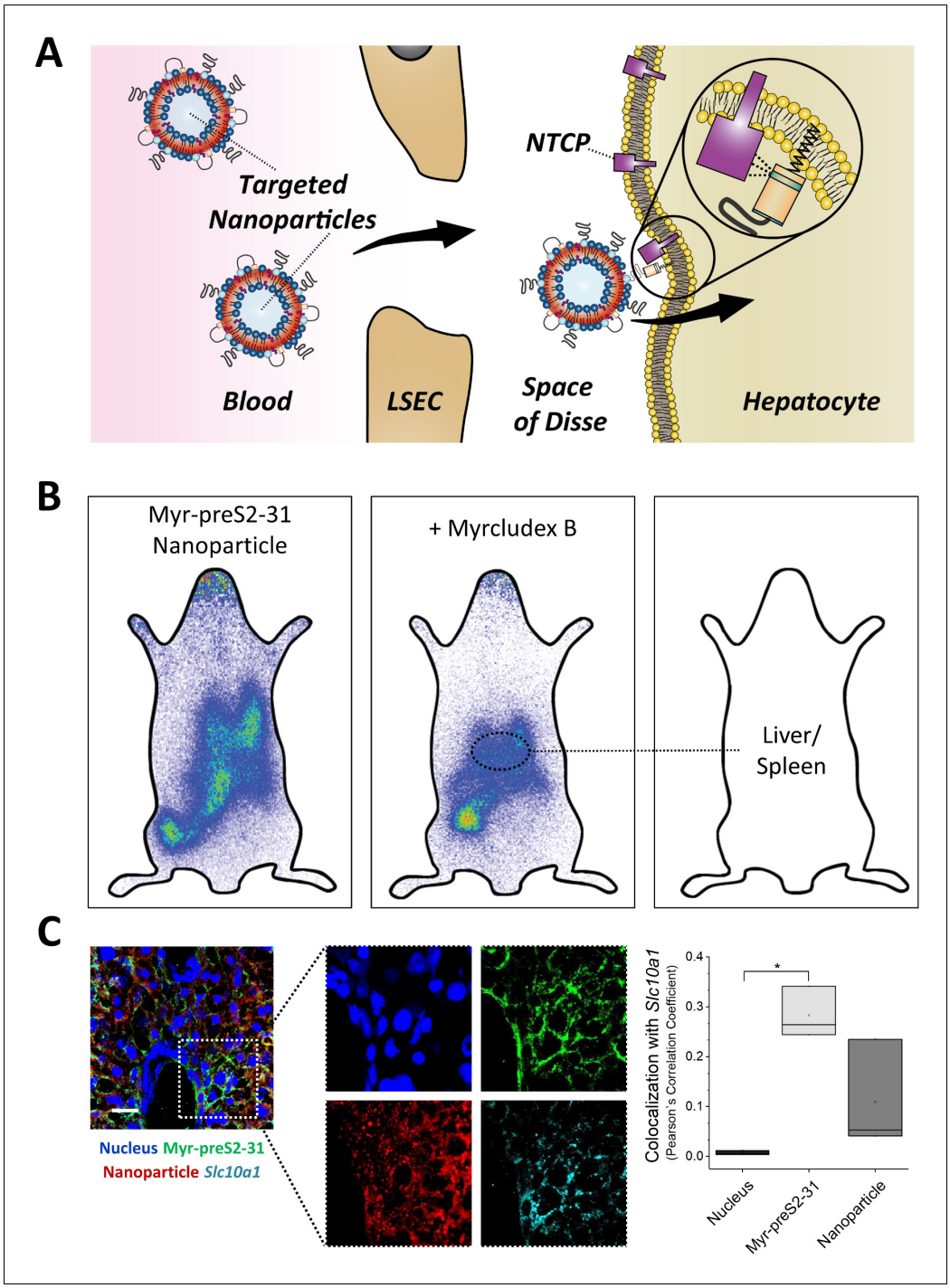

Figure 6. NTCP-specific uptake of Myr-preS2-31 conjugated nanoparticles into hepatocytes in vivo in mice. (**A**) Schematic representation of NTCP-targeted nanoparticle binding to hepatocytes. Circulating nanoparticles pass the fenestrae of liver sinusoidal endothelial cells (LSEC) and subsequently bind to the NTCP in the basolateral membrane of hepatocytes facing the space of Disse. Prior to Myr-preS2-31 mediated NTCP binding, the myristoyl chain is inserted into the lipid bilayer. In close proximity to hepatocytes, acyl chain switches into cellular membrane due to high affinity of essential

Figure 6 continued on next page

Figure 6 continued

peptide sequence to NTCP binding site, thereby consolidating target transporter binding. (**B**) Nanoparticles were modified with 0.25 mol% of Myr-preS2-31 and labeled with radioactive ^{111}In and fluorescent membrane dye (DiI, red signal). Planar imaging of mice 1 h post-injection. Competitive inhibition of liver binding by co-injection of free Myrcludex B clearly demonstrates NTCP-specific binding. Positions of liver and spleen are indicated by small circles. (**C**) Immunofluorescence staining of nanoparticles (red signal), targeting ligand (Myr-preS2-31, green signal, antibody staining), and *Slc10a1* (cyan signal, antibody staining) in liver cryosections. Nuclei staining (blue signal) served as control for complete internalization; no overlap with *Slc10a1*. Scale bar = 20 μm. Colocalization analysis with *Slc10a1* is represented by Pearson´s Correlation Coefficient (PCC). All values are shown as box plots of biological replicates (n = 3 independent experiments). *p<0.05. Numerical data for all graphs are shown in ***Figure 6—source data 1***.

DOI: https://doi.org/10.7554/eLife.42276.037

The following source data is available for figure 6:

Source data 1. Internalization into hepatocytes.

DOI: https://doi.org/10.7554/eLife.42276.038

To reveal the localization of nanoparticles, we performed a confocal microscopy analysis of liver cryo-sections (***Figure 6C***). We stained liver cryo-sections using antibodies against *Slc10a1* and Myr-preS2-31 (MA 18/7). Interestingly, nanoparticles that were internalized into parenchymal liver cells did not co-localize with *Slc10a1* fluorescent signals. Myr-preS2-31 still colocalized with *Slc10a1* suggesting that the targeting ligand was separated from the nanoparticle during cellular internalization as already observed in in vitro experiments. This phenomenon was confirmed by a colocalization analysis (***Figure 6C***). The observed cellular uptake is a surprising finding since HBV possesses pronounced host species specificity with regard to binding and infectivity. HBV binds to murine hepatocytes but cannot infect mice due to the lack of host cell dependency factors (***Lempp et al., 2016***). Therefore, chimeric mice transplanted with primary human hepatocytes have been developed to study anti-HBV drugs (***Petersen et al., 2008***; ***Lütgehetmann et al., 2012***). In humans or chimpanzees only, HBV specifically binds to hepatocytes and subsequently infects the host.

Importantly, our NTCP-targeted nanoparticles apparently lack this species specificity. In contrast to HBV, our hepatotropic nanoparticles specifically bind to mouse hepatocytes in a *Slc10a1*-dependent manner and are subsequently internalized. The exact molecular interactions behind this internalization process will require additional studies to elucidate structural determinants important for cellular uptake and to better understand viral entry mechanisms, which are still unknown (***Glebe and Urban, 2007***).

Conclusions

In conclusion, the combination of in vitro investigations, the zebrafish model and in vivo experiments in rodents offered a unique approach to optimize our targeting ligand modified nanoparticles. The zebrafish model demonstrated to be an excellent tool to pre-screen various nanoparticle formulations, to assess the effect of Myrcludex B modifications on their pharmacokinetics and biodistribution, and thus increase the accuracy of predictions for experiments in rodents. The developed delivery systems can increase liver uptake levels, decrease accumulation in off-target tissues and at the same time avoid clearance by the reticuloendothelial system by mimicking HBV targeting properties. Despite the fact that current liver targeting strategies such as ASGPR- or LDLR-targeted delivery systems have already demonstrated improved drug and gene delivery in various preclinical models, these systems also suffer from certain drawbacks including complex synthesis of multivalent glycans or strong evidence that a majority of endocytosed gene carriers is recycled back to the cell exterior thereby reducing activity (***Witzigmann et al., 2016a***; ***Sahay et al., 2013***). Due to the availability of efficient peptide manufacturing protocols, the proposed NTCP targeted delivery platform is an alternative and promising approach which warrants further investigation. For future clinical applications, optimized Myr-preS2-31 conjugated nanoparticles entrapping small molecule drugs, nucleic acids or proteins need to be studied in appropriate animal models of disease. In particular, we see a great potential for our nanoparticle targeting strategy in the field of metabolic diseases of the liver.

Materials and methods

Key resources table

Reagent type (species) or resource	Designation	Source or reference	Identifiers	Additional information
Cell line (*H. sapiens*)	HepG2 WT	DOI: 10.1111/hepr.12599	RRID:CVCL_0027	Cell depository of the Institute of Pathology (University Hospital of Basel, Switzerland)
Cell line (*H. sapiens*)	HepG2 *SLC10A1*	DOI: 10.1053/j.gastro.2013.12.024	RRID:CVCL_JY40	Prof. Dr. Stephan Urban (University Hospital Heidelberg)
Cell line (*H. sapiens*)	HuH7 WT	DOI: 10.1111/hepr.12599	RRID:CVCL_0336	RIKEN Cell Bank (Ibaraki, Japan)
Cell line (*H. sapiens*)	HuH7 *SLC10A1*	DOI: 10.1053/j.gastro.2013.12.024		Prof. Dr. Stephan Urban (University Hospital Heidelberg)
Cell line (*H. sapiens*)	HeLa WT	-	RRID:CVCL_0030	Prof. Dr. Jörg Huwyler (University of Basel)
Cell line (*H. sapiens*)	HEK293-GFP	DOI: 10.1021/acsami.5b01684		Prof. Dr. Jörg Huwyler (University of Basel)
Cell line (*Cricetulus griseus*)	CHO	DOI: 10.1021/bi702258z	RRID:CVCL_0214	Prof. Dr. Joachim Seelig (University of Basel)
Cell line (*Cricetulus griseus*)	psgA745	DOI: 10.1021/bi702258z		Prof. Dr. Joachim Seelig (University of Basel)
Genetic reagent (*Danio rerio*)	kdrl:EGFPs843 zebrafish	DOI: 10.1016/j.jconrel.2017.08.023	https://zfin.org/ZDB-TGCONSTRCT-070117-47	Prof. Dr. Markus Affolter (University of Basel)
Antibody	anti-Myr-preS2-31 antibody (MA18/7)	-	-	Prof. Dr. Wolfram Gerlich (Justus-Liebig-Universität Gießen); monoclonal human, 1:100 dilution
Antibody	anti-Slc10a1 (anti-Ntcp)	-	-	Prof. Bruno Stieger (University of Zurich); polyclonal rabbit, 1:100 dilution
Antibody	anti-FITC antibody	Invitrogen - ThermoFisher Scientific	Catalog # 71–1900	polyclonal rabbit, 1:100 dilution
Software	OriginPro 9.1 software	-	RRID:SCR_014212	OriginLab Corporation
Software	FlowJo VX software	-	RRID:SCR_008520	TreeStar
Software	ImageJ Fiji	-	RRID:SCR_002285	ImageJ

Synthesis of Myrcludex B-derived peptides

Different peptides were synthesized by fluorenylmethoxycarbonyl/t-butyl (Fmoc/tBu) solid-phase synthesis using an Applied Biosystems 433A peptide synthesizer and modified with acyl chains as described previously (***Schieck et al., 2013***). Atto fluorescence dyes were either linked to the distal cysteine residue by maleimide chemistry or to the ε-amino group of an additionally introduced D-lysine at position two by NHS chemistry for mechanistic studies based on a triple fluorescence labeling strategy. In contrast to all other amino acids of Myrcludex B-derived lipopeptides, a D-amino acid was introduced in the latter case due to the chemical synthesis strategy used. Peptides were purified using preparative reverse-phase high performance liquid chromatography (HPLC, LaPrep P110, VWR International GmbH) with a Reprosil-Gold 120 C18 4 µm column (Dr. Maisch GmbH) and a variable gradient adapted to the peptides properties in a range of 100% H_2O to 100% acetonitrile, both containing 0.1% TFA. Peptide identity was verified using an analytical Agilent 1100 HPLC system equipped with a Chromolith Performance RP-C18e column (Merck KGaA) coupled to a mass spectrometer (Exactive, Thermo Fisher Scientific).

Preparation of hepatotropic nanoparticles

Hepatotropic nanoparticles based on liposomes were prepared using the film rehydration extrusion method as described previously (***Detampel et al., 2014***). The lipid membrane composition of nanoparticles consisted of DSPC (Lipoid AG), cholesterol (Sigma-Aldrich), DSPE-PEG2000 (Lipoid AG) at a molar ratio of 52.7:42.3:5. For the conjugation of HBV-derived peptides, DSPE-PEG2000 was replaced by DSPE-PEG2000-maleimide (Avanti Polar Lipids) at indicated molar ratios. For fluorescence labeling of lipid membrane, 1 mol% DiI (Thermo Fisher Scientific) was added to the lipid composition replacing DSPC. For radioactive labeling with ^{111}In, DSPC was replaced by 3 mol% DSPE-DTPA (Avanti Polar Lipids). Desired ratios of lipids were mixed; a homogenous thin film was prepared and dried using a Rotavapor A-134 (Büchi). Lipid films were rehydrated using 0.01 M PBS pH 7.2 containing 1 mM EDTA (Sigma-Aldrich) to prevent metal ion catalyzed maleimide oxidation. For passive loading and fluorescence labeling of inner core, a 60 mM 5 (6)-carboxyfluorescein (Sigma-Aldrich) solution (pH 7.4) was used for the rehydration step. At this concentration >98% of the fluorescence is self-quenched (***Figure 1—figure supplement 3***). Resulting multilamellar vesicles were subjected to five freeze-thaw cycles and extruded 11 times through a polycarbonate membrane (Avanti Polar Lipids) with a pore size of 100 nm followed by 11 times through a polycarbonate membrane with a 50 nm pore size 10˚C above transition temperature (i.e. 65˚C for DSPC-based formulations). For functionalization with HBV-derived peptides, nanoparticles were mixed with peptides at molar maleimide-to-cysteine ratio of 1:1 and incubated at RT overnight. To remove non-conjugated peptides and/or free hydrophilic dye, size exclusion chromatography using a Sephadex G50 column (GE Healthcare) eluted with 0.01 M PBS pH 7.4 was performed. The size exclusion chromatography column was coupled to an UV detector to analyze recovery of nanoparticles based on peak areas. Hepatotropic nanoparticles were concentrated to a final lipid concentration of 10 mM using Amicon Ultra-4 centrifugal filter units with a 100 kDa molecular weight cut-off (Millipore). DiI and cholesterol were used as marker lipids to quantify total lipid content. DiI content was quantified based on relative fluorescence signals as compared to liposome standards and in combination with Triton X-100 treatment to account for potential DiI self-quenching. Samples were excited at 561 nm and fluorescence signals were recorded using a Spectramax M2 microplate reader (Molecular Devices). The cholesterol content was determined using the Cholesterol E cholesterol assay kit from Wako following the manufacturer's protocol.

Loading of compounds into hepatotropic nanoparticles

FITC-peptide loading

For passive loading of FITC-Ahx-yKKEEEK into nanoparticles, a 2 mg/mL FITC-peptide solution in a mixture of PBS/DMSO/EtOH at pH 7.0 was used for the rehydration step of the homogenous lipid film. Resulting multilamellar vesicles were processed as described in the Materials and methods section.

Propidium iodide loading

For passive loading of propidium iodide into nanoparticles, a 10 mg/mL propidium iodide solution in PBS was used for the rehydration step of the homogenous lipid film. Resulting multilamellar vesicles were processed as described in the Materials and methods section including a final purification step.

Doxorubicin loading

For loading of doxorubicin, an active drug loading strategy based on a citrate gradient was used as previously described (***Mayer et al., 1990***). The homogenous lipid film was rehydrated using a 300 mM citrate buffer at pH 4.0 and multilamellar vesicles were processed as described in the Materials and methods section. The pH of the external buffer solution was adjusted to pH 7.0 and nanoparticles were incubated with 2 mg/mL doxorubicin at 65˚C for 15 min. Free doxorubicin was removed by size exclusion chromatography.

DNA vector loading

Lipid nanoparticles entrapping DNA were prepared as previously described with modifications (***Kulkarni et al., 2019***; ***Kulkarni et al., 2018***; ***Kulkarni et al., 2017***). Briefly, lipids

(ionizable lipid, cholesterol, DSPC, DSPE-PEG2000, and DSPE-PEG2000-Maleimide at a molar ratio of 50:39:10:0.75:0.25 mol%) were dissolved in ethanol at a total lipid concentration of 15 mM. The DNA vector was dissolved in 25 mM sodium acetate (pH 4.0) at an N/P ratio of 6. After T-junction mixing at a flow rate ratio of 3:1 v/v, the pH was neutralized using a 5x excess of D-PBS, the appropriate amount of Myr-preS2-31 was added, and the resulting suspension was dialyzed against D-PBS to remove residual ethanol.

Physicochemical characterization of hepatotropic nanoparticles

Dynamic light scattering

Size and size distribution (polydispersity index, PDI) of nanoparticles were analyzed using a Delsa Nano C Particle Analyzer (Beckman Coulter) equipped with a 658 nm laser. Samples were measured in D-PBS at RT and a measurement angle of 165˚. Data were converted using the CONTIN particle size distribution analysis (Delsa Nano V3.73/2.30, Beckman Coulter Inc).

Electrophoretic light scattering

Zeta potential of nanoparticles was analyzed using a Delsa Nano C Particle Analyzer. Samples were measured in D-PBS at RT and a measurement angle of 15˚. Data were converted using the Smoluchowski equation (Delsa Nano V3.73/2.30).

Transmission electron microscopy

Size and morphology of nanoparticles were analyzed using transmission electron microscopy (TEM) as described previously (***Witzigmann et al., 2015a***). In brief, samples were deposited on a 400-mesh carbon-coated copper grid, negatively stained with 2% uranylacetate, and analyzed using a CM-100 electron microscope operating at 80 kV (Philips).

Fluorescence correlation spectroscopy

Fluorescence correlation spectroscopy (FCS) analysis of nanoparticles was performed as described previously (***Uhl et al., 2017***). In brief, Atto488, Myr-preS2-48-Atto488 and Myr-preS2-48-Atto488 conjugated nanoparticles were analyzed using an inverted confocal fluorescence laser scanning microscope (Zeiss LSM 510-META/Confocor 2) equipped with a 40 × water immersion objective lens (Zeiss C-Apochromat 40×, numerical aperture 1.2). Fluorescence intensity fluctuations were measured for three independent samples and each measurement was repeated 20–30 times. Autocorrelation functions were fitted using a two-component model and diffusion times were calculated.

Cell culture

Cell lines were purchased from ATCC or other recognized cell depositories (Institute of Pathology, University Hospital of Basel, Switzerland and RIKEN Cell Bank, Ibaraki, Japan) who perform authentication and quality-control tests on all distribution lots of cell lines (***Witzigmann et al., 2016b***). In addition, we performed authentication tests for all cell lines based on morphology check by microscope. All human cell lines were cultured at 37˚C under 5% CO_2 and saturated humidity in Dulbecco's modified Eagle's culture medium high glucose (DMEM, Sigma-Aldrich) supplemented with 10% fetal calf serum (Amimed), penicillin (100 units/mL, Sigma-Aldrich), and streptomycin (100 µg/mL, Sigma-Aldrich). Stable NTCP expressing liver derived cell lines, that is HepG2 *SLC10A1* and HuH7 *SLC10A1*, were created by lentiviral transduction as published previously (***Ni et al., 2014***). For uptake experiments, different cell lines were seeded at a density of 2.5×10^4 cells/cm^2 and allowed to adhere for 24 h. For confocal laser scanning microscopy experiments, cells were grown on poly-D-lysine (Sigma-Aldrich) coated glass cover slips (#1.5, Menzel) or well plates (TPP).

Transfection of cell lines

For transient expression of the transporter, plasmids encoding for mNtcp (*Slc10a1*) or hNTCP (*SLC10A1*) were generated, amplifying the coding sequence from commercially obtained mRNA (Amsbio) by PCR. The following primers were used:

*SLC10A1*_for: 5′-ATGGAGGCCCACAACGCGTCT-3′,
*SLC10A1*_rev 5′-CTAGGCTGTGCAAGGGGA-3′;
*Slc10a1*_for 5′-GTGTTCACTGGGTCGGAGGATG-'3,

*Slc10a1*_rev1 5'-CAGGTCCAGAGCAAATACTCATAGGAG-'3.

Subsequently the amplicons were ligated into pEF6-V5/HIS (Invitrogen), followed by sequence verification (Microsynth). The resulting plasmids *Slc10a1*-pEF6 and *SLC10A1*-pEF6 and Lipofectamine 3000 (Sigma-Aldrich) were used for transfection of human cell lines. A standard transfection protocol was developed as follows: Plasmid DNA and P3000 reagent were diluted in Opti-MEM (Sigma-Aldrich) and rapidly mixed with Lipofectamine 3000 diluted Opti-MEM using a DNA-to-Lipofectamine 3000 w/V ratio of 3. After 5 min incubation, the transfection mix was added to adhered cells at a plasmid DNA concentration of 1 µg/mL. Control cells were either transfected with empty pEF6 vector or treated with Opti-MEM alone.

Assessment of cytocompatibility of nanoparticles

To assess the cytocompatibility of nanoparticles modified with different Myrcludex B derived peptides a MTT cell viability assay was performed. Wild type HeLa cells, liver-derived wild type HepG2 cells and HepG2 *SLC10A1* were seeded and cultured as described above. Nanoparticles were added to cells at final concentrations of 0.25 mM – 8 mM. After 24 h, MTT reagent (Sigma-Aldrich) was added to cells for 4 h. Formazan dye crystals were solubilized for 2 h using a mixture containing 3% (v/v) sodium dodecyl sulfate (Sigma-Aldrich) and 40 mM hydrochloric acid in isopropanol (Sigma-Aldrich). Absorption of reduced MTT and background signals was measured using a Spectramax M2 microplate reader at 570 nm and 670 nm, respectively. Control cells treated with buffer were used to calculate relative cell viability.

Uptake of nanoparticles in vitro

To assess the uptake rate and intracellular localization of nanoparticles, cell lines were incubated with different concentrations of nanoparticles at 37˚C or 4˚C. Nanoparticles were loaded with 5 (6)-carboxyfluorescein (payload) and/or incorporated DiI in their phospholipid-membrane. Myrcludex B derived peptides were fluorescently labeled if necessary as indicated above. At the indicated time points, confocal laser scanning microscopy or flow cytometry were used for qualitative and quantitative analysis, respectively.

Competitive inhibition experiments in vitro

NTCP-specific uptake of nanoparticles was investigated by pre-incubation with 400 nM free Myrcludex B fluorescently labeled with Atto-565 or Atto-488 as indicated.

Binding mechanism studies in vitro

The hepatic cell dependent binding mechanism of nanoparticles was investigated by pre-incubation with 300 µg/mL heparin sulfate.

Uptake mechanism studies on NTCP mediated internalization in vitro

The uptake mechanism of nanoparticles into HepG2 *SLC10A1* cells was investigated using different pharmacological pathway inhibitors as described previously (***Lunov et al., 2011***). Cells were pre-incubated using 100 µg/mL colchicine (micropinocytosis inhibitor), 10 µg/mL chlorpromazine (inhibitor of clathrin-mediated endocytosis), or 25 µg/mL nystatine (inhibitor of caveolin-mediated endocytosis) for 30 min before addition of nanoparticles.

Confocal laser scanning microscopy

At indicated time points, cell nuclei were counterstained for 5 min using 1.0 µg/mL Hoechst 33342 (Sigma-Aldrich), washed with PBS and embedded using ProLong Gold antifading reagent (Invitrogen Life Technologies). For live cell imaging, cell nuclei were counterstained with Hoechst 33342, and if indicated cell membranes were stained with Cell Mask Deep Red Plasma Membrane Stain (1.0 µg/mL, Thermo Fisher Scientific) and NTCP was stained using fluorescently labeled Myrcludex B. Confocal laser scanning microscopy analysis was performed using an Olympus FV-1000 inverted microscope (Olympus Ltd.), equipped with a 60 × PlanApo N oil-immersion objective (numerical aperture 1.40).

Flow cytometry analysis

To quantify the uptake rate of nanoparticles into non-hepatic and hepatic cell lines with different NTCP expression levels, flow cytometry analysis was performed. Cells were detached using 0.25% trypsin/EDTA (Sigma-Aldrich), washed twice with PBS and re-suspended in PBS containing 1% fetal calf serum, 0.05% NaN3, and 2.5 mM EDTA. At least 10,000 cells per setting were analyzed using a FACS Canto II flow cytometer (Becton Dickinson). Doublets were excluded and DiI or CF signals were measured. Relative mean fluorescence intensities (MFI) of DiI or CF signals normalized to untreated cells were calculated using Flow Jo VX software (TreeStar).

High-content screening

To quantify the transfection of HepG2 cells deficient or expressing NTCP using DNA loaded nanoparticles, high-content screening was performed as described previously.(***Lin et al., 2013***) Cells were seeded in 96-well cell culture dishes, were allowed to adhere for 24 h, and treated with lipid nanoparticles at a DNA concentration of 1.5 µg/mL. To assess the transfection efficacy using high-content screening, cells were fixed with 3% paraformaldehyde 24 h post treatment and cell nuclei were counterstained with Hoechst 33342. Plates were scanned and analyzed using a Cellomics ArrayScan VTI (Thermo Scientific).

Zebrafish embryo culture

Zebrafish embryos (*Danio rerio*) are a well-established vertebrate screening model for engineered nanomaterials (***Campbell et al., 2018***; ***Einfalt et al., 2018***; ***Sieber et al., 2017***). They were maintained in accordance with Swiss animal welfare regulations as described previously (***Sieber et al., 2017***). In brief, eggs from wild type ABC/TU and transgenic kdrl:EGFPs843 adult zebrafish were maintained in media at 28˚C. Formation of pigment cells was prevented by 1-phenyl 2-thiourea (PTU, Sigma-Aldrich).

Injection of nanoparticles into zebrafish embryos

To assess the systemic circulation of nanoparticles, samples were injected into transgenic kdrl:EGFPs843 zebrafish embryos (two dpf) as described previously (***Sieber et al., 2017***). In brief, calibrated volumes of 1 nL were injected into the duct of Cuvier of anesthetized and agarose-embedded zebrafish embryos using a micromanipulator (Wagner Instrumentenbau KG), a pneumatic Pico Pump PV830 (WPI), and a Leica S8APO microscope (Leica). The tail region of zebrafish embryos was imaged 1 h post injection (hpi) using an Olympus FV-1000 inverted confocal laser scanning microscope equipped with a 20 × UPlanSApo (numerical aperture 0.75) objective.

Targeting of xenotransplanted human cells in the zebrafish model

Human HEK293 cells deficient or overexpressing *SLC10A1* were detached from 6-well cell culture dishes using 1 mL pre-warmed DMEM, washed (5 min at 200 g) and resuspended in 10 µL DMEM. Human cells (3 nL) were injected into the duct of Cuvier of ABC/TU zebrafish embryos. As soon as transgenic human cells stopped circulating and remained in the caudal vasculature tail region (after approximately two hpi), nanoparticles (1 nL) were injected as described above. Brightfield and fluorescence images of the tail region were taken 1 hpi of nanoparticles.

Colocalization analysis. Binding of nanoparticles to HEK293 cells was analyzed using the JaCoP plug-in Fiji. Therefore, Pearson´s Correlation Coefficient (PCC) was determined to assess the extent of colocalization (***Bolte and Cordelières, 2006***).

Radioactive labeling of nanoparticles with ^{111}In

Labeling of nanoparticles with ^{111}In was performed with modifications as described previously (***van der Geest et al., 2015***). Nanoparticles were prepared as described above in PBS at a total lipid concentration of 60 mM (including 3 mol% DSPE-DTPA). Size exclusion chromatography was used to exchange the buffer system to citrate buffered saline pH 5.4, fractions were pooled and finally concentrated using Amicon Ultra-4 centrifugal filter units (100 kDa size exclusion). Nanoparticles (30 µmol) were incubated with 40 µl of $^{111}InCl_3$ (Mallinckrodt Pharmaceuticals) at 37˚C for 45 min using a thermocycler. After incubation, ^{111}In labeled nanoparticles were purified using NAP-5

columns (GE Healthcare) by elution with sterile saline (B. Braun Medical Inc). Fractions of 250 µL were collected and activity of each fraction was determined.

Planar imaging of mice in vivo

All mice experiments were carried out in accordance with German legislation on animal welfare. Female NMRI mice (6–8 weeks) were obtained from Janvier Laboratories. For planar imaging, mice were anesthetized with Isoflurane (Baxter) and ^{111}In labeled nanoparticles with a total activity of 8–10 MBq (corresponding to 100 µL) were intravenously injected into the tail vein. Afterwards, the animals were placed in prone position (see ***Figure 5—figure supplements 2A*** and ***3A***) on a planar gamma-imager (Biospace) equipped with a high energy collimator as described previously (***Müller et al., 2013***; ***Wischnjow et al., 2016***). Images were recorded at the indicated time points with 10 min acquisition time.

Planar imaging of harvested organs from mice and rats ex vivo

For planar imaging of organs, animals were anesthetized with Isoflurane (Baxter) and ^{111}In labeled nanoparticles were intravenously injected into the tail vein. Animals were sacrificed 15 min or 1 h post injection, organs were harvested and placed on a planar gamma-imager (Biospace) equipped with a high energy collimator. Images were recorded at the indicated time points with 10 min acquisition time.

Quantitative organ biodistribution of nanoparticles in mice ex vivo

For biodistribution studies, ^{111}In labeled nanoparticles with a total activity of 1–2 MBq (corresponding to 100 µL) were intravenously injected into the tail vein of wild type mice. Animals were sacrificed (n = 3 per nanoparticle administration) 1 h post injection, organs were harvested and the radioactivity in each organ was measured with a Berthold LB 951G gamma counter. Each organ-associated activity was related to the injected dose. The percentage of injected dose (%ID) per organ was calculated using standard values for organ weights (***Mühlfeld et al., 2003***).

Fluorescence imaging of nanoparticles in tissue cryo-sections

Nanoparticles incorporating 1 mol% DiI were intravenously injected into the tail vein of wildtype mice. Animals were sacrificed 1 h post injection and organs were snap-frozen in liquid nitrogen. Cryo-sections of 16 µm were mounted on Superfrost Plus Ultra microscope slides (Thermo Fisher Scientific) and counterstained with Hoechst 33342 (2 µg/mL). Slides were embedded in Prolong Gold Antifade Mountant (Thermo Fisher Scientific), sealed with nail polisher and analyzed using an Olympus FV-1000 inverted confocal laser scanning microscope equipped with a 40x UPlanFL N oil-immersion objective (numerical aperture 1.30).

Immunohistochemistry of targeting ligand in tissue sections

After intravenous tail vein injection of nanoparticles, the mice were euthanized, organs were harvested, rinsed with PBS and immediately placed in a 4% formaldehyde solution in PBS. After fixation for 24 h, organs were dehydrated and embedded in paraffin. Sections of 5 µm thicknesses were cut using a microtome MICROM HM 355, placed onto a microscope slide and dried at 37˚C. After dewaxing and rehydration, epitope retrieval was performed. The primary antibody against Myr-preS2-31 (MA18/7, kind gift from Wolfram Gerlich) was added overnight at 4˚C, before incubation with the secondary antibody. Finally, slides were counterstained with hemalum (Merck KGaA) for 10 min, blued with tap water and mounted using Aquatex (Merck Millipore).

Immunofluorescence imaging of liver cryo-sections

Animals were sacrificed 3 h post injection of nanoparticles and liver cryo-sections (16 µm) were prepared as described above. Slides were stained using primary antibodies against Myr-preS2-31 (MA18/7, 1:100 dilution) and *Slc10a1* (provided by Prof. Bruno Stieger, University Zürich, 1:100 dilution). Finally, cell nuclei were counterstained with Hoechst 33342 (2 µg/mL) and analyzed by confocal microscopy as described above.

Statistical analysis

Statistical analysis for all experiments was performed by one-way analysis of variance (ANOVA) followed by Bonferroni post-hoc test using OriginPro 9.1 software (OriginLab Corporation). Differences between groups were considered to be statistically significant at the indicated p-values.

Acknowledgements

We thank M Affolter, HG Belting and N Schellinx for providing zebrafish eggs, K Leotta for support with mice experiments, S Meßnard for sectioning of paraffin-embedded tissue, P Scheiffele and L Burklé for support with cryo-sectioning, and H Heerklotz and D Eckhardt for DSC and PPC measurements.

Additional information

Funding

Funder	Grant reference number	Author
Swiss National Science Foundation	174975	Dominik Witzigmann
Swiss National Science Foundation	173057	Jonas Buck Jörg Huwyler
Deutsche Forschungsgemeinschaft	209091148	Stephan Urban
German Center for Infection Research	5.704	Stephan Urban
German Center for Infection Research	5.807	Stephan Urban
Freiwillige Akademische Gesellschaft	FAG Basel	Dominik Witzigmann Sandro Sieber Jörg Huwyler
Stiftung zur Förderung des pharmazeutischen Nachwuchses in Basel		Sandro Sieber
University of Basel	Novartis University Basel Excellence Scholarship for Life Sciences	Dominik Witzigmann
Novartis	Novartis University Basel Excellence Scholarship for Life Sciences	Dominik Witzigmann

The funders had no role in study design, data collection and interpretation, or the decision to submit the work for publication.

Author contributions

Dominik Witzigmann, Conceptualization, Resources, Formal analysis, Supervision, Funding acquisition, Validation, Visualization, Methodology, Writing—original draft, Project administration, Writing—review and editing; Philipp Uhl, Conceptualization, Formal analysis, Supervision, Funding acquisition, Validation, Investigation, Visualization, Methodology, Writing—original draft, Project administration, Writing—review and editing, Design and aquisition of rodent experiments; Sandro Sieber, Conceptualization, Formal analysis, Investigation, Methodology, Writing—review and editing, Design and aquisition of zebrafish experiments; Christina Kaufman, Conceptualization, Formal analysis, Investigation, Methodology, Writing—review and editing, Conception and design of HBV derived peptides and aquisition of rodent experiments; Tomaz Einfalt, Conceptualization, Formal analysis, Investigation, Methodology, Writing—original draft, Writing—review and editing, Physicochemical nanocarrier characterisation; Katrin Schöneweis, Formal analysis, Investigation, Methodology, Writing—original draft, Acquisition of tissue staining, Analysis and interpretation of

data; Philip Grossen, Formal analysis, Investigation, Methodology, Writing—original draft, Conception and design of nanocarrier; Jonas Buck, Investigation, Methodology, Writing—original draft, Acquisition of uptake mechanism studies; Yi Ni, Conceptualization, Resources, Methodology, Conception and design of NTC expressing cell lines; Susanne H Schenk, Conceptualization, Resources, Investigation, Methodology, Writing—original draft, Writing—review and editing, Design of DNA vectors; Janine Hussner, Resources, Formal analysis, Methodology, Contributed unpublished essential data; Henriette E Meyer zu Schwabedissen, Conceptualization, Methodology, Writing—review and editing, Design of NTCP encoding DNA vectors; Gabriela Québatte, Conceptualization, Investigation, Contributed unpublished essential data; Walter Mier, Stephan Urban, Conceptualization, Resources, Formal analysis, Funding acquisition, Writing—review and editing; Jörg Huwyler, Conceptualization, Resources, Formal analysis, Funding acquisition, Writing—original draft, Project administration, Writing—review and editing

Author ORCIDs
Dominik Witzigmann https://orcid.org/0000-0002-8197-8558
Philip Grossen http://orcid.org/0000-0002-3416-5570
Henriette E Meyer zu Schwabedissen http://orcid.org/0000-0003-0458-4579
Jörg Huwyler https://orcid.org/0000-0003-1748-5676

Ethics
Animal experimentation: Animal experimentation: Zebrafish embryo (*Danio rerio*) studies were performed in strict accordance with Swiss animal welfare regulations. Mouse and rat experiments were carried out in accordance with German legislation on animal welfare. All of the animals were handled according to approved institutional animal care and use protocol of the University of Basel and University of Heidelberg.

Decision letter and Author response
Decision letter https://doi.org/10.7554/eLife.42276.041
Author response https://doi.org/10.7554/eLife.42276.042

Additional files
Supplementary files
• Transparent reporting form
DOI: https://doi.org/10.7554/eLife.42276.039

Data availability
All data generated or analysed during this study are included in the manuscript and supporting files. Numerical data for all quantitative graphs are provided in the Figure source data.

References
Akinc A, Goldberg M, Qin J, Dorkin JR, Gamba-Vitalo C, Maier M, Jayaprakash KN, Jayaraman M, Rajeev KG, Manoharan M, Koteliansky V, Röhl I, Leshchiner ES, Langer R, Anderson DG. 2009. Development of lipidoid-siRNA formulations for systemic delivery to the liver. *Molecular Therapy* **17**:872–879. DOI: https://doi.org/10.1038/mt.2009.36, PMID: 19259063

Akinc A, Querbes W, De S, Qin J, Frank-Kamenetsky M, Jayaprakash KN, Jayaraman M, Rajeev KG, Cantley WL, Dorkin JR, Butler JS, Qin L, Racie T, Sprague A, Fava E, Zeigerer A, Hope MJ, Zerial M, Sah DW, Fitzgerald K, et al. 2010. Targeted delivery of RNAi therapeutics with endogenous and exogenous ligand-based mechanisms. *Molecular Therapy* **18**:1357–1364. DOI: https://doi.org/10.1038/mt.2010.85, PMID: 20461061

Asabe S, Wieland SF, Chattopadhyay PK, Roederer M, Engle RE, Purcell RH, Chisari FV. 2009. The size of the viral inoculum contributes to the outcome of hepatitis B virus infection. *Journal of Virology* **83**:9652–9662. DOI: https://doi.org/10.1128/JVI.00867-09, PMID: 19625407

Barenholz Y. 2012. Doxil–the first FDA-approved nano-drug: lessons learned. *Journal of Controlled Release* **160**: 117–134. DOI: https://doi.org/10.1016/j.jconrel.2012.03.020, PMID: 22484195

Barpe DR, Rosa DD, Froehlich PE. 2010. Pharmacokinetic evaluation of doxorubicin plasma levels in normal and overweight patients with breast Cancer and simulation of dose adjustment by different indexes of body mass.

European Journal of Pharmaceutical Sciences **41**:458–463. DOI: https://doi.org/10.1016/j.ejps.2010.07.015, PMID: 20688160

Barrett SE, Burke RS, Abrams MT, Bason C, Busuek M, Carlini E, Carr BA, Crocker LS, Fan H, Garbaccio RM, Guidry EN, Heo JH, Howell BJ, Kemp EA, Kowtoniuk RA, Latham AH, Leone AM, Lyman M, Parmar RG, Patel M, et al. 2014. Development of a liver-targeted siRNA delivery platform with a broad therapeutic window utilizing biodegradable polypeptide-based polymer conjugates. *Journal of Controlled Release* **183**:124–137. DOI: https://doi.org/10.1016/j.jconrel.2014.03.028, PMID: 24657948

Blank A, Markert C, Hohmann N, Carls A, Mikus G, Lehr T, Alexandrov A, Haag M, Schwab M, Urban S, Haefeli WE. 2016. First-in-human application of the novel hepatitis B and hepatitis D virus entry inhibitor myrcludex B. *Journal of Hepatology* **65**:483–489. DOI: https://doi.org/10.1016/j.jhep.2016.04.013, PMID: 27132172

Bogomolov P, Alexandrov A, Voronkova N, Macievich M, Kokina K, Petrachenkova M, Lehr T, Lempp FA, Wedemeyer H, Haag M, Schwab M, Haefeli WE, Blank A, Urban S. 2016. Treatment of chronic hepatitis D with the entry inhibitor myrcludex B: first results of a phase ib/IIa study. *Journal of Hepatology* **65**:490–498. DOI: https://doi.org/10.1016/j.jhep.2016.04.016, PMID: 27132170

Bolte S, Cordelières FP. 2006. A guided tour into subcellular colocalization analysis in light microscopy. *Journal of Microscopy* **224**:213–232. DOI: https://doi.org/10.1111/j.1365-2818.2006.01706.x, PMID: 17210054

Braet F, Wisse E. 2002. Structural and functional aspects of liver sinusoidal endothelial cell fenestrae: a review. *Comparative Hepatology* **1**. PMID: 12437787

Brown HK, Schiavone K, Tazzyman S, Heymann D, Chico TJ. 2017. Zebrafish xenograft models of Cancer and metastasis for drug discovery. *Expert Opinion on Drug Discovery* **12**:379–389. DOI: https://doi.org/10.1080/17460441.2017.1297416, PMID: 28277839

Campbell F, Bos FL, Sieber S, Arias-Alpizar G, Koch BE, Huwyler J, Kros A, Bussmann J. 2018. Directing nanoparticle biodistribution through evasion and exploitation of Stab2-Dependent nanoparticle uptake. *ACS Nano* **12**:2138–2150. DOI: https://doi.org/10.1021/acsnano.7b06995, PMID: 29320626

Chen RF, Knutson JR. 1988. Mechanism of fluorescence concentration quenching of carboxyfluorescein in liposomes: energy transfer to nonfluorescent dimers. *Analytical Biochemistry* **172**:61–77. DOI: https://doi.org/10.1016/0003-2697(88)90412-5, PMID: 3189776

Detampel P, Witzigmann D, Krähenbühl S, Huwyler J. 2014. Hepatocyte targeting using pegylated asialofetuin-conjugated liposomes. *Journal of Drug Targeting* **22**:232–241. DOI: https://doi.org/10.3109/1061186X.2013.860982, PMID: 24328572

Einfalt T, Witzigmann D, Edlinger C, Sieber S, Goers R, Najer A, Spulber M, Onaca-Fischer O, Huwyler J, Palivan CG. 2018. Biomimetic artificial organelles with in vitro and in vivo activity triggered by reduction in microenvironment. *Nature Communications* **9**:1127. DOI: https://doi.org/10.1038/s41467-018-03560-x, PMID: 29555899

Evensen L, Johansen PL, Koster G, Zhu K, Herfindal L, Speth M, Fenaroli F, Hildahl J, Bagherifam S, Tulotta C, Prasmickaite L, Mælandsmo GM, Snaar-Jagalska E, Griffiths G. 2016. Zebrafish as a model system for characterization of nanoparticles against Cancer. *Nanoscale* **8**:862–877. DOI: https://doi.org/10.1039/C5NR07289A, PMID: 26648525

Glebe D, Urban S. 2007. Viral and cellular determinants involved in hepadnaviral entry. *World Journal of Gastroenterology* **13**:22–38. DOI: https://doi.org/10.3748/wjg.v13.i1.22, PMID: 17206752

Harrington KJ, Rowlinson-Busza G, Syrigos KN, Uster PS, Abra RM, Stewart JS. 2000. Biodistribution and pharmacokinetics of 111In-DTPA-labelled pegylated liposomes in a human tumour xenograft model: implications for novel targeting strategies. *British Journal of Cancer* **83**:232–238. DOI: https://doi.org/10.1054/bjoc.1999.1232, PMID: 10901376

He S, Lamers GE, Beenakker JW, Cui C, Ghotra VP, Danen EH, Meijer AH, Spaink HP, Snaar-Jagalska BE. 2012. Neutrophil-mediated experimental metastasis is enhanced by VEGFR inhibition in a zebrafish xenograft model. *The Journal of Pathology* **227**:431–445. DOI: https://doi.org/10.1002/path.4013, PMID: 22374800

Ishiwata H, Suzuki N, Ando S, Kikuchi H, Kitagawa T. 2000. Characteristics and biodistribution of cationic liposomes and their DNA complexes. *Journal of Controlled Release* **69**:139–148. DOI: https://doi.org/10.1016/S0168-3659(00)00293-5, PMID: 11018552

Karmali PP, Simberg D. 2011. Interactions of nanoparticles with plasma proteins: implication on clearance and toxicity of drug delivery systems. *Expert Opinion on Drug Delivery* **8**:343–357. DOI: https://doi.org/10.1517/17425247.2011.554818, PMID: 21291354

Kettiger H, Schipanski A, Wick P, Huwyler J. 2013. Engineered nanomaterial uptake and tissue distribution: from cell to organism. *International Journal of Nanomedicine* **8**:3255–3269. DOI: https://doi.org/10.2147/IJN.S49770, PMID: 24023514

Kulkarni JA, Myhre JL, Chen S, Tam YYC, Danescu A, Richman JM, Cullis PR. 2017. Design of lipid nanoparticles for in vitro and in vivo delivery of plasmid DNA. *Nanomedicine: Nanotechnology, Biology and Medicine* **13**:1377–1387. DOI: https://doi.org/10.1016/j.nano.2016.12.014

Kulkarni JA, Darjuan MM, Mercer JE, Chen S, van der Meel R, Thewalt JL, Tam YYC, Cullis PR. 2018. On the formation and morphology of lipid nanoparticles containing ionizable cationic lipids and siRNA. *ACS Nano* **12**:4787–4795. DOI: https://doi.org/10.1021/acsnano.8b01516, PMID: 29614232

Kulkarni JA, Witzigmann D, Leung J, van der Meel R, Zaifman J, Darjuan MM, Grisch-Chan HM, Thöny B, Tam YYC, Cullis PR. 2019. Fusion-dependent formation of lipid nanoparticles containing macromolecular payloads. *Nanoscale* **11**:9023–9031. DOI: https://doi.org/10.1039/C9NR02004G, PMID: 31021343

Lempp FA, Mutz P, Lipps C, Wirth D, Bartenschlager R, Urban S. 2016. Evidence that hepatitis B virus replication in mouse cells is limited by the lack of a host cell dependency factor. *Journal of Hepatology* **64**:556–564. DOI: https://doi.org/10.1016/j.jhep.2015.10.030, PMID: 26576481

Lin PJ, Tam YY, Hafez I, Sandhu A, Chen S, Ciufolini MA, Nabi IR, Cullis PR. 2013. Influence of cationic lipid composition on uptake and intracellular processing of lipid nanoparticle formulations of siRNA. *Nanomedicine: Nanotechnology, Biology and Medicine* **9**:233–246. DOI: https://doi.org/10.1016/j.nano.2012.05.019, PMID: 22698807

Lin G, Manghnani PN, Mao D, Teh C, Li Y, Zhao Z, Liu B, Tang BZ. 2017. Robust red organic nanoparticles for in vivo fluorescence imaging of Cancer cell progression in xenografted zebrafish. *Advanced Functional Materials* **27**:1701418. DOI: https://doi.org/10.1002/adfm.201701418

Liu Q, Somiya M, Kuroda S. 2016. Elucidation of the early infection machinery of hepatitis B virus by using bio-nanocapsule. *World Journal of Gastroenterology* **22**:8489–8496. DOI: https://doi.org/10.3748/wjg.v22.i38.8489, PMID: 27784961

Lunov O, Syrovets T, Loos C, Beil J, Delacher M, Tron K, Nienhaus GU, Musyanovych A, Mailänder V, Landfester K, Simmet T. 2011. Differential uptake of functionalized polystyrene nanoparticles by human macrophages and a monocytic cell line. *ACS Nano* **5**:1657–1669. DOI: https://doi.org/10.1021/nn2000756, PMID: 21344890

Lütgehetmann M, Mancke LV, Volz T, Helbig M, Allweiss L, Bornscheuer T, Pollok JM, Lohse AW, Petersen J, Urban S, Dandri M. 2012. Humanized chimeric uPA mouse model for the study of hepatitis B and D virus interactions and preclinical drug evaluation. *Hepatology* **55**:685–694. DOI: https://doi.org/10.1002/hep.24758, PMID: 22031488

Maurer N, Fenske DB, Cullis PR. 2001. Developments in liposomal drug delivery systems. *Expert Opinion on Biological Therapy* **1**:923–947. DOI: https://doi.org/10.1517/14712598.1.6.923, PMID: 11728226

Mayer LD, Tai LCL, Bally MB, Mitilenes GN, Ginsberg RS, Cullis PR. 1990. Characterization of liposomal systems containing doxorubicin entrapped in response to pH gradients. *Biochimica Et Biophysica Acta (BBA) - Biomembranes* **1025**:143–151. DOI: https://doi.org/10.1016/0005-2736(90)90091-2

Meier A, Mehrle S, Weiss TS, Mier W, Urban S. 2013. Myristoylated PreS1-domain of the hepatitis B virus L-protein mediates specific binding to differentiated hepatocytes. *Hepatology* **58**:31–42. DOI: https://doi.org/10.1002/hep.26181, PMID: 23213046

Milla P, Dosio F, Cattel L. 2012. PEGylation of proteins and liposomes: a powerful and flexible strategy to improve the drug delivery. *Current Drug Metabolism* **13**:105–119. DOI: https://doi.org/10.2174/138920012798356934, PMID: 21892917

Mühlfeld AS, Segerer S, Hudkins K, Carling MD, Wen M, Farr AG, Ravetch JV, Alpers CE. 2003. Deletion of the fcgamma receptor IIb in thymic stromal lymphopoietin transgenic mice aggravates membranoproliferative glomerulonephritis. *The American Journal of Pathology* **163**:1127–1136. DOI: https://doi.org/10.1016/S0002-9440(10)63472-4, PMID: 12937154

Müller T, Mehrle S, Schieck A, Haberkorn U, Urban S, Mier W. 2013. Liver imaging with a novel hepatitis B surface protein derived SPECT-tracer. *Molecular Pharmaceutics* **10**:2230–2236. DOI: https://doi.org/10.1021/mp400038r, PMID: 23601010

Ni Y, Lempp FA, Mehrle S, Nkongolo S, Kaufman C, Fälth M, Stindt J, Königer C, Nassal M, Kubitz R, Sültmann H, Urban S. 2014. Hepatitis B and D viruses exploit sodium taurocholate co-transporting polypeptide for species-specific entry into hepatocytes. *Gastroenterology* **146**:1070–1083. DOI: https://doi.org/10.1053/j.gastro.2013.12.024, PMID: 24361467

Park K. 2017. Cover story: zebrafish as a screening tool for the systemic circulation of nanoparticles. *Journal of Controlled Release* **264**:342. DOI: https://doi.org/10.1016/j.jconrel.2017.09.037, PMID: 28987218

Petersen J, Dandri M, Mier W, Lütgehetmann M, Volz T, von Weizsäcker F, Haberkorn U, Fischer L, Pollok JM, Erbes B, Seitz S, Urban S. 2008. Prevention of hepatitis B virus infection in vivo by entry inhibitors derived from the large envelope protein. *Nature Biotechnology* **26**:335–341. DOI: https://doi.org/10.1038/nbt1389, PMID: 18297057

Poelstra K, Prakash J, Beljaars L. 2012. Drug targeting to the diseased liver. *Journal of Controlled Release* **161**:188–197. DOI: https://doi.org/10.1016/j.jconrel.2012.02.011, PMID: 22370583

Reddy LH, Couvreur P. 2011. Nanotechnology for therapy and imaging of liver diseases. *Journal of Hepatology* **55**:1461–1466. DOI: https://doi.org/10.1016/j.jhep.2011.05.039, PMID: 21801699

Rothkopf C, Fahr A, Fricker G, Scherphof GL, Kamps JAAM. 2005. Uptake of phosphatidylserine-containing liposomes by liver sinusoidal endothelial cells in the serum-free perfused rat liver. *Biochimica Et Biophysica Acta (BBA) - Biomembranes* **1668**:10–16. DOI: https://doi.org/10.1016/j.bbamem.2004.10.013

Sahay G, Querbes W, Alabi C, Eltoukhy A, Sarkar S, Zurenko C, Karagiannis E, Love K, Chen D, Zoncu R, Buganim Y, Schroeder A, Langer R, Anderson DG. 2013. Efficiency of siRNA delivery by lipid nanoparticles is limited by endocytic recycling. *Nature Biotechnology* **31**:653–658. DOI: https://doi.org/10.1038/nbt.2614, PMID: 23792629

Sauer I, Nikolenko H, Keller S, Abu Ajaj K, Bienert M, Dathe M. 2006. Dipalmitoylation of a cellular uptake-mediating apolipoprotein E-derived peptide as a promising modification for stable anchorage in liposomal drug carriers. *Biochimica Et Biophysica Acta (BBA) - Biomembranes* **1758**:552–561. DOI: https://doi.org/10.1016/j.bbamem.2006.03.017

Schieck A, Müller T, Schulze A, Haberkorn U, Urban S, Mier W. 2010. Solid-phase synthesis of the lipopeptide Myr-HBVpreS/2-78, a hepatitis B virus entry inhibitor. *Molecules* **15**:4773–4783. DOI: https://doi.org/10.3390/molecules15074773, PMID: 20657392

Schieck A, Schulze A, Gähler C, Müller T, Haberkorn U, Alexandrov A, Urban S, Mier W. 2013. Hepatitis B virus hepatotropism is mediated by specific receptor recognition in the liver and not restricted to susceptible hosts. *Hepatology* **58**:43–53. DOI: https://doi.org/10.1002/hep.26211, PMID: 23292963

Schulze A, Schieck A, Ni Y, Mier W, Urban S. 2010. Fine mapping of pre-S sequence requirements for hepatitis B virus large envelope protein-mediated receptor interaction. *Journal of Virology* **84**:1989–2000. DOI: https://doi.org/10.1128/JVI.01902-09, PMID: 20007265

Shan D, Li J, Cai P, Prasad P, Liu F, Rauth AM, Wu XY. 2015. RGD-conjugated solid lipid nanoparticles inhibit adhesion and invasion of αvβ3 integrin-overexpressing breast cancer cells. *Drug Delivery and Translational Research* **5**:15–26. DOI: https://doi.org/10.1007/s13346-014-0210-2, PMID: 25787336

Shih BB, Chang YF, Cheng CC, Yang HJ, Chang KW, Ho AS, Lin HC, Yeh C, Chang CC. 2017. SPECT imaging evaluation of ^{111}indium-chelated cetuximab for diagnosing EGFR-positive tumor in an HCT-15-induced colorectal xenograft. *Journal of the Chinese Medical Association* **80**:766–773. DOI: https://doi.org/10.1016/j.jcma.2017.02.010, PMID: 28969991

Sieber S, Grossen P, Detampel P, Siegfried S, Witzigmann D, Huwyler J. 2017. Zebrafish as an early stage screening tool to study the systemic circulation of nanoparticulate drug delivery systems in vivo. *Journal of Controlled Release* **264**:180–191. DOI: https://doi.org/10.1016/j.jconrel.2017.08.023, PMID: 28851572

Sieber S, Grossen P, Bussmann J, Campbell F, Kros A, Witzigmann D, Huwyler J. 2019a. Zebrafish as a preclinical in vivo screening model for nanomedicines. *Advanced Drug Delivery Reviews*. DOI: https://doi.org/10.1016/j.addr.2019.01.001, PMID: 30615917

Sieber S, Grossen P, Uhl P, Detampel P, Mier W, Witzigmann D, Huwyler J. 2019b. Zebrafish as a predictive screening model to assess macrophage clearance of liposomes in vivo. *Nanomedicine: Nanotechnology, Biology and Medicine* **17**:82–93. DOI: https://doi.org/10.1016/j.nano.2018.11.017, PMID: 30659929

Somiya M, Sasaki Y, Matsuzaki T, Liu Q, Iijima M, Yoshimoto N, Niimi T, Maturana AD, Kuroda S. 2015. Intracellular trafficking of bio-nanocapsule-liposome complex: identification of fusogenic activity in the pre-S1 region of hepatitis B virus surface antigen L protein. *Journal of Controlled Release* **212**:10–18. DOI: https://doi.org/10.1016/j.jconrel.2015.06.012, PMID: 26074149

Somiya M, Liu Q, Yoshimoto N, Iijima M, Tatematsu K, Nakai T, Okajima T, Kuroki K, Ueda K, Kuroda S. 2016. Cellular uptake of hepatitis B virus envelope L particles is independent of sodium taurocholate cotransporting polypeptide, but dependent on heparan sulfate proteoglycan. *Virology* **497**:23–32. DOI: https://doi.org/10.1016/j.virol.2016.06.024, PMID: 27420796

Steffan AM, Gendrault JL, Kirn A. 1987. Increase in the number of fenestrae in mouse endothelial liver cells by altering the cytoskeleton with cytochalasin B. *Hepatology* **7**:1230–1238. DOI: https://doi.org/10.1002/hep.1840070610, PMID: 3679088

Uhl P, Pantze S, Storck P, Parmentier J, Witzigmann D, Hofhaus G, Huwyler J, Mier W, Fricker G. 2017. Oral delivery of vancomycin by tetraether lipid liposomes. *European Journal of Pharmaceutical Sciences* **108**:111–118. DOI: https://doi.org/10.1016/j.ejps.2017.07.013, PMID: 28716758

Urban S, Bartenschlager R, Kubitz R, Zoulim F. 2014. Strategies to inhibit entry of HBV and HDV into hepatocytes. *Gastroenterology* **147**:48–64. DOI: https://doi.org/10.1053/j.gastro.2014.04.030, PMID: 24768844

van der Geest T, Laverman P, Gerrits D, Franssen GM, Metselaar JM, Storm G, Boerman OC. 2015. Comparison of three remote radiolabelling methods for long-circulating liposomes. *Journal of Controlled Release* **220**:239–244. DOI: https://doi.org/10.1016/j.jconrel.2015.10.043, PMID: 26514291

Veinotte CJ, Dellaire G, Berman JN. 2014. Hooking the big one: the potential of zebrafish xenotransplantation to reform Cancer drug screening in the genomic era. *Disease Models & Mechanisms* **7**:745–754. DOI: https://doi.org/10.1242/dmm.015784, PMID: 24973744

Verrier ER, Colpitts CC, Bach C, Heydmann L, Weiss A, Renaud M, Durand SC, Habersetzer F, Durantel D, Abou-Jaoudé G, López Ledesma MM, Felmlee DJ, Soumillon M, Croonenborghs T, Pochet N, Nassal M, Schuster C, Brino L, Sureau C, Zeisel MB, et al. 2016. A targeted functional RNA interference screen uncovers glypican 5 as an entry factor for hepatitis B and D viruses. *Hepatology* **63**:35–48. DOI: https://doi.org/10.1002/hep.28013, PMID: 26224662

Wagner DS, Delk NA, Lukianova-Hleb EY, Hafner JH, Farach-Carson MC, Lapotko DO. 2010. The in vivo performance of plasmonic nanobubbles as cell theranostic agents in zebrafish hosting prostate Cancer xenografts. *Biomaterials* **31**:7567–7574. DOI: https://doi.org/10.1016/j.biomaterials.2010.06.031, PMID: 20630586

Webb MS, Saxon D, Wong FMP, Lim HJ, Wang Z, Bally MB, Choi LSL, Cullis PR, Mayer LD. 1998. Comparison of different hydrophobic anchors conjugated to poly(ethylene glycol): effects on the pharmacokinetics of liposomal vincristine. *Biochimica Et Biophysica Acta (BBA) - Biomembranes* **1372**:272–282. DOI: https://doi.org/10.1016/S0005-2736(98)00077-7

Wertman J, Veinotte CJ, Dellaire G, Berman JN. 2016. The zebrafish xenograft platform: evolution of a novel Cancer model and preclinical screening tool. *Advances in Experimental Medicine and Biology* **916**:289–314. DOI: https://doi.org/10.1007/978-3-319-30654-4_13, PMID: 27165359

Williams R, Aspinall R, Bellis M, Camps-Walsh G, Cramp M, Dhawan A, Ferguson J, Forton D, Foster G, Gilmore SI, Hickman M, Hudson M, Kelly D, Langford A, Lombard M, Longworth L, Martin N, Moriarty K, Newsome P, O'Grady J, et al. 2014. Addressing liver disease in the UK: a blueprint for attaining excellence in health care and reducing premature mortality from lifestyle issues of excess consumption of alcohol, obesity, and viral hepatitis. *The Lancet* **384**:1953–1997. DOI: https://doi.org/10.1016/S0140-6736(14)61838-9

Wischnjow A, Sarko D, Janzer M, Kaufman C, Beijer B, Brings S, Haberkorn U, Larbig G, Kübelbeck A, Mier W. 2016. Renal targeting: peptide-based drug delivery to proximal tubule cells. *Bioconjugate Chemistry* **27**:1050–1057. DOI: https://doi.org/10.1021/acs.bioconjchem.6b00057, PMID: 26999755

Wisse E, Jacobs F, Topal B, Frederik P, De Geest B. 2008. The size of endothelial fenestrae in human liver sinusoids: implications for hepatocyte-directed gene transfer. *Gene Therapy* **15**:1193–1199. DOI: https://doi.org/10.1038/gt.2008.60, PMID: 18401434

Witzigmann D, Sieber S, Porta F, Grossen P, Bieri A, Strelnikova N, Pfohl T, Prescianotto-Baschong C, Huwyler J. 2015a. Formation of lipid and polymer based gold nanohybrids using a nanoreactor approach. *RSC Advances* **5**:74320–74328. DOI: https://doi.org/10.1039/C5RA13967H

Witzigmann D, Wu D, Schenk SH, Balasubramanian V, Meier W, Huwyler J. 2015b. Biocompatible polymer-Peptide hybrid-based DNA nanoparticles for gene delivery. *ACS Applied Materials & Interfaces* **7**:10446–10456. DOI: https://doi.org/10.1021/acsami.5b01684, PMID: 25907363

Witzigmann D, Detampel P, Porta F, Huwyler J. 2016a. Isolation of multiantennary N-glycans from glycoproteins for hepatocyte specific targeting via the asialoglycoprotein receptor. *RSC Advances* **6**:97636–97640. DOI: https://doi.org/10.1039/C6RA18297F

Witzigmann D, Quagliata L, Schenk SH, Quintavalle C, Terracciano LM, Huwyler J. 2016b. Variable asialoglycoprotein receptor 1 expression in liver disease: implications for therapeutic intervention. *Hepatology Research* **46**:686–696. DOI: https://doi.org/10.1111/hepr.12599, PMID: 26422581

Xiao K, Li Y, Luo J, Lee JS, Xiao W, Gonik AM, Agarwal RG, Lam KS. 2011. The effect of surface charge on in vivo biodistribution of PEG-oligocholic acid based micellar nanoparticles. *Biomaterials* **32**:3435–3446. DOI: https://doi.org/10.1016/j.biomaterials.2011.01.021, PMID: 21295849

Yan H, Zhong G, Xu G, He W, Jing Z, Gao Z, Huang Y, Qi Y, Peng B, Wang H, Fu L, Song M, Chen P, Gao W, Ren B, Sun Y, Cai T, Feng X, Sui J, Li W. 2012. Sodium taurocholate cotransporting polypeptide is a functional receptor for human hepatitis B and D virus. *eLife* **1**:e00049. DOI: https://doi.org/10.7554/eLife.00049, PMID: 23150796

Yin B, Li KHK, Ho LWC, Chan CKW, Choi CHJ. 2018. Toward understanding in vivo sequestration of nanoparticles at the molecular level. *ACS Nano* **12**:2088–2093. DOI: https://doi.org/10.1021/acsnano.8b00141, PMID: 29485854

Zhang X, Zhang Q, Peng Q, Zhou J, Liao L, Sun X, Zhang L, Gong T. 2014. Hepatitis B virus preS1-derived lipopeptide functionalized liposomes for targeting of hepatic cells. *Biomaterials* **35**:6130–6141. DOI: https://doi.org/10.1016/j.biomaterials.2014.04.037, PMID: 24797877

Zhang Q, Zhang X, Chen T, Wang X, Fu Y, Jin Y, Sun X, Gong T, Zhang Z. 2015. A safe and efficient hepatocyte-selective carrier system based on myristoylated preS1/21-47 domain of hepatitis B virus. *Nanoscale* **7**:9298–9310. DOI: https://doi.org/10.1039/C4NR04730C, PMID: 25945919

5.3.2 Chapter 3.2

Poly(Sarcosine) Surface Modification Imparts Stealth-Like Properties to Liposomes

Stefan Bleher, **Jonas Buck**, Christian Muhl, Sandro Sieber, Sabine Barnert, Dominik Witzigmann, Jörg Huwyler, Matthias Barz, Regine Süss

Small. 2019 Dec 1;15(50):1904716.
doi: 10.1002/smll.201904716.

Highlights: Prolonged blood circulation half-life time is a prerequisite for successful nano-particle-based therapies. The most common approach to extend blood circulation lifetime is the decoration of nanoparticles with polyethylene glycol (PEG). However, immune reactions to PEG may significantly reduce treatment efficiency, especially in the case of repeated administration. In this study, we describe the synthesis and use of a possible alternative to PEG: bisalkyl polysarcosine (BA-pSar). We show that BA-pSar can be synthesized with defined chain lengths and low polydispersity. BA-pSar was successfully incorporated into liposomal formulations and enhanced circulation behavior while reducing macrophage recognition in a similar manner to PEG, as determined in the zebrafish embryo animal model. Moreover, BA-pSar can be end group modified to reduce complement activation and thereby reduces immune reactions compared to PEG.

NANO · MICRO small
www.small-journal.com

Poly(Sarcosine) Surface Modification Imparts Stealth-Like Properties to Liposomes

Stefan Bleher, Jonas Buck, Christian Muhl, Sandro Sieber, Sabine Barnert, Dominik Witzigmann, Jörg Huwyler, Matthias Barz, and Regine Süss**

Circulation lifetime is a crucial parameter for a successful therapy with nanoparticles. Reduction and alteration of opsonization profiles by surface modification of nanoparticles is the main strategy to achieve this objective. In clinical settings, PEGylation is the most relevant strategy to enhance blood circulation, yet it has drawbacks, including hypersensitivity reactions in some patients treated with PEGylated nanoparticles, which fuel the search for alternative strategies. In this work, lipopolysarcosine derivatives (BA-pSar, bisalkyl polysarcosine) with precise chain lengths and low polydispersity indices are synthesized, characterized, and incorporated into the bilayer of preformed liposomes via a post insertion technique. Successful incorporation of BA-pSar can be realized in a clinically relevant liposomal formulation. Furthermore, BA-pSar provides excellent surface charge shielding potential for charged liposomes and renders their surface neutral. Pharmacokinetic investigations in a zebrafish model show enhanced circulation properties and reduction in macrophage recognition, matching the behavior of PEGylated liposomes. Moreover, complement activation, which is a key factor in hypersensitivity reactions caused by PEGylated liposomes, can be reduced by modifying the surface of liposomes with an acetylated BA-pSar derivative. Hence, this study presents an alternative surface modification strategy with similar benefits as the established PEGylation of nanoparticles, but with the potential of reducing its drawbacks.

1. Introduction

Nanomedicines have been investigated and used intensely over the past decades for several biomedical applications.[1] With numerous products already approved and a variety of preparations in clinical trials, liposomes are the most advanced and successful nanomedicine in clinic.[2–4]

Thereby, one of the main goals of liposomes is to protect the entrapped drug while also reducing its off-site toxicity, as shown for multiple formulations.[5–8] To this end, increasing on-target tissue concentration is a key aspect which can be achieved both by nontargeted and targeted liposomes.[9–12] In this regard, a crucial point is the prolongation of systemic circulation lifetime. It is well-known that upon injection the majority of conventional (plain) liposomes are cleared rapidly from the blood stream by cells of the mononuclear phagocyte system.[13–15] To enhance circulation times, a variety of approaches to modify the surface of liposomes emerged,[16–18] yet ultimately polyethylene glycol (PEG) established itself as gold standard in the early 1990s aiming at decreasing opsonization.[19–21] PEGylation not only reduces but also alternates the recognition of nanoparticles by complement factors and opsonins, resulting in a decreased nanoparticle recognition and clearance by macrophages.[22,23] Manipulating opsonization, including the reduction of complement activation thus is one of the main goals in preventing rapid clearance.

Today, surface modifications of liposomes are mostly realized with amphiphilic lipid-polymer conjugates like 1,2-distearoyl-*sn*-glycero-3-phosphoethanolamine-*N*-[methoxy(polyethylene glycol)-2000] (DSPE-mPEG2k).[24,25] Despite the benefits and being considered mostly nonimmunogenic, phospholipid-PEG conjugates have also demonstrated some drawbacks over the

S. Bleher, S. Barnert, Prof. R. Süss
Department of Pharmaceutical Technology and Biopharmacy
and Freiburger Materialforschungszentrum (FMF)
Institute of Pharmaceutical Sciences
Albert Ludwig University of Freiburg
79104 Freiburg, Germany
E-mail: stefan.bleher@pharmazie.uni-freiburg.de;
regine.suess@pharmazie.uni-freiburg.de

The ORCID identification number(s) for the author(s) of this article can be found under https://doi.org/10.1002/smll.201904716.

DOI: 10.1002/smll.201904716

J. Buck, Dr. S. Sieber, Dr. D. Witzigmann, Prof. J. Huwyler
Division of Pharmaceutical Technology
Department of Pharmaceutical Sciences
University of Basel
4056 Basel, Switzerland

C. Muhl, Dr. M. Barz
Institute of Organic Chemistry
Johannes Gutenberg University Mainz
55128 Mainz, Germany

Dr. D. Witzigmann
Department of Biochemistry and Molecular Biology
University of British Columbia
Health Sciences Mall, Vancouver V6T 1Z3, British Columbia, Canada

last decade. Anti-PEG antibodies are a major concern regarding the clearance of intravenously administered liposomes modified with PEG,[26,27] frequently culminating in the rapid clearance of injected liposomes.[28,29] The occurrence of pre-existing anti-PEG antibodies even in healthy individuals has increased in everyday life due to exposure to PEG-containing products.[30] Besides this so-called accelerated blood clearance phenomenon, it transpired that both, the anchoring phospholipid and PEG itself are likely to cause specific and nonspecific[31] immune reactions. Such reactions are often caused by complement activation[32,33] and can lead to hypersensitivity reactions (HSRs) possibly triggering anaphylaxis.[34]

The negative charge at the phosphate group of DSPE-PEG derivatives is predominantly linked to this complement induction.[35,36]

Conclusively, the development of alternative surface modifications offers an interesting possibility to circumvent the above-mentioned limitations of PEG derivatives.[37–39] For this purpose, a multitude of hydrophilic materials has been proposed.[40–45]

In this work, we report the synthesis of the lipid-like amphiphile bisalkyl polysarcosine (BA-pSar) and its successful incorporation into the lipid bilayer of preformed liposomes. It was demonstrated earlier that pSar has properties similar to PEG, comprising high water-solubility, flexibility, and low immunogenicity in vitro,[46,47] making it a promising candidate for surface modification of liposomes.[48] The aim of this study was to demonstrate that surface modification using pSar-lipopolymers is a valuable strategy to increase circulation half-life of liposomes while also ensuring good biocompatibility (i.e., low complement activation). After synthesis, physicochemical properties of pSar-modified liposomes were compared with PEGylated and nonsurface-modified liposomes regarding their size, polydispersity, and zeta potential. To evaluate the extend of BA-pSar inserted into the bilayer, we determined the incorporation efficiency via high performance liquid chromatography (HPLC) with increasing amounts of BA-pSar added to preformed liposomes using the post-insertion method.

In order to study the pharmacokinetics of liposomes with different surface modifications, we selected the zebrafish model as a validated in vivo tool to assess circulation properties and macrophage clearance.[49]

Addressing the occurrence of HSR, we also investigated the complement activation potential of liposomes modified with BA-pSar and an optimized acetylated derivative of pSar ($pSar_{102}Ac$) with net-neutral charge.

2. Results and Discussion

2.1. Synthesis of Bisalkylated Lipopolysarcosine

One part of the present work was the synthesis of a bisalkylated polysarcosine. The synthesis (**Scheme 1**) was adapted and modified from the literature.[45] The sarcosine-*N*-carboxyanhydride was synthesized and purified before the polymerization was started by the addition of the bisalkylamine. In contrast to monoalkylated pSar lipopolymers, solvent condition had to be adjusted due to the hydrophobicity of the initiator. Thus, polymerizations were performed in benzonitrile. After completion of the reaction, which was assured by Fourier-transform infrared spectroscopy, the polymer was precipitated in cold diethylether and purified via dialysis (**Figure 1**).

^{1}H NMR experiments demonstrate that the deviation between obtained and calculated degrees of polymerization is below 10% (**Table 1** and Figure 1A). In line with MALDI-TOF MS (matrix-assisted laser desorption/ionization-time of flight mass spectrometry) ^{1}H DOSY (diffusion-ordered spectroscopy) NMR shows the presence of only one diffusing species confirming the absence of free initiator and water-initiated polymer (Figure 1B). The discrepancy between the molecular weights determined by HFIP-GPC (hexafluoro-2-isopropanol-gel permeation chromatography) and NMR can be explained with the uncommonly high values of polymethylmethacrylate (PMMA) in HFIP.[46]

The reported method is a simple way to vary lipopolymer architectures in a one-step polymerization. Moreover, polysarcosine bears the potential for further end group modification, due to the terminal amine end group (Scheme 1). To maintain the nonionic nature of the polymer, pSar end groups were acetylated with acetic anhydride in a post-polymerization manner without any influence on the molecular weight distribution or chemical integrity of the polymer (**Figure 2**A,B). In addition, MALDI-ToF analysis of $BA\text{-}pSar_{102}$ was performed and is displayed in Figure 2C. Despite severe mass discrimination, the spectrum reveals the full incorporation of the bisalkyl amine initiator (dioctadecylamine) without any detectable side products, i.e., initiation by traces of water or other impurities. Enlargement of the most intense peaks (Figure 2D) shows degrees of polymerization of X_n = 19,20 and sub-populations due to sodium and potassium ionization.

The second part of this work was focused on the incorporation of synthesized pSar derivatives into the lipid bilayer of

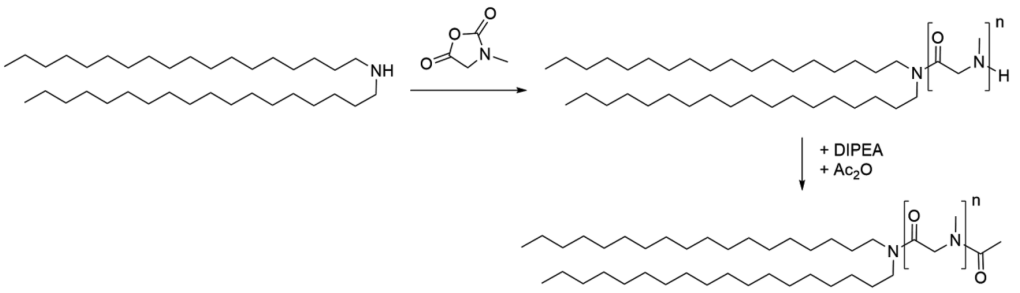

Scheme 1. Synthesis of $BA\text{-}pSar_{102}$ based on nucleophilic ring opening polymerization of sarcosine NCA and formation of $BA\text{-}pSar_{102}Ac$ via end group modification (acetylation).

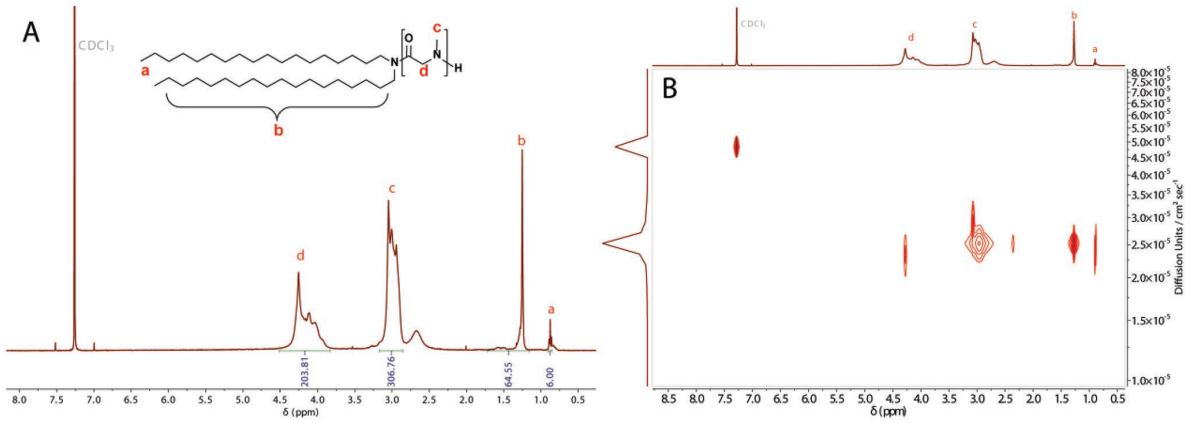

Figure 1. A) ^{1}H NMR spectrum of BA-pSar$_{102}$ in $CDCl_3$ with assignment of peaks. B) DOSY NMR spectrum of BA-pSar$_{102}$ in $CDCl_3$.

liposomes and the comparison with DSPE-mPEG2k. Therefore, BA-pSar$_{102}$, BA-pSar$_{102}$Ac, and DSPE-mPEG2k were used to modify the surface of preformed 1,2-distearoyl-*sn*-glycero-3-phosphocholine (DSPC)/cholesterol (Chol) liposomes. The lipid ratios were chosen to be similar to the formulation of an approved PEGylated liposome formulation, namely, Doxil. Doxil is composed of hydrogenated soya phosphatidylcholine, Chol, and DSPE-mPEG2k at a molar ratio of 57:38:5.[50]

2.2. Characterization of Liposomes

The hydrodynamic diameter and polydispersity index (PDI) of different liposome formulations were determined before and after purification of liposomes from noninserted lipopolymer conjugates using dynamic light scattering (DLS). Zeta potential was measured after purification. Results for size and PDI before and after post-insertion of lipopolymers followed by purification are displayed in **Table 2**. Within the estimated errors, results obtained for size and PDI were comparable for all preparations and did not change over the process of post-insertion. Size was approximately 120 nm and PDI was ≤0.1, indicating homogenous size distributions for all formulations.

Figure 3 shows Cryo-TEM (cryogenic transmission electron microscopy) images displaying the morphology of representative liposomes which were selected for further in vitro and zebrafish experiments. Unmodified as well as surface-modified formulations show a narrow size distribution. Neither PEGylation nor modification with BA-pSar$_{102}$ induced significant changes in liposomal morphology or size distribution. Cryo-TEM images are in good agreement with size values obtained by DLS measurements.

Table 1. Synthesized sarcosine-based lipopolymers with an initial monomer to initiator ratio of $M/I = 90$, molecular weights and dispersity indices.

Polymer	Initiator/end-group	M_n (Calc)[a] [kg mol^{-1}]	M_n(GPC)[b] [kg mol^{-1}]	M_n(NMR)[c] [kg mol^{-1}]	PDI
BA-pSar$_{102}$	DODA/H	6.9	38.5	7.8	1.2
BA-pSar$_{102}$Ac	DODA/Ac	7.0	38.7	7.8	1.2

[a]Calculated molecular weight (based on M/I ratio); [b]Determined by HFIP-GPC using PMMA-standards; [c]Determined by ^{1}H NMR via end-group analysis.

2.3. Zeta Potential of Liposomes

To assess the surface charge shielding potential of the different surface modifications, an additional set of liposomal formulations was prepared containing the cationic lipid 1,2-dioleoyl-3-trimethylammonium-propane (DOTAP, 10 mol%) (**Figure 4**A). Measurements of liposomes without DOTAP (Figure 4B) revealed only slight differences in zeta potential due to the neutral character of the formulation. Addition of DOTAP allowed to compare the influence on surface charge shielding of different formulations using zeta potential measurements. Notably, size characteristics for all preparations were comparable (Supporting Information, Figure S1). Unmodified liposomes showed a relatively high zeta potential of about +46 mV. In contrast, the zeta potential for liposomes modified with DSPE-mPEG2k and BA-pSar$_{102}$ was reduced drastically, as already reported previously.[51] PEGylation resulted in a zeta potential of about −6 mV, whereas liposomes modified with pSar had a zeta potential around +9 mV, suggesting an effective shielding of charge. The slightly negative zeta potential for PEGylated liposomes on the one hand is probably due to the negative charge at the phosphate moiety of DSPE-mPEG2k. The slightly positive charge of BA-pSar$_{102}$-modified liposomes on the other hand can be attributed to the terminal secondary amine of pSar, which is protonated at physiological pH. Measurements of liposomes modified with end-capped pSar (BA-pSar$_{102}$Ac) displayed a zeta potential of around +2 mV. Since BA-pSar$_{102}$Ac bears no charge, this suggests that an effective shielding of the positive charge introduced by DOTAP was achieved with this formulation.

2.4. Incorporation Efficiency

For all surface-modified liposomes, DSPE-mPEG2k, BA-pSar$_{102}$, and BA-pSar$_{102}$Ac incorporation efficiency into the liposomal bilayer was monitored via HPLC.

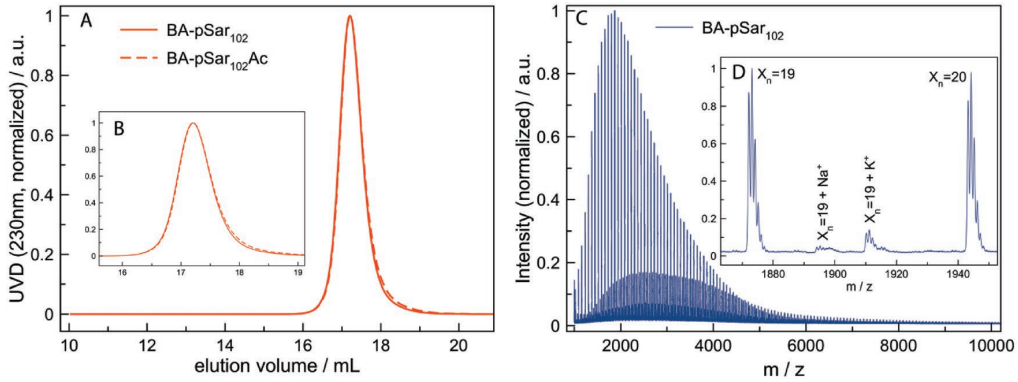

Figure 2. A) Normalized HFIP-GPC traces of BA-pSar$_{102}$ and BA-pSar$_{102}$Ac. B) Enlarged HFIP-GPC traces of BA-pSar$_{102}$ and BA-pSar$_{102}$Ac for a better comparison. C) Normalized MALDI-ToF spectrum of BA-pSar$_{102}$. D) Enlargement of the most intensive peaks of MALDI-ToF spectrum of BA-pSar$_{102}$.

In preliminary tests, different amounts of BA-pSar$_{102}$ (1–15 mol%) were dried from stock solutions, hydrated with preformed liposomes, and post-insertion into the liposomal bilayer was analyzed. Thereby, incorporation of at least 4.5 mol% was achieved by hydrating 7.5 mol% dried BA-pSar$_{102}$ or BA-pSar$_{102}$Ac with preformed liposomes. Excess conjugate was removed by ultrafiltration. These results correspond to an incorporation efficiency of approximately 60% of added conjugate. All further experiments therefore were conducted using the same setup, adding preformed liposomes to 7.5 mol% of dried BA-pSar$_{102}$ or BA-pSar$_{102}$Ac, respectively. When hydrating 5 mol% of dried DSPE-mPEG2k in an analogous manner, complete incorporation was observed. Incorporation efficiency results obtained after purification are shown in **Table 3**.

In summary, BA-pSar$_{102}$ and BA-pSar$_{102}$Ac were successfully incorporated into the lipid bilayer, resulting in liposomes with a narrow size distribution. Liposomes modified with lipopolysarcosines also showed effective surface charge shielding, comparable with findings for PEGylated liposomes. To further evaluate the potential use of BA-pSar$_{102}$-modified liposomes, clearance by macrophages and circulation properties were investigated in vivo in the zebrafish model.

2.5. Assessment of Liposome Pharmacokinetics In Vivo

Fluorescently labeled liposomes with different surface modifications (i.e., DSPE-mPEG2k as positive control for stealth properties or BA-pSar$_{102}$) and unmodified (conventional) liposomes (negative control) were injected into the blood circulation of zebrafish larvae. No acute signs of toxicity (i.e., denaturation of tissue fluids or yolk, heart failure) nor long-term effects including malformations or increased mortality were observed (data not shown), indicating the biocompatibility of all liposome formulations including both surface modifications.

Table 2. Physicochemical characterization of liposomal formulations after purification. Values are means ± SD, $n = 3$.

Formulation	Hydrodynamic diameter [nm]	PDI
DSPC/Chol/DiI	107 ± 10	0.05 ± 0.02
DSPC/Chol/DiI/DSPE-mPEG2k	113 ± 9	0.06 ± 0.02
DSPC/Chol/DiI/BA-pSar$_{102}$	123 ± 10	0.09 ± 0.02
DSPC/Chol/DiI/BA-pSar$_{102}$Ac	130 ± 2	0.05 ± 0.02

At 3 h post injection (hpi), all liposome formulations demonstrated a diffusive fluorescence staining without accumulations in the posterior caudal vein (PCV) region (**Figure 5**). Recently, it has been shown that endothelial cells in the PCV express stabilin receptors which can scavenge liposomes and thereby prevent blood circulation.[52] However, an increased colocalization (yellow) of conventional liposomes (red) and macrophages (green) was already detected at this time point indicating macrophage clearance (white arrows, Figure 5).

A clear difference in circulation characteristics of different liposome formulations was observed 24 hpi (Figure 5). Unmodified DSPC/Chol liposomes demonstrated decreased circulation properties indicated by a dotted staining pattern (i.e., clearance by stabilin scavenger receptors). In contrast, both surface-modified liposomes (i.e., DSPE-mPEG2k and BA-pSar$_{102}$) still demonstrated a prolonged circulation lifetime.[53] Strikingly, macrophage clearance of unmodified liposomes increased significantly as compared to surface-modified liposomes (indicated by yellow color of colocalization).[54] Both PEG and pSar prevented macrophage clearance signifying their ability to confer a stealth effect to the liposomes (Figure 5). This can be explained by the advantageous properties of lipopolymer surface modification including decreased opsonization and steric stabilization. In addition, this prevents time-dependent formation of aggregates via steric stabilization preferentially sequestered by macrophages. Conclusively, BA-pSar$_{102}$-modified liposomes outperformed unmodified control liposomes (i.e., DSPC/Chol) with favorable pharmacokinetic characteristics—an improved blood circulation lifetime and a decreased macrophage clearance. Moreover, BA-pSar$_{102}$-modification of liposomes resulted in similar in vivo properties as DSPE-mPEG2k liposomes, which are considered as the gold standard for long circulating, stealth liposomes.

2.6. In Vitro Complement Activation

Figure 6 shows the elevated sC5b-9 levels after incubation of liposomes and controls with three individual serum samples.

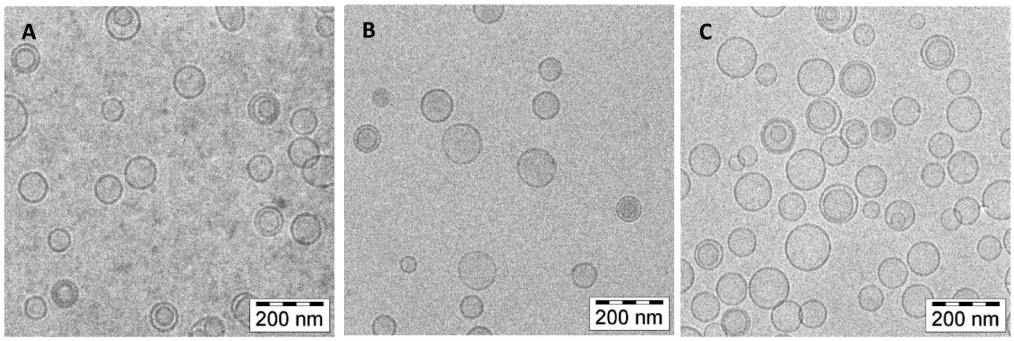

Figure 3. Cryo-TEM images showing the morphology of different liposomal formulations. A) DSPC/Chol/DiI, B) DSPC/Chol/DiI/DSPE-mPEG2k, and C) DSPC/Chol/DiI/BA-pSar$_{102}$.

As expected there are variations in sC5b-9 levels in the sera of different donors, as can be seen for the negative control (HBS, HEPES buffered saline). Compared to HBS, PEGylated liposomes induced a 1.5- to 2.5-fold increase in complement activation (C activation) in all tested sera, which is in good accordance with values obtained from literature.[36] For BA-pSar$_{102}$-modified liposomes, an increase in C activation was observed, resulting in 2.5- to 5-fold higher sC5b-9 levels as compared to HBS. Charged liposomes are known to elicit the complement system and cationic liposomes are known to do so via the alternative pathway.[55] Thus, C activation enhancement by BA-pSar$_{102}$ compared to DSPE-mPEG2k comes as no surprise as the N-terminus of the polymeric chain bears a secondary amine, which is present in its ammonium salt form under physiological conditions. In a similar manner, the negative charge at the phosphate moiety of DSPE-PEG is well known to stimulate C activation.[35] In order to exploit the advantageous synthetic features of lipopolysarcosine, the optimized end-capped BA-pSar$_{102}$Ac derivative was incorporated into liposomes. Interestingly, BA-pSar$_{102}$Ac-modified liposomes demonstrated improved properties with decreased complement activation. Compared to HBS only a 2.5-fold increase in sC5b-9 levels in serum C, and only 1.5-fold increase in serum A and strikingly no increase in serum B was observed.

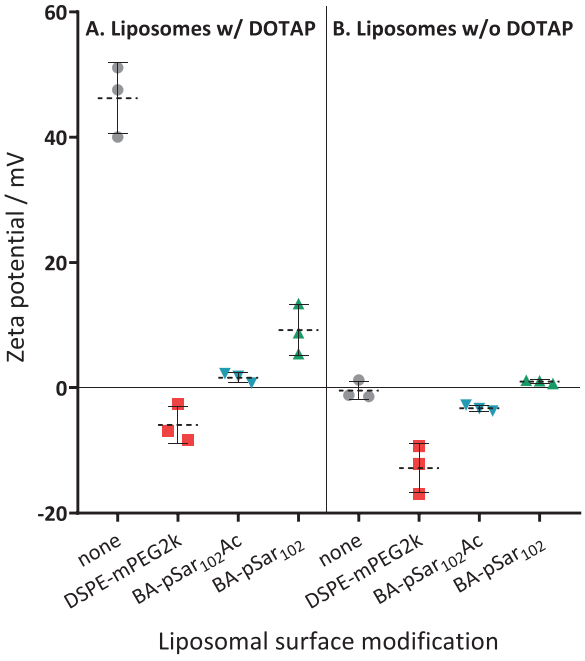

Figure 4. Surface charge shielding of liposomes. Zeta potential of different liposomal formulations containing A) 10 mol% DOTAP or B) no DOTAP. ● nonsurface-modified liposomes, ■ PEGylated liposomes, ▼ liposomes modified with BA-pSar$_{102}$Ac, and ▲ liposomes modified with BA-pSar$_{102}$. Symbols depict measured values, dashed lines show mean values ± SD, $n = 3$.

Our findings show that replacing the anchoring DSPE with dioctadecylamine and subsequent end-capping of pSar with a neutral acetyl moiety results in a significantly decreased C activation in two of the three tested sera when comparing DSPE-mPEG2k with BA-pSar$_{102}$Ac. This most likely is a result of omitting the charges both at the anchor (hydrophilic–hydrophobic interface) and the polymeric chain, as it was previously demonstrated for free (nonliposomal incorporated) polymers.[47]

3. Conclusion

In this study, we present the one step synthesis of a lipopolysarcosine derivative enabling controlled modification of liposomes to enhance systemic circulation. The controlled polymerization conditions allow for an accurate degree of polymerization resulting in the precise tailoring of pSar chain length while keeping polydispersity low. Due to the reactive

Table 3. Efficiency of conjugate insertion. Percent of incorporated polymer-conjugates determined by HPLC analysis after purification. Values are means ± SD, $n = 3$.

Formulation	Incorporation efficiency [%]
DSPC/Chol/DiI/BA-pSar$_{102}$	63 ± 6
DSPC/Chol/DiI/BA-pSar$_{102}$Ac	57 ± 4
DSPC/Chol/DiI/DSPE-mPEG2k	96 ± 6

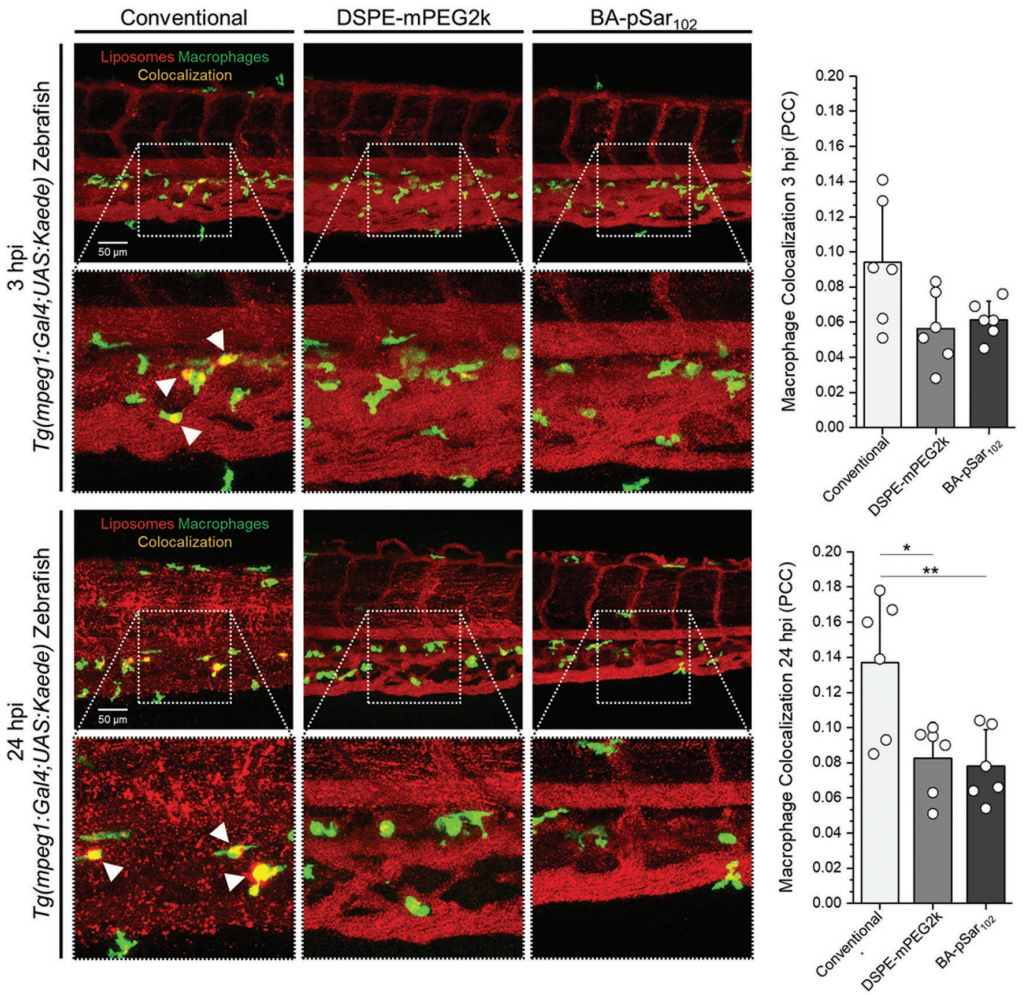

Figure 5. Assessment of liposome pharmacokinetics in transgenic zebrafish. Conventional liposomes and liposomes surface-modified with DSPE-mPEG2k or BA-pSar$_{102}$ were injected into the blood circulation of zebrafish (2 days post fertilization). Confocal images of tail region were acquired 3 and 24 hpi. White arrows indicate macrophage clearance of liposomes assessed by colocalization (yellow color) of green fluorescent macrophages (*KAEDE*) and fluorescently labeled liposomes (DiI, red). Quantitative analysis of macrophage clearance was performed using PCC. Values are means ± SD, $n = 6$. $^{*}p < 0.05$ or $^{**}p < 0.01$ (one-way analysis of variance (ANOVA) followed by Bonferroni post hoc test) as compared to conventional liposomes composed of DSPC/Chol/DiI.

amino group, further diversification can be achieved in a simple post-polymerization modification step without altering the polydispersity of the precursor polymer. Using this approach, the positive net charge of BA-pSar$_{102}$ was omitted by acetylation of the terminal amine. Subsequently, we were able to successfully incorporate BA-pSar$_{102}$ and BA-pSar$_{102}$Ac into the lipid bilayer of preformed liposomes using post-insertion technique.

Liposome characterization including the determination of size and morphology revealed a monodisperse size distribution with mostly unilamellar vesicles. Zeta potential measurements of surface-modified liposomes demonstrated an effective shielding of surface charge. In contrary to modification with DSPE-mPEG2k and BA-pSar$_{102}$, which still resulted in a slightly negative or positive zeta potential, BA-pSar$_{102}$Ac-modified liposomes unveiled an almost net-neutral surface charge. Furthermore, the alternative hydrophobic anchor not only circumvents the negative charge that comes with the widely used DSPE-PEG derivatives but also provides sufficiently firm binding for the relatively large pSar chain into the bilayer. Moreover, BA-pSar-modified liposomes also featured prolonged circulation properties and decreased recognition by macrophages in the zebrafish model similar to PEGylated liposomes. Finally, liposome-mediated C activation could be reduced by modification of liposomes with an end-capped pSar derivative. All these results confirm that surface modification of liposomes with pSar or its derivatives is a promising alternative to well-established PEGylation strategies, especially in regard of reducing potential HSR. Equipped with an easily modifiable

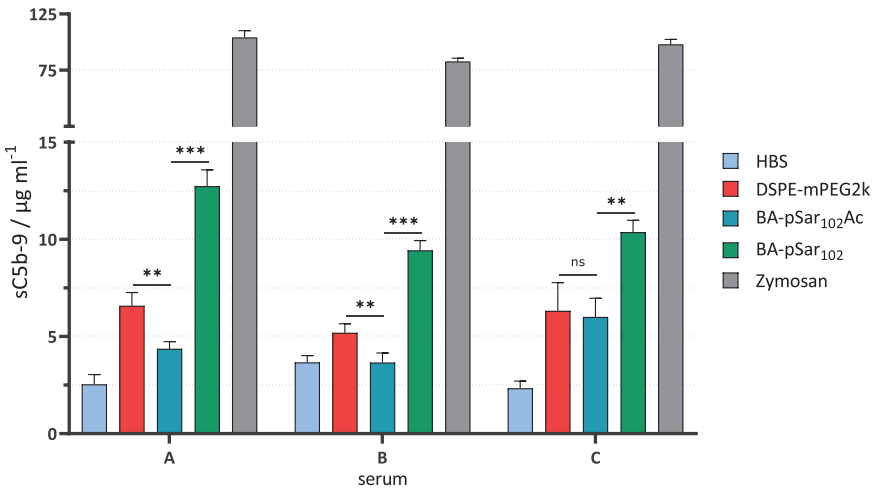

Figure 6. Complement activation of different liposomal formulations and controls. A–C) Samples were incubated for 1 h with human serum of three individuals. Values are means ± SD, $n = 2–3$. ns: not significant, $^{**}p < 0.01$ or $^{***}p < 0.001$ (one-way ANOVA followed by Bonferroni post hoc test) as compared to liposomes modified with BA-pSar$_{102}$Ac.

end-group, incorporation of lipopolysarcosine and further functionalization is also a promising option for the exploitation of active drug targeting or combination therapies.

4. Experimental Section

Materials: *n*-Hexane (Fischer Scientific, Waltham, USA) was distilled from Na/K. Benzonitrile was purchased from Sigma Aldrich (Steinheim, Germany), dried over CaH_2, and freshly distilled prior to use. Tetrahydrofuran (THF) and toluene were purchased from Fischer Scientific (Waltham, USA), dried over Na, and freshly distilled prior to use. HFIP was purchased from Fluorochem (Hadfield Derbyshire, UK). Dioctadecylamine was purchased from Fluka (St. Gallen, Switzerland) and dried at 40 °C under vacuum (1×10^{-3} mbar) for 24 h. Diphosgene was purchased from Alfa Aesar (Ward Hill, MA, USA) and deuterated solvents from Deutero GmbH (Kastellaun, Germany).

DSPC and DSPE-mPEG2k were generously donated by Lipoid GmbH (Ludwigshafen, Germany). DOTAP was obtained from Merck (Darmstadt, Germany). 1,1′-dioctadecyl-3,3,3′,3′-tetramethylindocarbocyanine perchlorate (DiI) was purchased from Invitrogen (Thermo Fisher Scientific, Waltham, USA). Chol was purchased from Sigma Aldrich (Steinheim, Germany). Other chemicals were purchased from Sigma-Aldrich (Steinheim, Germany) and used as received unless stated otherwise. Human serum samples of ten healthy donors were obtained from the University Medical Center Freiburg. Sera were stored at a temperature of –80 °C until used.

Synthesis of Sarcosine N-Carboxyanhydride: A total of 14.92 g (167.4 mmol) sarcosine, dried under vacuum for 1 h, was weighed into a pre-dried, three-neck, round-bottom flask. A total of 300 mL of absolute THF was added under a steady flow of nitrogen, 16.2 mL (134 mmol) of diphosgene was added slowly via syringe, and the nitrogen stream was reduced. The colorless suspension was mildly refluxed for 3 h, yielding a clear solution. Afterward, a steady flow of dry nitrogen was led through the solution for another 3 h while the outlet was connected to two gas washing bottles filled with aqueous NaOH solution to neutralize phosgene. The solvent was evaporated under reduced pressure, yielding a brownish oil as a crude reaction product. The oil was dried under reduced pressure (1×10^{-3} mbar for 2 h) to obtain an amorphous solid, free of phosgene and HCl, confirmed by testing against a silver nitrate solution. The crude product was redissolved in 40 mL of THF and precipitated with 300 mL of dry n-hexane. The solution was cooled to –18 °C and stored for 18 h to complete precipitation. The solid was filtered under dry nitrogen atmosphere and dried in a stream of dry nitrogen for 60–90 min and afterward under high vacuum for 2 h in the sublimation apparatus. The crude product was sublimated at 85 °C and 1×10^{-3} mbar. The product was collected from the sublimation apparatus in a glovebox on the same day. The purified product (110 mmol, 65% yield, colorless crystallites; melting point: 102–104 °C (lit: 102–105 °C)) was stored in a Schlenk tube at –80 °C.

^{1}H NMR (300 MHz, $CDCl_3$): δ/ppm = 4.22 (2H, s, –CH_2–CO–), 2.86 (3H, s, –CH_3).

Synthesis of Polysarcosine: Sarcosine NCA was transferred into a pre-dried Schlenk tube equipped with a stir bar under nitrogen counter flow and again flame-dried under high vacuum for 1 h. Subsequently, the NCA was dissolved in dry benzonitrile to yield a solution of 100 mg mL^{-1} with respect to the NCA. 1/*n* equivalent of dioctadecylamine was dispersed in pre-dried toluene and added to the NCA solution. The solution was stirred at room temperature and kept at a constant pressure of 1.25 bar of dry nitrogen via a schlenk line to prevent impurities from entering the reaction vessel while allowing CO_2 to escape. Completion of the reaction was confirmed by Fourier transform infrared (FT-IR) spectroscopy (disappearance of the NCA related peaks (1853 and 1786 cm^{-1})). After completion of the reaction, the polymer was precipitated in cold diethylether and centrifuged (4500 rcf at 4 °C for 15 min). After discarding the liquid fraction, new ether was added and the polymer was resuspended in a sonication bath. The suspension was centrifuged again and the procedure was repeated. The polymer was dissolved in water, dialyzed against MilliQ water and lyophilized, obtaining a colorless, stiff and porous solid. The yield after purification was 91% of the theoretically achievable mass of the polymer.

^{1}H NMR (400 MHz; $CDCl_3$): δ/ppm: 4.51–3.80 (204H; br; (2n)–CO–CH_2–NMe–); 3.12–2.62 (306H; br; (3n)–N–CH_3–); 1.83–1.00 (64H; br; (–CH_2–$(CH_2)_{16}$–$CH_3)_2$); 0.87 (6H; t; (–CH_2–$(CH_2)_{16}$–$CH_3)_2$).

Acetylation of Polysarcosine: 100 mg of polysarcosine (BA-pSar$_{102}$) was dissolved in 0.5 mL dimethylformamide (DMF), 10 equivalents (in respect to the calculated molecular mass of the polymer) of diisopropylamine were added and the solution was stirred for 30 min at room temperature. Afterward, 5 equivalents of acetic acid anhydride were added and the solution was stirred overnight at room temperature. The polymer was precipitated in cold ether and centrifuged (4500 rcf at 4 °C for 15 min). After discarding the liquid fraction, fresh ether was added, the polymer was resuspended in a sonication bath and

Table 4. Lipid compositions of prepared formulations.

Formulation	Initial molar ratio	Ratio after purification
DSPC/Chol/DiI	60:39:1	–
DSPC/Chol/DiI/DSPE-mPEG2k	55:39:1:5	55:39:1:4.8
DSPC/Chol/DiI/BA-pSar$_{102}$	57:39:1:7.5	57:39:1:3.2
DSPC/Chol/DiI/BA-pSar$_{102}$Ac	57:39:1:7.5	57:39:1:3.4
DSPC/Chol/DOTAP	50:40:10	–
DSPC/Chol/DOTAP/ DSPE-mPEG2k	45:40:10:5	45:40:10:4.9
DSPC/Chol/DOTAP/BA-pSar$_{102}$	47:40:10:7.5	47:40:10:3.1
DSPC/Chol/DOTAP/BA-pSar$_{102}$Ac	47:40:10:7.5	47:40:10:3.3

centrifuged afterward. This procedure was repeated. The polymer was dissolved in water, dialyzed against MilliQ water to remove excess of acetic acid and residual traces of DMF. After lyophilization, a colorless, stiff, and porous solid was obtained.

^{1}H NMR (400 MHz; $CDCl_3$): δ/ppm: 4.51–3.80 (204H; br; (2n)–CO–CH_2–NH–); 3.12–2.62 (306H; br; (3n)–N–CH_3–); 1.83–1.00 (64H; br; –CH_2–$(CH_2)_{16}$–CH_3); 0.87 (6H; t; –CH_2–CH_3).

^{1}H NMR spectra were recorded on a Bruker (Billerica, MA, USA) AC 400 at a frequency of 400 MHz, respectively. 2D NMR spectra as ^{1}H DOSY were recorded on a Bruker Avance III HD 400 at 400 MHz. All spectra were recorded at room temperature (25 °C) and calibrated using the solvent signals. Melting points were measured using a Mettler FP62 melting point apparatus at a heating rate of 2.5 °C min^{-1}. GPC was performed with HFIP containing 3 g L^{-1} potassium trifluoroacetate as the eluent at 40 °C and a flow rate of 0.8 mL min^{-1}. The columns were packed with modified silica (PFG column particle size: 7 µm, porosity: 100 and 1000 Å). PMMA standards (Polymer Standards Services GmbH, Mainz, Germany) were used for calibration and toluene was used as the internal standard. A refractive index detector (G1362A RID) and an UV-vis detector (at 230 nm unless otherwise stated; Jasco, Gross-Umstadt, Germany, UV-2075 Plus) were used for polymer detection.

Preparation of Liposomes: Liposomes were prepared using the thin-film hydration method. For zebrafish experiments, 1 mol% DiI was added as a fluorescent label. Briefly, stock solutions of all components were prepared by dissolving dry powders in $CHCl_3$ and/or MeOH. Stock solutions were mixed in molar ratios according to **Table 4**. Organic stocks were removed using a rotary evaporator (Rotavapor R, Büchi, Essen, Germany) and lipid films were dried for at least 2 h to ensure complete removal of organic solvents. Lipid films were hydrated with HBS (140 mmol L^{-1} NaCl, 10 mmol L^{-1} Hepes (4-(2-hydroxyethyl)-1-piperazineethanesulfonic acid), pH 7.4) resulting in a lipid concentration of 20 mmol L^{-1}. Dispersions were extruded 41 times through an 80 nm polycarbonate membrane. All steps were conducted at 65 °C. Phospholipid content was determined using Bartlett's Assay.[56] For exact compositions of liposomes, see Table 4.

Post-Insertion of PEG- and pSar-Conjugates: DSPE-mPEG2k, BA-pSar$_{102}$, and BA-pSar$_{102}$Ac were inserted into preformed liposomes using the post-insertion technique.[57,58] Briefly, organic stock solutions containing defined amounts of DSPE-mPEG2k, BA-pSar$_{102}$, and BA-pSar$_{102}$Ac were evaporated for several hours using an evaporation centrifuge (Concentrator 5301, Eppendorf, Hamburg, Germany). Dispersions of preformed liposomes then were added to the residue, vortex mixed, and incubated at 65 °C for 1 h under constant agitation (Thermomixer comfort, Eppendorf, Hamburg, Germany). To remove any noninserted conjugates, liposomes were washed three times with HBS using Vivaspin Turbo 4 ultrafiltration devices (100 kDa MWCO PES membranes, Sartorius, Göttingen, Germany) at 3000 rcf for 30 min. For molar ratios after purification see Table 4.

Particle Size and Zeta Potential Measurements: Mean hydrodynamic diameter, size distribution, and zeta potential were assessed using a Zetasizer Nano ZS (Malvern Instruments, Malvern, UK) and ZetaPals instrument (Brookhaven Instruments Corp., Holtsville, USA). For size measurements, samples were diluted with HBS to 0.1 mmol L^{-1} in disposable plastic cuvettes. Zeta potential was measured using a high concentration cell (Malvern Instruments, Malvern, UK) as described earlier.[59] Liposomes were diluted to 1 mmol L^{-1} with 10 mmol L^{-1} HBS and measured immediately after dilution.

Cryo-TEM: Liposomes were diluted with HBS to achieve a final concentration of 5 to 10 mmol L^{-1} lipid. About 3 µL were applied on a 400 × 100 mesh Quantifoil S 7/2 holey carbon film on a copper grid (Quantifoil Micro Tools GmbH, Jena, Germany). Excess liquid on the grid was removed with filter paper. The sample then was flash frozen by injection into liquid ethane. All sample preparation steps were conducted in a climate-controlled room using a CryoBox 340719 (Carl Zeiss, Oberkochen, Germany). Subsequent fixation of the grid on the sample rod (626-DH, Gatan, Warrendale, USA) and transfer of the rod into the TEM (Leo 912 Ω-mega, Carl Zeiss, Oberkochen, Germany) were conducted under nitrogen atmosphere at –183 °C. The instrument was operated at 120 kV and camera pictures (Proscan HSC 2, Oxford Instruments, Abingdon, USA) were taken with a 6300- to 12 500-fold magnification from different positions of the grid.[60]

Quantification of Conjugate Incorporation: Using a Waters Alliance 2695 separation module (Waters, Milford, USA), mounted with RP-8 (Kinetex 5 µm C8 100 Å, 250 × 4.6 mm) and HILIC (hydrophilic interaction liquid chromatography, Luna 5 µm HILIC 200 Å, 250 × 4.6 mm; both Phenomenex, Torrance, USA) columns, an HPLC method was developed to separate polymer-conjugates from other lipid components. Standards were dissolved in MeOH, samples were diluted to approximately 0.5 mmol L^{-1} with MeOH. DSPE-mPEG2k content was analyzed on an RP-8 column at 45 °C with the gradient shown in **Table 5**. BA-pSar$_{102}$ and BA-pSar$_{102}$Ac contents were analyzed on an HILIC column at 25 °C running the gradient as depicted in **Table 6**. The incorporation efficiency

Table 5. RP-8 column gradient. A: MeOH, B: NH_4OAc buffer pH 4.0, C: ACN. A methanol/water/acetonitrile (7:2:1) to methanol/acetonitrile (9:1) gradient was used to separate PEGylated samples on a C8 reversed phase column. Solvents contained 4 mmol L^{-1} ammonium acetate.

Time	Flow [mL]	%A	%B	%C
0	0.75	70	20	10
5	0.75	70	20	10
15	0.75	90	0	10
25	0.75	90	0	10
30	0.75	70	20	10

Table 6. HILIC column gradient. A: MeOH, B: H_2O, C: NH_4OAc buffer (100 mmol L^{-1} ammonium acetate buffer at pH 5.0), D: ACN. A complex gradient containing 5 mmol L^{-1} ammonium acetate buffer was used to separate samples containing lipopolysarcosines.

Time	Flow [mL]	%A	%B	%C	%D
0	1	0	0	5	95
4	1	0	0	5	95
7	1	10	3	5	82
10	1	10	3	5	82
14	1	40	25	5	30
17	1	40	25	5	30
19	1	40	50	5	5
21	1	40	50	5	5
22	1	0	0	5	95
25	1	0	0	5	95

of both polymer-conjugates was quantified with a Corona charged aerosol detector (Corona CAD ESA 542, Dionex, Sunnyvale, USA) after performing the post-insertion technique followed by a purification step. Data were analyzed with Empower 3.0 software (Waters, Milford, USA). Incorporation efficiency was calculated using the formula shown in Equation (1).

Equation (1). Incorporation efficiency of polymer-conjugates

$$IE = \frac{c_{cp} \times c_{lt}}{c_{ct} \times c_{lp}} \times 100\% \quad (1)$$

c_{cp}: polymer-conjugate concentration after purification
c_{ct}: theoretical polymer-conjugate concentration
c_{lp}: lipid concentration after purification
c_{lt}: theoretical lipid concentration

Zebrafish Experiments: Zebrafish larvae originating from adult Tg(mpeg1:Gal4;UAS:Kaede) were raised at 28 °C in zebrafish culture media.[61] Pigment cell formation was prevented by the addition of 1-phenyl-2-thiourea to the zebrafish culture media at 24 h post fertilization. All zebrafish experiments were performed in accordance with Swiss animal welfare regulations. Calibrated volumes of 1 nL at 5 mmol L^{-1} lipid concentration were injected directly into blood circulation via the duct of Cuvier. All injections were performed using a pneumatic PicoPump PV830 (WPI, Sarasota, Florida), and a Leica S8APO microscope (Leica, Wetzlar, Germany). Successfully injected zebrafish embryos (no yolk or heart injections) were kept at 28 °C and imaged 3 and 24 hpi using an Olympus FV-1000 inverted confocal laser scanning microscope (Olympus Ltd., Tokyo, Japan) equipped with a 20 × UPlanSApo (NA 0.75) objective. Macrophage clearance of liposomes was quantitatively assessed using colocalization analysis based on Pearsons's correlation coefficient (PCC) using the JaCoP plugin from Fiji ImageJ.[62,63]

Complement Activation: Activation of the complement cascade was analyzed by determining SC5b-9 (Protein S-bound terminal complement complex c5b-9) levels using an immunoassay kit (MicroVue SC5b-9 Plus EIA, Quidel, Santa Clara, USA).

In preliminary tests, liposome-mediated complement activation was investigated in freshly prepared human sera of 20 healthy donors. Sera of the three most sensitive individuals were chosen for further testing.

Applying the findings by Moghimi et al.[64] where concentrations of 3–4 mg lipid mL^{-1} serum were found to raise SC5b-9 levels the most, liposomes were diluted to 14.5 mmol L^{-1} (approximately 14 mg mL^{-1}) with HBS. HBS was used as a negative control, Zymosan (0.5 mg mL^{-1}) served as positive control. All samples were incubated by mixing 1 part liposome dispersion with 4 parts human serum for 1 h at 37 °C under constant agitation. Following the incubation samples were diluted 100-fold (700-fold for Zymosan) with manufacturers dilution buffer and the assay was conducted as described in the manufacturers protocol.

Supporting Information

Supporting Information is available from the Wiley Online Library or from the author.

Acknowledgements

The research project was supported by the Swiss National Science Foundation grants no. 174975 (D.W.) and no. 173057 (J.H.).

Conflict of Interest

The authors declare no conflict of interest.

Keywords

complement activation, liposomes, pharmacokinetics, polysarcosine, surface modification

Received: August 21, 2019
Revised: October 23, 2019
Published online:

[1] B. S. Pattni, V. V. Chupin, V. P. Torchilin, *Chem. Rev.* **2015**, *115*, 10938.
[2] T. M. Allen, P. R. Cullis, *Adv. Drug Delivery Rev.* **2013**, *65*, 36.
[3] U. Bulbake, S. Doppalapudi, N. Kommineni, W. Khan, *Pharmaceutics* **2017**, *9*, 12.
[4] A. Wicki, D. Witzigmann, V. Balasubramanian, J. Huwyler, *J. Controlled Release* **2015**, *200*, 138.
[5] A. Gabizon, A. Meshorer, Y. Barenholz, *J. Natl. Cancer Inst.* **1986**, *77*, 459.
[6] Y. Barenholz, *J. Controlled Release* **2012**, *160*, 117.
[7] J. Adler-Moore, R. T. Proffitt, *J. Antimicrob. Chemother.* **2002**, *49*, 21.
[8] R. T. Mehta, T. J. McQueen, A. Keyhani, G. Lopez-Berestein, *J. Infect. Dis.* **1991**, *164*, 1003.
[9] V. P. Torchilin, *J. Mol. Recognit.* **1996**, *9*, 335.
[10] J. Jakoby, F. Beuschlein, S. Mentz, C. Hantel, R. Süss, *Oncotarget* **2015**, *6*, 43698.
[11] D.-K. Chang, P.-C. Li, R.-M. Lu, W.-N. Jane, H.-C. Wu, *PLoS One* **2013**, *8*, e83239.
[12] C. Kelly, C. Jefferies, S.-A. Cryan, *J. Drug Delivery* **2011**, *2011*, 727241.
[13] J. Senior, J. C. W. Crawley, G. Gregoriadis, *Biochim. Biophys. Acta, Gen. Subj.* **1985**, *839*, 1.
[14] J. Senior, *Crit. Rev. Ther. Drug Carrier Syst.* **1986**, *3*, 123.
[15] T. M. Allen, C. Hansen, J. Rutledge, *Biochim. Biophys. Acta, Biomembr.* **1989**, *981*, 27.
[16] A. Chonn, P. R. Cullis, *J. Liposome Res.* **1992**, *2*, 397.
[17] T. M. Allen, A. Chonn, *FEBS Lett.* **1987**, *223*, 42.
[18] A. Gabizon, D. Papahadjopoulos, *Proc. Natl. Acad. Sci. U. S. A.* **1988**, *85*, 6949.
[19] A. L. Klibanov, K. Maruyama, V. P. Torchilin, L. Huang, *FEBS Lett.* **1990**, *268*, 235.
[20] S. I. Jeon, J. H. Lee, J. D. Andrade, P. G. De Gennes, *J. Colloid Interface Sci.* **1991**, *142*, 149.
[21] T. M. Allen, *Trends Pharmacol. Sci.* **1994**, *15*, 215.
[22] X. Yan, G. L. Scherphof, J. A. A. M. Kamps, *J. Liposome Res.* **2005**, *15*, 109.
[23] S. Schöttler, G. Becker, S. Winzen, T. Steinbach, K. Mohr, K. Landfester, V. Mailänder, F. R. Wurm, *Nat. Nanotechnol.* **2016**, *11*, 372.
[24] T. M. Allen, C. Hansen, F. Martin, C. Redemann, A. Yau-Young, *Biochim. Biophys. Acta, Biomembr.* **1991**, *1066*, 29.
[25] J. Senior, C. Delgado, D. Fisher, C. Tilcock, G. Gregoriadis, *Biochim. Biophys. Acta, Biomembr.* **1991**, *1062*, 77.
[26] T. Ishida, M. Ichihara, X. Wang, K. Yamamoto, J. Kimura, E. Majima, H. Kiwada, *J. Controlled Release* **2006**, *112*, 15.
[27] T. Ishida, M. Ichihara, X. Wang, H. Kiwada, *J. Controlled Release* **2006**, *115*, 243.
[28] E. T. M. Dams, P. Laverman, W. J. G. Oyen, G. Storm, G. L. Scherphof, J. W. M. van der Meer, F. H. M. Corstens, O. C. Boerman, *J. Pharmacol. Exp. Ther.* **2000**, *292*, 1071.
[29] T. Ishida, M. Harada, X. Y. Wang, M. Ichihara, K. Irimura, H. Kiwada, *J. Controlled Release* **2005**, *105*, 305.
[30] R. P. Garay, J. P. Labaune, *Open Conf. Proc. J.* **2011**, *2*, 104.
[31] H. F. Smyth, C. P. Carpenter, C. S. Weil, *J. Am. Pharm. Assoc., Sci. Ed.* **1950**, *39*, 349.

[32] A. Chanan-Khan, J. Szebeni, S. Savay, L. Liebes, N. M. Rafique, C. R. Alving, F. M. Muggia, *Ann. Oncol.* **2003**, *14*, 1430.
[33] J. Szebeni, *Toxicology* **2005**, *216*, 106.
[34] J. Szebeni, L. Baranyi, S. Sávay, M. Bodó, J. Milosevits, C. R. Alving, R. Bünger, *Am. J. Physiol.: Heart Circ. Physiol.* **2006**, *290*, H1050.
[35] S. M. Moghimi, I. Hamad, T. L. Andresen, K. Jørgensen, J. Szebeni, *FASEB J.* **2006**, *20*, 2591.
[36] J. Szebeni, L. Baranyi, S. Savay, J. Milosevits, R. Bunger, P. Laverman, J. M. Metselaar, G. Storm, A. Chanan-Khan, L. Liebes, F. M. Muggia, R. Cohen, Y. Barenholz, C. R. Alving, *J. Liposome Res.* **2002**, *12*, 165.
[37] P. H. Kierstead, H. Okochi, V. J. Venditto, T. C. Chuong, S. Kivimae, J. M. J. Fréchet, F. C. Szoka, *J. Controlled Release* **2015**, *213*, 1.
[38] Y.-C. Hsieh, H.-E. Wang, W.-W. Lin, S. R. Roffler, T.-C. Cheng, Y.-C. Su, J.-J. Li, C.-C. Chen, C.-H. Huang, B.-M. Chen, J.-Y. Wang, T.-L. Cheng, F.-M. Chen, *Theranostics* **2018**, *8*, 3164.
[39] R. P. Garay, R. El-Gewely, J. K. Armstrong, G. Garratty, P. Richette, *Expert Opin. Drug Delivery* **2012**, *9*, 1319.
[40] K. Knop, R. Hoogenboom, D. Fischer, U. S. Schubert, *Angew. Chem., Int. Ed.* **2010**, *49*, 6288.
[41] O. K. Nag, V. Awasthi, *Pharmaceutics* **2013**, *5*, 542.
[42] K. R. Whiteman, V. Subr, K. Ulbrich, V. P. Torchilin, *J. Liposome Res.* **2001**, *11*, 153.
[43] V. P. Torchilin, T. S. Levchenko, K. R. Whiteman, A. A. Yaroslavov, A. M. Tsatsakis, A. K. Rizos, E. V. Michailova, M. I. Shtilman, *Biomaterials* **2001**, *22*, 3035.
[44] J. M. Metselaar, P. Bruin, L. W. T. de Boer, T. de Vringer, C. Snel, C. Oussoren, M. H. M. Wauben, D. J. A. Crommelin, G. Storm, W. E. Hennink, *Bioconjugate Chem.* **2003**, *14*, 1156.
[45] M. Barz, R. Luxenhofer, R. Zentel, M. J. Vicent, *Polym. Chem.* **2011**, *2*, 1900.
[46] B. Weber, C. Seidl, D. Schwiertz, M. Scherer, S. Bleher, R. Süss, M. Barz, *Polymers* **2016**, *8*, 427.
[47] B. Weber, A. Birke, K. Fischer, M. Schmidt, M. Barz, *Macromolecules* **2018**, *51*, 2653.
[48] A. Birke, J. Ling, M. Barz, *Prog. Polym. Sci.* **2018**, *81*, 163.
[49] S. Sieber, P. Grossen, J. Bussmann, F. Campbell, A. Kros, D. Witzigmann, J. Huwyler, *Adv. Drug Delivery Rev.* **2019**.
[50] M. L. Immordino, F. Dosio, L. Cattel, *Nanomedicine* **2006**, *1*, 297.
[51] M. C. Smith, R. M. Crist, J. D. Clogston, S. E. McNeil, *Anal. Bioanal. Chem.* **2017**, *409*, 5779.
[52] F. Campbell, F. L. Bos, S. Sieber, G. Arias-Alpizar, B. E. Koch, J. Huwyler, A. Kros, J. Bussmann, *ACS Nano* **2018**, *12*, 2138.
[53] S. Sieber, P. Grossen, P. Detampel, S. Siegfried, D. Witzigmann, J. Huwyler, *J. Controlled Release* **2017**, *264*, 180.
[54] S. Sieber, P. Grossen, P. Uhl, P. Detampel, W. Mier, D. Witzigmann, J. Huwyler, *Nanomed.: Nanotechnol., Biol. Med.* **2019**, *17*, 82.
[55] A. Chonn, P. R. Cullis, D. V. Devine, *J. Immunol.* **1991**, *146*, 4234.
[56] G. R. Bartlett, *J. Biol. Chem.* **1959**, *234*, 466.
[57] D. L. Iden, T. M. Allen, *Biochim. Biophys. Acta, Biomembr.* **2001**, *1513*, 207.
[58] T. Ishida, D. L. Iden, T. M. Allen, *FEBS Lett.* **1999**, *460*, 129.
[59] C. Drechsler, M. Markones, J.-Y. Choi, N. Frieling, S. Fiedler, D. R. Voelker, R. Schubert, H. Heerklotz, *Biophys. J.* **2018**, *115*, 1509.
[60] M. Holzer, S. Barnert, J. Momm, R. Schubert, *J. Chromatogr. A* **2009**, *1216*, 5838.
[61] S. Sieber, S. Siegrist, S. Schwarz, F. Porta, S. H. Schenk, J. Huwyler, *Macromol. Biosci.* **2017**, *17*, 1700015.
[62] S. Bolte, F. P. Cordelières, *J. Microsc.* **2006**, *224*, 213.
[63] E. M. Manders, J. Stap, G. J. Brakenhoff, R. van Driel, J. A. Aten, *J. Cell Sci.* **1992**, *103*, 857.
[64] S. M. Moghimi, I. Hamad, *J. Liposome Res.* **2008**, *18*, 195.

5.4 Chapter 4

5.4.1 Chapter 4.1

Bacteria vs. antibiotics – Bridging infection modeling in Danio rerio

Jonas Buck, Patrick Hauswirth, Sandro Sieber, Beatrice Claudi, Dirk Bumann, Jörg Huwyler.

Manuscript ready for submission.

Highlights: Growing inefficiency of known antibiotic compounds towards pathogenic microorganism is a serious problem and the development of novel antibiotic compounds is very expensive. The zebrafish embryo animal model can serve as a tool to bridge the gap between *in vitro* and *in vivo* experiments in the development of nanomedicines. Here we describe the establishment of a zebrafish embryo *Salmonella* infection model for the screening of antibiotic compounds. Various model parameters (*i.e.*, the bacteria dose, the site of injection and temperature) were investigated. The optimized model was validated using two antibiotic compounds and could discriminate the antibiotics based on physicochemical properties of these compounds.

Bacteria vs. antibiotics – Bridging infection modeling in Danio rerio

Authors: J. Buck[1], P. Hauswirth[1], S. Sieber[1], Beatrice Claudi[2], Dirk Bumann[2], Jörg Huwyler[1*]

1 Department of Pharmaceutical Sciences, Division of Pharmaceutical Technology, University of Basel, Switzerland

2 Biozentrum, University of Basel, Switzerland

*suggested Journals: Science Advances: https://advances.sciencemag.org/content/5/11/eaax0063 , https://advances.sciencemag.org/content/4/8/eaat1273,

Or: Cell host & microbe, PLoS pathogen

*corresponding author. Email: Joerg.huwyler@unibas.ch

Abstract

Growing inefficiency of antimicrobial compounds due to increasingly emerging antibiotic resistance has the potential to become one of the most serious challenges in modern medical practice. Due to poor biodistribution and pharmacokinetic properties *in vitro* test often do not mirror the efficiency of antibiotic compounds *in vivo*. A significant contributor to the low number of newly introduced antibiotic compounds is high costs of animal trials. This study presents the generation and evaluation of a novel bridging, animal infection model using zebrafish embryos. Zebrafish embryos were chosen due to their transparency, allowing fluorescence-based methods to assess the progression of the infection. The investigation included different doses of bacteria, different sites of injection, different temperatures and the antibiotics ceftriaxone and tobramycin. The resulting model is tunable to a certain degree and allows to discriminate between different antibiotic interventions and can thereby be used as a valuable screening tool for novel antibiotic compounds.

Introduction

Salmonella is the leading cause of bloodstream infections in low- and middle-income countries and costs millions of lives each year across the globe every year.[1] Based on epidemiological data it represent a major health burden. Salmonella enterica spp. are extremely versatile and can infect different hosts. Moreover, Salmonella can survive and even replicate intracellularly within Salmonella containing vacuoles (SCV) in many cellular types including macrophages.[2] This information is especially problematic because a number of regularly used antibiotics is unable to cross cell membranes and therefore cannot reach their site of action (i.e. within macrophages).[3] After termination of the antibiotic intervention, these persistent intracellular pathogens can reemerge and lead to a fatal reinfection of the organism. Another serious problem is the growing development of antibiotic resistance (ABR) towards a large number the currently used antibiotics.[4] This phenomenon in combination with a very limited number of novel antibiotic compounds introduced into medical practice [5], [6] is a serious concern and burden for healthcare systems. It is even hypothesized that these developments could lead to a post-antibiotic era in which bacterial infectious diseases could reemerge as one of the leading causes of death like in the pre-antibiotic era.[6]–[8] Consequently, there is an urgent need for novel antibiotics or treatment regimens to avoid such a scenario. However, the development of antibiotics is expensive, however return of investment is relatively small, as efficient antibiotics rarely do get used in the end.[9] In addition to *in vitro* testing, novel antibiotics need to prove effectiveness in expensive *in vivo* trials. To reduce the costs of development of novel antibiotic compounds or treatment regimens and to increase the throughput of compound screenings, the zebrafish embryo animal model is suggested here as a viable alternative to costly rodent animal trials. Due to its unique properties, the zebrafish embryo animal model was already proposed as an early-stage screening tool to study the circulation behavior and macrophage clearance of nanoparticulate drug delivery systems.[10]–[12] The

zebrafish embryo animal model allows for fluorescence-based imaging (confocal) due to its transparency and for high throughput due to its high reproduction rate. Moreover, zebrafish embryos are classified as cell culture trials up to 5 days post-fertilization, thereby avoiding the administrative efforts associated with animal trials.[13] Furthermore, besides qualitative data from confocal imaging, survival analysis allows for quantification of the observed effects. It was therefore the aim of the present study to generate a zebrafish embryo infection model and to evaluate it as potential screening tool for antibiotic compounds

Results and Discussion

In order to develop and verify a Salmonella infection model in zebrafish embryos, the first important question to be answered was the number of colony-forming units (CFU) that need to be injected. A series of 30.000, 20.000, 10.000, 7.500, 5.000, 3.000, and 1.500 CFU were injected into zebrafish embryos and the fish were kept at 28°C.

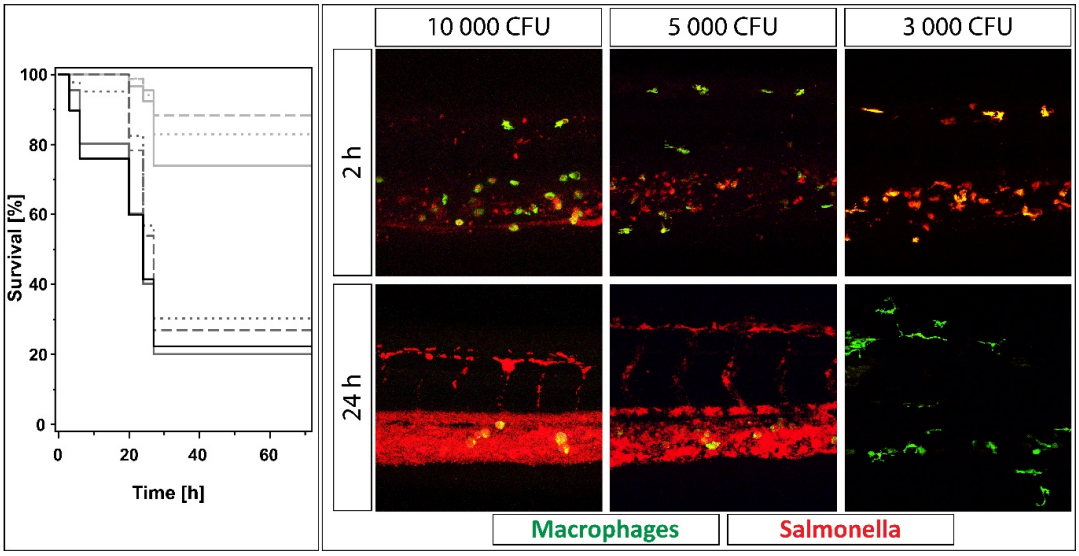

Figure 1: Evaluation of the dose of injected bacteria. The confocal images on the right side show representative images of different doses of bacteria after 2 and 24 h. While the fish survive a dose of 3.000 CFU, higher doses are associated with massive replication of bacteria within the vasculature after 24 h. The Kaplan-Meier survival plot on the left side shows the survival of zebrafish treated with different doses of bacteria. Light grey dotted line: 1.500 CFU, light grey dashed line: 3.000 CFU, light grey solid line: 5.000 CFU, dark grey dotted line: 7.500 CFU, dark grey dashed line: 10.000 CFU, dark grey solid line: 20.000 CFU, black solid line: 30.000 CFU. While 1.500 CFU, 3.000 CFU, and to a certain extent 5.000 CFU are still well tolerated, higher doses are associated with rapid death of fish. The survival analysis showed a dose-dependency.

At low dose low-dose injections (3.000 CFU, but also 1.500 CFU) Salmonella were still easily detectable within the whole zebrafish embryo using confocal imaging (Figure 1; An overview of the zebrafish and the location where imaging was carried out is provided by Supplementary Figure S1) Especially after

2 h and in the low CFU settings, most macrophages were infected with Salmonella as indicated by the fluorescence colocalization of the green (GFP of the macrophages) and the red (mCherry of Salmonella) dye, resulting in yellow color. Salmonella were efficiently cleared from the circulation by the zebrafish innate immune system and only present in macrophages after 24 h at a dose of 3.000 CFU. Furthermore, there was a clear dose-dependency of the survival. Doses higher than 5.000 CFU lead to rapid death of fish within 24 h. However, such high doses might not properly reflect the situation *in vivo.* Therefore, the next experiments were carried out at 28°C and with 1.500 CFU injected. The next question was whether it is possible to increase the number of infected macrophages and reduce the number of bacteria in circulation compared to the previous trials using different injection sites, such as the neural tube (a zebrafish embryo scheme depicting the injection sites is provided by Supplementary Figure S2). In order to study the intracellular infection, the vasculature of the fish should ideally be free of bacteria and all the bacteria present only in the macrophages. This way, the influence of bacteria replication within the vasculature on the survival of zebrafish embryos can be minimized and the influence of bacteria replication within macrophages can be maximized.

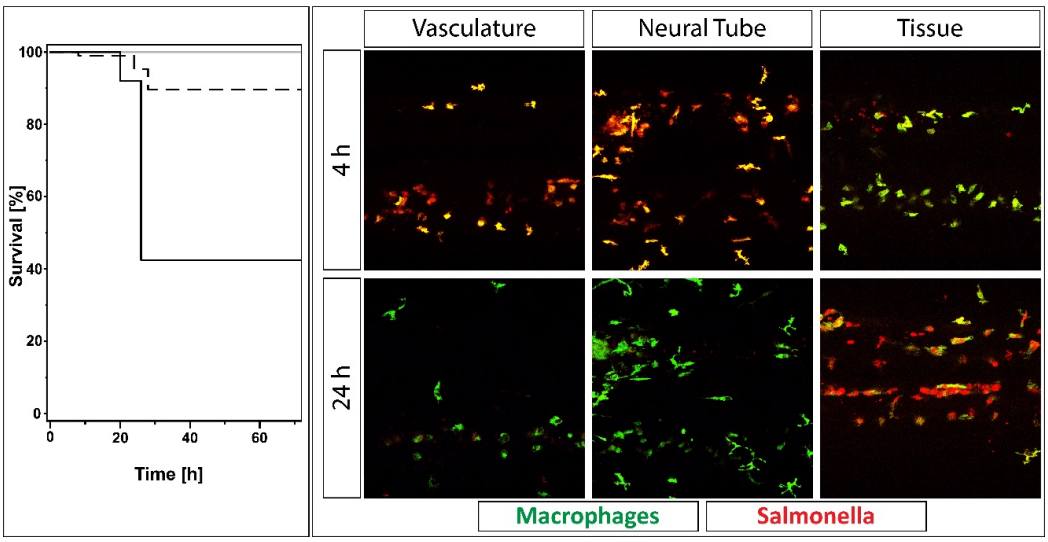

Figure 2: Site of injection evaluation. The figure shows representative confocal images and the survival analysis for the three injection sites (Vasculature refers to the Duct of Cuvier). A fluorescence colocalization of the green (GFP, macrophages) and red (mCherry, Salmonella) is indicated by yellow color. Predominant accumulation of bacteria within macrophages was observed with the neural tube injection and vasculature injection while. Neural tube injection was associated with complete survival while tissue injection showed the lowest survival which is reflected by confocal imaging. The survival plot on the left side shows the survival following neural tube injection (solid light grey line), vasculature injection (dashed black line), and tissue injection (solid black line).

The evaluation of the site of injection showed that injections into the neural tube led to almost exclusive accumulation of bacteria in tissue macrophages whereas the difference between tissue injection and vasculature (Duct of Cuvier) injection was only minor (Figure 2.) However, with respect to survival,

zebrafish subjected to neural tube injection showed complete survival. This leaves no space for improvement. Therefore, and because neural tube injection is very delicate and difficult to reproduce, the neural tube injection was discarded. Similarly to neural tube injection, because tissue injection is hardly reproducible and has the potential for severe injury of the zebrafish while offering no clear benefit, further experiments were carried out using vasculature injection. We observed that bacterial replication was hampered when fish were kept at 28ºC. Optimally fish would be kept at 37ºC, however at this temperature all fish died. 35ºC was therefore selected as a bridging temperature to allow both fish survival and bacterial growth. The results of this trial showed that the injected dose needs to be massively reduced due to the accelerated replication of bacteria at this temperature compared to 28°C.

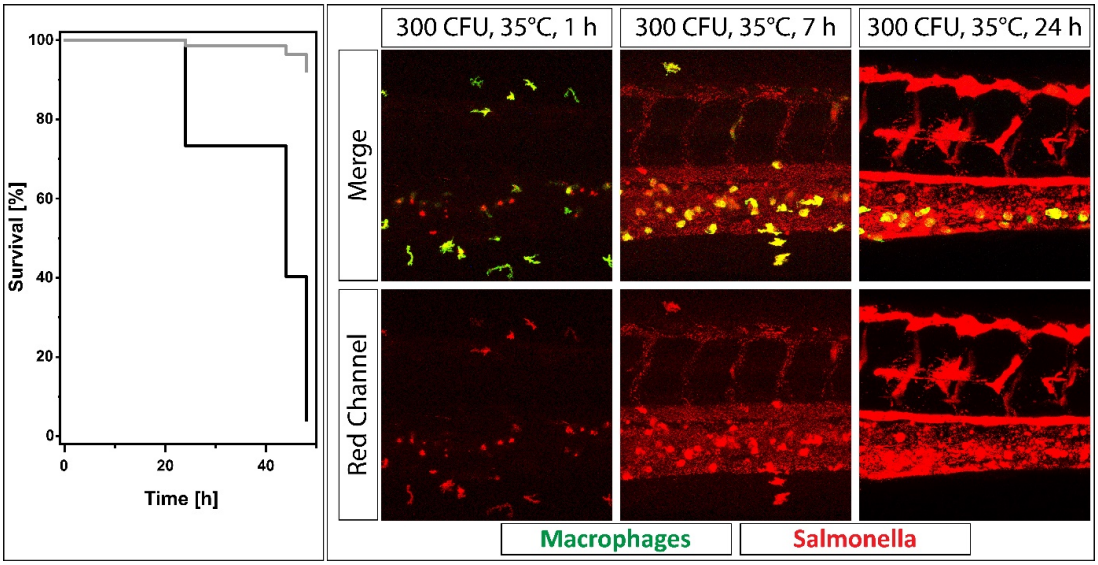

Figure 3: Temperature evaluation. The figure shows confocal images (right) and the survival analysis (upper left) of zebrafish embryos injected with 300 CFU and maintained at 35°C. Despite the lower dose injected into zebrafish embryos, Salmonella replication is accelerated due to the higher temperature. Consequently, images taken after 24 h are similar for 300 CFU at 35°C and 5.000 - 10.000 CFU at 28°C. Moreover, survival analysis showed a lower survival at 35°C (solid black line) compared to zebrafish maintained at 28°C (solid grey line), which reflects the observations during confocal imaging well.

The results of the temperature evaluation showed that zebrafish embryos survive well at 35°C but that the injected dose needs to be massively reduced (Figure 3). In order not to kill the majority of zebrafish embryos within the first few hours, the injected dose had to be reduced to 300 CFU (as compared to 3000 or 1500 CFU at 28ºC). At 35°C, confocal images taken after 24 h were very similar to images taken at the same time with 3.000 CFU at 28°C. However, it is important to note that at 35°C the development of zebrafish embryos or larvae is visibly accelerated. Therefore, further experiments were terminated after a maximum of 48 h to avoid conflicts with the animal trial regulations. After establishment of the model parameters, the validation of the model was carried out using the two antibiotics ceftriaxone and tobramycin. Ceftriaxone (logP = -1.7[14]) exhibits a higher membrane

permeability[15] than tobramycin (logP = -5.8[16]). Consequently, treatment with ceftriaxone is expected to eradicate all bacteria whereas treatment with tobramycin is expected not to kill bacteria persistent within macrophages. The results of the ceftriaxone and tobramycin trials are displayed in Figure 4.

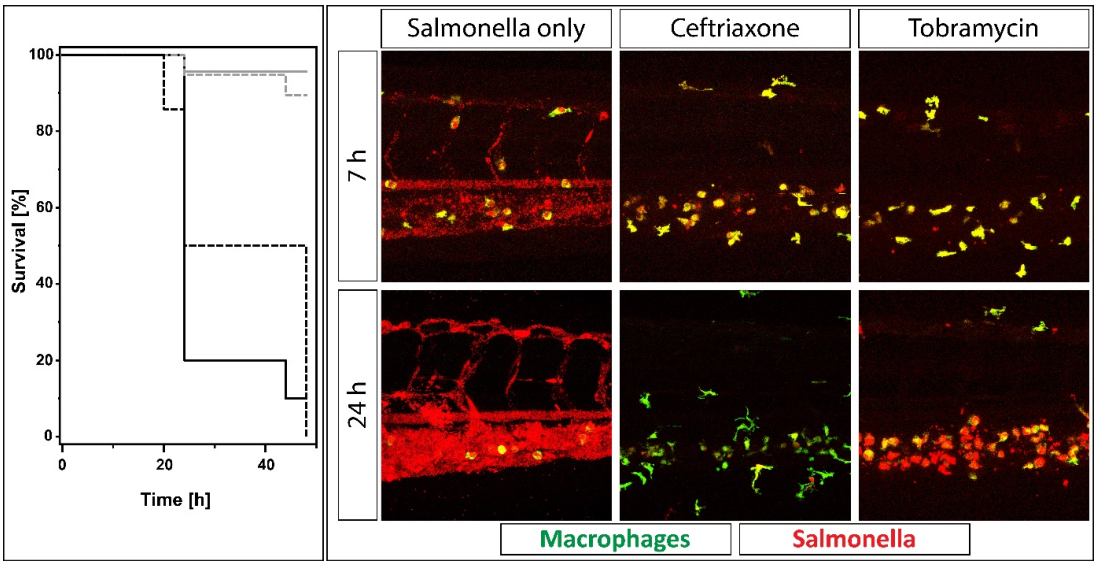

Figure 4: Treatment of Salmonella infection with ceftriaxone or tobramycin. The figure shows confocal images (right side) of Salmonella infected zebrafish (300 CFU) treated with either ceftriaxone or tobramycin (both 600 pg/zebrafish). Confocal imaging allows for a qualitative and survival analysis (left) for a quantitative assessment. Solid light grey line: Untreated zebrafish; Dashed dark grey line: Ceftriaxone; Dashed black line: Tobramycin; Solid black line: Salmonella only. Ceftriaxone was highly efficient in bacteria eradication with almost 100% survival at 24h. Furthermore, bacteria in circulation were almost completely eradicated. Tobramycin on the other hand was unable to eradicate bacteria in circulation and macrophages, leading to a survival of around 50% after 24 h.

The results of the validation trials were able to reflect the different permeabilities of the two antibiotic compounds. While ceftriaxone-treated zebrafish showed a high survival and almost no residual bacteria in circulation or macrophages, tobramycin-treated zebrafish showed a much lower survival of around 50% after 24 h and confocal imaging revealed that the fish were still infected with a large number of bacteria. Moreover, large red dots indicate Salmonella replication within macrophages followed by a burst of the macrophages and subsequent reemergence of Salmonella infection in the vasculature. The presented zebrafish animal infection model is capable of discrimination between the two different antibiotics. Moreover, during this study, Salmonella infections of zebrafish were highly reproducible. Conclusively, the presented model is suitable for testing of novel antibiotic compounds and can be a valuable alternative screening tool for preselection of promising candidates prior to expensive trials in higher vertebrate species.

Conclusion

Growing emergence of antibiotic resistance has the potential to become one of the major burdens for healthcare systems in the 21st century. The search for novel antibiotics is expensive and revenues are at risk to be further reduced due to increasingly strict regulations. A large contributor to high costs are expensive animal trials. We successfully developed a zebrafish animal infection model for the evaluation of novel antibiotic compounds. The zebrafish embryo is an inexpensive animal model that allows for high-throughput screening and fluorescence-based evaluation. We therefore believe that the presented model can be a valuable tool in basic research for novel antibiotic compounds, antibiotic adjuvants, or treatment regimens.

Materials and Methods

Zebrafish embryos (Danio rerio) were obtained from adult Tg(mpeg1:Gal4;UAS:Kaede)[17], [18] fish and were kept at 28°C in zebrafish culture medium supplemented with 1-phenyl-2-thiourea (PTU). Fish were kept in accordance with Swiss animal welfare regulations. 2 days post-fertilization (dpf) zebrafish embryos were dechorionized and injected with indicated amounts of the Salmonella strain SDB15 expressing mCherry. After indicated timepoints, infected zebrafish embryos were injected with indicated amounts of antibiotics, or adjuvant where applicable. Zebrafish were then kept at 35°C and at indicated timepoints, zebrafish were imaged using confocal microscopy and the survival was counted. The presence of heartbeat was chosen as the survival criterion. Zebrafish were injected in the Duct of Cuvier (if not stated differently) using a micromanipulator (Wagner Instrumentenbau KG, Schöffengrund, Germany), a pneumatic PicoPump PV830 (WPI, Sarasota, Florida), and a Leica S8APO microscope (Leica, Wetzlar, Germany). Confocal microscopy was carried out using a LEICA POINT SCANNING CONFOCAL “SP5-II-MATRIX“ (Leica, Wetzlar, Germany) equipped with a 25x HCX IRAPO L (NA 0.95) objective. Image analysis was carried out using Fiji ImageJ v. 1.52n. A minimum of three zebrafish embryos were imaged in all settings. Survival analysis was carried out using OriginPro 2018 (64-bit) SR1 b9.5.1.195 (Academic) Software (OriginLab Corporation, Northampton, MA, USA). A minimum of 15-20 zebrafish embryos were used for survival analysis.

Acknowledgements

We thank the Imaging Core facility (IMCF, University of Basel) and in particular Alexia Ferrand for the technical assistance provided on the confocal microscope.

References

[1] J. A. Crump, M. Sjölund-Karlsson, M. A. Gordon, and C. M. Parry, "Epidemiology, Clinical Presentation, Laboratory Diagnosis, Antimicrobial Resistance, and Antimicrobial Management of Invasive Salmonella Infections," *Clin. Microbiol. Rev.*, vol. 28, no. 4, pp. 901–937, Oct. 2015, doi: 10.1128/CMR.00002-15.

[2] P. Garai, D. P. Gnanadhas, and D. Chakravortty, "Salmonella enterica serovars Typhimurium and Typhi as model organisms," *Virulence*, vol. 3, no. 4, pp. 377–388, Jul. 2012, doi: 10.4161/viru.21087.

[3] P. J. Van Den Broek, P. S. Hiemstra, and C. Bril-Bazuin, "Uptake of antibiotics by monocytes and macrophages," in *Mononuclear Phagocytes: Biology of Monocytes and Macrophages*, R. van Furth, Ed. Dordrecht: Springer Netherlands, 1992, pp. 550–553.

[4] P. Guilfoile and I. E. Alcamo, *Antibiotic-Resistant Bacteria*. Infobase Publishing, 2007.

[5] M. S. Butler, M. A. Blaskovich, and M. A. Cooper, "Antibiotics in the clinical pipeline in 2013," *J. Antibiot. (Tokyo)*, vol. 66, no. 10, pp. 571–591, Oct. 2013, doi: 10.1038/ja.2013.86.

[6] M. E. Falagas and I. A. Bliziotis, "Pandrug-resistant Gram-negative bacteria: the dawn of the post-antibiotic era?," *Int. J. Antimicrob. Agents*, vol. 29, no. 6, pp. 630–636, Jun. 2007, doi: 10.1016/j.ijantimicag.2006.12.012.

[7] A. J. Alanis, "Resistance to Antibiotics: Are We in the Post-Antibiotic Era?," *Arch. Med. Res.*, vol. 36, no. 6, pp. 697–705, Nov. 2005, doi: 10.1016/j.arcmed.2005.06.009.

[8] C. T. Kåhrström, "Entering a post-antibiotic era?," *Nat. Rev. Microbiol.*, vol. 11, no. 3, pp. 146–146, Mar. 2013, doi: 10.1038/nrmicro2983.

[9] E. Power, "Impact of antibiotic restrictions: the pharmaceutical perspective," *Clin. Microbiol. Infect.*, vol. 12, no. s5, pp. 25–34, 2006, doi: 10.1111/j.1469-0691.2006.01528.x.

[10] S. Sieber, P. Grossen, P. Detampel, S. Siegfried, D. Witzigmann, and J. Huwyler, "Zebrafish as an early stage screening tool to study the systemic circulation of nanoparticulate drug delivery systems in vivo," *J. Control. Release Off. J. Control. Release Soc.*, vol. 264, pp. 180–191, Oct. 2017, doi: 10.1016/j.jconrel.2017.08.023.

[11] S. Sieber *et al.*, "Zebrafish as a predictive screening model to assess macrophage clearance of liposomes in vivo," *Nanomedicine Nanotechnol. Biol. Med.*, vol. 17, pp. 82–93, 2019, doi: 10.1016/j.nano.2018.11.017.

[12] S. Sieber *et al.*, "Zebrafish as a preclinical in vivo screening model for nanomedicines," *Adv. Drug Deliv. Rev.*, vol. 151–152, pp. 152–168, Nov. 2019, doi: 10.1016/j.addr.2019.01.001.

[13] R. Geisler, A. Köhler, T. Dickmeis, and U. Strähle, "Archiving of zebrafish lines can reduce animal experiments in biomedical research," *EMBO Rep.*, vol. 18, no. 1, pp. 1–2, Jan. 2017, doi: 10.15252/embr.201643561.

[14] PubChem, "Ceftriaxone." [Online]. Available: https://pubchem.ncbi.nlm.nih.gov/compound/5479530. [Accessed: 04-Mar-2020].

[15] B. J. Bennion *et al.*, "Predicting a Drug's Membrane Permeability: A Computational Model Validated With in Vitro Permeability Assay Data," *J. Phys. Chem. B*, vol. 121, no. 20, pp. 5228–5237, May 2017, doi: 10.1021/acs.jpcb.7b02914.

[16] PubChem, "Tobramycin." [Online]. Available: https://pubchem.ncbi.nlm.nih.gov/compound/36294. [Accessed: 04-Mar-2020].

[17] F. Ellett, L. Pase, J. W. Hayman, A. Andrianopoulos, and G. J. Lieschke, "mpeg1 promoter transgenes direct macrophage-lineage expression in zebrafish," *Blood*, vol. 117, no. 4, pp. e49–e56, Jan. 2011, doi: 10.1182/blood-2010-10-314120.

[18] E. K. Scott *et al.*, "Targeting neural circuitry in zebrafish using GAL4 enhancer trapping," *Nat. Methods*, vol. 4, no. 4, pp. 323–326, Apr. 2007, doi: 10.1038/nmeth1033.

Supporting Information

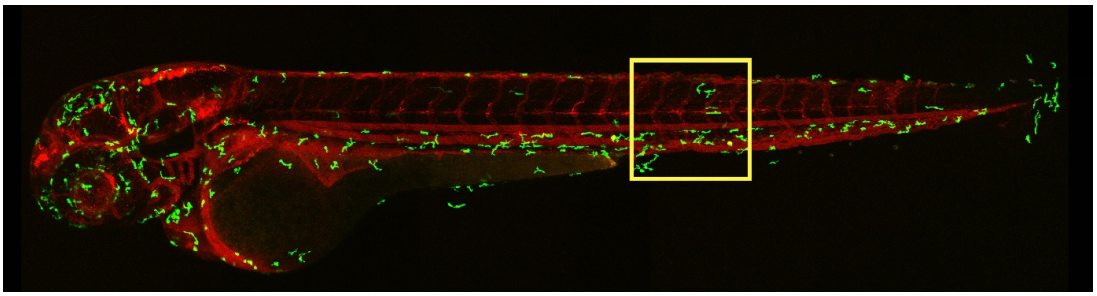

Figure S1: Overview image of the zebrafish embryo animal model. The yellow box indicates the location where zebrafish imaging was carried out. The picture shows the macrophages (green) and a freely-circulating DiI-labeled liposomal formulation (red) to visualize the vasculature.

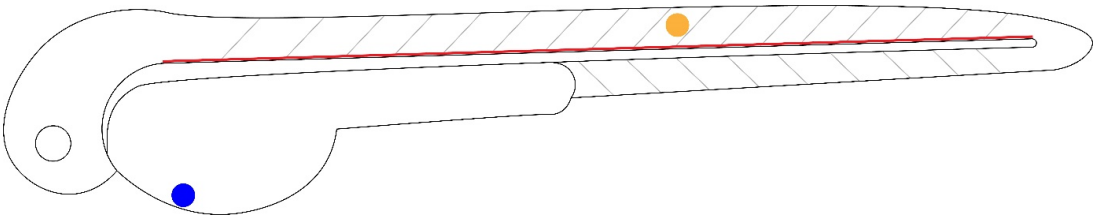

Figure S2: Zebrafish embryo scheme depicting the different injection sites. The scheme shows the three different injection sites. Blue: Injection into the Duct of Cuvier (termed vasculature injection in this study); Yellow: Injection into the tissue; Red: Injection into the neural tube, a tiny tube directly above the spinal cord.

5.4.2 Chapter 4.2

The Use of 4-Hexylresorcinol as Antibiotic Adjuvant

Y.A. Nikolaev, A.V. Tutel'yan, N.G. Loiko, **J. Buck**, S.V. Sidorenko, I. Lazareva, V. Gostev, O.Y. Manzen'yuk, I.G. Shemyakin, R. A. Abramovich, J. Huwyler, G. I. El'-Registan.

Manuscript submitted to PLOS One

Highlights: Emergence of antibiotic resistance in pathogenic bacteria is a severe problem. Many attempts have been made to overcome the widespread development of antibiotic resistances. The two most promising approaches include the search for novel antibiotic compounds and the search for substances that potentiate the effect of already existing antibiotics (antibiotic adjuvants). In this study, we investigated the potential use of 4-hexylresorcinol (4-HR), an alkylresorcinol, as antibiotic adjuvant to improve the effect of various antibiotics against a selection of microorganisms. We could demonstrate that 4-HR significantly reduced minimum inhibitory concentrations (MICs) of various antibiotics. The combination of 4-HR and antibiotics even reestablished susceptibility of bacteria to antibiotics against which they had already acquired antibiotic resistance and was highly efficient in eradication of persister cells. Moreover, *in vivo* experiments in mice showed high cure rates and even complete sanitation (absence of pathogenic microorganisms) of test animals in 75% of all cases.

PLOS ONE

RESEARCH ARTICLE

The use of 4-Hexylresorcinol as antibiotic adjuvant

Y. A. Nikolaev[1]*, A. V. Tutel'yan[2], N. G. Loiko[1], J. Buck[3], S. V. Sidorenko[5,6], I. Lazareva[5,6], V. Gostev[5,6], O. Y. Manzen'yuk[7], I. G. Shemyakin[7], R. A. Abramovich[4], J. Huwyler[3], G. I. El'-Registan[1]

1 Federal Research Centre "Fundamentals of Biotechnology", Russian Academy of Sciences, Moscow, Russia, **2** Central Research Institute of Epidemiology of Russian Federal Service for Surveillance on Consumer Rights Protection and Human Wellbeing (Rospotrebnadzor) and I.M. Sechenov First Moscow State Medical University of the Ministry of Health of the Russian Federation (Sechenov University), Moscow, Russia, **3** Department of Pharmaceutical Sciences, University of Basel, Basel, Switzerland, **4** Peoples' Friendship University of Russia (RUDN University), Moscow, Russia, **5** Pediatric Research and Clinical Center for Infectious Diseases, Saint Petersburg, Russia, **6** I.I. Mechnikov North Western State Medical University, St Petersburg, Russia, **7** State Research Center for Applied Microbiology and Biotechnology of Russian Federal Service for Surveillance on Consumer Rights Protection and Human Welfare (Rospotrebnadzor), Obolensk, Russia

* nikolaevya@mail.ru

Citation: Nikolaev YA, Tutel'yan AV, Loiko NG, Buck J, Sidorenko SV, Lazareva I, et al. (2020) The use of 4-Hexylresorcinol as antibiotic adjuvant. PLoS ONE 15(9): e0239147. https://doi.org/10.1371/journal.pone.0239147

Editor: Surajit Bhattacharjya, Nanyang Technological University, SINGAPORE

Received: April 24, 2020

Accepted: August 31, 2020

Published: September 22, 2020

Data Availability Statement: All relevant data are within the manuscript and its Supporting Information files.

Funding: This work was supported by internal funding from the Russian Academy of Sciences and the University of Basel. JB and JH were supported by the Swiss National Science Foundation (SNF grant No. 173057).

Competing interests: The authors have declared that no competing interests exist.

Abstract

Ever decreasing efficiency of antibiotic treatment due to growing antibiotic resistance of pathogenic bacteria is a critical issue in clinical practice. The two generally accepted major approaches to this problem are the search for new antibiotics and the development of antibiotic adjuvants to enhance the antimicrobial activity of known compounds. It was therefore the aim of the present study to test whether alkylresorcinols, a class of phenolic lipids, can be used as adjuvants to potentiate the effect of various classes of antibiotics. Alkylresorcinols were combined with 12 clinically used antibiotics. Growth-inhibiting activity against a broad range of pro- and eukaryotic microorganisms was determined. Test organisms did comprise 10 bacterial and 2 fungal collection strains, including *E. coli* and *S. aureus*, and clinical isolates of *K. pneumoniae*. The highest adjuvant activity was observed in the case of 4-hexylresorcinol (4-HR), a natural compound found in plants with antimicrobial activity. 50% of the minimal inhibitory concentration (MIC) of 4-HR caused an up to 50-fold decrease in the MIC of antibiotics of various classes. Application of 4-HR as an adjuvant revealed its efficiency against germination of bacterial dormant forms (spores) and prevented formation of antibiotic-tolerant persister cells. Using an *in vivo* mouse model of *K. pneumoniae*-induced sepsis, we could demonstrate that the combination of 4-HR and polymyxin was highly effective. 75% of animals were free of infection after treatment as compared to none of the animals receiving the antibiotic alone. We conclude that alkylresorcinols such as 4-HR can be used as an adjuvant to increase the efficiency of several known antibiotics. We suggest that by this approach the risk for development of genetically determined antibiotic resistance can be minimized due to the multimodal mode of action of 4-HR.

Introduction

Growing inefficiency of known medical preparations due to antibiotic resistance (ABR) of pathogenic microorganisms is a serious problem. [1] Mechanisms of ABR and approaches to minimize (or prevent) these phenomena are therefore a focus of basic research in antibiotic therapy.

ABR may emerge as a result of mutagenesis with subsequent inheritance of genetic determinants, or acquisition of antibiotic resistance determinants via lateral transfer between microorganisms. Overcoming ABR is an important albeit difficult task. [2] Historically, research on suppression of antibiotic resistance and enhancement of the efficiency of antibiotic treatment mainly focused on the search for new antibiotics. However, the number of new antibiotics introduced into medical practice is quite low, with only two new antibiotics registered during the 2000-2013 period. [3] Development of new drug products by combining established or new antibiotics may partially compensate for this insufficient introduction of new compounds. Such combinations may consist of antibiotic hybrids [4] or combinations of two or more antimicrobial agents with different targets in microbial cells to exploit synergistic effects. [5] Alternatively, the effect of an antibiotics can be enhanced by concomitant interference with mechanisms of bacterial resistance. For example, clavulanic acid inhibits beta-lactamases, the enzymes degrading beta-lactam antibiotics, and thus increases the effect of the latter. [6, 7] Substances such as clavulanic acid are adjuvants. They have *per se* no (or only a limited) antibacterial activity but they nevertheless potentiate the effect of antibiotics. [8–11]

Another mechanism of therapy evasion consists of emergence of a small subpopulation of nondividing persister cells in a growing microbial population. [12–18] Persister cells are by definition insensitive (tolerant) to antibiotics. Such cells survive an antimicrobial intervention, germinate after termination of the treatment, and form a new population of antibiotic-sensitive cells. They will have similar properties as the original population and are similarly capable of forming persister cells again. [12–15, 18] The phenotypic transition from a vegetative to a persistent state is associated with development of stress responses and mutations due to low-accuracy reparation of damaged DNA. It should be noted that in the case of resistance-related mutations, this may lead to emergence of genetically determined (inherited) ABR. [19]. More recently, approaches to minimize the formation of persister cells or to prevent germination were introduced. [8, 20–22] Persisters may be targeted by antibiotics or combined antimicrobial preparations either at the stage of their formation, in order to minimize their numbers, [23] or at the stage of their germination, in order to sensitize them to the action of antibiotics and to prevent reverse phenotypic transition. For example, quorum-sensing autoinducer AIA-1 potentiates the therapeutic effect of an antibiotic during treatment of experimental murine *Pseudomonas aeruginosa* infection by decreasing the numbers of antibiotic-tolerant persister cells. [23]

It was the aim of the present study to identify novel antibiotic adjuvants to enhance the effect of various classes of antibiotics. Our work was based on two assumptions: decreased metabolic activity in the cells of pathogenic microorganisms caused by an adjuvant will result in suppressed mechanisms of antibiotic resistance and minimization of the number of surviving persister cells (up to their possible elimination). This will decrease the risk of reinfection and the formation of genetic resistance determinants. Alkylresorcinols were identified to have the required properties. These phenolic lipids are secondary metabolites of plants and can as well be found in some microorganisms. [24] They have a weak antimicrobial activity. 4-hexylresorcinol (4-HR) (Fig 1) is a synthetic derivative used as topical drug in antibacterial oral gargles and throat lozenges. [25] Recently, an incorporation of 4-HR within PLGA polymer composite films was proposed as a strategy to obtain biomedical and packaging products with

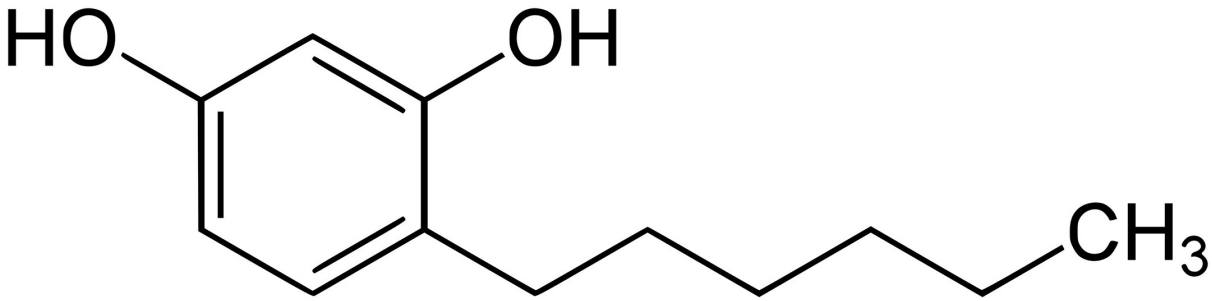

Fig 1. Chemical structure of 4-hexylresorcinol (4-HR). 4-hexylbenzene-1,3-diol has a molecular weight of 194.27 g/mol, a solubiliy in water of 800 mg/L, and an octanol-water partition coefficient of 3.9.

https://doi.org/10.1371/journal.pone.0239147.g001

antimicrobial properties. [25] In food industry, 4-HR is frequently used as a preservative and to prevent browning. [26] The widespread use in food industry and the antiseptic activity of 4-HR give rise to the assumption that 4-HR might be a safe adjuvant for antibiotic combination therapies.

Materials and methods

Alkylresorcinols

4-hexylresorcinol (Fig 1) was purchesed from Sigma- Aldrich (St. Louis, MO, USA) while other alkylresorcinols were provided by Carboshale Ltd. (Virumaa, Estonia). Phenolic lipids were added as stock solutions in ethanol (3% vol/vol) or dimethyl-sulfoxide (DMSO) (3% vol/vol).

Microorganisms

Nonpathogenic strains of pathogenic microorganisms such as gram negative *E. coli* K12 and gram positive *S. aureus* 209P were obtained from the fungal and bacterial collection of the All-Russian Collection of Microorganisms (Pushchino, Moscow Region, Russian Federation, see Table 1). For the chequerboard method and the *in vivo* experiments, the following strains from the collection of the Research Institute on Infant Infections (St. Petersburg, Russia) were

Table 1. Effect of 4-hexylresorcinol (4-HR) on a selection of various microorganisms. MIC values are means of two series of experiments.

Classification	Microorganism	Strain No.	MIC (mg/L)
Prokaryota (Gram positive)	*Bacillus subtilis*	VKM-B436	20
Prokaryota (Gram positive)	*Lactococcus lactis*	B-1662	20
Prokaryota (Gram positive)	*Micrococius luteus*	VKM-Ac2230	20
Prokaryota (Gram positive)	*Streptococcus faecalis*	B-602	20
Prokaryota (Gram positive)	*Staphylococcus aureus*	209P	25
Prokaryota (Gram positive)	*Streptomyces coelicolor*	Ac-738	30
Prokaryota (Gram positive)	*Lactobacillus acidophilus*	B-1660	50
Prokaryota (Gram negative)	*Pseudomonas carboxydaflava*	Z-1107	65
Prokaryota (Gram positive)	*Mycobacterium smegmatis*	Ac-1239	70
Prokaryota (Gram negative)	*Escherichia coli*	MC4100	200
Eukaryota	*Aspergillus niger*	F-2039	300
Eukaryota	*Saccharomyces cerevisiae*	Y-375	300

https://doi.org/10.1371/journal.pone.0239147.t001

used: *Staphylococcus aureus* ATCC 29213 (reference strain) and isolates MRSA *S. aureus* (SA0077, SA0206, SA0411 SA0318); clinical isolates *Enterococcus faecalis* E23 and E28; *Escherichia coli* ATCC 25922 (reference strain) and *Escherichia coli* isolates (1273, 1263); clinical isolates of *Klebsiella pneumoniae* (1191, 204, 895); *Pseudomonas aeruginosa* (1215, 56); *Acinetobacter baumannii* (121, 1308); as well as clinical isolate *Klebsiella pneumoniae* KPM9 from the collection of the State Research Center for Applied Microbiology and Biotechnology (Obolensk, Russia). Bacterial cultures were grown in LB medium for 18-20 hours. Fungal cultures were grown in wort medium for 36 hours (to the stationary growth phase). Second cycle cultures were inocculated and grown for 1 hour to the early exponential phase in 250 mL flasks with 50 mL of LB medium. Samples were dispensed (2 mL) into glass test tubes containing the indicated amounts of antibiotics and adjuvants (phenolic lipids). Starting concentration was 5 x 10^5 cells/mL. The test tubes were incubated for 24 hours at 30˚C on a rotary shaker (100 rpm) to determine the minimal growth-inhibiting concentrations (MIC) of saprophytic organisms or non-pathogenic strains of bacteria (Table 1). Bacterial growth was assessed spectrophotometrically by OD_{600} measurements on a Jenway Spectrophotometer 7315 (Jenway, Staffordshire, UK).

Determination of antibacterial activity of alkylresorcinols

The tested antibiotics are listed in S1 Table. The degree of prolongation of alkylresorcinol bactericidal action was determined by the use of a mixed culture of gram positive *B. subtilis*, gram negative *P. fluorescens*, and yeasts *S. cerevisiae*. Individual cultures were grown to the stationary phase and mixed in equal amounts to prepare the inoculum. The inoculum (5% vol/vol) was added to the medium consisting of a mixture (1:1) of LB medium and wort. Flasks were incubated and bacterial growth was assessed spectrophotometrically as described above.

Minimal growth-inhibiting concentrations (MIC)

Antibiotics were characterized by their minimal growth-inhibiting concentrations (MIC), which were determined for every test organism using conventional serial dilution in liquid media followed by plating. Phenolic lipids were used at concentrations of $\frac{1}{2}$ MIC; the latter was determined for each test organism. The criteria for adjuvant efficiency were as follows: decreased MIC of a given antibiotic in combination with AR ($\frac{1}{2}$ MIC), which was determined as the absence of growth of a test organism after 24 hour incubation in liquid medium; decreased number of viable persister cells (colony-forming units, CFU) retaining viability after 24 hour incubation at high antibiotic concentration (10 MIC and above, by [27]). CFU numbers were determined by plating serial ten-fold dilutions on agar (1.5%) LB medium. All values represent means of three independent sets of experiments with three repetitions each.

Chequerboard method

Stock solutions of the tested antibiotics were prepared to obtain two-fold serial dilutions in vertical rows 1-8 of a 96-well plate. 4-HR stock solutions were prepared to cover final concentrations of 8 to 512 μg/mL. 0.1 mL of antibiotic and/or 4-HR solution in broth (or broth only) was added to a well, then 0.1 mL of bacteria suspension was added to a final concentration of 5 x 10^5 cells/mL. Cultivation temperature was 35-37˚C. Results were assessed by measuring bacterial growth in the vertical and horizontal rows. MIC was defined as the minimal concentration at which bacterial growth was absent. The type of interaction of antibiotics (AB) and

4-HR was calculated using the FICI coefficient (Eq 1) as recommended: [28]

$$FICI = \frac{MIC(AB + 4 - HR)}{MIC(AB)} + \frac{MIC(AB + 4 - HR)}{MIC(4 - HR)} \quad (1)$$

Apart from the recommended coefficients, one more was introduced (K1), showing the MIC decrease for the monopreparation compared to the binary one:

$$K1 = \frac{MIC(AB)}{MIC(AB + 4 - HR)} \quad (2)$$

With K1 reflecting the decrease in the effective dose of antibiotic in the presence of an ineffective concentration of 4-HR.

K. pneumoniae KPM9 induced experimental sepsis

Outbred female white mice (18-21 g; Andreevka Farm, Scientific Center for Biomedical Technologies, Russia) were infected intraperitoneally by *K. pneumoniae* (clinical isolate KPM9) cell suspensions (0.5 mL, 50 × LD_{50}). The LD_{50} value was calculated according to Cerber in the modification by Ashmarin and Vorov'ev [29] according to survival duration after infection. The average LD_{50} values for *K. pneumoniae* KPM9 were 21 cells.

Mice were treated with polymyxin B (Pm; Bharat Sirams and Vaksins Ltd., India) and/or 4-HR. The doses were calculated as recommended. [29, 30] Treatment began 24 hours after infection (day 0). Pm was administered intramuscularly. 4-HR was administered *per os* twice a day for five days as as solution in 50% ethanol using an oral gavage needle (0.2 mL). Mice were monitored for 14 days. Criteria of treatment efficiency were survival and contamination of internal organs with bacteria (S3 Table). Severity of the infection was assessed using the overall condition of the animals (behavior, mobility, appetite, weight, and lymph node size). Surviving animals were euthanized, and bacteriological and postmortem study of their organs was carried out, including plating of the lungs, spleen, and blood samples onto solid HRM medium followed by a 48 hour incubation at 37˚C.

Laboratory animal welfare

Animals were kept under standard conditions according to guidelines of the US National Institutes of Health (NIH Publication No. 8023, revised 1978). Mice had free access to water and food (Laboratorkorm, Moscow, Russia) and were kept in polycarbonate cages (LabProducts, Seaford, DE) in groups of up to 10 animals. Animal health and behavior was monitored twice daily. Animals were handled by animal caretakers, which were trained in accordance to protocols established by the USAMRIID, WRIAR and UHSUS. Animal experiments were approved by the Bioethics Commission, State Research Center for Applied Microbiology & Biotechnology. Animal experiments involved fast spreading mice sepsis with a lethality of 100% without treatment within 5 days. Surviving animals were euthanized after 14 days. There is no alternative to these experiments since only an animal experiment can model all aspects of the bacterial infection [31, 32]. Studies were designed to measure survival percentages. In view of the severity and rapid progression of the infection, animals were bound to die from the disease. This provides a very small window of opportunity to intervene and to decide whether animals have reached a humane end point and should be euthanized. The number of animals was 60, 25 of which were found dead and 35 were euthanized.

Results

Antimicrobial activity of alkylresorcinols and phenolic lipids

Based on the hypothesis that phenolic lipids (Figs 1 and 2) can be used as adjuvants for antibiotic therapy, screening experiments were performed to study their impact on bacterial growth (MIC determinations) and subsequently synergistic effects with different classes of antibiotics (S1 Table). The MIC of phenolic lipid preparations were determined using as test organisms *S. aureus* 209P (a nonpathogenic *S. aureus* strain) and *M. smegmatis* AC-1239 (a nonpathogenic

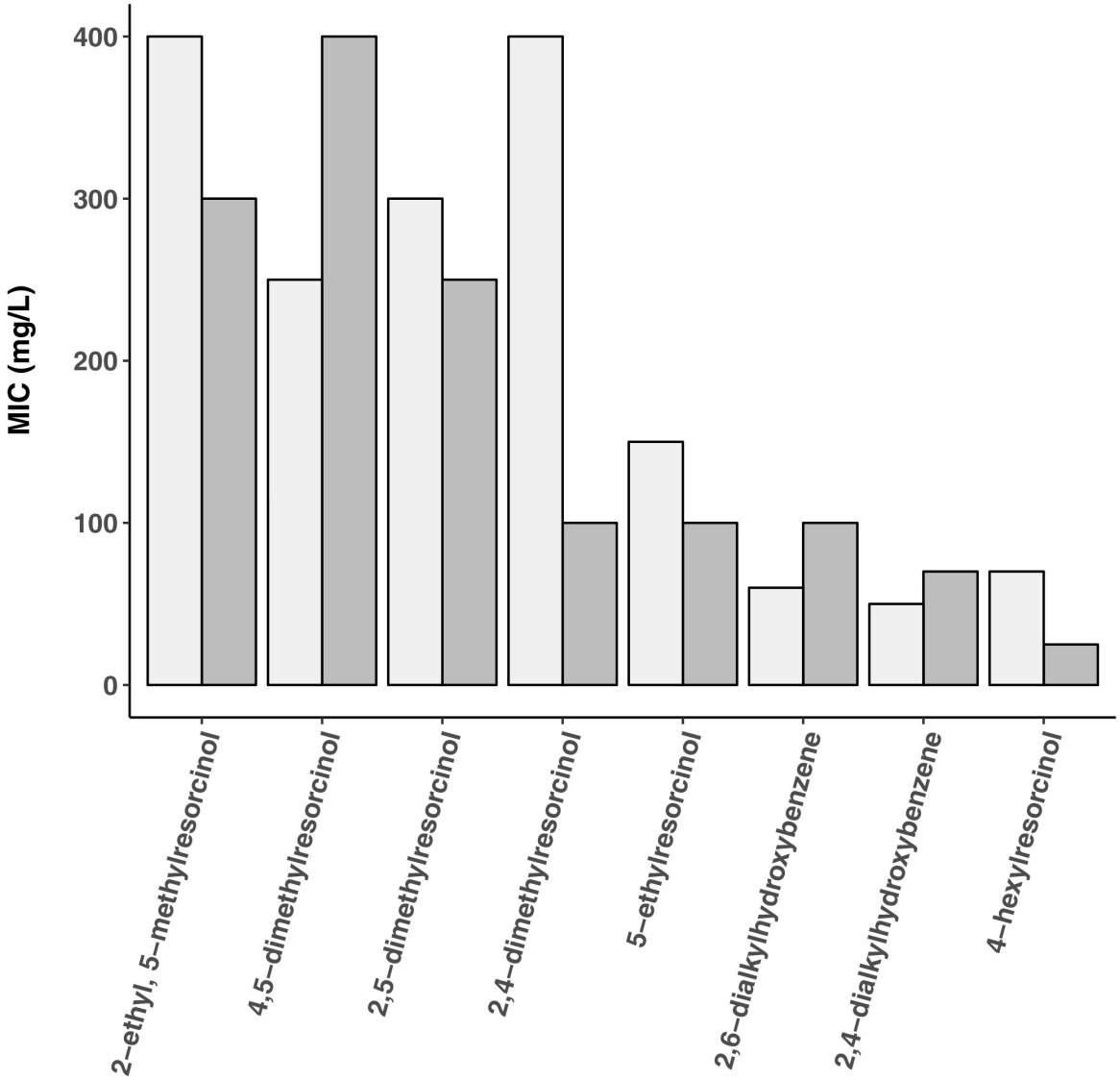

Fig 2. Minimal growth-inhibiting concentrations (MIC) of alkylresorcinols. 5-methylresorcinol showed poor activity against *M. smegmatis* (MIC = 300 mg/L, light grey bars) and *S. aureus* (MIC >5000 mg/L, dark grey bars). Values are means of two independent series of screening experiments.

https://doi.org/10.1371/journal.pone.0239147.g002

analog of the pathogen *M. tuberculosis*) (Fig 2). Different types of alkylresorcinols, amphiphilic 2,4- and 2,6-dialkylhydroxybenzenes and the more hydrophobic 4-hexylresorcinol (4-HR) were tested. In view of the high activity of 4-HR, its antimicrobial activity was subsequently studied using a broad range of microorganisms (Table 1). Gram positive bacteria were found to be most sensitive to 4-HR, with MICs of 20-50 mg/L. *M. smegmatis* was characterized by a MIC of 70 mg/L. Gram negative bacteria, yeasts and fungi were less sensitive.

Effect of 4-hexylresorcinol as antibiotic adjuvant

In the next series of experiments, MIC was determined for each antibiotic supplemented with 4-HR at the concentration of $\frac{1}{2}$ MIC, which was insignificant for preventing growth of the test organisms, but suppressed their metabolic activity. The results are presented in Tables 2 and 3. In the case of *S.aureus* 209P, the presence of 4-HR ($\frac{1}{2}$ MIC) enhanced the antimicrobial action of all tested antibiotics, especially of polymyxin, vancomycin, capremabol, levomycetin, and ampicillin (5- to 10-fold increase). In the case of *E. coli* K12, a significant intensification of the antimicrobial action was as well observed in presence of 4-HR ($\frac{1}{2}$ MIC). 4-HR had the greatest effect on activity of polymyxin, gentamicin, azithromycin, and levomycetin (MIC decreased 10- to 50-fold). The lowest effect (2- to 3-fold) was observed for cyclosporine, vancomycin, and rubomycin. In the case of a yeast-like organism (i.e. *C. utilis*), two antibiotics were tested:

Table 2. MIC of various antibiotics against gram positive *S. aureus*. MIC of antibiotics alone or antibiotics combined with 15 mg/L 4-HR corresponding to $\frac{1}{2}$ MIC are shown. Values are means of two series of experiments.

Antibiotic	MIC antibiotic (μg/L)	Fold decrease of MIC in presence of 4-HR
Capremabol	40	10
Ampicillin	0.25	5
Vancomycin	0.5	5
Levomycetin	2.5	5
Polymyxin	10	5
Gentamicin	0.2	4
Doxycycline	0.4	4
Rubomycin	200	4
Ciprofloxacin	3	3

https://doi.org/10.1371/journal.pone.0239147.t002

Table 3. MIC of various antibiotics against gram negative *E.coli*. MIC of antibiotics alone or antibiotics combined with 100 mg/L 4-HR corresponding to $\frac{1}{2}$ MIC are shown. Values are means of two series of experiments.

Antibiotic	MIC antibiotic (μg/L)	Fold decrease of MIC in presence of 4-HR
Polymyxin	5	50
Gentamicin	1	10
Azithromycin	1	10
Levomycetin	12.5	10
Ciprofloxacin	0.75	5
Doxycycline	5	5
Capremabol	100	5
Ampicillin	40	4
Tobramycin	60	4
Rubomycin	300	3
Vancomycin	200	2

https://doi.org/10.1371/journal.pone.0239147.t003

ciprofloxacin and naftifine hydrochloride. However, their MIC decreased insignificantly in presence of 4-HR. Antimicrobial action of the studied antibiotics against both tested bacteria increased in the presence of $\frac{1}{2}$ MIC of 4-heptylresorcinol leading to similar albeit weaker effects as observed with 4-HR. In view of the higher potency of 4-HR, only this compound was used for the next series of experiments.

Effect of 4-hexylresorcinol on germination

Dormant microbial forms lack metabolic activity and therefore targets of many biocidal agents. Moreover, they exhibit high resistance to damaging factors. Suppression of their germination is therefore a challenge. Addition of 4-HR for the indicated period of time to liquid medium prior to inoculation inhibited germination of *B. cereus* spores (Table 4). The decrease in the titer of viable spores (CFU) depended both on 4-HR concentration and exposure duration. We conclude that 4-HR exhibits antimicrobial activity against both bacterial vegetative cells and their dormant forms. Pretreatement of spores impairs their ability to germinate.

Effect of 4-hexylresorcinol on persister cells

4-HR was combined with antibiotics to study the effect of 4-HR on viability of persister cells, i.e. cells remaining viable in the presence of biocidal concentrations of antibiotics [18]. The test strain *E. coli* K12 was treated with ampicillin and ciprofloxacin (antibiotics inhibiting different targets in bacterial cells, i.e. cell wall synthesis and DNA synthesis, respectively). Their concentrations of 60 and 100 μg/mL, respectively, was above their MIC. The results presented in Table 5 demonstrate a decrease in the numbers of surviving persister cell in presence of 4-HR ($\frac{1}{2}$ MIC). No viable cells were found after 2 days (for ampicillin) and 7 days (for ciprofloxacin) if antibiotics were combined with 4-HR. A neglegible amount of viable cells (i.e. 32 CFU/ml) was detected after 1 day of incubation with ampicillin in the presence of 4-HR. This is in contrast to incubations with the antibiotics alone, which did not lead to complete eradication of the microorganisms under all tested conditions (viable cell count was $>3 \times 10^3$ CFU/mL).

Effects of 4-HR on clinical isolates of pathogenic bacteria

Synergistic effects of antibiotics and 4-HR were studied using clinical isolates of pathogenic bacteria causing infections associated with medical interventions. The chequerboard method

Table 4. Impact of 4-hexylresorcinol on germination of *B. cereus* spores. Liquid medium containing *B. cereus* B-504 spores was pretreated with 4-HR for the indicated period of time. Germination was in absence ((-); 100% control without 4-HR corresponds to $6.0 \pm 1.0 \times 10^7$ CFU/mL) or presence ((+); 100% control without 4-HR corresponds to $9.5 \pm 0.5 \times 10^7$ CFU/mL) of 4-HR. Values are means of two series of experiments.

Treatment	4-HR (mg/L)	% rate of germination
No pretreatment (+)	5	95 ± 15%
	10	77 ± 13%
	25	0%
1 hour pretreatment (-)	50	100 ± 18%
	100	98 ± 16%
	500	83 ± 14%
	1000	51 ± 11%
2 days pretreatment (-)	50	75 ± 16%
	100	75 ± 14%
	500	55 ± 11%
	1000	20 ± 3%

https://doi.org/10.1371/journal.pone.0239147.t004

Table 5. Effect of 4-HR on persister cells. CFU of *E.coli* were determined after incubation for the indicated period of time with biocidal antibiotic concentrations (60 μg/mL of ampicillin and 100 μg/mL of ciprofloxacin) in presence and absence of 4-HR ($\frac{1}{2}$ MIC). Initial cell titer was 10^9 CFU/mL. Values indicate fold change as compared to control (absence of antibiotics). $>10^6$: <500 remaining CFU/mL detected. Values are means ± SD, n = 3.

Antibiotic	Incubation	Fold reduction w/o 4-HR	Fold reduction with 4-HR
Ampicillin	3 hours	40	900'000
Ampicillin	24 hours	125	$>10^6$
Ampicillin	48 hours	4'000	$>10^6$
Ciprofloxacin	3 hours	40	200'000
Ciprofloxacin	48 hours	1'600	$>10^6$
Ciprofloxacin	168 hours	300'000	$>10^6$

https://doi.org/10.1371/journal.pone.0239147.t005

was applied to calculate a fractional inhibitory concentration index (FICI). [28] FICI values were categorized into three groups: Synergy (FICI $\leq$ 0.5), indifference, or absence of interaction, (0.5 $\leq$ FICI $\leq$ 4.0), and antagonism (FICI $\geq$ 4.0). Additionally, the coefficient K1 was calculated. With this coefficient, the decrease in the effective dose of antibiotic in the presence of 4-HR (K1) can be determined.

For this assessment, clinical isolates of gram positive bacteria (*S. aureus* and *E. faecium*) as well as gram negative bacteria (*E. coli*, *K. pneumoniae*, *A. baumannii*, *P. aeruginosa*) were selected (S2 Table). In 26% of the studied antibiotic with 4-HR combinations, no effect of 4-HR on the MIC of antibiotics was observed. But in the remaining 74%, the MIC of the studied antibiotics decreased 2- to 512-fold, with a fourfold and more pronounced MIC decrease found in 33% of the combinations and an eightfold and more pronounced MIC decrease occurred in 12% of the groups. Importantly, potentiation of antibiotic activity (strong synergistic effects as indicated by the FICI parameter and decrease in their effective doses in combination with 4-HR as indicated by the K1 parameter) was observed for both sensitive and resistant strains. 4-HR exhibited synergism and caused a significant decrease in the MIC of antibiotics in the case of interactions with ciprofloxacin (7 combinations), polymyxin (5 combinations), and amikacin (4 combinations). 4-HR efficiency varied depending on microbial taxa and was higher in the case of gram negative bacteria. 4-HR in combination with polymyxin showed synergism against *A. baumannii*, *P. aeruginosa* and *K. pneumoniae* with different levels of sensitivity. As a representative example, results for clinical isolates of *K. pneumoniae* KPM9 (covering both sensitive and resistant strains) are shown in Table 6. In the case of polymyxin, for example, strong synergistic effects were observed (FICI = 0.07 μg/L) with a 16-fold decrease in the effective dose of antibiotic in the presence of 4-HR.

In vivo proof of concept using an experimental mouse sepsis model

Based on the results of the chequerboard analysis (Table 6), a mouse experimental sepsis model was developed to demonstrate *in vivo* effects of a combination of polymyxin and 4-HR in infections caused by clinical isolates of pathogenic *K. pneumoniae*. For our model of mouse klebsiellosis, ten outbred mice per group were infected by intraperitoneal injection of a culture of antibiotics sensitive *K. pneumoniae* KPM9 (0.5 mL, ≈ 50 LD_{50}, 1000 CFU/mouse). Treatment of groups started 24 hours after infection and continued for five days. Since oral polymyxin (Pm) preparations are not well tolerated in mice, Pm was applied as intramuscular injection (1 mg/kg). The 4-HR preparation was administered twice a day *per os* (PO). Total daily 4-HR doses were 30 mg/kg. A representation of the survival data for Pm in combination with 4-HR is shown in Fig 3. On day 14 of the experiment, surviving animals were euthanized. Their spleen, blood, and lungs were examined to determine viable cell titers (CFU) of *K. pneumoniae* by plating serial dilutions on solid media.

Table 6. Assessment of interactions between 4-HR and various groups of antibiotics against clinical isolates of gram negative pathogenic *K. pneumoniae*. The chequerboard method yields FICI values (Eq 1) as well as the coefficient K1 (decrease in the effective dose of antibiotic in the presence of 4-HR; Eq 2). Synergy is defined by FICI $\leq$ 0.5, absence of interaction by 0.5 $\leq$ FICI $\leq$ 4.0, and antagonism by FICI $\geq$ 4.0. For the resistant pathogen, 4-HR concentrations were 512 μg/L. For the sensitive strain, 4-HR concentrations were 64 μg/L. Unit of MIC is μg/L. MIC AB designates MIC of the antibiotic alone.

Antibiotic	Phenotype	MIC AB	K1	FICI
Amikacin	Sensitive	1	1	2
Ampicillin	Sensitive	8	0.25	5
Cefotaxim	Sensitive	0.5	2	1.5
Ciprofloxacin	Sensitive	0.06	4	0.26
Meropenem	Sensitive	0.03	4	0.26
Polymyxin	Sensitive	0.25	16	0.07
Tigecycline	Sensitive	0.12	1	2
Amikacin	Resistant	128	16	0.09
Ampicillin	Resistant	256	0.1	8.06
Cefotaxim	Resistant	128	8	0.25
Ciprofloxacin	Resistant	128	16	0.09
Meropenem	Resistant	16	2	0.56
Tigecycline	Resistant	2	2	0.56

https://doi.org/10.1371/journal.pone.0239147.t006

Indications of the *Klebsiella* infection (adynamia, anorexia, and loss of weight) were observed during the experiment and resulted in a decrease in the body mass as well as death of animals. Treatment of animals with the Pm + 4-HR combination showed high efficiency when the 4-HR preparation was administered *per os*. Survival rate in the group treated with Pm + 30 mg/kg/day 4-HR was the highest (80%), while all the mice in the control group died. Moreover, life duration (9 days) of animals treated with Pm + 30 mg/kg/day 4-HR was more than twice that of the control mice (4 days). Approximately 75% of surviving animals in this group were sanified, as demonstrated by an absence of viable *K. pneumoniae* in inner organs. In the remaining mice, bacterial numbers in the spleen and lungs were approximately 3.2×10^2 and approximately 5.4×10^2 CFU/mL, respectively (S3 Table). No bacteria were found in the blood. Surprisingly, survival rates actually decreased to 60% in groups treated with higher 4-HR doses (i.e. 50 or 75 mg/kg/day). Higher doses of 4-HR did as well reduce the percentage of sanified mice (40% and 30% of surviving mice treated with 50 and 75 mg/kg/day, respectively). It should be noted that intraperitoneal administration of 4-HR was abandoned since it showed low efficiency and caused pain. Treatment of animals with 1 mg/kg Pm alone did not result in complete recovery of mice: in 40% of surviving animals, inner organs were contaminated with *K. pneumoniae*. None of the surviving animals receiving 4-HR alone were sanified.

Discussion

Research on microbial growth autoregulation revealed microorganisms (both pro- and eukaryotic) to produce low-molecular mass compounds acting as density regulators, which in a number of bacteria are phenolic lipids of the alkylresorcinol group. [33] Alkylresorcinols were subsequently shown to act as autoinducers of the quorum-dependent regulatory system. [33, 34] This is in agreement with literature confirming this function of alkylresorcinols. [35] At increasing concentrations of alkylresorcinol, population growth of microorganisms is restricted and the development of a hypometabolic and then anabiotic state is induced. [33, 34] This motivated us in the present study to explore a possible role of alkylresorcinols and other phenolic lipids as antibiotic adjuvants.

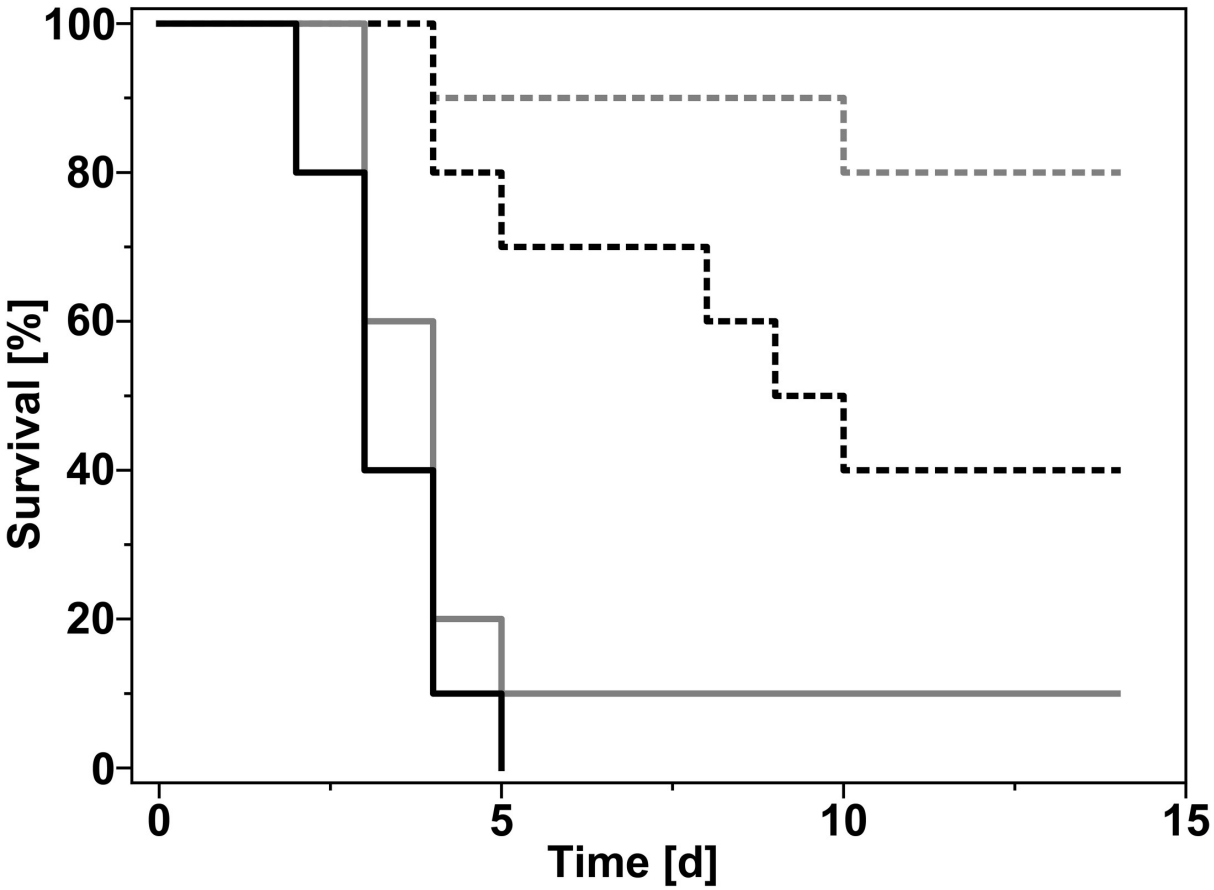

Fig 3. Effect of 4-hexylresorcinol in a mouse bacterial sepsis model. A total of 10 mice per group were infected with *K. pneumoniae* (clinical isolate KPM9; 1000 CFU/mouse). Treatment started 24 hours after infection (day 0). Mice were treated with polymyxin (1 mg/kg, intramuscular) and/or 4-HR (15 mg/kg twice a day for five days, *per os*). Dashed grey line: polymyxin and 4-HR combined. Dashed black line: polymyxin alone. Solid grey line: 4-HR alone. Solid black line: untreated control.

https://doi.org/10.1371/journal.pone.0239147.g003

4-HR (4-hexylresorcinol) was identified in screening experiments to have the strongest effects on bacterial growth. In these experiments, antimicrobial activity of alkylresorcinols with methyl-, ethyl-, and hexyl groups was found to increase with increasing hydrophobicity. Comparison of 4-HR and 2-ethyl-5-methylresorcinol revealed that the absence of screening of hydroxyl groups by a large alkyl group was important for antimicrobial activity. Thus, while the more hydrophobic compound 2-ethyl-5-methylresorcinol could have been expected to have higher antimicrobial activity than 4-HR, it was in fact less toxic to the test organisms. Comparison of 2,4- and 2,5-dimethylresorcinols revealed hydroxyl group screening to be less important for *S. aureus* (MIC 100 and 250 mg/L, respectively) than to *M. smegmatis* (400 and 300 mg/L, respectively).

Antimicrobial activity of 4-HR on microorganisms seem to depend on cell wall properties. High sensitivity was associated with a peptidoglycan-based outer cell wall structure of gram positive bacteria. The additional outer lipid membrane of gram negative bacteria, as well as the complex chitin and polysaccharide-based cell wall structure of yeast and fungi, seems to confer

some degree of resistance. High resistance to 4-HR in *M. smegmatis* might be due to the presence of lipid structures and mycolic acids, causing high hydrophobicity of their cell surface. Dependence of antimicrobial activity of phenolic lipids on their hydrophobicity is in agreement with literature, [36] which reports increased antimicrobial activity of n-alkylphenols with increasing length of the alkyl chain and higher resistance of microorgansisms with lipid-enriched cell membranes to alkylphenols. Based on these results, 4-HR was selected for further characterization.

The utility of 4-HR as potent adjuvant for the treatment of bacterial infections was demonstrated in combination with several antibiotics. The biocidal effects of these antibiotics to *S. aureus* and *E. coli* were potentiated 5- to 50-fold in the presence of $\frac{1}{2}$ MIC 4-HR. This result opens the opportunity for novel treatment regimens against bacterial infections. For instance, a higher bactericidal effect obtained with the combination of antibiotic and 4-HR could result in lower doses of antibiotics to be applied to a patient while still maintaining the same effectiveness. Consequently, antibiotics that are rarely used in humans due to side effects associated with bactericidal doses (such as polymyxin) might become a viable alternative when combined with 4-HR. In view of the challenges related to antibiotics resistance, this strategy could help to delay the hypothesized post-antibiotics era.

In addition to vegetative forms, bacteria can undergo transformation into a dormant form, leading to the emergence of persister cells. These dormant forms or endospores are characterized by the absence of metabolic activity and therefore possess a high resistance towards environmental insults including radiation, temperature, and chemicals. Previous studies [12, 37–39] suggest that persister cells are responsible for the chronic nature of many bacterial infections and that their formation is induced by prolonged use of antibiotics. [40, 41] This is due to selective pressure on the pathogens promoting persistence. [42, 43] Efficiency of antibiotic therapy can therefore be compromised by the development of antibiotic-resistant clones. Furthermore, persister cells surviving antibiotic treatment may transfer genetic information, e.g. plasmid encoded resistance genes, vertically from parent to offspring or transfer genetic information to another species of bacteria within the same generation by means of transduction, transformation and conjugation (horizontal gene transfer). It is therefore important to eliminate antibiotics-insensitive, dormant persister cells. Based on these considerations, we measured the synergisitc effect of a combination therapy using antibiotics-resistant persister cells. It was indeed possible to demonstrate that the addition of 4-HR significantly decreases the number of germinating *B. cereus* spores in liquid medium, as well as on agar medium. This in contrast to treatment with antibiotics alone. The observed effect was dependent on 4-HR concentration and duration of exposure. Moreover, the number of viable spores after prolonged treatment (14 days) was below the limit of detection. Thus, the risk of reemergence of an infection after termination of the antibiotic treatment due to germination of persister cells can be minimized. This result demonstrates that bacterial strains, that already acquired ABR, can become sensitive to the antibiotic compound again when 4-HR is co-administered. It is therefore tempting to speculate that antibiotics, that are rarely used due to widespread resistance towards that antibiotic, can become a viable treatment alternative again.

To systematically study interactions of 4-HR and antibiotics with clinical isolates of pathogenic bacteria, we used the chequerboard method. A FICI parameter of ≤ 0.5 [28] is thereby indicative of synergism. This classification is confirmed if the MIC of the antibiotic decreases at least fourfold in the presence of 4-HR ($K1 \geq 4$). Strong synergism was observed both for gram negative and gram positive bacteria. 4-HR combinations with fluoroquinolones, polymyxin, and amikacin with gram negative bacteria as targets were the most promising variants S2 Table. Interestingly, 4-HR may have both synergistic as well as antagonistic effects. These

results emphasize the importance of FICI values and the coefficient K1, which have to be determined for each new combination of antibiotic, 4-HR and pathogen. Importantly, 4-HR enhanced antibiotic activity equally well in both antibiotic sensitive and resistant bacterial strains.

In vitro efficiency of antibiotics in 4-HR binary compositions was determined for the gram negative bacterium *Klebsiella pneumoniae*, which causes various forms of klebsiellosis infections. Death rate in humans with the generalized klebsiellosis infection may be as high as 60%. Emergence of antibiotic-resistant *K. pneumoniae* strains is a major problem. [44] Therapy of nosocomial infections is often difficult due to high resistance of the causative agents to most known antibiotics, which develops in 30-50% of the patients in the course of monotherapy. Since the virulence of *K. pneumoniae* depends significantly on its ability to form a polysaccharide capsule preventing phagocytosis, the hypermucoid strain *K. pneumoniae* KPM9 was selected for the development of an animal model. *In vitro* results showed a significant effect of 4-HR on antibiotic efficiency with a FICI value of 0.07 and a 16-fold decrease of the polymyxin MIC in combinations with 4-HR (Table 6). In view of these pronounced synergistic effects, we decided to focus for the following series of experiments on combinations of *K. pneumoniae*, polymyxin, and 4-HR. With respect to selection of the antibiotic, it should be noted that previous *in vitro* studies reported synergistic effects of polymyxin with other antibiotics in that bactericidal activity was enhanced and bacterial heteroresistance was suppressed. [45–47] Clinical studies revealed that a combination therapy including polymyxin has a better clinical outcome as compared to a monotherapy. This can be attributed to a decreased risk of Pm associated side effects and offers interesting options with respect to the use of adjuvants such as 4-HR. [48]

Klebsiellosis treatment is often based on an assessment of the activity of preparations in treatment of experimental *Klebsiella* infections in animals. Mice are highly sensitive to this infection. Mouse klebsiellosis is characterized by an acute generalized disease, with *K. pneumonia* and sepsis in virulent forms. Death due to infection-related toxic shock occurs within a week after infection. Successful antibiotic treatment results in elimination of the infectious agent and normalization of clinical laboratory parameters. In the present study, it was indeed possible to eradicate *K. pneumoniae* in a mouse sepsis model by a combination of polymyxin and 4-HR. Combined therapy resulted in 80% survival rate compared to 40% for the polymyxin monotherapy. Interestingly, 4-HR doses of 30 mg/kg/day were in our experiments more effective than higher doses of 50 or 75 mg/kg/day. It is tempting to speculate that side-effects due to overdosing of 4-HR had a negative impact on the recovery of infected animals. Bacteriological analysis of parenchymatous organs of the animals euthanized 9 days after the end of combined treatment revealed absence of *K. pneumoniae* KPM9 cells in 75% of surviving animals, while all animals treated with the antibiotic alone were still carriers of the infection. Thus, the antibacterial preparation containing 4-HR suppressed formation of persister cells. We therefore propose that 4-HR might be an interesting alternative to sulfonamides and tetracyclines presently used as adjuvants for the treatment of klebsiellosis in humans.

The mechanism of action of 4-HR is polymodal and complex. Similar to other alkylresorcinols, the biological activity of 4-HR may be attributed to its action as a structural modifier of biopolymers and supramolecular structures such as membranes. [33, 34, 36, 49, 50] The amphiphilic nature of 4-HR seems to be responsible for its partitioning into and diffusion across cell membranes. Unlike cationic peptides, however, membrane integrity is not impaired by 4-HR. [51, 52] It has therefore been proposed that formation of complexes with macromolecules and membrane lipids results in increased microviscosity of the membrane lipids, which causes inhibition of their functional activity. [33, 36, 53] This membranotropic action of 4-HR explains the high efficiency of its combinations with the following antibiotics: polymyxin

(affecting membranes of gram negative bacteria), fluoroquinolones (inhibiting the activity of helicases located at the initial site of DNA replication), and amikacin, the effect of which depends on the transmembrane potential of bacterial cells. Besides its actions on membranes, 4-HR interacts with DNA [54] and proteins. The latter was demonstrated by studies using enzymes and immune system proteins as models. Effects were dose-dependent and linked to protein conformation and thus functional activity. [34, 50, 55, 56] Increased intracellular 4-HR concentrations induce a stress response leading to generation of reactive oxygen species (ROS) and RpoS (RNA polymerase, sigma factor S) activation. [57]

Due to their unspecific mode of action, 4-HR (and other alkylresorcinols) have unique properties in that they act on bacteria as well as on protozoans and helminths. [36] The outer membrane of gram negative bacteria seems to be the first target for 4-HR, which enables it to affect such forms of intracellular persistence as SCV-variants [58] and L-forms, [59] and to accumulate in phagocytes. [60] Model experiments *in vitro* revealed HR effect on biofilm formation and disintegration of mature biofilms. [61] It is tempting to speculate that the multimodal mode of action of alkylresorcinols prevents habituation or resistance. In fact, 4-HR-induced changes in microbial cells are similar to those observed under low-temperature stress (increased membrane viscosity and decreased enzymatic activity). Thus, adaptation of microbial cells both to low temperature and to elevated levels of alkylresorcinols is unlikely.

Conclusion

Alkylresorcinols are widespread in nature and are natural compounds present in large amounts in agricultural products (up to 1.5 g/kg in grain). Their daily consumption with food is 10-20 mg and is not considered harmful. [62] Alkylresorcinols are therefore considered to be bioactive nutrition components, [63] which are part of human metabolism without having negative consequences. [64] In experiments with mice, hexylresorcinol doses of up to 125 mg/kg were shown to have no carcinogenic properties. [65] Moreover, they exhibited antimutagenic [66] and antitumor properties. [67, 68] Consequently, 4-HR obtained regulatory authorization to be used for medical applications in human, [65] as well as in cosmetics and food industry. [69, 70] This status as safe compounds is an important advantage of alkylresorcinols, including 4-HR, and paves the way towards their clinical application as proposed antibiotic adjuvants. Our findings suggest that this strategy will allow for a more efficient use of established antibiotics and thereby reduce the risk of bacterial resistance.

Supporting information

S1 Table. Antibiotics used in the present study.
(PDF)

S2 Table. Interactions between 4-HR and various groups of antibiotics against clinical isolates of pathogenic gram negative bacteria.
(PDF)

S3 Table. Actual numbers of K. pneumoniae KPM9 cells in organs (cells/mL) from euthanized mice. Organs were analyzed 14 days after inoculation and treatment with the indicated doses of Polymixin B (PmB) and 4-HR for 5 days. For each organ, the range of bacterial counts in contaminated surviving animals (cells/mL) is indicated. Numbers in parenthesis: number of contaminated surviving animals / number of total surviving animals. Total number of animals was 10 per group. A ratio of 1/8 would thus describe a situation where 8 out of 10 mice did survive. From these 8 surviving animals, the respective organ of only one animal was still

contaminated.
(PDF)

Acknowledgments

The publication has been prepared with the support of the "RUDN University Program 5-100". Animal Research was supported by the Sectoral Scientific Program of the Russian Federal Service for Surveillance on Consumer Rights Protection and Human Wellbeing. We thank Viktoria Schreiner for editorial support. The authors declare that they have no conflict of interest.

Author Contributions

Conceptualization: Y. A. Nikolaev, J. Buck, J. Huwyler, G. I. El'-Registan.

Data curation: S. V. Sidorenko.

Formal analysis: J. Buck, I. Lazareva, V. Gostev, I. G. Shemyakin.

Funding acquisition: J. Huwyler.

Investigation: N. G. Loiko, J. Buck, O. Y. Manzen'yuk, I. G. Shemyakin.

Methodology: A. V. Tutel'yan, J. Buck, S. V. Sidorenko, I. Lazareva, V. Gostev, J. Huwyler.

Project administration: Y. A. Nikolaev, A. V. Tutel'yan, O. Y. Manzen'yuk, R. A. Abramovich, J. Huwyler.

Resources: J. Huwyler.

Supervision: Y. A. Nikolaev, J. Huwyler.

Validation: N. G. Loiko, J. Buck.

Visualization: J. Buck, J. Huwyler.

Writing – original draft: Y. A. Nikolaev, J. Buck.

Writing – review & editing: Y. A. Nikolaev, A. V. Tutel'yan, J. Buck, R. A. Abramovich, J. Huwyler, G. I. El'-Registan.

References

1. Guilfoile P. Antibiotic-resistant bacteria. Chelsea House. 2007; ISBN 978-0-7910-9188-3
2. Brooks B, Brooks A. Therapeutic Strategies to Combat Antibiotic Resistance. Advanced Drug Delivery Reviews. 2014; 78:14–27. https://doi.org/10.1016/j.addr.2014.10.027 PMID: 25450262
3. Butler MS, Blaskovich MA, Cooper MA. Antibiotics in the clinical pipeline in 2013. The Journal of Antibiotics. 2013 Sep; 66:571–591. https://doi.org/10.1038/ja.2013.86 PMID: 24002361
4. Domalaon R, Idowu T, Zhanel GG, Schweizer F. Antibiotic Hybrids: the Next Generation of Agents and Adjuvants against Gram-Negative Pathogens? Clinical Microbiology Reviews. 2018 Mar; 31:e00077–17. https://doi.org/10.1128/CMR.00077-17 PMID: 29540434
5. Eliopoulos GM, Eliopoulos CT. Antibiotic Combinations: Should They Be Tested? Clinical Microbiology Reviews. 1988; 1:139–156. https://doi.org/10.1128/cmr.1.2.139 PMID: 3069193
6. Finlay J, Miller L, Poupard JA. A review of the antimicrobial activity of clavulanate. Journal of Antimicrobial Chemotherapy. 2003 Jul; 52:18–23. https://doi.org/10.1093/jac/dkg286 PMID: 12775671
7. Gordon D. Amoxicillin–Clavulanic Acid (Co-Amoxiclav). Kucers' the Use of Antibiotics. 2010 Oct; 1:187–203.
8. Brown D. Antibiotic resistance breakers: can repurposed drugs fill the antibiotic discovery void?. Nature Reviews Drug Discovery. 2015 Dec; 14:821–832. https://doi.org/10.1038/nrd4675 PMID: 26493767

9. Wright GD. Antibiotic Adjuvants: Rescuing Antibiotics from Resistance. Trends in Microbiology. 2016; 24:862–871. https://doi.org/10.1016/j.tim.2016.06.009 PMID: 27430191

10. Kalan L, Wright GD. Antibiotic Adjuvants: Multicomponent Anti-Infective Strategies. Expert Reviews in Molecular Medicine. 2011; 13:e5. https://doi.org/10.1017/S1462399410001766 PMID: 21342612

11. Douafer H, Andrieu V, Phanstiel O, Brunel JM. Antibiotic Adjuvants: Make Antibiotics Great Again!. Journal of Medicinal Chemistry. 2019; 62:8665–8681. https://doi.org/10.1021/acs.jmedchem.8b01781 PMID: 31063379

12. Helaine S, Kugelberg E. Bacterial persisters: formation, eradication, and experimental systems. Trends in Microbiology. 2014 Jul; 22:417–424. https://doi.org/10.1016/j.tim.2014.03.008 PMID: 24768561

13. Grant SS and Hung DT. Persistent bacterial infections, antibiotic tolerance, and the oxidative stress response. Virulence. 2013 May; 4:273–283. https://doi.org/10.4161/viru.23987 PMID: 23563389

14. Michiels J and Fauvart M. Bacterial Persistence: Methods and Protocols. Humana Press. 2016. ISBN 978-1-4939-2853-8

15. Cabral DJ, Wurster JI, Belenky P. Antibiotic Persistence as a Metabolic Adaptation: Stress, Metabolism, the Host, and New Directions. Pharmaceuticals. 2018 Feb; 11. https://doi.org/10.3390/ph11010014 PMID: 29389876

16. Levin-Reisman I, Ronin I, Gefen O, Braniss I, Shoresh N, Balaban NQ. Antibiotic tolerance facilitates the evolution of resistance. Science. 2017 24; 355(6327):826–30. https://doi.org/10.1126/science.aaj2191 PMID: 28183996

17. Windels EM, Michiels JE, Fauvart M, Wenseleers T, den Bergh BV, Michiels J. Bacterial persistence promotes the evolution of antibiotic resistance by increasing survival and mutation rates. ISME J. 2019 May; 13(5):1239–51. https://doi.org/10.1038/s41396-019-0344-9 PMID: 30647458

18. Lewis K. Persister Cells. Annual Review of Microbiology. 2010; 64:357–372. https://doi.org/10.1146/annurev.micro.112408.134306 PMID: 20528688

19. Cohen NR, Lobritz MA, Collins JJ. Microbial persistence and the road to drug resistance. Cell host & microbe. 2013 Jun; 13:632–642. https://doi.org/10.1016/j.chom.2013.05.009 PMID: 23768488

20. Gill EE, Franco OL, Hancock REW. Antibiotic Adjuvants: Diverse Strategies for Controlling Drug-Resistant Pathogens. Chemical Biology & Drug Design. 2015 Jan; 85:56–78. https://doi.org/10.1111/cbdd.12478 PMID: 25393203

21. González-Bello C. Antibiotic adjuvants—A strategy to unlock bacterial resistance to antibiotics. Bioorganic & Medicinal Chemistry Letters. 2017 Sep; 27:4221–4228. https://doi.org/10.1016/j.bmcl.2017.08.027 PMID: 28827113

22. Mehta KC, Dargad RR, Borade DM, Swami OC. Burden of Antibiotic Resistance in Common Infectious Diseases: Role of Antibiotic Combination Therapy. Journal of Clinical and Diagnostic Research. 2014 Jun; 8:ME05–ME08. https://doi.org/10.7860/JCDR/2014/8778.4489 PMID: 25121020

23. Amoh T, Murakami K, Kariyama R, Hori K, Viducic D, Hirota K, et al. Effects of an autoinducer analogue on antibiotic tolerance in Pseudomonas aeruginosa. Journal of Antimicrobial Chemotherapy. 2017 Aug; 72:2230–2240. https://doi.org/10.1093/jac/dkx132 PMID: 28510695

24. Luís Â, Domingues F, Duarte AP Biological Properties of Plant-Derived Alkylresorcinols: Mini-Review. Mini Reviews in Medicinal Chemistry. 2016; 16:851–854. https://doi.org/10.2174/1389557516666160211121437 PMID: 26864549

25. Kemme M and Heinzel-Wieland R. Quantitative Assessment of Antimicrobial Activity of PLGA Films Loaded with 4-Hexylresorcinol. Journal of Functional Biomaterials. 2018 Mar; 9:4. https://doi.org/10.3390/jfb9010004 PMID: 29324696

26. Hao Y, Gao X, Xia W. Determination of 4-Hexylresorcinol in Shrimp Samples by Solid Phase Extraction Ultra Performance Liquid Chromatography-Tandem Mass Spectrometry. Molecules. 2018 Sep; 23:2173. https://doi.org/10.3390/molecules23092173 PMID: 30158429

27. Keren I, Kaldalu N, Spoering A, Wang Y, Lewis K. Persister cells and tolerance to antimicrobials. FEMS Microbiology Letters. 2004; 230:13–18. https://doi.org/10.1016/S0378-1097(03)00856-5 PMID: 14734160

28. Odds FC. Synergy, antagonism, and what the chequerboard puts between them. Journal of Antimicrobial Chemotherapy. 2003 Jul; 52(1):1–1. https://doi.org/10.1093/jac/dkg301 PMID: 12805255

29. Ashmarin IP and Vorob'ev AA Statistical methods in microbiological research [in Russian]. Leningrad, 1962

30. Morris TH Antibiotic Therapeutics in Laboratory Animals. Laboratory Animals. 1995 Jan; 29(1):16–36. https://doi.org/10.1258/002367795780740393 PMID: 7707675

31. Franco NH, Correia-Neves M, Olsson IS How "Humane" Is Your Endpoint?—Refining the Science-Driven Approach for Termination of Animal Studies of Chronic Infection, PLOS Pathogens. 2012; 8: e1002399. https://doi.org/10.1371/journal.ppat.1002399 PMID: 22275862

32. Seok Junhee, Shaw Warren H., Cuenca Alex G., Mindrinos Michael N., Baker Henry V., Xu Weihong, et al. Genomic Responses in Mouse Models Poorly Mimic Human Inflammatory Diseases. Proceedings of the National Academy of Sciences of the United States of America. 2013; 110:3507–12. https://doi.org/10.1073/pnas.1222878110 PMID: 23401516

33. El'-Registan GI, Mulyukin A, Nikolaev Y, Suzina NE, Gal'chenko VF, Duda VI. Adaptogenic functions of extracellular autoregulators of microorganisms. Microbiology. 2006 Jul; 75:380–389. https://doi.org/10.1134/S0026261706040035 PMID: 17025168

34. Nikolaev YA, Mulyukin AL, Stepanenko IY, El'-Registan GI. Autoregulation of stress response in microorganisms. Microbiology. 2006 Jul; 75:420–426. https://doi.org/10.1134/S0026261706040096 PMID: 17025174

35. Brameyer S, Kresovic D, Bode HB, Heermann R. Dialkylresorcinols as bacterial signaling molecules. Proceedings of the National Academy of Sciences of the United States of America. 2015 Jan; 112:572–577. https://doi.org/10.1073/pnas.1417685112 PMID: 25550519

36. Stasiuk M and Kozubek A. Biological activity of phenolic lipids. Cellular and Molecular Life Sciences. 2010 Mar; 67:841–860. https://doi.org/10.1007/s00018-009-0193-1 PMID: 20213924

37. Balaban NQ, Merrin J, Chait R, Kowalik L, Leibler S. Bacterial Persistence as a Phenotypic Switch. Science. 2004 Sep 10; 305(5690):1622–5. https://doi.org/10.1126/science.1099390 PMID: 15308767

38. Fisher RA, Gollan B, Helaine S. Persistent bacterial infections and persister cells. Nat Rev Microbiol. 2017 Aug; 15(8):453–64. https://doi.org/10.1038/nrmicro.2017.42 PMID: 28529326

39. den Bergh BV, Michiels JE, Wenseleers T, Windels EM, Boer PV, Kestemont D, et al. Frequency of antibiotic application drives rapid evolutionary adaptation of Escherichia coli persistence. Nat Microbiol. 2016 Mar 7; 1(5):1–7. https://doi.org/10.1038/nmicrobiol.2016.20 PMID: 27572640

40. Blango MG, Mulvey MA. Persistence of Uropathogenic Escherichia coli in the Face of Multiple Antibiotics. Antimicrob. Agents Chemother. 2010 May 1; 54(5):1855–63. https://doi.org/10.1128/AAC.00014-10 PMID: 20231390

41. Goneau LW, Yeoh NS, MacDonald KW, Cadieux PA, Burton JP, Razvi H, et al. Selective Target Inactivation Rather than Global Metabolic Dormancy Causes Antibiotic Tolerance in Uropathogens. Antimicrob. Agents Chemother. 2014 Apr 1; 58(4):2089–97. https://doi.org/10.1128/AAC.02552-13 PMID: 24449771

42. Ren H, He X, Zou X, Wang G, Li S, Wu Y. Gradual increase in antibiotic concentration affects persistence of Klebsiella pneumoniae. J Antimicrob Chemother. 2015 Dec; 70(12):3267–72. https://doi.org/10.1093/jac/dkv251 PMID: 26311842

43. Brauner A, Fridman O, Gefen O, Balaban NQ. Distinguishing between resistance, tolerance and persistence to antibiotic treatment. Nat. Rev. Microbiol. 2016 May; 14(5):320–30. https://doi.org/10.1038/nrmicro.2016.34 PMID: 27080241

44. Gomez-Simmonds A, Greenman M, Sullivan SB, Tanner JP, Sowash MG, Whittier S, et al. Population Structure of Klebsiella pneumoniae Causing Bloodstream Infections at a New York City Tertiary Care Hospital: Diversification of Multidrug-Resistant Isolates. J. Clin. Microbiol. 2015 Jul; 53(7):2060–7. https://doi.org/10.1128/JCM.03455-14 PMID: 25878348

45. O'Hara JA, Ambe LA, Casella LG, Townsend BM, Pelletier MR, Ernst RK, et al. Activities of Vancomycin-Containing Regimens against Colistin-Resistant Acinetobacter baumannii Clinical Strains. Antimicrob. Agents Chemother. 2013 May 1; 57(5):2103–8. https://doi.org/10.1128/AAC.02501-12 PMID: 23422916

46. Lee HJ, Bergen PJ, Bulitta JB, Tsuji B, Forrest A, Nation RL, et al. Synergistic Activity of Colistin and Rifampin Combination against Multidrug-Resistant Acinetobacter baumannii in an In Vitro Pharmacokinetic/Pharmacodynamic Model. Antimicrob. Agents Chemother. 2013 Aug; 57(8):3738–45. https://doi.org/10.1128/AAC.00703-13 PMID: 23716052

47. Chung J-H, Bhat A, Kim C-J, Yong D, Ryu C-M. Combination therapy with polymyxin B and netropsin against clinical isolates of multidrug-resistant Acinetobacter baumannii. Sci Rep. 2016 16; 6:28168 https://doi.org/10.1038/srep28168 PMID: 27306928

48. Cai B, Cai Y, Liew YX, Chua NG, Teo JQ-M, Lim T-P, et al. Clinical Efficacy of Polymyxin Monotherapy versus Nonvalidated Polymyxin Combination Therapy versus Validated Polymyxin Combination Therapy in Extensively Drug-Resistant gram Negative Bacillus Infections. Antimicrob. Agents Chemother. 2016 Jul 1; 60(7):4013–22. https://doi.org/10.1128/AAC.03064-15 PMID: 27090177

49. Kozubek A, Tyman JHP. Resorcinolic Lipids, the Natural Non-isoprenoid Phenolic Amphiphiles and Their Biological Activity. Chem Rev. 1999 Jan 13; 99(1):1–26. https://doi.org/10.1021/cr970464o PMID: 11848979

50. Krupyanskii YF, Abdulnasyrov EG, Loiko NG, Stepanov AS, Tereshkina KB, El'-Registan GI. Possible mechanisms of the influence of hexylresorcinol on the structure-dynamic and functional properties of lysozyme protein. Russ J Phys Chem B. 2012 Mar 1; 6(2):301–14. https://doi.org/10.1134/S1990793112020078

51. Chen X, Zhang M, Zhou C, Kallenbach NR, Ren D. Control of Bacterial Persister Cells by Trp/Arg-Containing Antimicrobial Peptides. Appl. Environ. Microbiol. 2011 Jul 15; 77(14):4878–85. https://doi.org/10.1128/AEM.02440-10 PMID: 21622798

52. Omardien S, Brul S, Zaat SAJ Antimicrobial Activity of Cationic Antimicrobial Peptides against Gram-Positives: Current Progress Made in Understanding the Mode of Action and the Response of Bacteria. Front. Cell Dev. Biol. [Internet]. 2016 Oct 14 [cited 2020 Feb 14];4.

53. Kaprelyants AS, Suleimenov MK, Sorokina AD, Deborin GA, El-Registan GI, Stoyanovich FM, et al. Structural and functional changes in bacterial and model cell membranes under phenolic lipids actions. Biological membranes. 1987 Mar; 4:254–262.

54. Davydova OK, Deryabin DG, El'-Registan GI. IR spectroscopic research on the impact of chemical analogues of autoregulatory d1 factors of microorganisms on structural changes in DNA. Microbiology. 2007 Jun 1; 76(3):266–72. https://doi.org/10.1134/S0026261707030022 PMID: 17633405

55. Martirosova EI, Karpekina TA, El'-Registan GI. Enzyme Modification by Natural Chemical Chaperons of Microorganisms. Microbiology. 2004 Sep; 73:609–615. https://doi.org/10.1023/B:MICI.0000044252.10568.08 PMID: 15595523

56. Deryabin DG, Romanenko NA, El'-Registan GI. Change of the specificity of antibodies in the presence of alkylphenylalkohol, chemical analog of bacterial autoregulation molecules. Immunologiya. 2013. V. 34, Iss. 1, P. 27–30.

57. Golod NA, Loiko NG, Lobanov KV, Mironov AS, Voieikova TA, Gal'chenko VF, et al. Involvement of alkylhydroxybenzenes, microbial autoregulators, in controlling the expression of stress regulons. Microbiology. 2009 Dec; 78:678. https://doi.org/10.1134/S0026261709060034

58. Grant SS, Hung DT. Persistent bacterial infections, antibiotic tolerance, and the oxidative stress response. Virulence. 2013 May 15; 4(4):273–83. https://doi.org/10.4161/viru.23987 PMID: 23563389

59. Kawai Y, Mickiewicz K, Errington J. Lysozyme Counteracts β-Lactam Antibiotics by Promoting the Emergence of L-Form Bacteria. Cell. 2018 22; 172(5):1038–1049.e10. https://doi.org/10.1016/j.cell.2018.01.021 PMID: 29456081

60. Sviridova TG, Slobodchikov SV, Deryabin DG, Shmagel KV, Chereshnev VA. The influence of alkyl phenyl alcohol on absorbing and secretory function of human peripheral blood neutrophils. Immunologiya. 2013. V. 34, Iss. 2, P. 84–88.

61. Mart'yanov SV, Zhurina MV, El'-Registan GI, Plakunov VK. Activating effect of Azytromycin on bacterial biofilms formation and prevention of this phenomenon. Microbiology. 2015. V. 84. Iss. 1. P. 27–36.

62. Ross AB, Kamal-Eldin A, Åman P. Dietary Alkylresorcinols: Absorption, Bioactivities, and Possible Use as Biomarkers of Whole-grain Wheat–and Rye–rich Foods. Nutrition Reviews. 2004 Mar; 62:81–95. https://doi.org/10.1111/j.1753-4887.2004.tb00029.x PMID: 15098855

63. Linko AM and Adlercreutz H. Whole-grain rye and wheat alkylresorcinols are incorporated into human erythrocyte membranes. British Journal of Nutrition. 2005 Jan; 93:11–13. https://doi.org/10.1079/BJN20041281 PMID: 15705219

64. Liukkonen KH, Katina K, Wilhelmsson A, Myllymaki O, Lampi AM, Kariluoto S, et al. Process-induced changes on bioactive compounds in whole grain rye. Proceedings of the Nutrition Society. 2003 Feb; 62:117–122. https://doi.org/10.1079/PNS2002218 PMID: 12740066

65. Chhabra RS. Toxicology and Carcinogenesis Studies of 4-Hexylresorcinol (CAS No 136-77-6) in F344/N Rats and B6C3F1 Mice (Gavage Studies). Natl Toxicol Program Tech Rep Ser. 1988 May; 330:1–166. PMID: 12732906

66. Yen GC, Duh PD, Lin CW. Effects of Resveratrol and 4-hexylresorcinol on Hydrogen Peroxide-induced Oxidative DNA Damage in Human Lymphocytes. Free Radical Research. 2003 Jan; 37:509–514. https://doi.org/10.1080/1071576031000083099 PMID: 12797471

67. Sumino M, Sekine T, Ruangrungsi N, Igarashi K, Ikegami F. Ardisiphenols and Other Antioxidant Principles from the Fruits of Ardisia colorata. J-STAGE Chemical and Pharmaceutical Bulletin. 2002; 50:1484–1487. https://doi.org/10.1248/cpb.50.1484 PMID: 12419914

68. Kim SG, Lee SW, Park YW, Jeong JH, Choi JY. 4-hexylresorcinol inhibits NF-κB phosphorylation and has a synergistic effect with cisplatin in KB cells. Oncology Reports. 2011 Dec; 26:1527–1532. https://doi.org/10.3892/or.2011.1436 PMID: 21874263

69. González-Aguilar GA, Wang CY, Buta JG. Maintaining Quality of Fresh-Cut Mangoes Using Antibrowning Agents and Modified Atmosphere Packaging. Journal of Agricultural and Food Chemistry. 2000 Sep; 48:4204–4208. https://doi.org/10.1021/jf991384j PMID: 10995338

70. Buta JG, Moline HE, Spaulding DW, Wang CY. Extending Storage Life of Fresh-Cut Apples Using Natural Products and Their Derivatives. Journal of Agricultural and Food Chemistry. 1999 Jan; 47:1–6. https://doi.org/10.1021/jf980712x PMID: 10563838

6 Discussion and Outlook

In the context of the presented PhD thesis, strategies to improve non-viral gene delivery have been investigated on three levels. These levels are from innermost to the outside: The lipid composition of the nanoparticle, the interactions of lipid-based nanoparticles with DNA, and the decoration of the lipid nanoparticle surface with shielding and targeting moieties. On top, strategies to improve the preclinical investigation of nanomedicines using the zebrafish embryo animal model have been proposed. Selected points of these four working packages shall be discussed and put into a larger context in the following sections.

6.1 Lipid-based Gene Delivery Vehicles

The first attempts towards lipid-based gene delivery were made in the late 70's and involved phosphatidylcholine. [102] This report inspired a number of researchers to use different phosphatidylcholine-based formulations to deliver genetic materials to a wide variety of organisms. [103–106] However, phosphatidylcholine, a zwitterionic molecule, showed poor gene delivery efficiency compared to lipid compounds developed later. The next important discovery was made in the late 80's when Felgner et al. synthesized the first cationic lipid N-[1-(2,3-dioleyloxy)-propyl]-N,N,N-trimethylammonium chloride (DOTMA). [107] Compared to previous compounds, this cationic lipid was highly effective in gene delivery. As a consequence, cationic lipid-based gene delivery gained momentum and in the following years, a number of cationic lipids were synthesized and published. [108–110] It seemed as if cationic lipids were the way gene delivery is done. In fact, cationic lipids offer a number of advantages, including very high DNA condensation capacity, and thereby a good protection of the encapsulated nucleic acids, [111] and facilitated interactions between the pos-

itively charged nanoparticle and the negatively charged cell membranes. [112] Up to this day, cationic lipids represent the most commonly used gene delivery systems due to these advantages and the simplicity of nanoparticle/DNA complexation. [113, 114] However, cationic lipids also suffer from some severe drawbacks, including unspecific interactions with cell membranes, [115] accumulation in highly negatively charged tissues such as the lungs, [116, 117] and interactions with cellular proteins leading to cytotoxicity. [118–120] It is therefore very important to weigh between efficiency and toxicity of a cationic lipid-based gene delivery system.

A solution to this problem came in the early 2000's with the synthesis of novel ionizable lipids for gene delivery. [121, 122] Ionizable lipids do not carry a permanent cationic charge but are designed to be positively charged only where necessary (*e.g.*, during complex formation) and uncharged when a cationic charge is detrimental (*e.g.*, in the blood circulation). For the design ionizable lipids, the pKa value plays a very important role. For example, the most efficient ionizable lipidoids of the Anderson group and ionizable lipids of the Cullis group both show pKa values in the range of 6.0 - 6.8. [9, 123, 124] This way, ionizable lipid/nucleic acid nanoparticles can be formed at low pH (*e.g.*, pH 4) where the lipid is ionized and therefore carries a cationic charge to ensure proper DNA condensation. Upon injection into the blood stream (or after buffer change to pH 7.4), the complex is neutral and does therefore not interact with serum components or cell membranes, thereby ensuring a prolonged circulation half life. After (targeted) uptake into the cell, the lipid becomes charged again due to the acidification of the endosome. The ionized lipids can then interact with negatively charged lipids of the endosomal membrane, leading to a lipid flip-flop and subsequent displacement of the negatively charged nucleic acids, resulting in endosomal escape of the encapsulated cargo. [125,126] Additionally, ionizable lipids often show reduced cytotoxicity due to their transient

charge as opposed to permanently charged cationic lipids. [127]
However, the synthesises of such sophisticated lipid compounds are complex, include several reaction steps and are therefore often associated with low yields. It was therefore the goal in **Chapter 1.2** to evaluate the feasibility of a one-pot approach based on double-reactive amination to obtain short-chain aminolipid compounds for gene delivery. The molecular structure of lipids for gene delivery can generally be divided into three categories: The headgroup, the tailgroup, and a linker functionality that connects head- and tailgroup. The linker functionality can have an important influence on the flexibility of charge presentation and biodegradability. [128] Owing to the nature of the reaction, however, the presented library consisted only of head- and tailgroups, whereas a linker functionality was not introduced. In this study, we could show that short-chain aminolipids are successfully synthesized using double-reactive amination and that methoxy-headgroups and C_{12} tails are superior to other headgroups and C_{10} tails. Because the study was focused on the feasibility of the reaction and the influence of a small number head- and tailgroups on transfection efficiency, no emphasis was paid on the pKa of the final products, which is considered an important factor nowadays. This flaw became obvious when combining our potentially ionizable aminolipids with cholesterol. The aim of replacing the permanently charged cationic lipid 1,2-dioleoyl-3-(trimethylammonium) propane (DOTAP) with aminolipids was not achieved. There was no particle formation, probably due to the absence of any charge that could condense DNA within the nanoparticle. Surprisingly, when DOTAP was combined with aminolipids instead of cholesterol, a number of candidates were able to improve the transfection efficiency compared to conventional DOTAP:cholesterol nanoparticles. A possible explanation for this phenomenon could be the small size of aminolipid headgroups and their short tailgroups. This facilitates lipid rearrangement within the membrane leaflets

of small multilamellar nanoparticles, which in turn reduces the nanoparticle membrane rigidity compared to cholesterol. It was shown for biological membranes that the reduction of the cholesterol content results in higher membrane fluidity, [129, 130] and therefore, increased likelihood of membrane rearrangements. Additionally, it was shown that cholesterol contents in membranes above 20 mol% decrease the the rate of membrane lipid translocation between membrane leaflets of a bilayer. [131] Therefore, the replacement of cholesterol with aminolipids could increase the rate of lipid rearrangement within the membrane which also facilitates lipid flip-flop between the bilayer of membranes. An additional explanation could be the ionization of aminolipids. It can be assumed that the nitrogen in aminolipids is ionized at lower pH, therefore increasing the net cationic charge of the nanoparticle. Anionic lipids of the endosomal membrane can then displace anionic DNA inside the nanoparticle and pair with the cationic lipids to form non-bilayer structures, [127] thereby disrupting the endosomal membrane and facilitating endosomal escape. The observed improvement of transfection efficiency could as well be the result of the combination of both effects. A further improvement of endosomal escape and therefore, improved transfection efficiency, could be achieved by introducing unsaturated lipid tails to aminolipids. Unsaturated lipid tails were shown to promote increased membrane fluidity, [132] thereby further increasing the likelihood of membrane rearrangements.

For DOTAP-based nanoparticles, aminolipids can be an interesting option to improve the transfection efficiency of said nanoparticles. However, some open questions remain. Cholesterol is a natural component of cell membranes whereas aminolipids are not. The toxic potential of aminolipids, and especially their long-term toxic potential, remains largely unclear. Therefore, the replacement of cholesterol with aminolipids is an effective but not necessarily safe option to improve the performance of DOTAP-based nanoparti-

cles. Moreover, the increase in transfection efficiency was only observed for DOTAP-based nanoparticles, but not for nanoparticles based on the ionizable lipid dilinoleylmethyl-4-dimethylaminobutyrate (DLin-MC3-DMA). This shows once more that there is no "one size fits it all approach" and that further research is necessary to improve our understanding of lipid components and their influence on interactions between nanoparticles and cells or even organisms. To improve our understanding of the underlying principles, further research with an expanded lipid library, including longer lipid tail lengths (*e.g.*, C_{14}, C_{16}, C_{18}) and unsaturated lipid tails, as well as a larger number of headgroups is needed. Regarding the headgroup, special emphasis should be put on the pKa value of the nitrogen group to obtain ionizable lipids that are able to form nanocomplexes together with DNA without the need for the cationic lipid DOTAP. Conclusively, the presented data demonstrates the validity of our approach to improve a clinically relevant nanoparticle formulation and deepens our understanding of the influence of molecular structures on lipid-based gene delivery.

6.2 DNA-Nanoparticle Interaction

Besides the lipid composition of nanoparticles, the type of DNA is another major contributor to gene delivery efficiency. Optimized DNA molecules such as minicircle DNA, which are devoid of the bacterial backbone that usually present in plasmid DNA, are associated with higher gene delivery efficiency and transgene expression levels, [133, 134] which was also observed in our study. (**Chapter 2.1**) [44] There are a number of explanations for the superior performance of minicircle DNA compared to its parental plasmid counterpart. These include for example the reduction of immunogenicity and epigenetic silencing due to removal of sequences of bacterial origin, [41,42,135] the increased mobility of smaller nucleic acid moieties in the cytoplasm and thereby improved nu-

clear translocation, [136–140] or higher numbers of minicircle DNA molecules delivered compared to its larger parental plasmid when the same mass of DNA is used. [141]

There are a number of papers in which the total amount of delivered DNA was quantified using quantitative polymerase chain reaction (qPCR) [142–145] or in which equimolar amounts of plasmids were delivered to remove the numerical bias on the superiority of minicircle DNA over parental plasmid DNA. [146–149] However, neither of these methods are able to provide information on the interactions between DNA molecules and nanoparticles and the latter approach is additionally biased by the fact that calculations might not properly reflect the actual experimental conditions. To improve the understanding of DNA-nanoparticle interactions, fluorescence cross-correlation spectroscopy (FCCS) was applied in **Chapter 2.1**. The investigation of lipoplexes of DNA and either a cationic lipid (DOTAP), an ionizable lipid (DLin-MC3-DMA), or a commercially available transfection reagent (Lipofectamine 3000) showed that DNA-nanoparticle interactions were different for each formulation. This observation can be explained by the structural differences of nanoparticles depending on the nanoparticle formulation. While DOTAP- and DLin-MC3-DMA-based formulations both adopt a small multilamellar vesicle structure where the nucleic acid is sandwiched between the lipid bilayers (Figure 1 and [36]), Lipofectamine 3000 is a liposomal formulation. According to the manufacturer, nucleic acids are mainly attached to the surface of the liposome but are not internalized. [150] However, the information on Lipofectamine 3000 is sparse due to its proprietary status. Therefore, it is difficult to draw further conclusions. Interestingly, our FCCS experiments correlate with these data since high DNA binding was observed for the multilamellar DOTAP- and DLin-MC3-DMA-based formulations and only weak binding was observed for Lipofectamine 3000-DNA interactions. Furthermore, the method allows to

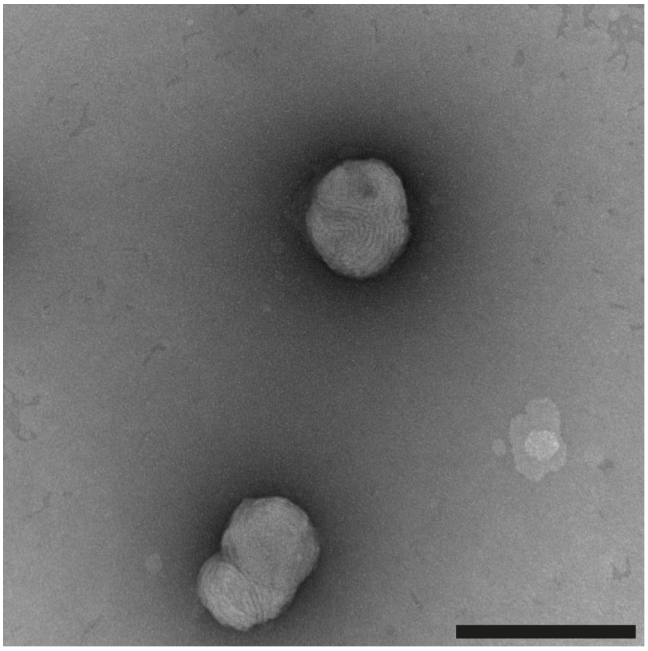

Figure 1: Transmission electron microscopy of DOTAP:cholesterol nanoparticles. The figure shows that DOTAP:cholesterol lipid nanoparticles (LNPs) adopt a small multilamellar vesicle structure. Nucleic acids are not only attached to the surface of the LNP but are mainly sandwiched between lipid bilayers by means of electrostatic interactions between the anionic phosphate backbone of DNA and cationic lipids. Scale bar = 200 nm.

determine the number of DNA molecules per nanoparticle after lipoplex formation. This number has so far only been calculated.

However, the method has some limitations as well. First, the method aims to determine interactions between nanoparticles and DNA. The method gives no information on where possible losses of DNA or nanoparticles occur but can only provide information on the final product after complexation (*i.e.*, lipoplexes). Second, the method provides only information on the interaction between DNA and nanoparticles but it cannot provide information on interactions between DNA and specific lipid components of the formulation. To improve our understanding of lipid-based gene delivery, it would be very interesting to determine which components of a formulation interact with DNA. For example, Kulkarni et al. applied cryo-TEM and molecular modeling to de-

termine interactions between formulation components and nucleic acids. [36] A method that could elucidate this question could improve formulation development, particularly when fine-tuning of a formulations towards specific needs is required. Conclusively, the measurements demonstrated that assumptions based on calculations are flawed and therefore, may lead to wrong conclusions. Furthermore, it is not possible to draw universally applicable conclusions that are valid for all lipid-based transfection reagents but the interactions have to be determined for each individual formulation.

FCCS is a very powerful technique with a wide variety of possible applications. An excellent in-depth discussion of FCCS and its possible applications is provided by Naredi-Rainer. [151] In addition to DNA-nanoparticle interactions after complex formation, FCCS can also be applied to elucidate the behavior of lipoplexes in contact with serum proteins, [152–154] or the extracellular matrix, [155,156] and to characterize drug-loaded nanocarriers in the blood circulation. [157] Further applications include the determination of nanoparticle uptake into cells, [158,159] and, importantly, the intracellular fate of lipoplexes and DNA molecules. [158,160–163] The latter is of special importance because additional information on the behavior of lipoplexes following uptake into cells is highly needed. The method can provide information about the extent and the duration of protection of nucleic acids by lipid-based nanoparticles after uptake into cells. It is known that nucleic acids need to be protected by the nanocarrier also within the endo-/lysosome and that the composition of the nanocarrier influences endosomal escape. [164] However, nucleic acids must dissociate from the lipid-based nanocarrier prior to nuclear translocation in order to successfully transfect a cell. It was shown that the nucleus is inaccessible to DNA complexed with cationic lipids (in contrast to DNA complexed with cationic polymers). [165, 166] The lipoplex of DNA and nanocarrier is considered unable to cross the nuclear membrane due to the small size of the

nuclear pore of approximately 25 nm, [166,167] but even if it is injected directly into the nucleus, no gene expression is observed for cationic lipid/DNA complexes. [112,168] This is due to the fact that the nanocarrier not only protects the nucleic acid from nucleases but by the same mechanism makes it inacessible to the transcription machinery of the cell as well. Therefore, the timepoint and the location of lipoplex dissociation are important characteristics to understand successful transfection. It was shown that the distance between the place of lipoplex dissociation and the nucleus of the cell is crucial [169] and that only 1‰ of DNA injected into the cytosol arrives in the nucleus, [165,168,170] likely due to degradation of DNA by cytosolic nucleases. [111] FCCS could monitor DNA and nanoparticles and allow to determine the spatial and temporal point at which they dissociate, thereby improving our understanding of intracellular processes crucial for successful transfection.

6.3 Targeting and Blood Circulation Properties

One of the major advantages of nanoparticulate drug or gene delivery systems is the possibility to direct these nanomedicines to specific cell populations within the body using a targeting approach. The first conceptualization for targeted medicines was made over a century ago. It was in 1906 when Paul Ehrlich formulated the concept of a 'magic bullet' that would enable site-specific drug delivery while simultaneously eliminating off-target toxicity. [171] However, the translation from the concept to its actual application took a long time. It was in the field of oncology where the usefulness of nanoparticle-mediated targeted drug delivery first became apparent to the wider scientific community after the discovery of the Enhanced Permeation and Retention (EPR) effect by Matsumura and Maeda in 1986. [172] According to this publication, exploiting this effect would enable accumulation of nanoparticulate drug delivery systems in solid tumors. Despite the fact that the extent of this

effect is still debated until today (the effect is pronounced in mice models but not generally applicable to human tumors [173,174]), the field of nanomedicine gained popularity and experienced a rapid growth following this discovery and up to this day, the majority of nanoparticulate drug delivery systems still rely (or claim to rely) on the EPR effect. [174, 175]

Targeting approaches can be categorized into two distinct categories: passive targeting and active targeting. Passive targeting does not require targeting ligands but relies on the properties of the nanoparticulate delivery system or the targeted tissue. Consequently, passive targeting approaches show reduced batch-to-batch variability and facilitated synthesis, formulation and characterization. [176] Properties enabling passive targeting include for example the size and the surface charge of nanoparticulate delivery systems or inherent properties of the target tissue (or tumor) such as the EPR effect. The size of a nanoparticulate delivery system influences its biodistribution and thereby enables passive targeting. For example, nanoparticles exceeding 200-250 nm are predominantly cleared by spleen and liver-resident macrophages of the reticuloendothelial system (RES), leading to accumulation in these organs. [177–181] Interestingly, the extent of serum opsonization after injection in the blood circulation is influenced by the size as well. It was shown that nanoparticles with a diameter below 100 nm are less susceptible to opsonization by serum proteins, thereby prolonging the blood circulation half-life *in vivo*. [182, 183] The surface charge of a nanoparticle can influence its biodistribution as well with highly positively charged nanoparticles accumulating predominantly in the lungs and highly negatively charged nanoparticles being cleared by cells expressing scavenger receptors such as liver endothelial cells. [184,185] Finally, the exploitation of the EPR effect is possible due to two characteristics of solid tumors: First, tumor growth requires accelerated formation of blood vessels (neovascularization) to provide the tumor with nutrients and oxygen. Be-

cause normal vascularization requires a fine balance of pro- and antiangiogenic factors which is shifted towards proangiogenic factors in tumors, novel blood vessels supplying the tumor are often leaky. [186, 187] This enables nanoparticle extravasation from the blood vessel and accumulation in the tumor tissue. Second, the tumor growth impairs lymphatic drainage that would normally lead to nanoparticle clearance from the tumor, thereby pronouncing nanoparticle accumulation in the tumor tissue. [188, 189] However, discussions on this topic are ongoing and in many tumors in humans, including pancreatic cancer, the EPR effect is not observed. [189]

In contrast, active targeting relies on one or more targeting ligands. On the one hand, this increases variability and complexity of the system. On the other hand, active targeting allows for much more specific direction of nanoparticles to desired cell populations. [190] There is a wide variety of targeting ligands from small molecules, over peptides, to antibodies, and antibody fragments. [50–62] Interestingly, an advantage of antibody fragments is the lack of the Fc domain, resulting in reduced uptake by phagocytic cells of the RES, thereby increasing blood circulation time. [191–193] Active targeting relies on cellular surface structures (*e.g.*, receptors) that are overexpressed or exclusively expressed in the targeted cell population. [194, 195] The targeting ligand is then responsible for the specific uptake into the targeted cell population through interaction with the targeted receptor. Moreover, in the case of internalizing receptors, improved uptake into cells through specific pathways is another advantage of targeting approaches. [196]

With respect to liver targeting, a large majority of targeting approaches rely on either the asialoglycoprotein receptor (ASGPR) or the low density lipoprotein receptor (LDLR). [66, 197, 198] However, both of these approaches suffer from drawbacks. Targeting to the ASGPR requires complex synthesises to obtain the multivalent glycans that interact with the ASGPR [199] and

for LDLR targeting, it was shown that a majority of nanoparticles are recycled back to the cell exterior after uptake, thereby reducing the delivery efficiency. [200] Consequently, novel targeting approaches are needed. The proposed strategy presented in **Chapter 3.1** relies on peptide sequences of viral origin, namely sequences of the large envelope protein of hepatitis B virus (HBVpreS). It was shown that this peptide sequence interact with the sodium-taurocholate cotransporting polypeptide (NTCP). The HBV specifically targets and infects hepatocytes in a highly efficient manner. [63] Optimization of the targeting peptide showed improved systemic circulation behavior of shorter myristoylated peptide sequences (Myr-preS2-31) as opposed to longer peptide sequences (Myr-preS2-48). This can be attributed to the increased immunogenicity of longer peptides [201–204] resulting in a reduced circulation half life. Furhermore, the ligand density plays an important role in efficient delivery. Too low ligand densities (*i.e.*, $\leq$ 0.125 mol%) do not promote sufficient uptake into hepatocytes, probably due to a decreased number of interactions between targeting ligand and NTCP. Too high ligand densities (*i.e.*, $\geq$ 0.5 mol%) showed increased clearance from the blood circulation, probably due to immune responses. A ligand density of 0.25 mol% (corresponding to around 80 maleimide-conjugated Myr-preS2-31 moieties per nanoparticle) showed an optimal balance between targeting efficiency and circulation properties. Interestingly, the high species-dependency of HBV (which is unable to infect murine hepatocytes [205]) was not observed for this targeting peptide. Indeed, Myr-preS2-31-modified liposomes showed a pronounced uptake into murine hepatocytes. Finally, the presented lipopeptide can be synthesized by standard solid phase peptide synthesis in high yields and purity. This eliminates complex synthesises like in the case of ASGPR targeting. [65, 206, 207] Taken together, these results demonstrate the viability of the approach to exploit targeting mechanisms found in pathogens for successful drug or gene therapy.

Moreover, this viral peptide allows specific targeting of hepatocytes whereas other pathogens such as *Plasmodium spp.* initially target Kupffer cells before they are able to infect hepatocytes. [208]

Efficient targeting is only one aspect of successful drug or gene delivery using nanoparticles. Another important aspect comprises the blood circulation properties. Prolonged systemic circulation half-life is a prerequisite for successful targeted delivery of nanomedicines because it extends the timeframe during which nanomedicines can interact with the targeted surface structures. Even the most sophisticated and efficient targeting approaches are likely to result in clinical failure if the nanocarriers are rapidly cleared from circulation following intravenous injection. Unshielded nanoparticles are characterized by low systemic circulation half-life *in vivo* [209, 210] due to opsonization of the nanoparticle surface with opsonin proteins (complement compounds, immunoglobulins, fibronectin, and apolipoproteins [211]) and subsequent recognition by and uptake into phagocytic cells of the RES. [212] Hydrophobic surfaces are particularly prone to opsonization due to hydrophobic interactions with opsonins. A possible solution to this problem consists of surface modification with hydrophilic substances. [213] The first reports on the use of polyethylene glycol (PEG), a hydrophilic polymer, were published in 1977. In their study, Abuchowski et al. demonstrated prolonged systemic circulation half-life of bovine serum albumin and liver catalase following PEG modification (PEGylation). [214] The successful demonstration of prolonged blood circulation properties of PEGylated proteins inspired several researchers to investigate the applicability of the PEGylation concept to improve the circulation behavior of nanoparticles in the 80's and 90's. [72, 215, 216] The first PEGylated protein product, Adagen®, an adenosine deaminase enzyme for the treatment of severe-combined immunodeficiency (SCID) was approved by the FDA in 1990 [217] and the first PEGylated nanoparticle product, Doxil®,

in 1995. [47] Since that time, enhancement of circulation properties using PEGylation has been established as the most widely applied strategy to increase the blood circulation time of nanomedicines. [210, 218]

Advantages of PEGylation include not only reduced opsonization, but also reduced tendency of nanoparticles to aggregate due to the steric hindrance provided by PEG [219, 220] and, to a certain extent, shielding of excessive surface charge due to an increased distance between nanoparticle core surface and nanoparticle PEG brush surface, resulting in so-called 'stealth' nanoparticles. [221] Despite these advantages, an increasing number of researchers raise concerns towards PEGylation strategies due to the emergence of Anti-PEG antibodies. [222–225] There is increasing evidence that the phenomenon of accelerated blood clearance (ABC), *i.e.*, the gradual reduction in efficacy of PEGylated nanoparticles following repeated administration, is closely connected to the emergence of Anti-PEG antibodies. [226, 227] The reduced efficacy of PEGylated nanomedicines due to immune reactions to PEG is even more concerning considering the fact that Anti-PEG antibodies were even found in healthy individuals who were not treated with PEGylated nanomedicines so far. The emergence of Anti-PEG antibodies in healthy individuals is likely attributable to exposure to PEG moieties in products of everyday life such as cosmetics. [228, 229] Furthermore, there is indication that the anchoring phospholipid causes specific and nonspecific immune reactions as well, [82] likely due to the negative charge at the phosphate group of DSPE-PEG variants. [230, 231]

Taken together, these findings demonstrate the need to search for alternatives to PEG. Alternatives to PEG which exhibit similar properties with respect to water solubility or immunogenicity include, for example, hyperbranched polyglycerol (hbPG) [232–237] and polysarcosine (pSar) moieties. [238, 239] The applicability of the latter to enhance blood circulation properties of lipo-

somes was investigated in **Chapter 3.2**, whereas the former motivated us to establish a zebrafish Salmonella infection model **(Chapter 4.1)** as discussed later. We could show that bisalkyl polysarcosine (BA-pSar) is a valuable alternative to PEG. BA-pSar (more precisely: BA-pSar$_{102}$) was successfully and reproducibly synthesized with high yields ($\geq$90%) in a controllable one-step reaction. As discussed for lipid synthesis in the section 6.1 Lipid-based Gene Delivery Vehicles, polymer synthesis often involves multi-step reactions as well, leading to high variations between different batches. Batch-to-batch variability is a serious problem in polymer chemistry for nanoparticles, especially when it comes to scale-up. [240, 241] The obtained BA-pSar was successfully incorporated into liposomes based on the Doxil® formulation, yielding nanoparticles comparable to their DSPE-mPEG2k-modified counterparts with respect to size and polydispersity index (PDI) and with similar charge shielding properties. BA-pSar was firmly anchored in the lipid bilayer via its bisalkyl tails, thereby omitting the charged DSPE moiety, one of the structural properties responsible for complement activation. Further end group modification (*i.e.*, acetylation, BA-pSar$_{102}$Ac) removed the positive charge of the terminal amine group present in unmodified BA-pSar. As a consequence of this modification, uncharged BA-pSar$_{102}$Ac showed reduced immunogenicity in the complement activation assay with the immunogenicity increasing in the following order: BA-pSar$_{102}$Ac < DSPE-mPEG2k < BA-pSar$_{102}$. Notably, pSar is the polymer of sarcosine, an intermediate in glycine metabolism which is classified to be of low concern by the United States Environmental Protection Agency (EPA). [246] Therefore, immune responses to sarcosine are unlikely to occur. However, the ethylene glycol monomer is considered non-immunogenic as well, [224] showing that polymeric materials do not necessarily share the immunogenic properties of their respective monomer. This in combination with the large gap between first applications of PEGylated nanomedicines and the

discovery of immune reactions against PEG shows that long-term trials would be needed to rule out possible immune reactions to pSar-modified nanoparticles. Interestingly, the terminal amine end group of unmodified BA-pSar allows its modification with different moieties as well, thereby enabling straightforward coupling of *e.g.*, targeting moieties directly to BA-pSar. For example, the terminal amine of BA-pSar could be modified with maleimide [242] enabling coupling of thiolated moieties as described for Myr-preS2-31. [66] This way, the liver targeting approach described before could also be applied to BA-pSar-modified liposomes. Alternatively, BA-pSar could be synthesized with shorter alkyl chains and incorporated into ionizable lipid formulations based on DLin-MC3-DMA or DLin-KC2-DMA. Similar to short chain PEG anchors, the short chain alkyl anchor would allow rapid dissociation of BA-pSar shielding from the lipid nanoparticle, leading to interactions with apolipoprotein E (ApoE), thereby enabling targeted uptake into hepatocytes. [9, 127, 243] Finally, in the highly predictive zebrafish animal model, BA-pSar-modified liposomes circulated freely similar to DSPE-mPEG2k-modified liposomes whereas unmodified liposomes were cleared from circulation after 24h. [244, 245] Conclusively, the presented results demonstrate that BA-pSar moieties can be a valuable alternative to PEG when it comes to the improvement of systemic circulation properties of and the reduction of immune reactions to lipid-based nanomedicines.

6.4 Zebrafish Embryo *Salmonella* Infection Model

There are other possibilites to improve the circulation behavior of liposomes in a similar manner to PEG. One proposed class of substance is hyperbranched polyglycerol (hbPG). [232–237] In cooperation with the group of Prof. Mark Helm at the University of Mainz, we were asked to evaluate the blood circulation behavior of hbPG-modified liposomes in our zebrafish embryo animal

model (Figure 2). To our surprise, the hbPG-modified liposomes exhibited a

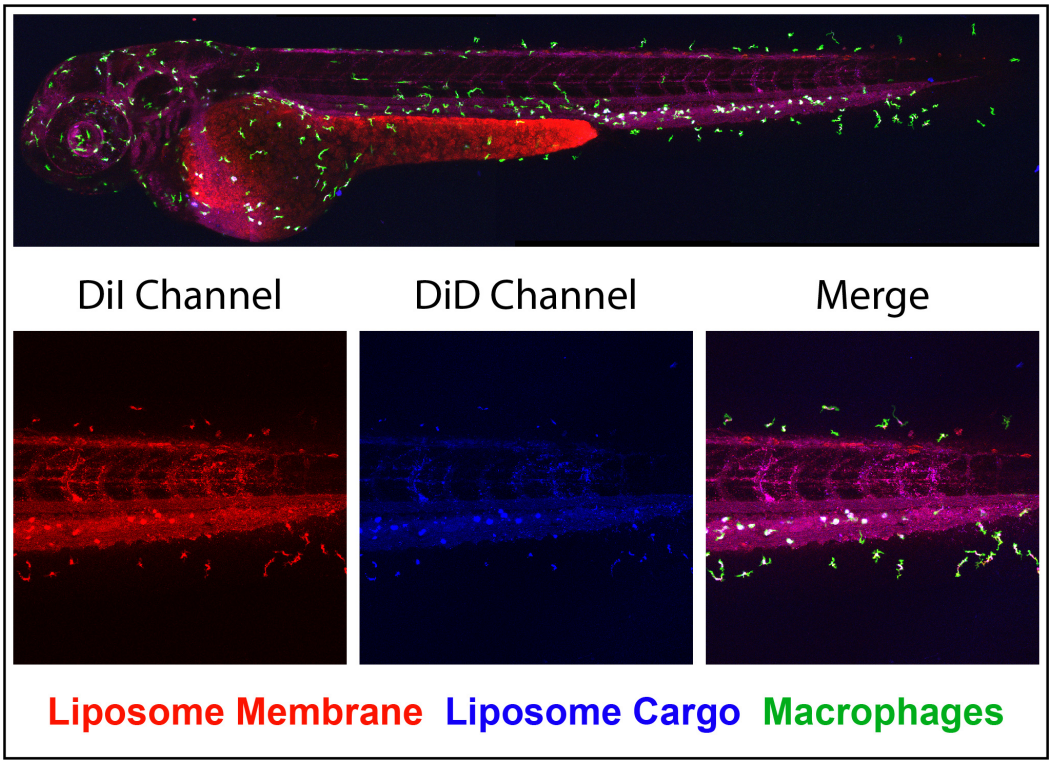

Figure 2: Macrophage accumulation of hbPG-modified liposomes. The figure shows the accumulation of hbPG-modified liposomes in macrophages four hours after injection. The labeled liposomes (red) encapsulating DiD (blue) as a liposome cargo model clearly accumulate in macrophages (green) of Tg(mpeg:Gal4;UAS:Kaede) zebrafish visualized by fluorescence colocalization of red, green, and blue dye, resulting in white color within the macrophages.

rapid uptake not only into macrophages with access to the blood circulation (round shape) but also into tissue-resident (star shape) macrophages. Except for the predominant uptake into macrophages, image analysis revealed a favorable blood circulation behavior, indicated by the diffuse staining pattern of the liposome membrane dye. [85] Therefore, hbPG-modification of liposomes represents a means to target macrophages. These unexpected results motivated us to investigate the applicability of hbPG-modified, antibiotics-loaded liposomes to treat systemic infections of pathogenic microorganisms that per-

sist within macrophages. *Salmonella spp.*, along with other pathogenic microorganisms such as *Mycobacterium tuberculosis* possess the ability to persist and even replicate within macrophages within so-called Salmonella containing vacuoles (SCV). [93–96, 247] This behavior is very problematic because these pathogenic microorganisms can evade an antibiotic treatment by this strategy, especially if the used antibiotics show poor cell membrane penetration properties (such as tobramycin). [248] After termination of the antibiotic treatment, theses microorganisms can reemerge due to uncontrolled replication within the macrophage leading to a burst of the macrophage and release of the microorgansims. This behavior was observed time and again during our experiments. Consequently, novel treatment approaches are needed to tackle macrophage-persistent pathogenic microorganisms. Another serious problem in the field of antibiotic treatment is the emergence of antibiotic resistance. In fact, the increasing inefficiency of antibiotic compounds for the treatment of infectious diseases caused by pathogenic microorganism is potentially one of the most serious problems of our century. [86] Widespread antibiotic resistance could well render present treatment regimens inefficient, leading to a relapse into a situation similar to the pre-antibiotic era during which infectious diseases caused by pathogenic microorganisms were one of the major causes of death. [249–251] However, at the same time the development of novel antibiotic compounds is unattractive to the pharmaceutical industry due to concerns that return of investment cannot be achieved because of strict regulations and due to the high costs associated with the development of novel antibiotic compounds. [252] One of the drivers of high costs are expensive animal trials. We therefore proposed the relatively inexpensive zebrafish animal model as a pre-selection tool for screenings. Not only does the high reproduction rate of zebrafish allow for high-throughput screenings but the pharmacokinetics of fluorescent liposomal antibiotic formulations can be assessed as well due to the transparency of this

animal model.

In view of this, we developed a zebrafish embryo *Salmonella* infection model (**Chapter 4.1**) to assess the applicability of hbPG-modified liposomes encapsulating antibiotics and of 4-hexylresorcinol as an antibiotic adjuvant (**Chapter 4.2**). To establish the *Salmonella* infection model, the dose of bacteria, the site of injection, and the temperature at which zebrafish embryos were kept, were assessed. Optimal results were obtained with a bacteria dose of 300 CFU injected into the Duct of Cuvier (termed vasculature injection) and when zebrafish were kept at 35°C. This temperature was chosen because it is the best compromise between human body temperature (37°C) and ideal zebrafish culture temperature (28°C). Unfortunately, zebrafish embryos did not survive at 37°C. The model was then validated using two antibiotics with different membrane penetration properties: Ceftriaxone (membrane penetrating) and tobramycin (no membrane penetrating). Survival analysis clearly showed the difference between the two antibiotics. Ceftriaxone-treated zebrafish exhibited high survival rates (almost 100%) and tobramycin-treated zebrafish showed reduced survival rates of only 50%. The results of the survival analysis were confirmed by qualitative fluorescence-based confocal imaging: Macrophages were almost completely free of *Salmonella* in ceftriaxone-treated zebrafish embryos whereas in tobramycin-treated zebrafish the majority of macrophages was still infected with large amounts of bacteria. Both treatments showed rapid clearance of bacteria in circulation. Therefore, we attributed the observed effects to the different penetration properties of the antibiotics.

However, despite the successful establishment of an animal model we were unable to demonstrate the superiority of either hbPG-modified liposomal formulation. There are several reasons for this failure: First, compared to free ceftriaxone, liposomal ceftriaxone did not improve bacteria eradication within macrophages and therefore, survival of the zebrafish (Figure 3). This is at-

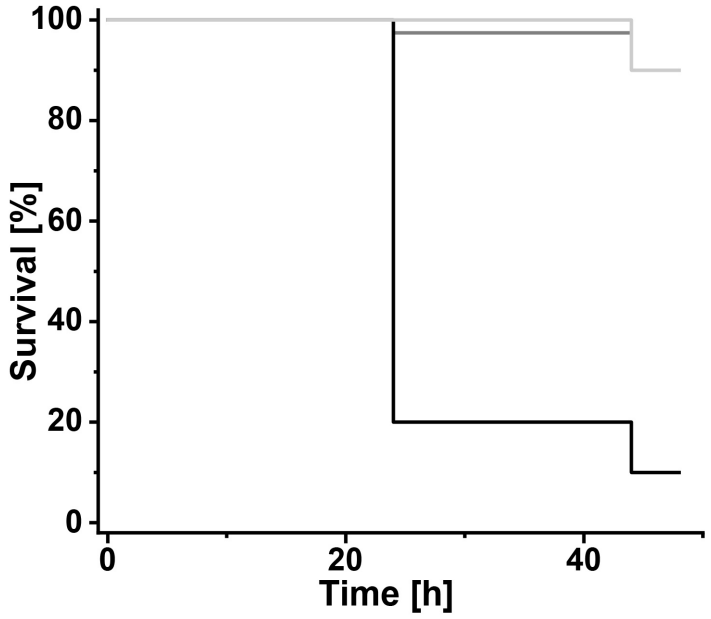

Figure 3: Survival analysis of zebrafish embryos infected with *Salmonella* treated with free or liposomal ceftriaxone. The figure shows the survival analysis of zebrafish embryos infected with 300 CFU *Salmonella*. Zebrafish were either treated ceftriaxone-loaded hbPG-modified liposomes (light grey), free ceftriaxone (dark grey) or PBS (black). There is no significant difference between liposomal and free ceftriaxone. (n=20).

tributed to the ability of free ceftriaxone to penetrate membranes. Therefore, macrophage-targeting liposomes are not necessary to eliminate bacteria within macrophages. Second, tobramycin encapsulated within macrophage-targeting liposomes was unable to eradicate bacteria in circulation following its intracellular release from the liposomes within the macrophages. Consequently, the bacteria in circulation were able to replicate and led to rapid death of treated zebrafish. Generally, bacteria replication in the vasculature had a much more pronounced influence on the survival of zebrafish embryos compared to replication within the macrophages. Therefore, eradication of bacteria in circulation is necessary to determine the treatment efficiency of liposomal tobramycin. Third, if zebrafish were treated with a combination of free and liposomal tobramycin, the bacteria in the vasculature were successfully eradicated after

four hours. However, accumulation of hbPG-modified liposomes was not effective enough to eradicate bacteria in all macrophages within a short timeframe. Tobramycin shows a short circulation half-life of only 2-3 h and is predominantly eliminated renally in humans (93% within 24 h). [253] The half-life of tobramycin in zebrafish embryos is likely similar to that in humans due to the close analogy between zebrafish and mammalian kidneys. [254] Very few untreated macrophages are therefore sufficient to allow *Salmonella* survival and replication, leading to rapid reinfection. The high bacteria load in circulation in combination with the presence of bursted macrophages after 24 hours indicate such an effect. Fourth, polymer chemistry is, as already mentioned in the section 6.3 Targeting and Blood Circulation Properties, associated with high batch-to-batch variabilities. Indeed, accumulation of hbPG-modified liposomes and circulation behavior varied to a large extent among the different experiments. These observations were made independent of the lipid composition of the formulation (Figure 4). Therefore, it is reasonable to assume that these differences are caused by the polymer. On top of that, our collaboration partner in Mainz had to change the supplier of educts for hbPG synthesis, thereby further increasing the variability of the synthesized polymers. Consequently, our fine-tuned animal model that allowed differentiation of free antibiotics struggled with the high variations inherent to the hbPG-modified liposomes (RSD up to 140% for survival after 24 h).

Possible solutions to these problems could be the decoration of liposomes with PEG350 and the use of a different strain of bacteria. First, decoration with short-chain PEG moieties such as PEG350 was shown to promote macrophage accumulation as well, as demonstrated by Sieber and co-workers. [245] An advantage of PEG350 is that it is commercially available as a well characterized, high quality product, thereby eliminating issues associated with high variability of small-scale polymer synthesis. Another possbility is the infection

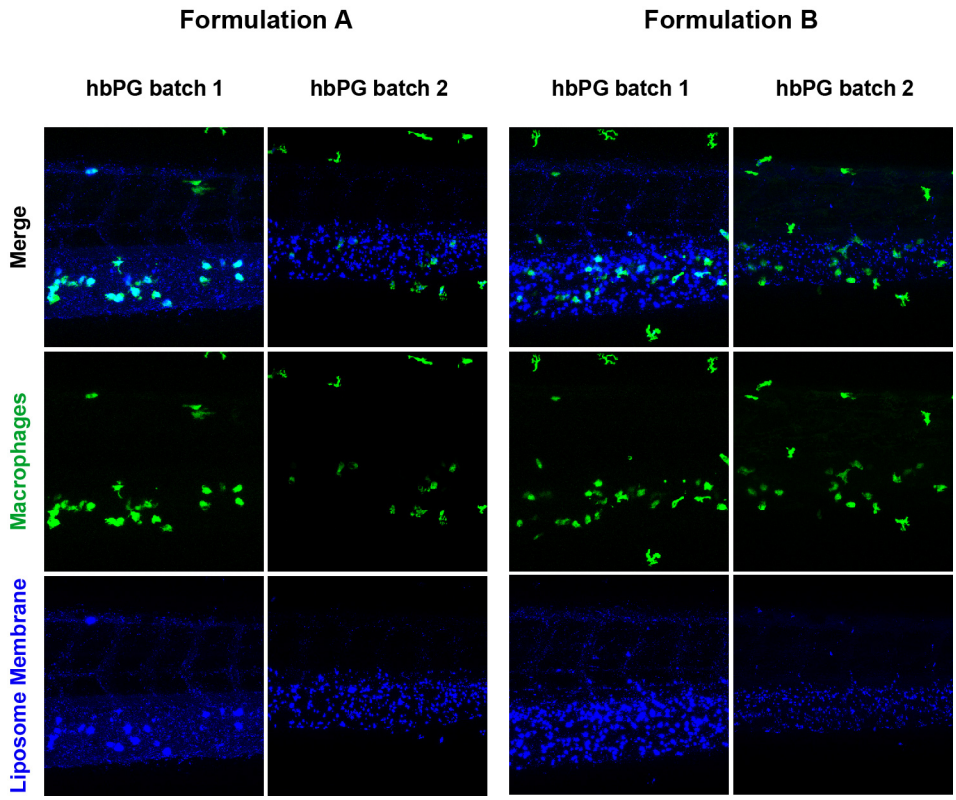

Figure 4: Confocal images showing the variability in macrophage accumulation and circulation behavior between two batches of hyperbranched polyglycerol (hbPG). The different hbPG batches lead to different macrophage accumulation and circulation behavior. Liposomes modified with hbPG batch 1 colocalized well with macrophages whereas liposomes modified with hbPG batch 2 showed only poor colocalization.

of zebrafish embryos with a different bacteria strain, namely the TIMER^{bac} strain, a strain of *Salmonella enterica* serovar Typhimurium SL1344 published by Claudi et al. in 2014. [255] This bacteria strain expresses two different fluorescent proteins depending on the growth rate. Briefly, the bacteria express green fluorescent proteins in their replication phase and orange fluorescent proteins in the non-replicative status. Thus, TIMER^{bac} can be used as a growth reporter. Using this strain, the effect of liposomal formulations of antibiotics on the intracellular replication of bacteria can be assessed qualitatively. This strategy does not allow for quantification of the effect but it could qualita-

tively demonstrate the applicability of the approach to eradicate intracellular pathogens *in vivo*.

In addition to the assessment of liposomal formulations of antibiotics, we employed our zebrafish embryo *Salmonella* infection model to assess the use of 4-hexylresorcinol (4-HR) as an antibiotic adjuvant, as well. Alkylresorcinols, including 4-HR, can be found in agricultural products such as grain and are considered safe bioactive nutrition components. [256] Doses up to 125 mg/kg showed no carcinogenic properties in mice [257] but possess antimutagenic [258] and antitumor properties. [259, 260] Alkylresorcinols are widely used in cosmetics and food industry [261, 262] and are authorized to be used in medical applications in humans. [257] 4-HR potentiated the activity of a selection of widely used antibiotics *in vitro* and *in vivo* as demonstrated in **Chapter 4.2**. Moreover, inclusion of 4-HR in antibiotic treatment was also highly efficient in eradicating persister cells and in preventing germination of spore forms. Both of these forms do not possess acquired antibiotic resistance but are considered an important link in the chain of antibiotic resistance development. The zebrafish *Salmonella* infection model was used to the assess the benefit of combination therapy. The zebrafish was chosen as a model organism because it allows to monitor the survival of a large number of animals, thereby increasing the reliability of the data and decreasing the impact of outliers. 4-HR is poorly water soluble with a solubility of only 800 mg/L (determined experimentally by Nikolaev and co-workers). Therefore, preliminary experiments aimed to assess the tolerability of dimethyl sulfoxide (DMSO) injections into zebrafish embryos. Injections of 100% DMSO were not well-tolerated by zebrafish embryos (survival 60%; denaturation of the tissue surrounding the injection site) but the survival drastically improved when the DMSO concentration was lowered. Injections of 50% DMSO in Dulbecco's phosphate-buffered saline (DPBS) were better tolerated in zebrafish embryos with a survival of 100% of the treated fish

after 24 h. However, the transparent surrounding tissue shifted to a black/grey color upon injection, possibly due to interactions of DMSO with serum proteins and cellular proteins (denaturation). Consequently, DMSO concentrations had to be reduced further. Color shifts were not observed anymore for a concentration of 25% DMSO in DPBS (survival 100%), a concentration which allowed to dissolve 2 mg/mL 4-HR. Therefore, injections of the maximum volume possible in zebrafish embryos (5 nL) enabled treatment with concentrations of up to 100 mg/L 4-HR within the zebrafish. Concentrations of 4-HR up to 60 mg/L were tolerated by zebrafish (survival 100% after 28 h). However, the combination of *Salmonella* injection, antibiotics injection (polymyxin), and 4-HR injection led to a drop in survival below 25% after 24 h. We speculated that this drop is caused by the injuries inflicted to zebrafish embryos by three injections. Therefore, 4-HR and antibiotics were combined in one sample in further experiments to reduce the number of injections. However, zebrafish embryos did not tolerate these conditions as well. Even a reduction of 4-HR concentration in the zebrafish embryos to 10 and 20 mg/L did not improve the survival (25% after 24 h). Although 4-HR is toxic especially to water organisms, the initial experiments indicating tolerability up to a concentration of 60 mg/L seemed promising at first. However, the combination of all interventions likely led to a synergistic reduction in survival that was not observed for the single factors alone. Finally, we aimed to improve the survival by eliminating 4-HR from the injection schedule. Zebrafish embryos were injected only with *Salmonella* and polymyxin and the fish were maintained in zebrafish culture medium supplemented with 10 or 20 mg/L 4-HR. However, zebrafish embryos did not tolerate the presence of 4-HR in the culture medium at all: All fish died within 4 hours irrespective of the 4-HR concentration (Figure 5). Probably, zebrafish embryos do not tolerate 4-HR in doses as high as 10 mg/L over prolonged periods of time. It is reasonable to assume that the difference in tol-

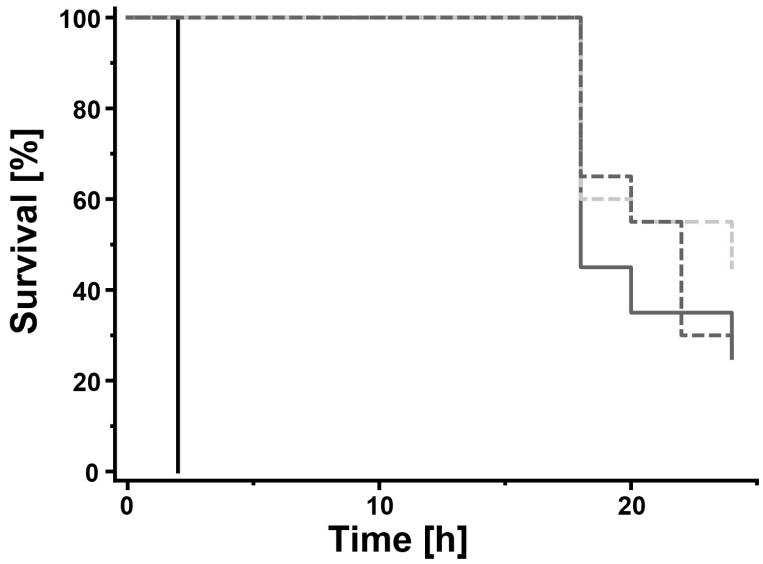

Figure 5: Survival analysis of zebrafish embryos treated with 4-hexylresorcinol (4-HR), Polymyxin, or combinations thereof. *Salmonella* infected zebrafish were treated with 100 pg Polymyxin (light grey dashed line), 20 mg/L 4-HR alone (dark grey solid line), 100 pg Polymyxin + 20 mg/L 4-HR (dark grey dashed line), or 100 pg Polymyxin in the presence of 20 mg/L 4-HR in the zebrafish culture medium (black solid line). Injected doses are given as the final concentration of 4-HR in the zebrafish embryos. (n=20).

erability between the two treatment variants (*i.e.*, 4-HR injection and addition of 4-HR to the medium) is caused by the different resulting plasma concentrations. The concept of absorption, distribution, metabolism, and excretion (ADME) can explain the observed effects. After injections of 2 ng 4-HR into zebrafish (total volume at the day of injection of up to 100 nL [263], resulting in a concentration of 20 mg/L in the fish), 4-HR is subjected to rapid elimination. The clearance of 4-HR in zebrafish can occur by several ways: Biliary elimination via the gall bladder and subsequent excretion via the intestine, renal excretion via the urine, elimination via the skin, and possibly elimination via the gills. Furthermore, a contribution of metabolism cannot be excluded. We therefore assume that intravenous injection of 4-HR results in transient exposure only. Compared to the volume of zebrafish culture medium (25 mL),

the total dose of 4-HR injected into all zebrafish embryos present in said volume of culture medium is negligible (40 ng). Injection of 4-HR is therefore in contrast to experiments in which the culture medium is supplemented with 4-HR. In this case, topical absorption of 4-HR from the culture medium overcomes excretion, resulting in a rapid increase of 4-HR plasma concentrations in the zebrafish. Additionally, accumulation of 4-HR in lipophilic environments cannot be excluded (logP = 3.45 [264]). As a consequence, zebrafish embryos are exposed to 4-HR over a prolonged period of time and die rapidly due to toxic effects. A drawback of the zebrafish embryo model is the fact that we could not determine the contributions of metabolism and elimination to the clearance of 4-HR. Therefore, clearance mechanisms for 4-HR need to be elucidated in different animal models (*e.g.*, mice or rats) because the measurement of plasma concentrations in zebrafish embryos is very challenging. In fact, novel methods sensitive enough to perform pharmacokinetic measurements in zebrafish embryos have been published only very recently. [265, 266] The technological advance may therefore enable pharmacokinetic studies in zebrafish in the near future.

Conclusively, our zebrafish embryo *Salmonella* infection model is probably the wrong animal model to investigate the effect of 4-HR (or other alkylresorcinols that share the specific toxicity towards water organisms) on the treatment of pathogenic microorganisms with antibiotics. Furthermore, the high variabilities in polymer chemistry resulted in highly variable circulation behavior and macrophage clearance for hbPG-modified liposomes. Therefore, the shortcomings in the preparation process of modified liposomes made it difficult to demonstrate the applicability of liposomal antibiotics formulations for the treatment of intracellular pathogens. Despite these setbacks, the established zebrafish embryo *Salmonella* infection model could be an interesting research tool for the screening of novel antibiotics because it was able to clearly differen-

tiate the two antibiotics. The differences in effectiveness of the two antibiotic compounds were reflected by both, survival analysis and confocal imaging and are in good accordance with the physicochemical properties of the antibiotic compounds. Moreover, the model can provide deeper insights into mechanisms of antibiotic therapy, especially if the established model were combined with the bacterial growth reporter *Salmonella* strain TIMER^{bac}.

7 Conclusion

In the context of this PhD thesis, four major working packages (**Chapters 1-4**) were investigated. The presented working packages cover four areas of lipid-based gene and drug delivery from the inside to the outside, starting with nanoparticle lipid composition and ending with the application of the zebrafish embryo animal model.

First, an overview of the current state of lipid-based gene delivery was provided and factors influencing gene delivery *in vitro* and *in vivo* were discussed. Furthermore, the successful application of a simplified lipid synthesis for DNA delivery was demonstrated. Short-chain aminolipids synthesized in a straightforward one-pot synthesis improved the gene delivery efficiency of a clinically relevant lipoplex formulation. Moreover, molecular structures important for gene delivery were discussed theoretically and evaluated practically in a Structure-Activity-Relationship experiment (**Chapter 1**).

Second, a fluorescence-based tool to investigate DNA-nanoparticle interactions was evaluated. The investigation of fluorescently-labeled DNA and nanoparticles using FCCS enabled the determination of the number of DNA molecules per nanoparticle. Moreover, the tool revealed qualitatively different interactions with DNA depending on the type of lipid-based gene delivery vehicles. These results demonstrate that ideally, DNA-nanoparticle interactions should be evaluated for each individual formulation (**Chapter 2**).

Third, novel approaches towards targeted delivery and enhancement of circulation properties of nanomedicines were evaluated. The presented targeting strategy relying on peptides derived from hepatitis B virus promoted highly efficient and selective uptake into hepatocytes. Enhancement of circulation properties similar to PEG but with reduced immunogenicity was achieved using a shielding strategy based on bisalkyl polysarcosines (**Chapter 3**).

Fourth, a zebrafish embryo animal model for the screening of antibiotic compounds was established and validated. The model was used to evaluate liposome-based antibiotic therapy and antibiotic adjuvants. Shortcomings of polymer synthesis for liposome-based antibiotic therapy and high toxicity of the adjuvant to zebrafish embryos prevented further examinations. Despite these drawbacks, the basic model could be very useful for the screening of novel antibiotic compounds and, when combined with bacterial growth reporters, for mechanistic investigations of antibiotic treatments as well (**Chapter 4**).

Conclusively, the the findings of this PhD thesis aim to improve our understanding of lipid nanoparticle-based gene and drug delivery and to provide additional tools for their preclinical investigation.

Abbreviations

4-HR	4-hexylresorcinol
ABC	Accelerated blood clearance
ABR	Antibiotic resistance
ADME	Absorption, distribution, metabolism, and elimination
ASGPR	Asialoglycoprotein receptor
BA-pSar	Bisalkyl polysarcosine
Cas9	CRISPR-associated protein 9
CRISPR	Clustered regularly interspaced short palindromic repeats
DLin-MC3-DMA	Dilinoleylmethyl-4-dimethylaminobutyrate
DMSO	Dimethyl sulfoxide
DOTAP	1,2-dioleoyl-3-(trimethylammonium) propane
DOTMA	N-[1-(2,3-dioleyloxy)-propyl]-N,N,N-trimethylammonium chloride
DPBS	Dulbecco's phosphate-buffered saline
DSPE-mPEG2k	1,2-distearoyl-sn-glycero-3-phosphoethanolamine-N-[methoxy(polyethylene glycol)-2000]
EPR effect	Enhanced permeation and retention effect
FCS	Fluorescence correlation spectroscopy
FCCS	Fluorescence cross-correlation spectroscopy
hbPG	Hyperbranched polyglycerol
GOI	Gene of interest
HBV	Hepatitis B virus
HBVpreS	Large HBV envelope protein
LDLR	Low density lipoprotein receptor

LNP	Lipid nanoparticle
MIC	Minimum inhibitory concentration
MPS	Mononuclear phagocytic system
mRNA	Messenger RNA
NTCP	Sodium-taurocholate cotransporting polypeptide
ORI	Origin of replication
PDI	Polydispersity index
PEG	Polyethylene glycol
polyA	Polyadenylation
pSar	Polysarcosine
qPCR	Quantitative polymerase chain reaction
RES	Reticuloendothelial system
RISC	RNA-induced silencing complex
RNAi	RNA interference
SCID	Severe-combined immunodeficiency
SCV	Salmonella containing vacuole
siRNA	Small interfering RNA

Bibliography

[1] Cox DBT, Platt RJ, Zhang F: *Therapeutic genome editing: prospects and challenges*. Nat Med. 2015 Feb;21(2):121–31, doi: 10.1038/nm.3793.

[2] Clayton PT: *Inborn errors presenting with liver dysfunction*. Semin Neonatol. 2002 Feb 1;7(1):49–63, doi: 10.1053/siny.2001.0086.

[3] Jansen PLM: *Diagnosis and management of Crigler-Najjar syndrome*. Eur J Pediatr. 1999 Nov 1;158(2):S089–94, doi: 10.1007/PL00014330.

[4] Marcuello E, Altés A, Menoyo A, del Rio E, Gómez-Pardo M, Baiget M: *UGT1A1 gene variations and irinotecan treatment in patients with metastatic colorectal cancer*. Br J Cancer. 2004 Aug 16;91(4):678–82, doi: 10.1038/sj.bjc.6602042.

[5] Kadakol A, Ghosh SS, Sappal BS, Sharma G, Chowdhury JR, Chowdhury NR: *Genetic lesions of bilirubin uridine-diphosphoglucuronate glucuronosyltransferase (UGT1A1) causing Crigler-Najjar and Gilbert syndromes: Correlation of genotype to phenotype*. Hum Mutat. 2000 Oct 1;16(4):297–306, doi: 10.1002/1098-1004(200010)16:4<297::AID-HUMU2>3.0.CO;2-Z.

[6] Schuchman EH, Wasserstein MP: *Types A and B Niemann-Pick disease*. Best Pract Res Clin Endocrinol Metab. 2015 Mar 1;29(2):237–47, doi: 10.1016/j.beem.2014.10.002.

[7] Marciniuk DD, Hernandez P, Balter M, Bourbeau J, Chapman KR, Ford GT, et al.: *Alpha-1 antitrypsin deficiency targeted testing and augmentation therapy: a Canadian Thoracic Society clinical practice guideline*. Can Respir J. 2012 Apr;19(2):109–16, doi: 10.1155/2012/920918.

[8] Winter J, Jung S, Keller S, Gregory RI, Diederichs S: *Many roads to maturity: microRNA biogenesis pathways and their regulation.* Nat Cell Biol. 2009 Mar;11(3):228–34, doi: 10.1038/ncb0309-228.

[9] Tam YYC, Chen S, Cullis PR: *Advances in Lipid Nanoparticles for siRNA Delivery.* Pharmaceutics. 2013 Sep 18;5(3):498–507, doi: 10.3390/pharmaceutics5030498.

[10] Sands MS, Davidson BL: *Gene therapy for lysosomal storage diseases.* Mol Ther. 2006 May 1;13(5):839–49, doi: 10.1016/j.ymthe.2006.01.006.

[11] Gaspar V, Melo-Diogo D de, Costa E, Moreira A, Queiroz J, Pichon C, et al.: *Minicircle DNA vectors for gene therapy: advances and applications.* Expert Opin Biol Ther. 2015 Mar 4;15(3):353–79, doi: 10.1517/14712598.2015.996544.

[12] Scherman D: *Advanced Textbook on Gene Transfer, Gene Therapy and Genetic Pharmacology: Principles, Delivery and Pharmacological and Biomedical Applications of Nucleotide-Based Therapies.* Imperial College Press 2014, doi: https://doi.org/10.1142/p820.

[13] Cameron JR, Philippsen P, Davis RW: *Analysis of chromosomal integration and deletions of yeast plasmids.* Nucleic Acids Res. 1977 Jun 1;4(5):1429–48, doi: 10.1093/nar/4.5.1429.

[14] Casey J, Daly C, Fitzgerald GF: *Chromosomal integration of plasmid DNA by homologous recombination in Enterococcus faecalis and Lactococcus lactis subsp. lactis hosts harboring Tn919.* Appl Environ Microbiol. 1991 Sep 1;57(9):2677–82.

[15] Lea A, Niakan KK: *Human germline genome editing.* Nat Cell Biol. 2019;21(12):1479–89, doi: 10.1038/s41556-019-0424-0.

[16] Hill IRC, Garnett MC, Bignotti F, Davis SS: *Determination of Protection from Serum Nuclease Activity by DNA–Polyelectrolyte Complexes Using an Electrophoretic Method.* Anal Biochem. 2001 Apr 1;291(1):62–8, doi: 10.1006/abio.2001.5004.

[17] Conway JW, McLaughlin CK, Castor KJ, Sleiman H: *DNA nanostructure serum stability: greater than the sum of its parts.* Chem Commun. 2013 Jan 14;49(12):1172–4, doi: 10.1039/C2CC37556G.

[18] Dimmock NJ, Easton AJ, Leppard KN: *Introduction to modern virology.* 6th ed., Malden, MA: Blackwell Pub, 2007, p. 10.

[19] Nayerossadat N, Maedeh T, Ali PA: *Viral and nonviral delivery systems for gene delivery.* Adv. Biomed. Res., vol. 1, Jul. 2012, doi: 10.4103/2277-9175.98152.

[20] del Pozo-Rodríguez A, Delgado D, Solinís MA, Gascón AR, Pedraz JL: *Solid lipid nanoparticles: Formulation factors affecting cell transfection capacity.* Int J Pharm. 2007 Jul 18;339(1):261–8.

[21] Szybalska EH, Szybalski W: *Genetics of human cell lines, IV. DNA-mediated heritable transformation of a biochemical trait.* Proc Natl Acad Sci U S A. 1962 Dec;48(12):2026–34.

[22] Wicki A, Witzigmann D, Balasubramanian V, Huwyler J: *Nanomedicine in cancer therapy: challenges, opportunities, and clinical applications.* J Control Release Off J Control Release Soc. 2015 Feb 28;200:138–57, doi: 10.1016/j.jconrel.2014.12.030.

[23] Reichmuth AM, Oberli MA, Jaklenec A, Langer R, Blankschtein D: *mRNA vaccine delivery using lipid nanoparticles.* Ther Deliv. 2016 May;7(5):319–34, doi: 10.4155/tde-2016-0006.

[24] Ramamoorth M, Narvekar A: *Non Viral Vectors in Gene Therapy - An Overview.* J Clin Diagn Res JCDR. 2015 Jan;9(1):GE01–6, doi: 10.7860/JCDR/2015/10443.5394.

[25] Cheng X, Lee RJ: *The role of helper lipids in lipid nanoparticles (LNPs) designed for oligonucleotide delivery.* Adv Drug Deliv Rev. 2016 Apr 1;99:129–37, doi: 10.1016/j.addr.2016.01.022.

[26] Cheow WS, Hadinoto K: *Factors affecting drug encapsulation and stability of lipid–polymer hybrid nanoparticles.* Colloids Surf B Biointerfaces. 2011 Jul 1;85(2):214–20, doi: 10.1016/j.colsurfb.2011.02.033.

[27] Gebauer JS, Malissek M, Simon S, Knauer SK, Maskos M, Stauber RH, et al.: *Impact of the Nanoparticle–Protein Corona on Colloidal Stability and Protein Structure.* Langmuir. 2012 Jun 26;28(25):9673–9, doi: 10.1021/la301104a.

[28] Ginn SL, Amaya AK, Alexander IE, Edelstein M, Abedi MR: *NGene therapy clinical trials worldwide to 2017: An update.* J Gene Med. 2018;20(5):e3015, doi: 10.1002/jgm.3015.

[29] Lu C, Stewart DJ, Lee JJ, Ji L, Ramesh R, Jayachandran G, et al.: *Phase I clinical trial of systemically administered TUSC2(FUS1)-nanoparticles mediating functional gene transfer in humans.* PloS One. 2012;7(4):e34833, doi: 10.1371/journal.pone.0034833.

[30] Rimkus T, Sirkisoon S, Harrison A, Lo H-W: *Tumor suppressor candidate 2 (TUSC2, FUS-1) and human cancers.* Discov Med. 2017;23(128):325–30.

[31] Buck J, Grossen P, Cullis PR, Huwyler J, Witzigmann D: *Lipid-Based DNA Therapeutics: Hallmarks of Non-Viral Gene Delivery.* ACS Nano. 2019 Apr 23;13(4):3754–82, doi: 10.1021/acsnano.8b07858.

[32] Buck J, Mueller D, Mettal U, Ackermann M, Grisch-Chan HM, Thöny B, et al.: *Improvement of DNA Vector Delivery of DOTAP Lipoplexes by Short Chain Aminolipids.* Manuscript in Revision, ACS Omega

[33] Habrant D, Peuziat P, Colombani T, Dallet L, Gehin J, Goudeau E, et al.: *Design of Ionizable Lipids To Overcome the Limiting Step of Endosomal Escape: Application in the Intracellular Delivery of mRNA, DNA, and siRNA.* J Med Chem. 2016 Apr 14;59(7):3046–62, doi: 10.1021/acs.jmedchem.5b01679.

[34] Fenton OS, Kauffman KJ, McClellan RL, Appel EA, Dorkin JR, Tibbitt MW, et al.: *Bioinspired Alkenyl Amino Alcohol Ionizable Lipid Materials for Highly Potent In Vivo mRNA Delivery.* Adv Mater. 2016;28(15):2939–43, doi: 10.1002/adma.201505822.

[35] Zhang J-S, Liu F, Huang L: *Implications of pharmacokinetic behavior of lipoplex for its inflammatory toxicity.* Adv Drug Deliv Rev. 2005 Apr 5;57(5):689–98, doi: 10.1016/j.addr.2004.12.004.

[36] Kulkarni JA, Darjuan MM, Mercer JE, Chen S, van der Meel R, Thewalt JL, et al.: *On the Formation and Morphology of Lipid Nanoparticles Containing Ionizable Cationic Lipids and siRNA.* ACS Nano. 2018 May 22;12(5):4787–95, doi: 10.1021/acsnano.8b01516.

[37] Scholz C, Wagner E: *Therapeutic plasmid DNA versus siRNA delivery: Common and different tasks for synthetic carriers.* J Controlled Release. 2012 Jul 20;161(2):554–65, doi: 10.1016/j.jconrel.2011.11.014.

[38] Wolff JA, Ludtke JJ, Acsadi G, Williams P, Jani A: *Long-term persistence of plasmid DNA and foreign gone expression in mouse muscle.* Hum Mol Genet. 1992 Sep 1;1(6):363–9, doi: 10.1093/hmg/1.6.363.

[39] Gill DR, Pringle IA, Hyde SC: *Progress and Prospects: The design and production of plasmid vectors*. Gene Ther. 2009 Feb;16(2):165–71, doi: 10.1038/gt.2008.183.

[40] Chen ZY, He CY, Meuse L, Kay MA: *Silencing of episomal transgene expression by plasmid bacterial DNA elements in vivo*. Gene Ther. 2004 May;11(10):856–64, doi: 10.1038/sj.gt.3302231.

[41] Chen ZY, Riu E, He CY, Xu H, Kay MA: *Silencing of Episomal Transgene Expression in Liver by Plasmid Bacterial Backbone DNA Is Independent of CpG Methylation*. Mol Ther. 2008 Mar 1;16(3):548–56, doi: 10.1038/sj.mt.6300399.

[42] Gracey Maniar LE, Maniar JM, Chen Z-Y, Lu J, Fire AZ, Kay MA: *Minicircle DNA Vectors Achieve Sustained Expression Reflected by Active Chromatin and Transcriptional Level*. Mol Ther. 2013 Jan;21(1):131–8, doi: 10.1038/mt.2012.244.

[43] Viecelli HM, Harbottle RP, Wong SP, Schlegel A, Chuah MK, VandenDriessche T, et al.: *Treatment of phenylketonuria using minicircle-based naked-DNA gene transfer to murine liver*. Hepatology. 2014;60(3):1035–43, doi: 10.1002/hep.27104.

[44] Buck J, Witzigmann D, Schenk SH, Einfalt T, Zweifel L, Grisch-Chan HM, et al.: *Characterization and Optimization of Lipoplexes: How to standardize Assays and avoid Pitfalls*. Manuscript ready for submission.

[45] Yun YH, Lee BK, Park K: *Controlled Drug Delivery: Historical perspective for the next generation*. J Controlled Release. 2015 Dec 10;219:2–7, doi: 10.1016/j.jconrel.2015.10.005.

[46] Vasir JK, Labhasetwar V: *Targeted Drug Delivery in Cancer Therapy.* Technol. Cancer Res. Treat. 2016, doi: 10.1177/153303460500400405.

[47] Barenholz Y: *Doxil®–the first FDA-approved nano-drug: lessons learned.* J Control Release Off J Control Release Soc. 2012 Jun 10;160(2):117–34, doi: 10.1016/j.jconrel.2012.03.020.

[48] Safary A, Akbarzadeh Khiavi M, Omidi Y, Rafi MA: *Targeted enzyme delivery systems in lysosomal disorders: an innovative form of therapy for mucopolysaccharidosis.* Cell Mol Life Sci. 2019 Sep 1;76(17):3363–81, doi: 10.1007/s00018-019-03135-z.

[49] Schellmann N, Deckert PM, Bachran D, Fuchs H, Bachran C: *Targeted enzyme prodrug therapies.* Mini Rev Med Chem. 2010 Sep;10(10):887–904, doi: 10.2174/138955710792007196.

[50] Cheung A, Bax HJ, Josephs DH, Ilieva KM, Pellizzari G, Opzoomer J, et al.: *Targeting folate receptor alpha for cancer treatment.* Oncotarget. 2016 May 27;7(32):52553–74, doi: 10.18632/oncotarget.9651.

[51] Fernández M, Javaid F, Chudasama V: *Advances in targeting the folate receptor in the treatment/imaging of cancers.* Chem Sci. 2017 Dec 18;9(4):790–810, doi: 10.1039/c7sc04004k.

[52] Li J, Zhang J, Zhang Q, Bai Z, Zhao Q, He D, et al.: *Syntheses and anti-cancer activity of CO-releasing molecules with targeting galactose receptors.* Org Biomol Chem. 2018 Nov 7;16(43):8115–29, doi: 10.1039/C8OB01921E.

[53] Sonoke S, Ueda T, Fujiwara K, Kuwabara K, Yano J: *Galactose-modified cationic liposomes as a liver-targeting delivery system for*

small interfering RNA. Biol Pharm Bull. 2011;34(8):1338–42, doi: 10.1248/bpb.34.1338.

[54] Asati S, Pandey V, Soni V: *RGD Peptide as a Targeting Moiety for Theranostic Purpose: An Update Study*. Int J Pept Res Ther. 2019 Mar 1;25(1):49–65, doi: 10.1007/s10989-018-9728-3.

[55] Garanger E, Boturyn D, Dumy P: *Tumor targeting with RGD peptide ligands-design of new molecular conjugates for imaging and therapy of cancers*. Anticancer Agents Med Chem. 2007 Sep;7(5):552–8, doi: 10.2174/187152007781668706.

[56] Johnsen KB, Burkhart A, Thomsen LB, Andresen TL, Moos T: *Targeting the transferrin receptor for brain drug delivery*. Prog Neurobiol. 2019;181:101665, doi: 10.1016/j.pneurobio.2019.101665.

[57] Daniels TR, Bernabeu E, Rodríguez JA, Patel S, Kozman M, Chiappetta DA, et al.: *The transferrin receptor and the targeted delivery of therapeutic agents against cancer*. Biochim Biophys Acta. 2012 Mar;1820(3):291–317, doi: 10.1016/j.bbagen.2011.07.016.

[58] Chen D, Parayath N, Ganesh S, Wang W, Amiji M: *The role of apolipoprotein- and vitronectin-enriched protein corona on lipid nanoparticles for in vivo targeted delivery and transfection of oligonucleotides in murine tumor models*. Nanoscale. 2019 Oct 17;11(40):18806–24, doi: 10.1039/C9NR05788A.

[59] Radwan AA, Alanazi FK: *Targeting cancer using cholesterol conjugates*. Saudi Pharm J SPJ. 2014 Jan;22(1):3–16, doi: 10.1016/j.jsps.2013.01.003.

[60] Attarwala H: *Role of antibodies in cancer targeting*. J Nat Sci Biol Med. 2010;1(1):53–6, doi: 10.4103/0976-9668.71675.

[61] Carter T, Mulholland P, Chester K: *Antibody-targeted nanoparticles for cancer treatment.* Immunotherapy. 2016;8(8):941–58, doi: 10.2217/imt.16.11.

[62] Richards DA, Maruani A, Chudasama V: *Antibody fragments as nanoparticle targeting ligands: a step in the right direction.* Chem Sci. 2016 Dec 19;8(1):63–77, doi: 10.1039/C6SC02403C.

[63] Asabe S, Wieland SF, Chattopadhyay PK, Roederer M, Engle RE, Purcell RH, et al.: *The Size of the Viral Inoculum Contributes to the Outcome of Hepatitis B Virus Infection.* J Virol. 2009 Oct 1;83(19):9652–62, doi: 10.1128/JVI.00867-09.

[64] Meier A, Mehrle S, Weiss TS, Mier W, Urban S: *TMyristoylated PreS1-domain of the hepatitis B virus L-protein mediates specific binding to differentiated hepatocytes.* Hepatology. 2013;58(1):31–42, doi: 10.1002/hep.26181.

[65] Schieck A, Schulze A, Gähler C, Müller T, Haberkorn U, Alexandrov A, et al.: *Hepatitis B virus hepatotropism is mediated by specific receptor recognition in the liver and not restricted to susceptible hosts.* Hepatology. 2013;58(1):43–53, doi: 10.1002/hep.26211.

[66] Witzigmann D, Uhl P, Sieber S, Kaufman C, Einfalt T, Schöneweis K, et al.: *Optimization-by-design of hepatotropic lipid nanoparticles targeting the sodium-taurocholate cotransporting polypeptide.* eLife. 2019 Jul 23;8:e42276, doi: 10.7554/eLife.42276.

[67] Liu F, Frick A, Yuan X, Huang L: *Dysopsonin activity of serum DNA-binding proteins favorable for gene delivery.* J Pharmacol Exp Ther. 2010 Feb;332(2):500–4, doi: 10.1124/jpet.109.159541.

[68] Immordino ML, Dosio F, Cattel L: *Stealth liposomes: review of the basic science, rationale, and clinical applications, existing and potential.* Int J Nanomedicine. 2006 Sep;1(3):297–315.

[69] Senior J, Crawley JC, Gregoriadis G: *Tissue distribution of liposomes exhibiting long half-lives in the circulation after intravenous injection.* Biochim Biophys Acta. 1985 Mar 29;839(1):1–8, doi: 10.1016/0304-4165(85)90174-6.

[70] Senior JH: *Fate and behavior of liposomes in vivo: a review of controlling factors.* Crit Rev Ther Drug Carrier Syst. 1987;3(2):123–93.

[71] Allen TM, Hansen C, Rutledge J: *Liposomes with prolonged circulation times: factors affecting uptake by reticuloendothelial and other tissues.* Biochim Biophys Acta. 1989 May 19;981(1):27–35, doi: 10.1016/0005-2736(89)90078-3.

[72] Klibanov AL, Maruyama K, Torchilin VP, Huang L: *Amphipathic polyethyleneglycols effectively prolong the circulation time of liposomes.* FEBS Lett. 1990;268(1):235–7, doi: 10.1016/0014-5793(90)81016-H.

[73] Jeon SI, Lee JH, Andrade JD, De Gennes PG: *Protein—surface interactions in the presence of polyethylene oxide: I. Simplified theory.* J Colloid Interface Sci. 1991 Mar 1;142(1):149–58, doi: 10.1016/0021-9797(91)90043-8.

[74] Allen TM: *Long-circulating (sterically stabilized) liposomes for targeted drug delivery.* Trends Pharmacol Sci. 1994 Jul;15(7):215–20, doi: 10.1016/0165-6147(94)90314-x.

[75] Yan X, Scherphof GL, Kamps JAAM: *Liposome opsonization.* J Liposome Res. 2005;15(1–2):109–39, doi: 10.1081/lpr-64971.

[76] Schöttler S, Becker G, Winzen S, Steinbach T, Mohr K, Landfester K, et al.: *Protein adsorption is required for stealth effect of poly(ethylene glycol)- and poly(phosphoester)-coated nanocarriers*. Nat Nanotechnol. 2016 Apr;11(4):372–7, doi: 10.1038/nnano.2015.330.

[77] Garay RP, Labaune JP: *Immunogenicity of Polyethylene Glycol (PEG)*. Open Conf Proc J. 2011 Oct 3;2(1), doi: 10.2174/2210289201102010104.

[78] Garay RP, El-Gewely R, Armstrong JK, Garratty G, Richette P: *Antibodies against polyethylene glycol in healthy subjects and in patients treated with PEG-conjugated agents*. Expert Opin Drug Deliv. 2012 Nov 1;9(11):1319–23, doi: 10.1517/17425247.2012.720969.

[79] Armstrong JK, Hempel G, Koling S, Chan LS, Fisher T, Meiselman HJ, et al.: *Antibody against poly(ethylene glycol) adversely affects PEG-asparaginase therapy in acute lymphoblastic leukemia patients*. Cancer. 2007;110(1):103–11, doi: 10.1002/cncr.22739.

[80] Hershfield MS, Ganson NJ, Kelly SJ, Scarlett EL, Jaggers DA, Sundy JS: *Induced and pre-existing anti-polyethylene glycol antibody in a trial of every 3-week dosing of pegloticase for refractory gout, including in organ transplant recipients*. Arthritis Res Ther. 2014 Mar 7;16(2):R63, doi: 10.1186/ar4500.

[81] Lipsky PE, Calabrese LH, Kavanaugh A, Sundy JS, Wright D, Wolfson M, et al.: *Pegloticase immunogenicity: the relationship between efficacy and antibody development in patients treated for refractory chronic gout*. Arthritis Res Ther. 2014 Mar 4;16(2):R60, doi: 10.1186/ar4497.

[82] Smyth HF, Carpenter CP, Weil CS: *The toxicology of the polyethylene glycols.* J Am Pharm Assoc Am Pharm Assoc. 1950 Jun;39(6):349–54, doi: 10.1002/jps.3030390615.

[83] Bleher S, Buck J, Muhl C, Sieber S, Barnert S, Witzigmann D, et al.: *Poly(Sarcosine) Surface Modification Imparts Stealth-Like Properties to Liposomes.* Small. 2019 Dec 1;15(50):1904716, doi: 10.1002/smll.201904716.

[84] Geisler R, Köhler A, Dickmeis T, Strähle U: *Archiving of zebrafish lines can reduce animal experiments in biomedical research.* EMBO Rep. 2017 Jan 1;18(1):1–2, doi: 10.15252/embr.201643561.

[85] Sieber S, Grossen P, Detampel P, Siegfried S, Witzigmann D, Huwyler J: *Zebrafish as an early stage screening tool to study the systemic circulation of nanoparticulate drug delivery systems in vivo.* J Control Release Off J Control Release Soc. 2017 Oct 28;264:180–91, doi: 10.1016/j.jconrel.2017.08.023.

[86] Guilfoile P, Alcamo IE: *Antibiotic-resistant bacteria.* Infobase Publishing, 2007. ISBN 978-0-7910-9188-3.

[87] Ochman H, Lawrence JG, Groisman EA: *Lateral gene transfer and the nature of bacterial innovation.* Nature. 2000 May;405(6784):299–304, doi: 10.1038/35012500.

[88] Hotopp JCD, Clark ME, Oliveira DCSG, Foster JM, Fischer P, Torres MCM, et al.: *Widespread Lateral Gene Transfer from Intracellular Bacteria to Multicellular Eukaryotes.* Science. 2007 Sep 21;317(5845):1753–6, doi: 10.1126/science.1142490.

[89] Lewis K: *Persister Cells.* Annu Rev Microbiol. 2010;64(1):357–72, doi: 10.1146/annurev.micro.112408.134306.

[90] Helaine S, Kugelberg E: *Bacterial persisters: formation, eradication, and experimental systems.* Trends Microbiol. 2014 Jul 1;22(7):417–24, doi: 10.1016/j.tim.2014.03.008.

[91] Grant SS, Hung DT: *Persistent bacterial infections, antibiotic tolerance, and the oxidative stress response.* Virulence. 2013 May 15;4(4):273–83, doi: 10.4161/viru.23987.

[92] Cabral DJ, Wurster JI, Belenky P: *Antibiotic Persistence as a Metabolic Adaptation: Stress, Metabolism, the Host, and New Directions.* Pharmaceuticals. 2018 Mar;11(1):14, doi: 10.3390/ph11010014.

[93] Alpuche-Aranda CM, Racoosin EL, Swanson JA, Miller SI: *Salmonella stimulate macrophage macropinocytosis and persist within spacious phagosomes.* J Exp Med. 1994 Feb 1;179(2):601–8, doi: 10.1084/jem.179.2.601.

[94] Nandre RM, Chaudhari AA, Matsuda K, Lee JH: *Immunogenicity of a Salmonella Enteritidis mutant as vaccine candidate and its protective efficacy against salmonellosis in chickens.* Vet Immunol Immunopathol. 2011 Dec 15;144(3):299–311, doi: 10.1016/j.vetimm.2011.08.015.

[95] Nandre RM, Mahajan P: *Salmonella Survival Inside the Macrophage.* Res & Rev: J Vet Sci. 2018 Mar;11(1):14.

[96] Newson JP: *Salmonella in Australia: understanding and controlling infection.* Microbiol Aust. 2017 Aug 9;11(1):14, doi: 10.1071/MA17044.

[97] McKinney JD, Bentrup KH zu, Muñoz-Elías EJ, Miczak A, Chen B, Chan W-T, et al.: *Persistence of Mycobacterium tuberculosis in macrophages and mice requires the glyoxylate shunt enzyme isocitrate lyase.* Nature. 2000 Aug;406(6797):735–8, doi: 10.1038/35021074.

[98] Chan J, Fan XD, Hunter SW, Brennan PJ, Bloom BR: *Lipoarabinomannan, a possible virulence factor involved in persistence of Mycobacterium tuberculosis within macrophages*. Infect Immun. 1991 May 1;59(5):1755–61.

[99] Gao L-Y, Pak M, Kish R, Kajihara K, Brown EJ: *A Mycobacterial Operon Essential for Virulence In Vivo and Invasion and Intracellular Persistence in Macrophages*. Infect Immun. 2006 Mar 1;74(3):1757–67, doi: 10.1128/IAI.74.3.1757-1767.2006.

[100] Buck J, Hauswirth P, Sieber S, Claudi B, Bumann D, Huwyler J: *Bacteria vs. antibiotics – Bridging infection modeling in Danio rerio*. Manuscript ready for submission.

[101] Nikolaev YA, Tutel'yan AV, Loiko NG, Buck J, Sidorenko SV, Lazareva I, et al.: *The Use of 4-Hexylresorcinol as Antibiotic Adjuvant*. Manuscript submitted to PLOS One.

[102] Mukherjee AB, Orloff S, Butler JD, Triche T, Lalley P, Schulman JD: *Entrapment of Metaphase Chromosomes into Phospholipid Vesicles (Lipochromosomes): Carrier Potential in Gene Transfer*. Proc Natl Acad Sci U S A. 1978;75(3):1361–5, doi: 10.2307/68000.

[103] Fraley RT, Fornari CS, Kaplan S: *Entrapment of a bacterial plasmid in phospholipid vesicles: potential for gene transfer*. Proc Natl Acad Sci U S A. 1979 Jul;76(7):3348–52.

[104] Fraley RT, Subramani S, Berg P, Papahadjopoulos D: *Introduction of liposome-encapsulated SV40 DNA into cells*. J Biol Chem. 1980 Nov 10;255(21):10431–5.

[105] Lurquin PF: *Entrapment of plasmid DNA by liposomes and their interactions with plant protoplasts.* Nucleic Acids Res. 1979 Aug 24;6(12):3773–84.

[106] Nicolau C, Le Pape A, Soriano P, Fargette F, Juhel MF: *In vivo expression of rat insulin after intravenous administration of the liposome-entrapped gene for rat insulin I.* Proc Natl Acad Sci U S A. 1983 Feb;80(4):1068–72.

[107] Felgner PL, Gadek TR, Holm M, Roman R, Chan HW, Wenz M, et al.: *Lipofection: a highly efficient, lipid-mediated DNA-transfection procedure.* Proc Natl Acad Sci U S A. 1987 Nov;84(21):7413–7.

[108] Gao X, Huang L: *A novel cationic liposome reagent for efficient transfection of mammalian cells.* Biochem Biophys Res Commun. 1991 Aug 30;179(1):280–5, doi: 10.1016/0006-291X(91)91366-K.

[109] Kurzchalia TV, Dupree P, Parton RG, Kellner R, Virta H, Lehnert M, et al.: *VIP21, a 21-kD membrane protein is an integral component of trans-Golgi-network-derived transport vesicles.* J Cell Biol. 1992 Sep;118(5):1003–14.

[110] Lee ER, Marshall J, Siegel CS, Jiang C, Yew NS, Nichols MR, et al.: *Detailed Analysis of Structures and Formulations of Cationic Lipids for Efficient Gene Transfer to the Lung.* Hum Gene Ther. 1996 Sep 10;7(14):1701–17, doi: 10.1089/hum.1996.7.14-1701.

[111] Lechardeur D, Sohn KJ, Haardt M, Joshi PB, Monck M, Graham RW, et al.: *Metabolic instability of plasmid DNA in the cytosol: a potential barrier to gene transfer.* Gene Ther. 1999 Apr;6(4):482–97, doi: 10.1038/sj.gt.3300867.

[112] Xu Y, Szoka FC: *Mechanism of DNA release from cationic liposome/DNA complexes used in cell transfection.* Biochemistry (Mosc). 1996 May 7;35(18):5616–23, doi: 10.1021/bi9602019.

[113] Zhao Y, Huang L: *Lipid Nanoparticles for Gene Delivery.* Adv Genet. 2014;88:13–36, doi: 10.1016/B978-0-12-800148-6.00002-X.

[114] Wang Y, Miao L, Satterlee A, Huang L: *Delivery of oligonucleotides with lipid nanoparticles.* Adv Drug Deliv Rev. 2015 Jun 29;87:68–80, doi: 10.1016/j.addr.2015.02.007.

[115] Wonder E, Simón-Gracia L, Scodeller P, Majzoub RN, Kotamraju VR, Ewert KK, et al.: *Competition of charge-mediated and specific binding by peptide-tagged cationic liposome-DNA nanoparticles in vitro and in vivo.* Biomaterials. 2018 Jun;166:52–63, doi: 10.1016/j.biomaterials.2018.02.052.

[116] Mansour HM, Rhee Y-S, Wu X: *Nanomedicine in pulmonary delivery.* Int J Nanomedicine. 2009;4:299–319.

[117] Sakurai F, Nishioka T, Yamashita F, Takakura Y, Hashida M: *Effects of erythrocytes and serum proteins on lung accumulation of lipoplexes containing cholesterol or DOPE as a helper lipid in the single-pass rat lung perfusion system.* Eur J Pharm Biopharm Off J Arbeitsgemeinschaft Pharm Verfahrenstechnik EV. 2001 Sep;52(2):165–72.

[118] Kunath K, von Harpe A, Fischer D, Petersen H, Bickel U, Voigt K, et al.: *Low-molecular-weight polyethylenimine as a non-viral vector for DNA delivery: comparison of physicochemical properties, transfection efficiency and in vivo distribution with high-molecular-weight polyethylenimine.* J Controlled Release. 2003 Apr 14;89(1):113–25, doi: 10.1016/S0168-3659(03)00076-2.

[119] Hsu CYM, Uludağ H: *A simple and rapid nonviral approach to efficiently transfect primary tissue-derived cells using polyethylenimine*. Nat Protoc. 2012 May;7(5):935–45, doi: 10.1038/nprot.2012.038.

[120] Godbey WT, Wu KK, Hirasaki GJ, Mikos AG: *Improved packing of poly(ethylenimine)/DNA complexes increases transfection efficiency*. Gene Ther. 1999 Aug;6(8):1380–8, doi: 10.1038/sj.gt.3300976.

[121] Heyes J, Palmer L, Bremner K, MacLachlan I: *Cationic lipid saturation influences intracellular delivery of encapsulated nucleic acids*. J Control Release Off J Control Release Soc. 2005 Oct 3;107(2):276–87, doi: 10.1016/j.jconrel.2005.06.014.

[122] Semple SC, Klimuk SK, Harasym TO, Dos Santos N, Ansell SM, Wong KF, et al.: *Efficient encapsulation of antisense oligonucleotides in lipid vesicles using ionizable aminolipids: formation of novel small multilamellar vesicle structures*. Biochim Biophys Acta. 2001 Feb 9;1510(1–2):152–66, doi: 10.1016/s0005-2736(00)00343-6.

[123] Whitehead KA, Dorkin JR, Vegas AJ, Chang PH, Veiseh O, Matthews J, et al.: *Degradable lipid nanoparticles with predictable in vivo siRNA delivery activity*. Nat Commun. 2014 Jun 27;5(1):1–10, doi: 10.1038/ncomms5277.

[124] Jayaraman M, Ansell SM, Mui BL, Tam YK, Chen J, Du X, et al.: *Maximizing the potency of siRNA lipid nanoparticles for hepatic gene silencing in vivo*. Angew Chem Int Ed Engl. 2012 Aug 20;51(34):8529–33, doi: 10.1002/anie.201203263.

[125] Chan H, Král P: *Nanoparticles Self-Assembly within Lipid Bilayers*. ACS Omega. 2018 Sep 5;3(9):10631–7, doi: 10.1021/acsomega.8b01445.

[126] Degors IMS, Wang C, Rehman ZU, Zuhorn IS: *Carriers Break Barriers in Drug Delivery: Endocytosis and Endosomal Escape of Gene Delivery Vectors*. Acc Chem Res. 2019 Jul 16;52(7):1750–60, doi: 10.1021/acs.accounts.9b00177.

[127] Cullis PR, Hope MJ: *Lipid Nanoparticle Systems for Enabling Gene Therapies*. Mol Ther. 2017 Jul 5;25(7):1467–75, doi: 10.1016/j.ymthe.2017.03.013.

[128] Sun S, Wang M, Knupp SA, Soto-Feliciano Y, Hu X, Kaplan DL, et al.: *Combinatorial Library of Lipidoids for In Vitro DNA Delivery*. Bioconjug Chem. 2012 Jan 18;23(1):135–40, doi: 10.1021/bc200572w.

[129] Cooper RA: *Influence of increased membrane cholesterol on membrane fluidity and cell function in human red blood cells*. J Supramol Struct. 1978;8(4):413–30, doi: 10.1002/jss.400080404.

[130] Fernández-Pérez EJ, Sepúlveda FJ, Peters C, Bascuñán D, Riffo-Lepe NO, González-Sanmiguel J, et al.: *Effect of Cholesterol on Membrane Fluidity and Association of Aβ Oligomers and Subsequent Neuronal Damage: A Double-Edged Sword*. Front Aging Neurosci. 2018;10, doi: 10.3389/fnagi.2018.00226.

[131] Allhusen JS, Kimball DR, Conboy JC: *Structural Origins of Cholesterol Accelerated Lipid Flip-Flop Studied by Sum-Frequency Vibrational Spectroscopy*. J Phys Chem B. 2016 Mar 31;120(12):3157–68, doi: 10.1021/acs.jpcb.6b01254.

[132] Leekumjorn S, Cho HJ, Wu Y, Wright NT, Sum AK, Chan C: *The Role of Fatty Acid Unsaturation in Minimizing Biophysical Changes on the Structure and Local Effects of Bilayer Membranes*. Biochim Biophys Acta. 2009 Jul;1788(7):1508–16, doi: 10.1016/j.bbamem.2009.04.002.

[133] Kreiss P, Cameron B, Rangara R, Mailhe P, Aguerre-Charriol O, Airiau M, et al.: *Plasmid DNA size does not affect the physicochemical properties of lipoplexes but modulates gene transfer efficiency*. Nucleic Acids Res. 1999 Oct 1;27(19):3792–8, doi: 10.1093/nar/27.19.3792.

[134] Ribeiro S, Mairhofer J, Madeira C, Diogo MM, Lobato da Silva C, Monteiro G, et al.: *Plasmid DNA size does affect nonviral gene delivery efficiency in stem cells*. Cell Reprogramming. 2012 Apr;14(2):130–7, doi: 10.1089/cell.2011.0093.

[135] Chen Z-Y, He C-Y, Ehrhardt A, Kay MA: *Minicircle DNA vectors devoid of bacterial DNA result in persistent and high-level transgene expression in vivo*. Mol Ther. 2003 Sep 1;8(3):495–500, doi: 10.1016/S1525-0016(03)00168-0.

[136] Vaughan EE, DeGiulio JV, Dean DA: *Intracellular Trafficking of Plasmids for Gene Therapy: Mechanisms of Cytoplasmic Movement and Nuclear Import*. Curr Gene Ther. 2006 Dec;6(6):671–81.

[137] Nafissi N, Alqawlaq S, Lee EA, Foldvari M, Spagnuolo PA, Slavcev RA: *DNA Ministrings: Highly Safe and Effective Gene Delivery Vectors*. Mol Ther - Nucleic Acids. 2014 Jan 1;3, doi: 10.1038/mtna.2014.16.

[138] Lukacs GL, Haggie P, Seksek O, Lechardeur D, Freedman N, Verkman AS: *Size-dependent DNA Mobility in Cytoplasm and Nucleus*. J Biol Chem. 2000 Jan 21;275(3):1625–9, doi: 10.1074/jbc.275.3.1625.

[139] Akita H, Kurihara D, Schmeer M, Schleef M, Harashima H: *Effect of the Compaction and the Size of DNA on the Nuclear Transfer Efficiency after Microinjection in Synchronized Cells*. Pharmaceutics. 2015 Jun 9;7(2):64–73, doi: 10.3390/pharmaceutics7020064.

[140] Vacik J, Dean BS, Zimmer WE, Dean DA: *Cell-specific nuclear import of plasmid DNA*. Gene Ther. 1999 Jun;6(6):1006–14, doi: 10.1038/sj.gt.3300924.

[141] Hardee CL, Arévalo-Soliz LM, Hornstein BD, Zechiedrich L: *Advances in Non-Viral DNA Vectors for Gene Therapy*. Genes. 2017 Feb;8(2):65, doi: 10.3390/genes8020065.

[142] Munye MM, Tagalakis AD, Barnes JL, Brown RE, McAnulty RJ, Howe SJ, et al.: *Minicircle DNA Provides Enhanced and Prolonged Transgene Expression Following Airway Gene Transfer*. Sci Rep. 2016 Mar 15;6:23125, doi: 10.1038/srep23125.

[143] Narsinh KH, Jia F, Robbins RC, Kay MA, Longaker MT, Wu JC: *Generation of adult human induced pluripotent stem cells using nonviral minicircle DNA vectors*. Nat Protoc. 2011 Jan;6(1):78–88, doi: 10.1038/nprot.2010.173.

[144] Stenler S, Wiklander OP, Badal-Tejedor M, Turunen J, Nordin JZ, Hallengärd D, et al.: *Micro-minicircle Gene Therapy: Implications of Size on Fermentation, Complexation, Shearing Resistance, and Expression*. Mol Ther - Nucleic Acids. 2014 Jan 1;3, doi: 10.1038/mtna.2013.67.

[145] Jia F, Wilson KD, Sun N, Gupta DM, Huang M, Li Z, et al.: *A nonviral minicircle vector for deriving human iPS cells*. Nat Methods. 2010 Mar;7(3):197–9, doi: 10.1038/nmeth.1426.

[146] Kobelt D, Schleef M, Schmeer M, Aumann J, Schlag PM, Walther W: *Performance of High Quality Minicircle DNA for In Vitro and In Vivo Gene Transfer*. Mol Biotechnol. 2013 Jan 1;53(1):80–9, doi: 10.1007/s12033-012-9535-6.

[147] Yin W, Xiang P, Li Q: *Investigations of the effect of DNA size in transient transfection assay using dual luciferase system.* Anal Biochem. 2005 Nov 15;346(2):289–94, doi: 10.1016/j.ab.2005.08.029.

[148] Dietz WM, Skinner NEB, Hamilton SE, Jund MD, Heitfeld SM, Litterman AJ, et al.: *Minicircle DNA is Superior to Plasmid DNA in Eliciting Antigen-specific CD8+ T-cell Responses.* Mol Ther. 2013 Aug;21(8):1526–35, doi: 10.1038/mt.2013.85.

[149] Kanada M, Kim BD, Hardy JW, Ronald JA, Bachmann MH, Bernard MP, et al.: *Microvesicle-Mediated Delivery of Minicircle DNA Results in Effective Gene-Directed Enzyme Prodrug Cancer Therapy.* Mol Cancer Ther. 2019;18(12):2331–42, doi: 10.1158/1535-7163.MCT-19-0299.

[150] ThermoFisher N: *How Cationic Lipid Mediated Transfection Works.* [[Internet]. Available from: https://www.thermofisher.com/uk/en/home/references/gibco-cell-culture-basics/transfection-basics/gene-delivery-technologies/cationic-lipid-mediated-delivery/how-cationic-lipid-mediated-transfection-works.html. [cited 2020 Mar 22].

[151] Naredi-Rainer N: *Advanced confocal microscopy.* [Text.PhDThesis]. Ludwig-Maximilians-Universität München; 2014 [cited 2020 Mar 2], Available from: https://edoc.ub.uni-muenchen.de/16834/.

[152] Röcker C, Pötzl M, Zhang F, Parak WJ, Nienhaus GU: *A quantitative fluorescence study of protein monolayer formation on colloidal nanoparticles.* Nat Nanotechnol. 2009 Sep;4(9):577–80, doi: 10.1038/nnano.2009.195.

[153] Milani S, Baldelli Bombelli F, Pitek AS, Dawson KA, Rädler J: *Reversible versus Irreversible Binding of Transferrin to Polystyrene Nanoparticles: Soft and Hard Corona.* ACS Nano. 2012 Mar 27;6(3):2532–41, doi: 10.1021/nn204951s.

[154] Nienhaus GU, Maffre P, Nienhaus K: *Studying the protein corona on nanoparticles by FCS.* Methods Enzymol. 2013;519:115–37, doi: 10.1016/B978-0-12-405539-1.00004-X.

[155] Kihara T, Ito J, Miyake J: *Measurement of Biomolecular Diffusion in Extracellular Matrix Condensed by Fibroblasts Using Fluorescence Correlation Spectroscopy.* PLoS ONE. 2013 Nov 28;8(11), doi: 10.1371/journal.pone.0082382.

[156] Leroux C-E, Monnier S, Wang I, Cappello G, Delon A: *Fluorescent correlation spectroscopy measurements with adaptive optics in the intercellular space of spheroids.* Biomed Opt Express. 2014 Sep 29;5(10):3730–8, doi: 10.1364/BOE.5.003730.

[157] Negwer I, Best A, Schinnerer M, Schäfer O, Capeloa L, Wagner M, et al.: *Monitoring drug nanocarriers in human blood by near-infrared fluorescence correlation spectroscopy.* Nat Commun. 2018 Dec 13;9(1):1–9, doi: 10.1038/s41467-018-07755-0.

[158] Bacia K, Majoul IV, Schwille P: *Probing the Endocytic Pathway in Live Cells Using Dual-Color Fluorescence Cross-Correlation Analysis.* Biophys J. 2002 Aug 1;83(2):1184–93, doi: 10.1016/S0006-3495(02)75242-9.

[159] Treuel L, Brandholt S, Maffre P, Wiegele S, Shang L, Nienhaus GU: *Impact of Protein Modification on the Protein Corona on*

Nanoparticles and Nanoparticle–Cell Interactions. ACS Nano. 2014 Jan 28;8(1):503–13, doi: 10.1021/nn405019v.

[160] Sasaki A, Kinjo M: *Fluorescence Cross-Correlation Spectroscopy for Real-Time Monitoring of Exogenous DNA Behavior in Living Cells*. Gene Ther Appl. 2011 Aug 23, doi: 10.5772/18970.

[161] Di Silvio D, Silvestri A, Lay L, Polito L, Moya SE: *Impact of ConcanavalinA affinity in the intracellular fate of Protein Corona on Glucosamine Au nanoparticles*. Sci Rep. 2018 Jun 13;8(1):1–11, doi: 10.1038/s41598-018-27418-w.

[162] Martinez-Moro M, Di Silvio D, Moya SE: *Fluorescence correlation spectroscopy as a tool for the study of the intracellular dynamics and biological fate of protein corona*. Biophys Chem. 2019 Oct 1;253:106218, doi: 10.1016/j.bpc.2019.106218.

[163] Di Silvio D, Martínez-Moro M, Salvador C, de los Angeles Ramirez M, Caceres-Velez PR, Ortore MG, et al.: *Self-assembly of poly(allylamine)/siRNA nanoparticles, their intracellular fate and siRNA delivery*. J Colloid Interface Sci. 2019 Dec 1;557:757–66, doi: 10.1016/j.jcis.2019.09.082.

[164] Gottfried LF, Dean DA: *Extracellular and Intracellular Barriers to Non-Viral Gene Transfer*. Nov Gene Ther Approaches. 2013 Feb 13, doi: 10.5772/54699.

[165] Pollard H, Remy J-S, Loussouarn G, Demolombe S, Behr J-P, Escande D: *Polyethylenimine but Not Cationic Lipids Promotes Transgene Delivery to the Nucleus in Mammalian Cells*. J Biol Chem. 1998 Mar 27;273(13):7507–11, doi: 10.1074/jbc.273.13.7507.

[166] Ditto AJ, Shah PN, Yun YH: *Non-viral gene delivery using nanoparticles*. Expert Opin Drug Deliv. 2009 Nov 1;6(11):1149–60, doi: 10.1517/17425240903241796.

[167] Liu G, Li D, Pasumarthy MK, Kowalczyk TH, Gedeon CR, Hyatt SL, et al.: *NNanoparticles of Compacted DNA Transfect Postmitotic Cells*. J Biol Chem. 2003 Aug 29;278(35):32578–86, doi: 10.1074/jbc.M305776200.

[168] Zabner J, Fasbender AJ, Moninger T, Poellinger KA, Welsh MJ: *Cellular and Molecular Barriers to Gene Transfer by a Cationic Lipid*. J Biol Chem. 1995 Nov 8;270(32):18997–9007, doi: 10.1074/jbc.270.32.18997.

[169] Zhou R, Geiger RC, Dean DA: *Intracellular trafficking of nucleic acids*. Expert Opin Drug Deliv. 2004 Nov;1(1):127–40, doi: 10.1517/17425247.1.1.127.

[170] Labat-Moleur F, Steffan AM, Brisson C, Perron H, Feugeas O, Furstenberger P, et al.: *An electron microscopy study into the mechanism of gene transfer with lipopolyamines*. Gene Ther. 1996 Nov;3(11):1010–7, doi: 10.1517/17425247.1.1.127.

[171] Strebhardt K, Ullrich A: *Paul Ehrlich's magic bullet concept: 100 years of progress*. Nat Rev Cancer. 2008 Jun;8(6):473–80, doi: 10.1038/nrc2394.

[172] Matsumura Y, Maeda H: *A new concept for macromolecular therapeutics in cancer chemotherapy: mechanism of tumoritropic accumulation of proteins and the antitumor agent smancs*. Cancer Res. 1986 Dec;46(12 Pt 1):6387–92.

[173] Lammers T, Kiessling F, Hennink WE, Storm G: *Drug targeting to tumors: Principles, pitfalls and (pre-) clinical progress*. J Controlled Release. 2012 Jul 20;161(2):175–87, doi: 10.1016/j.jconrel.2011.09.063.

[174] Nehoff H, Parayath NN, Domanovitch L, Taurin S, Greish K: *Nanomedicine for drug targeting: strategies beyond the enhanced permeability and retention effect*. Int J Nanomedicine. 2014 May 22;9:2539–55, doi: 10.2147/IJN.S47129.

[175] Pearce AK, O'Reilly RK: *Insights into Active Targeting of Nanoparticles in Drug Delivery: Advances in Clinical Studies and Design Considerations for Cancer Nanomedicine*. Bioconjug Chem. 2019 Sep 18;30(9):2300–11, doi: 10.1021/acs.bioconjchem.9b00456.

[176] Dahlman JE, Kauffman KJ, Langer R, Anderson DG: *Chapter Three - Nanotechnology for In vivo Targeted siRNA Delivery*. In: Advances in Genetics. Academic Press; 2014. p. 37–69.

[177] Porter CJ, Moghimi SM, Illum L, Davis SS: *The polyoxyethylene/polyoxypropylene block co-polymer poloxamer-407 selectively redirects intravenously injected microspheres to sinusoidal endothelial cells of rabbit bone marrow*. FEBS Lett. 1992 Jun 22;305(1):62–6, doi: 10.1016/0014-5793(92)80655-z.

[178] Choi HS, Liu W, Misra P, Tanaka E, Zimmer JP, Ipe BI, et al.: *Renal clearance of quantum dots*. Nat Biotechnol. 2007 Oct;25(10):1165–70, doi: 10.1038/nbt1340.

[179] Jain RK, Stylianopoulos T: *Delivering nanomedicine to solid tumors*. Nat Rev Clin Oncol. 2010 Nov;7(11):653–64, doi: 10.1038/nrclinonc.2010.139.

[180] Kettiger H, Schipanski A, Wick P, Huwyler J: *Engineered nanomaterial uptake and tissue distribution: from cell to organism*. Int J Nanomedicine. 2013;8:3255–69, doi: 10.2147/IJN.S49770.

[181] Raza K, Kumar P, Kumar N, Malik R: *9 - Pharmacokinetics and biodistribution of the nanoparticles*. In: Advances in Nanomedicine for the Delivery of Therapeutic Nucleic Acids. Woodhead Publishing; 2017. p. 165–86.

[182] Fang C, Shi B, Pei Y-Y, Hong M-H, Wu J, Chen H-Z: *In vivo tumor targeting of tumor necrosis factor-α-loaded stealth nanoparticles: Effect of MePEG molecular weight and particle size*. Eur J Pharm Sci. 2006 Jan 1;27(1):27–36, doi: 10.1016/j.ejps.2005.08.002.

[183] Bertrand N, Grenier P, Mahmoudi M, Lima EM, Appel EA, Dormont F, et al.: *Mechanistic understanding of in vivo protein corona formation on polymeric nanoparticles and impact on pharmacokinetics*. Nat Commun. 2017 Oct 3;8(1):1–8, doi: 10.1038/s41467-017-00600-w.

[184] Ishiwata H, Suzuki N, Ando S, Kikuchi H, Kitagawa T: *Characteristics and biodistribution of cationic liposomes and their DNA complexes*. J Controlled Release. 2000 Oct 3;69(1):139–48, doi: 10.1016/S0168-3659(00)00293-5.

[185] Rothkopf C, Fahr A, Fricker G, Scherphof GL, Kamps JAAM: *Uptake of phosphatidylserine-containing liposomes by liver sinusoidal endothelial cells in the serum-free perfused rat liver*. Biochim Biophys Acta BBA - Biomembr. 2005 Feb 1;1668(1):10–6, doi: 10.1016/j.bbamem.2004.10.013.

[186] Jain RK: *Barriers to drug delivery in solid tumors*. Sci Am. 1994 Jul;271(1):58–65, doi: 10.1038/scientificamerican0794-58.

[187] Jain RK: *Normalization of tumor vasculature: an emerging concept in antiangiogenic therapy.* Science. 2005 Jan 7;307(5706):58–62, doi: 10.1126/science.1104819.

[188] Boucher Y, Baxter LT, Jain RK: *Interstitial pressure gradients in tissue-isolated and subcutaneous tumors: implications for therapy.* Cancer Res. 1990 Aug 1;50(15):4478–84.

[189] Villaverde G, Baeza A: *Targeting strategies for improving the efficacy of nanomedicine in oncology.* Beilstein J Nanotechnol. 2019 Jan 14;10:168–81, doi: 10.3762/bjnano.10.16.

[190] Kumar Khanna V: *Targeted Delivery of Nanomedicines.* ISRN Pharmacol. 2012;2012:571394, doi: 10.5402/2012/571394.

[191] Maruyama K, Takahashi N, Tagawa T, Nagaike K, Iwatsuru M: *Immunoliposomes bearing polyethyleneglycol-coupled Fab' fragment show prolonged circulation time and high extravasation into targeted solid tumors in vivo.* FEBS Lett. 1997 Aug 11;413(1):177–80, doi: 10.1016/S0014-5793(97)00905-8.

[192] Chapman AP: *PEGylated antibodies and antibody fragments for improved therapy: a review.* Adv Drug Deliv Rev. 2002 Jun 17;54(4):531–45, doi: 10.1016/S0169-409X(02)00026-1.

[193] Marcucci F, Lefoulon F: *Active targeting with particulate drug carriers in tumor therapy: fundamentals and recent progress.* Drug Discov Today. 2004 Mar 1;9(5):219–28, doi: 10.1016/S1359-6446(03)02988-X.

[194] Allen TM: *Ligand-targeted therapeutics in anticancer therapy.* Nat Rev Cancer. 2002 Oct;2(10):750–63, doi: 10.1038/nrc903.

[195] Lammers T, Hennink WE, Storm G: *Tumour-targeted nanomedicines: principles and practice.* Br J Cancer. 2008 Aug;99(3):392–7, doi: 10.1038/sj.bjc.6604483.

[196] Byrne JD, Betancourt T, Brannon-Peppas L: *Active targeting schemes for nanoparticle systems in cancer therapeutics.* Adv Drug Deliv Rev. 2008 Dec 14;60(15):1615–26, doi: 10.1016/j.addr.2008.08.005.

[197] Wu J, Nantz MH, Zern MA: *Targeting hepatocytes for drug and gene delivery: emerging novel approaches and applications.* Front Biosci J Virtual Libr. 2002 Mar 1;7:d717-725.

[198] Mishra N, Yadav NP, Rai VK, Sinha P, Yadav KS, Jain S, et al.: *Efficient hepatic delivery of drugs: novel strategies and their significance.* BioMed Res Int. 2013;2013:382184, doi: 10.1155/2013/382184.

[199] Witzigmann D, Quagliata L, Schenk SH, Quintavalle C, Terracciano LM, Huwyler J: *Variable asialoglycoprotein receptor 1 expression in liver disease: Implications for therapeutic intervention.* Hepatol Res. 2016;46(7):686–96, doi: 10.1111/hepr.12599.

[200] Sahay G, Querbes W, Alabi C, Eltoukhy A, Sarkar S, Zurenko C, et al.: *Efficiency of siRNA delivery by lipid nanoparticles is limited by endocytic recycling.* Nat Biotechnol. 2013 Jul;31(7):653–8, doi: 10.1038/nbt.2614.

[201] Srinivasan M, Domanico SZ, Kaumaya PT, Pierce SK: *Peptides of 23 residues or greater are required to stimulate a high affinity class II-restricted T cell response.* Eur J Immunol. 1993 May;23(5):1011–6, doi: 10.1002/eji.1830230504.

[202] Zwaveling S, Ferreira Mota SC, Nouta J, Johnson M, Lipford GB, Offringa R, et al.: *Established human papillomavirus type 16-*

expressing tumors are effectively eradicated following vaccination with long peptides. J Immunol Baltim Md 1950. 2002 Jul 1;169(1):350–8, doi: 10.4049/jimmunol.169.1.350.

[203] Bijker MS, van den Eeden SJF, Franken KL, Melief CJM, van der Burg SH, Offringa R: *Superior induction of anti-tumor CTL immunity by extended peptide vaccines involves prolonged, DC-focused antigen presentation*. Eur J Immunol. 2008 Apr;38(4):1033–42, doi: 10.1002/eji.200737995.

[204] Slingluff CL: *The Present and Future of Peptide Vaccines for Cancer: Single or Multiple, Long or Short, Alone or in Combination?* Cancer J Sudbury Mass. 2011 Sep;17(5):343–50, doi: 10.1097/PPO.0b013e318233e5b2.

[205] Lempp FA, Mutz P, Lipps C, Wirth D, Bartenschlager R, Urban S: *Evidence that hepatitis B virus replication in mouse cells is limited by the lack of a host cell dependency factor*. J Hepatol. 2016 Mar 1;64(3):556–64, doi: 10.1016/j.jhep.2015.10.030.

[206] Schieck A, Müller T, Schulze A, Haberkorn U, Urban S, Mier W: *Solid-Phase Synthesis of the Lipopeptide Myr-HBVpreS/2-78, a Hepatitis B Virus Entry Inhibitor*. Molecules. 2010 Jul;15(7):4773–83, doi: 10.3390/molecules15074773.

[207] Müller T, Mehrle S, Schieck A, Haberkorn U, Urban S, Mier W: *Liver Imaging with a Novel Hepatitis B Surface Protein Derived SPECT-Tracer*. Mol Pharm. 2013 Jun 3;10(6):2230–6, doi: 10.1021/mp400038r.

[208] Protzer U, Maini MK, Knolle PA: *Living in the liver: hepatic infections*. Nat Rev Immunol. 2012 Mar;12(3):201–13, doi: 10.1038/nri3169.

[209] Gref R, Minamitake Y, Peracchia MT, Trubetskoy V, Torchilin V, Langer R: *Biodegradable long-circulating polymeric nanospheres*. Science. 1994 Mar 18;263(5153):1600–3, doi: 10.1007/s13346-019-00631-4.

[210] Hussain Z, Khan S, Imran M, Sohail M, Shah SWA, de Matas M: *PEGylation: a promising strategy to overcome challenges to cancer-targeted nanomedicines: a review of challenges to clinical transition and promising resolution*. Drug Deliv Transl Res. 2019 Jun 1;9(3):721–34, doi: 10.1126/science.8128245.

[211] Vonarbourg A, Passirani C, Saulnier P, Benoit J-P: *Parameters influencing the stealthiness of colloidal drug delivery systems*. Biomaterials. 2006 Aug 1;27(24):4356–73, doi: 10.1016/j.biomaterials.2006.03.039.

[212] Frank MM, Fries LF: *The role of complement in inflammation and phagocytosis*. Immunol Today. 1991 Sep 1;12(9):322–6, doi: 10.1016/0167-5699(91)90009-I.

[213] van Vlerken LE, Vyas TK, Amiji MM: *Poly(ethylene glycol)-modified Nanocarriers for Tumor-targeted and Intracellular Delivery*. Pharm Res. 2007 Aug 1;24(8):1405–14, doi: 10.1007/s11095-007-9284-6.

[214] Abuchowski A, McCoy JR, Palczuk NC, van Es T, Davis FF: *Effect of covalent attachment of polyethylene glycol on immunogenicity and circulating life of bovine liver catalase*. J Biol Chem. 1977 Jun 10;252(11):3582–6.

[215] Arturson P, Laakso T, Edman P: *Acrylic microspheres in vivo IX: Blood elimination kinetics and organ distribution of microparticles with different surface characteristics*. J Pharm Sci. 1983 Dec;72(12):1415–20, doi: 10.1002/jps.2600721213.

[216] Tan JS, Butterfield DE, Voycheck CL, Caldwell KD, Li JT: *Surface modification of nanoparticles by PEO/PPO block copolymers to minimize interactions with blood components and prolong blood circulation in rats.* Biomaterials. 1993 Sep;14(11):823–33, doi: 10.1016/0142-9612(93)90004-l.

[217] Weissig V, Pettinger TK, Murdock N: *Nanopharmaceuticals (part 1): products on the market.* Int J Nanomedicine. 2014;9:4357–73, doi: 10.2147/IJN.S46900.

[218] Suk JS, Xu Q, Kim N, Hanes J, Ensign LM: *PEGylation as a strategy for improving nanoparticle-based drug and gene delivery.* Adv Drug Deliv Rev. 2016 Apr 1;99(Pt A):28–51, doi: 10.1016/j.addr.2015.09.012.

[219] Woodle MC, Lasic DD: *Sterically stabilized liposomes.* Biochim Biophys Acta. 1992 Aug 14;1113(2):171–99, doi: 10.1016/0304-4157(92)90038-c.

[220] Stolnik S, Illum L, Davis SS: *Long circulating microparticulate drug carriers.* Adv Drug Deliv Rev. 1995 Sep 1;16(2):195–214, doi: 10.1016/0169-409X(95)00025-3.

[221] Jokerst JV, Lobovkina T, Zare RN, Gambhir SS: *Nanoparticle PEGylation for imaging and therapy.* Nanomed. 2011 Jun;6(4):715–28, doi: 10.2217/nnm.11.19.

[222] Ishida T, Ichihara M, Wang X, Yamamoto K, Kimura J, Majima E, et al.: *Injection of PEGylated liposomes in rats elicits PEG-specific IgM, which is responsible for rapid elimination of a second dose of PEGylated liposomes.* J Control Release Off J Control Release Soc. 2006 May 1;112(1):15–25, doi: 10.1016/j.jconrel.2006.01.005.

[223] Ishida T, Ichihara M, Wang X, Kiwada H: *Spleen plays an important role in the induction of accelerated blood clearance of PEGylated liposomes.* J Control Release Off J Control Release Soc. 2006 Oct 27;115(3):243–50, doi: 10.1016/j.jconrel.2006.08.001.

[224] Zhang P, Sun F, Liu S, Jiang S: *Anti-PEG antibodies in the clinic: Current issues and beyond PEGylation.* J Control Release Off J Control Release Soc. 2016 28;244(Pt B):184–93, doi: 10.1016/j.jconrel.2016.06.040.

[225] Neun BW, Barenholz Y, Szebeni J, Dobrovolskaia MA: *Understanding the Role of Anti-PEG Antibodies in the Complement Activation by Doxil in Vitro.* Mol J Synth Chem Nat Prod Chem. 2018 Jul 12;23(7), doi: 10.3390/molecules23071700.

[226] Dams ET, Laverman P, Oyen WJ, Storm G, Scherphof GL, van Der Meer JW, et al.: *Accelerated blood clearance and altered biodistribution of repeated injections of sterically stabilized liposomes.* J Pharmacol Exp Ther. 2000 Mar;292(3):1071–9.

[227] Ishida T, Harada M, Wang XY, Ichihara M, Irimura K, Kiwada H: *Accelerated blood clearance of PEGylated liposomes following preceding liposome injection: effects of lipid dose and PEG surface-density and chain length of the first-dose liposomes.* J Control Release Off J Control Release Soc. 2005 Jul 20;105(3):305–17, doi: 10.1016/j.jconrel.2005.04.003.

[228] Garay RP, El-Gewely R, Armstrong JK, Garratty G, Richette P: *Antibodies against polyethylene glycol in healthy subjects and in patients treated with PEG-conjugated agents.* Expert Opin Drug Deliv. 2012 Nov 1;9(11):1319–23, doi: 10.1517/17425247.2012.720969.

[229] Yang Q, Lai SK: *Anti-PEG immunity: emergence, characteristics, and unaddressed questions.* Wiley Interdiscip Rev Nanomed Nanobiotechnol. 2015 Oct;7(5):655–77, doi: 10.1002/wnan.1339.

[230] Szebeni J, Baranyi L, Savay S, Milosevits J, Bunger R, Laverman P, et al.: *Role of complement activation in hypersensitivity reactions to doxil and hynic PEG liposomes: experimental and clinical studies.* J Liposome Res. 2002 May;12(1–2):165–72, doi: 10.1081/lpr-120004790.

[231] Moghimi SM, Hamad I, Andresen TL, Jørgensen K, Szebeni J: *Methylation of the phosphate oxygen moiety of phospholipid-methoxy(polyethylene glycol) conjugate prevents PEGylated liposome-mediated complement activation and anaphylatoxin production.* FASEB J Off Publ Fed Am Soc Exp Biol. 2006 Dec;20(14):2591–3, doi: 10.1096/fj.06-6186fje.

[232] Lee CC, MacKay JA, Fréchet JMJ, Szoka FC: *Designing dendrimers for biological applications.* Nat Biotechnol. 2005 Dec;23(12):1517–26, doi: 10.1038/nbt1171.

[233] Wurm F, Nieberle J, Frey H: *Double-Hydrophilic Linear-Hyperbranched Block Copolymers Based on Poly(ethylene oxide) and Poly(glycerol).* Macromolecules. 2008 Feb 1;41(4):1184–8, doi: 10.1021/ma702308g.

[234] Wilms D, Stiriba S-E, Frey H: *Hyperbranched Polyglycerols: From the Controlled Synthesis of Biocompatible Polyether Polyols to Multipurpose Applications.* Acc Chem Res. 2010 Jan 19;43(1):129–41, doi: 10.1021/ar900158p.

[235] Hofmann AM, Wurm F, Frey H: *Rapid Access to Polyfunctional Lipids with Complex Architecture via Oxyanionic Ring-Opening*

Polymerization. Macromolecules. 2011 Jun 28;44(12):4648–57, doi: 10.1021/ma200367c.

[236] Müller SS, Dingels C, Hofmann AM, Frey H: *Polyether-Based Lipids Synthesized with an Epoxide Construction Kit: Multivalent Architectures for Functional Liposome*. In: Tailored Polymer Architectures for Pharmaceutical and Biomedical Applications. American Chemical Society; 2013. p. 11–25. (ACS Symposium Series; vol. 1135).

[237] Fritz T, Hirsch M, Richter FC, Müller SS, Hofmann AM, Rusitzka KAK, et al.: *Click Modification of Multifunctional Liposomes Bearing Hyperbranched Polyether Chains*. Biomacromolecules. 2014 Jul 14;15(7):2440–8, doi: 10.1021/bm5003027.

[238] Weber B, Seidl C, Schwiertz D, Scherer M, Bleher S, Süss R, et al.: *Polysarcosine-Based Lipids: From Lipopolypeptoid Micelles to Stealth-Like Lipids in Langmuir Blodgett Monolayers*. Polymers. 2016 Dec 9;8(12), doi: 10.3390/polym8120427.

[239] Weber B, Birke A, Fischer K, Schmidt M, Barz M: *Solution Properties of Polysarcosine: From Absolute and Relative Molar Mass Determinations to Complement Activation*. Macromolecules. 2018 Apr 10;51(7):2653–61, doi: 10.1021/acs.macromol.8b00258.

[240] Gdowski A, Johnson K, Shah S, Gryczynski I, Vishwanatha J, Ranjan A: *Optimization and scale up of microfluidic nanolipomer production method for preclinical and potential clinical trials*. J Nanobiotechnology. 2018 Feb 12;16(1):12, doi: 10.1186/s12951-018-0339-0.

[241] Mülhopt S, Diabaté S, Dilger M, Adelhelm C, Anderlohr C, Bergfeldt T, et al.: *Characterization of Nanoparticle Batch-To-Batch Variability*. Nanomaterials. 2018 May 8;8(5), doi: 10.3390/nano8050311.

[242] Sharpless NE, Flavin M: *The Reactions of Amines and Amino Acids with Maleimides. Structure of the Reaction Products Deduced from Infrared and Nuclear Magnetic Resonance Spectroscopy.* Biochemistry. 1966 Sep;5(9):2963–71, doi: 10.1021/bi00873a028.

[243] Mui BL, Tam YK, Jayaraman M, Ansell SM, Du X, Tam YYC, et al.: *Influence of Polyethylene Glycol Lipid Desorption Rates on Pharmacokinetics and Pharmacodynamics of siRNA Lipid Nanoparticles.* Mol Ther - Nucleic Acids. 2013 Jan 1;2:e139, doi: 10.1038/mtna.2013.66.

[244] Sieber S, Grossen P, Bussmann J, Campbell F, Kros A, Witzigmann D, et al.: *Zebrafish as a preclinical in vivo screening model for nanomedicines.* Adv Drug Deliv Rev. 2019 Dec;151–152:152–68, doi: 10.1016/j.addr.2019.01.001.

[245] Sieber S, Grossen P, Uhl P, Detampel P, Mier W, Witzigmann D, et al.: *Zebrafish as a predictive screening model to assess macrophage clearance of liposomes in vivo.* Nanomedicine Nanotechnol Biol Med. 2019;17:82–93, doi: 10.1016/j.nano.2018.11.017.

[246] PubChem [Online]: *"Sarcosine"*. Available from: https://pubchem.ncbi.nlm.nih.gov/compound/1088. [Accessed: 13-Mar-2020].

[247] Garai P, Gnanadhas DP, Chakravortty D: *Salmonella enterica serovars Typhimurium and Typhi as model organisms.* Virulence. 2012 Jul 1;3(4):377–88, doi: 10.4161/viru.21087.

[248] Van Den Broek PJ, Hiemstra PS, Bril-Bazuin C: *Uptake of antibiotics by monocytes and macrophages.* In: Mononuclear Phagocytes. Dordrecht: Springer Netherlands; 1992 p. 550–3.

[249] Adedeji WA: *THE TREASURE CALLED ANTIBIOTICS*. Ann Ib Postgrad Med. 2016 Dec;14(2):56–7.

[250] Friedman ND, Temkin E, Carmeli Y: *The negative impact of antibiotic resistance*. Clin Microbiol Infect. 2016 May 1;22(5):416–22, doi: 10.1016/j.cmi.2015.12.002.

[251] Shatzkes K, Connell ND, Kadouri DE: *Predatory bacteria: a new therapeutic approach for a post-antibiotic era*. Future Microbiol. 2017 May 1;12(6):469–72, doi: 10.2217/fmb-2017-0021.

[252] Power E: *Impact of antibiotic restrictions: the pharmaceutical perspective*. Clin Microbiol Infect. 2006;12(s5):25–34, doi: 10.1111/j.1469-0691.2006.01528.x.

[253] Swissmedicinfo [Online]: *"Obracin"*. Available from: https://www.swissmedicinfo.ch/. [Accessed: 19-Mar-2020].

[254] Outtandy P, Russell C, Kleta R, Bockenhauer D: *Zebrafish as a model for kidney function and disease*. Pediatr Nephrol. 2019 May 1;34(5):751–62, doi: 10.1007/s00467-018-3921-7.

[255] Claudi B, Spröte P, Chirkova A, Personnic N, Zankl J, Schürmann N, et al.: *Phenotypic Variation of Salmonella in Host Tissues Delays Eradication by Antimicrobial Chemotherapy*. Cell. 2014 Aug 14;158(4):722–33, doi: 10.1016/j.cell.2014.06.045.

[256] Chen X, Zhang M, Zhou C, Kallenbach NR, Ren D: *Control of Bacterial Persister Cells by Trp/Arg-Containing Antimicrobial Peptides*. Appl. Environ. Microbiol. 2011 Jul 15;77(14):4878–85, doi: 10.1128/AEM.02440-10.

[257] Chhabra RS: *Toxicology and Carcinogenesis Studies of 4-Hexylresorcinol (CAS No 136-77-6) in F344/N Rats and B6C3F1 Mice (Gavage Studies).* Natl Toxicol Program Tech Rep Ser. 1988 May;330:1-166.

[258] Yen GC, Duh PD, Lin CW: *Effects of Resveratrol and 4-hexylresorcinol on Hydrogen Peroxide-induced Oxidative DNA Damage in Human Lymphocytes.* Free Radical Research. 2003 Jan;37:509-514, doi: 10.1080/1071576031000083099.

[259] Sumino M, Sekine T, Ruangrungsi N, Igarashi K, Ikegami F: *Ardisiphenols and Other Antioxidant Principles from the Fruits of Ardisia colorata.* J-STAGE Chemical and Pharmaceutical Bulletin. 2002;50:1484-1487, doi: 10.1248/cpb.50.1484.

[260] Kim SG, Lee SW, Park YW, Jeong JH, Choi JY: *4-hexylresorcinol inhibits NF-κB phosphorylation and has a synergistic effect with cisplatin in KB cells.* Oncology Reports. 2011 Dec;26:1527-1532, doi: 10.3892/or.2011.1436.

[261] Buta JG, Moline HE, Spaulding DW, Wang CY: *Extending Storage Life of Fresh-Cut Apples Using Natural Products and Their Derivatives.* Journal of Agricultural and Food Chemistry. 1999 Jan;47:1-6, doi: 10.1021/jf980712x.

[262] González-Aguilar GA, Wang CY, Buta JG: *Maintaining Quality of Fresh-Cut Mangoes Using Antibrowning Agents and Modified Atmosphere Packaging.* Journal of Agricultural and Food Chemistry. 2000 Sep;48:4204-4208, doi: 10.1021/jf991384j.

[263] Craig MP, Gilday SD, Dabiri D, Hove JR: *An Optimized Method for Delivering Flow Tracer Particles to Intravital Fluid Environments*

in the Developing Zebrafish. Zebrafish. 2012 Sep;9(3):108–19, doi: 10.1089/zeb.2012.0740.

[264] PubChem [Online]: *"Hexylresorcinol"*. Available from: https://pubchem.ncbi.nlm.nih.gov/compound/3610. [Accessed: 19-Mar-2020].

[265] Wijk RCV, Krekels EHJ, Kantae V, Ordas A, Kreling T, Harms AC, et al.: *Mechanistic and Quantitative Understanding of Pharmacokinetics in Zebrafish Larvae through Nanoscale Blood Sampling and Metabolite Modeling of Paracetamol*. J Pharmacol Exp Ther. 2019 Oct 1;371(1):15–24, doi: 10.1124/jpet.119.260299.

[266] Moraes JS, da Silva Nornberg BF, Castro MR de, Vaz B dos S, Mizuschima CW, Marins LFF, et al.: *Zebrafish (Danio rerio) ability to activate ABCC transporters after exposure to glyphosate and its formulation Roundup Transorb®*. Chemosphere. 2020 Jun 1;248:125959, doi: 10.1016/j.chemosphere.2020.125959.

Acknowledgements

First and foremost, I would like to thank **Prof. Jörg Huwyler** for the supervision of this PhD project and for giving me the opportunity to work in this exciting field. It was a great experience to work in his team and he always had time and gave great advice throughout the whole time. I am very grateful for the support and the feedback he provided and for the great working atmosphere in his lab. Thank you for the great time I had during my PhD.

For his co-referee, for his feedback on presentations and the PhD project in general, and for the uncomplicated collaboration, I would like to thank **Prof. Alex Odermatt**. Furthermore, I would like to express my gratitude to **Prof. Paola Luciani** for being the external expert in this doctoral committee and to **Prof. Daniel Ricklin** for his chair during my PhD defense.

A big thank you goes to **Dr. Dominik Witzigmann** for his great and constant support throughout the whole time of my PhD. I thank him for introducing me to the topic of gene delivery, for great discussions and ideas and for his most valuable feedback. He always had time for me and his enthusiastic and motivating kind provided great atmosphere during worktime. I very much appreciated the time I was working with him and under his supervision and I also enjoyed the occasional after-work beers.

I would like to thank **Dr. Philip Grossen**, **Dr. Stefan Siegrist**, and in particular, **Dr. Sandro Sieber** for the great atmosphere during the first three years of my PhD. It was a great experience to work with you and I also enjoyed our activities away from work very much. Thank you very much Sandro for introducing me to the zebrafish animal model and for all the feedback you gave during this whole time.

Furthermore, I would like to thank all collaborators from publication. In par-

ticular, I would like to thank **Prof. Andreas Zumbühl** for giving me the opportunity to synthesize aminolipids in his lab in Fribourg and for the warm and welcoming atmosphere during my trips to Fribourg. Also, I would like to express my gratitude to **Dr. Philipp Uhl** for the possibility to visit Heidelberg and to experience *in vivo* trials and radiolabeling first hand. Furthermore, I would like to thank **Prof. Beat Thöny** and his group, and in particular, **Nicole Rimann**, for introducing me to minicircle DNA amplification and **Prof. Mark Helm**, **Dr. Matthias Voigt**, and **Lukas Gleue**, as well as **Prof. Rimma Abramovich** and **Dr. Yury Nikolaev** for the opportunity to work in the field of antibiotics research.

I would like to thank **Dr. Susanne Schenk** for all the support I received from her. Thanks to her constant support and all the work she does for the whole lab, I had the privilege to be able to focus completely on research. Her valuable inputs and her advice helped me a lot. I would also like **Dr. Tomaz Einfalt** for his valuable inputs and for reviewing parts of the thesis, and, of course, I want to thank all the members of the **Pharmaceutical Technology** group. I had a great time in this lab and the members of the team all share a great open-minded attitude. Thanks for the fruitful discussions and valuable inputs and for the great time in general.

I would like to thank all my friends in Basel and in Hochdorf for always being there and for the great time away from work. In particular, I would like to thank my flat mates **Andreas Heilmann** and **Katja Fromm** for the great time I had living together with you. I would also like to thank my carnival group **Philharmoguuger Hochdorf** for the great times during carnival and throughout the year and for the (at times) welcome distraction from work at the weekends.

Special thanks go to my parents **Josef** and **Romy Buck**. They always sup-

ported me and were always there for me when I needed it. Without their support, I would not stand where I am now. In addition, I would also like to thank my brother **Kilian Buck** for being a brother but also a great friend to me.

Finally, the greatest thanks go to my girlfriend **Ursina Stadelmann** for always being there for me and for motivating me. Thank you for your endless support and for being by my side. I am indescribably happy to have you by my side and I am happily looking forward to our future.

Curriculum Vitae

January 2021

Personal Information:

Surname:	Buck
First name:	Jonas
Address:	Hauptstrasse 1, 6280 Hochdorf
Mobile:	079 718 98 44
E-Mail:	jonas.buck131@gmail.com
Date of birth:	03.09.1988
Civil status:	Unmarried
Nationality:	CH

Education:

08/2016 – 04/2020	PhD candidate at the University of Basel in the field of Drug Targeting supervised by Prof. Jörg Huwyler
09/2012 – 07/2014	Master of Pharmaceutical Sciences at the University of Basel
09/2009 – 07/2012	Bachelor of Pharmaceutical Sciences at the University of Basel
08/2001 – 07/2007	High school, Kantonale Mittelschule Seetal
08/1995 – 07/2001	Primary school, Hochdorf

Experience:

07/2020 – Today	Head Galenic Research & Development, Vesifact AG, Baar
08/2016 – 04/2020	PhD candidate at the University of Basel in the field of Drug Targeting supervised by Prof. Jörg Huwyler

05/2016 – 07/2016	Internship at the University of Basel in the field of Drug Targeting supervised by Prof. Jörg Huwyler
07/2014 – 12/2015	Principal Associate in the field of Formulation Research & Development, F. Hoffmann-La Roche AG, Basel
12/2013 – 06/2014	Master thesis project in the field of Formulation Research & Development, F. Hoffmann-La Roche AG, Basel
10/2013 – 11/2013	Internship in the field of Formulation Research & Development, F. Hoffmann-La Roche AG, Basel
2011 – 2013 (During semester break)	Employee in the field of plastic manufacturing, Plastika Balumag AG, Hochdorf
2009 – 2010 (During semester break)	Craftsman, Eiholzer AG, Baldegg
03/2008 – 01/2009	Military service, Swiss Armed Forces
08/2007 – 02/2008	Employee in the field of metalworking, Seven-Air Gebr. Meyer AG, Hitzkirch

Languages:

German	Native speaker
English	Fluent
French	High school knowledge

Personal Interests:

Traveling, trombone playing, member of a carnival music group, playing cards (Jass)

Conferences:

Poster presentation:	Swiss Pharma Science Day in Bern, August 2019
	Annual Research Meeting Pharmazentrum Uni Basel, Februar 2019
	Swiss Pharma Science Day in Bern, August 2018
	PhD Retreat Bio/Pharm Uni Basel in Engelberg, Juni 2018
	Annual Research Meeting Pharmazentrum Uni Basel, Februar 2018
	ILS Liposome Advances and Liposome Research Days Combined Conference in Athen, September 2017

Swiss Pharma Science Day in Bern, August 2017

PhD Retreat Bio/Pharm Uni Basel in Montreux, Juni 2017

6. EuPFi-Konferenz (European Paediatric Formulation Initiative) in Athen, September 2014

Awards:

Poster Award Special Prize	12. Swiss Pharma Science Day in Bern, 28. August 2019 for the poster: "Development of a Salmonella Infection Model in Zebrafish Embryos"
Best Poster Award	6. EuPFi-Konferenz (European Paediatric Formulation Initiative) in Athens, 17. – 18. September 2014 for the poster: "Development And Characterization of Dispersible Tablets Employing Novel Characterization Methods"

Publications:

First author

Buck J, Mueller D, Mettal U, Ackermann M, Grisch-Chan HM, Thöny B, Zumbuehl A, Huwyler J, Witzigmann D. *Improvement of DNA Vector Delivery of DOTAP Lipoplexes by Short-Chain Aminolipids.* ACS Omega. 2020 Sep 15;5(38):24724-24732. DOI: 10.1021/acsomega.0c03303.

Buck J, Grossen P, Cullis PR, Huwyler J, Witzigmann D. *Lipid-Based DNA Therapeutics: Hallmarks of Non-Viral Gene Delivery.* ACS Nano 2019, 13, 3754−3782. DOI: 10.1021/acsnano.8b07858

Buck J, Huwyler J, Dischinger A, Kühl P. *Pediatric Dispersible Tablets: A Modular Approach*. Pharm Res. 2016 Aug;33(8):2043-55. DOI: 10.1007/s11095-016-1946-9

Co-Autor

Nikolaev YA, Tutel'yan AV, Loiko NG, **Buck J**, Sidorenko SV, Lazareva I, Gostev V, Manzen'yuk OY, Shemyakin IG, Abramovich RA, Huwyler J, El'-Registan GI. *The use of 4-Hexylresorcinol as antibiotic adjuvant.* PLoS One. 2020 Sep 22;15(9):e0239147. DOI: 10.1371/journal.pone.0239147.

Fontana F, Lindstedt H, Correia A, Chiaro J, Kari OK, Ndika J, Alenius H, **Buck J**, Sieber S, Mäkilä E, Salonen J, Urtti A, Cerullo V, Hirvonen JT, Santos HA. *Influence of Cell Membrane Wrapping on the Cell-Porous Silicon Nanoparticle Interactions.* Adv Healthc Mater. 2020 Sep;9(17):e2000529. DOI: 10.1002/adhm.202000529.

Bleher S, **Buck J**, Muhl C, Sieber S, Barnert S, Witzigmann D, Huwyler J, Barz M, Süss R, *Poly(Sarcosine) Surface Modification Imparts Stealth-Like Properties to Liposomes.* Small 2019, 15 (50), 1904716. DOI: 10.1002/smll.201904716

Witzigmann D, Uhl P, Sieber S, Kaufman C, Einfalt T, Schöneweis K, Grossen P, **Buck J**, Ni Y, Schenk SH, Hussner J, Meyer zu Schwabedissen HE, Québatte G, Mier W, Urban S, Huwyler J, *Optimization-by-design of hepatotropic lipid nanoparticles targeting the sodium-taurocholate cotransporting polypeptide.* eLife 2019;8:e42276. DOI: https://doi.org/10.7554/eLife.42276

References:

Prof. Dr. Jörg Huwyler
Department of Pharmaceutical Sciences
Division of Pharmaceutical Technology
University of Basel
Klingelbergstr. 50
4056 Basel
Tel: +41 61 207 15 13
E-Mail: joerg.huwyler@unibas.ch

Dr. Susanne Page
PTDC-F, Formulation R&D Oral Dosage Forms
F. Hoffmann-La Roche AG
Building 97/O04.011
Grenzacherstr. 124
CH 4070 Basel
Tel: +41 61 688 70 98
E-Mail: susanne.page@roche.com